Melt migration and deformation in the upper mantle: An example of the Lanzo peridotite massif (Western Alps, Italy)

A dissertation submitted for the degree
of Doctor es Sciences

presented by

Mary-Alix Kaczmarek

April 23, 2007

Institut de Géologie et d'Hydrogéologie
Université de Neuchâtel

Jury members

Prof. Othmar Müntener, Lausanne, CH	PhD supervisor
Prof. Kalt Angelika, Neuchâtel, CH	rapporteur
Prof. Gianreto Manatschal, strasbourg, F	rapporteur
Dr. Rubatto Daniela, Canberra, AU	rapporteur
Prof. Jean-Louis Bodinier, Montpellier, F	rapporteur

From left to right and top to bottom: 1) microphotographs of mylonite, 2) clinopyroxene porphyroclast impregnated by melt with crystallization of plagioclase + orthopyroxene, 3) olivine porphyroclast replaced by interstitial orthopyroxene, and 4) sheared Fe-Ti-gabbro.

Université de Neuchâtel

FACULTE DES SCIENCES
Secrétariat-Décanat de la faculté
- Rue Emile-Argand 11
- CP 158
- CH-2009 Neuchâtel

IMPRIMATUR POUR LA THESE

Melt migration and deformation in the upper mantle : an example of the peridotite massif (Western Alps, Italy)

Mary-Alix Kaczmarek

UNIVERSITE DE NEUCHATEL

FACULTE DES SCIENCES

La Faculté des sciences de l'Université de Neuchâtel,
sur le rapport des membres du jury

Mmes A. Kalt (co-directrice de thèse), D. Rubatto (Canberra, AUS),
MM. O. Müntener (co-directeur de thèse, Lausanne),
G. Manatschal (Strasbourg F) et J.-L. Bodinier (Montpellier F)

autorise l'impression de la présente thèse.

Neuchâtel, le 23 août 2007

Le doyen :
T. Ward

UNIVERSITE DE NEUCHATEL
FACULTE DES SCIENCES
Secrétariat-décanat de la faculté
Rue Emile-Argand 11 - CP 158
CH-2009 Neuchâtel

KEYWORDS & ABSTRACT

KEYWORDS

Lanzo massif, ocean-continent transition, Piemont-Ligurian ocean, plagioclase peridotite, shear zone, mantle exhumation, melt impregnation, major element and trace element geochemistry, oxyde gabbros, zircon U-Pb dating.

MOTS-CLEF

Massif de Lanzo, transition océan-continent, océan Liguro-Piémontais, péridotite à plagioclase, zone de cisaillement, exhumation du manteau, imprégnation de liquide magmatique, géochimie des éléments majeurs et traces, gabbros différenciés, datation U-Pb sur zircon.

ABSTRACT

Mantle domains from present-day and ancient ocean-continent transition zones display signs of melt/rock reaction, but the relationships of the deformation processes during magma-starved periods of (ultra-)slow spreading are poorly understood. The transition from melt-poor to -rich regions is likely to be an important rheological boundary. The mylonitic mantle shear zones are commonly found in peridotite massifs and in the oceanic lithosphere and the grain size reduction is considered as an important process, but the role of melt-enhanced reactions is less well known.

This thesis is the result of field, petrologic and geochemical studies on a high temperature mantle shear zone in the Lanzo peridotite massif from the Western Alps (Northern Italy), and its interaction with melt migration are presented. The mantle shear zone between the northern and the central bodies of the Lanzo massif displays five rock types with different deformation fabrics: coarse grained secondary granular (CGSG), fine grained secondary granular (FGSG), proto-mylonite, mylonite, hydrous-mylonite and ultra-mylonite. The spatial distribution of deformation is asymmetric with respect to the mylonite, increases from SW to NE, and the northern body is composed of CGSG rocks. Discordant mafic dikes are asymmetrically distributed and concentrated in the southern part, which is interpreted as the footwall of the large mantle shear zone.

The high Al pyroxene porphyroclastic cores, indicate high temperatures (1100-1030°C). The low Al neoblasts, display substantially lower final equilibration temperatures at ~860°C. Spinel Cr# (molar Cr/Cr+Al) and TiO_2 concentrations are extremely variable and cover the entire range from spinel to plagioclase peridotite. The variability does not correlate with microstructures in a simple way. However, the CGSG spinel compositions from the central body are more variable than spinel from mylonite, hydrous-mylonite and spinel compositions from the northern body. The spinel compositions indicate local disequilibrium, argue for a rapid exhumation of the central relative to the northern peridotite body.

Melt impregnation textures such as dissolution of clinopyroxene and cotectic crystallization of orthopyroxene and plagioclase, and replacement of olivine by orthopyroxene are common in the massif. Melt impregnation textures largely disappear in the mylonite, indicating that deformation along the mylonite zone outlasted melt-rock reactions. Melt-rock reaction may cause grain size reduction, which in turn led to localization of deformation. The actively deforming peridotite mylonite acted as a permeability barrier for migrating liquid, and thus inhibiting the propagation of gabbroic dikes. This is supported by the observation that gabbros are asymmetrically distributed with respect to the shear zone and concentrate in the footwall of the high-temperature peridotite mylonite zone.

The whole rock major and trace element data of variably deformed peridotite display a large compositional variation from ‘super-fertile’ (e.g. higher than primitive upper mantle [PUM]) to refractory peridotite in the CGSG and, a homogeneous fertile composition in the deformed rocks, which can be explained

by grain size reduction. The incompatible elements show an enrichment in the order of 10-20% in the deformed rocks (proto-mylonite, mylonite and hydrous-mylonite) compared to the CGSG from the northern body. This supports the hypothesis that fine-grained rocks acted as a permeability barrier. The $(Ce/Yb)_N$ ratio display little variation and reinforces the hypothesis that the geochemical signature is not defined by fractionation processes. Simple models indicate that the plagioclase peridotite composition is more consistent with the refertilization processes. It can qualitatively be estimated, that about 5 to 10% of MORB-type liquid must be added to explain the variability of the Lanzo plagioclase peridotites. The enrichment of peridotites in the footwall of a major mantle shear zone indicates that melt accumulation must have been important: consistent with the permeability hypothesis.

Gabbroic rocks from the Lanzo peridotite massif form a cumulate sequence with about 3 orders of magnitude enrichment of incompatible elements. Fe-Ti gabbros dated from the central and the southern part of the massif provided middle Jurassic ages of 161 ± 2, 158 ± 2 and 163 ± 1 Ma, which argues for magmatic activity over a few millions of years. Zircon crystals are characterized by high but variable Th/U ratios, REE patterns enriched in HREE, pronounced positive Ce and negative Eu-anomalies consistent with crystallization after substantial plagioclase fractionation. The zircon trace element composition coupled with whole rock chemistry indicate that a number of gabbros crystallized in-situ, and zircon precipitated from trapped, intercumulus liquid, while other gabbros represent residual liquids that were extracted from a cumulus pile and crystallized along syn-magmatic shear zones. We propose a model, in which the emplacement mechanism of gabbroic rocks in ocean continent transition zones evolves from ‘early’ in-situ crystallization to ‘late’ stratified crystallization with efficient extraction of residual liquid along syn-magmatic shear zones. Such an evolution of the igneous crystallization is probably related to the thermal evolution of the underlying mantle lithosphere.

REMERCIEMENTS

REMERCIEMENTS

Cette aventure a débuté par le bel automne de 2002 et a duré un peu plus de 4 ans merveilleux à Neuchâtel, ville paradisiaque entre lac et montagne. Ce travail de longue haleine aurait été irréalisable sans la présence de nombreuses personnes qui m'ont accompagné durant ces années.

Tout d'abord, je souhaite te remercier **Othmar M.**, pour m'avoir donné l'opportunité de faire cette thèse et de travailler sur le manteau. Tu m'as fait confiance, tu m'as donné un large champ d'action et une indépendance précieuse. Ton optimisme et ton dynamisme, lors de nos meeting-discussions, ainsi que sur le terrain sont toujours un régal à partager. J'ai eu beaucoup de plaisir à travailler avec toi et j'ai beaucoup appris. Merci.

Merci au Fond National Suisse sans qui cette aventure n'aurait jamais été possible (projets 21-66923.01 et 200020-104636/1). Les fonds m'ont permis de faire de nombreuses analyses, de mener sereinement cette recherche et de pouvoir me déplacer dans de nombreux pays pour présenter mes résultats.
Je souhaite également remercier les membres du jury pour avoir accepté d'être rapporteur de mes travaux et de participer à ma thèse.

Ayant travaillé sur le massif de Lanzo en Italie, j'ai découvert une petite région du Piémont et fait mon apprentissage en Italien. Je suis très vite tombée amoureuse de cette région riche et verdoyante, avec une population très accueillante. Merci à l'Albergo delli Valli à Germagnano, cet hôtel familial qui est devenu mon refuge confortable où j'ai goutté les joies de la cuisine Piémontaise. Miam, la charcuterie, le fromage, la Pasta et la Grappa!

Gianreto M., je te remercie beaucoup pour ta spontanéité, pour m'avoir soutenue et pour m'avoir encouragé. Tes conseils ont été précieux dans l'élaboration de mes modèles. Merci également d'avoir pensé à moi et de m'avoir invité pour les whorkshops dans les Alpes où j'ai beaucoup appris et où j'ai rencontré tu sais qui…
Gracie **Daniela R.**, per averla tanto accolse in Australia, quest'esperienza è una memoria fantastica. Ho molto gradito lavorare con te. Grazie per il tu dinamismo, per avere condiviso tu esperienza e la fiducia che avevi per me. Grazie anche a **Jörg H.** per le discussioni sui miei risultati, e grazie ai ragazzi.

Un grand merci aux gens du labo de Neuchâtel. Il y en a tellement sans qui cette thèse ne serait pas ce qu'elle est aujourd'hui. Merci à **Angelika K.** pour ton soutien et pour t'être soucié de mon devenir. Merci à **Arjan D.** pour tes conseils et pour les discussions enrichissantes sur mes données. Merci aussi à **Martin B.**, qui avait toujours une oreille attentive pour une question et un café à proposer. **André V.**, merci pour toutes ces lames minces très précieuses que tu as préparé avec perfection. Un énorme merci à nos secrétaires épatantes : **Gianfranca C. et Sabine E.**, que deviendrions-nous sans vous ? Toujours l'oreille ouverte, prêtes à filer un tuyaux pour résoudre nos petits soucis. Merci aussi à **Eli K.**, notre bibliothécaire, qui a toujours trouvé rapidement les papiers introuvables. Merci aussi à toi **Manu**, le concierge irremplaçable, pour tes coucous pleins de soleil.

Un des avantages de travailler à l'Université de Neuchâtel (hormis la possibilité de se baigner l'été) est de pouvoir bénéficier du système BeNeFri. Entre Neuchâtel, Bern et Fribourg, j'ai profité des infrastructures et de nombreux Scientist. Merci beaucoup à **Massoud Dadrass** et à **Mireille Leboeuf**, du SCEM à

Neuchâtel, pour votre aide lors de l'utilisation du SEM et pour le capricieux EBSD. Mes déplacements m'ont permis de rencontrer et de discuter avec de nombreuses personnes. Merci à vous tous pour avoir été si accueillant. Je souhaite remercier en particulier, Marco Herweg, Igor Villa, Jan Kramers, Edwin Gnoss, Thomas Petke, Bernard Grobety.
Durant ma thèse, j'ai eu la chance de participer à beaucoup de rencontres et d'excursions Géologiques, merci à tous pour cette Science partagée, c'est très exaltant. Merci à Gianreto Manatschal, Brian Tucholke et Jean-Claude Sibuet. pour m'avoir invité et intégré dans les rencontres de géophysiciens et de l'ODP. Thanks to Nick Direen, who invited me at Adelaide for a week to present my research. Merci à Adolphe Nicolas et Françoise Boudier qui m'ont invité à visiter l'ophiolite majestueuse d'Oman et à partager leur connaissance.


Si le vin de Neuchâtel n'est pas ce qui se fait de mieux, le cru des thésards et assistants était extra.
Alex, mon grand ami. Tu étais toujours là pour moi, tu m'as soutenue dans les moments difficiles et nous avons partagé beaucoup de moments fantastiques. Merci pour ta grande gentillesse et ton amitié (et les choux à la crème). C'était génial de t'avoir pendant ces 4 années. **Virginie**, t'es mon côté Ch'Nord. Merci beaucoup pour tous ces moments passés ensemble et pour m'avoir toujours soutenue (ah mais c'est génial!). Au départ, nous avions 3 éléments essentiels en commun : jogging, bière, shopping. Mais maintenant il y en a plein d'autres: bière, shopping, raclette, bricolage, peinture, cuisine, les bains, escalade, jogging, Dominique, blablablablabla. **Charles,** merci d'avoir partagé, ton bureau, ton boulot, ton bordel, la montagne et la photo, c'était formidable. Merci d'avoir supporté les moments où je pétais les plombs ainsi que la mousik. Attention tortue, cochon, globe et pierres volantes! **Steph,** pas bien bavard mais toujours prêt pour les bêtises. Mais laissez-moi tranquillllllle! Je suis très heureuse que parachuté de ton Alsace chérie, tu sois venu faire la fête avec nous à Neuch.





Merci à l'équipe pétro avec qui les excus et les camps de carto étaient toujours des moments fantastiques. **Beni,** mon Swiss deutch préféré, Krlikr. J'ai adoré faire mes premiers pas dans les congrès avec toi, et tous les autres ! C'était super de partager ça. Merci aussi pour tous les petits tuyaux pétro. Chut, fait discret, on va boire une bière? **Laure,** merci pour ta gentillesse, ton enthousiasme et ta fraîcheur. Mais dit-moi, ils sont où les millions ? **Erwan,** tu passais souvent ta tête au bureau, ça va Mary aujourd'hui ? Merci pour ta disponibilité, ta gentillesse et vive le beurre en import direct. Enfin **Flu,** le joli coeur de ces dames, merci pour les tuyaux et les papiers. Ne change pas, j'adore ton parlé français.

Il y a aussi le reste de l'équipe de Neuchâtel qui a contribué à une ambiance de travail particulièrement joviale et détendue et qui m'a permis de rester motivé par tous temps (brouillard, soleil, pluie, neige). **Bast** (mon brother)**, Stafele** (plutôt déçu ou plutôt content?), **Cécile** (Ah, les questions existentielles

de thésardes), et aussi **Nico** (sympa le balcon), **François** (ça va, je t'ai pas fait trop peur?), **Laurent, Melody, Laurent C., Laure**, **Guillaume, J-D, Christophe, Karl, Thirrrry,** l'équipe dynamique de Biologie, tous les autres et les étudiants (et il y en a) avec qui les excus, les barbecs au bord du lac, les restos et toutes autres activités resteront des moments mémorables.

Une thèse c'est « faire de la Science », et si en même temps, il est possible d'avoir des amis dans le même domaine, c'est fantastique. Un grand merci à ma cop's **Mèl,** c'est super de pouvoir parler boulot, de pouvoir dévier sur la vie privée lors de week-end où de rapides coup de fils, hum hum. T'avoir comme amie est formidable. **Audrey** qui vogue sur un autre continent, et qu'il est bon de retrouver au détour d'un congrès ou d'un passage éclair en Europe. **Gwenn**, la meilleure des rencontres lors de ma thèse. Nous avons tellement de choses en commun : un goût certain pour la structure des marges et des rides, les programmes télévisés du dimanche matin, et tellement d'autres choses. Merci pour ta gentillesse, ton enthousiasme et tout ton toi, c'était formidable de passer tous ces moments ensemble.



Merci aussi à **Anne-Lise**, venir à Lausanne pour parler boulot, labo, vie et découvrir les restos sympas de Lausanne. J'adore. Je suis très heureuse de t'avoir rencontré par le biais de la Science. Merci aussi à **Pierre**, nos rencontres étaient très fructueuses autant au niveau Science que personnel, et j'adorais nos petites conférences téléphoniques. Merci aussi à **Alex T**. qui m'a fait mettre un pied en Suisse et découvrir Bâle. j'étais très heureuse de vous voir, toi ainsi que **Emilie** lors de mes virées Bernoises.

Merci aussi à tous mes amis éparpillés en France et dans le monde et où j'ai à chaque fois une petite partie de mon cœur. Ma grande copine Céline H., Arnaud, Séverine, Nico, Céline L., Alexandra, Bruno et Louis, Anne-Marie, Jean-Jean-Michel, Jean-Michel, Jean-Christian, Jean-David, Fred, Pédro, Isabelle, Laure, Sandrine, Agnès. Merci aussi à Greg qui m'a beaucoup soutenu pendant cette thèse. Merci aux copains de Nancy et à tous ceux que j'oublie…

Je ne peux pas terminer sans remercier mes parents qui m'ont permis de faire des études et qui m'ont toujours soutenu. Merci pour votre gentillesse, votre écoute et votre soutien. Je ne serai pas où j'en suis aujourd'hui sans vous. Merci aussi à ma sœur pour sa présence et aussi à vous mon fréro et Amélie, pour ces week-ends chez vous jardinage, déblais ou ski!

Enfin je terminerai par remercier mon Christian, pour m'avoir soutenu durant l'année 2006, année du grand changement. A nous 2007, qui je n'en doute pas sera encore plus formidable.

Merci à toutes celles et tous ceux que j'oublie…



Cette thèse est dédiée a tous ceux qui ont cru en moi.
Une pensée particulière pour ma marraine.

Merci à tous du fond du cœur.

TABLE OF CONTENT

ACRONYMS ALPHABETICAL LIST 23

CHAPTER 1: INTRODUCTION 25

1.1 BACKGROUND AND AIMS OF THIS STUDY 27
1.2 GEOGRAPHIC OVERVIEW 29
1.3 TECTONIC OVERVIEW ON THE LANZO MASSIF 29
1.4 PREVIOUS STUDIES ON THE LANZO MASSIF 31
1.4.1 Layering, foliation and grain size distribution 31
1.4.2 Melt impregnation 32
1.4.3 Gabbroic lenses related to the deformation 35
1.4.4 Early interpretations of the genesis of the Lanzo peridotite 35
1.5 ALPINE HISTORY AND METAMORPHISM OF THE LANZO MASSIF . . .36
1.6 OUTLINE OF THE THESIS 38
1.7 THE STUDY AREA 38

CHAPTER 2: JUXTAPOSITION OF MELT IMPREGNATION AND HIGH TEMPERATURE SHEAR ZONE IN THE UPPER MANTLE (LANZO, N-ITALY) I: TEXTURE AND MINERAL COMPOSITION 41

ABSTRACT 43
2. 1 INTRODUCTION 43
2.2 GEOLOGICAL SETTING 44
2.3 FIELD RELATIONS OF A HIGH TEMPERATURE MANTLE SHEAR ZONE . . 46
2.3.1 Mapping and distribution of peridotite microstructures 46
2.3.2 Spatial distribution of mafic dikes 49
2.4 PERIDOTITE MICROSTRUCTURES 49
2.4.1 Microstructures related to deformation 49
2.4.1.1 Coarse-grained secondary granular texture, CGSG 49
2.4.1.2 Fine grained secondary granular texture, FGSG 51
2.4.1.3 Proto-mylonite texture 51
2.4.1.4 Mylonite texture 51
2.4.1.5 Hydrous mylonite texture 52
2.4.2 Olivine grain size and shear sense 53

2.4.3 Microstructures related to melt impregnation 53

2.5 MINERAL CHEMISTRY 65
2.5.1 Clinopyroxene 67
2.5.2 Orthopyroxene 68
2.5.3 Spinel 70
2.5.4 Olivine 70
2.5.5 Plagioclase 72
2.5.6 Amphibole 72

2.6 THERMOMETRY 72

2.7 DISCUSSION 73
2.7.1 Fabric variation across the shear zone 73
2.7.2 Disequilibrium mineral compositions and relationship to microstructures . . .74
2.7.3 Partial melting, reactive melt percolation, deformation 75
2.7.4 Thermal constraints on the mantle shear zone 76
2.7.5 The mantle shear zone structure, dynamic and implications for the Lanzo massif 76

2.8 CONCLUSIONS AND GEODYNAMIC EVOLUTION 77

ACKNOWLEDGEMENTS 79

CHAPTER 3: JUXTAPOSITION OF MELT IMPREGNATION AND HIGH TEMPERATURE SHEAR ZONES IN THE UPPER MANTLE (LANZO PERIDOTITE, N-ITALY) II: WHOLE ROCK GEOCHEMISTRY 81

3.1 INTRODUCTION 83

3.2 THE LANZO MASSIF 83

3.3 SAMPLE SELECTION AND ANALYTICAL TECHNIQUES 85

3.4 RESULTS 88
3.4.1 Major elements 89
3.4.2 Trace elements 90
3.4.3 Other trace elements 92

3.5 DISCUSSION 93
3.5.1 Major element variability 93
3.5.2 Trace element variability 94
3.5.3 Melting and refertilization modeling 95
3.5.4 Chemical variability as a function of deformation 97
3.5.5 Implications 98

ACKNOWLEDGEMENTS 98

CHAPTER 4: TRACE ELEMENT CHEMISTRY AND U-PB DATING OF ZIRCONS FROM OCEANIC GABBROS AND THEIR RELATIONSHIP WITH WHOLE ROCK COMPOSITION 101

ABSTRACT 103
4.1 INTRODUCTION 103
4.2 GEOLOGICAL SETTING 104
4.3 FIELD OCCURRENCE OF MAFIC DIKES IN THE LANZO MASSIF 105
4.4 PETROGRAPHY OF ZIRCON BEARING GABBRO DIKES 105
4.5 ANALYTICAL TECHNIQUES 107
4.6 WHOLE ROCK MAJOR AND TRACE ELEMENT GEOCHEMISTRY . .109
4.6.1 Major and minor elements 109
4.6.2 Rare earth elements 111
4.7 ZIRCON DESCRIPTION 114
4.8 ZIRCON COMPOSITION 114
4.9 U-PB GEOCHRONOLOGY 115
4.10 DISCUSSION 119
4.10.1 Chemical differentiation of mafic rocks 119
4.10.2 Age interpretation and zircon chemistry 121
4.10.3 Tracking the thermal evolution of an ascent ultra-slow spreading system . .122
4.10.4 Paleogeographic consequences 122
4.11 CONCLUSIONS 123
ACKNOWLEDGEMENTS 123

CHAPTER 5: CONCLUSIONS AND OUTLOOKS 127

5.1 RESULTS AND CONCLUSIONS 129
5.1.1 Principal results 129
Deformation in the peridotite 129
Minerals and peridotite geochemistry 129
Mafic dikes in the Lanzo peridotite 129
5.1.2 What is new on the Lanzo massif ? 130
5.2 THE LANZO SHEAR ZONE IN RELATION TO OTHER MANTLE

PERIDOTITES 130
5.3 OUTLOOKS 131

APPENDIX 135

REFERENCES 189

APPENDIX 1: ANALYTICAL METHODS (CD)

APPENDIX 2: MAPS, TEXTURES AND MICROPROBE DATASET 137

A2.1 MICROTEXTURE DEFORMATION CLASSES 139

A2.2 LANZO MAPS AND SAMPLE LOCALIZATION 142

A2.2a Northern part 142

Outcrops and sample localization 142

Sample and microtexture classes 143

A2.2b Sample list from the northern part 144

A2.2c Southern part 145

Sample localization in Lanzo south 145

Foliation, layering and dike orientation 146

A2.3 L187 OUTCROP: HYDROUS- AND ULTRA-MYLONITE 147

A2.3.1 Microstructure of the hydrous-mylonite zone 147

A2.3.2 Hydrous-mylonite foliation and shearing 148

A2.3.3 Mineralogy of shear plane P4 150

A2.3.4 Mylonite and gabbros 150

A2.3.5 Conclusions on the hydrous-mylonite zone 153

A.2.3.6 Summary and conclusions on the shear zones 153

A2.4 MELT IMPREGNATION TEXTURES 155

A2.4a Clinopyroxene porphyroclastic replaced by oxp + plg 155

A2.4b Olivine porphyroclasts replaced by orthopyroxene 156

A2.4c Crystallization of feldspath close to spinel 157

A2.4d Recrystallization of ol, cpx, opx 157

A2.5 MICROPROBE DATASET (SEE CD)

A2.5a Orthopyroxene

A2.5b Clinopyroxene

A2.5c Olivine

A2.5d Spinel

A2.5e Plagioclase

A2.5f Hornblende

A2.6 PROFILES OF MINERALS (DATASET ASSOCIATED ON CD)

A2.6a Orthopyroxene 159

A2.6b Clinopyroxene 164

A2.6c Spinel 168

A2.6d Plagioclase 175

A2.7 THERMOMETRY (SEE CD)

A2.8 STRUCTURAL DATA SET (SEE CD)

A2.8a Northern part
A2.8b Southern part

APPENDIX 3 :DIKES AND ZIRCON 177

A3.1 LAYERING ON OUTCROPS 179

A3.2 OUTCROPS OF DIKES 180
A3.2a Dikelets 180
A3.2b Gabbros from the central and southern part 181
A3.2c Basalts 182

A3.3 SEM IMAGES OF ZIRCON 183

A3.4 CATHODOLUMINESCENCE IMAGES OF ZIRCON 185
A3.4a Sample L165 185
A3.4b Sample A71 185
A3.4c Sample A91 186

APPENDIX 4 : ZIRCON OF GRANULITE (B11) (CD)

A4.1 MICROPHOTOGRAPH

A4.2 ZIRCON CATHODO-LUMINESCENCE PICTURES

A4.3 TRACE ELEMENT OF ZIRCON

A4.4 ZIRCON U-PB GEOCHRONOLOGY

APPENDIX 5: PUBLICATION AND SELECTED COMMUNICATION (CD)

A5.1 LANZO FIELD GUIDE, KACZMAREK AND MÜNTENER, 2005 (OFIOLITI, 30, 125-134)

A5.2 SELECTED POSTER PRESENTATION

A5.2a Swiss Geosciences meeting (2003)
A5.2b Goldschmidt conference (2004)
A5.2c EGU (2005)
A5.2d Deformation Rheology and Tectonic conference (2005)
A5.2e AGU fall meeting (2006)

ACRONYMS ALPHABETICAL LIST

Minerals

An: anorthite
Ap: apatite
Chl: chlorite
Cpx: clinopyroxene
Grt:garnet
Hbl: hornblende
Ilm: ilmenite
Ol: olivine
Opx: orthopyroxene
Plg: plagioclase
Sp: spinel
Zr: zircon

CL: Cathodoluminesence
CGSG: Coarse Grained Secondary Granular
CGSGn: CGSG rocks from the northern body
CGSGc: CGSG rocks from the central body
DMM: Depleted MORB Mantle
EBSD: Electron Backscatter Diffraction
FGSG: Fine Grained Secondary Granular
H-M: Hydrous-Mylonite
HP: High Pressure
HFSE: High Field Strength Elements
HREE: Heavy Rare Earth Elements
ICP-MS: Inductively coupled plasma-mass spectrometer
LA: Laser Ablation analyze
LOI: Loss of Ignition
LOT: Lherzolite Ophiolite Type
LREE: Light Rare Earth Element
MORB: Mid Ocean Ridge Basalt
MSWD: Mean Square Weighted Deviate
OCTZ: Ocean Continent Transition Zone
PM: Primitive Mantle
PUM: Primitive Upper Mantle
REE: Rare Earth Elements
SEM: Scanning Electron Microscope
SHRIMP: Sensitive High Resolution Ion Microprobe
SWIR: South Western Indian Ridge
SZ I: Shear Zone I
SZ II: Shear Zone II
XRF: X-ray fluorescence spectroscopy
ZECM: Zone of Exhumed Continental Mantle

CHAPTER 1:

INTRODUCTION

Germagnano and Gran Costa

1.1 BACKGROUND AND AIMS OF THIS STUDY

Studies comparing field data from orogenic ophiolites with those derived from geophysical investigations and deep sea drilling from actual mid-ocean ridges were fundamental for the development of conceptual models of the oceanic lithosphere. Classic models for the structure of the oceanic lithosphere are described with a sedimentary sequence and a 4 to 6 km thick igneous crust overlying a peridotite basement. The igneous crust is produced by decompression melting of ascending asthenospheric mantle. However, in the last ten years, it has been shown that along slow and ultra-slow spreading ridges, magma supply is limited (Cannat, 1993; Cannat, 1996; Dick et al., 1984; Michael et al., 2003) and that exposure of crust-free mantle lithosphere is more common that previously supposed (Bonatti et al., 2001; Cannat, 1993; Cannat et al., 1997; Michael et al., 2003). Along mid-ocean ridges outcrop of peridotite on the ocean floor by mantle denudation occurs as fracture zones, magma-starved rift segments, and oceanic core complexes (Blackman et al., 1998; Tucholke et al., 1998).

The concept of ophiolite as defined at the Penrose conference (1972) is unlike of numerous ophiolite sections in the Alps, Corsica and Apennine. The Alpine-Apennine ophiolites display important volume of mantle that were serpentinized at the sea floor and very low volumes of gabbro and basalt, the absence of sheeted dike complex and a sedimentary stratigraphic sequence sitting directly on the top of the mantle (Lagabrielle and Lemoine, 1997). The peculiar stratigraphy of Alpine ophiolites suggests three classes of genetic models: (1) the slow spreading ridge system (Lagabrielle and Lemoine, 1997), (2) the transform fault model (Weissert and Bernoulli, 1985), and (3) the low angle detachment faulting model (Froitzheim and Eberli, 1990; Lemoine et al., 1987; Piccardo et al., 1990).

The processes controlling the margin architecture must be connected to mantle processes. The understanding of detachment faulting, mantle exhumation in the Ocean Continent Transition Zone (OCTZ) and the sediment architecture across the margin is important and is enhanced by the study of remnants of ancient margins preserved in the Alps (Lemoine et al., 1986; Manatschal, 2004; Manatschal and Bernoulli, 1999; Manatschal and Nievergelt, 1997). Based on the magmatic architecture and their relation to exhumed mantle rocks, the ophiolites exposed along the Franco/Italian Alps were interpreted to have formed within a slow-spreading ridge environment (Lagabrielle and Cannat, 1990; Lagabrielle and Lemoine, 1997). The conceptual model explaining Tethyan passive margin formation (Lavier and Manatschal, 2006; Manatschal, 2004) offers a schematic explanation of the evolution of different Alpine peridotites that formed some sort of a “Tethyan” oceanic crust during the middle Jurassic. These peridotite “massifs” record several evolutionary stages in the evolution of magma-poor passive margins (e.g. Desmurs, 2001; Müntener et al., 2000; Rampone et al., 1996). While the transition from continental crust to exhumed mantle has been studied in the Alps (e.g. Desmurs, 2001; Manatschal and Nievergelt, 1997), inferred in the Apennines (Marroni et al., 1998) and drilled off Iberia (Péron-Pinvidic et al., 2007; Whitmarsh et al., 2001), little is known at present about how the OCT evolves into unequivocal oceanic crust formed in a (slow) spreading system.

The detachment structures exhuming the mantle in the OCTZ are concave downward and are rooted in the mantle (Manatschal, 2004). The deformation associated with lithospheric extension and thinning is forming km-scale shear zones in the mantle lithosphere which are responsible for exhumation of mantle rocks to the ocean floor at mid-ocean ridges, in particular in slow-spreading oceans (Cannat, 1993; Jaroslow et al., 1996). Peridotite shear zones may control the strength of the upper mantle (Vissers et al., 1995; 1997) and therefore play a crucial role in lithosphere scale deformation processes. Mylonite shear zones are commonly found in peridotite massifs (Boudier et al., 1988; Ceuleneer et al., 1988; Dijkstra et al., 2002; Furusho and Kanagawa, 1999; Hoogerduijn Strating et al., 1993; Newman et al., 1999; Vissers et al., 1991) and in peridotite from the ocean floor (Beslier et al., 1996; Cannat et al., 1991; Jaroslow et al., 1996; Warren and Hirth, 2006). A consequence of low-angle detachment faulting models is that most of the exhumed mantle rocks have a subcontinental origin, as revealed by field evidences (Florineth and Froitzheim, 1994;

Manatschal, 2004; Müntener and Hermann, 1996; Trommsdorff et al., 1993) and petrologic and isotopic studies (Bodinier et al., 1991; Piccardo, 1976; Rampone et al., 1995; Rampone et al., 1996). It has been shown (South Lanzo and Erro-Tobbio, Ligurian Alps) that pristine mantle protoliths from the deep subcontinental lithosphere of the future Europe-Adria realm record a composite scenario of magmatic and tectonic-metamorphic events during lithospheric extension and pre-oceanic rifting in the Alpine Tethys (Piccardo et al., 2007). Two main processes dominating the extensional evolution are: 1) the progressive subsolidus decompressional upwelling of the lithospheric mantle (mainly peridotites close to the continent) and 2) the formation and migration of MORB-type melts from the underlying molten asthenosphere (mainly those that are at some distance from the continent). The peridotites from these two different settings show highly contrasted chemistries and are clearly linked in space and time.

Recent studies showed that Alpine peridotites, and in particular the Lanzo peridotites, record a wide variety of mantle processes, including melt percolation, melt/rock interaction and refertilization (Müntener et al., 2004; Müntener and Piccardo, 2003; Piccardo, 2003; Piccardo et al., 2004; Piccardo et al., 2006). Numerous plagioclase peridotites exhumed in OCTZ represent hybrid rocks composed of subcontinental mantle modified by reaction and partial crystallization of liquid produced during mantle upwelling and early stage of seafloor spreading (Müntener et al., 2004). The occurrence of trapped basaltic magmas in mantle peridotites is documented in present-day oceanic settings (Cannat et al., 1992; Dick, 1989; Girardeau and Mercier, 1992). Piccardo et al. (2007) show that many of the ophiolitic peridotites from the Ligurian Tethys underwent diffuse structural and compositional modification by various melt percolation and melt-rock interaction events, during their progressive exhumation from subcontinental lithospheric depths to shallow levels. The upward migration of the asthenospheric melts (from reactive percolation at spinel-facies conditions to melt impregnation at plagioclase-facies conditions) produced the compositional modification (both depletion and enrichment) of the extending lithospheric mantle, which underwent thermo-mechanical erosion, i.e. it was “asthenospherised” (Bodinier and Godard, 2003; Müntener and Piccardo, 2003; Müntener et al., 2005; Piccardo, 2003; Piccardo et al., 2004; Piccardo et al., 2007). The early asthenospheric melts that ascended in the extensional system were apparently trapped in the mantle, and the pre-oceanic rift stages are thus characterized by the lack of volcanics. Note, however, that a similar scenario can be inferred in the more Internal sequences, (e.g. Internal Ligurides and Corsica), which are equally characterized by significant melt storage in the extending mantle, via both impregnation and intrusion, but poorly documented volcanism. Thus, rifting and drifting in the Ligurian Tethys were mostly non-volcanic, but not a-magmatic, similarly to what is found for slow and ultra-slow spreading oceanic settings (Dick et al., 2003).

In the Lanzo massif, rapid cooling after mantle refertilization and a change in the melt extraction mechanism from pervasive porous flow to diking has been proposed (Müntener and Piccardo, 2003). The presence of gabbro dikes in the ancient margins allowed constraining the timing of continental break-up. Ages on gabbros from the zone of exhumed continental mantle (ZECM) show ages ranging between 162 and 156 Ma (Costa and Caby, 2001; Peters and Stettler, 1987; Rampone et al., 1998; Rampone et al., 2005; Schaltegger et al., 2002), and are interpreted as representing early (syn-rift) melt crystallization in lithospheric mantle peridotites. Gabbros from the Ligurian peridotites are slightly older (Borghini et al., 2007; Tribuzio et al., 2004). Finally, younger ages are recorded by some plagiogranites from the Ligurian peridotites and the Chenaillet massif (Borsi et al., 1996; Costa and Caby, 2001), ranging from 156 to 148 Ma. These rocks cut across breccias and basaltic rocks and thus clearly postdate continental breakup. The range of ages is consistent with a relatively short time period (<~15-20 Ma) implying that exhumation and cooling of the subcontinental mantle was associated with emplacement of gabbro bodies, and, finally, basalt extrusions.

The main objective of this PhD thesis is to better constrain the relative roles of the melt impregnation and its interplay with mantle deformation through tectonic processes during

mantle exhumation before the continental break-up. This study will address the following problems:
- The Lanzo massif was exhumed from spinel to plagioclase facies. This mantle shear zone involves structural and geochemical variations in the peridotite. What are the high-temperature deformation processes related to detachment faulting and mantle exhumation at the seafloor?
-The Lanzo south peridotite massif recorded a transitional scenario extending sub-continental lithosphere mantle with depleted compositions. The peridotite was both depleted and refertilized by early melts with MORB-affinity formed by decompression partial melting of the upwelling asthenosphere during pre-oceanic rifting and lithosphere thinning in the Ligurian Tethys (Piccardo et al., 2007). The Lanzo north is also interpreted as a sub-continental lithosphere (Bodinier et al., 1991), but the possibility of a refertilized peridotite has not be investigated. Is it possible that the northern part of the massif was both depleted and refertilized?
- What is the spatial and temporal relationship between deformation and the mode of melt migration in the mantle? How important are pervasive porous flow, focused melt flow and dikes with respect to deformation of the Lanzo peridotite? Are there feedback mechanisms between melt migration and deformation?
- The Lanzo massif is part of the oceanic crust in the Piemont-Ligurian ocean (Lagabrielle et al., 1989; Pelletier and Müntener, 2006). What are the fractionation processes and what are the timescales of oceanic crust accretion within the Lanzo massif? Dating of gabbro dikes, which represent the crystallization of melt during oceanic crust exhumation, will constrain the timing of melt percolation in the Lanzo massif.

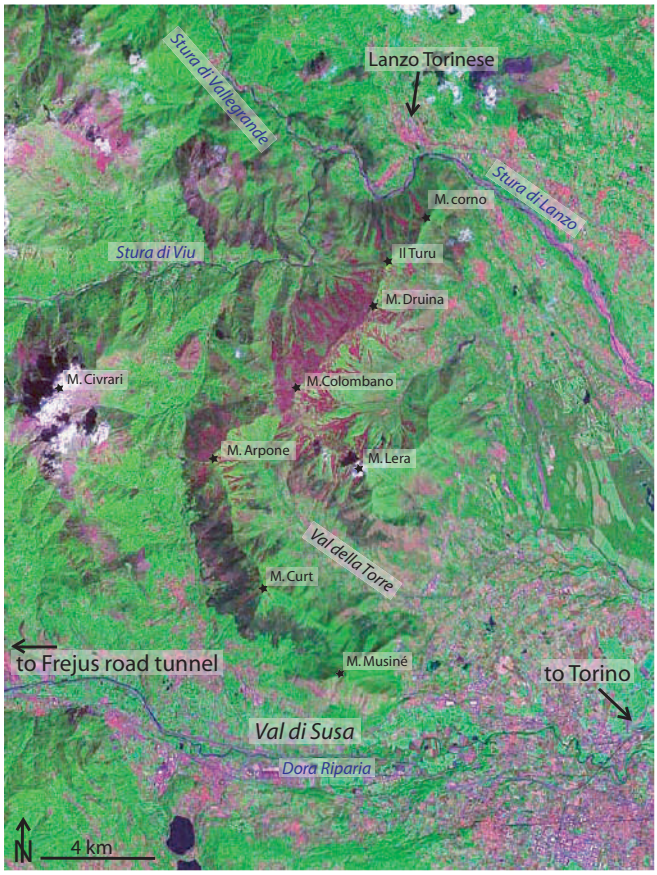

Fig. 1.1: The Landsat image represents the geographical location of the Lanzo massif near Torino (source NASA and Earth Satellite Corporation, https://zulu.ssc.nasa.gov/mrsid/, image: NASA N-32-45).

1.2 GEOGRAPHIC OVERVIEW

The Lanzo massif is located north-west of Torino in the Piemontese Alps, and between Lanzo-Torinese village to the north and Val di Susa to the south, just at the Po plain boundary (Fig. 1.1). The Landsat image shows that many parts of the Lanzo massif are covered by vegetation (green) and numerous rockslides (purple). The Landsat image also highlights Stura and Val della Torre, which separate the northern form the central body and the central from the southern body of the massif, respectively. The central and the southern bodies are underline by the crest line: the south part from NW (Monte Arpone) to SE (Monte Musiné), and the central part from north (Monte Corno) to south (Monte Lera). The altitude varies from 1658 m (Monte Colombano) to 500 m (Lanzo Torinese). The major summits are Monte Arpone (1600 m), Monte Lera (1371 m) and Monte Druina (1516 m).

1.3 TECTONIC OVERVIEW ON THE LANZO MASSIF

The Lanzo massif was first studied in detail during the seventies by a group of French researchers, principally by A. Nicolas and F. Boudier, who provided the first detailed maps and proposed a genetic model about this peridotite massif, which was influential for later studies on the structural petrology of the mantle rocks (Boudier,

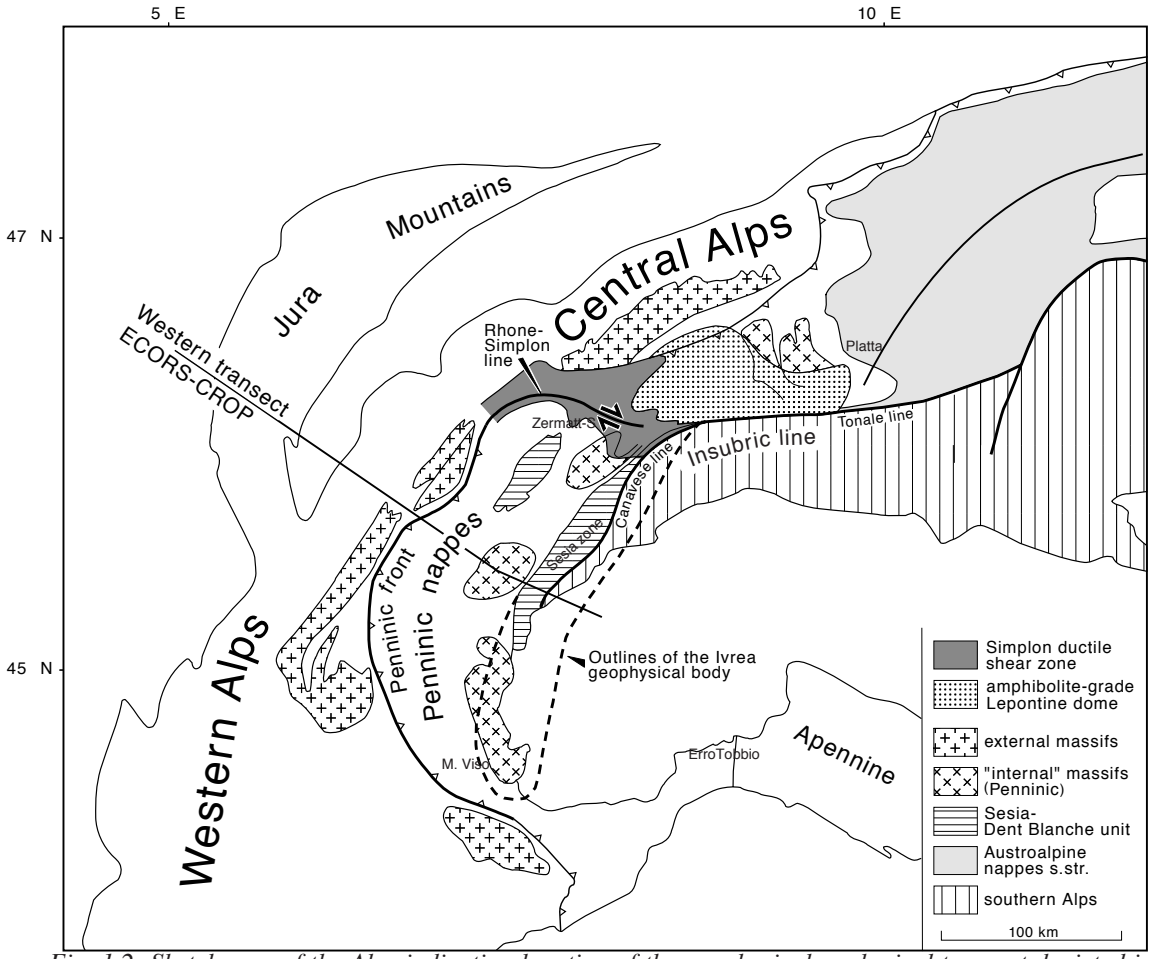

Fig. 1.2: Sketch map of the Alps indicating location of the geophysical-geological transect depicted in Fig. 1.) (modified after van der Pluijm and Marshak, 2004).

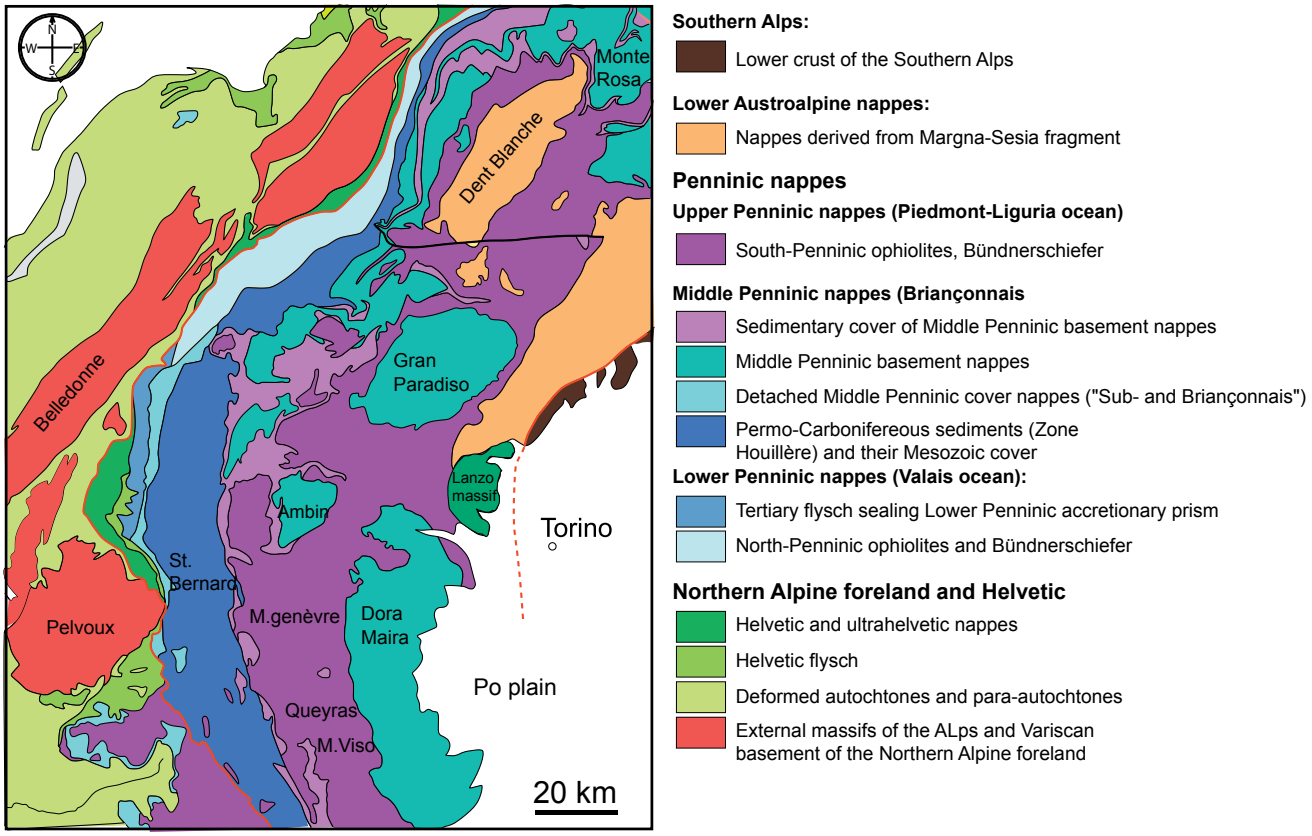

Fig. 1.3 Structural units of the Western Alps, after Schmid et al. (2004).

1978; Boudier and Nicolas, 1972; Nicolas et al., 1972; Nicolas et al., 1971). The Lanzo massif is surrounded by the Piemontese ophiolites (west), the Sesia zone (north) and is close to the Po plain (east) (Fig. 1.2 and 1.3). In the Penninic zone, the metamorphic conditions increase from west to east, from blueschist to eclogite facies respectively. Nicolas et al. (1972) proposed that the "Viu-Locana" zone corresponds to an older seismic zone plunging below the Adriatic plate. In his view, this zone was the limit between the European and the Adriatic plate, and would have allowed exhumation of the mantle roof during Alpine collision. The Lanzo massif was interpreted as the exposed mantle part of a mantle roof linked to the Ivrea zone, which developed a high-pressure paragenesis during final exhumation phase (Boudier and Nicolas, 1972, Fig. 1.3). However, the discovery of eclogite facies metamorphism in the Lanzo massif (Compagnoni

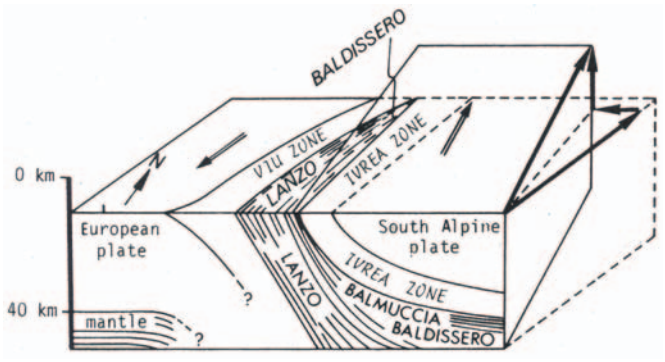

Fig. 1.4: Conceptual model of the relative displacement of South Alpine and European plates as inferred from the internal structures of the Lanzo massif (Boudier, 1978).

and Sandrone, 1979; Kienast and Pognante, 1988) argue for the subduction of the body during the Alpine orgenesis, and therefore the Lanzo massif cannot be directly linked to the geophysical Ivrea body. According to Boudier (1972), peridotite and gabbroic petrology indicates a ~ 100km depth origin of the peridotite massif and partial melting at 15 to 20 km at 1250°C during the exhumation. In the eighties, several studies (Bodinier et al., 1986; Lombardo and Pognante, 1982; Pognante et al., 1985) focused on the mafic rocks and highlighted the presence of N-MORB type magmas intruding the peridotite. Pognante et al. (1985) concluded that the Lanzo massif was not a residua after extraction of N-MORB type melts, but might be a section of sub-continental lithosphere, which recorded partial melting processes during exhumation and was later intruded by a N-MORB produced at depth. The Lanzo massif is considered as an integral part of the Piemont-Ligurian oceanic crust and forms the basement of an oceanic sequence. The oceanic sedimentary sequence of the Lanzo massif is very similar to those from the Piemontese ophiolite (Lagabrielle et al., 1989), which further support the hypothesis that the Lanzo massif was part of the Piemont Ligurian ocean floor. This hypothesis of exposure on the ocean floor is also indicated by the discovery of local ophicarbonate breccias (Pelletier, 2003; Pelletier and Müntener, 2006).

1.4 PREVIOUS STUDIES ON THE LANZO MASSIF

1.4.1 Layering, foliation and grain size distribution

The oldest structure in the Lanzo peridotite that is affected by high-temperature plastic deformation is a pyroxenitic layering (So). The layering is composed of variable amounts of spinel, pyroxene, olivine and plagioclase. The thickness varies from north to south in the massif: the layering seems to be thicker (from 1 cm up to 40 cm, (Boudier, 1972) and folded (Fig. 1.5a-b) in the northern and central bodies. In the southern part of the massif, the layering is thin and sometimes extremely reduced. Locally, ghost layering in dunite bodies can be observed, particularly in the southern part of the massif (Piccardo et al., 2007). Pyroxenite layering is overprinted by a high-temperature foliation (S1), which can be recognized in the field by the alignment of pyroxene, spinel and plagioclase. A series of maps realized on the entire Lanzo massif (Boudier, 1972) highlight pyroxenite banding and high temperature foliation. They are parallel in the southern body and discordant in the central and northern bodies (Fig. 1.6a). So the layering and the foliation tends to be parallel in the area between the northern and the central bodies. The grain size measured in this zone is small (0.2 mm), contrary to the grain size in the southern and northern bodies (> 500 μm, Fig. 1.6b, 1.7). Smaller grain size observed between the northern and the central bodies along a more than 4 km^2 area is also observed between the central and the southern bodies in a small area of ~1 km^2 (Nicolas et al., 1972). In the following, these 2 areas are

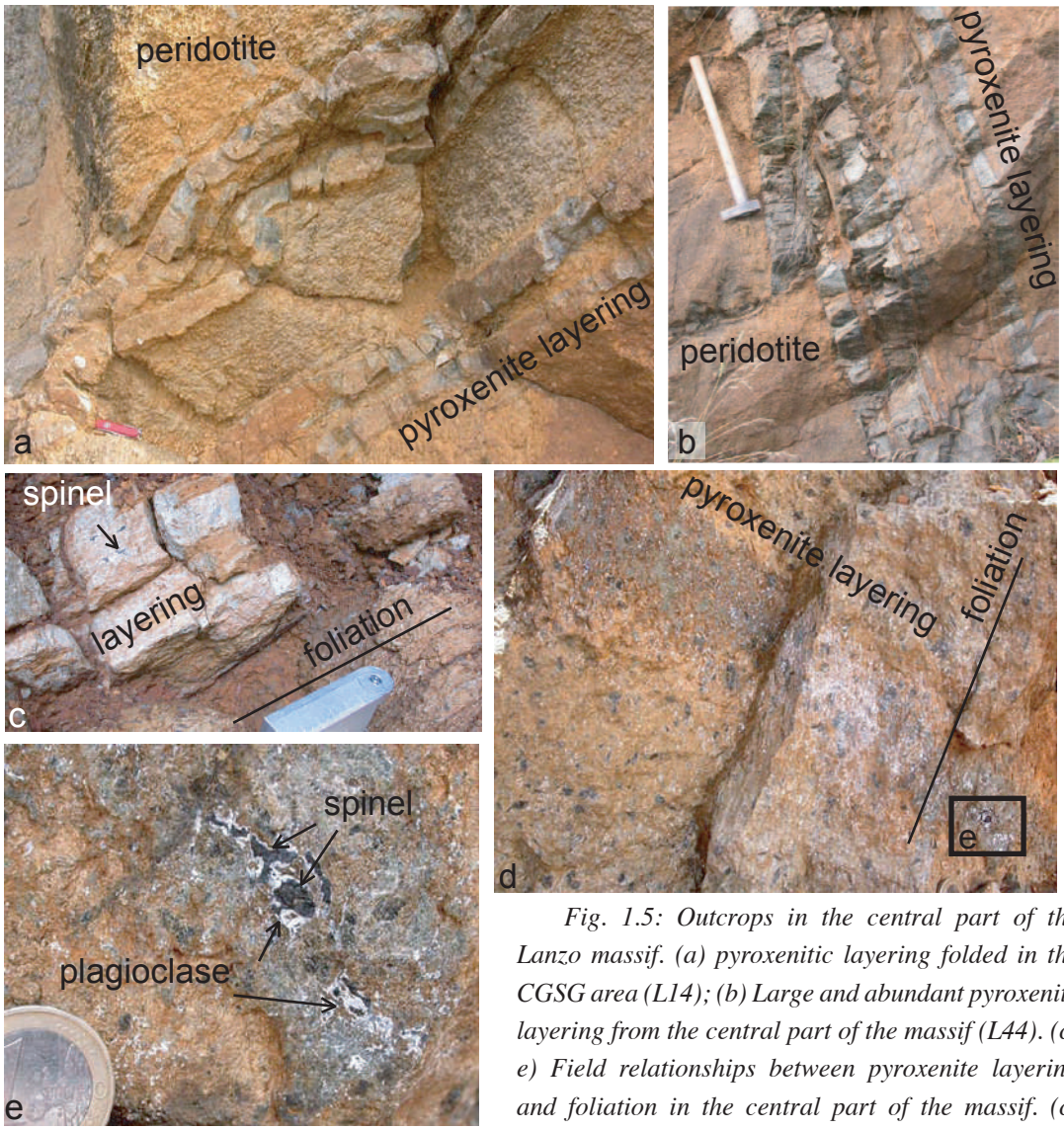

Fig. 1.5: Outcrops in the central part of the Lanzo massif. (a) pyroxenitic layering folded in the CGSG area (L14); (b) Large and abundant pyroxenite layering from the central part of the massif (L44). (c-e) Field relationships between pyroxenite layering and foliation in the central part of the massif. (c) In the mylonite area the layering is characterized by elongate spinel parallel to the foliation. (d) Granular peridotite with pyroxenite layering contains spinel surrouded by plagioclase. The foliation, outlined by plagioclase, is perpendicular to the layering. (e) Detail of pyroxenite layering composed of pyroxene, spinel and plagioclase.

called shear zone I (SZ I), and shear zone II (SZ II), respectively (Fig. 1.7). The grain size reduction in SZ I is concordant with the parallelization of the foliation with the layering, which contains elongate spinels underlining the foliation (Fig. 1.5c, see part. 2.2). To the south of SZ I, the peridotite is granular and foliation is discordant to layering (Fig. 1.5d-e). The pyroxenite layering shows diffuse contacts with the peridotite, this is the result of high temperature deformation, which overprints the layering and involves minerals recrystallization along the foliation.

Shear zone II is located in the south of the central body, and the boundary of the area is delimited by the grain size reduction. The zone indicates a NW-SE orientation, which is parallel to the SZ I orientation (Fig. 1.6b). The pyroxenite layering and foliation tend to be parallel in the SZ II but the orientation N-S is discordant to the orientation the foliation and the pyroxenite layering of the SZ I (NW-SE) (Fig. 1.6a).

1.4.2 Melt impregnation

The Lanzo massif is a lherzolitic body recording melt impregnation linked to melt migration (Müntener and Piccardo, 2003; Piccardo et al., 2007). Figure 1.8 represents a conceptual model of melt rock interaction processes with temperature variation, schematically illustrated by 5 successive events that are continuous in time

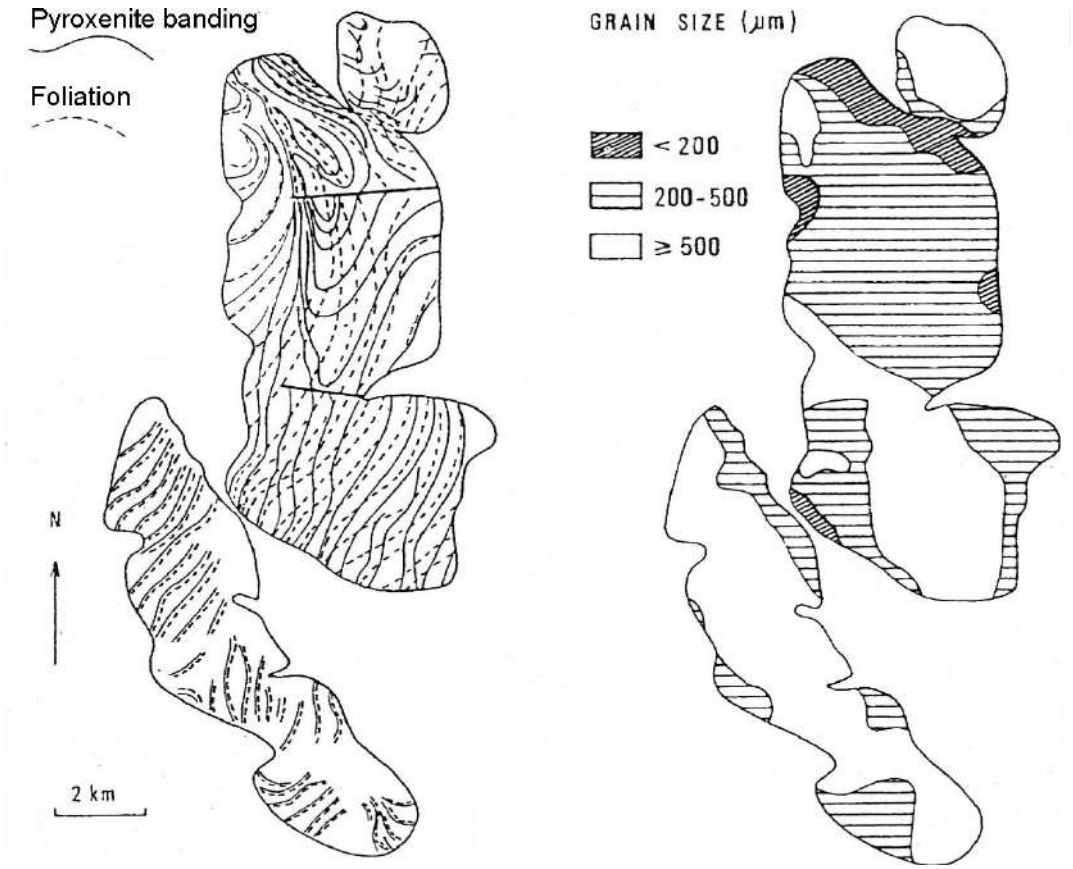

Fig. 1.6: Sketch map showing structural and textural variations in the Lanzo massif: (a) Structural pattern of the massif (Boudier and Nicolas, 1980). The pyroxenites are concordant in the southern and western part of the massif, whereas they are discordant in the eastern and northern part of the massif; (b) Grain size map (Boudier et Nicolas, 1980) grain size <200µm corresponds to mylonitic texture, 200-500 µm to intermediate textures and > 500µm to protogranular texture.

(Müntener and Piccardo, 2003).

The first sketch (a) illustrates the intersection of the high temperature foliation of the peridotite with the pyroxenite layering. The temperature is below the solidus of peridotite (~1100°C) and corresponds to a ± conductively cooled mantle. The second sketch (b) is characterized by pervasive melt infiltration and melt-rock reaction at high temperature (The temperature is below the solidus of peridotite (~1100°C) and corresponds to a ± conductively cooled mantle. The second sketch (b) is characterized by pervasive melt infiltration and melt-rock reaction at high temperature (ted from below reacts with the surrounding peridotite in a complex way, producing first pyroxene-undersaturated liquids followed by orthopyroxene and clinopyroxene saturated melt (Müntener and Piccardo, 2003). The quantities of melt increase and the melt flow changes from initially porous to focused. (c) The focused porous melt flow involves dunite channels at a thermal maximum close to the peridotite solidus (>1200°C). Reactive harzburgites and dunites are discordant to the foliation and the layering, and replace plagioclase peridotite and spinel websterite. The transition from porous to focused melt flow might indicates that the competing effects between heating of the mantle by ascending magmas from the underlying hot asthenosphere and cooling by exhumation are still dominated by the rising isotherms. (d) Beginning of cooling will create dunite conduits with interstitial cpx and plagioclase megacrysts, and eventually change the melt migration mechanisms from focused flow to cracks, which are represented by gabbroic veinlets. (e) Continued cooling (~1000°C) and exhumation leads to the formation of km-scale gabbroic dikes, discordant to the previous igneous features. These gabbroic dikes range from primitive troctolite to Fe-Ti gabbros, indicating the increasing effect of crystal fractionation on the evolution of magma at falling temperatures. This event has been dated by the U-Pb method on zircons from Fe-Ti gabbros to be between 163-158 Ma (chapter 4).

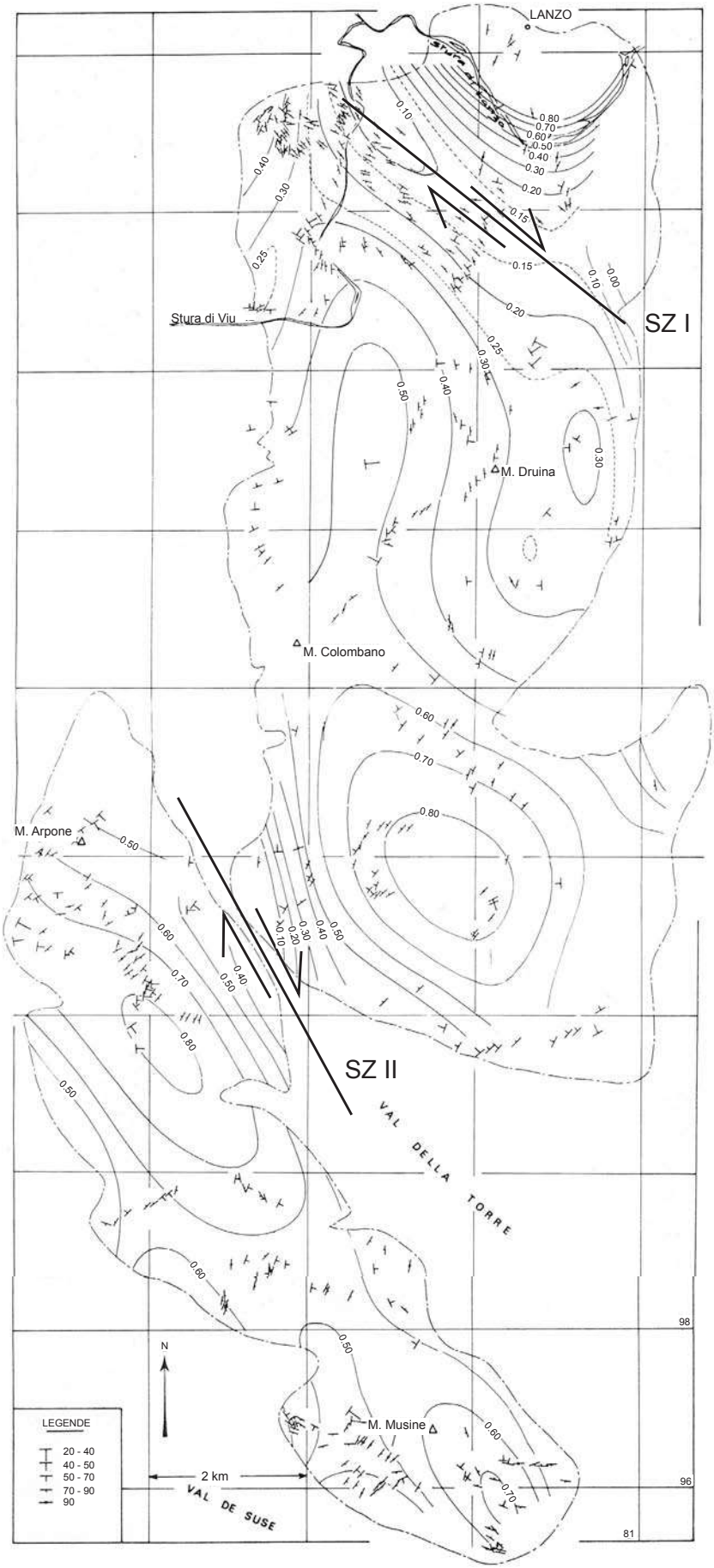

Fig. 1.7: Map of the foliation plane in the Lanzo massif superimposed: contours of equal grain-size illustrating the pattern of the plastic deformation in the massif (measurements in millimeters), from Nicolas et al. (1972).

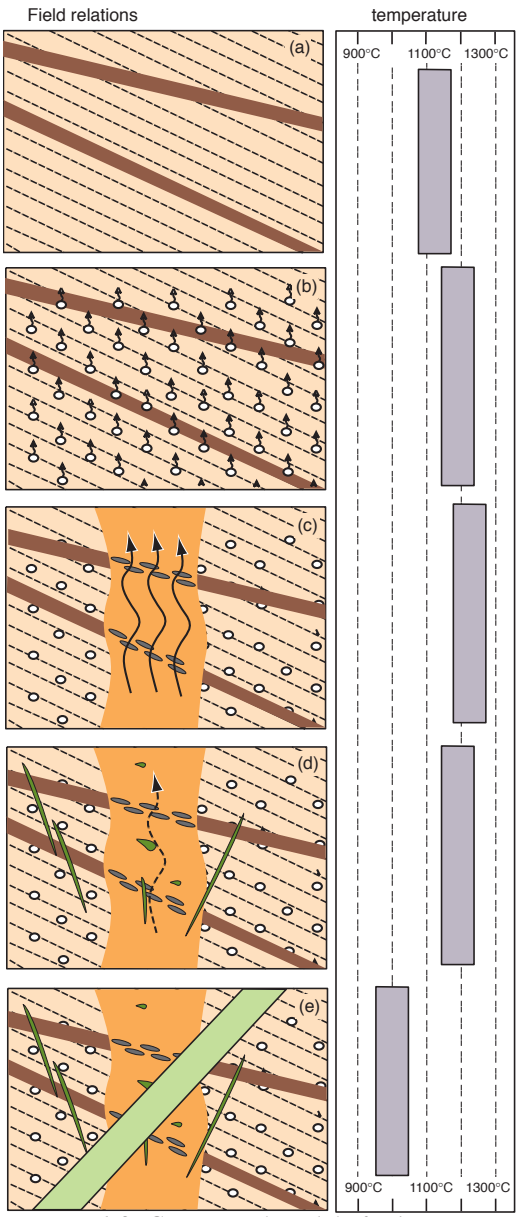

Fig. 1.8: Conceptual model of subcontinental peridotite evolution from embryonic ocean basins above an upwelling asthenosphere, as evidenced from the Piedmont Ligurian ophiolitic peridotite (modified from Müntener and Piccardo, 2003).

1.4.3 Gabbroic lenses related to the deformation

The simple field relation between deformation and accumulation of melt was used to determine the shear sense. Originally, the deformation was explained to be synchronous to gabbroic fusion at 1150 °C, and between 5 to 8 Kbar (Boudier, 1972; Boudier, 1978). However, the chemical composition of such gabbroic lenses are inconsistent with a liquid composition (see Chapter 4), and are now regarded as gabbro cumulates, from which a substantial amount of liquid escaped (Bodinier et al., 1991 and chapter 4). Gabbroic lenses formed oblique planes on the foliation and intersection of these two planes tend to be perpendicular to the transport direction (Nicolas et al., 1972). The Figure 1.9 represents the geometric relationship and shows the "en echelon" orientation of the gabbroic lenses from the Lanzo massif with respect to the high-temperature foliation. This geometry was interpreted as magma injection in tension planes linked to the shearing. This observation indicates a dextral sense of shearing.

1.4.4 Early interpretations of the genesis of the Lanzo peridotite

The Lanzo massif was interpreted as the exposed part of a mantle root linked to the Ivrea zone (Boudier and Nicolas, 1977). A map of internal movement of the Lanzo massif (shear planes, transport direction, shear senses and estimation of movement intensity) was used to interpret an intrusive origin of the Lanzo massif

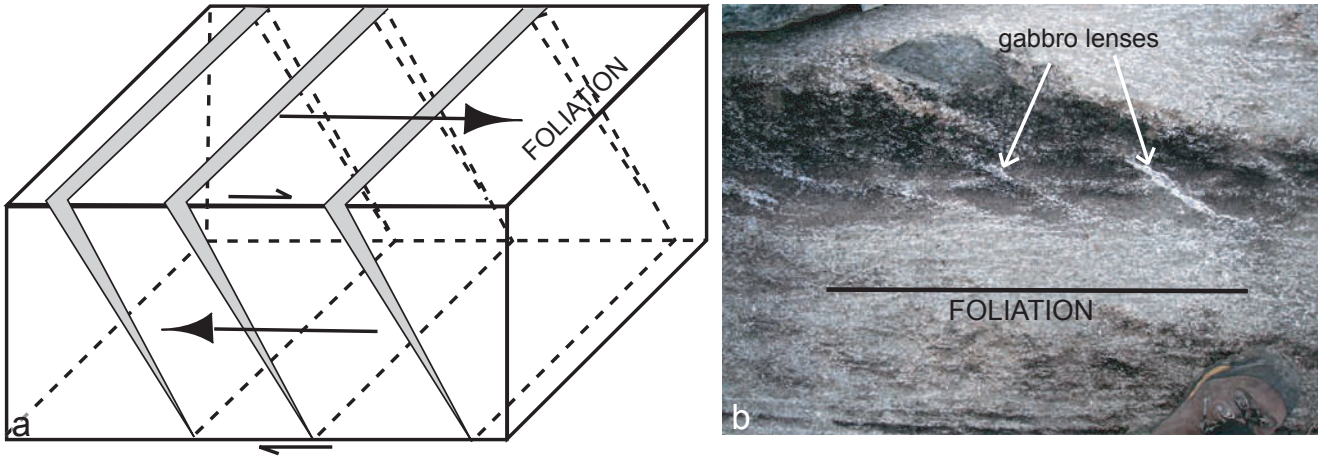

Fig. 1.9: (a) Relationships between tension planes (parallel shading) and a dextral simple shear in the horizontal plane (Nicolas et al. 1972). (b) Field photograph of gabbroic "echelon" dikelets.

(Nicolas et al., 1972) by simple shear (Nicolas et al., 1971). The grain size reduction at the boundaries of the body was interpreted as deformation during this intrusion. The shearing mechanisms were interpreted as intra-crystalline and especially intra-granular, which started when deformation strongly increased. These results considered grain size as the inverse proportion of deformation intensity and allowed extrapolation on a map of the entire Lanzo massif.

1.5 ALPINE HISTORY AND METAMORPHISM OF THE LANZO MASSIF

The oceanic sequence formation during the Jurassic was followed by inversion of the large scale plate movement involving the closure of the basin by subduction followed by Alpine collision (Dal Piaz, 1974). The paleogeographic position of the Lanzo peridotite was (and is) a matter of debate and in the following several arguments are put forth to test some hypotheses on the location of the Lanzo massif before the subduction.

Numerous studies of the eclogite facies rocks were performed to better constrain the timing of the subduction (Droop et al., 1990; Froitzheim et al., 1996; Gebauer et al., 1993; Lardeaux and Spalla, 1991). The Lanzo massif was subducted up to eclogite facies and recorded two contrasting metamorphic peaks: (i) the metasedimentary cover, located western of the massif, recorded 500 to 550 °C and 0.9 to 1.3 GPa conditions (ii) kyanite + talc assemblage from eclogite facies metagabbro in peridotite indicates 550 °C to 620°C to 2.5 Gpa (Pelletier and Müntener, 2006). The difference was interpreted as a retrograde metamorphic overprint erasing peak-metamorphic conditions and a metamorphic gradient from west to east. This metamorphic gradient is similar to the one is the Sesia zone indicating a possible common subduction history (Compagnoni, 1977; Lardeaux and Spalla, 1991; Pognante, 1989; Spalla et al., 1983).

Parts of the oceanic crust from the Piemontese-Ligurian ocean were subducted at different times. An important discontinuity will separate the internal Piemontese massifs (e.g. Lanzo, Mongenèvre, Monviso, Internal Liguride) and external Piemontese massifs (e.g. Chenaillet

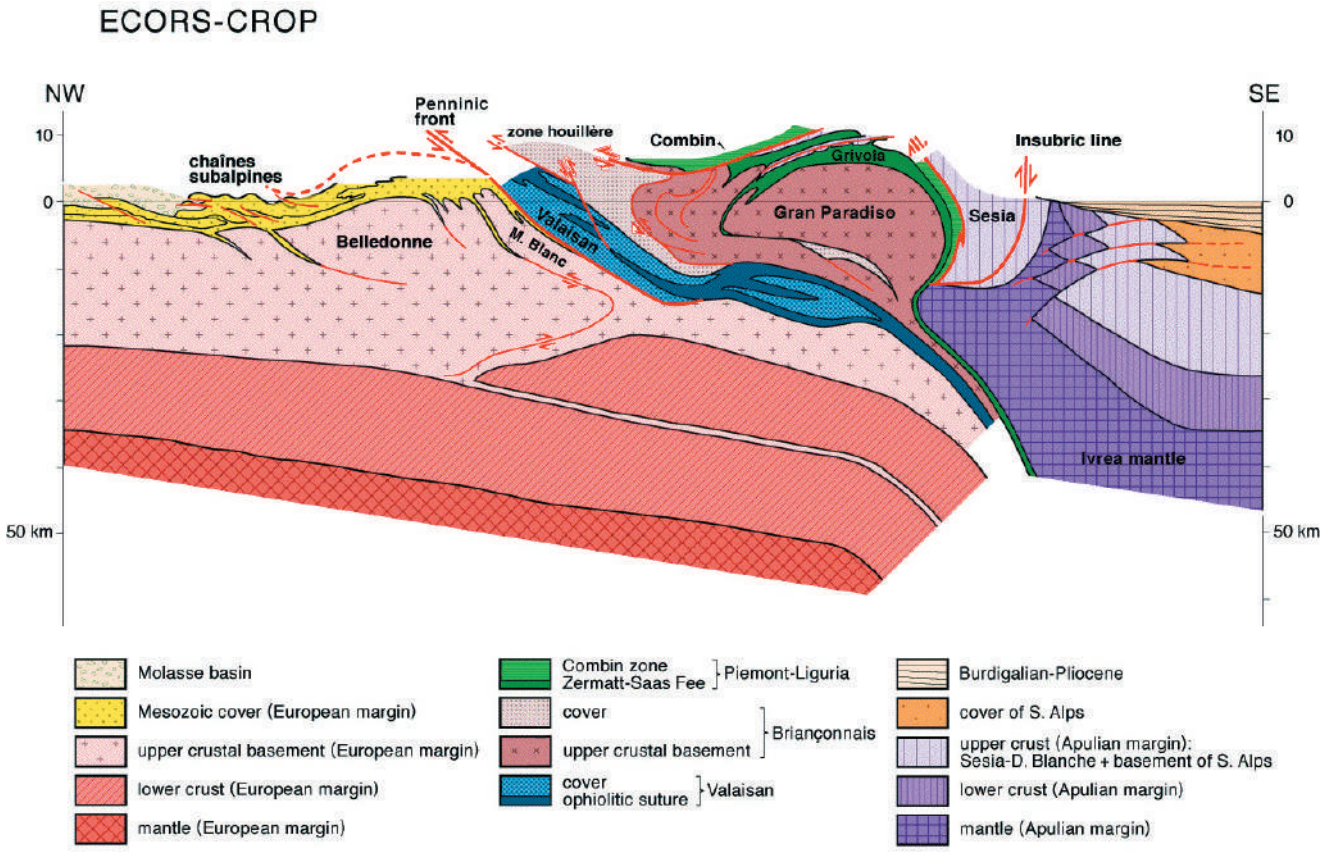

Fig. 1.10: Geophysical-geological cross section through the Western Alps (ECORS-CROP profile)(van der Pluijm and Marshak, 2004).

massif, External Liguride, Platta nappe). The position of the different massifs before subduction was discussed by severals studies, most notably by Froitzheim et al. (1996), which assume that the Sesia massif was an extensional allochton near the Apulian margin, and was thus the first continental unit subducted. However, Lagabrielle et al. (1989) discussed an alternative scenario that considers late Cretaceous subduction preceding subduction of the Sesia zone (Fig. 1.10).

The Lanzo massif is weakly serpentinized and is surrounded by a serpentinite belt (Boudier, 1972). In several places, serpentinization strongly overprinted the peridotite bodies: at the eastern part, the southern part, and particularly in the shear zone areas, which separate the three Lanzo massif bodies (Fig. 1.11). The serpentine zone is larger in the shear zone separating the central to the southern body (SZ II) than in those separating the northern to the central body (SZ I). The serpentinite-peridotite boundaries at the shear zone I area are revaluated in this study, completed by data from Pelletier (2003). Boudier and Nicolas (1977; 1982) consider the shear zones as Alpine deformation. They proposed a reconstruction before alpine time based on chemical composition, gabbro dikes and dunite occurrence (Fig. 1.11).

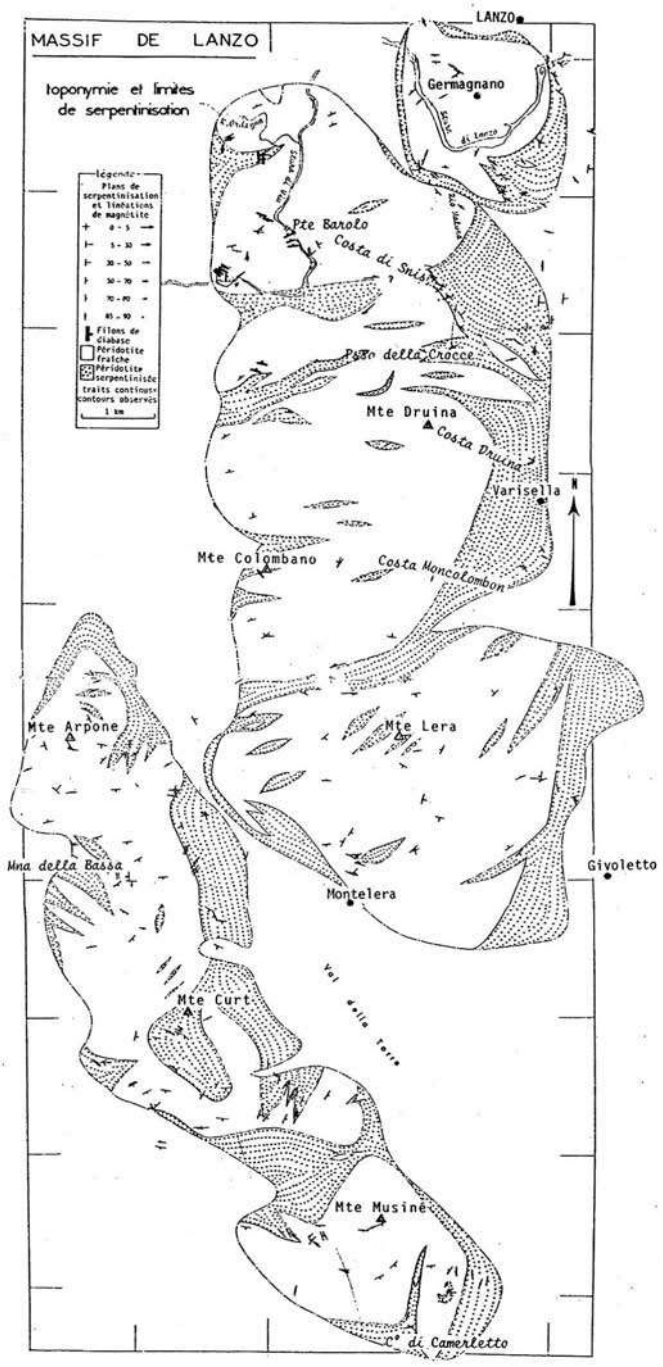

Fig. 1.11: Map of the Lanzo peridotite massif and the distribution of serpentinites (dotted areas) (Boudier, 1972).

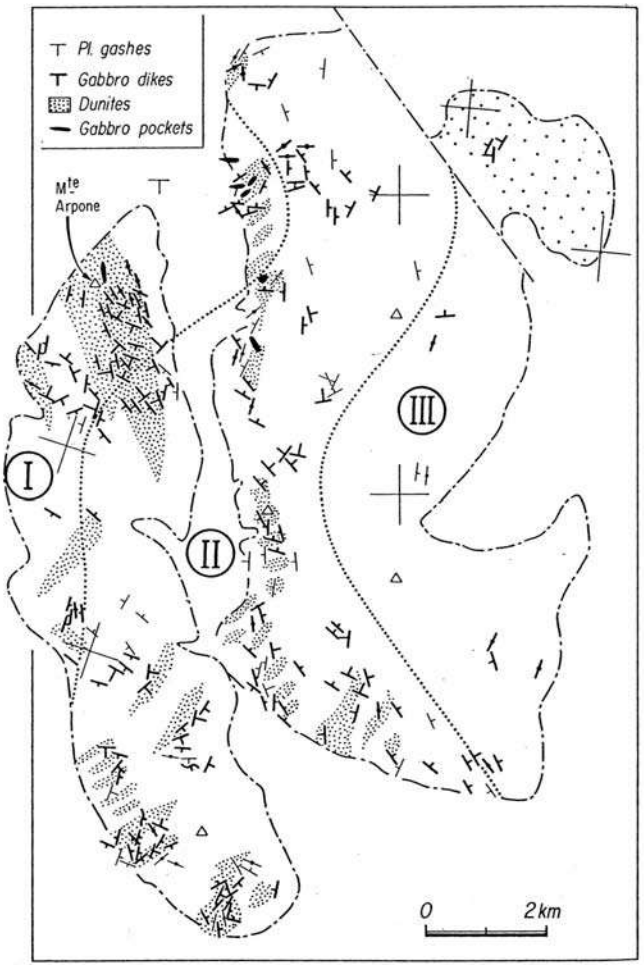

Fig. 1.12: Map of melt-related features in the Lanzo massif, after restration of the different bodies to their presumed pre-Alpine positions (Boudier and Nicolas, 1977; Boudier and Nicolas, 1982).

1.6 OUTLINE OF THE THESIS

This work is organized in five chapters: three parts of them are present as papers (one is accepted and two are sub-ready for submission). The **first chapter** is a general introduction to the geological history of the massif, the previous works and his geographic overview. The massif was first interpreted to be a mantle root of the Sesia zone and is now interpreted as a remnant of the oceanic crust of the Piemontese-Ligurian basin. The **second chapter** presents the characterization of a shear zone in the Lanzo massif. Fieldwork and structural investigations presented in this part will be used as a base of chemical analyses of minerals. This study will better constrain the interplay of melt processes and deformation at thin section and map scale (paper to be submitted to Journal of Petrology). The **third chapter** concerns the geochemistry of plagioclase peridotite from a mantle shear zone and highlights the relation between deformation and melt rock interaction. **Chapter four** provides time constraints on gabbros crystallization by U-Pb dating of zircons from Fe-Ti gabbros, completed by a geochemical study on mafic rocks. This chapter is accepted to Contributions to Mineralogy and Petrology. Finally, general conclusions are drawn from the new data **(chapter 5),** the Lanzo massif is compared to other peridotite shear zones and an outlook is presented to complete this study.

1.7 THE STUDY AREA

The grain size correlated with the high temperature foliation and with the pyroxenite layering highlights structural differences between the two shear zones, which separate the 3 bodies of the Lanzo massif. Shear zone II is clearly discordant to the pyroxenite layering and to the high temperature foliation and was mapped as a strongly serpentinized zone (Val della Torre, Fig. 1.5). Shear zone II might be interpreted as event contemporaneous to Alpine collision or strongly overprinted by deformation related to Alpine collision. This was the preferred interpretation of Nicolas et al. (1972), who describe the SZ II as Alpine strike slip fault. Shear zone I shows parallel foliation and pyroxenite layering, with grain size reduction and very little overprint by serpentinization. These initial observations motivated the detailed study of SZ I.

CHAPTER 2:

JUXTAPOSITION OF MELT IMPREGNATION AND HIGH TEMPERATURE SHEAR ZONE IN THE UPPER MANTLE (LANZO, N-ITALY) I: TEXTURE AND MINERAL COMPOSITION

Manuscript prepared for Journal of Petrology

Kaczmarek, M.-A.[1,2] and Müntener O.[2,3].

Il Turù from col Colmet

(1) Institute of Geology, University of Neuchâtel, rue Emile Argand, 2007 Neuchâtel, Switzerland. Mary-alix.kaczmarek@unine.ch, 0041 (0)3 27 18 27 12, Fax: 0041 (0)3 27 18 26 01
(2) Institute of Mineralogy and Geochemistry, University of Lausanne, Anthopole, CH-1015 Lausanne, Switzerland
(3) formerly at: Institute of Geological Sciences, University of Bern, Baltzerst. 1, 3012 Bern, Switzerland.

ABSTRACT

A mantle shear zone between the northern and the central bodies of the Lanzo peridotite massif (NW-Italy) has been investigated and displays five classes of deformation: coarse grained secondary granular (CGSG), fine grained secondary granular (FGSG), proto-mylonite, mylonite and hydrous-mylonite. CGSG shows weakly deformed porphyroclastic zones and domains of igneous recrystallization. Mylonite and hydrous-mylonite are characterized by stretched porphyroclasts, embedded between domains of fine-grained, polycrystalline matrix (ol, pl, cpx, opx, sp, Ti-hbl), and domains of polycrystalline olivine. The spatial distribution of deformation is asymmetric with respect to the mylonite, increasing from south-west to north-east, and the northern body is composed of CGSG rocks. Discordant gabbroic and basaltic dikes are asymmetrically distributed and concentrated in the southern part of the shear zone.

The pyroxene chemistry is correlated with grain size. The high-Al pyroxene porphyroclastic cores, indicate high temperatures (1100-1030°C), while the neoblasts with lower Al contents, display lower final equilibration temperatures (~860°C). This indicates a rapid exhumation from spinel to plagioclase facies coupled with incomplete chemical equilibration. Cr# (molar Cr/Cr+Al) and TiO_2 concentrations in mantle spinel show an extreme variability covering the entire range from spinel to plagioclase peridotite, which does not seem to be microstructurally controlled. The CGSG spinel compositions from the central body are more variable than spinel from mylonite, hydrous-mylonite and CGSG of the northern body. The spinel compositions indicating disequilibrium argue for a rapid exhumation and a faster exhumation of the central body relative to the northern body.

The microstructural analysis suggests that two types of melt impregnation textures are common in the Lanzo massif: (1) clinopyroxene porphyroclasts reacted with melt, and orthopyroxene plus plagioclase crystallized; (2) olivine porphyroclasts are corroded and surrounded by interstitial orthopyroxene. The melt impregnation textures tend to disappear in the mylonite zone, indicating that the mylonite formation postdates melt-rock reactions. Our results indicate that melt migration and high temperature deformation are juxtaposed both in time and space. Melt-rock reaction may cause grain size reduction, which in turn led to localization of deformation. Pinning inhibits substantial grain growth. Structural and geochemical observations indicate that actively deforming peridotite mylonite acted as a permeability barrier and that ascending gabbros might terminate and crystallize along actively deforming shear zones. This is supported by the observation that gabbros are asymmetrically distributed with respect to the shear zone and concentrate in the footwall of the high-temperature mylonitic shear zone. This is probably an important mechanism for explaining the discontinuous distribution of gabbros in ocean-continent transition zones and ultra-slow spreading ridges.

Keywords : Lanzo massif, plagioclase peridotite, shear zones, melt impregnation, deformation, thermometry.

2. 1 INTRODUCTION

Peridotite mylonite in the oceanic lithosphere is responsible for exhumation of mantle rocks to the ocean floor in ocean-continent transition zones and at mid-ocean ridges, in particular in slow-spreading oceans (Cannat, 1993; Jaroslow et al., 1996). Forsterite-rich olivine dominates the upper mantle composition and, being a relatively weak mineral, controls mantle rheology (Drury and Fitz Gerald, 1998; Drury et al., 1990). Peridotite mylonite may control the strength of the mantle lithosphere (Vissers et al., 1995; 1997) and therefore play a crucial role in lithosphere scale deformation processes such as continental rifting or mountain building. The processes that could induce substantial weakening of mantle peridotite are thermal weakening, reaction weakening and a change in the dominant reaction mechanism (Drury et al., 1990). Melt is known to lower the resistance

to stress in solid state flow (Hirth and Kohlstedt, 1995a; Hirth and Kohlstedt, 1995b) but on the other hand, promotes recrystallization and grain growth. Small amounts of melts (<6%) enhance recrystallization in dislocation creep, and may also produce weakening. Small melt fractions have an important influence on the physical properties of rocks (such as seismic velocities) that are sensitive to the grain-scale distribution of melt. In actively deforming polyphase rocks, like upper mantle peridotite, grain growth is often inhibited and a stable grain size develops depending on the grain size and volume fraction of the phases other than olivine (Olgaard and Evans, 1988). Dijkstra et al. (2002) conclude that grain size reduction by melt-rock reaction, combined with mechanical mixing of mineral phases, provides an important mechanism for weakening and strain localization in mantle rocks.

Evidence for melt rock reaction requires textural and detailed geochemical investigations. The presence of plagioclase in peridotite in particular facilities recognition of melt-rock reaction textures (Girardeau and Mercier, 1992; Nicolas, 1986) or as melt segregation (Menzies, 1973; Quick, 1981) i.e. in situ partial melting of the host rock and incomplete extraction. The Othris peridotite, Dijkstra et al (2001) interpreted plagioclase as cumulate phase of a basaltic melt that impregnate the harzburgite. In the Lanzo massif, plagioclase peridotite has originally been interpreted as melt segregation features, e.g. in-situ partial melting of the host-rock and incomplete melt extraction (Boudier, 1978b; Boudier and Nicolas, 1972; Nicolas, 1986; Nicolas et al., 1988). In recent years, the plagioclase peridotite microtextures has been challenged and are interpreted as related to melt impregnation processes is considered (Müntener and Piccardo, 2003; Piccardo et al., 2004; Piccardo et al., 2006). These studies demonstrate, that the Lanzo South peridotite record a progressive evolution of an igneous system from diffuse to focused porous flow and finally diking during cooling and exhumation of the massif.
To explore the effects of deformation on melt migration processes in the upper mantle we performed a detailed field and mineral chemistry study on deformed plagioclase peridotites from the Lanzo peridotite. This mantle shear zone has originally been interpreted as a zone that separates a mantle diapir (Lanzo South Central) from the surrounding peridotite (Boudier, 1978b; Boudier and Nicolas, 1972). We present a detailed structural map with different classes of peridotite microstructures that indicate that the footwall of the shear zone shows a ±gradual increase in deformation on a km-scale approaching a zone of ultramylonite that separates the Central from the coarse-grained Northern Lanzo body. We discuss the effects of variable deformation with respect to mineral composition, in particular spinel. We find that disequilibrium mineral compositions recorded in coarse-grained peridotites indicate melt infiltration in the thermal boundary layer followed by rapid exhumation of peridotite in the footwall of a major mantle shear zone. The strongly deformed rocks are compositionally much more homogeneous. We discuss the role of mantle shear zones with respect to melt migration, and argue that actively deforming high temperature shear zones might act as a permeability barrier for migrating liquid in the upper mantle.

2.2 GEOLOGICAL SETTING

The Lanzo massif is located in the Western Alps (Northern Italy), north-west of Torino (Italy), at the Po plain boundary, and forms part of the high pressure metamorphic belt of the internal Western Alps. It is located to the south of the "Sesia" high-pressure area and in the suture zone. To the west, the massif is separated from the Piemontese ophiolites by the "Viu Locana" tectonic zone and separated from the Po plain by the Insubric Line. Earlier studies divided the Lanzo massif in 3 parts: a northern (5 km^2), a central body (~90 km^2) and a southern body (55 km^2), each separated by partially serpentinized mylonitic shear zone (Nicolas et al., 1972) (Fig. 2.1). The entire massif is dominated by plagioclase peridotite and has mapped structurally by Boudier (1978b), who presented maps with the regional distribution of pyroxenite layering, high temperature foliations and gabbroic dikes. In the northern and central parts of the massif, pyroxenites and high temperature foliations are mostly discordant while in the southern body pyroxenite layering and high temperature foliations

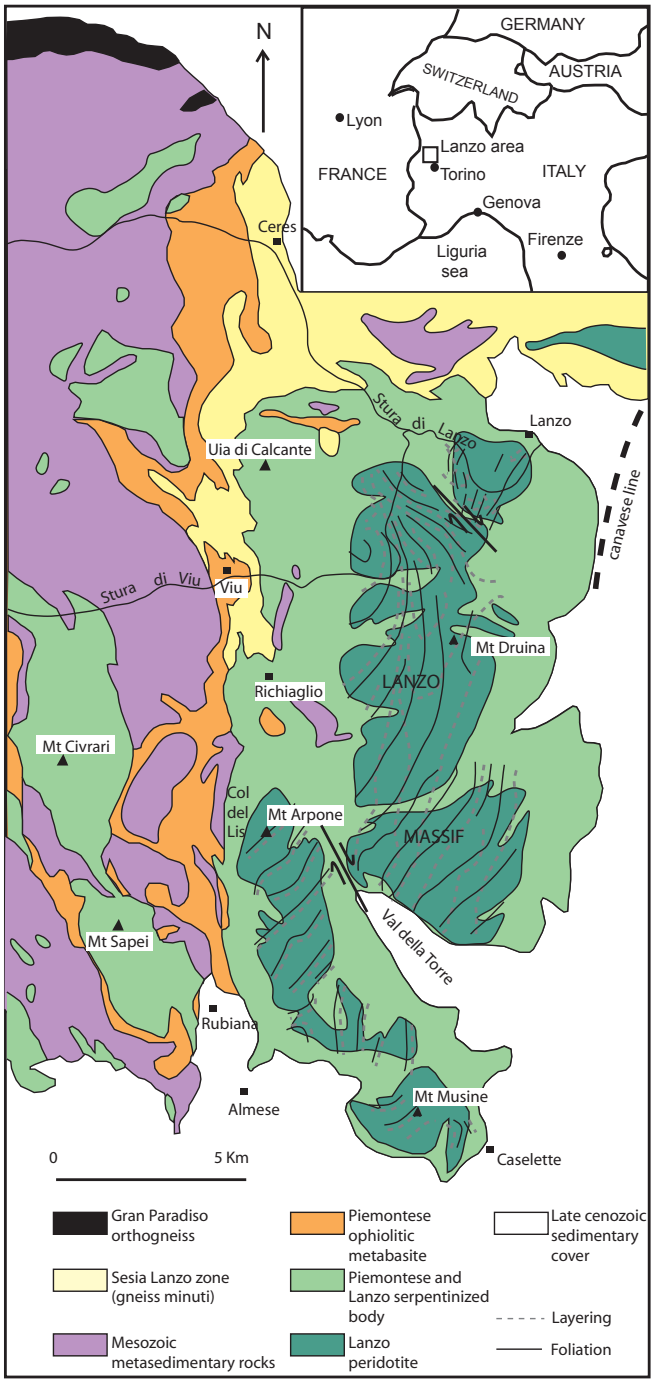

Fig. 2.1: Tectonic map of the Lanzo massif, (modified after Boudier 1972; Boudier 1978; Pognante 1989).

are concordant (Fig. 2.1). The pyroxenite layering is locally folded with the development of an axial plane foliation and presumably represents an old, lithospheric history of the massif (Boudier, 1978b). Previous works have defined two main domains: (i) the northern body, which is characterized by fertile lherzolitic composition, has been considered to represent a fragment of sub-continental lithosphere which became isolated from the convective mantle some 400-700 Ma ago (Bodinier et al., 1991); and (ii) The southern body, which displays more refractory compositions (Bodinier, 1988; Bodinier et al., 1991), and has been interpreted as an asthenospheric diapir that rose from the garnet stability field, and was emplaced in the early Mesozoic, during the opening of the Ligurian Tethys. The Lanzo peridotite has an overall fertile composition with respect to primitive mantle abundances, with calculated melt extraction of about 6% in the northern body and 6 to 12% in the southern body (Bodinier, 1988). The extracted melts are interpreted melt to have a T-MORB in the north and a T to N-MORB composition in the north and in the south, respectively (Bodinier, 1988), similar to basalts from the Ligurian Alps (Beccaluva et al., 1984). The Lanzo massif shows evidence of melt formation and melt extraction (Boudier, 1978b; Boudier and Nicolas, 1972; Nicolas, 1986) such as plagioclase-pyroxene clusters, plagioclase lenses and dunites. More recent studies emphazise the role of 'asthenospherisation' of a previous lithospheric mantle (Müntener and Piccardo, 2003; Müntener et al., 2005; Piccardo et al., 2004). The massif contains numerous igneous rocks cutting all previous events in the mantle, ranging from troctolite, olivine gabbro to oxides gabbros and porphyritic basaltic dikes (Bodinier et al., 1986; Boudier, 1978b; Boudier and Nicolas, 1972, chapter 4).

The high-temperature deformation history of the Lanzo massif has originally been related to the emplacement of mantle diapirs (Nicolas, 1986), and thus the shear zone structures may have developed in response to diapiric uprise of the lherzolite body in a more or less symmetric extensional geometry as suggested by Nicolas (1986). Alternatively, they may have developed in an asymmetric system (Froitzheim and Manatschal, 1996; Lemoine et al., 1985; Vissers et al., 1995). Peridotites and gabbroic dikes are partially transformed into eclogite facies paragenesis during Alpine metamorphism (Kienast and Pognante, 1988; Pelletier and Müntener, 2006). In the Lanzo north part, the peridotite core is surrounded by serpentinized peridotites and strongly foliated serpentinites, result of the eclogite to greenschist facies alpine metamorphism (Bente and Lensch, 1981). In places, the top of the mantle rocks is covered by ophicarbonate breccias (Pelletier and Müntener, 2006).

2.3 FIELD RELATIONS OF A HIGH TEMPERATURE MANTLE SHEAR ZONE

2.3.1 Mapping and distribution of peridotite microstructures

Detailed mapping was realized in an area of about 16 km^2, along the boundary between the northern and the central part of the Lanzo massif (Figs. 2.1, 2.2). The boundary represents a km-scale mantle shear zone, where high temperature foliation and pyroxenite layering are parallel, separating the central and northern part where foliation and layering are mostly discordant (Figs. 2.1, 2.2, see also Boudier, 1972). We systematically measured foliation, lineation, shear-sense and grain size in order to constrain the structural evolution along this important intra-mantle detachment.

Observations of deformation features in the field and the successive study of thin sections, allow to determine 5 different classes of microstructures (complete description micro-textures is detailed in part 2.2.4): (1) coarse grained secondary granular

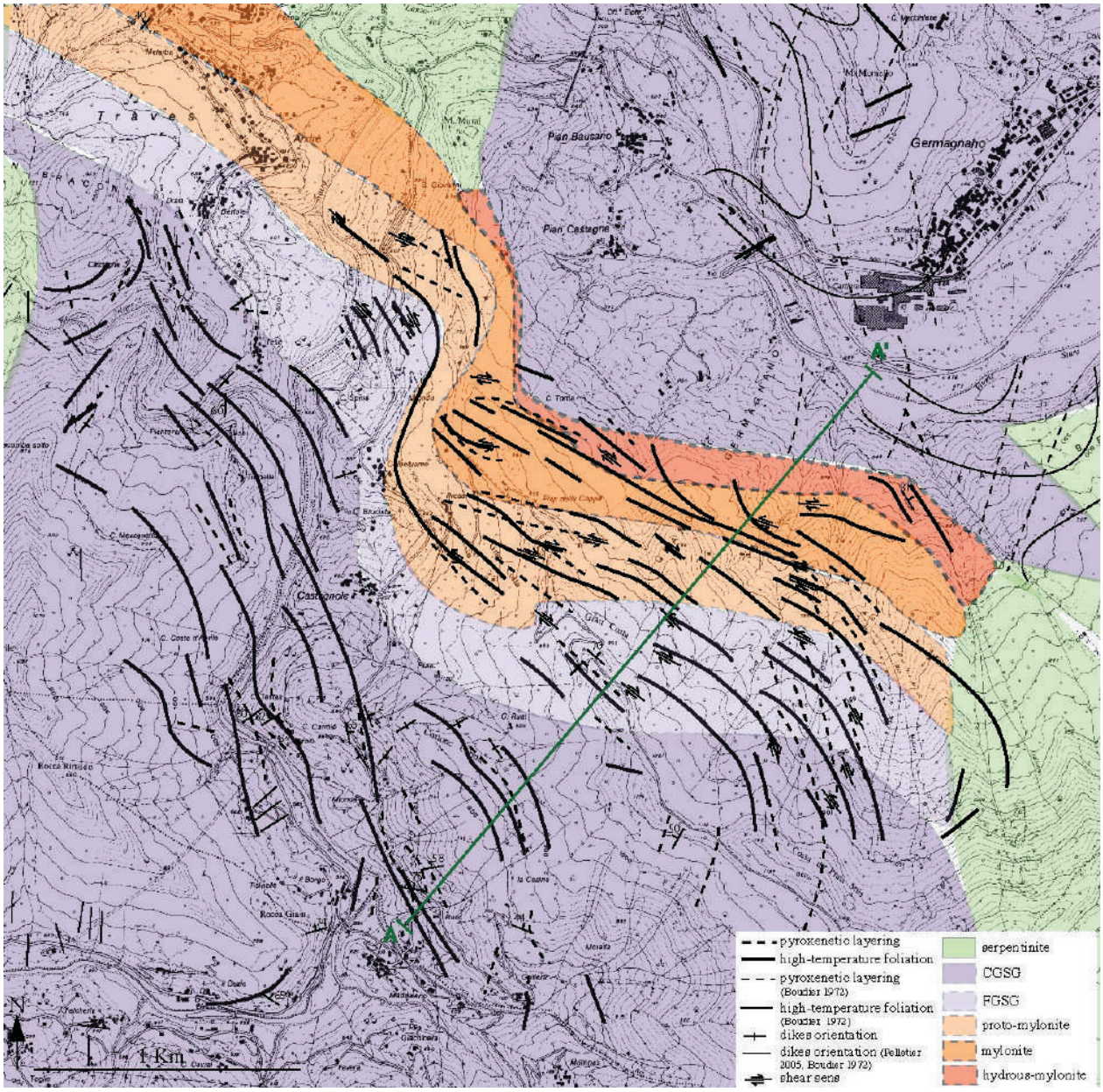

Fig. 2.2: Schematic map of the shear zone between the northern and the central part of the Lanzo massif. The high temperature foliation, and the pyroxenite layering are illustrated by lines. The variably deformed rocks have been separated into 5 deformation classes (coarse-grained secondary granular [CGSG], fine-grained secondary granular [FGSG], proto-mylonite, mylonite and hydrous mylonite) and are illustrated by grey-scale variations from darker to lighter grey with decreasing degree of deformation. The line corresponds to the localization of the cross section (see Fig. 2.9).

texture (CGSG), (2) fine grained secondary granular texture (FGSG), (3) proto-mylonite, (4) mylonite and (5) hydrous mylonite. The coarse grained secondary granular (CGSG) texture is characterized by large, cm-scale, weakly deformed orthopyroxene and clinopyroxene, embedded in an olivine matrix (Fig. 2.3a). Spinel grains are usually smaller (<5mm), and partially surrounded by a grayish and white, plagioclase rim. The fine-grained secondary granular rocks display a marked decrease in grain size and larger proportions of entirely recrystallized domains. However, we emphasize that in the field,

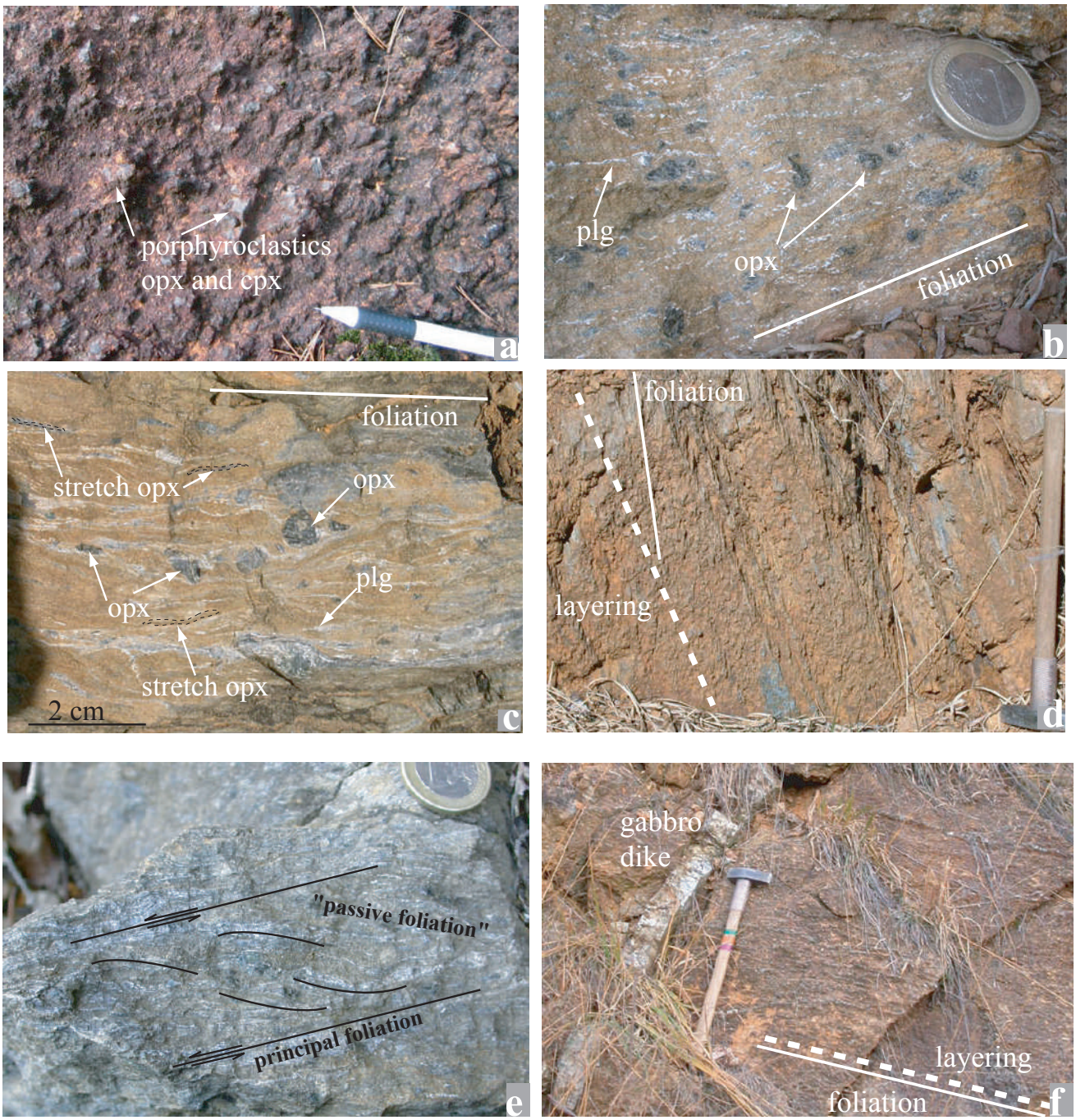

Fig. 2.3: Photographs of representative outcrops in the central part of the Lanzo massif. (a) Angular discordance between spinel pyroxenite layering and high-temperature foliation (Gran Costa). (b) Coarse-grained secondary granular texture with cm-scale pyroxenes weathering out from the surface (south of Pian Castagna). (c) Proto-mylonitic peridotite with pyroxene porphyroclasts and high temperature foliation underlined by white bands of plagioclase (East of Colbeltramo). (d) High temperature foliation and porphyroclasts in the mylonite rock, note that some of the orthopyroxene shows elongation, while others form ± rounded porphyroclasts (East of Colbeltramo). (e) Example of an internal oblique foliation (passive foliation), indicator of the shear sense in the mylonitic zone (Est of Colbeltramo). (f) Gabbro dike cross cut the deformed peridotite (northeastern of Maddalene). The minerals are slightly parallel to the orientation of the gabbro dike intrusion.

the distinction between (1) and (2) is sometimes arbitrary. In proto-mylonitic rocks (Fig. 2.3b), spinel and plagioclase are aligned parallel to the foliation, while orthopyroxene and clinopyroxene porphyroclasts are surrounded by the foliation. The transition to mylonite rocks is marked by a well-developed foliation and lineation. Orthopyroxene porphyroclasts might be extremely stretched, with aspect ratios exceeding 10:1 (Fig. 2.3c).

The high temperature foliation is reflected by elongated spinel, lenses of deformed plagioclase and elongated porphyroclasts of clinopyroxene and orthopyroxene. The well developed pyroxenitic layering, is composed of variable proportions of pyroxene, plagioclase, spinels and olivine, which are recrystallized and parallel to the foliation (Fig. 2.3b-c). The pyroxenite layering and the high temperature foliation are generally discordant with an angle of about 20° degrees between the foliation plane and the pyroxenite banding (Fig. 2.2 and Fig. 2.3d), both plunging steeply (50-90°) towards the NE. In the mylonite zone, however, the pyroxenite banding is extremely thinned (< 2cm), elongated and parallel to the foliation, which renders recognition and mapping of pyroxenite layers rather difficult. The lineation measured was sub-horizontal, parallel to the high temperature foliation. The Lanzo north massif, exposed on the northeastern side of the hydrous mylonite, is characterized by a clear discordance of pyroxenite banding and high-temperature foliation (Boudier, 1972). In addition the orientation of the foliation is nearly perpendicular to the one in the mylonite zone, thus further supporting the sharp transition from hydrous mylonites to weakly deformed peridotites on the northerneastern side of the shear zone.

The spatial distribution and the orientation of the different microstructures are illustrated on a map view (Fig. 2.2) where dashed lines separating different colors indicate the somewhat gradational transition between the different microstructures. The spatial distribution of microstructures is also illustrated along a cross section, together with stereographic projections of foliation and pyroxenite layering (Fig. 2.4). Along a transect of ~1.5 km,

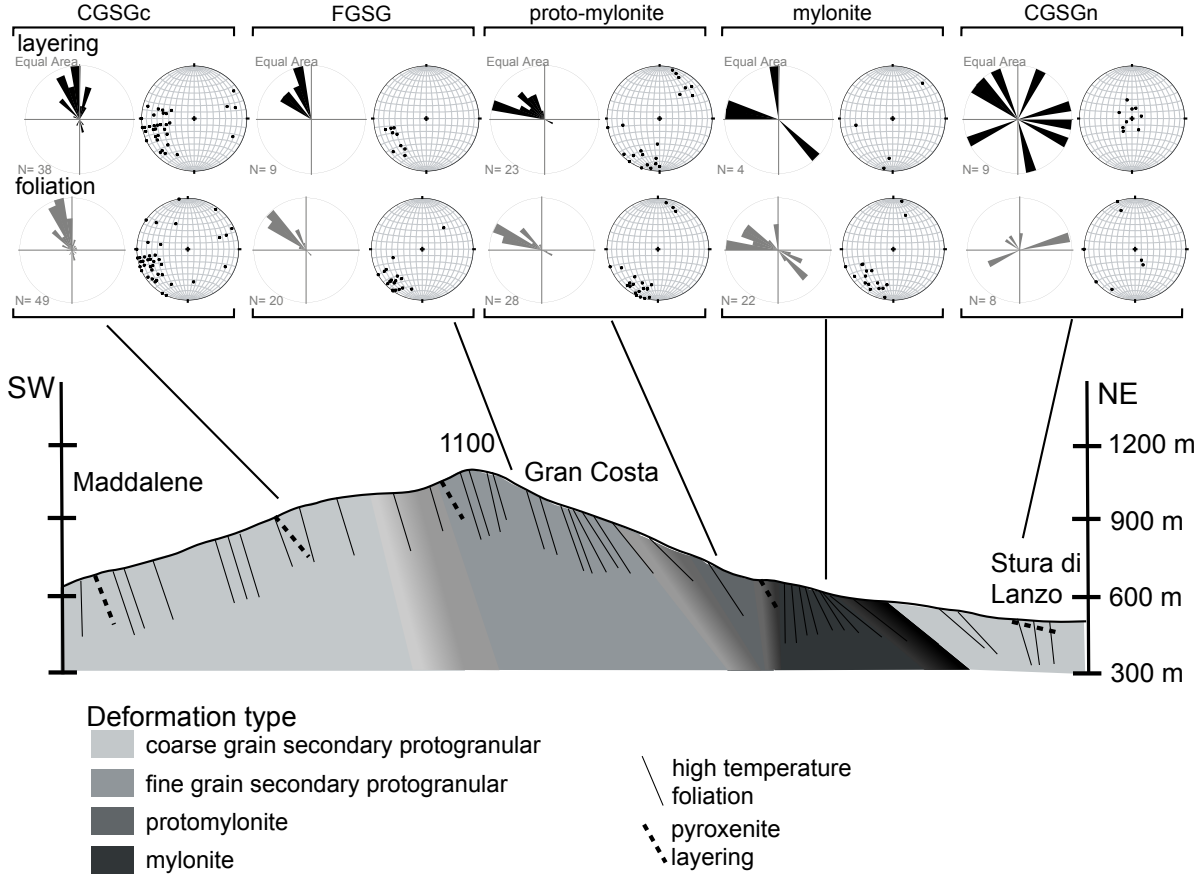

Fig. 2.4: Cross section of the shear zone illustrating layering and foliation relationship associated with the deformation type. Foliation and layering are represented by lower hemisphere, equal area projection. Roses stereographs represent plane orientation and the associated stereographs correspond to the pole of the foliation or pyroxenite layering (black dots). Note that the foliation of the Lanzo North peridotite is discordant to the mylonite zone.

there is a continuous increase of deformation from CGSG in the SW to the hydrous mylonite in the NE. In the SE part of the map, the high temperature foliation and the different microstructural domains are discordant to each other, indicating that the recrystallization related to the mylonite formation overprints an older peridotite foliation. In contrast to the southwestern part of the mylonite zone, the transition from the mylonite zone to the CGSG microstructure of the northern part of the Lanzo massif is relatively abrupt (~200m).

2.3.2 Spatial distribution of mafic dikes

The southwestern part of the mapped area contains numerous gabbroic dikes and lenses (Fig. 2.2), which are concentrated in the weakly deformed peridotites southwest of the mylonite zone. Most of the mafic rocks are undeformed, coarse-grained (>1cm), olivine gabbro dikes, with little evidence of syn-magmatic deformation. Dike thickness does not exceed 20 cm in fresh peridotite, while larger (several tens of meters thick) gabbroic bodies were found in the serpentinized, western part of the Lanzo peridotite. Fe-Ti gabbros are rare in the mapped area, however, they are more abundant in the southern part of the Lanzo massif. Rare, synmagmatic deformation is localized in the center of Fe-Ti gabbros. There, elevated concentrations of Ti-hornblende, ilmenite, apatite and zircon may be found, suggesting that interstitial liquids are preferentially extracted in zones of active deformation. Details on the igneous evolution, age determinations and whole rock geochemistry of the gabbros rocks will be discussed elsewhere (chapter 4).

Gabbroic dikes are not systematically oriented with respect to the peridotite structures (Fig. 2.2) and may be sub-parallel or discordant to the foliation/layering (Fig. 2.3f). However, we never observed gabbroic dikes crosscutting the peridotite mylonite, and we are not aware of any location in Lanzo North where gabbroic dikes have been found. This suggests that the mechanical contrast between the mylonite and the weakly deformed peridotite was high enough to prevent propagation of gabbroic dikes across the mylonite zone. The consequences of these observations will be discussed below.

2.4 PERIDOTITE MICROSTRUCTURES

As outlined above, the peridotite microstructures, based on field observations and microstructural investigations of ~100 thin sections (cut perpendicular to the foliation and parallel to the lineation). The classification of the microstructures is based on Mercier and Nicolas (1975), Sibson (1977), and Spry (1969). In addition, textures related to melt/rock interaction will be described separately.

2.4.1 Microstructures related to deformation

2.4.1.1 Coarse-grained secondary granular texture, CGSG (Fig. 2.5a):

The coarse grained secondary granular texture is characterized by a bimodal grain size distribution, containing weakly deformed porphyroclasts (olivine, orthopyroxene, clinopyroxene) with grain sizes exceeding 1 cm, embedded in matrix of recrystallized grains made of olivine, orthopyroxene, plagioclase, clinopyroxene and spinel. The development of equilibrium textures with 120° triple junctions can be observed (Fig. 2.5a). Exsolved mantle orthopyroxene porphyroclasts are sometimes kinked and show curvilinear grain boundaries, where they are partially replaced by new olivine, indicating replacement of mantle orthopyroxene by olivine. Occasionally, subhedral olivine crystals are included in large orthopyroxene. Olivine is characterized by deformation lamellae and embayment structures, where recrystallized olivine can be found. Porphyroclastic clinopyroxene with orthopyroxene exsolution lamellae is mostly recrystallized to smaller grains of ~0.5 mm. Recrystallized brown spinels (> 1 mm) are rounded or aligned parallel to the foliation, and are sometimes associated with plagioclase aggregates. Smaller dark brown spinels (<0.4 mm) are associated with new orthopyroxene and/or follow olivine grain boundaries. In most samples, vermicular, pargasitic Ti-hornblende crystallized (10 to 50 μm, Fig. 2.5b), rimming clinopyroxene porphyroclasts, indicating grain boundary migration of fluids/liquids.

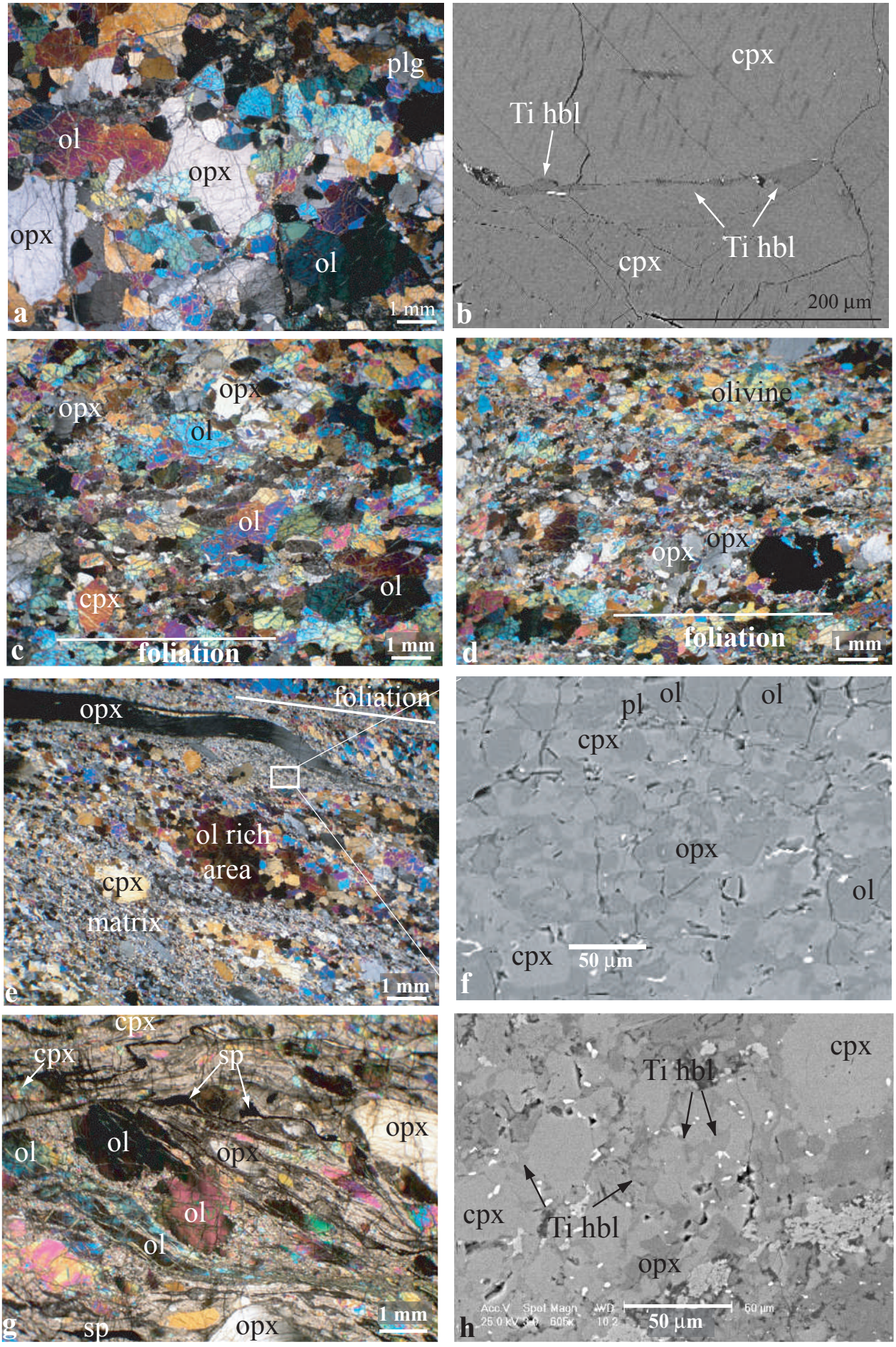
plg
ol
opx
opx
ol
a
1 mm
cpx
Ti hbl
Ti hbl
cpx
b
200 µm
opx
opx
ol
ol
cpx
ol
c
foliation
1 mm
olivine
opx
opx
d
foliation
1 mm
opx
foliation
ol rich
area
cpx
matrix
e
1 mm
pl
ol
ol
cpx
opx
ol
cpx
50 µm
f
cpx
cpx
sp
opx
ol
ol
opx
ol
ol
g
sp
opx
1 mm
cpx
Ti hbl
cpx
cpx
Ti hbl
opx
h
50 µm

Fig. 2.5

2.4.1.2 Fine grained secondary granular texture, FGSG (Fig. 2.5c):

This texture is characterized by an overall increase in the proportions of recrystallized grains compared to relict porphyroclasts (Fig. 2.5b), with the recrystallized grains being generally smaller than in the previous texture (CGSG). Porphyroclasts of exsolved orthopyroxene and clinopyroxene are less than 1 cm in size. Olivine porphyroclasts display an increase in subgrain bands and larger areas of dynamically recrystallized grains. Recrystallized olivine, orthopyroxene, clinopyroxene, spinel and plagioclase display a shape-preferred orientation subparallel to the foliation. Spinel shows different grain shapes according to their microstructural site: Rounded spinels (≤ 0.3 mm) might be included in olivine or orthopyroxene, while vermicular spinel is found along olivine grain boundaries. Elongate (long axis ~1mm), dark-brown spinel aligned in the foliation is usually associated with plagioclase. Twin lamellae of plagioclase (grain size ~0.2 mm) might be preferentially oriented parallel to the foliation, however, spinel-free plagioclase lenses have also been observed. As above, interstitial Ti-hornblende preferentially surrounding clinopyroxene clasts has been observed.

Fig. 2.5: Photomicrographs and backscattered electron (BSE) images of different rock types: (a) Coarse grained secondary granular texture (L147, crossed Nicols). (b) BSE image of Ti-hornblende at the border of porphyroclastic clinopyroxene (L13). Note that exsolution lamellae disappear on the last 20-30μm, indicating recrystallization of clinopyroxene along its borders. (c) Fine grained secondary granular texture (L110, crossed Nicols). (d) Proto-mylonite texture (L112, crossed Nicols). (e) Mylonite texture (L04), characterized by elongated orthopyroxene with aspect ratios exceeding 20:1, and recrystallized olivine oriented oblique to the main foliation (crossed Nicols). (f) BSE image of the fine-grained matrix in the mylonite (L04). (g) Hydrous mylonite localized in the north part of the shear zone (L187d). Note the flow of fine-grained polyphase matrix around olivine, orthopyroxene and spinel clasts that are rounded compared to Figure 2.10f (crossed Nicols). (h) BSE picture of Ti-hbl rich zone associated with clinopyroxene, orthopyroxene and spinel neoblasts in hydrous mylonite sample (L187d).

2.4.1.3 Proto-mylonite texture (Fig. 2.5d):

This texture is characterized by further grain size reduction of porphyroclasts and the first occurrence of elongate orthopyroxene, with gliding along (001) slip planes. Aspect ratios might approach 10:1. There is a small angle between the foliation and the shape-preferred orientation of olivine (Fig. 2.5d). The proportion of recrystallized matrix minerals (olivine, clinopyroxene, orthopyroxene, plagioclase, spinel, and Ti-hornblende) generally exceeds 25-30%. The grain size of the matrix minerals varies between 50 μm and 200 μm. Spinel (grain size exceeding 1mm) is aligned in the foliation and might be associated with plagioclase lenses or olivine. Spinel also forms inclusions in olivine and lobate at olivine boundary.

2.4.1.4 Mylonite texture (Fig. 2.5e):

The mylonitic texture is separated from the protomylonite by the occurrence of porphyroclasts embedded in a fine-grained matrix, and by the presence of extremely stretched orthopyroxene with aspect ratios exceeding 20:1. Olivine-rich areas are elongate, oblique to the foliation and composed of porphyroclastic relics with subgrain domains, surrounded by a matrix of dynamically recrystallized olivine (50 to 100 μm). Secondary phases are rare and restricted to small brown or black vermicular spinel pinning olivine grain boundaries. Plagioclase forms aggregates of several grains and occasionally surrounding porphyroclastic spinel (<2mm).

The fine-grained matrix is inhomogeneously distributed within the mylonite and is composed of olivine, clinopyroxene, orthopyroxene, plagioclase, spinel, and Ti hornblende (Fig. 2.5f). The recrystallized grain size varies from 50 μm to 5 μm, about one order of magnitude lower than in the olivine-rich areas. Minerals in the matrix have a weak shape preferred orientation, which defines the main foliation. Spinel is small (~10 μm), with black or brownish colors, aligned parallel to the foliation. Some plagioclase in the matrix is bigger than the other minerals (> 50 μm).

The mylonitic microstructure shows 3 distinctive zones that are separated from each other by variable grain size: (i) porphyroclastic zones, (ii) intermediate zones composed of smaller grains 100

to 200 μm, and (iii) very fine grained matrix (50 to 5 μm). Observations reveal that there is a sharp transition between the fine-grained matrix and the other two domains, indicating that strain strongly partitions into the fine-grained matrix.

2.4.1.5 Hydrous mylonite texture (Fig. 2.5g):

The hydrous mylonite is located in the northern part of the mylonite area, just at the limit of the northern body (Fig. 2.2), and is characterized by elongate or rounded orthopyroxene, clinopyroxene and olivine porphyroclasts (~1cm size) embedded in ultra-mylonite matrix (details and ultra-mylonite description in Appendix 2.3).

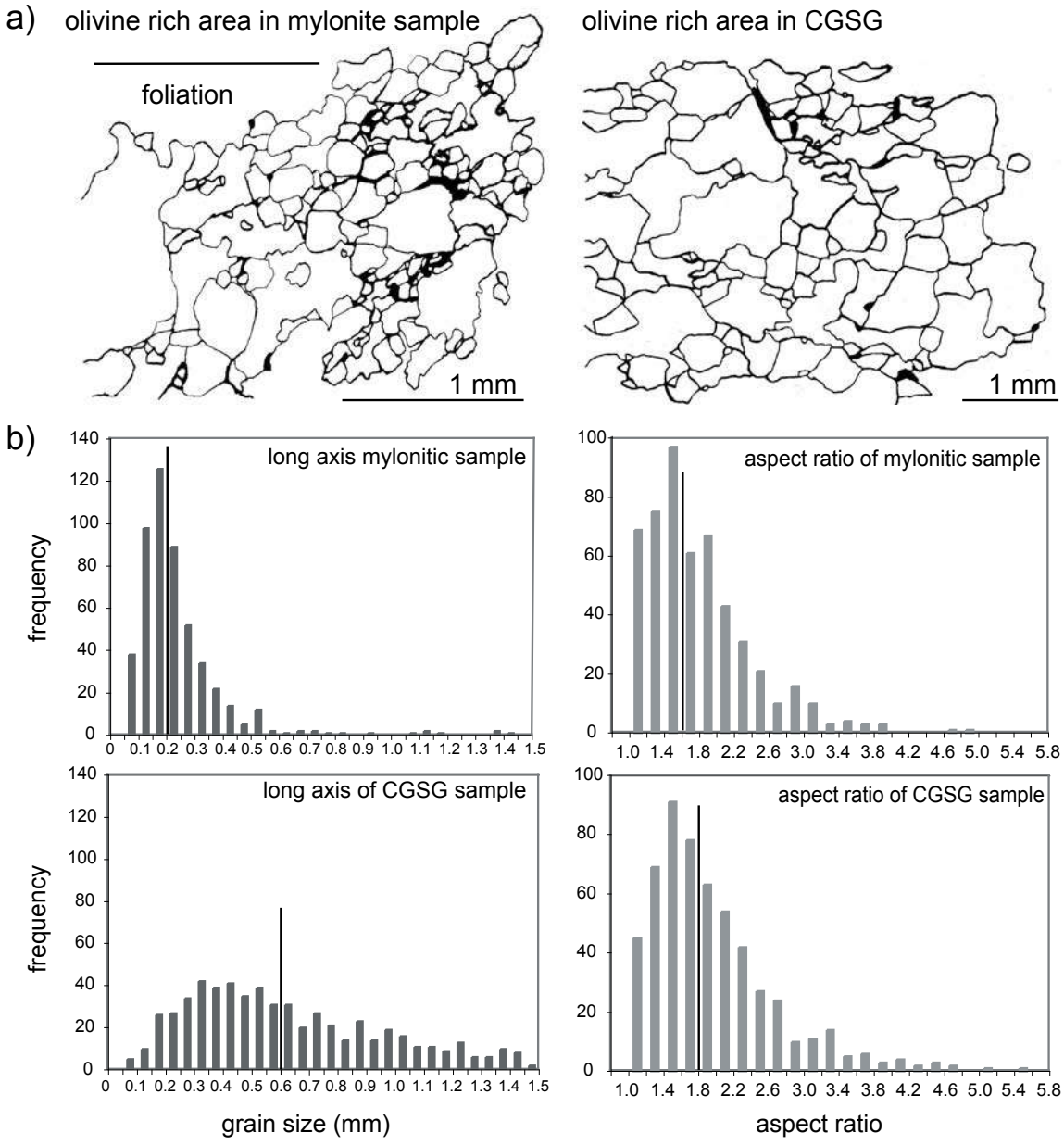

Fig. 2.6: (a) Tracing from microphotographs showing recrystallized olivine grain size and shape in mylonite and CGSG samples. Note that the orientation in the mylonite is oblique to the foliation, while in CGSG the elongation of the grains is rougly parallel to the foliation. (b) Results of grain size analysis (long axis (in mm) and aspect ratio) in mylonite (n=6) and CGSG sample (n=9) realized on ~600 grains (>100 per sample). Note that the mylonite sample shows a much tighter grain size distribution, with close correspondence of Median and maximum, while the CGSG sample has a median value of, which is substantially higher. Note also that the aspect ratio is not notably different between the two samples.

In some cases these porphyroclasts are relatively coarse-grained aggregates of recrystallized olivine (10 to 50 μm). Elongated olivine porphyroclasts exhibit deformation and kink bands. Exsolved orthopyroxene and clinopyroxene porphyroclasts are stretched and sometimes broken up in several pieces suggesting that gliding along (001) was no longer active. Porphyroclastic spinel size is between 200-400 μm. In most cases spinel grains are flattened and elongated along the foliation. Bands of disrupted spinel grains are formed in pressure shadows of larger porphyroclasts. (Fig. 2.5g). These microstructures indicate that the large porphyroclast grains behaved as hard inclusions during deformation.

The fine-grained ultra-mylonitic matrix is composed of orthopyroxene, clinopyroxene, spinel, plagioclase (completely altered), olivine and Ti-hornblende with grain size between <5 μm to 15 μm. Ti-hornblende is more abundant in these mylonites and partially replaces clinopyroxene neoblasts (Fig. 2.5h), suggesting the presence of interstitial melt and/or water during deformation. The matrix also contains hydrous minerals (chlorite, serpentine and amphibole), which replace anhydrous minerals.

This texture might be the results of a continuous dynamic recrystallization process, explained by 4 successive stages: The first (i) corresponds to an initial high temperature mylonite (presence of extremely stretched orthopyroxene and clinopyroxene). The second stage (ii) corresponds to intermediate deformation characterized by the presence of recrystallized rounded olivine grains close to olivine porphyroclasts. Next stage (iii) is the cooling and hydration (replacement of pyroxenes and olivine by amphibole and chlorite) and concomitant focusing of deformation in small-scale shear bands. The last stage (iv) corresponds to formation of the serpentinite veins cutting the high previous.

2.4.2 Olivine grain size and shear sense

Olivine grain size was determined with digitized optical images and treatment with SXimage software (Barrett S. 2005; Version 1.75) for each deformation type. The analysis was performed on recrystallized olivine-rich areas, which partially replaced olivine porphyroclasts. In the case of proto-mylonite and mylonite samples, recrystallized grains are smaller and show an oblique grain-shape preferred orientation (Fig. 2.6). Such an oblique grain-shape fabric, however, has generally not been observed in coarse- and fine-grained secondary granular samples. Results of aspect ratios and absolute length of olivine long axis for different deformation type (mylonite and CGSG) are illustrated in histograms in Fig. 2.6. The two categories show maximum aspect ratios close to 1.5, but might reach values up to 5.0 in mylonitic samples. However, the morphological olivine long axis is clearly different: the histogram clearly shows that most of the grains are smaller than 0.2 mm, with only a few grains exceeding 0.4 mm. In contrast, in the CGSG samples there is a large variability in olivine long axis with a median at 0.6 mm, however, maximum grain sizes reach 1.8 cm.

Peridotite shear sense indicators were either obtained from field observation (asymmetric porphyroclasts, asymmetric pressure shadows or secondary foliations within high strain zones, leading to lense shaped appearance of peridotite mylonite (Fig. 2.3e) or from oriented thin sections. Shape preferred orientation of olivine rich areas, stretched orthopyroxene porphyroclasts and dynamically recrystallized matrix minerals oblique to the foliation with an angle of 25-30° were used to derive the microscopic shear sense. Shear sense determinations indicate a preferential top to the northwest sense of shear, although top to the southeast has also been observed (Fig. 2.2). These microscopic shear sense determinations are consistent with the large-scale structures on a map scale (Fig. 2.2), which tend to be parallel to the mylonite in the northern and southern part and indicates a top to the northwest sense of shear.

2.4.3 Microstructures related to melt impregnation

Such textures are common all over the Lanzo massif, particularly in the southern part (Müntener and Piccardo, 2003), indicating that melt migration is a regional scale phenomenon.

The development of equilibrium texture with 120° triple junctions among recrystallized minerals

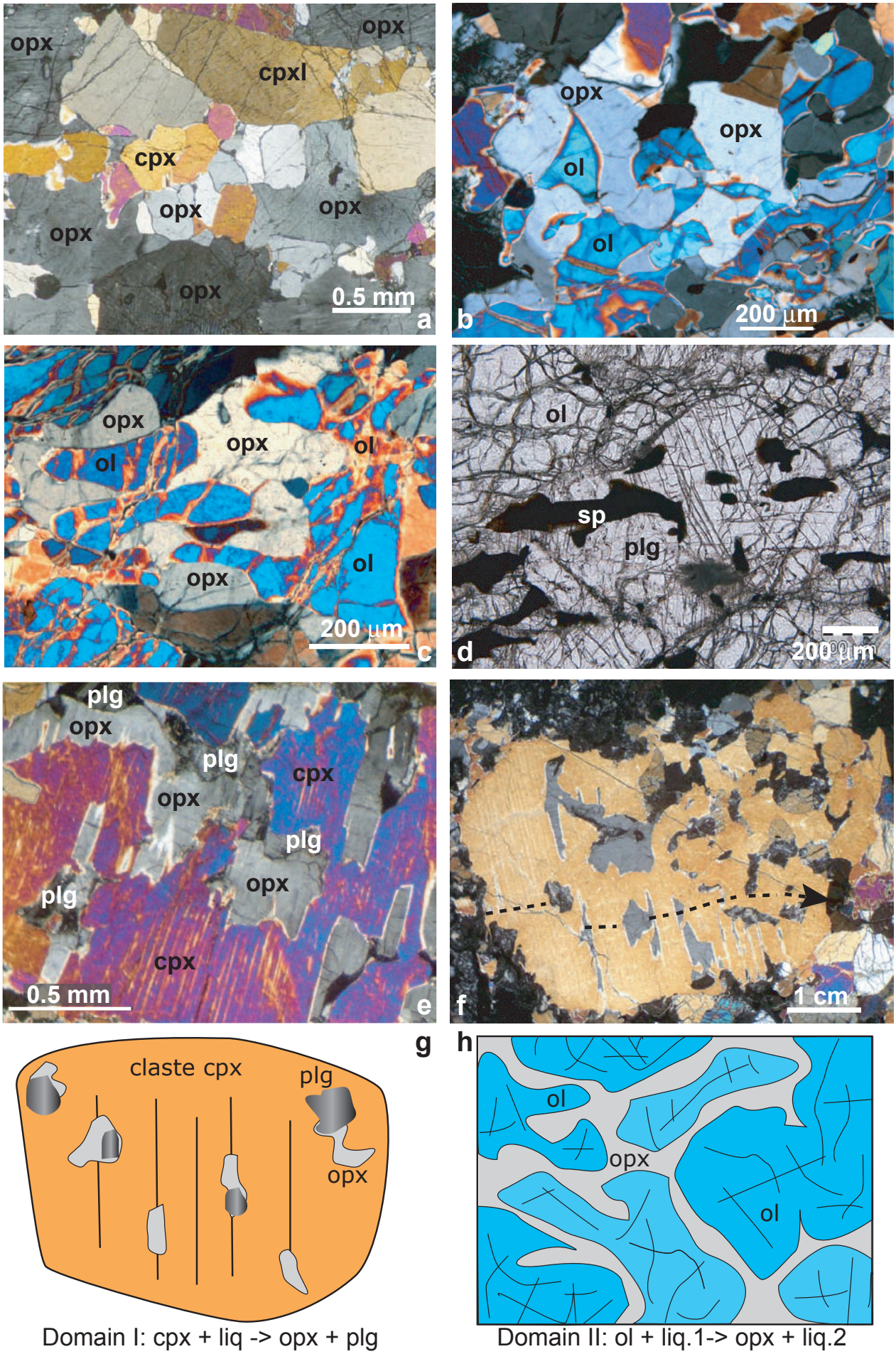
opx
opx
cpxl
cpx
opx
opx
opx
opx
0.5 mm
a
opx
opx
ol
ol
200 µm
b
opx
opx
ol
ol
opx
ol
200 µm
c
ol
sp
plg
200 µm
d
plg
opx
plg
cpx
opx
plg
plg
opx
cpx
0.5 mm
e
1 cm
f
g
claste cpx
plg
opx
Domain I: cpx + liq -> opx + plg
h
ol
opx
ol
Domain II: ol + liq.1-> opx + liq.2

Fig. 2.7

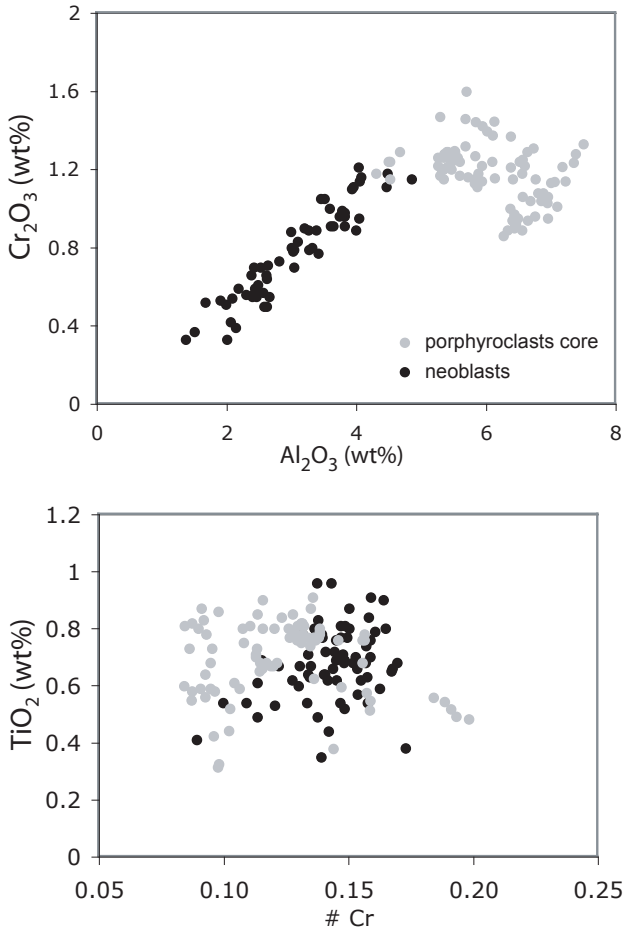

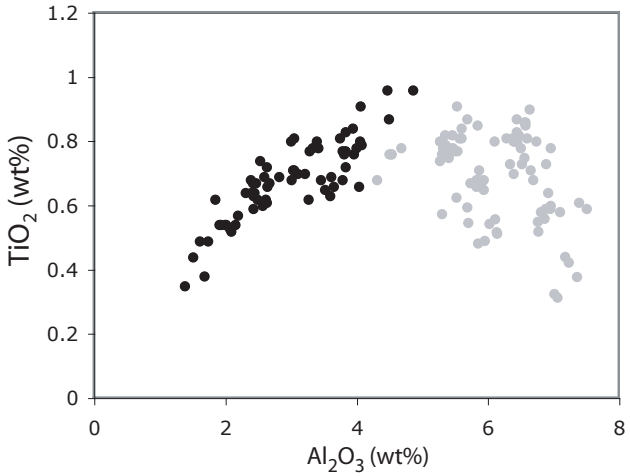

Fig. 2.8: Clinopyroxene composition from porphyroclasts (grey dots) and neoblasts (black dots). Porphyroclast analyses in 13 samples are from all rocks categories (CGSG, FGSG, proto-mylonite, mylonite). Neoblast analyses from 6 samples represented mylonite, proto-mylonite, FGSG rocks. Note increasing TiO_2 with decreasing Al_2O_3 for the porphyroclastic cpx (negative correlation), while for the neoblasts, Cr_2O_3 and TiO_2 correlate positively.

Fig. 2.7: Microphotographs of textures related to recrystallization, melt impregnation and melt/rock reaction. (a) Recrystallized zone of clinopyroxene and orthopyroxene between larger pyroxene porphyroclasts (L13, crossed Nicols). (b) Fine-grained olivine+orthopyroxene domain in pressure shadows of large olivine porphyroclasts. Note the interstitial occurrence of orthopyroxene (I2, crossed Nicols). (c) Undeformed plagioclase replacing deformed and elongated spinel, indicating crystallization of plagioclase after deformation of spinel (L241, plane polarized light). (d) Replacement of clinopyroxene porphyroclasts by orthopyroxene and plagioclase (L13), note that formation of orthopyroxene and plagioclase is irregular (crossed Nicols). (e) Clinopyroxene porphyroclast partially replaced by orthopyroxene and plagioclase, (L212, crossed Nicols). (f) Clinopyroxene porphyroclast, partially replaced by orthopyroxene and plagioclase. Arrow indicates microprobe traverse shown in Fig. 2.14 (crossed Nicols). (g) Schematic representation of clinopyroxene partially replaced by orthopyroxene and plagioclase in the presence of melt (domain I); (h) Sketch of interstitial orthopyroxene replacing olivine, according to the reaction ol+liq1 -> opx+liq2 (domain II).

(olivine + clinopyroxene + orthopyroxene ± plagioclase) in CGSG or FGSG samples indicate thermal equilibration in the presence of melt (Fig. 2.7a). Evidence for melt/rock reaction can be observed in all peridotite types, with vermicular and interstitial, mostly exsolution-free orthopyroxene, localized along the contact with olivine and/or crosscutting larger porphyroclastic olivine. Such microstructures probably indicate the reaction of SiO_2-saturated melts with olivine according to the peritectic reaction (1) (Fig. 2.7b-c-h).

(1) Liq. 1 + olivine -> orthopyroxene + Liq. 2

Plagioclase has been observed in 3 different microstructural sites: (i) Plagioclase surrounding dark Cr-rich spinel is oriented sub-parallel to the foliation in the mylonitic rocks (Fig. 2.7d). (ii) The plagioclase is not only associated to spinel, but also like aggregates parallel to the foliation associated with orthopyroxene, clinopyroxene and olivine.

(iii) Some exsolved porphyroclastic clinopyroxenes are partially replaced by orthopyroxene patches and/or by intergrowth of orthopyroxene and plagioclase (Fig. 2.7e-f-g), similar to observations from Lanzo south, where orthopyroxene and

Table 2.1: Clinopyroxene composition of neoblasts, porphyroclasts core and porphyroclast rim. (n= number of analyses). Mg# = (Mg / (Mg + Fe^{2+} + Fe^{3+})) and Cr# = (Cr/(Cr+Al)).

		hydrous-mylonite			**mylonite**						**proto-mylonite**						**FGSG**		
sample		L187d			L04			L104			L112			La-2002-5			L09		
		neoblast	*rim*	*core*	*neoblast*	*rim*	*core*	*neoblast*	*rim*	*core*	*neoblast*	*rim*	*core*	*neoblast*	*rim*	*core*	*neoblast*	*rim*	*core*
		n=4	*n=2*	*n=4*	*n=4*	*n=2*	*n=3*	*n=4*	*n=2*	*n=3*	*n=2*	*n=2*	*n=3*	*n=4*	*n=3*	*n=4*	*n=3*	*n=2*	*n=4*
wt%	SiO2	53.7(3)	52.0(4)	50.1(2)	53.2(3)	52.4(2)	50.1(3)	52.2(5)	51.6(1)	50.1(2)	52.9(0)	52.3(0)	50.4(2)	53.5(9)	52.3(4)	51.3(1)	52.1(1)	52.0(3)	49.7(3)
	TiO2	0.54(6)	0.85(7)	0.82(3)	0.66(4)	0.64(6)	0.60(3)	0.76(4)	0.79(0)	0.77(6)	0.66(2)	0.79(1)	0.84(3)	0.57(19)	0.68(4)	0.76(3)	0.67(1)	0.73(1)	0.84(5)
	Al2O3	1.8(1)	3.6(4)	6.5(1)	2.62(14)	3.38(7)	7.0(1)	3.7(4)	4.09(4)	6.6(1)	2.36(8)	3.3(3)	5.75(6)	2.2(7)	3.6(3)	4.6(1)	3.8(2)	3.21(1)	6.63(7)
	Cr2O3	0.39(5)	1.1(0)	0.92(3)	0.63(10)	0.93(2)	1.04(3)	0.91(6)	1.04(4)	1.1(0)	0.56(0)	0.83(6)	1.26(2)	0.56(19)	1.01(8)	1.2(1)	1.0(2)	1.1(2)	1.27(4)
	Fe2O3	1.0(4)	1.2(4)	1.8(4)	1.2(5)	1.92(4)	1.99(68)	1.8(5)	2.3(4)	2.1(5)	1.5(8)	1.0(0)	2.07(9)	0.69(58)	0.65(5)	1.3(3)	1.7(1)	1.57(6)	1.8(4)
	FeO	1.6(3)	1.5(2)	1.6(4)	1.5(4)	1.05(2)	1.37(50)	1.5(4)	0.71(23)	1.6(3)	1.4(9)	2.0(0)	1.37(24)	2.1(4)	2.24(4)	1.8(3)	1.8(2)	1.27(4)	1.5(3)
	MnO	0.08(3)	0.10(1)	0.14(4)	0.06(3)	0.11(3)	0.10(3)	0.08(3)	0.10(2)	0.08(2)	0.08(4)	0.10(3)	0.10(5)	0.09(2)	0.04(3)	0.08(2)	0.09(4)	0.10(4)	0.07(2)
	NiO	0.06(2)	0.04(3)	0.07(2)	0.02(2)	0.03(2)	0.04(2)	0.04(2)	-	-	0.06(1)	0.05(2)	0.02(1)	0.05(2)	0.05(3)	0.04(2)	0.03(2)	-	0.00(1)
	MgO	17.1(1)	16.1(2)	14.8(2)	17.2(1)	17.1(1)	15.1(2)	16.7(2)	16.3(0)	15.6(5)	16.9(1)	16.4(1)	15.1(2)	17.0(5)	16.3(2)	15.7(1)	16.9(2)	16.58(5)	15.0(2)
	CaO	24.0(1)	23.3(1)	22.8(1)	23.1(1)	22.5(4)	22.5(3)	22.4(3)	23.0(4)	21.7(5)	23.5(4)	23.0(2)	22.8(3)	23.2(3)	22.7(2)	22.7(1)	22.3(4)	22.85(2)	22.5(3)
	Na2O	0.40(3)	0.62(6)	0.73(3)	0.52(3)	0.57(2)	0.69(2)	0.64(4)	0.67(11)	0.71(2)	0.45(7)	0.55(2)	0.70(2)	0.44(8)	0.56(1)	0.65(1)	0.53(4)	0.58(4)	0.67(5)
	K2O	<0.01	<0.01	<0.01	<0.01	0.01(1)	0.01(1)	<0.01	<0.01	<0.01	0.01(1)	<0.01	0.01(1)	0.01(1)	<0.01	0.01(1)	<0.01	<0.01	<0.01
	Total	100.5(2)	100.3(0)	100.2(5)	100.7(1)	100.58(28)	100.4(1)	100.7(4)	100.6(1)	100.3(2)	100.2(5)	100.2(3)	100.4(3)	100.3(3)	100.1(4)	100.2(2)	100.5(1)	100.0(6)	99.9(5)
cation	Si	1.942	1.891	1.826	1.919	1.892	1.817	1.885	1.869	1.818	1.920	1.902	1.832	1.937	1.900	1.869	1.886	1.895	1.816
	Ti	0.014	0.023	0.022	0.018	0.017	0.017	0.021	0.022	0.021	0.018	0.021	0.023	0.015	0.019	0.021	0.018	0.020	0.023
	Al	0.076	0.152	0.278	0.111	0.144	0.298	0.159	0.174	0.283	0.101	0.141	0.246	0.092	0.155	0.196	0.163	0.138	0.285
	Cr	0.011	0.030	0.026	0.018	0.026	0.030	0.026	0.030	0.031	0.016	0.024	0.036	0.016	0.029	0.036	0.030	0.031	0.037
	Fe3+	0.028	0.033	0.050	0.033	0.052	0.054	0.048	0.062	0.057	0.040	0.027	0.057	0.019	0.018	0.035	0.037	0.043	0.048
	Fe2+	0.047	0.046	0.047	0.045	0.032	0.042	0.045	0.021	0.048	0.043	0.060	0.042	0.064	0.068	0.056	0.053	0.039	0.044
	Mn	0.002	0.003	0.004	0.002	0.003	0.003	0.003	0.003	0.002	0.002	0.003	0.003	0.003	0.001	0.003	0.003	0.003	0.002
	Ni	0.002	0.001	0.002	0.000	0.001	0.001	0.001	-	-	0.002	0.001	0.001	0.001	0.002	0.001	0.001	-	<0.001
	Mg	0.921	0.870	0.802	0.925	0.921	0.815	0.902	0.880	0.842	0.912	0.887	0.821	0.920	0.884	0.852	0.910	0.900	0.818
	Ca	0.928	0.907	0.890	0.892	0.872	0.875	0.865	0.892	0.846	0.915	0.895	0.889	0.901	0.886	0.886	0.863	0.892	0.879
	Na	0.028	0.044	0.051	0.036	0.040	0.049	0.045	0.047	0.050	0.032	0.038	0.049	0.031	0.039	0.046	0.037	0.041	0.047
	K	<0.001	<0.001	<0.001	<0.001	0.001	<0.001	<0.001	<0.001	<0.001	<0.001	<0.001	<0.001	<0.001	<0.001	<0.001	<0.001	<0.001	<0.001
	total	4.000	4.000	4.000	4.000	4.000	4.000	4.000	4.000	4.000	4.000	4.000	4.000	4.000	4.000	4.000	4.000	4.000	4.000
	# Mg	0.928	0.920	0.897	0.925	0.922	0.900	0.948	0.970	0.940	0.920	0.913	0.898	0.920	0.913	0.906	0.913	0.921	0.903
	# Cr	0.128	0.165	0.086	0.138	0.155	0.091	0.140	0.146	0.100	0.137	0.145	0.128	0.149	0.159	0.154	0.154	0.185	0.114

Table 2.1: Continued

		FGSG			**CGSG central**										**CGSG north**					
sample		L110			L13			L42		L147			L241			W2			L195	
		neoblast	*rim*	*core*	*neoblast*	*rim*	*core*	*rim*	*core*	*neoblast*	*rim*	*core*	*neoblast*	*rim*	*core*	*neoblast*	*rim*	*core*	*rim*	*co*
		n=3	*n=3*	*n=4*	*n=4*	*n=2*	*n=4*	*n=3*	*n=5*	*n=3*	*n=3*	*n=4*	*n=3*	*n=2*	*n=4*	*n=3*	*n=3*	*n=2*	*n=1*	*n=*
wt%	SiO2	53.0(8)	51.8(1)	50.0(1)	50.9(1)	52.4(1)	50.1(3)	51.0(1)	49.6(3)	50.9(2)	52.0(2)	50.7(2)	52.2(9)	51.4(4)	50.4(1)	52.0(7)	51.7(4)	50.5(1)	52.6	50.4
	TiO2	0.60(20)	0.91(4)	0.80(9)	1.01(3)	0.98(1)	0.55(3)	0.64(4)	0.49(6)	0.78(4)	0.91(4)	0.81(2)	0.72(13)	0.78(6)	0.68(3)	0.55(1)	0.68(9)	0.60(4)	0.45	0.38
	Al2O3	2.5(8)	3.7(1)	6.5(1)	4.9(1)	3.4(4)	7.35(3)	4.1(1)	6.0(1)	4.7(2)	4.0(4)	5.8(1)	3.2(1.0)	4.0(1)	6.0(1)	3.4(1)	3.7(3)	5.4(2)	3.8	7.2
	Cr2O3	0.64(15)	1.1(1)	0.98(3)	1.4(1)	0.99(10)	1.22(5)	1.2(1)	1.4(1)	1.2(1)	1.1(1)	1.2(0)	0.77(21)	0.97(8)	1.15(5)	0.96(4)	1.19(5)	1.4(1)	1.1	1.2
	Fe2O3	0.89(50)	0.65(29)	1.2(1.4)	1.7(2)	1.01(33)	1.4(5)	1.9(1.0)	2.7(5)	0.13(23)	0.81(42)	1.5(4)	1.5(5)	1.7(3)	2.1(5)	1.8(1.1)	1.8(7)	2.3(6)	<0.01	0.17
	FeO	2.0(2)	1.8(2)	1.7(1.2)	1.7(2)	2.2(4)	2.2(4)	0.92(85)	0.46(47)	2.9(2)	1.9(4)	1.8(3)	1.6(3)	1.5(2)	1.4(4)	1.1(8)	0.95(78)	0.83(57)	2.5	2.6
	MnO	0.07(3)	0.07(6)	0.09(5)	0.10(4)	0.14(5)	0.08(3)	0.12(1)	0.11(2)	0.06(3)	0.06(3)	0.08(4)	0.10(2)	0.08(1)	0.11(3)	0.09(1)	0.11(2)	0.11(3)	0.09	0.1
	NiO	0.06(4)	0.01(2)	0.04(1)	0.07(3)	0.05(0)	0.07(3)	0.05(4)	0.05(1)	0.03(4)	0.05(2)	0.06(2)	0.03(3)	0.02(0)	0.03(3)	0.04(2)	0.03(3)	0.05(0)	0.06	0.0
	MgO	16.8(4)	15.8(1)	15.6(1.8)	15.742)	16.5(2)	14.3(2)	16.0(6)	15.3(2)	15.3(1)	15.9(2)	15.2(1)	16.5(4)	16.0(1)	15.1(1)	16.3(1)	15.8(2)	15.0(2)	16.0	14.6
	CaO	23.2(3)	23.4(1)	22.0(1.2)	22.4(2)	22.7(6)	22.7(3)	22.6(6)	22.5(5)	23.0(2)	23.6(4)	23.0(1)	23.1(3)	23.1(5)	22.8(2)	23.3(1)	23.8(5)	23.2(3)	22.3	22.4
	Na2O	0.46(5)	0.58(1)	0.61(11)	0.68(7)	0.56(1)	0.72(5)	0.65(4)	0.67(2)	0.57(2)	0.51(9)	0.64(5)	0.51(8)	0.54(4)	0.70(3)	0.59(1)	0.61(5)	0.72(2)	0.52	0.6
	K2O	0.01(1)	0.01(1)	0.01(1)	0.01(1)	0.01(1)	0.01(1)	<0.01	0.01(1)	<0.01	0.01(1)	0.00(1)	<0.01	<0.01	0.01(2)	0.01(1)	<0.01	<0.01	0.01	0.01
	Total	100.2(2)	99.8(3)	99.5(6)	100.5(2)	101.0(0)	100.8(3)	99.2(6)	99.3(3)	99.5(2)	100.9(3)	100.7(2)	100.1(3)	100.0(5)	100.3(3)	100.0(3)	100.3(3)	100.1(5)	99.4	99.7
cation	Si	1.926	1.890	1.829	1.850	1.892	1.816	1.872	1.820	1.866	1.881	1.839	1.898	1.876	1.835	1.905	1.881	1.842	1.928	1.8
	Ti	0.016	0.025	0.022	0.028	0.027	0.015	0.018	0.013	0.022	0.025	0.022	0.020	0.021	0.019	0.015	0.019	0.016	0.012	0.0
	Al	0.106	0.162	0.279	0.208	0.147	0.314	0.179	0.261	0.201	0.172	0.248	0.138	0.170	0.252	0.027	0.034	0.040	0.164	0.3
	Cr	0.018	0.032	0.028	0.039	0.028	0.035	0.036	0.040	0.036	0.031	0.035	0.022	0.028	0.033	0.143	0.160	0.232	0.031	0.0
	Fe3+	0.024	0.018	0.032	0.045	0.027	0.039	0.053	0.075	0.004	0.022	0.039	0.041	0.046	0.057	0.033	0.049	0.063	0.000	0.0
	Fe2+	0.061	0.054	0.053	0.054	0.066	0.068	0.028	0.014	0.088	0.059	0.054	0.048	0.046	0.041	0.050	0.029	0.025	0.076	0.0
	Mn	0.002	0.002	0.003	0.004	0.004	0.002	0.004	0.003	0.002	0.002	0.002	0.003	0.002	0.003	0.003	0.003	0.003	0.003	0.0
	Ni	0.002	0.000	0.001	0.002	0.001	0.002	0.001	0.002	0.001	0.002	0.002	0.001	0.001	0.001	0.001	0.001	0.001	0.002	0.0
	Mg	0.909	0.860	0.847	0.852	0.888	0.774	0.875	0.837	0.837	0.856	0.820	0.893	0.872	0.821	0.883	0.854	0.818	0.872	0.7
	Ca	0.902	0.915	0.863	0.872	0.879	0.884	0.888	0.886	0.903	0.915	0.893	0.900	0.901	0.888	0.898	0.927	0.907	0.875	0.8
	Na	0.032	0.041	0.043	0.046	0.039	0.050	0.046	0.048	0.040	0.036	0.045	0.036	0.038	0.049	0.041	0.043	0.051	0.037	0.0
	K	<0.001	0.001	<0.001	0.001	<0.001	<0.001	<0.001	<0.001	<0.001	0.001	<0.001	<0.001	<0.001	<0.001	<0.001	<0.001	<0.001	<0.001	<0.0
	total	4.000	4.000	4.000	4.000	4.000	4.000	4.000	4.000	3.999	4.000	4.000	4.000	4.000	4.000	4.000	4.000	4.000	4.000	4.0
	# Mg	0.916	0.924	0.912	0.900	0.907	0.882	0.920	0.911	0.902	0.916	0.902	0.914	0.909	0.899	0.918	0.921	0.909	0.920	0.9
	# Cr	0.148	0.165	0.092	0.157	0.162	0.100	0.168	0.133	0.151	0.153	0.123	0.139	0.142	0.116	0.842	0.824	0.854	0.158	0.1

Table 2.2: Orthopyroxene composition of neoblasts, porphyroclasts core, porphyroclast rim, intermediate composition in porphyroclast (plateau), orthopyroxene of impregnation microtexture linked with olivine (imp (ol)) and replacive orthopyroxene in porphyroclastic clinopyroxene (imp (cpx)). (n= number of analyses). Mg# = (Mg / (Mg + Fe^{2+} + Fe^{3+})) and Cr# = (Cr/(Cr+Al)). Units in parentheses indicate standard deviation from average analysis.

		Hydrous mylonite				**mylonite**									**proto-mylonite**			
sample		L187d				L04				L104					L112			
		neoblast	*rim*	*core*	*imp (cpx)*	*neoblast*	*rim*	*core*	*imp (ol)*	*neoblast*	*rim*	*core*	*imp (ol)r*	*imp (ol)c*	*neoblast*	*rim*	*core*	*imp(ol)*
		n=4	*n=2*	*n=4*	*n=2*	*n=4*	*n=2*	*n=3*	*n=6*	*n=5*	*n=3*	*n=3*	*n=2*	*n=3*	*n=2*	*n=2*	*n=3*	*n=3*
wt%	SiO2	57.5(2)	56.4(3)	55.0(1)	54.4(4)	57.5 (4)	56.9(1)	54.2(2)	57.0(3)	57.1(2)	56.8(3)	54.6(1)	56.5(0)	56.2(1)	56.7(4)	56.3(5)	54.8(2)	55.7(3)
	TiO2	0.13(3)	0.16(5)	0.25(2)	0.19(1)	0.19(3)	0.18(5)	0.14(3)	0.18(1)	0.23(2)	0.20(3)	0.19(4)	0.23(4)	0.27(3)	0.23(2)	0.22(1)	0.23(1)	0.24(2)
	Al2O3	0.92(24)	2.2(2)	3.9(2)	5.0(9)	1.2(3)	1.1(1)	4.96(8)	1.4(2)	1.7(3)	1.8(3)	4.6(1)	2.0(1)	2.5(1)	1.5(5)	1.6(6)	3.88(8)	2.6(4)
	Cr2O3	0.12(3)	0.35(6)	0.76(1)	0.71(7)	0.24(7)	0.18(1)	0.78(4)	0.22(4)	0.34(8)	0.40(12)	0.84(7)	0.31(08)	0.47(2)	0.28(2)	0.32(16)	0.77(5)	0.57(8)
	Fe2O3	1.1(3)	0.80(21)	1.2(4)	0.91(59)	1.4(4)	0.21(3)	0.80(44)	0.13(28)	1.1(4)	0.84(58)	1.2(6)	1.6(3)	1.3(1)	0.58(18)	<0.01	<0.01	0.19(23)
	FeO	5.9(2)	6.2(5)	5.8(1)	6.1(6)	5.4(3)	6.4(1)	5.87(36)	6.27(31)	5.9(3)	6.2(8)	5.7(4)	5.6(3)	5.7(2)	6.0(5)	6.6(2)	6.5(2)	6.5(2)
	MnO	0.20(3)	0.19(1)	0.10(3)	0.18(0)	0.16(2)	0.16(7)	0.11(4)	0.18(1)	0.17(1)	0.19(5)	0.16(2)	0.15(1)	0.14(1)	0.17(6)	0.17(4)	0.15(4)	0.16(2)
	NiO	0.06(3)	0.08(2)	0.10(1)	0.11(4)	0.05(3)	0.04(2)	0.13(3)	0.07(2)	0.09(1)	-	-	0.07(4)	0.08(3)	0.09(2)	0.12(6)	0.12(3)	0.09(3)
	MgO	34.9(2)	34.1(0)	33.2(1)	32.6(6)	35.1(2)	34.2(1)	32.5(2)	34.2(1)	34.5(1)	34.2(6)	32.9(2)	34.4(1)	34.1(0)	34.1(5)	33.4(5)	32.3(2)	33.2(3)
	CaO	0.39(5)	0.35(1)	0.52(2)	0.47(1)	0.51(12)	0.44(8)	0.65(3)	0.45(4)	0.58(5)	0.45(9)	0.65(8)	0.54(2)	0.61(3)	0.57(4)	0.64(10)	0.87(6)	0.58(4)
	Na2O	0.01(1)	0.01(1)	0.02(2)	0.03(1)	0.02(1)	0.01(1)	0.03(2)	0.01(1)	0.01(1)	0.01(1)	0.03(1)	0.02(3)	0.02(1)	0.02(0)	0.02(3)	0.02(1)	0.01(1)
	Total	101.1(4)	100.8(4)	101.2(4)	100.6(2)	101.8(2)	99.8(3)	100.1(1)	100.1(3)	101.7(2)	101.1(3)	101.0(3)	101.4(2)	101.3(3)	100.2(1)	99.3(1)	99.7(4)	99.8(6)
cation	Si	1.963	1.937	1.890	1.874	1.949	1.969	1.876	1.967	1.942	1.943	1.876	1.931	1.921	1.953	1.961	1.908	1.934
	Ti	0.003	0.004	0.006	0.005	0.005	0.005	0.004	0.005	0.006	0.005	0.005	0.006	0.007	0.006	0.006	0.006	0.006
	Al	0.037	0.089	0.157	0.201	0.050	0.043	0.203	0.006	0.070	0.073	0.186	0.079	0.098	0.061	0.066	0.159	0.105
	Cr	0.003	0.009	0.021	0.019	0.007	0.005	0.021	0.056	0.009	0.011	0.023	0.008	0.013	0.007	0.009	0.021	0.016
	Fe3+	0.027	0.021	0.031	0.023	0.036	0.006	0.021	0.003	0.027	0.022	0.032	0.041	0.034	0.015	<0.001	<0.001	0.005
	Fe2+	0.169	0.178	0.168	0.176	0.153	0.185	0.170	0.181	0.169	0.178	0.164	0.159	0.162	0.174	0.191	0.190	0.190
	Mn	0.006	0.006	0.003	0.005	0.005	0.005	0.003	0.005	0.005	0.006	0.005	0.004	0.004	0.005	0.005	0.005	0.005
	Ni	0.002	0.002	0.003	0.003	0.001	0.001	0.003	0.002	0.002	-	-	0.002	0.002	0.002	0.003	0.003	0.003
	Mg	1.775	1.742	1.702	1.674	1.775	1.764	1.673	1.757	1.748	1.746	1.684	1.749	1.735	1.753	1.734	1.675	1.715
	Ca	0.014	0.013	0.019	0.017	0.018	0.016	0.024	0.016	0.021	0.017	0.024	0.020	0.022	0.021	0.024	0.033	0.022
	Na	0.001	<0.001	0.001	0.002	0.001	0.001	0.002	0.001	0.001	0.001	0.002	0.001	0.001	0.002	0.001	0.002	0.001
	K	<0.001	<0.001	<0.001	<0.001	<0.001	<0.001	0.001	0.000	<0.001	<0.001	<0.001	<0.001	<0.001	<0.001	<0.001	<0.001	<0.001
	total	4.000	4.000	4.000	4.000	4.000	4.000	4.000	4.000	4.000	4.000	4.000	4.000	4.000	4.000	4.000	4.000	4.000
	# Mg	0.902	0.899	0.897	0.895	0.905	0.903	0.899	0.905	0.911	0.907	0.910	0.915	0.913	0.903	0.901	0.898	0.898
	# Cr	0.080	0.095	0.116	0.087	0.116	0.101	0.095	0.901	0.117	0.129	0.109	0.096	0.115	0.109	0.116	0.117	0.129

Table 2.2: Continued

sample		proto-mylonite La2002-05				FGSG L09				L110			CGSG central L13					L42	
		neoblast n=4	*rim* n=2	*plateau* n=3	*core* n=4	*imp (ol)* n=3	*neoblast* n=3	*rim* n=2	*core* n=5	*neoblast* n=3	*rim* n=2	*core* n=4	*imp (ol)* n=5	*rim* n=3	*core* n=4	*imp (ol)* n=5	*imp (cpx)* n=5	*rim* n=2	*core* n=2
wt%	SiO2	57.0(6)	56.7(2)	55.6(1)	55.0(1)	56.0(1)	56.2(1)	56.9(2)	55.1(3)	56.8(1)	56.7(2)	55.5(1)	55.5(5)	56.7(2)	55.4(2)	56.3(4)	55.1(3)	56.5(3)	54.0(4)
	TiO2	0.20(4)	0.23(0)	0.25(1)	0.19(1)	0.27(2)	0.23(2)	0.16(8)	0.22(3)	0.21(5)	0.24(2)	0.25(3)	0.23(2)	0.31(2)	0.25(3)	0.33(3)	0.26(3)	0.22(3)	0.17(7)
	Al2O3	1.4(4)	1.6(1)	3.2(1)	3.84(2)	2.4(1)	2.7(1)	1.94(6)	4.12(17)	1.6(3)	1.8(1)	3.1(1)	2.6(2)	2.1(2)	3.28(6)	2.3(5)	3.8(2)	1.4(4)	4.2(0)
	Cr2O3	0.28(12)	0.35(1)	0.64(6)	0.77(2)	0.48(4)	0.48(5)	0.44(14)	0.81(6)	0.35(11)	0.47(5)	0.70(4)	0.59(3)	0.47(2)	0.70(2)	0.54(4)	0.89(12)	0.33(6)	0.89(8)
	Fe2O3	0.50(3)	1.0(1.2)	0.98(20)	1.0(2)	0.90(20)	1.1(4)	0.64(47)	0.47(36)	0.60(52)	<0.01	<0.01	0.84(17)	<0.01	0.27(25)	0.99(29)	1.4(2)	0.48(68)	2.0(1.6)
	FeO	6.5(1)	5.8(9)	6.0(2)	5.9(2)	6.1(2)	6.0(4)	6.16(6)	6.32(23)	6.5(2)	5.1(5)	5.4(1)	6.1(3)	6.9(1)	7.0(2)	6.1(2)	6.2(1)	6.4(1)	4.4(1.3)
	MnO	0.16(1)	0.17(1)	0.15(2)	0.14(4)	0.15(6)	0.17(3)	0.14(1)	0.15(4)	0.17(3)	0.10(4)	0.13(4)	0.13(7)	0.18(5)	0.13(3)	0.18(1)	0.18(5)	0.21(6)	0.19(1)
	NiO	0.07(1)	0.11(4)	0.09(1)	0.10(2)	0.08(1)	0.08(3)	0.08(1)	0.07(1)	0.07(3)	0.06(1)	0.08(2)	0.08(2)	0.10(0)	0.08(2)	0.07(3)	0.04(1)	0.08(3)	0.10(3)
	MgO	34.1(5)	34.4(3)	33.3(2)	32.9(1)	33.5(2)	33.7(3)	34.3(2)	32.9(2)	33.9(3)	33.4(2)	32.7(1)	32.8(5)	33.31(6)	32.7(1)	33.6(4)	32.8(4)	33.9(1)	33.1(7)
	CaO	0.58(10)	0.58(1)	0.80(6)	0.85(2)	0.86(6)	0.79(6)	0.50(11)	0.64(18)	0.50(9)	0.78(16)	0.78(9)	1.25(71)	0.69(13)	0.70(5)	0.92(18)	0.82(23)	0.45(26)	0.66(18)
	Na2O	0.01(1)	0.01(1)	0.02(1)	0.01(1)	0.02(2)	0.02(2)	0.03(3)	0.01(1)	0.01(1)	0.03(1)	0.02(1)	0.05(2)	0.02(1)	0.03(1)	0.03(2)	0.02(1)	0.02(1)	0.03(0)
	Total	100.8(3)	100.8(4)	101.0(1)	100.6(1)	100.7(2)	101.4(4)	101.2(1)	100.8(1)	100.7(2)	98.6(2)	98.7(3)	100.3(7)	100.74(7)	100.5(2)	101.3(3)	101.5(3)	100.0(2)	99.8(6)
cation	Si	1.958	1.945	1.908	1.894	1.927	1.921	1.944	1.895	1.952	1.984	1.944	1.922	1.951	1.915	1.927	1.888	1.956	1.873
	Ti	0.005	0.006	0.006	0.005	0.007	0.006	0.004	0.006	0.005	0.006	0.007	0.008	0.008	0.007	0.008	0.007	0.006	0.004
	Al	0.055	0.063	0.131	0.156	0.097	0.107	0.078	0.167	0.064	0.073	0.130	0.106	0.085	0.134	0.091	0.154	0.058	0.170
	Cr	0.008	0.009	0.017	0.021	0.013	0.013	0.012	0.022	0.010	0.013	0.019	0.016	0.013	0.019	0.015	0.024	0.009	0.024
	Fe3+	0.013	0.026	0.025	0.027	0.023	0.028	0.016	0.012	0.016	0.000	0.000	0.022	<0.001	0.007	0.025	0.035	0.013	0.053
	Fe2+	0.188	0.165	0.173	0.169	0.176	0.172	0.176	0.182	0.188	0.149	0.157	0.177	0.200	0.201	0.176	0.177	0.184	0.128
	Mn	0.005	0.005	0.004	0.004	0.004	0.005	0.004	0.004	0.005	0.003	0.004	0.004	0.005	0.004	0.005	0.005	0.006	0.005
	Ni	0.002	0.003	0.003	0.003	0.002	0.002	0.002	0.002	0.002	0.002	0.002	0.002	0.003	0.002	0.002	0.001	0.002	0.003
	Mg	1.745	1.756	1.702	1.690	1.717	1.715	1.746	1.688	1.739	1.739	1.706	1.693	1.710	1.684	1.714	1.677	1.748	1.712
	Ca	0.021	0.021	0.029	0.031	0.032	0.029	0.018	0.024	0.018	0.029	0.029	0.046	0.025	0.026	0.034	0.030	0.017	0.024
	Na	0.001	<0.001	0.001	0.001	0.001	0.002	0.002	0.001	0.001	0.002	0.001	0.003	0.001	0.002	0.002	0.002	0.001	0.002
	K	<0.001	<0.001	<0.001	<0.001	<0.001	<0.001	<0.001	<0.001	0.001	<0.001	<0.001	<0.001	<0.001	<0.001	0.001	<0.001	<0.001	<0.001
	total	4.000	4.000	4.000	4.000	4.000	4.000	4.002	4.002	4.000	4.000	4.000	4.000	4.000	4.000	4.000	4.000	4.000	4.000
	# Mg	0.898	0.903	0.897	0.898	0.897	0.897	0.902	0.898	0.896	0.921	0.916	0.896	0.895	0.890	0.896	0.889	0.899	0.907
	# Cr	0.121	0.129	0.117	0.119	0.118	0.109	0.133	0.116	0.130	0.150	0.130	0.133	0.131	0.125	0.140	0.136	0.136	0.126

Table 2.2: Continued

		CGSG central											CGSG north						
sample		L42	L147						L241				W2				L195		
		imp (ol)	*coarse*	*rim*	*plateau*	*core*	*imp (ol)c*	*imp (ol)r*	*neoblast*	*rim*	*plateau*	*core*	*imp (ol)*	*neoblast*	*rim*	*core*	*imp (ol)*	*rim*	*core*
		n=4	*n=1*	*n=3*	*n=4*	*n=2*	*n=4*	*n=2*	*n=3*	*n=3*	*n=4*	*n=4*	*n=7*	*n=1*	*n=4*	*n=2*	*n=4*	*n=5*	*n=5*
wt%	SiO2	54.8(6)	54.8	55.1(3)	54.4(2)	55.7(1)	55.5(1)	56.4(1)	56.4(4)	56.2(3)	55.3(2)	54.9(2)	56.7(7)	56.39	55.5(4)	54.1(2)	56.0(6)	56.2(5)	54.9(3)
	TiO2	0.16(2)	0.28	0.24(1)	0.21(1)	0.27(1)	0.29(2)	0.25(1)	0.19(5)	0.19(4)	0.22(1)	0.19(1)	0.19(8)	0.19	0.19(3)	0.13(0)	0.19(5)	0.12(4)	0.13(3)
	Al2O3	2.9(8)	3.0	1.30(5)	1.68(1)	3.8(3)	2.6(3)	1.7(3)	1.8(4)	2.4(2)	3.4(1)	4.1(0)	1.8(6)	2.15	2.4(3)	4.8(6)	2.1(6)	2.5(3)	4.5(1)
	Cr2O3	0.81(12)	0.69	0.58(5)	0.75(2)	0.80(7)	0.59(8)	0.29(6)	0.30(2)	0.57(2)	0.72(3)	0.79(3)	0.35(16)	0.44	0.51(4)	0.83(2)	0.32(11)	0.55(7)	1.0(8)
	Fe2O3	1.9(2)	0.02	<0.01	0.59(24)	0.54(8)	0.24(45)	0.00	1.8(3)	1.0(2)	1.5(2)	1.5(4)	1.0(4)	0.18	0.63(34)	0.85(54)	0.16(19)	0.04(6)	0.25(37)
	FeO	4.6(3)	6.6	6.8(1)	6.2(2)	6.3(0)	6.5(1)	6.62(4)	5.32(0)	6.1(2)	5.6(2)	5.6(4)	6.1(2)	6.34	6.0(4)	5.6(5)	6.5(2)	5.8(2)	5.6(3)
	MnO	0.17(0)	0.19	0.16(2)	0.14(3)	0.18(4)	0.16(3)	0.13(1)	0.18(3)	0.15(2)	0.16(3)	0.17(4)	0.18(4)	0.15	0.15(1)	0.15(2)	0.16(1)	0.16(1)	0.15(2)
	NiO	0.10(1)	0.08	0.08(2)	0.10(1)	0.13(4)	0.06(2)	0.07(5)	0.08(2)	0.09(1)	0.11(3)	0.12(3)	0.08(3)	0.09	0.08(2)	0.08(2)	0.07(1)	0.06(3)	0.05(4)
	MgO	33.4(3)	32.3	32.7(2)	32.3(1)	33.3(3)	32.8(2)	33.5(1)	34.4(3)	33.9(1)	33.4(1)	33.1(2)	34.1(5)	33.80	33.2(2)	32.4(1)	33.3(5)	33.7(3)	32.7(7)
	CaO	0.84(4)	0.94	0.72(8)	0.88(12)	0.65(8)	0.80(9)	0.62(1)	0.52(15)	0.54(4)	0.66(6)	0.60(4)	0.62(21)	0.57	0.7(1)	0.84(13)	0.67(22)	0.70(10)	0.78(9)
	Na2O	0.02(1)	0.03	0.01(1)	0.01(1)	0.02(1)	0.03(1)	0.01(1)	0.01(1)	0.01(1)	0.02(1)	0.01(1)	0.02(1)	0.01	0.01(1)	0.03(2)	0.01(1)	0.01(1)	0.01(1)
	Total	99.6(0)	99.01	97.7(4)	97.2(3)	101.7(0)	99.6(5)	99.6(6)	101.0(5)	101.1(1)	101.1(3)	101.0(4)	101.1(2)	100.31	99.4(3)	99.7(3)	99.5(1)	99.9(3)	100.1(4)
cation	Si	1.902	1.921	1.955	1.941	1.901	1.931	1.960	1.932	1.927	1.896	1.884	1.941	1.943	1.931	1.877	1.948	1.941	1.896
	Ti	0.004	0.008	0.006	0.006	0.007	0.008	0.006	0.005	0.005	0.006	0.005	0.005	0.005	0.005	0.003	0.005	0.003	0.003
	Al	0.119	0.125	0.055	0.071	0.151	0.106	0.068	0.073	0.095	0.139	0.165	0.073	0.087	0.099	0.195	0.084	0.104	0.183
	Cr	0.022	0.019	0.016	0.021	0.021	0.016	0.008	0.008	0.015	0.019	0.021	0.009	0.012	0.014	0.023	0.009	0.015	0.028
	Fe3+	0.049	0.001	<0.001	0.016	0.014	0.006	<0.001	0.047	0.026	0.039	0.037	0.026	0.005	0.017	0.022	0.004	0.001	0.007
	Fe2+	0.133	0.192	0.201	0.184	0.180	0.190	0.192	0.152	0.174	0.161	0.162	0.174	0.183	0.176	0.163	0.190	0.168	0.163
	Mn	0.005	0.006	0.005	0.004	0.005	0.005	0.004	0.005	0.004	0.005	0.005	0.005	0.004	0.004	0.004	0.005	0.005	0.004
	Ni	0.003	0.002	0.002	0.003	0.004	0.002	0.002	0.002	0.002	0.003	0.003	0.002	0.002	0.002	0.002	0.002	0.002	0.001
	Mg	1.730	1.689	1.735	1.720	1.691	1.704	1.736	1.756	1.730	1.707	1.695	1.740	1.736	1.725	1.676	1.727	1.735	1.684
	Ca	0.031	0.035	0.028	0.034	0.024	0.030	0.023	0.019	0.020	0.024	0.022	0.023	0.021	0.026	0.031	0.025	0.026	0.029
	Na	0.001	0.002	0.001	0.001	0.002	0.002	0.001	0.001	<0.001	0.001	0.001	0.001	0.001	0.001	0.002	0.001	0.001	<0.001
	K	<0.001	<0.001	<0.001	<0.001	0.001	<0.001	0.001	<0.001	<0.001	<0.001	<0.001	<0.001	<0.001	<0.001	<0.001	<0.001	0.001	<0.001
	total	4.000	4.000	4.004	4.000	4.000	4.000	4.000	4.000	4.000	4.000	4.000	4.000	4.000	4.000	4.000	4.000	4.000	3.998
	# Mg	0.907	0.897	0.896	0.897	0.898	0.897	0.900	0.900	0.898	0.897	0.897	0.898	0.903	0.900	0.902	0.899	0.912	0.909
	# Cr	0.157	0.132	0.232	0.230	0.124	0.133	0.105	0.102	0.139	0.123	0.115	0.114	0.120	0.123	0.104	0.096	0.126	0.131

Table 2.2: Continued

		CGSG north		
sample		L195		
		imp (cpx)	*imp (ol)c*	*imp (ol)r*
		n=5	*n=6*	*n=5*
wt%	SiO2	53.7(3)	56.5(4)	56.5(8)
	TiO2	0.07(2)	0.15(1)	0.14(2)
	Al2O3	6.2(3)	2.4(5)	2.2(6)
	Cr2O3	0.86(8)	0.50(12)	0.49(21)
	Fe2O3	0.26(34)	<0.01	0.41(57)
	FeO	6.0(4)	5.9(0)	5.5(6)
	MnO	0.16(1)	0.17(2)	0.16(0)
	NiO	0.10(1)	0.09(2)	0.08(2)
	MgO	32.1(3)	33.8(2)	33.9(5)
	CaO	0.55(11)	0.76(12)	0.74(10)
	Na2O	0.02(1)	0.02(0)	0.03(1)
	K2O	0.01(0)	0.01(0)	0.01(0)
	Total	100.1(2)	100.2(1)	100.2(4)
cation	Si	1.858	1.947	1.948
	Ti	0.002	0.004	0.004
	Al	0.254	0.097	0.088
	Cr	0.024	0.014	0.013
	Fe3+	0.007	<0.001	0.011
	Fe2+	0.174	0.168	0.158
	Mn	0.005	0.005	0.005
	Ni	0.003	0.002	0.002
	Mg	1.652	1.733	1.741
	Ca	0.020	0.028	0.027
	Na	0.001	0.001	0.002
	K	<0.001	<0.001	<0.001
	total	4.000	4.000	4.000
	# Mg	0.902	0.911	0.912
	# Cr	0.085	0.124	0.131

Table 2.3: Olivine composition composition of neoblasts, porphyroclasts core and porphyroclast rim. (n= number of analyses). Mg# = (Mg / (Mg + Fe^{2+} + Fe^{3+})) and Cr# = (Cr/(Cr+Al)).

		hydrous-mylonite			mylonite				proto-mylonite				FGSG		
sample		L187d			L04		L104		L112		La2002-5		L09		
		neoblast	*round neo*	*core*	*neoblast*	*core*	*neoblast*	*core*	*neoblast*	*core*	*neoblast*	*core*	*neoblast*	*core*
		n=4	*n=3*	*n=2*	*n=5*	*n=3*	*n=4*	*n=3*	*n=4*	*n=6*	*n=3*	*n=2*	*n=3*	*n=6*
wt%	SiO2	41.5(1)	40.8(1)	40.9(1)	41.5(2)	40.9(3)	40.9(2)	41.1(0)	40.9(1)	40.8(2)	41.1(3)	40.9(2)	41.3(2)	40.6(2)
	TiO2	0.02(1)	0.01(1)	0.02(2)	0.01(1)	0.01(2)	0.01(1)	0.01(1)	0.01(1)	0.04(7)	0.01(1)	0.02(2)	0.02(2)	0.00(1)
	Al2O3	0.01(1)	0.01(1)	0.01(1)	0.38(81)	<0.01	0.01(1)	0.01(1)	<0.01	<0.01	0.01(1)	0.01(1)	0.00(1)	<0.01
	Cr2O3	0.02(2)	0.01(2)	0.01(1)	0.03(3)	0.01(1)	<0.01	0.01(2)	0.04(4)	0.02(2)	0.07(9)	0.02(0)	0.06(5)	0.02(2)
	Fe2O3	-	-	-	-	-	-	-	-	-	-	-	-	-
	FeO	8.2(4)	10.0(2)	10.3(2)	9.41(22)	9.5(5)	11.5(8)	10.9(3)	9.7(2)	9.7(2)	9.6(3)	10.2(2)	9.8(2)	9.7(2)
	MnO	0.05(1)	0.15(3)	0.19(9)	0.14(4)	0.16(2)	0.26(7)	0.20(2)	0.17(4)	0.18(4)	0.14(2)	0.11(1)	0.15(3)	0.16(1)
	NiO	0.40(4)	0.37(2)	0.39(3)	0.38(5)	0.36(4)	0.26(10)	0.35(2)	0.38(1)	0.37(1)	0.36(4)	0.38(6)	0.37(1)	0.38(2)
	MgO	51.2(3)	49.4(1)	49.6(2)	49.9(8)	49.5(5)	48.3(6)	48.8(3)	49.0(2)	48.8(4)	49.9(4)	49.2(1)	49.8(2)	49.1(1)
	CaO	0.10(2)	<0.01	0.03(1)	0.21(28)	0.02(2)	0.01(1)	0.01(1)	0.02(1)	0.03(1)	<0.01	0.05(1)	0.02(1)	0.04(1)
	Na2O	0.01(1)	0.01(1)	0.01(1)	0.02(2)	0.01(1)	0.01(1)	0.00(1)	0.01(1)	<0.01	0.01(1)	0.01(1)	0.01(1)	0.00(1)
	K2O	<0.01	0.01(1)	0.01(1)	0.01	<0.01	<0.01	<0.01	<0.01	0.01(1)	0.00(1)	0.02(1)	0.00(1)	<0.01
	Total	101.5(2)	100.7(2)	101.4(3)	101.93(53)	100.5(4)	101.3(2)	101.4(1)	100.2(3)	100.0(6)	101.2(3)	100.9(1)	101.4(3)	100.0(2)
cation	Si	0.994	0.993	0.990	0.996	0.997	0.998	0.999	1.001	1.003	0.995	0.996	0.997	0.996
	Ti	<0.001	<0.001	<0.001	<0.001	<0.001	<0.001	<0.001	<0.001	0.001	<0.001	<0.001	<0.001	<0.001
	Al	<0.001	<0.001	<0.001	0.011	<0.001	<0.001	<0.001	<0.001	<0.001	<0.001	<0.001	<0.001	<0.001
	Cr	<0.001	<0.001	<0.001	0.001	<0.001	<0.001	<0.001	0.001	0.001	0.001	<0.001	0.001	<0.001
	Fe3+	-	-	-	-	-	-	-	-	-	-	-	-	-
	Fe2+	0.164	0.203	0.207	0.189	0.198	0.234	0.222	0.198	0.199	0.194	0.207	0.197	0.199
	Mn	0.001	0.003	0.004	0.003	0.003	0.005	0.004	0.004	0.004	0.003	0.002	0.003	0.003
	Ni	0.008	0.007	0.008	0.007	0.007	0.005	0.007	0.007	0.007	0.007	0.007	0.007	0.008
	Mg	1.829	1.793	1.789	1.786	1.794	1.757	1.767	1.788	1.785	1.799	1.785	1.793	1.793
	Ca	0.002	<0.001	0.001	0.005	0.001	0.000	<0.001	0.001	0.001	<0.001	0.001	0.001	0.001
	Na	0.001	<0.001	<0.001	0.001	<0.001	0.001	<0.001	<0.001	<0.001	<0.001	<0.001	<0.001	<0.001
	K	<0.001	<0.001	<0.001	<0.001	<0.001	<0.001	<0.001	<0.001	<0.001	<0.001	<0.001	<0.001	<0.001
	total	3.000	3.000	3.000	3.000	3.000	3.000	2.999	3.000	3.000	2.999	2.998	3.000	3.000
	# Mg	0.918	0.898	0.896	0.90	0.90	0.88	0.89	0.90	0.90	0.903	0.896	0.90	0.90

Table 2.3: Continued

		FGSG	CGSG central				CGSG north		
sample		L110	L13	L42	L147	L241	L195		W2
		neoblast	*core*	*core*	*core*	*neoblast*	*core*	*core*	*core*
		n=2	*n=4*	*n=2*	*n=3*	*n=3*	*n=3*	*n=8*	*n=3*	*n=4*
wt%	SiO2	41.0(2)	40.9(2)	41.1(1)	41.0(0)	40.7(0)	40.9(1)	41.0(1)	41.0(2)	40.6(8)
	TiO2	0.02(1)	0.01(1)	0.01(1)	0.01(1)	<0.01	<0.01	0.01(1)	<0.01	0.01(1)
	Al2O3	0.01(1)	0.01(1)	0.01(1)	0.04(6)	<0.01	<0.01	0.01(1)	0.01(1)	0.02(4)
	Cr2O3	0.02(3)	0.01(2)	<0.01	0.01(1)	0.01(1)	0.05(5)	0.03(1)	0.01(1)	0.01(1)
	Fe2O3	-	-	-	-	-	-	-	-	-
	FeO	10.3(6)	10.2(1)	10.9(2)	9.2(8)	10.0(3)	10.0(3)	8.6(1)	10.3(2)	9.57(5)
	MnO	0.12(7)	0.17(4)	0.19(3)	0.16(1)	0.14(2)	0.14(2)	0.14(1)	0.15(2)	0.14(1)
	NiO	0.38(0)	0.37(3)	0.35(1)	0.38(4)	0.35(2)	0.40(4)	0.40(3)	0.40(3)	0.39(2)
	MgO	49.1(3)	49.2(2)	49.1(1)	50.1(13)	48.9(5)	49.6(2)	50.0(3)	48.8(2)	49.15(6)
	CaO	0.07(4)	0.03(0)	0.03(1)	0.05(4)	0.02(1)	0.02(1)	0.03(2)	0.04(2)	0.02(2)
	Na2O	0.02(2)	0.01(1)	0.01(1)	0.01(1)	<0.01	0.01(1)	0.07(15)	0.01(1)	<0.01
	K2O	0.01(1)	0.01(1)	<0.01	<0.01	<0.01	<0.01	0.01(1)	0.01(1)	<0.01
	Total	101.0(0)	100.9(2)	101.73(3)	100.9(3)	100.1(7)	101.1(2)	100.2(4)	100.7(2)	99.9(1)
cation	Si	0.997	0.995	0.995	0.993	0.997	0.992	0.998	1.001	0.995
	Ti	<0.001	<0.001	0.000	0.000	<0.001	<0.001	0.000	<0.001	0.000
	Al	<0.001	<0.001	<0.001	0.001	<0.001	<0.001	0.00012	<0.001	<0.001
	Cr	<0.001	<0.001	<0.001	<0.001	<0.001	0.001	0.000	<0.001	<0.001
	Fe3+	-	-	-	-	-	-	-	-	-
	Fe2+	0.208	0.208	0.221	0.185	0.205	0.204	0.175	0.211	0.196
	Mn	0.003	0.004	0.004	0.003	0.003	0.003	0.003	0.003	0.003
	Ni	0.007	0.007	0.007	0.007	0.007	0.008	0.007	0.008	0.008
	Mg	1.781	1.784	1.771	1.808	1.787	1.792	1.813	1.776	1.797
	Ca	0.002	0.001	0.001	0.001	0.001	<0.001	0.001	0.001	<0.001
	Na	0.001	<0.001	0.001	<0.001	<0.001	<0.001	0.003	<0.001	<0.001
	K	<0.001	<0.001	<0.001	<0.001	<0.001	<0.001	0.000	<0.001	<0.001
	total	2.999	2.999	3.000	3.000	3.000	3.000	3.000	3.000	3.000
	# Mg	0.90	0.90	0.889	0.907	0.90	0.898	0.91	0.894	0.902

Table 2.4: Spinel composition of neoblasts, porphyroclasts core and porphyroclats rim. n is the number of analysis per grain type. Mg# = (Mg / (Mg + Fe^{2+} + Fe^{3+})) and Cr# = (Cr/(Cr+Al)).

		h-mylonite		mylonite		
sample		L187d		L04		L104
		neoblast	*core*	*neoblast*	*core*	*core*
		n=4	*n=2*	*n=4*	*n=4*	*n=5*
wt%	SiO2	0.03(1)	0.02(2)	0.06(3)	0.02(2)	0.08(15)
	TiO2	0.19(11)	0.44(17)	0.39(16)	0.59(5)	0.28(16)
	Al2O3	33.1(2.0)	35.1(1.4)	35.6(5.5)	32.0(4)	28.5(1.8)
	Cr2O3	29.3(1.4)	27.2(1.3)	26.7(5.7)	29.5(3)	30.6(1.6)
	Fe2O3	6.2(6)	6.2(2)	6.0(3)	7.0(1)	7.51(39)
	FeO	19.0(1.0)	16.9(7)	18.4(2.0)	14.7(2)	23.3(1.0)
	MnO	0.10(9)	0.11(1)	0.27(2)	0.13(4)	0.46(5)
	NiO	0.16(2)	0.25(1)	0.23(6)	0.24(1)	0.18(3)
	MgO	11.7(1.0)	13.3(6)	12.2(1.7)	14.3(2)	8.0(6)
	CaO	0.03(1)	<0.01	0.03(4)	0.01(1)	<0.01
	Na2O	0.01(1)	0.02(1)	-	0.02(2)	-
	K2O	0.00(1)	<0.01	-	0.00(1)	-
	ZnO	0.20(6)	0.25(2)	0.24(5)	0.16(7)	0.4(1)
	Total	100.0(1.0)	99.8(0)	100.1(6)	98.6(2)	99.4(1)
cation	Si	0.001	<0.001	0.002	0.000	0.003
	Ti	0.004	0.010	0.009	0.013	0.007
	Al	1.162	1.213	1.179	1.099	1.049
	Cr	0.689	0.631	0.668	0.712	0.756
	Fe3+	0.140	0.137	0.132	0.163	0.176
	Fe2+	0.472	0.414	0.455	0.367	0.609
	Mn	0.002	0.003	0.007	0.004	0.012
	Ni	0.004	0.006	0.005	0.006	0.005
	Mg	0.520	0.580	0.537	0.633	0.373
	Ca	0.001	<0.001	0.001	<0.001	<0.001
	Na	<0.001	0.001	-	<0.001	-
	K	<0.001	<0.001	-	<0.001	-
	Zn	0.004	0.005	0.005	0.003	0.010
	total	3.000	3.000	3.000	3.000	3.000
	# Mg	0.465	0.519	0.54	0.63	0.37
	# Cr	0.372	0.342	0.36	0.39	0.42

Table 2.4: Continued

		proto-mylonite				**FGSG**				**CGSG**						**CGSG north**		
sample		L112		La2002-05		L09		L110		L13	L42		L147	L241		W2	L195	
		neoblast	*core*	*neoblast*	*core*	*neoblast*	*core*	*neoblast*	*core*	*core*	*neoblast*	*core*	*core*	*neoblast*	*core*	*core*	*rim*	*core*
		n=3	*n=2*	*n=3*	*n=4*	*n=6*	*n=5*	*n=2*	*n=3*	*n=2*	*n=2*	*n=3*	*n=2*	*n=3*	*n=3*	*n=4*	*n=4*	*n=4*
wt%	SiO2	0.01(1)	<0.01	0.01(1)	<0.01	0.03(1)	0.01(0)	0.02(1)	<0.01	0.02(2)	0.04(1)	0.02(1)	0.05(1)	0.05(3)	0.03(2)	0.02(1)	0.03(1)	0.02(1)
	TiO2	0.57(22)	1.15(73)	0.50(8)	0.54(3)	0.40(13)	0.40(4)	0.54(16)	0.97(41)	0.64(2)	0.66(2)	0.62(4)	0.55(6)	0.29(2)	0.55(17)	0.43(24)	0.39(4)	0.38(7)
	Al2O3	27.4(4.5)	31.6(5)	27.2(2.3)	31.3(2)	32.7(6.8)	36.76(9)	30.2(2.3)	31.0(4)	25.8(0)	28.9(3)	28.5(6)	30.7(2)	33.5(1.3)	33.5(4)	28.5(9)	30.7(5)	32.8(1.0)
	Cr2O3	29.5(3.7)	31.3(1)	33.1(2.8)	31.0(2)	28.0(5.9)	27.56(31)	31.0(2.2)	30.4(5)	31.5(6)	33.0(1.2)	34.1(1.2)	31.1(4)	27.9(1.8)	29.3(5)	32.8(5)	31.5(7)	30.4(3)
	Fe2O3	10.2(1.2)	5.6(7)	7.0(3)	6.1(1)	6.5(1.0)	4.97(24)	5.8(0.3)	6.16(15)	9.47(58)	6.1(1)	6.5(7)	6.6(2)	6.2(2)	7.1(2)	7.4(9)	5.8(4)	5.9(5)
	FeO	23.0(2.2)	16.6(9)	19.5(4)	14.8(1)	19.0(2.5)	14.7(3)	17.4(2.0)	15.9(4)	23.0(6)	17.0(2)	18.0(1.2)	18.3(4)	19.0(2)	15.3(1)	22.0(1.1)	20.7(1.6)	17.1(2.7)
	MnO	0.24(9)	0.17(1)	0.16(3)	0.15(1)	0.23(7)	0.16(6)	0.21(4)	0.11(10)	0.14(2)	0.73(2)	0.68(3)	0.17(6)	0.20(5)	0.11(6)	0.77(4)	0.79(7)	0.68(06)
	NiO	0.19(2)	0.19(2)	0.18(6)	0.22(3)	0.21(4)	0.22(6)	0.15	0.23(7)	0.20(4)	0.17(4)	0.20(2)	0.20(3)	0.20(2)	0.28(2)	0.17(4)	0.20(3)	0.20(3)
	MgO	8.4(2.0)	13.7(3)	10.5(6)	14.1(1)	11.3(2.2)	14.0(2)	12.1(1.7)	13.7(2)	8.2(2)	12.2(3)	11.9(8)	12.0(5)	11.5(2)	14.5(1)	8.7(1.3)	9.8(1.5)	12.7(1.8)
	CaO	0.01(1)	<0.01	0.01(1)	0.01(1)	0.01(1)	<0.01	0.01(1)	<0.01	0.01(1)	0.01(1)	0.01(1)	0.02(1)	0.02(1)	0.00(1)	0.01(1)	0.00	0.00
	Na2O	0.02(2)	0.02(1)	0.01(1)	-	-	-	-	-	0.03(2)	<0.01	<0.01	0.02(2)	0.01(2)	0.01(1)	<0.01	0.00	0.00
	K2O	<0.01	<0.01	0.00(1)	-	-	-	-	-	0.02(0)	<0.01	<0.01	<0.01	<0.01	0.01(1)	<0.01	0.00	0.00
	ZnO	0.37(10)	0.17(1)	0.32(4)	0.13(10)	0.42(10)	0.18(7)	0.30(10)	0.20(4)	-	0.39(6)	0.19(20)	0.23(1)	0.29(7)	0.20(4)	1.4(7)	0.76(71)	0.21(9)
	Total	99.9(6)	100.5(0)	97.8(3)	98.4(3)	98.8(4)	99.9(4)	97.6(2)	98.6(3)	99.4(4)	99.2(9)	100.7(5)	99.9(5)	99.2(2)	100.8(2)	100.7(3)	100.8(6)	100.4(5)
cation	Si	<0.001	<0.001	0.001	<0.001	0.011	<0.001	0.001	<0.001	<0.001	0.001	0.001	0.001	0.002	0.001	0.001	0.001	0.001
	Ti	0.013	0.026	0.012	0.012	0.010	0.009	0.012	0.022	0.015	0.015	0.014	0.012	0.006	0.012	0.010	0.009	0.008
	Al	1.004	1.096	0.997	1.103	1.079	1.247	1.089	1.096	0.960	1.036	1.012	1.086	1.183	1.147	1.022	1.096	1.142
	Cr	0.730	0.729	0.816	0.734	0.732	0.627	0.751	0.721	0.787	0.792	0.811	0.739	0.662	0.673	0.789	0.754	0.709
	Fe3+	0.240	0.125	0.163	0.138	0.148	0.108	0.134	0.139	0.225	0.140	0.148	0.148	0.139	0.156	0.169	0.131	0.131
	Fe2+	0.602	0.410	0.508	0.370	0.492	0.354	0.445	0.398	0.607	0.431	0.454	0.461	0.476	0.372	0.560	0.525	0.423
	Mn	0.006	0.004	0.004	0.004	0.006	0.004	0.005	0.003	0.004	0.019	0.017	0.004	0.005	0.003	0.020	0.020	0.017
	Ni	0.005	0.004	0.004	0.005	0.005	0.005	0.004	0.005	0.005	0.004	0.005	0.005	0.005	0.007	0.004	0.005	0.005
	Mg	0.389	0.602	0.486	0.630	0.509	0.642	0.551	0.612	0.009	0.553	0.534	0.536	0.006	0.626	0.394	0.442	0.560
	Ca	0.000	<0.001	<0.001	<0.001	0.001	<0.001	0.000	<0.001	0.386	<0.001	<0.001	<0.001	0.514	<0.001	<0.001	0.000	0.000
	Na	0.001	0.001	0.001	-	-	-	-	-	<0.001	<0.001	<0.001	0.001	0.001	0.001	<0.001	0.000	0.000
	K	<0.001	<0.001	<0.001	-	-	-	-	-	0.002	<0.001	<0.001	<0.001	0.001	<0.001	<0.001	0.000	0.000
	Zn	0.008	0.004	0.007	0.003	0.008	0.004	0.007	0.005	-	0.009	0.004	0.005	<0.001	0.004	0.032	0.017	0.004
	total	3.000	3.000	3.000	3.000	3.000	3.000	3.000	3.000	3.000	3.000	3.000	3.000	3.000	3.000	3.000	3.000	3.000
	# Mg	0.32	0.54	0.426	0.561	0.45	0.59	0.49	0.54	0.011	0.50	0.48	0.47	0.010	0.550	0.043	0.41	0.51
	# Cr	0.42	0.40	0.450	0.400	0.40	0.33	0.41	0.40	0.451	0.43	0.44	0.40	0.359	0.370	0.436	0.41	0.38

Table 2.5: Plagioclase composition of neoblasts and porphyroclast cores. an is the anorthite percentage.

sample		mylonite L04 *neoblast* *n=7*	mylonite L04 core *n=11*	FGSG L09 *n=12*	proto-mylonite L112 *n=8*	proto-mylonite La2002-5 *n=7*	CGSG L241 *n=12*	pyrox La-2002-02 *core* *n=5*
wt%	SiO2	49.5(9)	50.4(4)	49.6(7)	49.9(6)	48.8(4)	48.5(5)	47.9(4)
	TiO2	0.05(3)	0.03(1)	-	-	-	-	-
	Al2O3	33.0(3)	33.1(2)	33.2(5)	32.6(5)	33.0(4)	33.6(4)	33.9(2)
	Fe2O3	<0.01	0.10(5)	0.16(13)	0.08(6)	0.12(6)	0.13(5)	0.16(7)
	FeO	0.12(3)	0.01(2)	0.02(4)	0.04(6)	<0.01	0.01(3)	0.02(5)
	MnO	<0.01	<0.01	-	-	-	-	-
	MgO	<0.01	<0.01	-	-	-	-	-
	CaO	15.2(7)	15.3(3)	14.9(5)	14.4(4)	15.7(4)	15.6(4)	16.0(2)
	Na2O	2.7(4)	3.1(2)	3.07(31)	3.3(2)	2.7(2)	2.6(2)	2.4(2)
	K2O	<0.01	0.01(1)	0.01(1)	0.01(1)	0.01(1)	0.01(1)	0.01(0)
	Total	100.6(4)	101.9(7)	100.9(3)	100.3(9)	100.4(3)	100.5(3)	100.3(4)
cation	Si	2.260	2.252	2.241	2.265	2.220	2.203	2.181
	Ti	0.001	0.001	-	-	-	-	-
	Al	1.758	1.743	1.764	1.740	1.769	1.798	1.821
	Fe3+	<0.001	0.003	0.005	0.003	0.004	0.005	0.006
	Fe2+	0.004	<0.001	0.001	0.002	<0.001	<0.001	0.001
	Mn	<0.001	<0.001	-	-	-	-	-
	Mg	<0.001	<0.001	-	-	-	-	-
	Ca	0.736	0.730	0.720	0.701	0.766	0.761	0.779
	Na	0.240	0.269	0.268	0.289	0.241	0.232	0.212
	K	<0.001	0.001	0.001	<0.001	<0.001	0.001	0.001
	total	5.000	5.000	5.000	5.000	5.000	5.000	5.000
	An	0.75	0.73	0.73	0.73	0.76	0.77	0.79

Table 2.6: Amphibole composition in plagioclase peridotite. Note that all amphiboles are K-poor Ti-pargasite.

sample		h-mylo L187d *n=4*	mylonite L04 *n=3*	proto-mylonite L112 *n=5*	proto-mylonite La2002-5 *n=3*	FGSG L09 *n=5*	CGSGc L110 *n=4*	CGSGc L13 *n=3*	CGSGc L147 *n=7*	CGSGc L241 *n=5*
wt%	SiO2	44.4(3)	43.0(6)	42.3(4)	43.3(1)	43.2(3)	42.7(4)	43.9(5)	42.5(5)	42.5(7)
	TiO2	3.0(3)	4.3(5)	4.2(2)	3.6(4)	2.7(2)	4.1(2)	3.4(7)	3.5(4)	3.3(6)
	Al2O3	12.1(3)	13.2(8)	11.5(3)	11.5(4)	11.8(4)	11.8(2)	12.2(4)	13.5(5)	12.0(4)
	Cr2O3	1.21(2)	1.53(2)	1.54(2)	1.78(4)	1.82(2)	1.61(2)	1.52(1)	1.39(2)	1.41(2)
	Fe2O3	0.00	<0.01	0.00	0.00	<0.01	-	0.00	0.00	0.00
	FeO	3.8(2)	4.3(5)	4.3(1)	4.2(2)	4.9(2)	4.5(2)	5.1(5)	4.1(1)	5.0(2)
	MnO	0.07(2)	0.04(2)	0.04(3)	0.10(4)	0.05(2)	0.06(2)	0.06(4)	0.08(1)	0.05(3)
	NiO	0.08(1)	-	0.1(3)	0.10(1)	0.10(3)	0.09(2)	-	0.09(2)	0.10(3)
	MgO	17.3(2)	17.0(2)	16.6(1)	16.9(3)	17.1(2)	16.6(2)	16.9(1)	16.4(4)	17.4(5)
	CaO	12.3(3)	12.1(1)	12.4(2)	12.3(1)	12.3(1)	12.3(3)	12.7(3)	12.4(2)	12.3(3)
	Na2O	3.5(2)	3.7(1)	3.4(1)	3.4(0)	3.3(1)	3.4(2)	3.3(1)	3.6(1)	3.3(1)
	K2O	0.01(1)	0.01(2)	0.01(2)	<0.01	0.00(1)	0.02(2)	0.05(1)	0.01(0)	0.00(1)
	H2O	2.1(1)	2.09(2)	2.0(0)	2.1(0)	2.0(0)	2.0(1)	2.1(0)	2.1(0)	2.1(1)
	Total	99.8(6)	101.1(6)	98.4(4)	99.2(3)	99.3(1)	99.2(3)	101.1(3)	99.7(4)	99.3(2)
cation	Si	6.391	6.149	6.223	6.313	6.270	6.235	6.263	6.163	6.161
	Ti	0.320	0.458	0.465	0.394	0.298	0.453	0.367	0.384	0.357
	Al	2.059	2.229	1.995	1.969	2.013	2.031	2.046	2.303	2.049
	Cr	0.141	0.174	0.173	0.206	0.206	0.188	0.164	0.164	0.154
	Fe3+	0.000	<0.001	0.000	0.000	0.000	0.000	0.000	0.000	0.000
	Fe2+	0.453	0.518	0.535	0.508	0.594	0.547	0.611	0.502	0.604
	Mn	0.008	0.005	0.006	0.012	0.007	0.007	0.008	0.009	0.007
	Ni	0.010		0.012	0.011	0.012	0.010	-	0.010	0.011
	Mg	3.724	3.617	3.638	3.671	3.687	3.614	3.597	3.537	3.751
	Ca	1.895	1.850	1.953	1.916	1.913	1.916	1.944	1.927	1.905
	Na	0.974	1.022	0.966	0.970	0.922	0.963	0.924	1.013	0.913
	K	0.002	0.002	0.002	<0.001	0.001	0.003	0.009	0.001	0.001
	H	2.000	2.000	1.908	2.000	2.000	2.000	2.000	2.000	2.000
	total	18.025	18.025	17.877	17.970	17.923	17.966	17.933	18.014	17.915
	# Mg	0.892	0.87	0.87	0.878	0.861	0.87	0.761	0.88	0.861
	# Cr	0.064	0.07	0.08	0.095	0.09	0.08	0.074	0.07	0.070

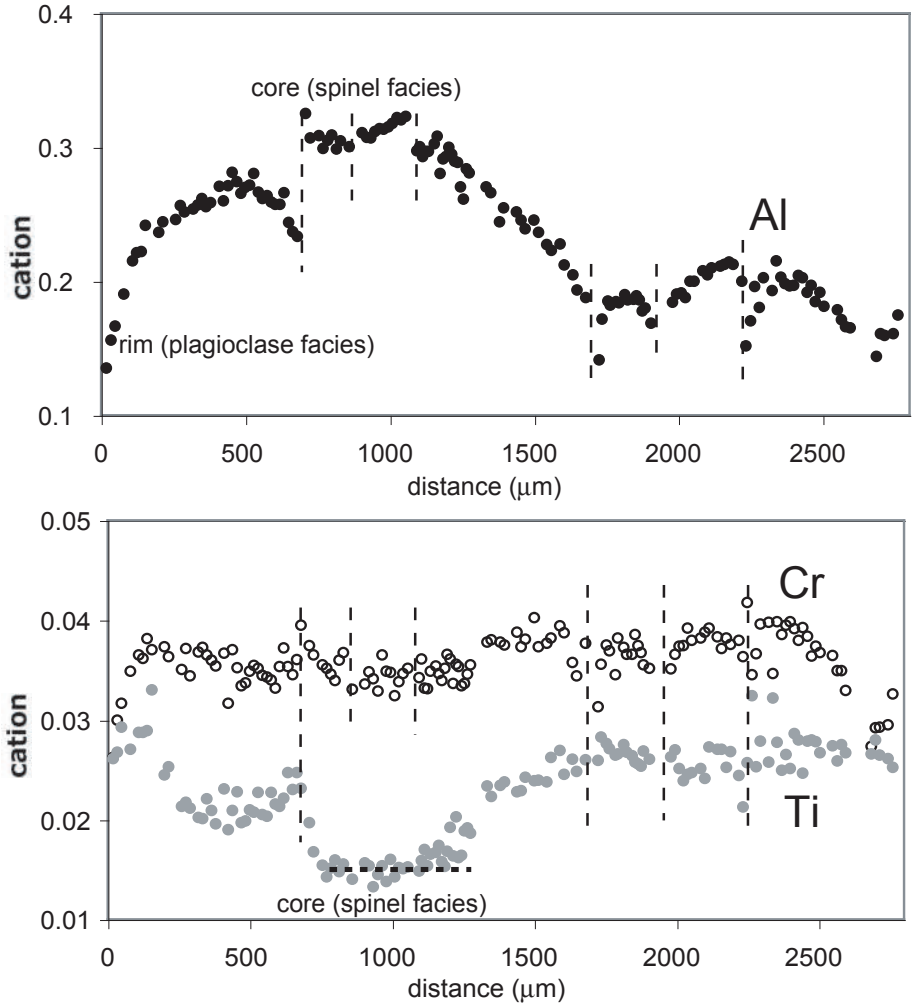

Fig. 2.9: Representative example of compositional variation of a cpx porphyroclast in terms of Al, Cr, and Ti (sample L13, CGSG). The core shows the highest Al and lowest Ti content, indicating equilibration within the spinel peridotite stability field. Decreasing Al is coupled to increasing Ti, while the Cr content shows little variation. The areas indicated by dash lines display orthopyroxene + plagioclase intergrowth (see location of cross section in Fig. 2.11f).

plagioclase show cotectic intergrowth (Müntener and Piccardo, 2003). This microstructure is preferentially observed in weakly deformed rocks, or within large porphyroclasts in proto-mylonite or mylonite. The liquid followed or cross cut the pre-existing exsolutions in the deformed and undeformed clinopyroxene and indicates melt-rock reaction before or during the shearing. This suggests that clinopyroxene became unstable in the presence of a clinopyroxene-undersaturated liquid (reaction (2): cpx + Liq -> opx + plg ± ol).

2.5 MINERAL CHEMISTRY

Mineral compositions were determined using a Cameca SX-50 and a Jeol JXA 8200 electron microprobe located at the Institute of Geological Sciences at the University of Bern (Switzerland), and a Cameca SX51 at the Institute of Mineralogy at the University of Heidelberg (Germany), equipped with four, or five wavelength-dispersive spectrometers, respectively. No systematic differences among the different electron microprobes have been observed. Operating conditions comprised an acceleration voltage of 15 kV and a 20 nA beam current. The spot size was about 3 μm for all minerals except plagioclase and amphibole, where a defocused beam has been used (~5 μm). Element peak and background counting time was 20 seconds, except for Al (30s), Mg (30s) and Na (10s). Natural and synthetic oxides were used as standards. Backscattered electron (BSE) images were obtained at the CSEM (Centre Suisse d'Electronique et de Microtechnique) in Neuchâtel (Switzerland), with an Environmental Scanning Electron Microscope, Philips XL-30, operated at 25 kV. Averages of minerals from different

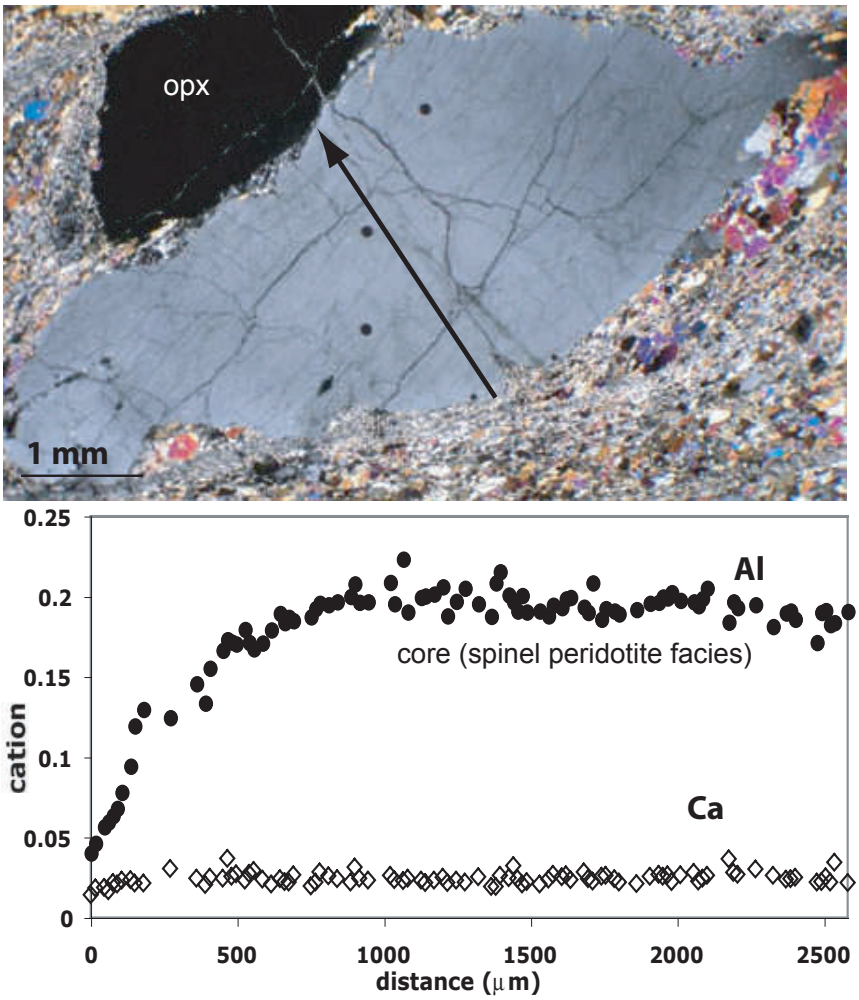

Fig. 2.10: Representative chemical zoning pattern of orthopyroxene from a peridotite mylonite (L04). Note the approximately 1000μm thick and decrease of Al towards the rim, while Ca shows only a weak zoning within the last 150μm. The contact to the matrix in the lower part of the photomicrograph is abrupt and does not exhibit gradational zoning towards the mylonitic matrix, indicating syn-mylonitic breaking-up of orthopyroxene porphyroclasts.

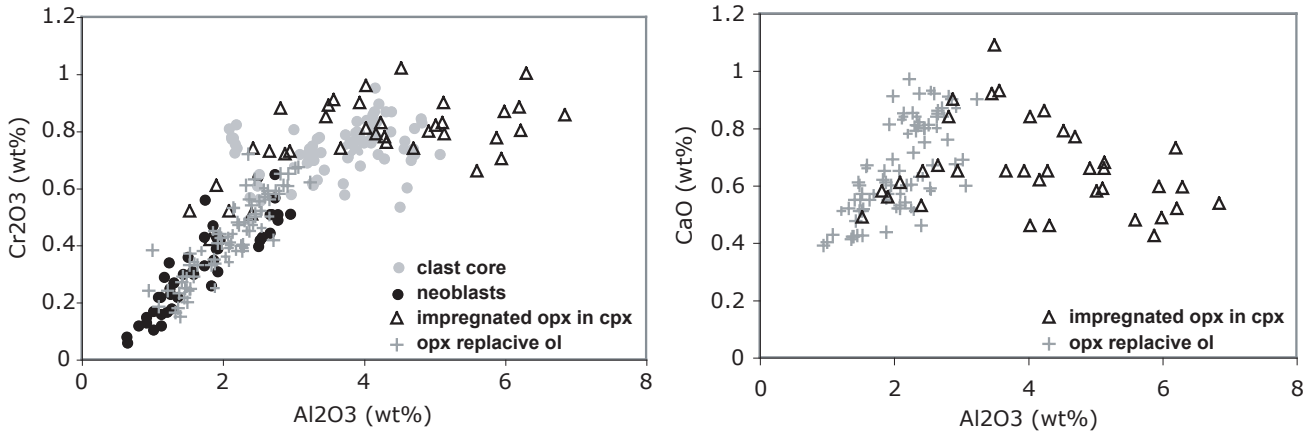

Fig. 2.11: (a) Major element chemistry of orthopyroxene, in terms of Al_2O_3 vs. Cr_2O_3 for porphyroclast cores (n=14), neoblasts (n=8) and opx replacing olivine (n=10), and opx replacing cpx (n=5). The lowest Al and Cr contents are from mylonitic neoblasts. (b)10-b: Al_2O_3 vs. CaO for opx related to melt/rock reaction processes. Note that opx replacing cpx (domain I) has higher Al_2O_3 contents than orthopyroxene replacing olivine (domain II), indicating that the high Al_2O_3 content is inherited from precursor clinopyroxene. Note also that the CaO content in 'reacted' orthopyroxene does not show significant differences between the microstructural sites, indicating some post-reaction thermal equilibration.

microstructural sites and their standard deviations are listed in Tables 2.1-2.6 and illustrated in Figures 2.13-2.17. A complete dataset is available from the authors upon request.

2.5.1 Clinopyroxene

Clinopyroxene from the northern part of the Lanzo massif shows large compositional variations (Tab. 2.1), which are dependent on the microstructural site, but are apparently independent of the regional structure. In all samples, the compositional variation is nearly as large as the entire dataset. Exsolution of orthopyroxene lamellae is common in clinopyroxene porphyroclasts, but less common in recrystallized grains. In addition to these representative textures, occasional clinopyroxene clasts show flame-like orthopyroxene and plagioclase inclusions, in proportions much higher that what can be exsolved from primary clinopyroxene (see Fig. 2.7f). These grains show large disequilibrium compositions.

Overall, the clinopyroxene data reflect two different compositional trends with decreasing Al content (Fig. 2.8). High-Al clinopyroxene is characterized by a negative correlation between Al and Ti or Cr, while low Al clinopyroxene show positive correlations between Al, Cr and Ti. In terms of absolute element concentrations, the Al_2O_3 content in clinopyroxene porphyroclast cores ranges from 4.3 to 7.5 wt% and is substantially higher than in neoblasts (1.37 to 4.85 wt%). Mg# are not correlated with Al_2O_3 and vary from ~0.9 to 0.94. CaO contents are generally high, as observed for orogenic and residual abyssal peridotites (Hellebrand et al., 2005) indicating substantial

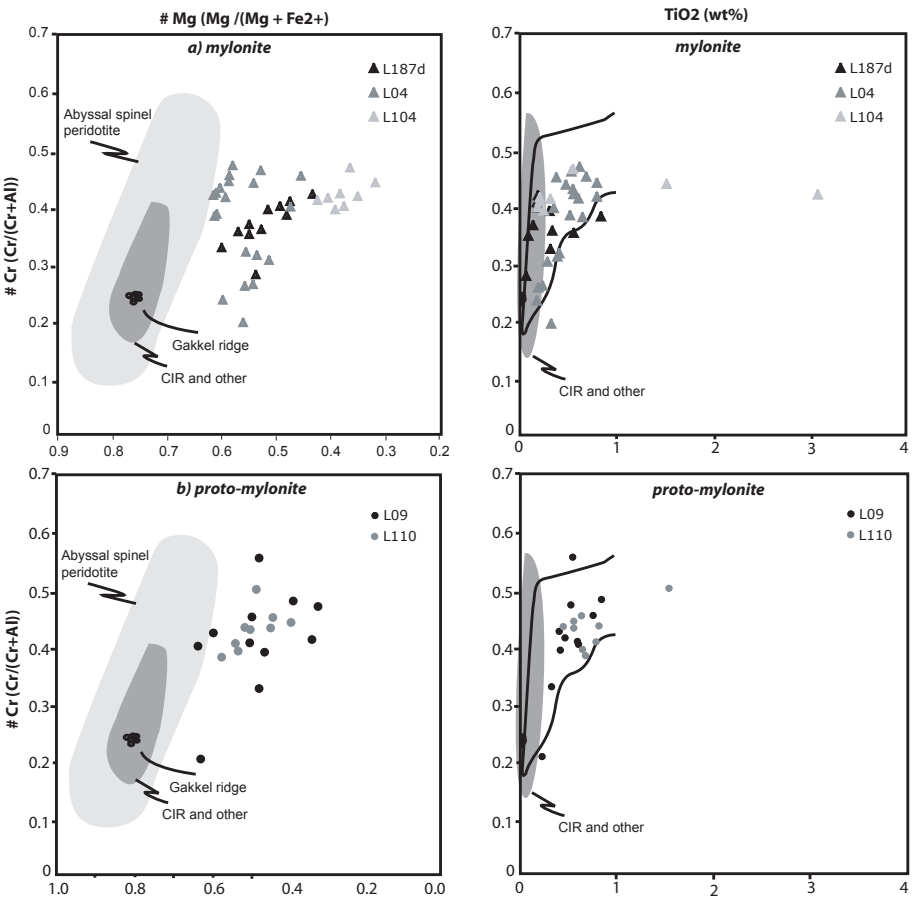

Fig. 2.12: (a-e) Cr# vs. Mg# of spinels from the Lanzo shear zone. Cr# of spinels from the investigated samples vary from 0.1 to 0.6. Most samples plot to the right of abyssal spinel peridotite (Hellebrand et al., 2002) consistent with equilibration in the plagioclase peridotite field and probable addition of olivine+plagioclase±orthopyroxene (Dick and Natland, 1996). (f-j) Weight % TiO_2 plotted against Cr#. Note that almost all spinel analyses exceed 0.2 wt% TiO_2. High TiO_2 in spinel is associated with the crystallization of spinel from migrating liquids and is a characteristic feature of Cr-spinel in dunite, troctolite and olivine gabbros (Cannat et al., 1997a; Dick and Natland, 1996). Note that the extreme variability of TiO_2 in CGSG and FGSG is greatly reduced in proto-mylonites and mylonites, suggesting 'homogenization' of compositional variability during deformation. Note also that spinels from the northern body seem more homogeneous than other classes.

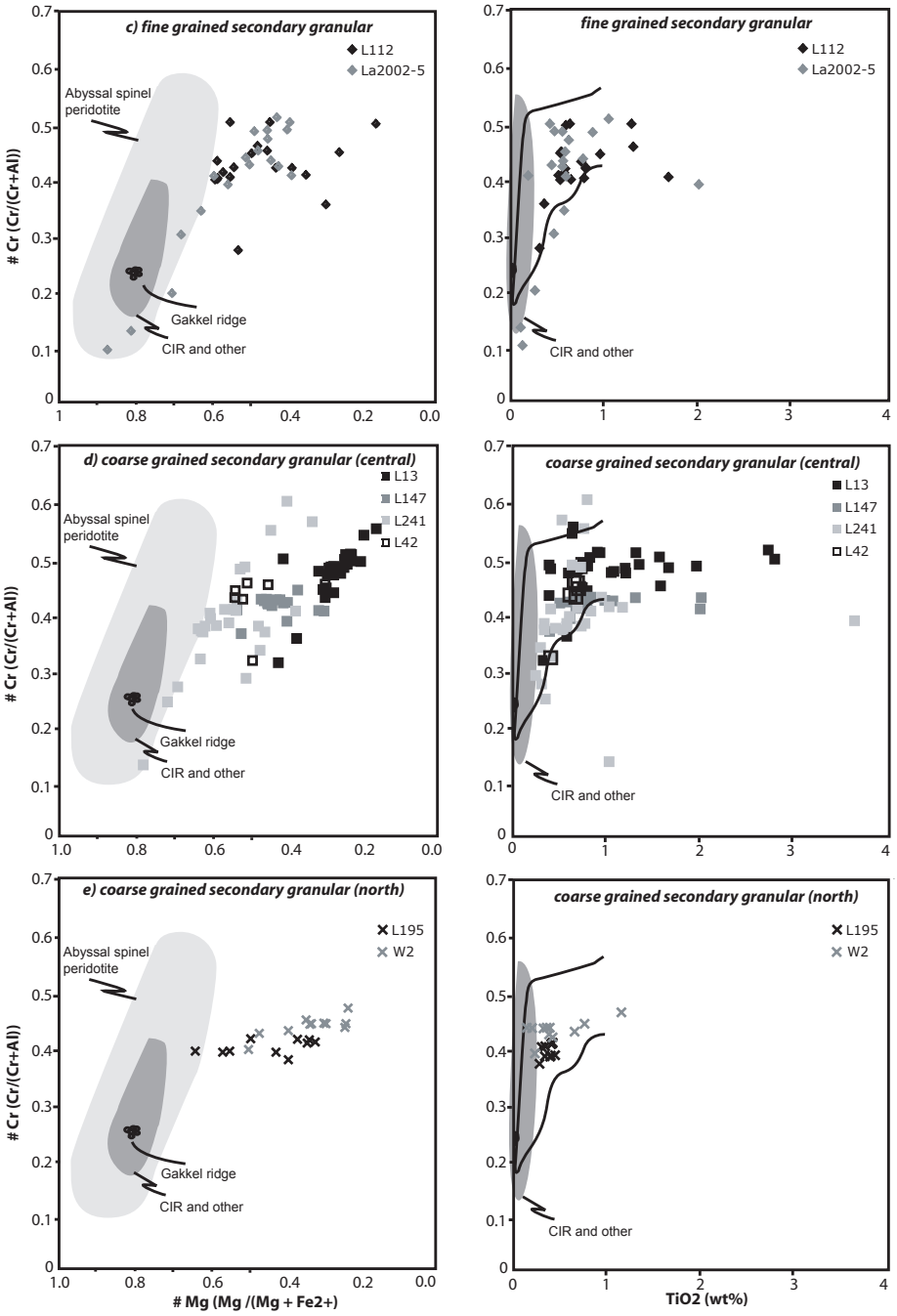

Fig. 2.12: continued

retrograde equilibration (see thermometry below). Chemical profiles in porphyroclastic clinopyroxene (L13) characterized by orthopyroxene + plagioclase intergrowth are heterogeneous and strongly zoned. This is illustrated in Fig. 2.9, where a plateau of high Al (0.31 Al p.f.u.), low Ti (0.015 p.f.u.) clinopyroxene is preserved, with compositions similar to clinopyroxene from fertile spinel peridotites (Ernst and Piccardo, 1979; Müntener et al., 2004). Towards the areas with orthopyroxene-plagioclase intergrowth (Fig. 2.7), Al is decreasing and Ti and to a lesser extent Cr is increasing (Fig. 2.9).

2.5.2 Orthopyroxene

All analyzed grains are enstatite-rich orthopyroxenes with Mg# ranging from 89.0 to 91.2 with no notable difference between cores and rims. Lower Mg# were only measured for pyroxenite layers. Clinopyroxene exsolution lamellae in orthopyroxene are generally very thin (<1μm) are too small to be analyzed by electron microprobe. Analyzing orthopyroxene with a beam size of 1 μm is used and exsolutions are not included in the chemical composition of the orthopyroxene. In

addition, most samples exhibit extensive dynamic recrystallization and therefore clinopyroxene exsolution lamellae have not been detected. CaO and Al_2O_3 contents are variable mainly due to mineral zoning and different microstructural sites (Fig. 2.11a). Orthopyroxene neoblasts show lower values in Al_2O_3 (0.64 to 2.95 wt%), in Cr_2O_3 (0.06 to 0.65 wt%) than in porphyroclast cores (2 to 5 wt% and 0.55 to 1 wt% respectively, Fig. 2.11a). The samples from the northern part of the massif (W2 and L195) exhibit high Al_2O_3 value for the core composition (up to 4.80 wt%), but also the recrystallized grains show high Al_2O_3 contents (2.2

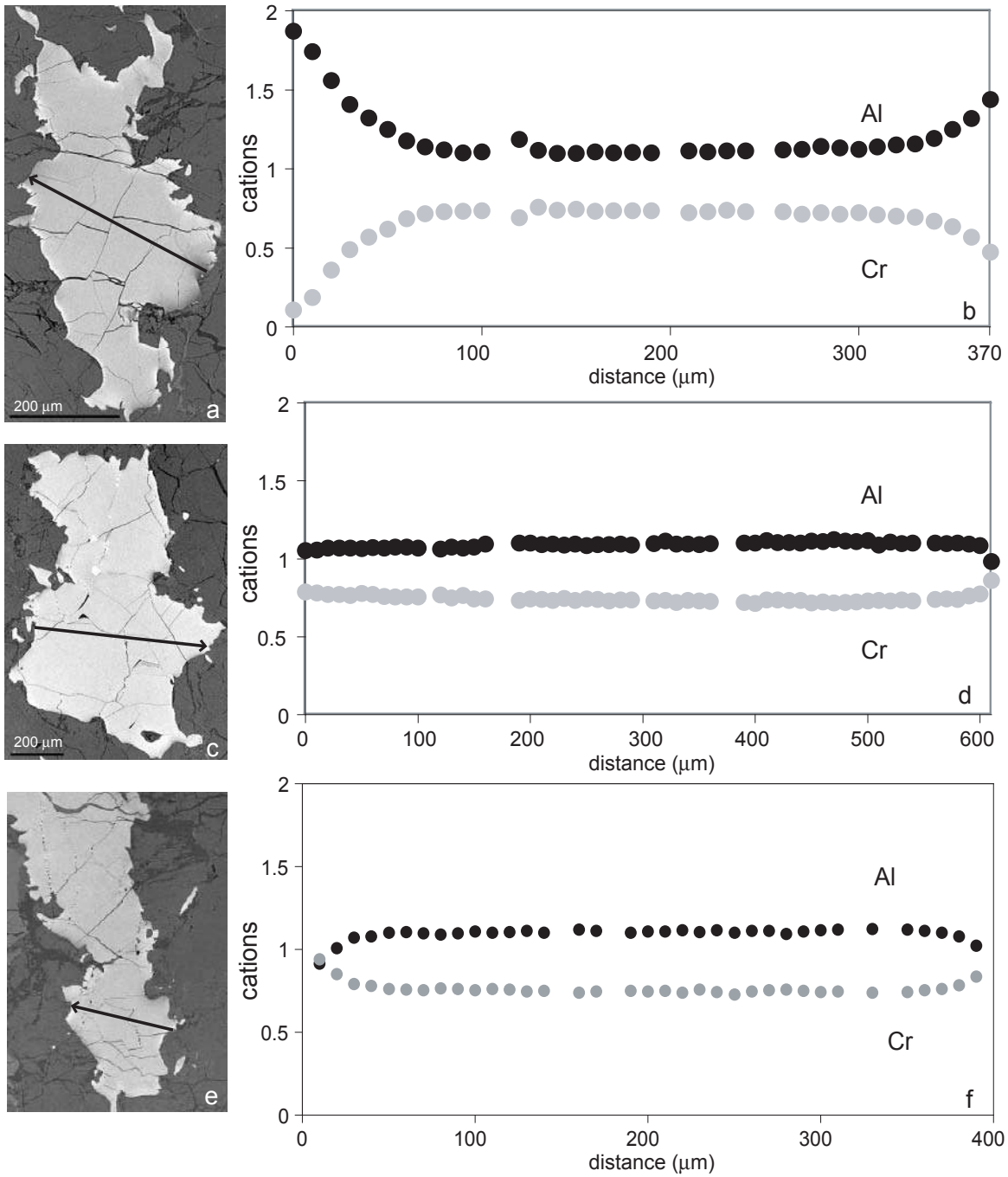

Fig. 2.13: Compositional cross-section of spinel grains from the FGSG and the proto-mylonite domain, with lines indicated on BSE images. (a-b) Zoning profile of a spinel grain surrounded by olivine (left) and orthopyroxene resulting in a Cr# variation between 0.10 and 0.40. Note that the spinel shows a distinct asymmetric zoning pattern inconsistent with overall equilibrium (La2002-5). (c-d) Zoning profile of spinel from a different microstructural domain, but from the same sample (La2002-5). The grain is surrounded by plagioclase (left) and olivine (right). Here Al exhibits a weak decrease coupled with a Cr increase (La2002-5). (e-f) Symmetric zonation of Al and Cr along the profile (L09). The grain is surrounded by plagioclase (left) and orthopyroxene (right).

and 3.7 wt%) compared to the other CGSG sample from the southern part (1.2 to 2 wt%).

Large porphyroclastic orthopyroxene (~2500 μm) display pronounced zoning from core to rim. In several orthopyroxene porphyroclasts, Al decreases from the core (0.15 – 0.20 p.f.u.) to the rim (0.04 – 0.09 p.f.u.). However, the Ca content is uniformly low and shows virtually no zoning (Fig. 2.10). In some porphyroclasts, a plateau of intermediate composition between the core and the rim can be recognized (L147, L241).

In most samples, orthopyroxene formed by melt-rock reaction, either displaying cotectic crystallization together with plagioclase, replacing clinopyroxene (domain I) or forming at the expense of olivine (domain II). In these samples the composition of orthopyroxene seems to be locally controlled: (1) high Al in orthopyroxene, but low Ca (which is buffered by coexisting plagioclase) is related to domain I, and (2) low Al, in domain II (Fig. 2.11-a-b-c). This translates into systematic temperature differences for both orthopyroxene populations, if Al-in orthopyroxene thermometry is applied (see below). The implications of these results are discussed below.

2.5.3 Spinel

Spinel analyses of different groups from Lanzo samples cover almost the entire compositional range for abyssal peridotites and indicate substantial variation in TiO_2 and Cr# among porphyroclasts and neoblasts (Fig. 2.12). The majority of spinel contains between 0.18 wt% TiO_2 and 1 wt%, although exceptionally high values up to 5.1 wt% were found in some samples. These values are much higher than those generally found in spinel peridotites (Dick and Bullen, 1984; Hellebrand et al., 2001), but TiO_2 up to 1 wt% is fairly common for plagioclase peridotite (Cannat et al., 1997b; Dick, 1989). TiO_2 contents exceeding 1 wt% is usually associated with the crystallization of trapped melt in troctolites or olivine gabbros. The enrichment and extreme variation of TiO_2 in some of the peridotites is remarkable, in particular when compared to the olivine compositions, which display a variation of Mg# between 88-91. This extreme variation cannot be explained by fractional crystallization in a closed system (Villiger et al., 2004), but must be related to large compositional variations of migrating liquid within a peridotite matrix. If one considers the spinel data split into the microstructural classes described above, it can be seen that the variability is correlated with the degree of deformation. Surprisingly, within one single sample, spinel composition covers almost the entire range of abyssal peridotite (Fig. 2.12). The largest variations can be observed in the CGSG, while spinel composition in strongly deformed rocks is more homogeneous in terms of TiO_2 and Cr#, suggesting a faster and more complete equilibration among small grains than in coarse-grained samples. However, the extreme variability is not restricted to a particular microstructure. The within-sample variation indicates that equilibrium on a thin section scale is not maintained. This is illustrated in Fig. 2.13, where two compositional cross sections from the same sample are shown. BSE images of spinel porphyroclasts show an irregular distribution of dark zones (corresponding to high Al spinel, maximum: 1.8 p.f.u.), surrounding brighter zones (Fig. 2.13a-b). Such an irregular distribution is best explained by melt-rock reaction. In contrast, there are more regular spinels, with a ±symmetrical inverse zonation, with a core to rim decrease of Al from 1.1 to 0.9 p.f.u. and corresponding Cr increase from 0.73 to 0.86 p.f.u (Fig. 2.13c-f). This is compatible with cooling during exhumation of the peridotites (Müntener et al., 2000). This also suggests that once the plagioclase peridotites completely crystallized, exhumation to shallower depth must have been rapid, in order to preserve disequilibrium chemical compositions. This feature will be discussed in detail below.

2.5.4 Olivine

Electron microprobe analyses were performed on cores and rims of large porphyroclasts, and neoblasts indicating a restricted chemical variation with respect to olivine Mg# (molar $Mg/Mg+Fe_{tot}$). There is a small range in Mg# composition between 0.89 and 0.905, and NiO between 0.30 and 0.45 wt%. Olivine from one mylonite sample (L104, more serpentinized than L04), displays slightly lower Mg# (0.88 to 0.89 in porphyroclastic core; and 0.88 in neoblasts). Olivine crystals show a NiO variation from the core (0.4 to 0.3 wt%) to neoblasts (0.15 to 0.2 wt%). The hydrous mylonite sample (L187d) contains different microstructural categories of olivine with different chemical composition:

thermometer	$T_{2\text{-pyx BK90}}$	$T_{\text{Ca-in-opx BK90}}$	$T_{\text{Al,Cr-in-opx WS91}}$	$T_{\text{ol-sp Bal.91}}$	
cores					
hydrous mylonite	825 ± 4	902 ± 7	1032 ± 7	944 ± 35	n=1
mylonite	924 ± 72	954 ± 4	1101 ± 7	1136 ± 65	n=2
proto-mylonite	846 ± 22	1017 ± 7	1063 ± 25	1051 ± 83	n=2
FGSG	901 ± 33	970 ± 36	1069 ± 23	972 ± 20	n=2
CGSG	836 ± 11	960 ± 23	1030 ±18	924 ± 188	n=3
CGSG north	853 ± 55	1003 ± 10	1070 ± 23	-	n=2
average	*872 ± 38*	*980 ± 28*	*1067 ± 23*	*1021 ± 93*	
rims					
hydrous mylonite	770 ± 5	798 ± 6	826 ± 24	-	n=1
mylonite	862 ± 80	841 ± 1	779 ± 65	-	n=2
proto-mylonite	855 ± 19	903 ± 19	791 ± 37	-	n=2
FGSG	830 ± 19	909 ± 70	887 ± 46	-	n=2
CGSG	809 ± 80	920 ± 43	901 ± 6	-	n=3
CGSG north	714 ± 130	764 ± 219	768 ± 192	-	n=2
average	*814 ± 60*	*867 ± 65*	*825 ± 63*	-	
core II plateau					
all categories	-	969 ± 38	976 ± 14	-	n=3
neoblasts					
hydrous mylonite	800 ± 25	825 ± 11	-	598 ± 1	n=1
mylonite	890 ± 44	879 ± 12	-	774 ± 53	n=2
proto-mylonite	806 ± 42	891 ± 2	-	760 ± 74	n=2
FGSG	888 ± 84	912 ± 69	-	794 ± 18	n=2
average	*861 ± 48*	*894 ± 17*	-	*776 ± 17*	
melt reaction: cpx + liq -> opx + plg					
all categories	-	950 ± 36	1095 ± 88	-	n=4
melt reaction: ol + liq1 -> opx + liq2					
all categories core	-	951 ± 62	889 ± 61	-	n=10
all categories rim	-	908 ± 28	821 ± 49	-	n=5

Table 2.7: Thermometry of Lanzo peridotite with pyroxenes and olivine-spinel systems: The averages are calculated without the hydrous-mylonite. The temperature for each category is an average on 3-6 neighboring grains and a minimum of 2 different samples (n), except for the hydrous-mylonite (n=1).

surprisingly the core porphyroclasts (Mg# 0.89 - 0.90; NiO 0.10 – 0.25 wt%) display lower Ni contents than small neoblasts (Mg# 0.915 - 0.925; NiO 0.40 - 0.45 wt%), and the rounded neoblasts observed in pressure shadows (Mg# 0.90; NiO 0.35 – 0.45 wt%). The pyroxenite sample (La2002-02) indicates a composition lower in NiO (0.2 to 0.3 wt%) and Mg# around 0.87.

2.5.5 Plagioclase

Plagioclase analyses were performed on 6 samples, one of them is a plagioclase-bearing pyroxenite. The chemical composition of plagioclase is heterogeneous and can be influenced by the microstructure, however the majority of plagioclase varies between An_{75} – An_{80} (Tab. 2.5). The major difference is a slightly higher Na_2O content (2.36 – 4.00 wt%) in the mylonite than in the CGSG samples (e.g., 2.0 – 3.5 wt% Na_2O, 14.5 to 16.5 wt% CaO).

2.5.6 Amphibole

Amphibole are all K-poor Ti-pargasites (Tab. 2.6), with TiO_2 contents of 2.7 – 4.3 wt%, and Cr_2O_3 contents of 1.21-1.82 wt%. Mg-numbers (86.1-89.2) are slightly lower than coexisting olivine and pyroxenes, with one exception with a Mg# of 76.2. Amphibole shows very low K_2O contents (<0.05 wt%) and is thus different than mantle amphiboles related to modal metasomatism in ophiolitic peridotites and mantle xenoliths (Vannucci et al., 1995).

2.6 THERMOMETRY

A large number of thermometers have been experimentally and empirically calibrated for upper mantle assemblages. Temperatures calculated in this study are based on the following formulations: (a) the experimental calibration of Brey and Köhler (1990), a thermometer based on coexisting clinopyroxene and orthopyroxene ($T_{2\text{-pyx BK90}}$), (b) on the Ca-in-opx thermometer, with opx in equilibrium with clinopyroxene ($T_{\text{Ca-in-opx BK90}}$), (c) on the Al and Cr contents in orthopyroxene ($T_{\text{Al,Cr-in-opx WS91}}$) as defined by Witt-Eickschen and Seck (1991) and (d) on the Fe^{2+}-Mg exchange between olivine and spinel (Ballhaus et al., 1991). Results of the thermometric calculations are given in Table 2.7. Pressures were assumed to be 10 Kbar, for cores, implying that equilibration took place in the spinel stability field, (Klemme and O'Neill, 2000), and 5 Kbar for rims and neoblasts (Gasparik, 1987).

The strong Al zoning in clino- and orthopyroxene indicates that bulk equilibration has not been attained. However, in porphyroclastic orthopyroxene (Fig. 2.10), there is a large plateau in terms of Al and diffusion related to cooling affected the outer 1000 μm only. Application of the Witt-Eickschen and Seck (1991) thermometer results in relatively homogeneous temperatures for orthopyroxene cores for all structural domains, ranging from 1030-1100°C. On average, these temperatures are ~80°C higher than those obtained by the Ca-in orthopyroxene thermometer of Brey and Köhler (1990) and approximately 200°C higher than was calculated with the two pyroxene thermometer (Brey and Köhler 1990). This discrepancy is readily explained by the much faster diffusive equilibration of Ca-in-opx compared to Al-in opx (Smith et al., 1999), and the tendency of clinopyroxene to recrystallize, especially in deformed samples such as the ones from Lanzo. Substantially slower diffusion of Al and Cr, compared to Fe, Mg and Ca, has also been observed by Ozawa and Takahashi (1995).

In contrast, thermometric estimates from orthopyroxene rims preserve a very different thermal history. Applying the Ca-in-opx thermometer of Brey and Köhler (1990), the Ca concentration would correspond to a mean temperature of ~880°C for CGSG, FGSG and the protomylonites (Tab. 2.7). Mylonites, hydrous mylonites and the peridotites from the Lanzo North record progressively lower temperatures, reaching ~770°C. Neoblasts provide similar results, with decreasing temperatures towards the hydrous mylonite zone. Independent of the accuracy of the absolute temperature, there is a temperature difference on the order of 150°C for neoblasts across the shear zone.

The temperature range for all exsolution-free orthopyroxene related to melt/rock reaction (e.g. domain I and II), lies around 950°C ($T_{\text{Al,Cr-in-opx WS91}}$), while temperatures obtained by applying the Witt-

Eickschen and Seck calibration ($T_{Al,Cr\text{-}in\text{-}opx\ WS91}$) results in 1095±88 °C and 890±61 °C for domain I and II, respectively. The temperature difference of ~200°C suggests that full equilibrium was attained in terms of Ca, but not in Al and Cr. The contrasting temperatures obtained by $T_{Al,Cr\text{-}in\text{-}opx\ WS91}$ are artifacts of the orthopyroxene-forming process and are locally controlled by the availability of Al (and Cr). One important observation is that the average Al content of orthopyroxene from domain II exceeds that of large orthopyroxene porphyroclasts (Fig. 2.10), which could be an inherited effect from mantle clinopyroxene, which is generally considered to accommodate higher Al and Cr contents than orthoypyroxene (e.g. Brey and Köhler 1990).

The calculations derived from olivine-spinel thermometry provide very different results. The highest temperatures are preserved in the mylonitic rocks (protomylonite and mylonite, 1051 and 1136°C, respectively), approaching the conditions obtained from orthopyroxene thermometry ($T_{Al,Cr\text{-}in\text{-}opx\ WS91}$). While the calculated values for CGSG and FGSG rocks approach those of Ca-in opx ($T_{Ca\text{-}in\text{-}opx\ BK90}$), this is not the case for the Lanzo north peridotite, where about 810°C have been obtained, suggesting relatively slow cooling for northern Lanzo, but relatively rapid cooling for the southern part (see discussion below). Calculated temperatures for neoblast provide similar results for all different rock types and vary between 760 and 800°C (Tab. 2.7).

2.7 DISCUSSION

2.7.1 Fabric variation across the shear zone

The inhomogeneous distribution of coarse- and fine-grained products across the mylonite zone and the variation of grain sizes over ~three orders of magnitude indicate that different deformation mechanisms operated during the development of the Lanzo shear zone. The presence of large, sometimes equant porphyroclasts across the peridotite shear zone indicates that the rheology of the mantle shear zone is grain size sensitive and that localization of deformation is an important process. The fine-grained, proto-mylonite and mylonite rocks have asymmetric bands of recrystallized grains, indicating dominantly non-coaxial deformation of the peridotites. An important observation is that grain size variation is correlated to the presence or absence of secondary phases.

Polyphase mylonitic bands are not unique to the Lanzo peridotites and have been found in several ophiolitic peridotites. Vissers et al. (1995; 1991) interpreted polyphase, fine-grained mantle shear zones in the Erro-Tobbio peridotites as resulting from hydration reactions and related grain size reduction, while Newman et al. (1999) identified the subsolidus plagioclase forming reaction as a major mechanism for grain size reduction in a Pyreenean peridotite shear zone. An alternative mechanism was proposed for the Othris peridotite (Greece), where grain-size reduction was in part induced by melt-present reactions (Dijkstra et al., 2002). As outlined above, plagioclase is present everywhere in the Lanzo peridotite, and its modal abundance is not related to peridotite mylonites. Thus an origin of the fine-grained, polyphase bands by subsolidus metamorphic processes is unlikely. Instead, the presence of reaction textures (Müntener and Piccardo, 2003) and the interstitial Ti-hornblende indicate that melt-enhanced deformation played a major role in the evolution of the Lanzo shear zone.

The occurrence of interstitial orthopyroxene associated to olivine (domain II, ol+opx) in the mylonite and the fine grained bands suggests two processes that control the evolution of grain size during ongoing deformation: (i) the chemistry of migrating basaltic liquids in the deformed peridotites, and (ii) the ongoing cooling to lower temperatures during deformation. Disequilibrium textures among different mantle minerals suggest that the chemistry of migrating liquid is locally controlled. Thus, the presence of ol+opx, the peridotite-melt system might not be multiply saturated and orthopyroxene-olivine reaction relationships dominate. This microstructure is presents in pressure shadows of polycrystalline olivine bands. From experimental petrology, the olivine-orthopyroxene equilibrium is extremely sensitive to small chemical, thermal or pressure variations (Villiger et al., 2004) and it is thus not surprising that olivine-producing and olivine-consuming microstructures have been observed in

the same samples (Dijkstra et al., 2002). Because olivine and orthopyroxene are in a peritectic reaction relationship, pinning might be less effective because opx grows at the expense of olivine (and vice versa), which is illustrated by grain sizes that are significantly larger than in polyphase mylonitic bands. To emphasize the conditions, where the polyphase mylonitic bands may form, one has to consider that the chemical composition of migrating basaltic liquid is efficiently buffered, if four or even five phases are present. Multiple saturation will lead to efficient crystallization of interstitial liquid, however, grain growth is inhibited by the presence of secondary phases. As deformation continues to lower temperatures and therefore higher stresses (Vissers et al., 1995), the initial small grain size decreases further as a consequence of dynamic recrystallization. Thus, we propose that a combination of melt-enhanced recrystallization coupled to the pinning effects of secondary phases (Herwegh et al., 2005; Olgaard and Evans, 1988) can explain the inhomogeneous fine-grained shear zones in the Lanzo peridotite.

2.7.2 Disequilibrium mineral compositions and relationship to microstructures

The chemical variation of orthopyroxene and clinopyroxene from core to rim (decrease in Al and Cr) is a marker of retrogression (decreasing P-T) within the plagioclase facies and is observed in all different rock types. Very little relicts of a precursor equilibration in the spinel peridotite field are preserved. However, the systematic chemical variation of orthopyroxene with respect to its microstructure indicates that overall chemical equilibrium on a thin section scale has not been achieved (see below). The associated thermometry study indicates a cooling history, which started at high temperatures in the spinel-lherzolite field (Pognante et al., 1985), and finally ending in the plagioclase lherzolite field. The widespread occurrence of Ti-hornblende in the recrystallized matrix of peridotite indicates the presence of a fluid/silicate melt during deformation, at temperatures not exceeding 1050°C at least for the final crystallization of hornblende (Niida and Green, 1999).

The spinel chemistry shows a large compositional variation observed on the grain to intra-sample scale. The chemical variation covers almost the entire field of abyssal spinel peridotites (Dick and Bullen, 1984), and indicates equilibrium in plagioclase facies (Cr- and Ti-rich spinel). The Cr# of spinel is a sensitive indicator for melt extraction (Dick, 1989; Dick and Bullen, 1984; Dick et al., 1984; Michael and Bonatti, 1985), melt peridotite reaction during focused porous flow (Allan and Dick, 1996; Dick and Natland, 1996; Kelemen et al., 1992; Kelemen et al., 1997) and melt wall rock reactions in the vicinity of intruding magmatic veins (Cannat et al., 1997a; Hellebrand et al., 1999). With increasing degree of melting, decreasing activity of Al in the peridotite leads to an increase in equilibrium Cr# in spinel. However, spinel formed by reaction with a migrating silicate liquid records enrichment of Al and concomitant decrease in Cr (Al-spinel + liq1 -> Cr-spinel + plagioclase + liq2). In addition the TiO_2 enrichment in spinel coexisting with plagioclase and variation of some peridotites cannot be explained by simple fractional crystallization in a closed system (e.g. Villiger et al. 2004), but must be related to large compositional variations of migrating and reacting silicate liquid within a peridotite matrix.

The most variable composition of spinel is found in the CGSG samples, and its high TiO_2 content strongly suggests in-situ crystallization of trapped liquid, producing (micro-) gabbroic assemblages. A characteristic feature is that the extreme variability is only recorded by mineral composition and not by whole rocks (chapter 3), which supports the hypothesis of nearly complete solidification without major escape of residual liquid out of the peridotite. The crystallization of trapped melt by reaction in the shallow mantle explains why some parameters show little compositional variation (e.g. Mg#), while others show extreme enrichment (e.g. TiO_2 in spinel). This process could potentially happen at near-isothermal conditions, however, the widespread interstitial crystallization of Ti-hornblende suggests a final crystallization temperature of less than 1050°C.

However in the northern part, the CGSG samples contain spinel of much more homogeneous composition in equilibrium in with plagioclase (Tab. 2.4). This remarkable difference between the CGSG south and CGSG north probably indicates

a different cooling history for the two peridotites bodies: the footwall records a relatively rapid exhumation with respect to the hanging-wall.
It is interesting to speculate about the effects of homogenization of spinel compositions by progressive localization of deformation and concomitant grain size reduction and simple cooling. It is possible that decreasing temperatures under subsolidus conditions coupled with grain size reduction erased most of the disequilibrium spinel compositions. However, an alternative is that melt migration along actively deforming shear zones precludes extreme fractionation of basaltic liquids, and thus extremely TiO_2-rich spinel compositions never developed.

2.7.3 Partial melting, reactive melt percolation, deformation

The presence of melt impregnation microtextures in the Lanzo massif, witness of an important melt percolation by diffuse porous flow (Müntener and Piccardo, 2003) and the particular texture of coarse and fine grained rocks, characterized by "secondary granular" corresponds to reheating and recrystallization at high temperature of a previous primary porphyroclastic texture.
The impregnation microtexture (e.g. Fig. 2.6) was observed in all classes of rocks, and is more abundant in the FGSG and CGSG than in the mylonite rocks. In the following we discuss several scenarios to explain our observations: (i) the melt impregnation event preceded the deformation and the progressive mylonitization and recrystallization progressively eliminated melt migration microstructures, or (ii) the melt impregnation was contemporaneous to the major shearing event. The presence of deformed microstructures of orthopyroxene and plagioclase replacing clinopyroxene argues for melt impregnation before the shearing. The development of vermicular, interstitial orthopyroxene with long axis parallel to the foliation, abundant in proto-mylonite and uncommon in the mylonite suggests melt/rock reaction preceding and/or during the shearing, followed by integration of the interstitial orthopyroxene in the fine grained matrix of the mylonite. Thus, the microtextural evidence indicates that reactive porous flow of melt is preceding high temperature deformation. The preferential orientation of plagioclase-bearing aggregates along the spinel foliation planes (Fig. 2.3) might indicate deformation-enhanced melt migration. This microtexture indicates a peritectic reaction (2): Al-rich spinel + Liq 1-> Cr-spinel + plagioclase + Liq 2. The plagioclase is not only associated to spinel, but also occurs as aggregates parallel to the foliation associated with olivine, orthopyroxene, and clinopyroxene. The high modal abundance of plagioclase, coupled with a chemical composition exceeding primitive upper mantle (chapter 3) suggests, that the top of the shear zone acts as 'melt-freezing area', with volumetrically abundant accumulation of melt.
Mineralogical and structural features (cpx + melt -> opx + plg and ol + melt -> opx) indicate lithospheric peridotite spinel facies were percolated by orthopyroxene-satured and clinopyroxene-undersaturated melts and by two pyroxenes saturated melts, suggesting progressive pyroxene saturation during upward migration of melts (Müntener and Piccardo, 2003; Piccardo et al., 2007). This interpretation is concordant with Kelemen et al. (1995) who argue for pyroxene undersaturated melt originated at depth, which migrates upwards by porous flow within the lithospheric mantle column.
The impregnated melt added basaltic components to the peridotite, from mm-scale gabbroic aggregates to gabbroic dikes with a MORB signature. The percolation of basaltic melts (> 1250°C) into a 'cold' mantle lithosphere (Müntener and Piccardo, 2003; Piccardo et al., 2004) requires that the thermal lithosphere was significantly heated by the rising asthenosphere. This thermal effect can explain the reheating zones in CGSG and FGSG rocks. The heating of the mantle lithosphere and the migration of the asthenospheric melts produced the compositional modification (both depletion and enrichment), which underwent thermo-chemical erosion, i.e it was "asthenospherized" (Müntener et al., 2005). During lithospheric extension, the mantle exhumation and the melt impregnation of the Lanzo massif is continuous. The host peridotite is cooling and dikes cross-cutting the high temperature foliation are emplaced (Müntener and Piccardo, 2003; Piccardo et al., 2004; Piccardo et al., 2007).

2.7.4 Thermal constraints on the mantle shear zone

In order to understand the significance of the temperature discrepancy between porphyroclasts and neoblasts and the discrepancy of the different thermometers (Tab. 2.7), it is important to briefly address the approximate relative equilibration velocity of different thermometers. Solid-state volume Fe-Mg exchange between olivine and spinel is considered to be a fast process (Ballhaus et al., 1991) compared to Ca-Mg or Al diffusion in pyroxene (Sautter et al., 1988). If we consider slow cooling, calculated temperatures will be controlled by the diffusion velocity of different chemical species, and will be lowest for Fe-Mg exchange between olivine and spinel and highest for Al in orthopyroxene. This is the case for the Lanzo North peridotite.

The observation that temperatures obtained by olivine-spinel thermometry ($T_{Fe\text{-}Mg,\ ol\text{-}spl\ B91}$) are highest in the most deformed rocks is counterintuitive to the above statement. Calculations using core compositions and using fast and slowly reacting thermometers ($T_{Al,Cr\text{-}in\text{-}opx\ WS91}$, $T_{Fe\text{-}Mg,\ ol\text{-}spl\ B91}$) result in similar temperatures, suggesting that cooling of the mylonites was fast enough to significantly affect core compositions by solid state diffusion. If we consider the results from the neoblasts (Tab. 2.7) Ca-in-opx provides temperatures that are ~100°C higher than the one from olivine-spinel thermometry, suggesting that cooling was slow enough to affect small neoblasts, but not large porphyroclasts. We thus conclude that equilibration within the mylonites is controlled by recrystallization, and not by solid-state diffusion. Therefore rapid exhumation is required to retain high temperatures in the porphyroclasts. We discuss the implications of these findings below.

The peridotite records a decreasing temperature gradient from porphyroclastic cores to neoblasts and by localization of the deformation. The grain size decrease continuously from CGSG to hydrous-mylonite rocks and the deformation became localized in ultra-mylonite bands (Fig. 2.14). The thermal history and the mineral chemistry of the CGSG, FGSG, proto-mylonite, mylonite and hydrous mylonite clearly indicate rapid exhumation from spinel to plagioclase facies. The complete equilibration in the plagioclase facies of spinel from the northern part of the massif, contrary to those from the central part indicates a faster exhumation of the central part, at least during the high-temperature deformation. We concluded that the central part of the Lanzo peridotite represents the footwall of a major mantle shear zone.

2.7.5 The mantle shear zone structure, dynamic and implications for the Lanzo massif

The deformation increased continuously from south (CGSG) to north (mylonite) (Fig. 2.4, 2.14). The high deformation (mylonite and hydrous-mylonite) is constrained in a zone of 200 meters width indicating the deformation localization. The localization of the deformation was also observed at the thin section scale with ultra-mylonite bands developed in the hydrous-mylonite. The localization of the deformation can be the result from a combination of effects. The localization

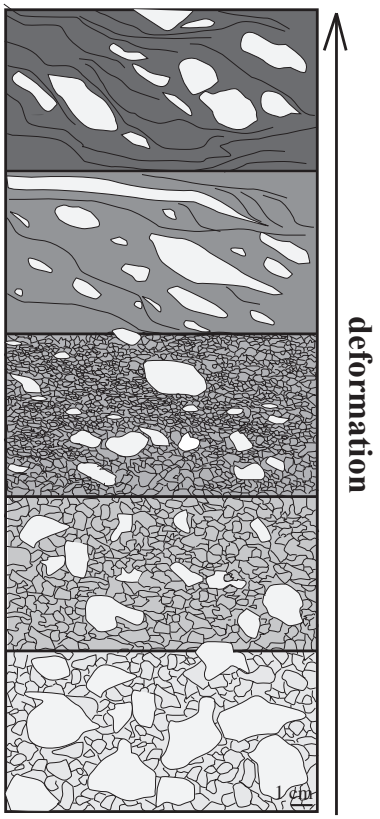

Fig. 2.14: Sketch representing the 5 classes of deformation and the continuous increase of the deformation form CGSG to hydrous-mylonite coeval with a decrease of temperature. The matrix micro-texture is represented by a grey gradation, which became darker when the grain size decrease.

of the deformation is involved by microphysical mechanisms that cause incipient localization into microscale zones that are mechanically weaker than the initial grain aggregates (Vissers et al., 1997). This result may be explained by (1) structural softening, induced by either a transition from dislocation creep to diffusion creep (Rutter and Brodie, 1988), or by the production of weak, new recrystallized grains (Drury et al., 1990); (2) semi-brittle deformation and (3) reaction softening (Drury et al., 1990; Handy, 1989; White and Knipe, 1978) induced by the formation of reaction products weaker than the precursor assemblage. Complementary to these softening and localization mechanisms, the development of plagioclase may have induced reaction softening: plagioclase is mechanically weak compared to olivine, pyroxene and spinel, and plagioclase intermixed with other phases stabilized the polyphase bands against grain growth such that lower stress (Vissers et al., 1997).

The profile realized on this zone (Fig. 2.4) highlights a fan foliation in the mylonitic zone, where the interpretation of the deformation continuity in depth is difficult. Considering the deformation localization, the increase of deformation and the dip foliation variation, one possibility is an anastomoze shear zone.

The Lanzo massif his chemically and structurally heterogeneous from the north to the south, respectively interpreted like sub-continental to asthenospheric mantle (Bodinier, 1988; Bodinier et al., 1991) and from east to west by increase of dikes and lenses presence (Boudier, 1972). As found in the entire massif, the study area shows heterogeneous repartition of gabbro dikes They are asymmetrically distributed and concentrate in the south and west (Figs. 2.6, 2.7). The basaltic and gabbroic dikes display MORB affinities (Bodinier et al., 1986; Piccardo et al., 2007; Pognante et al., 1985) suggesting that intrusion occurred at a late stage of continental rifting or an early stage of oceanic spreading. These results imply that the 'gabbro-rich zone' (central body) is the footwall of the mantle shear zone and the northern body is the hanging-wall. Moreover, the distribution of the dikes suggests that the mylonite zone is important barrier in inhibiting of the dikes. The nature of the barrier is not yet determinable, may be a rheological barrier and a terminator of dike propagation.

Interesting question should be to determine if the Lanzo north shear zone is a old history of the depth mantle and reactivate during the exhumation or a shear zone create during the Liguro-Piemontais basin formation. The presence of old pyroxenetic layering with recrystallization of mineral parallel to the high temperature foliation and presence of plagioclase rims around spinels indicates new history related to the exhumation.

2.8 CONCLUSIONS AND GEODYNAMIC EVOLUTION

The P-T data and petrology of the CGSG, FGSG, proto-mylonite, mylonite and hydrous mylonite clearly indicate exhumation of the Lanzo massif from spinel (1100 °C, porphyroclasts core) to plagioclase facies (860°C, neoblasts). The spinel facies is defined below 10 Kbr (Klemme and O'Neill, 2000) consequently the initial position of the Lanzo massif is represented at the Fig. 2.15a. There is no indication of inherited signatures from the garnet (Bodinier et al., 1991; Nicolas et al., 1972) was not relievable in this study and will not be considered here.

Melt impregnation features can be observed in the entire massif and initiates clearly before the bulk of the deformation (melt impregnation textures tend to disappear within highly deformed rocks, Fig. 2.15b). However, the melt infiltration should be continuous during the massif exhumation and the cooling involve melt focused in gabbroic lenses dikelets (Boudier, 1978a; Boudier and Nicolas, 1972) until dikes intrusions cutting the high temperature foliation (Fig. 2.15c-d). The chemistry and structural studies display a rapid exhumation of the Lanzo massif nevertheless a faster exhumation of the central body relatively to the northern body is suggested by the spinel composition.

The Lanzo shear zones are not consider as the major shear zone which exhumed the mantle until directly to the sea floor, but by is scale, as a secondary shear zones linked to the mantle exhumation. The geometry and the possible geodynamic evolution in depth were illustrated by two scenarios. The absolute movement between central and the northern bodies of the Lanzo peridotite cannot be quantified. The Lanzo massif was impregnated in first and the shearing take place

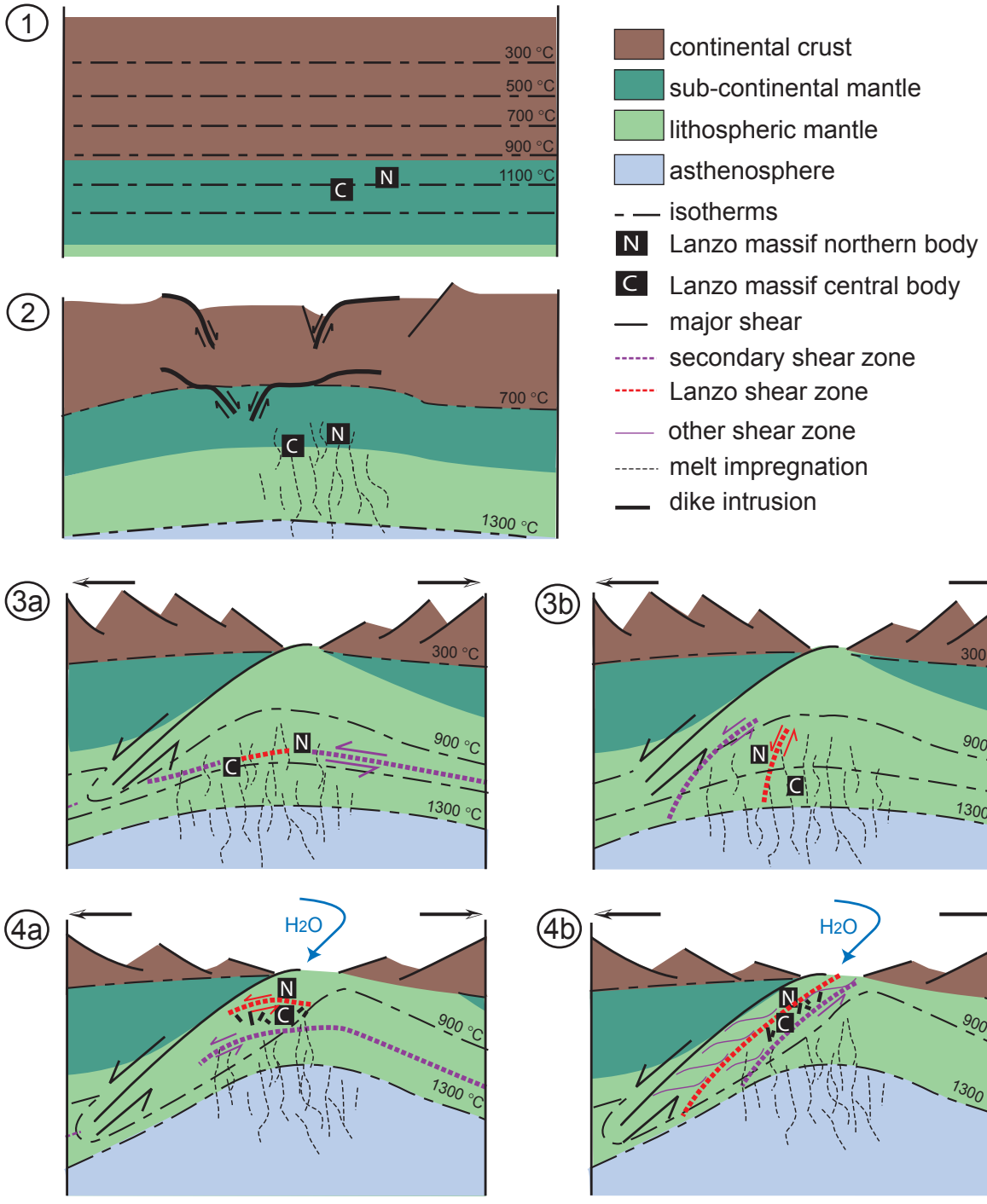

Fig. 2.15: A schematic model for the evolution of the high temperature mantle shear zone in the Lanzo peridotite, during the advanced stages of rifting. (a) and (b) schematically illustrate the approximate position of the Lanzo massif in the lithosphere during mantle exhumation before the break-up. Both the northern (N) and the central (C) body start as spinel peridotites. (1) Thermally equilibrated pre-rift lithosphere where the Lanzo massif is localized in the sub-continental mantle. (2) Initial extension of the crust initializes shear zones (stretching phase, after Lavier and Manatschal, 2006). (3) Exhumation and melt impregnation into the lithosphere; a) with initiation of the Lanzo shear zone parallel to the lithosphere or (b) parallel to the pre-existing extensional shear zone. (4) Rapid exhumation of mantle peridotites to shallow levels, hydration of the top of the shear zone by infiltrating fluids and formation of MORB type gabbro dikes crosscutting peridotite mylonites (Kaczmarek et al., Submitted).

in depth (Fig. 2.15-2-3). The initiation of the shear zone was parallel to the lithosphere as suggested by recent work of Manatschal (Manatschal, 2004) and Lavier and Manatschal (2006) or more simply by a conjugate shear zone parallel to the pre-existing major extensional shear zone suggesting a shear-zone system (Fig. 2.15-3). The rapid cooling, localization of the deformation, hydration of the peridotite and formation of MORB type gabbro dikes crosscutting peridotite mylonites (chapter 4) imply exhumation of the massif until shallow level (Fig. 2.15-4).

ACKNOWLEDGEMENTS

We thank the Microscopy Unit provided for access to the microprobe facilities: Bern (SX50 and Jeol JXA 8200) and Heidelberg (SX50). We thank Marco Herwegh, Uli Faul and Giovanni Piccardo for discussion. This research was financially supported by the Swiss National Foundation (Project 21-66923.01 and 200020-104636/1).

CHAPTER 3:

JUXTAPOSITION OF MELT IMPREGNATION AND HIGH TEMPERATURE SHEAR ZONES IN THE UPPER MANTLE (LANZO PERIDOTITE, N-ITALY) II: WHOLE ROCK GEOCHEMISTRY

Manuscript prepared forJournal of Petrology

Kaczmarek, M.-A.[1,2], Müntener O.[2,3].

North-West view from Monte Colombano

(1) Institute of Geology, University of Neuchâtel, rue Emile Argand, 2007 Neuchâtel, Switzerland. Mary-alix.kaczmarek@unine.ch, 0041 (0)3 27 18 27 12, Fax: 0041 (0)3 27 18 26 01

(2) Institute of Mineralogy and Geochemistry, University of Lausanne, Anthropôle, CH-1015 Lausanne, Switzerland

(3) formerly at: Institute of Geological Sciences, University of Bern, Baltzerst. 1, 3012 Bern, Switzerland.

3.1 INTRODUCTION

Studies on orogenic peridotites and mantle xenoliths proposed that melt migration and reaction is a major process in controlling the textures, mineralogy and geochemistry of mantle peridotite (e.g. Dijkstra et al., 2002; Garrido and Bodinier, 1999; Lenoir et al., 2001; Piccardo et al., 2007). Melt percolation in mantle peridotite can be detected by geochemical investigations if a LREE-enriched melt has percolated peridotites (e.g. Bedini et al., 1997), and by textural studies in plagioclase-bearing peridotites, in which micro-gabbroic pods and disequilibrium compositions are an indication of melt/rock reactions (Müntener and Piccardo, 2003; Piccardo et al., 2006; von der Handt et al., 2002).
Recently, it was recognized that textures and mineral chemistry of plagioclase peridotites are inconsistent with a residual origin and are interpreted as the product of impregnation with melt (Dijkstra et al., 2002; Müntener and Piccardo, 2003; Piccardo et al., 2006; von der Handt et al., 2002). A large portion of mantle minerals, like clinopyroxene, orthopyroxene, olivine and Al-phases reacted with, and partially recrystallized from migrating melt. Such a process was discussed by Elthon (1992) for some abyssal peridotites and by Dick (1989) for oceanic plagioclase peridotites. Recently, refertilization by basaltic or refractory melts has also been invoked for abyssal peridotites (Hellebrand et al., 2002; Kelemen et al., 2004), which conventionally have been interpreted as simple residues of partial melting (Johnson and Dick, 1992; Johnson et al., 1990). Reactive porous flow and refertilization are two important processes that are able to deeply modify textures, mineral modes and chemical compositions of peridotites (Bedini et al., 1997; Dijkstra et al., 2001; Godard et al., 2000; Müntener and Piccardo, 2003; Piccardo et al., 2004; Piccardo et al., 2006; Van der Wal and Bodinier, 1996).

The high temperature Alpine peridotites play a key role in identifying these processes. They have been classically considered as only slightly depleted upper mantle material that rose as asthenospheric diapirs (Boudier and Nicolas, 1972), and which could represent a source rock for MOR basalts (Beccaluva et al., 1984; Frey et al., 1985). Nicolas and Dupuy (1984) suggested that ophiolitic plagioclase lherzolite could be residual peridotite impregnated by a liquid with N-MORB composition. Heterogeneous composition of the oceanic lithosphere is influenced by a variety of melting processes (equilibrium vs. near fractional) and transport processes (pervasive porous flow vs. flow in chemically isolated conduits) (e.g. Kelemen et al., 1997; Kelemen et al., 1995; Nicolas, 1989).
Several studies from orogenic massifs or xenoliths highlight the relationship between composition, melt/rock interaction and texture of the peridotite (e.g. Godard et al., 2000; Lenoir et al., 2000; Lenoir et al., 2001; Van der Wal and Bodinier, 1996). For example, in Oman the high-temperature mantle deformation and the distance from the Moho are correlated with the chemical composition of peridotite (Godard et al., 2000). In the Ronda massif, peridotite texture and chemistry are controlled by pervasive melt front (Lenoir et al., 2001; Van der Wal and Bodinier, 1996), and peridotite from the Massif Central are originated from different lithospheric blocks underlain by two sub-continental lithospheric mantle domains, texturally and chemically distinct (refractory coarse granular and fertile protogranular peridotite, respectively Lenoir et al., 2000). Thus, chemical composition and texture of peridotite, should track the interplay between the melt percolation / impregnation, the source, the texture and the deformation.

In this paper we present the results of geochemical investigations on plagioclase peridotite, and its relationship with an actively deforming shear zone. Our results indicate a systematic relationship between incompatible element ratios and degree of deformation. We test the refertilization hypothesis of the Lanzo massif during its exhumation. We propose that actively deforming high temperature shear zones in the mantle act as permeability barriers for migrating liquid, and we discuss our results in the light of the asymmetric distribution of gabbro bodies in slowly accreted oceanic crust.

3.2 THE LANZO MASSIF

The Lanzo massif is located North-West

of Torino, at the Po plain boundary, just at the south of the Sesia zone (Fig. 3.1). The massif has been subdivised in three parts, the northern, the central and the southern body, separated by shear zones (Boudier, 1972; Boudier, 1978; Boudier and Nicolas, 1972, and chapter 2). The Lanzo massif presents relatively fresh peridotite surrounded by a serpentinite belt (Boudier, 1978; Boudier and Nicolas, 1972) and a chemical and structural variation from the central to the northern part (Bodinier, 1988, and chapter 2).

Modal and geochemical trends indicate the Lanzo peridotite to be a residual piece of upper mantle after MORB extraction (Bodinier, 1988). The northern body is less depleted in LREE and has lower Nd and Sr isotope ratios than in the southern body, which are similar to those of Atlantic MORB. The central body displays transitional geochemical features between the southern and the northern bodies (Bodinier et al., 1991). It was proposed by Bodinier (1988) that the northern body presents melt extraction lower than 6% and the lherzolite were equilibrated with T-MORB. The central and southern domains present a variable percentage from 6% (central part) to 12% (south part) and have affinities with T to N-MORB (Bodinier, 1988; Bodinier et al., 1991; Pognante et al., 1985). The southern body was interpreted as asthenosphere, which rose as a diapir shortly before the massif emplacement at shallow levels. The northern body is interpreted as older depleted MORB mantle (DMM) material separated from the convective mantle ~700 Ma years ago and accreted to sub-continental lithosphere (Bodinier et al., 1991). The presence of refractory peridotite at shallow depth, are interpreted as band of melt percolation.

The structural and study of the shear zone between the northern and the central part of the massif highlights increase of deformation from south to north (chapter 2). This increase in deformation is ±continuous and we mapped 5 different classes of deformation: Coarse Grained Secondary Granular (CGSG), Fine Grained Secondary Granular (FGSG), proto-mylonite, mylonite and hydrous-mylonite (Fig. 3.2). The granular rocks are characterized by centimetric porphyroclasts of olivine, orthopyroxene and clinopyroxene, and recrystallized domains of these minerals. The abundance of porphyroclasts and their grain size, decrease with the increase of the deformation towards the mylonite zone. The mylonite texture is characterized by extremely stretched orthopyroxene and small neoblasts (grain size < 50 μm). The coarse granular rocks are localized at the south of the shear zone in the central body (CGSG central) and form the bulk of the northern body of the massif (CGSG north) (Fig. 3.2). From the north part of the mylonite (hydrous-mylonite zone) to the northern body, the deformation is discontinuous and change from mylonitic to coarse granular by a very small distance of a few tens to hundreds of meters.

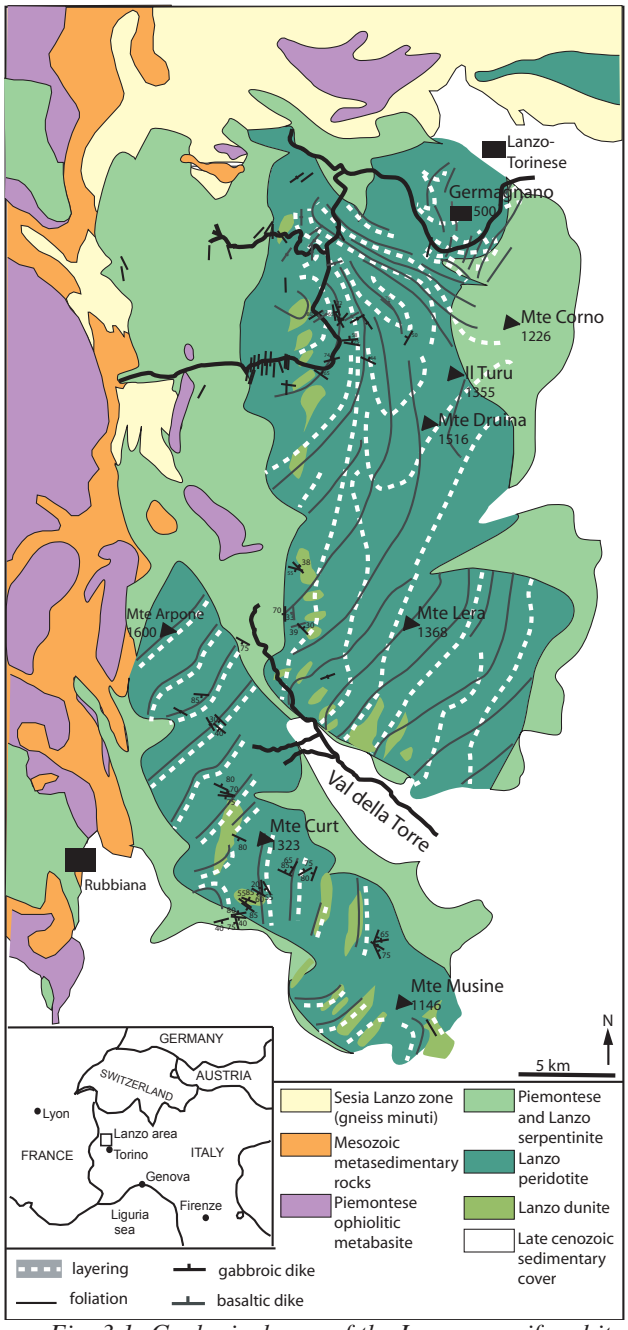

Fig. 3.1: Geological map of the Lanzo massif and its environment, after Kaczmarek et al. (Submitted).

3.3 SAMPLE SELECTION AND ANALYTICAL TECHNIQUES

36 samples of plagioclase peridotite were selected by localization across the shear zone in relation with the deformation gradient, from hydrous-mylonite to Coarse Grained Secondary Granular peridotite in the northern and central part of the massif (Fig. 3.2). The samples where selected for a preferentially low degree of serpentinization and a minimum distance from pyroxenite layering. Samples were crushed and finally powdered in an agate mill to reduce trace contamination. Whole rock glasses were prepared with the addition of Li-Tetraborate (dilution at 1:10). Peridotites were analyzed by Wavelength-dispersive X-ray fluorescence spectroscopy (XRF, Phillips PW 1404) at the University of Fribourg (Switzerland) and the results are presented in Table 3.1. Trace element precision is generally better than 5%. Peridotite whole rock trace elements (REE, Cs, Rb, Th, U, Nb, Ta, Sr, Zr, Hf) were analyzed by a VG-PQ2 Turbo + Inductively Coupled Plasma-Mass Spectrometer (ICP-MS) at ISTEEM (Université Montpellier II, Montpellier, France) and are reported in Table 3.2. REE, Cs, Rb,

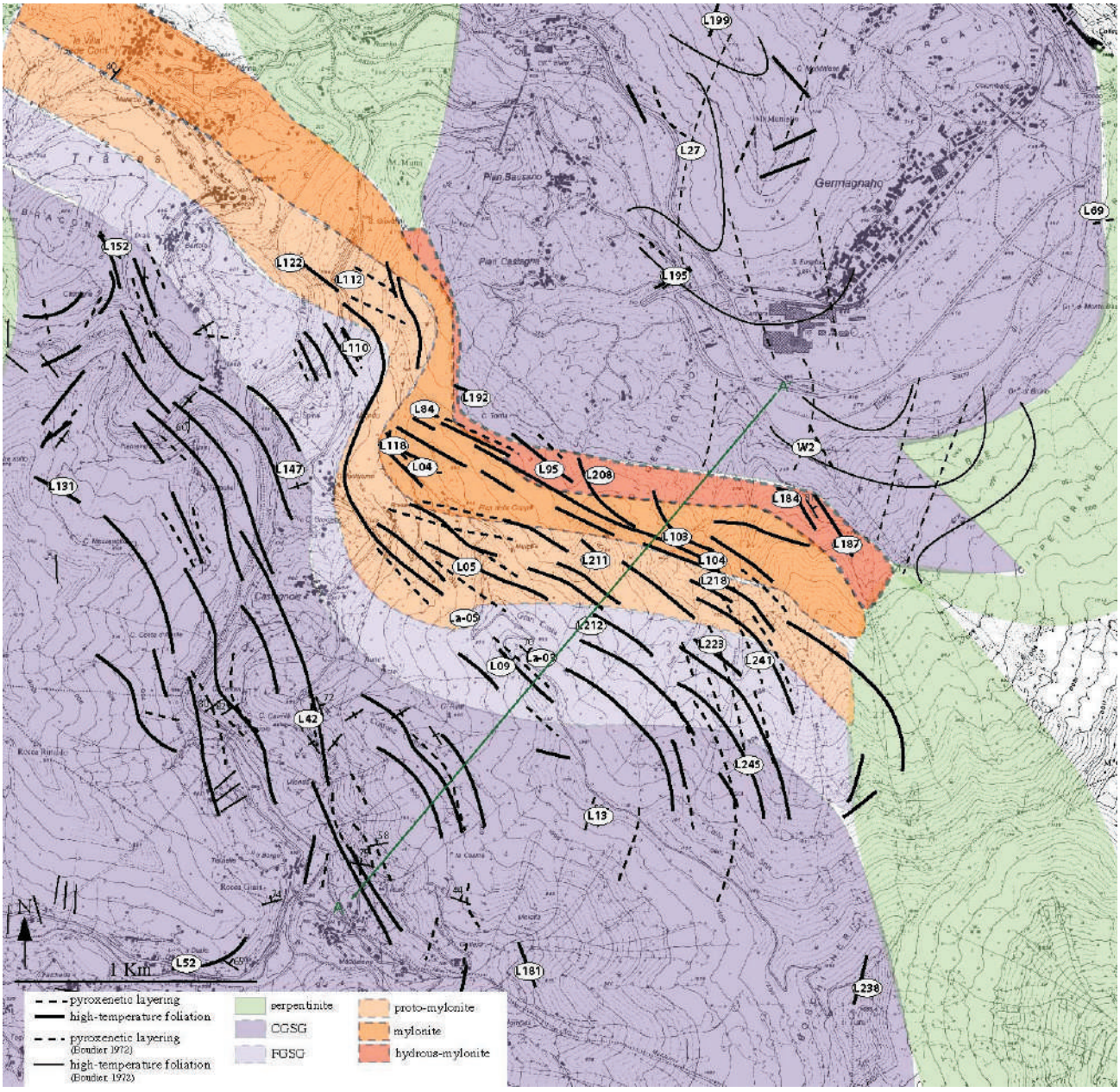

Fig. 3.2: Topographic map of the shear zone between the northern and the central part of the Lanzo massif. The peridotite and serpentinite boundaries, the 5 deformation zones, and the main high temperature foliation are represented (Kaczmarek et al., Submitted). The samples studied are plotted on the map.

Table 3.1: XRF major and trace element analyses of plagioclase peridotite. Mg# = (Mg / (Mg + Fe^{2+} + Fe^{3+})) and Cr# = (Cr/(Cr+Al)).

	hydrous mylonite				**mylonite**					**proto-mylonite**						**FGSG**		
sample	L95	L184	L187d	L208	L04	L84	L103	L104	L118	L05	L112	L122A	L211	L218	La2002-5	L09	L110	L212
SiO2	44.8	44.3	45.0	45.0	43.8	44.3	43.9	44.7	45.0	44.3	45.0	43.9	44.3	45.1	44.5	45.1	44.3	44.9
TiO2	0.10	0.11	0.15	0.12	0.09	0.12	0.11	0.14	0.18	0.15	0.14	0.11	0.18	0.16	0.12	0.14	0.14	0.16
Al2O3	3.37	3.30	3.64	3.18	3.09	2.84	3.20	3.21	4.42	3.32	3.33	2.64	4.01	3.63	3.27	3.34	3.16	3.34
FeO tot	8.96	9.22	8.82	8.82	8.98	9.42	9.12	9.33	8.76	8.99	9.00	9.11	9.23	9.03	9.12	9.01	9.27	9.05
MnO	0.13	0.14	0.13	0.13	0.13	0.13	0.13	0.13	0.13	0.14	0.13	0.13	0.10	0.13	0.13	0.13	0.13	0.13
MgO	38.9	38.5	38.0	39.0	40.1	39.8	39.6	38.6	36.6	38.3	38.7	40.9	38.3	37.9	39.0	38.4	39.2	38.0
CaO	2.86	2.80	3.31	3.00	3.04	2.72	2.69	2.81	4.09	3.22	2.92	2.55	2.64	3.24	3.03	3.09	2.99	3.61
Na2O	0.35	1.12	0.50	0.23	0.28	0.23	0.74	0.61	0.30	1.19	0.30	0.20	0.58	0.26	0.29	0.31	0.31	0.31
K2O	0.01	0.02	0.01<	0.01<	0.01<	0.01<	0.02	0.03	0.01<	0.01	0.01<	0.01<	0.02	0.01<	0.01<	0.01<	0.01<	0.01<
P2O5	0.01<	0.02	0.01<	0.02	0.01<	0.02	0.01<	0.01<	0.04	0.03	0.01<	0.01<	0.03	0.02	0.01	0.02	0.01<	0.03
Total	99.5	100.2	99.6	99.8	99.0	99.7	99.5	100.1	99.7	100.6	99.8	99.3	99.8	99.7	99.6	99.7	99.4	99.9
LOI	1.69	1.87	1.12	1.35	1.16	1.35	3.95	6.35	2.63	1.39	1.14	1.68	9.46	1.80	0.68	1.36	1.63	1.23
Mg#	0.89	0.88	0.88	0.89	0.89	0.88	0.89	0.88	0.88	0.88	0.88	0.89	0.88	0.88	0.88	0.88	0.88	0.88
Cr#	0.068	0.076	0.065	0.079	0.071	0.070	0.070	0.068	0.057	0.064	0.068	0.083	0.069	0.065	0.073	0.072	0.072	0.065
Cr	2520	2748	2589	2787	2416	2183	2472	2395	2736	2315	2472	2421	3046	2584	2636	2651	2501	2378
Ni	2462	2186	2115	2137	2131	2255	2270	2130	1910	1988	2028	2192	2789	1977	2091	1995	2061	2021
Cu	31	46	55	2<	24	26	2<	27	22	29	31	25	70	49	35	26	41	24
Zn	47	55	47	48	48	52	45	53	53	49	48	51	49	50	49	51	54	49
Pb	7<	7<	7<	7<	7<	7<	7<	7<	7<	7<	7	7<	22	7<	7<	9	8	7<
Rb	2<	2<	2<	2<	2<	2<	2<	4	2<	2<	3	2<	2<	3	2<	2<	2<	2<
Sr	13	10	10	11	10	8	12	16	10	9	11	8	8	10	7	14	7	10
Y	1<	1<	2<	1<	1<	1<	1<	1<	2<	2<	1<	1<	1<	1<	1<	2<	2<	2<
Zr	12	16	14	13	13	13	13	16	17	14	14	12	17	16	12	14	8	17
Nb	1<	1<	1<	1<	1<	1<	1<	1<	1<	1<	1<	1<	1<	1<	1<	1<	1<	1<

Table 3.1: continued.

	FGSG continued			CGSG north						CGSG central								
sample	L223	L241	La2002-3	L27	L69	L192	L195	L199	W2	L13	L42	L52	L131	L147	L152	L181	L238	L245
SiO2	43.9	43.7	44.5	44.6	44.5	44.3	43.1	45.4	42.9	44.2	44.6	44.0	44.3	44.4	45.1	43.8	43.1	43.8
TiO2	0.09	0.10	0.13	0.14	0.12	0.12	0.07	0.13	0.06	0.11	0.10	0.14	0.16	0.14	0.16	0.12	0.07	0.10
Al2O3	2.95	2.89	3.17	4.19	2.96	4.94	1.97	3.37	1.20	3.09	2.19	3.01	3.90	3.41	3.42	2.55	1.72	3.22
FeO tot	9.15	9.46	9.09	8.91	9.09	8.51	8.75	9.26	10.15	9.39	9.12	9.54	8.85	8.99	9.26	9.43	9.98	9.00
MnO	0.13	0.13	0.13	0.13	0.14	0.13	0.12	0.14	0.13	0.14	0.13	0.14	0.13	0.13	0.14	0.13	0.14	0.13
MgO	40.3	40.5	39.0	37.4	40.1	37.6	42.3	38.1	44.5	39.2	40.7	39.8	37.1	38.6	38.0	40.8	42.9	39.8
CaO	2.61	2.54	2.66	3.58	2.31	3.29	1.98	2.50	0.55	3.03	2.40	2.75	3.77	3.50	3.21	2.32	1.13	2.97
Na2O	0.31	0.21	0.82	0.41	0.30	0.58	1.19	0.63	0.08	0.33	0.13	0.22	1.35	0.37	0.17	0.24	0.48	0.54
K2O	0.01<	0.01<	0.01<	0.01<	0.03	0.01<	0.03	0.02	0.01<	0.01<	0.01<	0.02	0.03	0.04	0.01	0.01<	0.01<	0.01<
P2O5	0.01	0.02	0.01<	0.00<	0.01<	0.01	0.02	0.02	0.01<	0.05	0.01	0.01<	0.02	0.01	0.01<	0.05	0.01<	0.03
Total	100.0	99.7	100.3	99.6	99.6	100.9	100.5	99.8	99.9	99.8	99.7	99.3	100.0	99.6	99.3	99.9	100.2	99.8
LOI	1.89	1.13	1.11	2.61	5.80	2.17	3.18	9.57	3.03	1.35	1.21	5.49	4.40	2.51	3.24	3.55	1.86	1.73
Mg#	0.89	0.88	0.88	0.88	0.89	0.89	0.90	0.88	0.89	0.88	0.89	0.88	0.88	0.88	0.88	0.89	0.88	0.89
Cr#	0.078	0.079	0.074	0.067	0.089	0.058	0.108	0.066	0.121	0.081	0.125	0.076	0.057	0.071	0.064	0.075	0.081	0.071
Cr	2545	2529	2588	3059	2952	3093	2428	2412	1687	2779	3199	2517	2426	2642	2395	2106	1546	2493
Ni	2196	2161	2040	1987	2093	2327	2398	2019	2444	2071	2615	2115	1975	2052	2158	2181	2318	2146
Cu	29	24	21	36	2<	63	24	9	2<	20	21	31	2<	29	24	14	12	19
Zn	50	51	51	51	56	53	50	47	54	53	51	55	50	49	48	51	56	48
Pb	7<	7<	7<	7<	7<	7<	7<	10	24	7<	7<	7<	11	8	7<	7<	7<	7<
Rb	2<	2<	2<	3	2<	2<	2<	2<	2<	2<	2<	2<	2<	2<	2<	2<	5	4
Sr	10	7	6	16	10	14	7	13	7	9	7	13	11	26	11	8	5	11
Y	1<	1<	1<	1<	1<	1<	1<	1<	1<	1<	1<	1<	1<	1<	1<	1<	1<	1<
Zr	13	11	12	15	13	16	8	16	9	12	11	12	15	16	18	12	9	15
Nb	1<	1<	1<	1<	1<	1<	1<	1<	1<	1<	1<	1<	1<	1<	1<	1<	1<	1<

Table 3.2: Trace element composition of plagioclase peridotite, measurements by ICP-MS. Resultsa are in ppm.

	Cs	Rb	Ba	Th	U	Nb	Ta	La	Ce	Pb	Pr	Sr	Nd
hydrous-mylonite													
L95	0.0012	0.111	6.949	0.0003	0.0003	0.007	0.0005	0.186	0.24	0.011	0.065	8.58	0.433
L184	0.0035	0.058	1.327	0.0022	0.0026	0.017	0.0019	0.124	0.42	0.056	0.085	8.47	0.520
L187d	0.0019	0.061	2.059	0.0013	0.0012	0.012	0.0013	0.143	0.47	0.057	0.109	9.42	0.719
L208	0.0014	0.076	2.923	0.0012	0.0007	0.019	0.0019	0.109	0.44	0.051	0.093	8.10	0.601
mylonite													
LO4	<0.0001	0.012	0.041	0.0006	0.0001	0.009	0.0008	0.074	0.35	0.021	0.076	6.73	0.500
L84	0.0085	0.053	0.892	0.0002	0.0001	0.007	0.0008	0.095	0.38	0.069	0.088	5.67	0.573
L103	0.0181	0.127	2.302	0.0009	0.0005	0.012	0.0006	0.156	0.22	0.000	0.061	6.85	0.391
L104	0.0070	0.145	25.62	0.0002	0.0004	0.006	0.0004	0.318	0.42	0.022	0.132	14.9	0.766
L118	0.0216	0.202	1.174	0.0002	0.0001	0.007	0.0006	0.080	0.50	0.017	0.118	8.26	0.840
proto-mylonite													
LO5	0.0002	0.011	0.034	0.0004	0.0001	0.008	0.0006	0.074	0.39	0.011	0.086	5.26	0.589
L112	0.0020	0.018	0.661	0.0004	0.0004	0.007	0.0012	0.095	0.44	0.038	0.090	8.31	0.574
L122	0.0012	0.029	0.042	0.0005	0.0010	0.010	0.0008	0.064	0.32	0.031	0.074	5.41	0.506
L211	0.0549	0.273	11.24	0.0003	0.0008	0.014	0.0007	0.126	0.47	0.110	0.111	4.85	0.733
L218	0.0008	0.032	0.036	0.0009	0.0006	0.014	0.0012	0.078	0.42	0.036	0.095	6.38	0.656
La2002-5	0.0005	0.035	0.039	0.0006	0.0014	0.014	0.0011	0.062	0.31	0.044	0.073	5.44	0.483
FGSG													
LO9	0.0151	0.042	0.828	0.0002	<0.0001	0.007	0.0011	0.094	0.46	0.021	0.097	10.6	0.640
L110	0.0141	0.051	1.049	0.0021	0.0027	0.008	0.0008	0.091	0.51	0.214	0.102	4.41	0.681
L212	0.0052	0.196	0.277	0.0014	0.0013	0.019	0.0538	0.095	0.52	0.070	0.118	6.21	0.804
L223	0.0003	0.024	0.052	0.0009	0.0009	0.014	0.0010	0.062	0.30	0.039	0.068	6.11	0.446
L241	0.0031	0.087	0.031	0.0008	0.0007	0.014	0.0009	0.038	0.21	0.065	0.049	5.55	0.346
La2002-3	0.0005	0.022	0.100	0.0018	0.0015	0.016	0.0012	0.064	0.34	0.164	0.076	5.03	0.494
CGSG central													
L13	0.0003	0.018	0.040	0.0014	0.0007	0.026	0.0021	0.096	0.38	0.024	0.074	6.24	0.492
L42	0.0026	0.073	1.328	0.0007	0.0002	0.010	0.0013	0.128	0.33	0.024	0.073	3.30	0.474
L52	0.0328	0.064	0.672	0.0001	0.0001	0.006	0.0007	0.075	0.34	0.033	0.071	10.1	0.489
L131	0.0056	0.151	2.409	0.0010	0.0011	0.010	0.0008	0.089	0.45	0.056	0.106	8.75	0.719
L147	0.2006	0.225	14.30	0.0014	0.0010	0.014	0.0011	0.104	0.46	0.117	0.105	21.6	0.678
L152	0.0038	0.201	2.733	0.0013	0.0017	0.013	0.0022	0.204	0.66	0.028	0.138	8.28	0.856
L181	0.0281	0.090	0.317	0.0016	0.0021	0.010	0.0010	0.070	0.33	0.027	0.073	5.43	0.479
L228	0.0004	0.024	0.019	0.0009	0.0016	0.011	0.0007	0.027	0.12	0.039	0.025	2.02	0.156
CGSG north													
L27	0.0039	0.031	0.147	0.0008	0.0001	0.011	0.0013	0.121	0.52	0.026	0.105	11.6	0.679
L69	0.0573	0.133	1.092	0.0008	0.0006	0.011	0.0010	0.083	0.37	0.044	0.073	8.17	0.448
L192	0.0031	0.060	2.391	0.0023	0.0015	0.017	0.0021	0.195	0.50	0.148	0.105	9.96	0.645
L195	0.0043	0.027	0.227	0.0020	0.0017	0.013	0.0011	0.038	0.12	0.057	0.030	5.05	0.228
L199	0.1259	0.891	25.88	0.0018	0.0024	0.017	0.0018	0.110	0.43	0.027	0.095	8.23	0.623
W2	0.0092	0.021	0.683	0.0006	0.0007	0.015	0.0014	0.037	0.09	0.025	0.013	3.58	0.077

Pb, Th, U, Sr, Zr, and Hf concentrations were determined by external calibration following the $HF/HClO_4$ dissolution and analytical procedure described in detail by Ionov et al. (1992). To avoid memory effects due to the intake of concentrated Nb–Ta solutions in the instrument, Nb and Ta concentrations were determined by using Zr and Hf, respectively, as internal standards. This technique is an implementation to ICP-MS analysis of the method described by Jochum et al. (1990). Detection limits obtained by long-term analyses of chemical blanks at ISTEEM can be found in Ionov et al. (1992) and Godard et al. (2000).

3.4 RESULTS

Peridotite from each deformation category was analyzed. The samples are localized on Fig. 3.2: hydrous-mylonite (4 samples), mylonite (5 samples), proto-mylonite (6 samples), Fine Grained Secondary Granular (FGSG, 6 samples), CGSG from the central part of the massif (9 samples, CGSGc) and CGSG from the northern part of the massif (6 samples, CGSGn).

Table 3.2: continued.

	Sm	Zr	Hf	Eu	Gd	Tb	Dy	Y	Ho	Er	Tm	Yb	Lu
hydrous-mylonite													
L95	0.186	3.00	0.109	0.085	0.339	0.065	0.490	2.72	0.111	0.320	0.049	0.331	
L184	0.210	3.98	0.132	0.097	0.345	0.065	0.495	2.66	0.109	0.327	0.050	0.328	
L187d	0.308	5.82	0.203	0.127	0.507	0.094	0.707	3.81	0.153	0.459	0.067	0.446	
L208	0.243	5.17	0.154	0.104	0.426	0.079	0.606	3.25	0.132	0.382	0.056	0.375	
mylonite													
LO4	0.210	3.72	0.130	0.091	0.362	0.070	0.532	2.72	0.116	0.343	0.051	0.322	
L84	0.242	4.61	0.150	0.105	0.408	0.076	0.584	3.10	0.126	0.372	0.054	0.360	
L103	0.162	3.04	0.104	0.067	0.295	0.056	0.423	2.29	0.094	0.269	0.042	0.260	
L104	0.286	4.21	0.153	0.119	0.465	0.086	0.636	3.24	0.133	0.391	0.059	0.378	
L118	0.374	6.77	0.238	0.156	0.629	0.120	0.896	4.57	0.188	0.546	0.082	0.512	
proto-mylonite													
LO5	0.268	4.93	0.174	0.115	0.460	0.088	0.661	3.38	0.146	0.425	0.064	0.420	
L112	0.241	5.12	0.168	0.104	0.401	0.078	0.566	2.99	0.123	0.363	0.056	0.373	
L122	0.222	4.03	0.139	0.094	0.379	0.070	0.520	2.45	0.115	0.335	0.048	0.314	
L211	0.319	5.99	0.201	0.123	0.556	0.102	0.757	4.16	0.165	0.467	0.069	0.436	
L218	0.285	5.93	0.191	0.120	0.481	0.089	0.665	3.72	0.147	0.422	0.064	0.418	
La2002-5	0.211	4.08	0.140	0.097	0.384	0.072	0.552	3.06	0.122	0.359	0.054	0.351	
FGSG													
LO9	0.262	5.21	0.182	0.114	0.456	0.087	0.647	3.37	0.147	0.425	0.066	0.434	
L110	0.277	4.61	0.175	0.112	0.444	0.086	0.637	3.23	0.137	0.404	0.060	0.390	
L212	0.337	6.77	0.215	0.142	0.570	0.105	0.794	4.27	0.169	0.490	0.070	0.470	
L223	0.197	3.96	0.126	0.084	0.339	0.064	0.474	2.61	0.104	0.302	0.044	0.300	
L241	0.168	3.72	0.119	0.079	0.315	0.059	0.463	2.58	0.103	0.299	0.044	0.297	
La2002-3	0.208	4.47	0.135	0.092	0.348	0.064	0.491	2.73	0.109	0.314	0.048	0.328	
CGSG central													
L13	0.204	3.77	0.131	0.090	0.349	0.070	0.520	2.70	0.115	0.328	0.052	0.334	
L42	0.202	3.75	0.114	0.077	0.353	0.068	0.529	2.71	0.115	0.333	0.052	0.334	
L52	0.213	3.49	0.125	0.086	0.360	0.069	0.517	2.72	0.110	0.326	0.051	0.322	
L131	0.321	3.02	0.159	0.139	0.534	0.099	0.742	3.57	0.161	0.466	0.068	0.434	
L147	0.299	4.62	0.176	0.123	0.483	0.089	0.663	3.31	0.142	0.419	0.060	0.399	
L152	0.333	6.20	0.210	0.141	0.522	0.095	0.699	3.64	0.153	0.449	0.066	0.418	
L181	0.204	3.96	0.138	0.084	0.344	0.063	0.477	2.51	0.106	0.309	0.046	0.304	
L228	0.065	1.84	0.053	0.030	0.107	0.021	0.168	1.02	0.040	0.121	0.021	0.151	
CGSG north													
L27	0.284	5.47	0.182	0.126	0.469	0.088	0.666	3.28	0.140	0.405	0.061	0.390	
L69	0.175	3.73	0.116	0.079	0.293	0.057	0.431	2.29	0.096	0.274	0.042	0.278	
L192	0.268	4.78	0.164	0.116	0.452	0.082	0.617	3.31	0.135	0.385	0.055	0.365	
L195	0.136	2.05	0.077	0.054	0.250	0.047	0.372	2.03	0.081	0.242	0.037	0.233	
L199	0.261	4.43	0.148	0.097	0.455	0.082	0.628	3.77	0.138	0.407	0.060	0.386	
W2	0.033	1.72	0.042	0.014	0.056	0.012	0.092	0.54	0.023	0.073	0.012	0.087	

3.4.1 Major elements

Similar to many other suites of mantle peridotite, the studied samples show overall trends of increasing MgO, Ni and Cr, with decreasing incompatible elements (e.g. Bodinier and Godard, 2003), with some notable exceptions. The studied peridotites display a range of MgO contents between 36.57 and 40.83 wt% that are negatively correlated with SiO_2 (Fig. 3.3a). The data of Bodinier (1988) present generally higher SiO_2 (~46 wt%) than our analyses. The analyzed samples show a high Al_2O_3/SiO_2 ratio (0.049 to 0.090) similar to depleted plagioclase peridotite (Bodinier, 1988; Piccardo et al., 2006; Rampone et al., 2005). However, few samples from the CGSG rocks display low ratios (> 0.028) similar to the refractory rocks of abyssal peridotite (Godard et al., 2000) and some samples provide a very high ratio (0.098 and 0.112). Peridotite also have a typical plagioclase peridotite MgO/SiO_2 ratio except for few samples, which are enriched in Al_2O_3 and depleted in SiO_2 (Fig. 3.3b). The Al_2O_3 content scatters from 1.2 to 4.98 wt% (Tab. 3.1) and the major variation is recorded in the CGSG rocks type, particularly from the northern part of the massif. Three samples, from the CGSG, have very low Al_2O_3 content (below 2 wt%) close to the harzburgitic or dunitic composition. Our data are close to the primitive mantle (PM) line (Jagoutz et al., 1979). On the contrary, the data of Piccardo

et al. (2006) in MgO/SiO_2 present systematically higher composition compared to the PM line, and might reflect a too high MgO content. The peridotite analyzed by Bodinier (1988) show a trend parallel to our analyses and lightly lower, as a consequence of a genrally higher SiO_2 content at a given MgO. The reason for this apparent discrepancy is not known. The Mg# content is independent of the deformation and ranging between 90 and 89 forsterite content (Fig. 3.3c). Similar to other suites of mantle rocks the Al_2O_3/CaO is constant and close to primitive mantle estimates (Fig. 3.3d). Few samples of plagioclase peridotite plot above the PM line with high content in Al_2O_3.

3.4.2 Trace elements

The normalized REE and trace element patterns of the analyzed samples are shown in Figures 3.4 and 3.5, respectively. The plagioclase lherzolites present trace element signatures characterized by weak LREE depletion and a relatively flat M-HREE pattern (Fig. 3.4). The patterns are similar in shape in all classes of deformation with little variation in the $(Ce/Yb)_N$ ratio (0.2-0.4). Only a few samples display remarkable variations. The primitive mantle composition plotted on the diagrams highlights HREE enrichment for one (mylonite group) or several (CGSG central group)

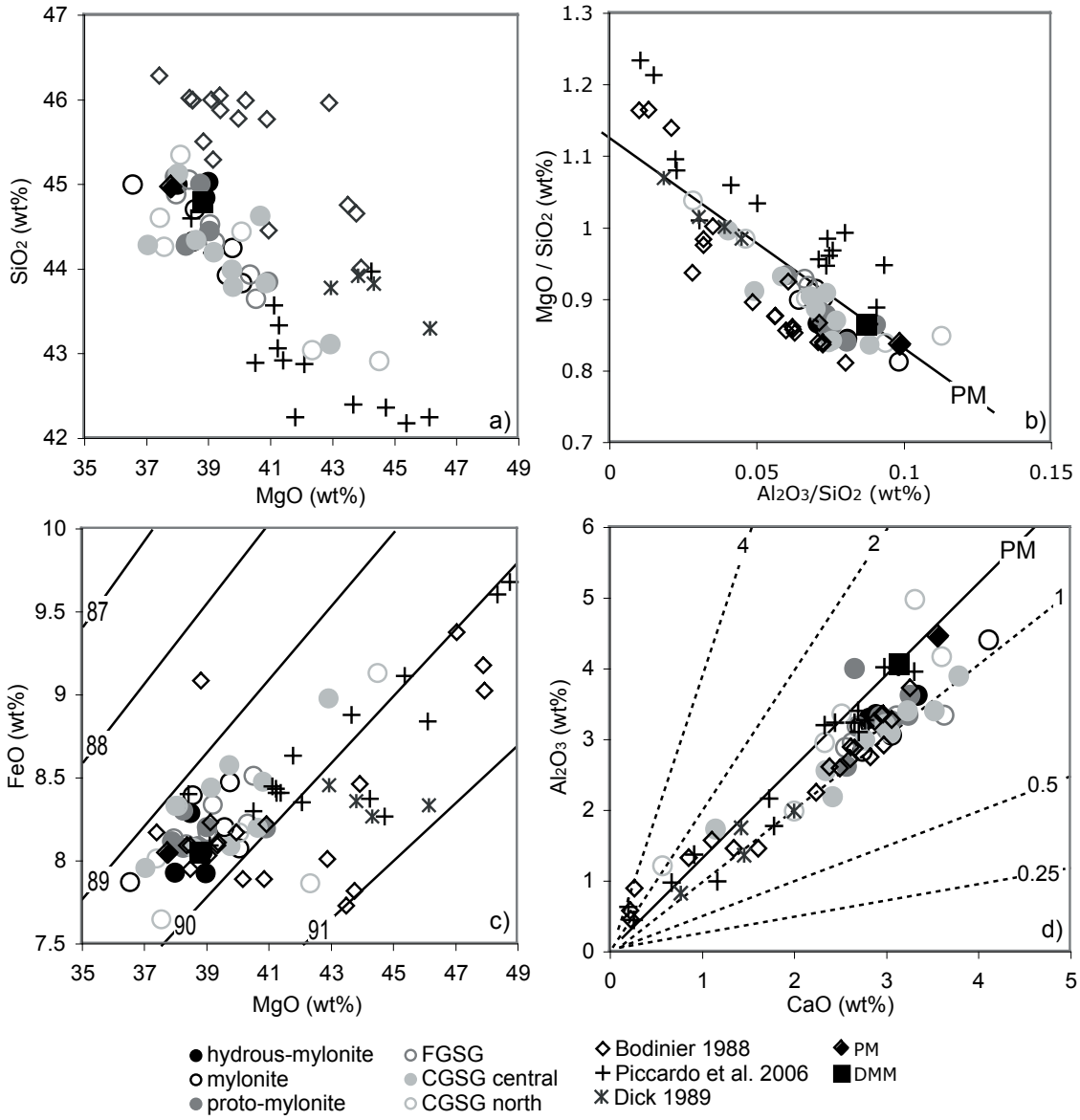

Fig. 3.3: Whole rock major element composition of the shear zone illustrated in (a) Al_2O_3/SiO_2 vs. MgO/SiO_2 (wt%), (b) CaO vs. Al_2O_3 (wt%) and (c) MgO vs. FeO (wt%) diagrams. Published data from the Lanzo massif are shown for comparison: Bodinier, (1988), Piccardo et al., (2006). Abyssal peridotites are from Dick (1989). In diagram d, dashed lines represent the constant CaO/Al_2O_3 ratios and the black line represents the silicate Earth differentiation trend and the primitive mantle ratio (PM) (Jagoutz et al., 1979). The solid lines in diagram c show constant Mg# values.

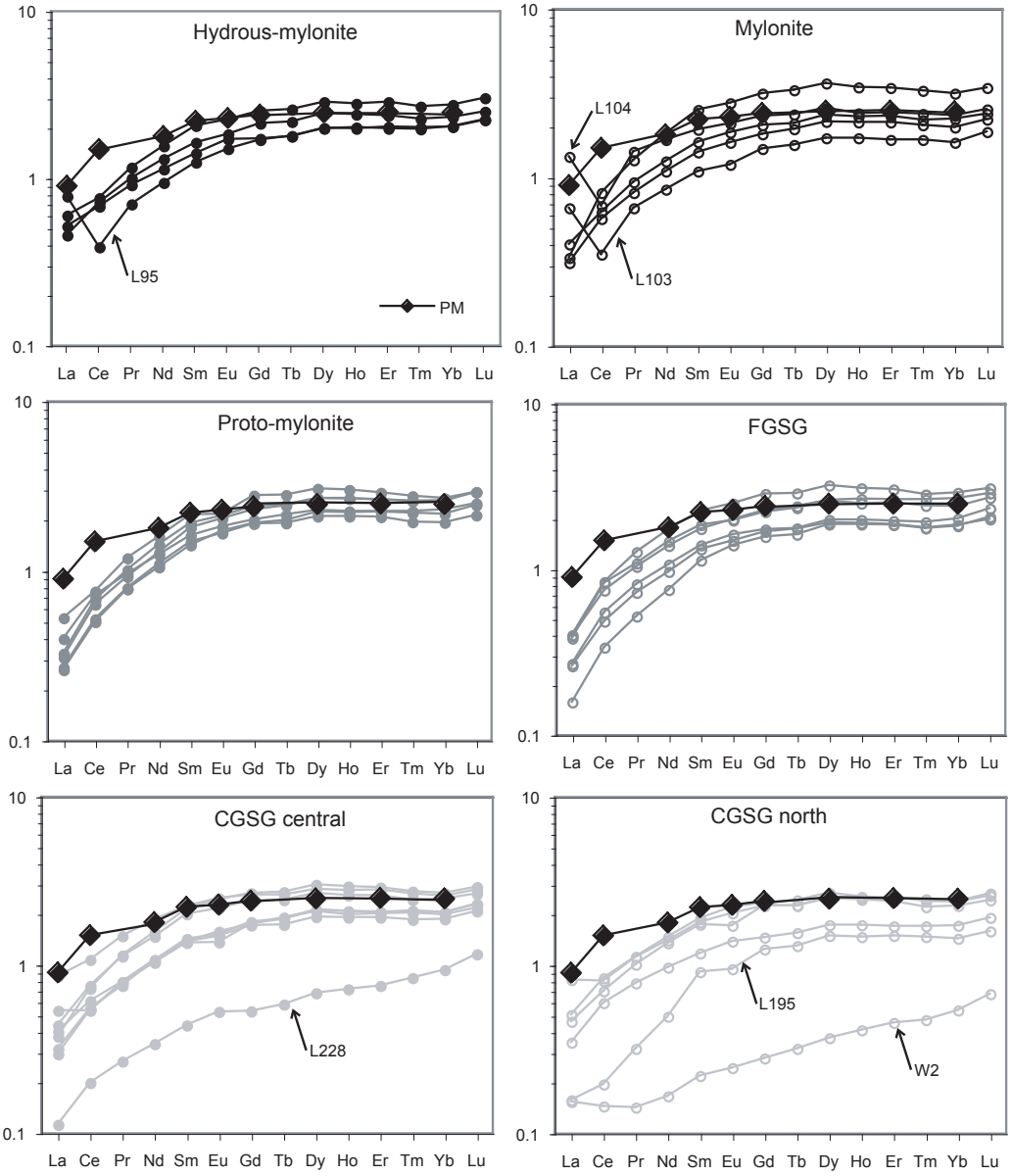

Fig. 3.4: Plagioclase peridotite trace element diagrams normalized to chondrite. The analyses are separated by classes of deformation from (a) hydrous-mylonite, (e-f) to coarse-grained secondary granular samples. PM: Primitive mantle (Sun and McDonough, 1989). Symbols as in Figure 3.3.

samples for deformation categories, except for the CGSG rocks from the northern part of the massif. For example, L118 sample from the mylonite group is enriched from Sm_N (2.5) to HREE elements (e.g. Lu_N: 3.4).

Hydrous mylonite samples display a rather homogeneous composition except sample L95, which is depleted in Ce and enriched in La. Two other samples (L104 and L103) from the mylonite group show a similar behavior with $(La/Ce)_N > 1$, apparently independent of the degree of serpentinization.

The FGSG samples present a large variation in LREE, from samples L241 with 0.038 ppm to sample L212 with 0.095 ppm as La content. The LREE shape, from sample L241 increases until to tend to be parallel with the other samples of this category.

The coarse grained peridotites from the northern and the central body display a larger variation recorded in the analyses. The sample L228 from the CGSGc presents general low content in all trace elements and increases from LREE to HREE elements. The pattern is similar to clinopyroxene-poor lherzolite described by Bodinier (1988) in the southern part of the massif.

In the CGSG from the northern part of the massif, the sample L195 presents a rapid enrichment in LREE and content in HREE are closed to the other plagioclase lherzolites. Sample W2 is clearly

different from the general trend of plagioclase lherzolite, displaying low contents in all elements and a much smoother increase from La to Lu.

3.4.3 Other trace elements

Similar to fertile and depleted peridotites from different places (e.g. Bodinier and Godard, 2003), the Lanzo peridotites are characterized by U-shaped normalized incompatible trace element patterns, with slight depletions of Zr, Hf and LREE with respect to M- and HREE. The trace element pattern show small but significant positive spikes in Pb, with $(Ce/Pb)_N$ of 0.08 to 1.40, that are not accompanied by Sr spikes. The Nb/Ta ratio is below the primitive mantle estimate (11.4±3.1). U/Th ratios, normalized to primitive mantle are between 0.08 and 1.39.

Plagioclase lherzolite from all different categories have homogeneous and flat patterns from Pr to Lu, except to clinopyroxene-poor lherzolites samples L228 and W2, which generally show a lower concentration in all trace elements (Fig. 3.5). The elements Cs, Rb and Ba present large variations on primitive mantle normalized diagrams (from < 0.1 to > 1). Several samples from the CGSG rocks have a relatively high LOI (from 2.5 to 9.5) and display either low or high contents in Ba, Cs and Rb (Tab. 3.2). We conclude that serpentinization had a minor influence on these highly incompatible elements.

Figures 3.6 and 3.7 illustrate the chemical variation with respect to deformation in terms of Al_2O_3, Na_2O, TiO_2, Ce, Sm and Yb. It is apparent that the variability decreases from coarse granular to mylonitic rocks. In particular, the Al_2O_3 content, illustrates a decrease from coarse granular rocks (1.20 to 4.98 wt%), proto-mylonite and FGSG rocks (2.62 to 4.00 wt%) to hydrous-mylonite and mylonite samples (2.83 to 3.62 wt%). The Na_2O variability is similar in the mylonitic, proto-mylonite and FGSG samples and the majority of peridotite samples have a higher content than the coarse granular rocks (Fig. 3.6a). The hydrous-mylonite samples are, on average, higher Na_2O enriched compared to the mylonite rocks (0.53 and 0.43 wt% respectively). The Ni content is uniform with increasing deformation and is higher in the hydrous-mylonite and mylonite (from 2100 to 2400 ppm, Fig. 3.6c).

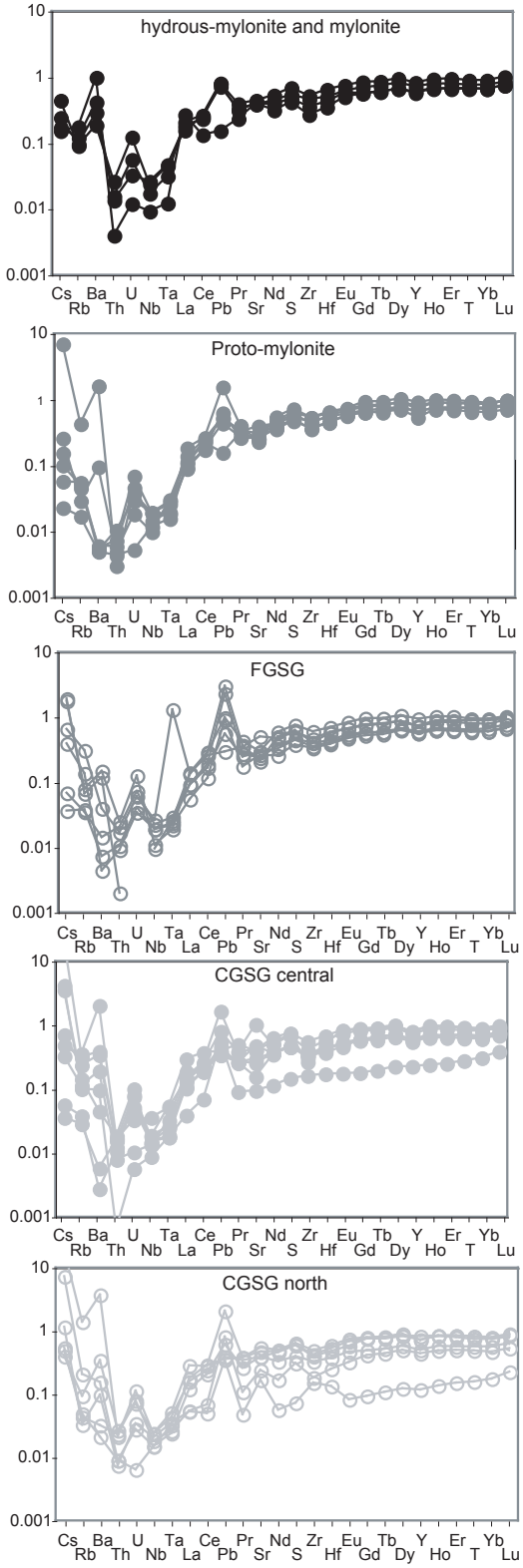

Fig. 3.5: Abundances of incompatible trace element diagrams of all classes of rocks from the Lanzo peridotite, normalized to primitive mantle (Sun and McDonough 1989). Symbols as in Figure 3.3.

The REE Ce, Sm and Yb, indicate homogeneous composition when the deformation increases (Fig. 3.7a, b, c). From Ce (LREE) element to Yb (HREE)

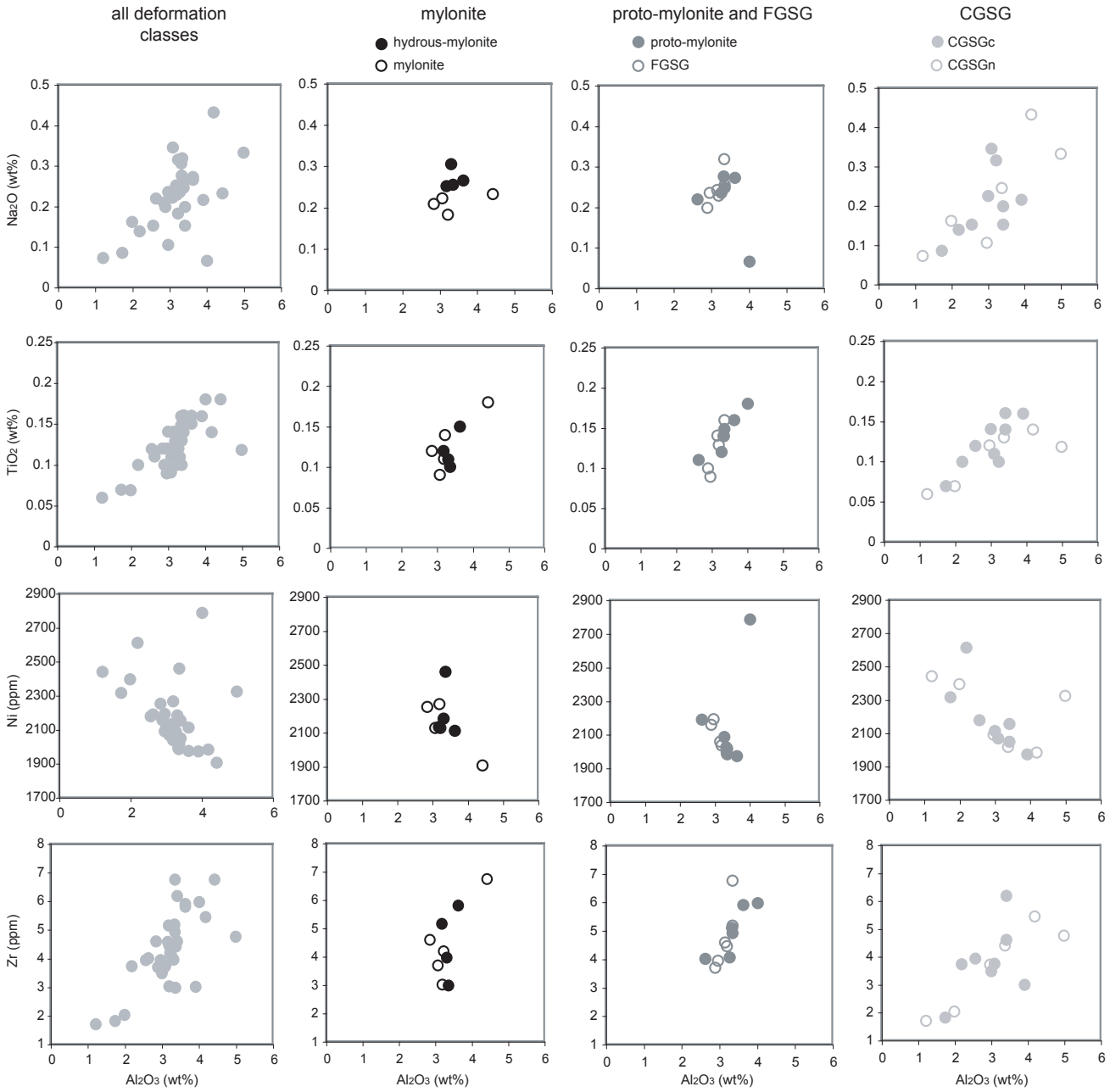

Fig. 3.6: Element diagrams of Rb (ppm), Na_2O (wt%), TiO_2 (wt%), Ni (ppm) and Zr (ppm) vs. Al_2O_3. The first column summarizes the whole dataset, while the 2nd to 4th columns present the data according to microstructural criteria. Note that there is almost no correlation between Al_2O_3 and a variety of trace elements within the mylonite/hydrous mylonite.

element, the Yb is highly homogeneous than the Ce in the mylonitic rocks. This indicates a slower diffusion of the Ce than the Yb, and the possible presence of liquid during the deformation. Looking at the Ce_N vs. Yb_N highlight the variation between both elements, the Ce became progressively independent of Yb element.

3.5 DISCUSSION

3.5.1 Major element variability

The whole rock composition of peridotites is clearly linked to the type of deformation, more the peridotite is deformed, the more the composition is homogeneous (Al_2O_3, TiO_2, Na_2O, NiO). This might be explained by the influence of the grain size reduction. The granular peridotites from the central and northern body show heterogeneous compositions and, the presence of few samples

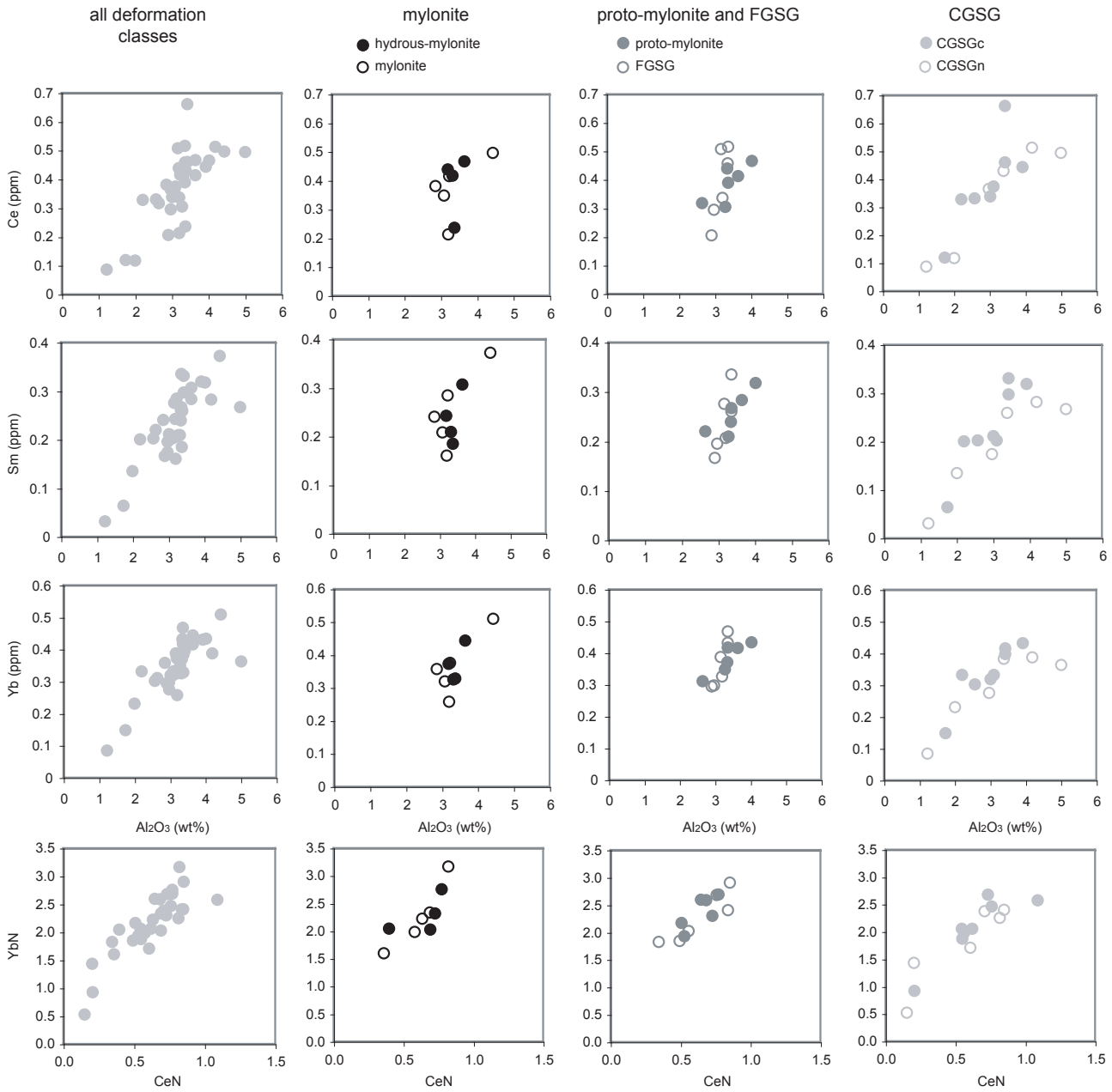

Fig. 3.7: Element diagrams of Ce, Sm and Yb vs. Al_2O_3 and YbN vs. CeN. The analyses are represented by a general diagram with all classes of deformation and indicate the general trend of the analyses and after 3 diagrams correspond to the classes of deformation.

depleted, are the proof of very heterogeneous mantle before the deformation.

Plagioclase lherzolite from the Lanzo massif, already analyzed, display Al_2O_3 content between 2-4 wt% and those with less of 1% are dunite rocks (Bodinier, 1988). Some plagioclase peridotite from this study reflect a refractory composition. Major elements, indicative of peridotite fertility (e.g. Al and Ca), show high content in deformed rocks, and a low content in the case of CGSG rocks from the northern part of the massif. The Al_2O_3 average realized on each category of sample highlights a clearly higher content in hydrous-mylonite, mylonite and proto-mylonite than in the granular rocks (Fig. 3.8). The same type of behaviour is observed with CaO average content. This may indicate the possibility of melt addition in the peridotite and preferentially in the deformed rocks. The deformation will occur in presence of melt and the shear zone is expected like melt accumulation.

3.5.2 Trace element variability

The plagioclase peridotites of the Northern and Central Lanzo massif are distinguished

from Lanzo South peridotite by overall higher REE content, a far less frequent occurrence of refractory harzburgite and dunite, and a remarkable constant $(Ce/Yb)_N$ ratio. In addition, each class of deformation contains samples that are enriched in REE compared to primitive mantle estimates (Fig. 3.4). These features are not consistent with simple melting models.

This 'superfertile' composition might be explained by a "marble cake" peridotite composed of heterogeneously distributed pyroxenites mixed with peridotite as suggested by Allègre and Turcotte (1986). In their view, pyroxenites might represent stretched stripes of 'oceanic crust' that was recycled through the mantle. However, there is no major element evidence for the involvement of oceanic crust in the pyroxenite compositions (Bodinier, 1988) and the pyroxenite layers were excluded from the sampling. In the case of mylonite, it might be difficult to identify small remnants of disrupted pyroxenite layering in the field, but careful inspection of mineral chemistry indicate that spinel from pyroxenites is generally rich in Al, and could clearly be distinguished from peridotite spinel (chapter 2). Such samples have been excluded from our dataset. An alternative hypothesis to explain the HREE enrichment in plagioclase peridotite is refertilization by diffuse porous melt flow. The melt/rock reaction and the melt migration textures are frequent in the Lanzo peridotite massif (chapter 2, Müntener and Piccardo, 2003; Piccardo et al., 2004) and commonly illustrated by i) the occurrence of orthopyroxene + plagioclase symplectite replacing clinopyroxene and ii) vermicular orthopyroxene replacing olivine porphyroclasts. For a complete description see chapter 2 and Piccardo et al. (2004). Recent textural and geochemical investigations proposed that refertilization by basaltic or refractory melts is also an important process in abyssal peridotites (Hellebrand et al., 2002; Kelemen et al., 2004), which have been conventionally interpreted as simple residues of partial melting (Johnson and Dick, 1992; Johnson et al., 1990). Reactive porous flow and refertilization are two important processes that are able to deeply modify textures, mineral modes and chemical compositions of peridotites (Bedini et al., 1997; Godard et al., 2000; Müntener and Piccardo, 2003; Piccardo et al., 2004; Piccardo et al., 2006; Van der Wal and Bodinier, 1996). The rocks do not reveal a substantial Ce/Yb fractionation, which is concordant with a refertilization hypothesis. This indicates addition of melt fraction of closely constant composition.

The content of Ce, Yb and Y as an average in each class of deformation (e.g. Yb on Fig. 3.8) indicate a depleted composition of the northern body compared to the central body. This suggests that deformation controls the chemical composition and the mylonite zone acted as a impermeable barrier, and will be discussed in details below.

The highly incompatible elements (Cs, Rb and Ba) enrichment is unrelated to the deformation categories. LREE enrichment in ophiolitic peridotite is generally attributed to secondary processes as serpentinization, oceanic alteration or contamination by crustal fluids (Gruau et al. 1988, Sharma and Wasserburg, 1996). Moreover, the La enrichment should be linked to the serpentinization degree of the peridotite.

3.5.3 Melting and refertilization modeling

In the following, melting models will be discussed, in order to evaluate how the trace element signatures of the plagioclase peridotite could be explained. Peridotite modes, partition coefficients and melting modes are reported in Table 3.3. We used the partition coefficients compiled by Suhr et al. (1998), which are similar to many other partition coefficient determinations for mantle melting (Hart and Dunn, 1993). Two simple melting models, batch melting and fractional melting are illustrated in Figure 3.9, simulating melting in the stability field of spinel peridotite, using a DMM source (Depleted MORB Mantle, Workman and Hart, 2005, Fig. 3.9a) and a PUM source (Primitive Mantle, McDonough and Sun, 1995, Fig. 3.9b).

The two fractional melting trajectories are shown, using different source compositions. Melt extraction will lead to rapidly decreasing $(Ce/Yb)_N$ ratios at near constant Yb concentrations in the peridotites. After a few % of melting (about 2% for a DMM source and about 4% using a PUM source) most plagioclase peridotites have $(Ce/Yb)_N$ that are too high to be explained by fractional melting

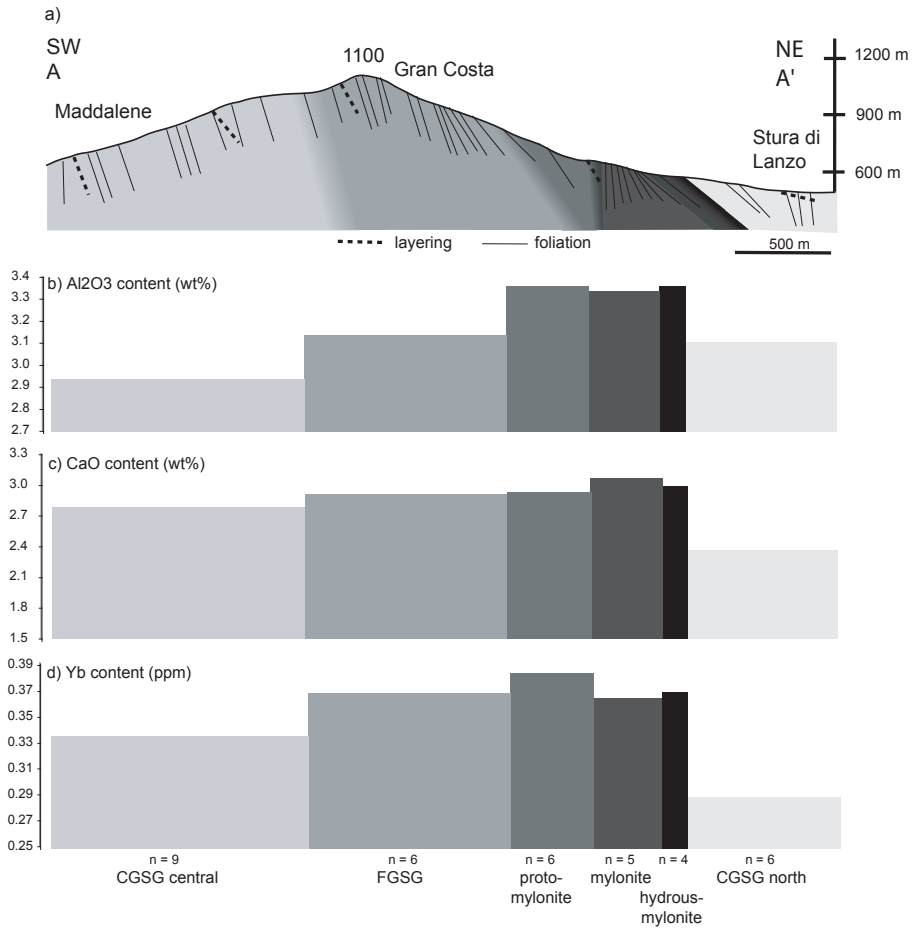

Fig. 3.8: Average of major element compositions of peridotite along a cross section of the shear zone from SW (A) to NE (A'). a) Schematic topography of the shear zone cross section (after chapter 2). b) Histogram of average Al_2O_3 (wt%) content and standard deviations for peridotites with different microstructures. c) Histogram of average CaO (wt%) content and standard deviations for peridotites with different microstructures. Note that block classes correspond to the distance in the shear zone.

alone. And, more importantly, more than 60% of the samples have Yb concentrations that are too high to be consistent with a fractional melting process. We have tested critical melting models, with residual melt porosities up to 5%, but these calculations do not significantly change the results. Batch melting models yield a much more moderate fractionation of LREE compared to HREE, which is shown by the relatively high $(Ce/Yb)_N$ ratio after 15-20% melting, and a slower decrease of Yb for a given degree of melting. In contrast to fractional melting, the $(Ce/Yb)_N$ ratio is much less fractionated (e.g. between 10 and 20 % melting: $0.1<(Ce/Yb)_N<0.15$) and only slightly lower than the Lanzo peridotites. However, more than 70% of the data have Yb concentrations that are significantly higher than those obtained by melting models, (except assuming a value of Yb_N for the depleted or primitive mantle, that is far higher than any proposed value; e.g. Workman and Hart 2005, McDonough and Sun 1995). We have tested garnet field and plagioclase field melting models (not shown), but the results are essentially the same.

In summary, more than 50% of the Lanzo plagioclase peridotites cannot be explained by any kind of melting model, but require addition of melt with a relatively constant $(Ce/Yb)_N$ ratio. Given the clinopyroxene poor lherzolite as a protolith before refertilization (e.g. L228) and assuming a normal mid-ocean ridge basalt with $(Ce/Yb)_N$ ~0.8 and Yb_N ~24 from (MORB values from Hofmann, 1988; McDonough and Sun, 1995), as a potential refertilization agent, simple melt entrapment calculations have been performed. We added N-MORB basalt in steps of 1%, followed by equilibrium trace element distribution. Minor amounts of MORB-type melt added to the residue will produce a rapid increase of Yb_N values exceeding estimates of DMM and PUM, without modifying substantially the $(Ce/Yb)_N$ ratio. It can

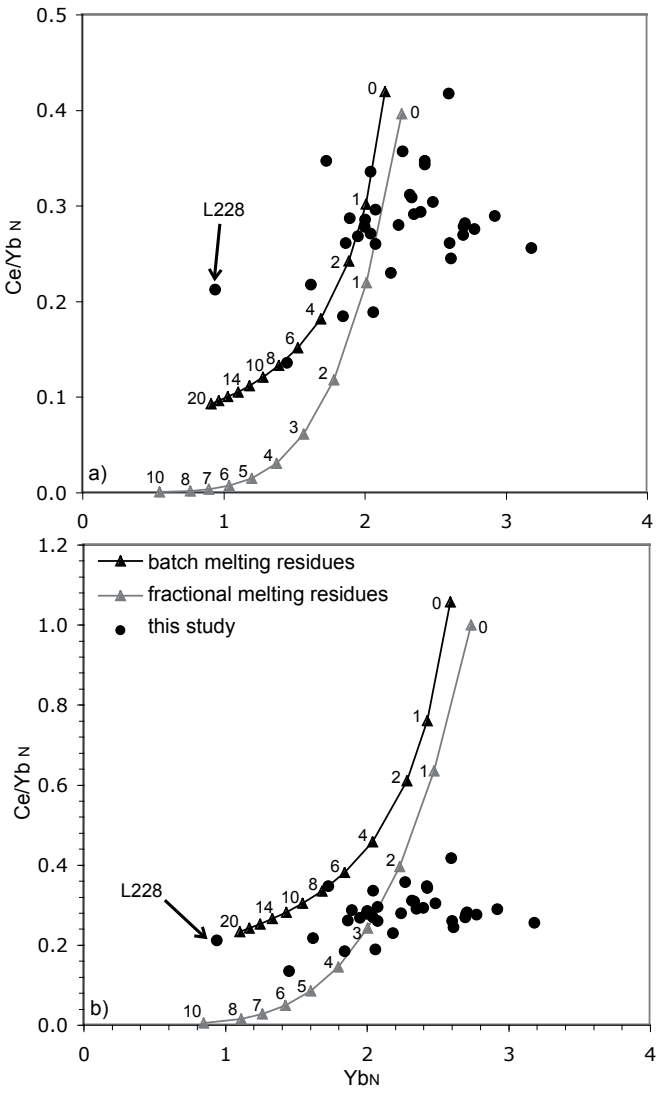

Fig. 3.9: Illustrations of simple melting model of Yb_N vs. $(Ce/Yb)_N$. (a) Model calculated with DMM source (Depleted MORB Mantle, Workman and Hart, 2005). Symbols on the modeling curve represent fractionation steps in %. (b) Model calculated with a PUM source (Primitive Mantle, McDonough and Sun, 1995). Modeling parameters and partition coefficients are listed in Table 3.3.

qualitatively be estimated (Fig. 3.9b), that about 5 to 10% of MORB-type liquid must be added to explain the variability of the Lanzo plagioclase peridotites. These results are qualitatively similar to those obtained by Elthon (1992), which were based on the Na_2O content of depleted peridotite. Obviously, it remains difficult to determine whether complete redistribution occurred, or whether some of the incompatible elements escaped to higher crustal levels.

Table 3.3: Parameters to melting models: Modal composition are from Johnson (1998). Partition coefficient as compiled by Suhr et al. (1998), Melting modes are from Kinzler (1997).

Modal composition of peridotite

Olivine	0.57
Orthospyroxene	0.28
Clinopyroxene	0.13
Spinel	0.02

Partition coefficient

	Ce	Yb
Olivine	0.00001	0.014
Orthospyroxene	0.005	0.09
Clinopyroxene	0.1	0.41
Spinel	0.0006	0.005

Melting modes

Olivine	-0.06
Orthospyroxene	0.28
Clinopyroxene	0.67
Spinel	0.11

3.5.4 Chemical variability as a function of deformation

The peridotites from the Lanzo shear zone are characterized by spatial variations with respect to mineral chemistry and microtextures (chapter 2). The authors discussed the effects of deformation on the compositional homogeneity of peridotite minerals. Here we illustrated the whole rock variability as a function of distance to the shear zone (Fig. 3.2, 3.6-7). The results display a large compositional variation at the Lanzo massif scale, and a tendency of enrichment in the footwall of the mantle shear zone. The incompatible elements show an enrichment in the order of 10-20% in the more deformed rocks (proto-mylonite, mylonite and hydrous-mylonite) compared to the CGSG from the northern body (Fig. 3.8). Considering a large variety of trace elements as function of Al_2O_3, we can observe a systematic variation relative to the micro-textures: most incompatible elements are well correlated with Al_2O_3 in the coarse- and fine-grained rocks. This positive correlation is progressively lost between Al_2O_3 and REE and other incompatible elements (e.g. Zr, Na, Ti) with increasing deformation (Figs. 3.6 and 3.7). The inverse is observed with compatible elements such as Ni: the correlation with Al_2O_3 is negative, and this correlation tends to be lost in the mylonitic rocks.

Interestingly, the Ce_N concentration tends to be more homogeneous with respect to Yb_N with increasing deformation. This has two important implications: first, the homogenization is unlikely to be caused by simple mechanical mixing, as this process would tend to eliminate the compositional variability of all incompatible elements; second, it is also unlikely, that solid state diffusion can explain the data, as Ce diffuses orders of magnitudes slower than Yb (Van Orman et al. 2001). If diffusion would be the dominant mechanism one would expect homogenization of Yb rather than Ce. For these reasons, we prefer the interpretation that deformation occurred in the presence of small melt fractions, which preferentially homogenizes the more incompatible LREE with respect to HREE.
If our refertilization model is correct, then the infiltrating liquid in the Lanzo massif is most probably of N-MORB composition and thus very different from many xenoliths studies, and also vary different from liquid that formed the Ronda recrystallization front (Lenoir et al., 2001; Van der Wal and Bodinier, 1996). In contrast to the recrystallization front of the Ronda peridotite, which is related to km-scale pervasive melt percolation (Van der Wal and Bodinier, 1996) and chromatographic trace element fractionation in the deformed peridotites, the Lanzo mantle shear zone does not show chromatographic effects. We attribute this to the combined effects of active deformation, rapid cooling and exhumation of the Lanzo peridotites, so that the remaining melt fractions rapidly freeze. The stagnating melt probably acts as a lubricant for deformation during the early high temperature stages and at the same time the fine grained rocks efficiently inhibit upwards migration of melt.

3.5.5 Implications

This study highlights the geochemical variability in peridotite in the footwall of actively deforming shear zones. Initial pervasive porous flow of melt became focused in time and space (e.g. chapter 2, Müntener and Piccardo, 2003): as documented by impregnation textures in the entire zone, and gabbroic dikes that are much abundant in the footwall of the shear zone (Fig. 3.10). Our new results, together with previously published data (e.g. Piccardo et al., 2007) confirm that

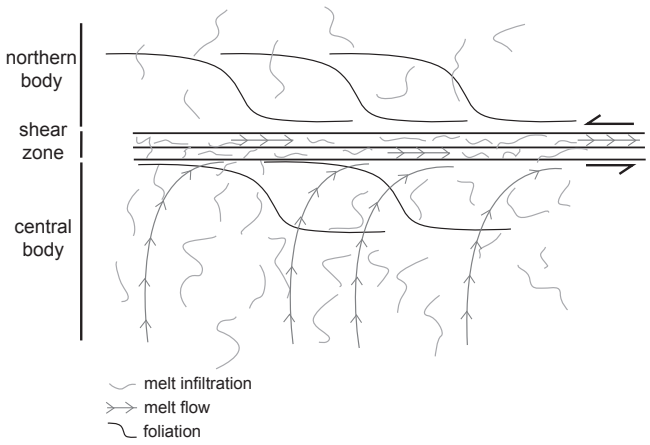

Fig. 3.10: Conceptual model of melt migration and stagnation with respect to deformation along a high-temperature mantle shear zone. Pervasive melt flow is focused and concentrated along the shear zone. Note that younger gabbroic dikes are almost exclusively found in the footwall of the shear zone, suggesting that the shear zone acted as a permeability barrier to dikes.

melt migration occurred on a km-scale over the entire Lanzo massif, but local differences exist. The southern Lanzo peridotite displays a large range of composition, from fertile plagioclase peridotite to refractory harzburgite and dunite, while the footwall of the shear zone is relatively homogeneous, accentuated by important grain size reduction within the mylonite zone. The northern body is less enriched than the central body. An important question is to understand whether the first event is the melt accumulation or the high temperature deformation and shear zones formation. The presence of melt in the rock will change the rheological behavior and increase the weakening. In any case deformation involves grain size reduction and allowed important melt rock interaction. One hypothesis is the possibility of a pre-existant shear zone from the old history in the mantle, which reacted as a permeability barrier. The second hypothesis is the formation of the shear zone during the mantle exhumation. We propose that a combination of existing heterogeneities (pre-existing shear zones, pyroxenite layers) and thermal gradients might induce the formation of an intra-mantle permeability barrier.

ACKNOWLEDGEMENTS

We thank V. Serneels for helping with

the XRF analyses and J.L. Bodinier for ICP-MS analyses at ISTEEM (Université Montpellier II, Montpellier, France). This research was financially supported by the Swiss National Foundation (Project 21-66923.01 and 200020-104636/1).

CHAPTER 4:

TRACE ELEMENT CHEMISTRY AND U-PB DATING OF ZIRCONS FROM OCEANIC GABBROS AND THEIR RELATIONSHIP WITH WHOLE ROCK COMPOSITION (LANZO, ITALIAN ALPS).

Manuscript in press in Contributions to Mineralogy and Petrology

Val Della Torre

Kaczmarek, M.-A.[1,2], Müntener O.[2,3], and Rubatto, D.[4]

(1) Institute of Geology, University of Neuchâtel, rue Emile Argand, 2007 Neuchâtel, Switzerland. Mary-alix.kaczmarek@unine.ch, 0041 (0)3 27 18 27 12, Fax: 0041 (0)3 27 18 26 01
(2) Institute of Mineralogy and Geochemistry, University of Lausanne, Anthopole, CH-1015 Lausanne, Switzerland
(3) formerly at: Institute of Geological Sciences, University of Bern, Baltzerst. 1, 3012 Bern, Switzerland.
(4) Research School of Earth Sciences, The Australian National University, Canberra ACT 0200, Australia.

ABSTRACT

The U-Pb ages and the trace element content of zircon U-Pb along with major and trace element whole rock data on gabbroic dikes from the Lanzo lherzolitic massif, N-Italy, have been determined to constrain crustal accretion in ocean-continent transition zones. Three Fe-Ti gabbros were dated from the central and the southern part of the massif providing middle Jurassic ages of 161 ± 2, 158 ± 2 and 163 ± 1 Ma, which argue for magmatic activity over few millions of years. Zircon crystals are characterized by high but variable Th/U ratios, rare earth element patterns enriched in heavy rare earths, pronounced positive Ce and negative Eu-anomalies consistent with crystallization after substantial plagioclase fractionation. The zircon trace element composition coupled with whole rock chemistry was used to reconstruct the crystallization history of the gabbros. A number of gabbros crystallized in-situ, and zircon precipitated from trapped, intercumulus liquid, while other gabbros represent residual liquids that were extracted from a cumulus pile and crystallized along syn-magmatic shear zones. We propose a model in which the emplacement mechanism of gabbroic rocks in ocean-continent transition zones evolves from in-situ crystallization to stratified crystallization with efficient extraction of residual liquid along syn-magmatic shear zones. Such an evolution of the crystallization history is probably related to the thermal evolution of the underlying mantle lithosphere.

Keywords: Zircon, oxyde gabbros, trace element geochemistry, peridotite, Lanzo massif, Piemont-Ligurian ocean, SHRIMP, U-Pb dating.

4.1 INTRODUCTION

The processes and mechanisms determining accretion of oceanic crust widely differ among the global mid-ocean ridge systems, and are mainly dependant on spreading rates (Bown and White 1994; Dick 1994; Dick et al. 2000; Langmuir et al. 1993). At spreading rates lower than about 20 mm/y (ultra-slow spreading ridges), additional parameters such as the thermal structure and the composition of the underlying mantle dramatically affect crustal production rates (Dick et al. 2003). Similar observations are made for the accretion of oceanic crust in ocean–continent transition zones (Müntener and Manatschal 2006; Tucholke et al. 2006). Ophiolites in general do not provide direct constraints on spreading rates. However, the predominance of lherzolite and harzburgite subtypes (Nicolas 1989) has been taken as a proxy for magma production rates from which paleo-spreading rates might be inferred.

Results from a variety of studies indicate that the (ultra-) slow spreading oceanic crust of the Jurassic-Cretaceous Piemont-Ligurian ocean is dominated by the emplacement of small-scale gabbroic bodies of generally less than 500 m in thickness (Desmurs et al. 2002), intruded into mantle rocks that are partly subcontinental in origin (Decandia and Elter 1972; Piccardo 1976). This association of subcontinental mantle and gabbroic rocks is covered either by small volumes of effusive basaltic rocks (pillow lavas, pillow breccias, Desmurs et al. 2002; Dietrich 1969) or directly by mid-Jurassic sediments. The overall volume of basaltic rocks is small and discontinuous. Geochronological data across the remnants of the Piemont-Ligurian ocean suggest that the gabbroic bodies crystallized over a short period of time, from ~170 to 150 Ma (Rubatto et al. 1998; Rubatto and Hermann 2003; Schaltegger et al. 2002; Tribuzio et al. 2004). However, there is some discrepancy between ages inferred from Sm-Nd isochrons and ages determined by U-Pb on zircon. Sm-Nd mineral isochrons have been determined on a few Mg-gabbro samples from Ligurian gabbros ranging from ~180-164 Ma (Rampone et al. 1998; Tribuzio et al. 2004). U-Pb ages on zircon, however, indicate generally younger ages ranging from 166-148 (e.g. Bill et al. 1997; Costa and Caby 2001; Rubatto et al. 1998; Rubatto and Hermann 2003; Schaltegger

et al. 2002). However, few attempts have been made so far to quantify the duration of MOR-type magmatism in a spatially restricted area.

In this paper we present the results of U-Pb age determinations on zircons from mafic rocks distributed over more than 20km^2 within the Lanzo peridotite massif, in order to constrain the time interval over which gabbro emplacement was active. We combine whole rock major and trace element data, with zircon trace element chemistry, to discuss possible crystallization mechanisms of zircon in gabbroic rocks. We infer, that over time, the formation of highly differentiated, zircon-saturated liquid evolved from dominantly intercumulus, in-situ crystallization, to extraction along shear zones, leaving at depth the primitive cumulates from where such fractionated liquids originated. This means that the stratification of mafic oceanic crust is an evolving process that likely depends on the thermal evolution of the oceanic lithosphere during late rifting to (ultra-) slow seafloor spreading.

4.2 GEOLOGICAL SETTING

The Lanzo massif is located in the Western Alps, north-west of Torino (Italy), and is bounded to the north by the continental Sesia-Lanzo zone and to the east by the Piemont-Ligurian ophiolite zone (Fig. 4.1). The northern part of the massif consists of peridotite surrounded by strongly foliated serpentinites, which are the combined result of ocean-floor alteration and Alpine metamorphism. Many gabbroic dikes were metamorphosed and rodingitized during ocean floor alteration and Alpine metamorphism. However, in less serpentinized areas gabbroic dikes were partially transformed into eclogites during Alpine subduction in Alpine times (Kienast and Pognante 1988; Pelletier and Müntener 2006). Locally the massif is overlain by minor ophicarbonates, MORB type volcanic rocks and metasediments (Lagabrielle et al. 1989; Pelletier and Müntener 2006). The core of the Lanzo massif is dominated by fertile plagioclase lherzolite and minor volumes of spinel harzburgite and dunite (Boudier 1972; Boudier 1978; Piccardo et al. 2004) The peridotite body is characterized by a high temperature foliation and pyroxenite layering (Boudier 1978, Fig. 4.1). In addition, the massif contains numerous intrusive rocks (Boudier

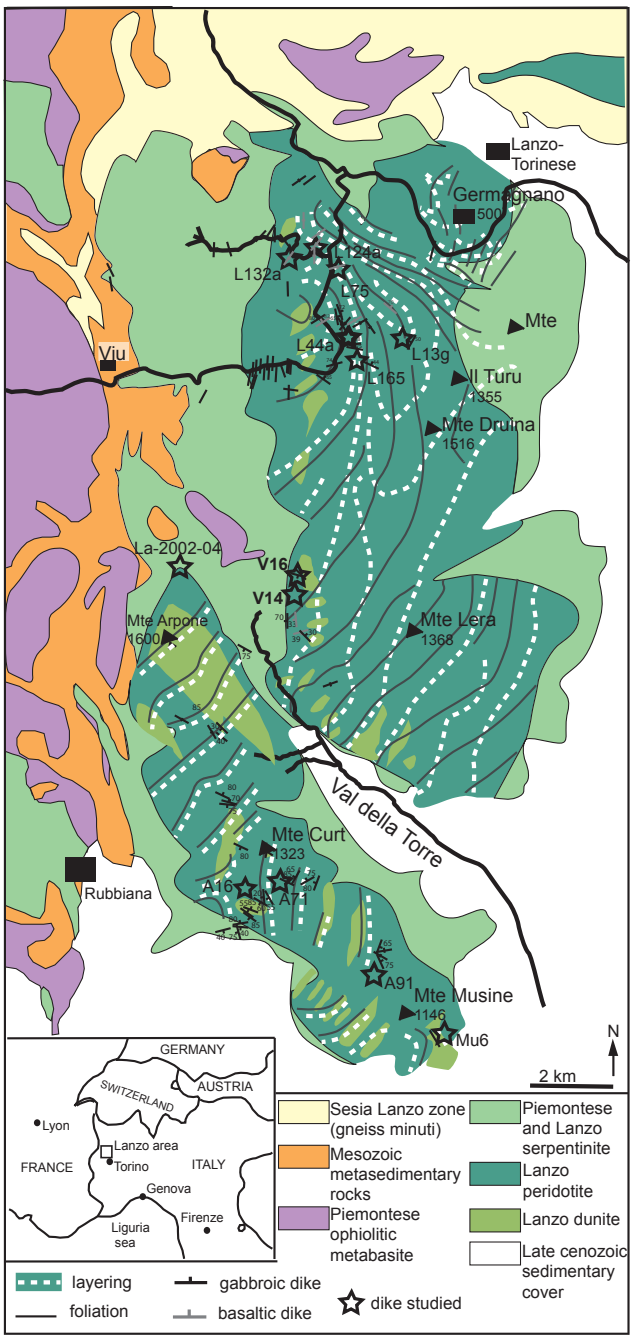

Fig. 4.1: Geological map of the Lanzo massif and the surrounding areas (compiled after Boudier 1972; Boudier 1978; Boudier and Nicolas 1972; Pelletier 2003; Pognante 1989). The location of gabbroic and basaltic dikes is indicated with black stars. Additional gabbro dikes and basaltic rocks are compiled from Boudier (1972), Boudier (1978), Pognante (1989) and Pelletier (2003).

1978; Boudier and Nicolas 1972) that may be classified into three groups according to their relative timing (Boudier and Nicolas 1972): (i) an "indigenous" group which consist of plagioclase to gabbroic veinlets, frequently occurring in "echelon", and thin mm to cm scale olivine gabbro dikes. (ii) An "intrusive" group consisting of olivine gabbros, gabbronorite to ferro-gabbros

and rare plagiogranites occurring as several meters thick dikes. (iii) Fine grained gabbro dikes parallel to swarms of basaltic dikes and cutting across the gabbros of the "intrusive" group and the high temperature foliation. Recent studies refined this model and proposed a conceptual model from porous to focused melt flow to explain the various igneous features in the Lanzo peridotite (Müntener and Piccardo 2003; Müntener et al. 2005; Piccardo et al. 2004): (a) a pervasive porous melt flow leading to the formation of impregnated peridotites; (b) focused porous flow where melt transport is mainly focused in replacive harzburgites and dunites; (c) initial crystallization and formation of megacrysts and small dikes corresponding to the "indigenous" group of Boudier and Nicolas (1972) and (d) ubiquitous formation of km-scale, discordant gabbroic and basaltic dikes. Previous studies (Bodinier 1988; Bodinier et al. 1986; Pognante et al. 1985) indicate that gabbro and basaltic dikes are derived from T-MORB to T- to N-MORB type magmas from the north to the south, respectively, and are compositionally similar to ophiolitic basalts of the Ligurian, Western and Eastern Central Alps (e.g. Beccaluva et al. 1984; Bill et al. 2000; Desmurs et al. 2002).

The Lanzo massif is considered a part of the lithospheric mantle exhumed at the ocean floor during opening of the Jurassic-Piedmont Ligurian ocean (Lagabrielle et al. 1989; Pognante et al. 1985). Recent studies demonstrate that the presence of a high-temperature mantle shear zone between the north and the central part of the massif is related to rapid mantle exhumation. This exhumation is presumably active during the earliest stages of the formation of embryonic oceanic crust (chapter 2).

4.3 FIELD OCCURRENCE OF MAFIC DIKES IN THE LANZO MASSIF

The Lanzo massif contains numerous intrusive rocks ranging from coarse-grained troctolites, olivine-gabbros to fine-grained basaltic dikes. A geological map illustrates the heterogeneous spatial distribution of gabbroic and basaltic dike and their relative orientation with respect to the high-temperature foliation in the peridotite (Fig. 4.1). In the northern part of the massif, gabbro dikes are not observed. From the central to the southern part of the massif, mafic dikes are progressively more abundant, increase in size and are preferentially found toward the west (Fig. 4.1). The structurally earliest gabbros are represented by small dikelets or lenses of gabbro in the central part of the massif within granular lherzolite (Fig. 4.2a). Gabbro to gabbronorite dikelets are one to four centimeters thick and rarely exceed 10 to 40 cm in length. In the south part of the massif, dikelets are more abundant than in the central part and are composed of cm-scale clinopyroxene and plagioclase (Fig. 4.2b). The dikelets show fuzzy contacts with the country-rock peridotite and can be surrounded by a dunitic zone (Fig. 4.2b) where euhedral to subhedral spinel is preserved. The presence of dikelets and mega-crystals of clinopyroxene associated to plagioclase in dunite are precursors to gabbroic dikes (Müntener and Piccardo 2003; Müntener et al. 2005; Piccardo et al. 2004). The dikelets of cm-scale with fuzzy contacts are clearly different to intrusive dikes, which show sharp and discordant contacts with the pyroxenite layering and the high-temperature foliation. The thickness of gabbros varies from 5 to 40 cm (locally exceeding 1m) while basalts vary between 15 and 30 cm (Fig. 4.2c and 4.2d). Gabbro dikes are generally thicker in the southern part of the massif (10 cm to several meters, Fig. 4.2d; 4.2e). Most of the dikes are troctolite, to olivine gabbros, to kaersutite and Fe-Ti gabbro with rare plagiogranites. In the southern part of the massif, gabbroic dikes may be flanked by symmetric dunitic zones, which are proportional in size to the gabbro dikes (Fig. 4.2e). Basaltic dikes are rare throughout the massif and mostly present in the western central part (close to the shear zone in Fig. 4.1) where they cut and have sharp contact with the undeformed to mylonitic peridotite (Fig. 4.2d).

4.4 PETROGRAPHY OF ZIRCON BEARING GABBRO DIKES

Five samples from the Lanzo peridotitic massif (four ferro-gabbros and one plagiogranite) were selected for geochronological investigations because of their high modal zircon content. Two gabbros (L165, V14) and the plagiogranite (V16) were sampled in the central part and the two other gabbros (A71, A91) are from the south part of the

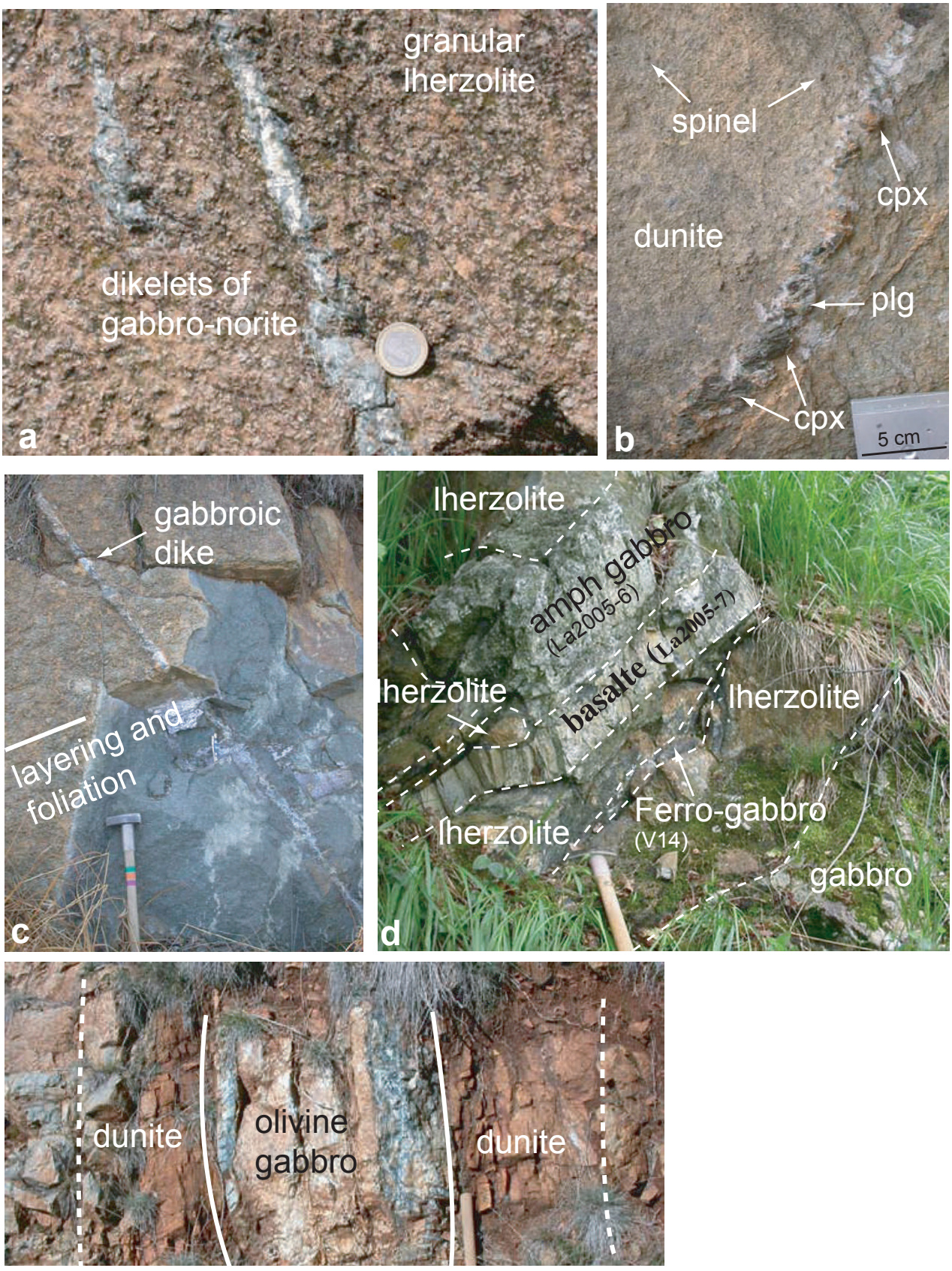

Fig. 4.2: Field photographs of gabbroic and basaltic dikes. (a) Dikelets of gabbro-norite within lherzolite from the central part of the Lanzo massif (diameter of coin is: 2 cm); (b) Dikelet of gabbro within dunite from the south part of the Lanzo massif; (c) Gabbroic dikes cross cut the pyroxenite layering and the high-temperature foliation in the central part of the massif; (d) The peridotite is cross cut by a Fe-Ti gabbro (V14) and a gabbro body (La2002-06) which in turn is cross cut by a basaltic dike (La2002-07). Central part of the massif (for location see Fig. 4.1); (e) Gabbroic dike with symmetric dunite zones from the southern part of the massif.

massif (for location see Fig. 4.1).

The Fe-gabbro **L165** is located in the footwall of a km-scale shear zone that separates the north from and the central part of the Lanzo massif (Fig. 4.1). The outcrop is located along the road between the villages of Castagnole and Maddalene (Fig. 4.2), where ferro-gabbros, several olivine gabbro dikes and a basaltic dike cut the peridotite (Kaczmarek and Müntener 2005). The 5 cm thick dike has sharp contacts to the host peridotite. The dike contains a mylonitic shear zone in the central part underlined by the crystallization of oriented kaersutite, plagioclase and ilmenite (Fig. 4.3a). Two parts can be distinguished: (i) a light coloured domain, which corresponds to former plagioclase, now present as a fine-grained symplectite of jadeite and quartz, associated with zoisite and garnet; (ii) a brown to greenish domain mainly composed of magmatic amphibole and ilmenite. The amphibole is partially replaced by a corona of white or green amphibole and ilmenite, which is probably exsolved from the primary Ti-rich hornblende (Fig. 4.3c). The minerals are parallel to the shear zone in the central part of the sample and indicate shearing close to the boundary (Fig. 4.3a). The shear zone concentrates brown, Ti-rich hornblende, ilmenite, zircon and apatite (Fig. 4.3a and 4.3c). Hypidiomorphic zircon crystals are concentrated in the central shear zone and generally range from 100 μm to 250 μm in size with some smaller grains (20 μm) also found.

Sample **A91** is from the southern part of the Lanzo massif (Fig. 4.1) and was sampled in a gabbro-rich area (1km long) containing numerous mostly undeformed troctolite and olivine gabbros, and several Fe-Ti gabbros. The dike is ~7 cm thick and shows a syn-magmatic shear zone in the central part (Fig. 4.3b and 4.3d). Ti-hornblende, ilmenite, apatite and zircon are concentrated within the shear zone with large T-hornblende crystals concentrated at the border. The white domains (Fig. 4.3d) represents former igneous plagioclase and now consists of metamorphic jadeite + quartz symplectites associated with ilmenite and garnet. The white matrix contains garnet, zoisite, tremolite, titanite, chlorite and plagioclase. Zircons are concentrated in the shear zone (grain size between 60 μm and 250 μm) suggesting localized flow of Zr-saturated, differentiated melt.

V14a is a hornblende-gabbro (7 cm thickness) cross cutting a peridotite associated with a gabbro body (Fig. 4.2e). The sample is composed of cm-scale, magmatic Ti-hornblende with ilmenite inclusions parallel to the contact with the host peridotite and surrounded by a matrix of granoblastic hornblende (mm grain size). Small zircons and apatite (~20 μm) are found in the granoblastic hornblende matrix. The white domains are ghosts of igneous plagioclase now transformed into jadeite + quartz symplectites plus zoisite and/or clinozoisite.

The ferro-gabbro **A71** (60 cm thickness) shows a mineralogical variation expressed by a higher concentration of Fe-Ti minerals (e.g. ilmenite) close to the walls. Similar to smaller Fe-Ti gabbros, this sample is composed of white and black spots containing both magmatic and metamorphic parageneses. The white areas, are composed of a matrix of chlorite and chloritoid, and contain relics of rutile rimmed by titanite. The black areas are composed of centimetric ilmenite replaced along grain boundaries by zoisite, garnet and chlorite. The relict magmatic paragenesis is represented by igneous clinopyroxene and euhedral zircons (20 to 150 μm in length Fig. 4.3e).

V16b is a white to greenish fine-grained meta-plagiogranite about 8 cm thick that has sharp contacts with the host peridotite. The meta-plagiogranite is composed of a matrix of omphacite, zoisite, chlorite, clinozoisite, and symplectite areas of jadeite + quartz. The sample is extremely rich in euhedral zircons (Fig. 4.3f) intergrown with inclusion-rich apatite. The presence of allanite, rutile and omphacite in the matrix suggests partial recrystallization at high-pressure conditions.

4.5 ANALYTICAL TECHNIQUES

The samples were crushed with an agate mill to reduce trace element contamination. Whole rock glasses were prepared with the addition of Li-Tetraborate (dilution at 1:10). Gabbros and basalts were analyzed by wavelength-dispersive X-ray fluorescence spectroscopy (XRF, Phillips PW 1404) at the University of Fribourg (Switzerland). Trace element precision is generally better than 5%. All trace element analyses for basalts and Fe-Ti gabbros were obtained by Laser Ablation ICP-MS on the glasses using a pulsed 193nm Excimer Laser system (Lambda Physik, Geolas 200M), coupled with an ICP-MS (Perkin Elmer DRC 6200), at the

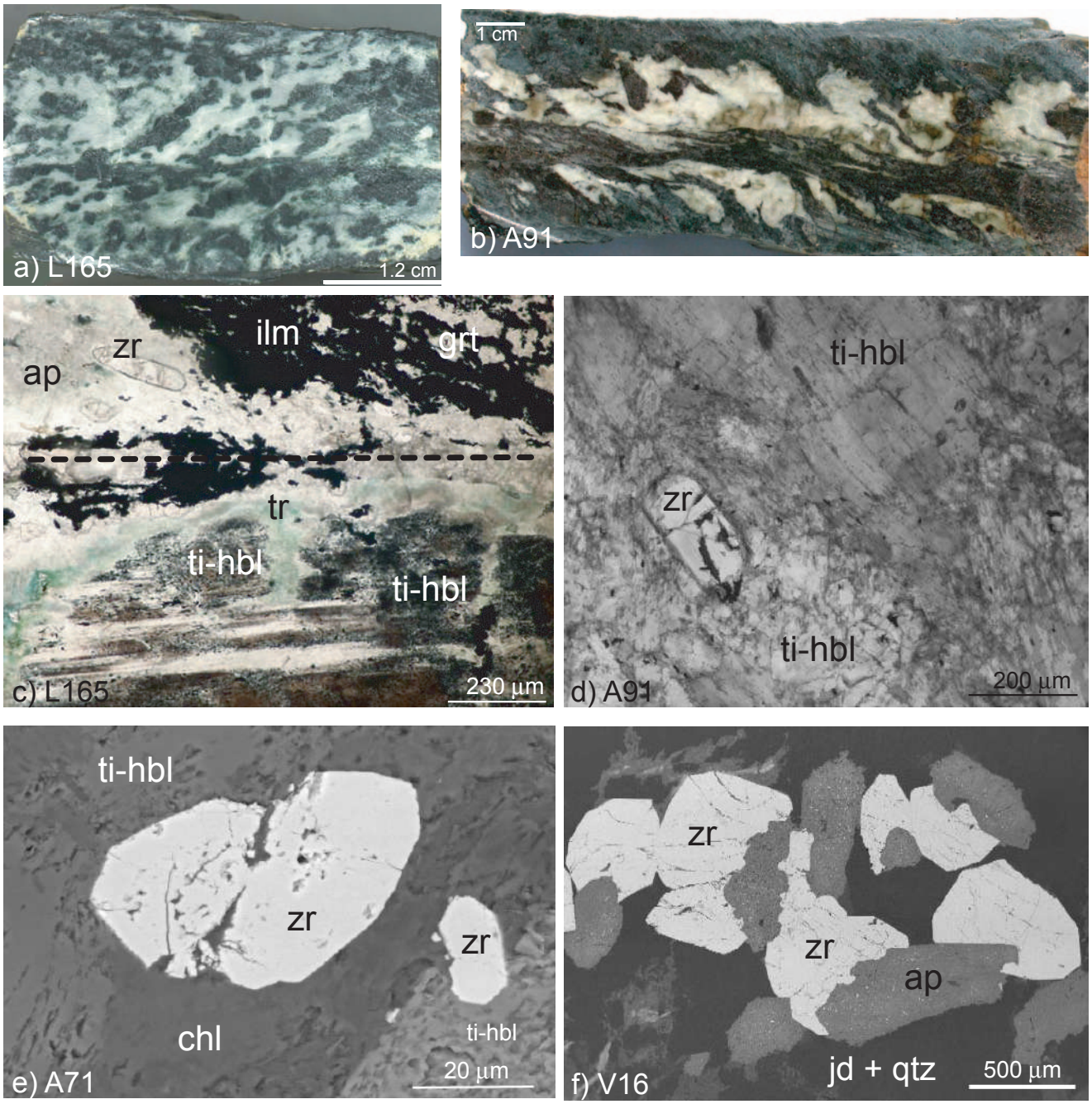

Fig. 4.3: Macro- and microscopic textures of gabbros: (a) Ferro-gabbro (L165) with a central fine-grained shear zone (dashed line; see photomicrograph in c) and syn-magmatic orientation of minerals; (b) Ferro-gabbro (A91) with zircon-ilmenite-hornblende-rich central shear zone discordant to igneous clinopyroxene and plagioclase; (c) Microphotograph (plane polarized light) of the shear zone within sample L165 (dashed line) with enrichment of ilmenite, apatite and zircon; (d) Photomicrograph of sample A91 showing a large zircon crystal associated with hornblende, in the central part of the sample (plane polarized light); (e) SEM image of idiomorphic zircon crystals (sample A71); (f) SEM image of plagiogranite (V16) with euhedral zircon and apatite, embedded in a matrix of metamorphic jadeite and quartz. Abbreviations are: Ti-hbl: Ti-rich hornblende; ilm: ilmenite; ap: apatite; zr: zircon; tre: tremolite; grt: garnet; chl: chlorite; jad: jadeite; qtz: quartz.

University of Lausanne, with operating conditions of 27kV, and 10Hz repetition rate, yielding a flux of ca 12J/cm^2 on the ablation site. Helium was used as a carrier gas. The NIST 610 glass was chosen as an external standard, and Ca as the internal standard. BCR2 basaltic glass was used to monitor the reproducibility and accuracy of the system.

Olivine gabbros and troctolite whole rock trace elements (REE, Cs, Rb, Th, U, Nb, Ta, Sr, Zr, Hf) were analyzed by a VG-PQ2 Turbo + Inductively Coupled Plasma-Mass Spectrometer (ICP-MS) at ISTEEM (Université Montpellier II, Montpellier,

France) and are reported in Table 4.2. REE, Cs, Rb, Pb, Th, U, Sr, Zr, and Hf concentrations were determined by external calibration following the $HF/HClO_4$ dissolution and analytical procedure described in detail by Ionov et al. (1992). To avoid memory effects due to the intake of concentrated Nb–Ta solutions in the instrument, Nb and Ta concentrations were determined by using Zr and Hf, respectively, as internal standards. This technique is an implementation to ICP-MS analysis of the method described by Jochum et al. (1990). Detection limits obtained by long-term analyses of chemical blanks at ISTEEM can be found in Ionov et al. (1992).

For zircon separation all samples were crushed and sieved to less than 250 μm. Zircons were separated according to magnetic properties and density and finally selected by hand picking. Zircons separated were mounted on a 25 mm epoxy discs and polished down to expose the grain centers. The internal zoning was investigated by a cathodoluminescence (CL) detection system at the Electron Microscope Unit at the Australian National University (ANU) with a HITACHI S2250-N scanning electron microscope operating at 15kv accelerating potential, ~60 μA current and 20 mm working distance.

Trace element analyses on zircons were performed by Laser Ablation ICP-MS at the Research School of Earth Sciences, ANU using a pulsed 193-nm ArF Excimer laser, with 100mJ energy at a repetition rate of a 5Hz, coupled to an Agilent 7500 quadrupole ICP-MS (Eggins et al. 1998). During the time-resolved analysis, the contamination from inclusions, fractures and zones of different composition was detected by monitoring several elements. It might, however, not have been possible to eliminate all contaminations from micro inclusions whose signal was spread over the entire analysis. In specific cases it was chosen to present analyses containing inclusions in order to identify the compositions of the inclusions and/or have information on the elements not affected by the inclusions (e.g. Y will not be affected by a plagioclase inclusion). Analysis spot size was 24 or 32 μm in diameter. External calibration was performed relative to NIST 612 glass using the concentration given in Pearce et al. (1996). Internal standard was Si.

U-Th-Pb analyses of zircons were performed with a Sensitive High Resolution Ion Microprobe (SHRIMP II) at the ANU using a beam size of ~25 μm. Analytical procedures were similar as described by Compston et al. (1984). The measured U-Pb ratios were corrected using the standard zircon TEM (417 Ma, Black et al. 2003), which was analyzed each fourth analysis. A zircon of knows composition (SL13) has been used to determine the U content of zircon. The data were corrected for common Pb on the basis of the measured $^{207}Pb/^{206}Pb$ ratios as described in Compston et al. (1992) and assuming a common Pb composition according to the model of Stacey and Kramers (1975). The analytical uncertainty in the reproducibility of the U-Pb age of the standard was between 2.2 and 2.4 % (2σ). Age calculations were done using the software Isoplot/Ex (Ludwig 2003). Mean ages are intercept ages in uncorrected $^{207}Pb/^{206}Pb$ versus $^{238}U/^{206}Pb$ (Tera Wasserburg) diagrams and are given at 95% confidence level.

4.6 WHOLE ROCK MAJOR AND TRACE ELEMENT GEOCHEMISTRY

The whole rock analyses were performed on discordant mafic dikes, on the entire compositional spectrum of oceanic gabbros, ranging from troctolite (L44a, La2002-4) to olivine gabbro (L13g, Mu6, A16) to Fe-Ti gabbro (A91, L165, A71, La2005-6). We also analyzed one plagiogranite (V16), and two basalts (L132a, La2005-7), although these rocks are strongly overprinted by Alpine metamorphism. Results on major and trace element chemistry are summarized in tables 4.1 and 4.2, additional analyses might be found elsewhere (Bodinier et al. 1986; Piccardo et al. 2007; Pognante et al. 1985).

4.6.1 Major and minor elements

The chemical evolution of the Lanzo gabbros is well reflected by the variation of bulk Mg# (calculated as molar $Mg/Mg+Fe_{tot}$, all Fe as Fe^2). Some gabbros have elevated Mg# at relatively high Zr content indicating substantial exchange with the host peridotite (Tab. 4.1). The Al_2O_3 content varies from ~12 to 21 wt% and is highest for troctolite (27.84 wt%). Basalts, ferro-gabbros and amphibole gabbro have high TiO_2 contents compared to olivine-gabbros and troctolite, but olivine-gabbros

are particularly rich in Ni (368 and 524 ppm).
Ferro-gabbros have high Zr contents (150-314 ppm) and an exceptionally high Zr value is reported for the plagiogranite (3352 ppm, not shown in Fig. 4.4b). In contrast to ferro-gabbros, the olivine-gabbro and troctolite have low Zr contents (<10 ppm), in agreement with Zr concentration known from previous studies of the Lanzo gabbros (Bodinier et al. 1986; Pognante et al. 1985). The Mg# shows a large variation: from 0.47 to 0.88, with the higher Mg# and Al_2O_3 contents are observed in the olivine-gabbro, troctolite and plagiogranite (Tab. 4.1). The TiO_2 increase reflects the differentiation of the different gabbro types, from olivine-gabbros and troctolite (0.05 to 0.21 wt%) to ferro-gabbros (1.99 to 4.65 wt%, Fig. 4.4c and Tab. 41). The plagiogranite shows low concentration of TiO_2 (0.32 wt%), low SiO_2 and very high Mg#, indicating substantial metasomatic exchange with the peridotite, either during ocean floor alteration, or during high-pressure metamorphism. The composition in Ti and P of troctolite, olivine-gabbros and plagiogranite are depleted compared to ferro-gabbros (Tab. 4.1 and Fig. 4.4). The general trend, from olivine-gabbros to ferro-gabbros, shows a Zr, Ti, Y enrichment and a Ni decrease.
The basaltic dikes show little variation in terms of their Mg# (0.55-0.62), except for the rodingite sample (L124a) which has a Mg# of 0.68 (Tab. 4.1) and contain elevated Zr contents (110 to 279 ppm, Fig. 4.4b). The Al_2O_3 and TiO_2 contents are similar to basalts from the Western Alps and from the Lanzo massif (Bodinier et al. 1986; Pognante et al. 1985, Fig. 4.4c). The Lanzo basalts display a positive correlation of Mg# with Ni and a negative correlation with TiO_2.

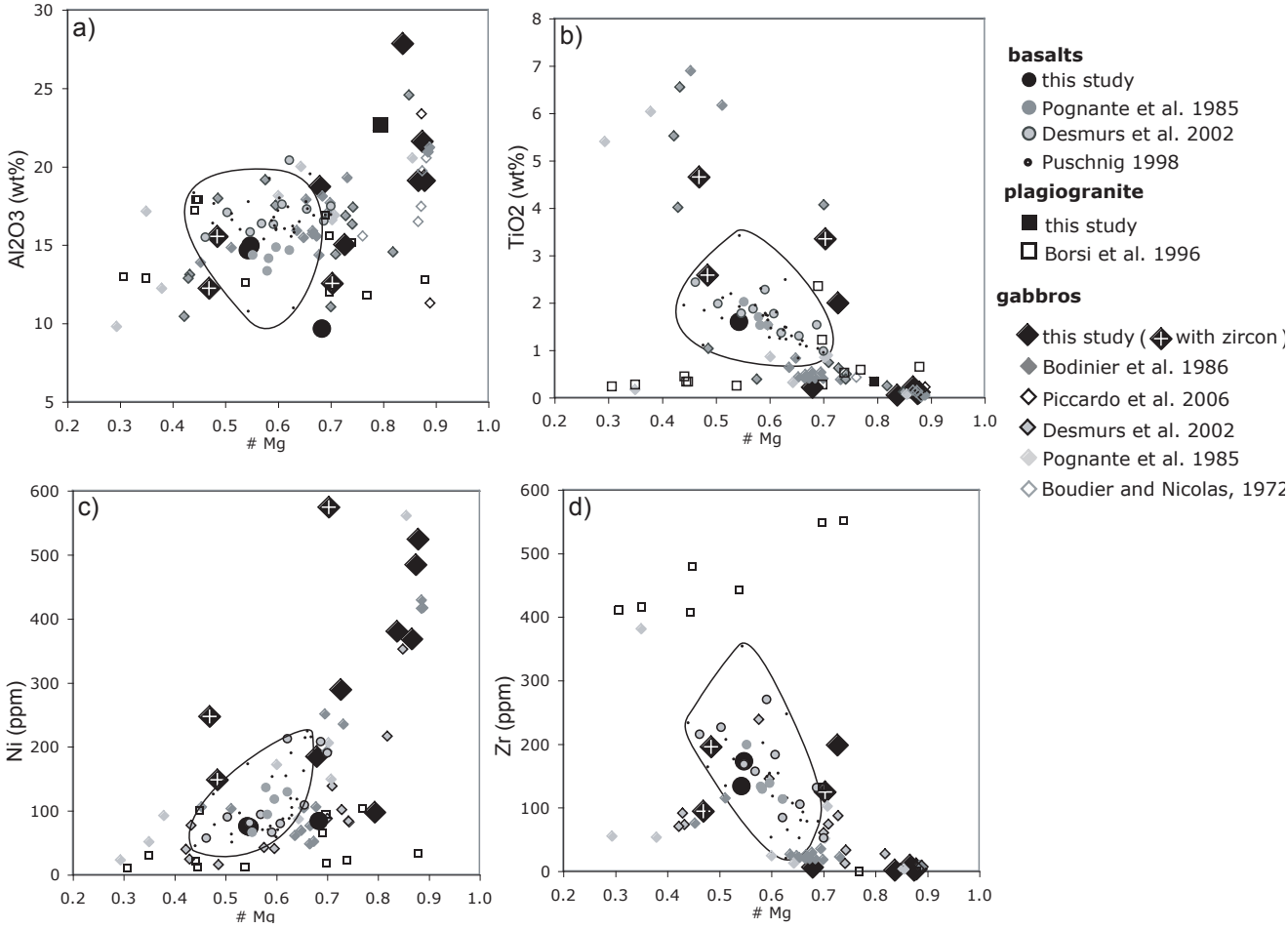

Fig. 4.4: Major and trace element variation diagrams of mafic rocks from the Lanzo massif: (a) Mg# (molecular Mg/(Mg+Fe_{tot})) vs Al_2O_3; (b) Mg# vs TiO_2; (c) Mg# vs Ni (ppm); (d) Mg# vs Zr (ppm). Additional data from the Lanzo massif are from Boudier and Nicolas (1972), Piccardo et al. (2007), Bodinier et al. (1986) and Pognante et al. (1985); Additional data from the Alpine-Apennine system are plotted for comparison (Borsi et al. 1996; Desmurs et al. 2002; Puschnig 1998). The black line encloses the basalt field.

4.6.2 Rare earth elements

Lanzo troctolites to olivine-gabbros display a large positive Eu anomaly (Eu/Eu* = Eu_N /(Sm_N + Gd_N)/2 from 6.8 to 2.0). The positive Eu anomaly illustrates that the Lanzo troctolites and olivine-gabbros are cumulates from which substantial amounts of derivative liquid has been extracted. The $(Ce/Yb)_N$ varies from < 1 to 2.8 and suggests variable proportions of clinopyroxene and plagioclase, and possibly variable amounts of trapped liquids, as illustrated by interstitial Ti-hornblende in some samples. The exceptionally high $(La/Yb)_N$ at very low heavy REE (e.g. Yb_N: 0.54) indicates plagioclase-rich troctolite layers in some places supporting the cumulate nature of much of the primitive Lanzo gabbros.

Fe-Ti gabbros are characterized by a relatively flat REE pattern with a weak fractionation of light to middle REE, and $(Gd/Yb)_N$ > 1 (Fig. 4.5a). The chondrite normalized REE diagram of zircon-bearing rocks highlights two samples (A91 and La2005-6) with a negative Eu anomaly, one sample relatively flat in REE pattern (L165) and one sample with a positive Eu anomaly (A71, Fig. 4.5a and Tab. 4.2). From sample A71 to La2005-6, the overall distribution is similar and shows REE enrichment. The Sr content correlates positively with the Eu anomalies suggesting that plagioclase controls the Sr budget of the whole rocks (Tab. 4.1).

The plagiogranite is enriched in incompatible elements and has a U-shaped REE pattern with a very low and a pronounced negative Eu anomaly (0.30), indicating plagioclase fractionation prior to crystallization. In addition, the plagiogranite is enriched in HFSE and Sr (Fig. 4.5a, Tab. 4.1).

Basalt analyses are plotted in figure 4.5b, together with previously published Instrumental Neutron Activation Analysis data (Bodinier et al. 1986; Pognante et al. 1985) and compared to other basalt occurrences in the Alps (Desmurs et al. 2002). The basalts from Lanzo are homogeneous in REE, show $(La/Yb)_N$ close to unity and are analogue to N-MORB compositions. The general trend is close to those of ferro-gabbros but the REE content is lower (Tab. 4.2). In contrast to basalts from various places from the Alps (Desmurs et al. 2002) the variation in REE is rather limited and T- to E-MORB compositions have not been found.

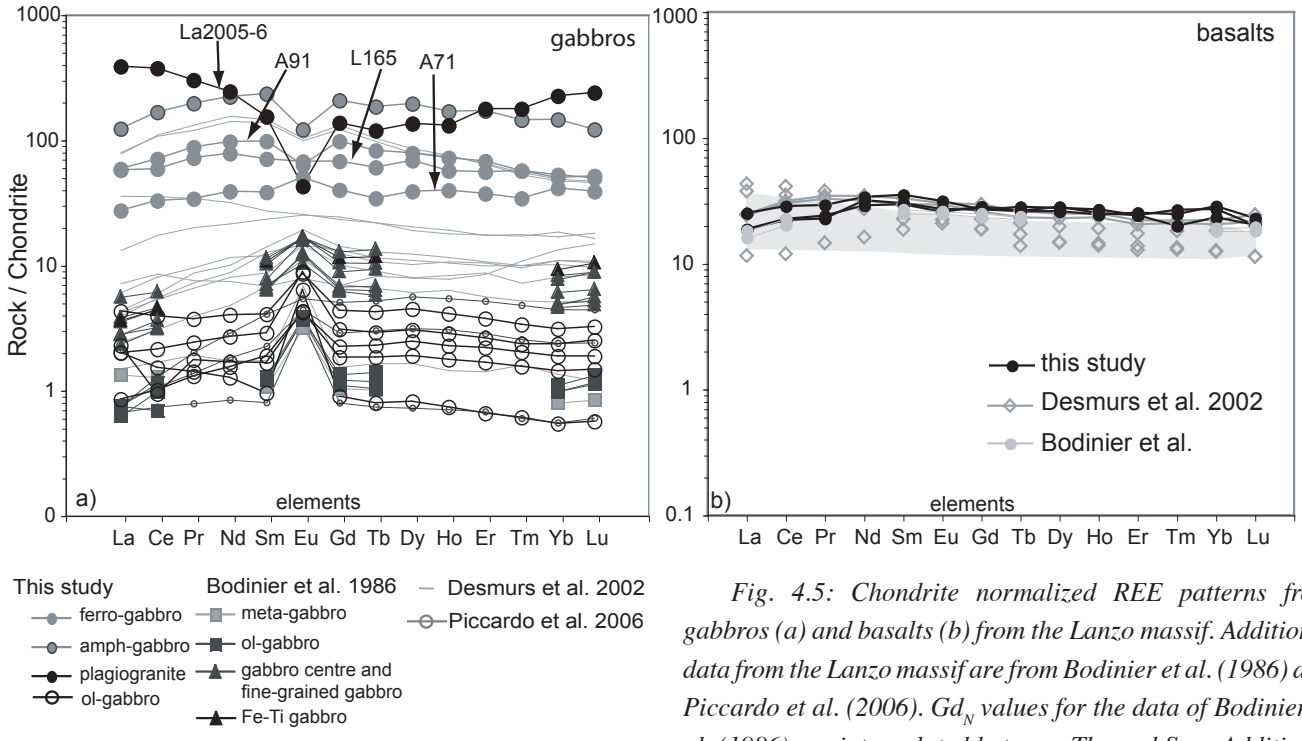

Fig. 4.5: Chondrite normalized REE patterns from gabbros (a) and basalts (b) from the Lanzo massif. Additional data from the Lanzo massif are from Bodinier et al. (1986) and Piccardo et al. (2006). Gd_N values for the data of Bodinier et al. (1986) are interpolated between Tb_N and Sm_N. Additional data sources are Desmurs et al. (2002) and Beccaluva et al. (1984, grey area). Normalization values for chondrite are taken from Sun and McDonough (1989).

Table 4.1: XRF major and trace element analyses of basalts and gabbros. Basalts (L132a, La2005-7), rodiginte (L124a), ferro-gabbro with zircon (L165, A71b, A91a), amphibole-gabbro (La2005-6), olivine-gabbro (L13g, Mu6, A16), meta-troctolite (L44a) and leuco-troctolite (La2002-4), and plagiogranite (V16). For Zr analyzed by XRF, values below 10ppm are considered unreliable. In Fig. 4.4b, we used data from laser ablation ICP-MS (Zr).*

	basalt			**ferro-gabbro + Z**			**amph-g**	**ol gabbro**			**troctolite**		**plg-granite**
sample	L132A	LA2005-7	L124a	L165	A71	A91	LA2005-6	L13G	Mu6	A16	L44A	LA2002-4	V16
SiO2	50.78	51.74	46.93	55.43	39.08	46.47	55.00	50.86	50.70	51.58	40.84	52.22	51.78
TiO2	1.69	1.80	1.61	2.57	4.65	3.34	1.99	0.22	0.11	0.08	0.05	0.21	0.34
Al2O3	14.71	14.99	9.71	15.54	12.23	12.53	15.01	19.09	19.10	21.60	27.84	18.71	22.69
FeO tot	10.02	9.32	7.52	7.40	18.74	8.68	4.84	2.90	2.85	2.16	2.47	7.25	1.33
MnO	0.17	0.19	0.25	0.14	0.36	0.15	0.09	0.06	0.05	0.04	0.09	0.12	0.05
MgO	6.65	6.31	9.07	3.91	9.30	11.59	7.23	10.58	11.59	8.49	7.17	8.64	2.87
NiO	0.00	0.00	0.00	0.00	0.00	0.00	0.00	0.00	0.00	0.00	0.00	0.00	0.00
CaO	9.94	8.23	23.75	5.87	15.03	9.81	7.50	12.79	12.25	12.00	20.87	8.18	14.33
Na2O	5.61	6.91	0.97	8.52	0.36	5.77	7.01	3.36	3.01	3.75	0.37	4.55	5.62
K2O	0.11	0.10	0.00	0.06	0.02	0.03	0.10	0.06	0.03	0.03	0.00	0.04	0.01
P2O5	0.19	0.24	0.18	0.45	0.04	1.44	1.09	0.00	0.00	0.00	0.00	0.02	0.45
LOI	-0.13	0.52	0.31	0.17	1.81	2.01	1.12	2.34	1.34	1.19	3.5	0.12	1.17
Total	99.1	100.2	99.2	99.0	99.4	99.9	99.0	99.1	99.0	99.1	99.5	99.2	98.7
Mg#	0.54	0.55	0.68	0.48	0.47	0.70	0.73	0.87	0.88	0.88	0.84	0.68	0.79
Cr	193	126	180	47	-7<	162	160	139	1988	1489	293	25	9
Ni	77	75	85	148	247	574	289	368	524	484	380	184	97
Cu	70	19	77	95	15	6	3	8	12	-3<	-1<	41	9
Zn	70	53	45	47	54	34	21	15	13	12	44	39	13
Pb	16	3<	6<	5<	14	9	17	2<	2<	2<	4<	3<	2<
Rb	5	-2<	-1<	5	3	0<	3	-1<	-0<	1<	-2<	3<	-1<
Sr	124	616	16	237	228	270	509	499	247	297	2294	260	1340
Y	32	36	33	74	49	107	250	1<	-1<	-2<	-3<	1<	281
Zr	*201*	*279*	*12*	*263*	*150*	*192*	*314*	*56*	*31*	*33*	*195*	*35*	*3352*
Zr*	135	173	153.4	195	94	124	198	8.5	3.0	1.3	1.1	5.9	3040
Nb	<1	-1<	<1	6	2<	6	19	-1<	-3<	-2<	-3<	-3<	25

Table 4.2: Trace element composition of basalts and gabbros measurements by LA-ICP-MS. Abbreviations as in table 4.1.

	basalt			**ferro-gabbro + Z**			**amph-g**	**ol gabbro**			**troctolite**		**plg-gran**
sample	L132A	LA2005-7	L124a	L165	A71	A91	LA2005-6	L13G	Mu6	A16	L44A	LA2002-4	V16
Sc	41	39	38	28	70	46	38	29	21	14	3	17	3
V	283	300	261	109	388	205	211	105	94	72	45	76	41
Rb	0.75	0.43	0.16	0.58	2.15	0.29	0.79	0.41	0.24	0.73	0.21	0.31	0.38
Sr	117	613	15	229	226	258	477	486.5	239	290	2191	253	1241
Y	37	40	37	87	52	108	256	5.8	4	4	1	4	248
Zr	135	173	153	195	94	124	198	9.4	3	2	1	5	3040
Nb	2.0	2.5	2.1	5.9	3.6	4.1	11.0	0.1	0.1	-	0.1	0.0	13.7
Cs	0.04	0.05	0.13	0.19	0.10	0.01	0.05	0.09	0.03	0.04	0.10	0.01	0.00
Ba	6.7	17.7	3.9	4.2	11.7	5.8	13.2	14.5	2.4	6.2	7.6	13.9	9.0
Cr	343	216	260	155	112	262	219	205	1948	1645	352	79	100
Ni	79	79	73	131	216	549	251	325	410	474	355	168	94
Co (wt%)	31	32	27	16	59	34	18	19	26	19	17	41	7
Zn	63	51	40	43	49	29	23	17	10	15	44	39	20
Pb	13	1.6	4	2.3	12	10	9	2.6	1.7	1.1	1.8	2.3	8
Th	0.14	0.20	0.24	0.30	0.18	0.14	0.2	0.00	-0.06	-0.02	0.07	0.05	3.2
U	0.13	0.05	0.06	0.08	0.10	0.06	0.3	0.08	-0.05	-0.01	0.05	0.02	1.0
La	4.4	6.0	4.5	13.8	6.5	14.0	29.5	1.02	0.20	0.55	0.48	0.48	92.2
Ce	13.6	17.6	13.9	36.2	20.3	43.8	103.4	2.43	0.62	0.58	0.94	1.32	231.6
Pr	2.1	2.7	2.2	6.7	3.2	8.2	18.4	0.35	0.12	0.16	0.13	0.23	28.2
Nd	14.6	15.5	13.3	36.0	17.9	44.6	102.3	1.86	0.71	0.78	0.58	1.24	112.7
Sm	4.5	5.2	4.4	10.6	5.7	14.6	35.0	0.61	0.28	0.25	0.14	0.43	23.0
Eu	1.5	1.8	1.5	3.8	2.9	3.6	6.9	0.49	0.24	0.24	0.36	0.50	2.4
Gd	5.3	5.4	5.7	13.6	8.0	19.7	41.5	0.87	0.45	0.37	0.18	0.62	27.5
Tb	1.0	0.9	1.0	2.2	1.2	3.0	6.7	0.15	0.08	0.07	0.03	0.11	4.3
Dy	6.8	6.4	6.9	17.1	9.6	19.5	48.4	1.11	0.61	0.47	0.20	0.75	33.6
Ho	1.5	1.3	1.4	3.1	2.2	4.0	9.3	0.23	0.13	0.10	0.04	0.16	7.2
Er	3.9	4.1	3.9	9.0	6.0	10.9	27.7	0.61	0.35	0.27	0.11	0.42	28.7
Tm	0.5	0.6	0.7	1.4	0.9	1.4	3.6	0.08	0.05	0.04	0.02	0.06	4.4
Yb	3.7	4.6	4.4	8.1	6.7	8.6	23.6	0.50	0.30	0.23	0.09	0.38	36.5
Lu	0.5	0.6	0.5	1.3	1.0	1.2	3.0	0.08	0.05	0.04	0.01	0.06	5.9
Hf	3.0	4.0	2.9	6.5	2.4	2.9	6.0	0.11	0.08	0.09	0.06	0.08	64.5
Ta	0.10	0.22	0.15	0.55	0.22	0.35	0.41	0.56	0.25	-	-	0.19	0.82

4.7 ZIRCON DESCRIPTION

The zircon grains from mylonitic ferro-gabbro **L165** are transparent and 200 to 300 μm in size. They often appear like fragments of larger euhedral crystals. Oscillatory zoning can be present, but the majority of crystals are characterized by irregular sectors with different CL emission or patchy zoning (Fig. 4.6a). They often present a network of sealed fractures that cut across the zoning and along which low luminescence zircon is present (Fig. 4.6b).

Fe-gabbro **A71** contains transparent light pink zircon fragments between 80 to 400μm in size, which only occasionally preserve pyramidal faces. Growth zoning is rare (Fig. 4.6c) and most of the crystals are CL-dark and either unzoned (Fig. 4.6d) or patchy zoned and rich in mineral inclusions (Fig. 4.6e). In the mylonitic Fe-gabbro **A91**, zircons are similar to A71 for size and shape, but more often preserve growth zoning. One remarkable zircon from A91 has a more complex structure with a dark center with remnants of growth zoning that is cross cut by fractures and surrounded by an unzoned, bright rim (Fig. 4.6f). Several larger crystal display patchy zoning (Fig. 4.6g), but the majority of grains corresponds to small, unzoned fragments (ca. 100 μm), with moderate CL emission. The plagiogranite (**V16**) contains euhedral zircons (100-500 μm) that are clear and transparent with a well-developed oscillatory-sector growth zoning (Fig. 4.6h-i).

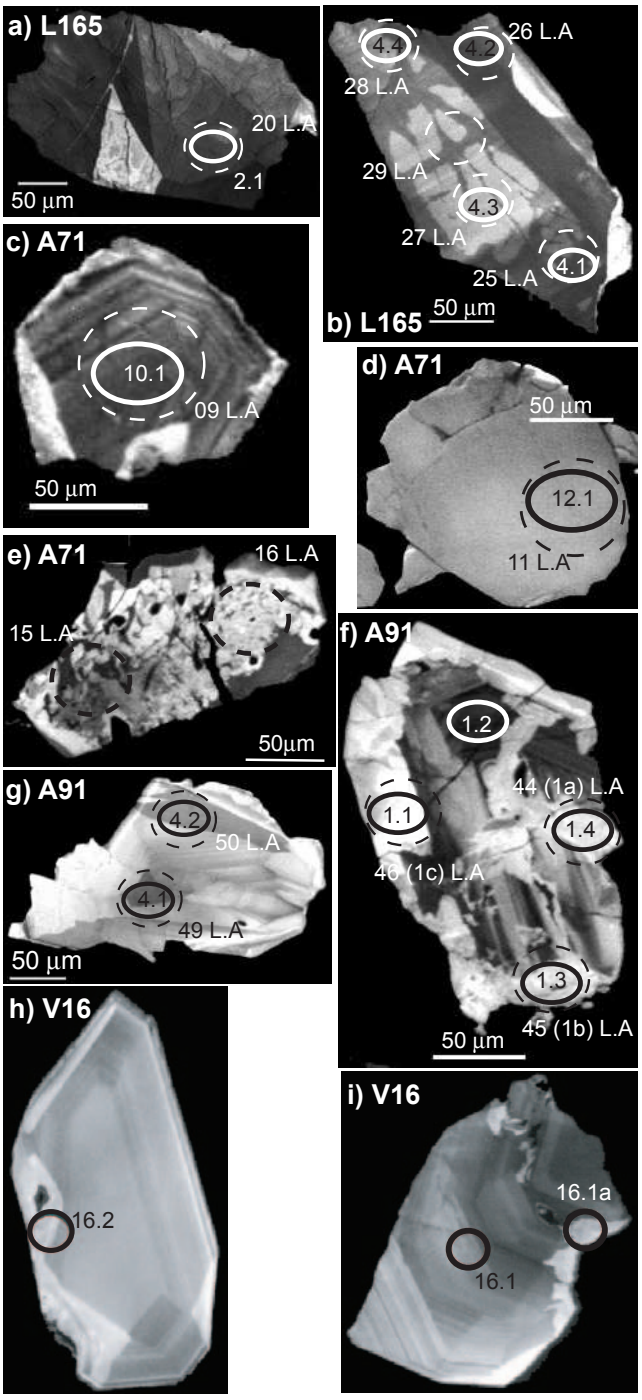

Fig. 4.6: Cathodoluminescence images of dated zircons from three ferro-gabbros (L165 in a-b, A71 in c-e and A91 in f-g) and the plagiogranite V16 (h-i). Solid circles: SHRIMP analyses and numbering associated (e.g. 2.1); dotted circles: LA-ICPMS analyses and numbering associated (e.g. 20 LA, and reported in Tab. 4.3). See text for discussion.

4.8 ZIRCON COMPOSITION

Zircon crystals from three of the dated samples were analyzed for their trace element composition by LA-ICPMS (Tab. 4.3, Fig. 4.7 and 4.8). Th and U contents were also measured during SHRIMP analysis (Tab. 4.4) and values are generally comparable to LA-ICPMS results. Occasionally, higher Th and U contents were measured by SHRIMP because the limited volume of the analysis allowed targeting small CL-dark and thus U and Th-rich domains.

Zircon in the three samples have U and Th contents from low (a few ppm) to moderate (several hundreds of ppm), which vary significantly even within a sample, particularly in L165 and A71. Zircons in gabbro A91 are the most homogeneous with the lowest contents in Th, U and P. Zircons from all samples contain comparable average Ti concentrations around 15-25 ppm. However, similarly to U and Th, significant variations in Ti are detected in zircons from sample A71 and A91 where an extreme value of 145 ppm was

measured.

Zircons from sample A71 show a strong variation in a number of elements including P, Ti, Sr, Y and Yb. Some of these variations might be due to the presence of micro inclusions of apatite (Sr and P) and/or xenotime (P, Y and Yb). In fact, analyses performed on patchy-zoned and inclusion-rich zircon (such as those shown in Fig. 4.6e) resulted in irregular trace-element distribution throughout the analyses. For comparison, two of these analyses are plotted in figures 4.7 and 4.8 (A71 inclusion-rich) and show systematically high Y, Sr, Ca, Yb and P contents. On the other hand, zircons from sample A91, which display well-developed growth zoning and are generally free of fractures and inclusions, have a more homogeneous trace element composition. This suggests that their composition is effectively reflecting crystallization from the melt and is not contaminated by micro-inclusions.

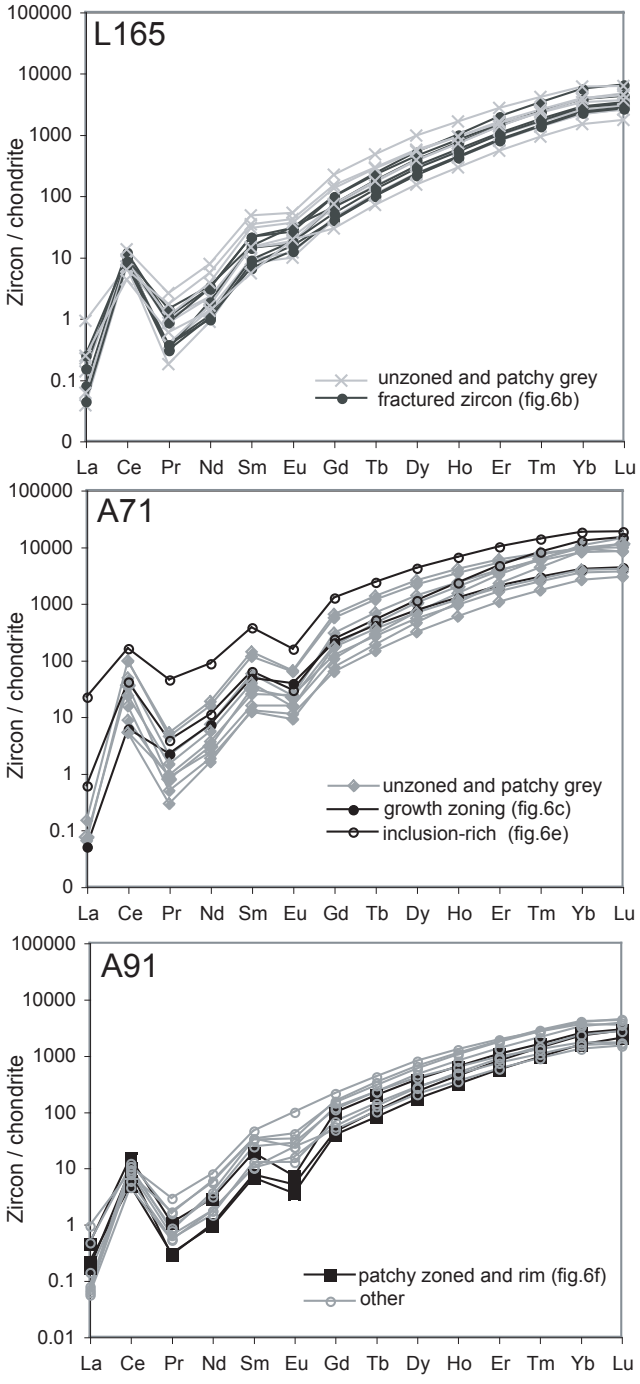

Fig. 4.7: Chondrite normalized REE diagrams of zircons from Fe-gabbros L165, A 91, and A 71. Normalization values for chondrite are taken from Sun and McDonough (1989).

The chemical composition of the zircons follows the differentiation trend defined by bulk rock composition (A91 to A71). There is a slight increase of incompatible elements in zircon from sample A91 and L165 to A71 ($\Sigma_{(Sm\text{-}Lu)}$)= 869, 1075 and 2490, respectively). The chondrite-normalized REE pattern of zircons from the three samples (Fig. 4.8) is enriched in heavy-REE with respect to the light-REE, as typical for magmatic zircon (Hinton and Upton 1991). Despite the variation within a single sample, HREE enrichment in zircon is broadly decreasing with differentiation (i.e. from sample A91 to L165 and A71), whereas the negative Eu anomaly increases (Tab. 4.3 and Fig. 4.7) and correlates with Y contents (Fig. 4.8a). The Eu anomaly suggests plagioclase fractionation in the magma and is in line with a magmatic origin of the zircon. Two analyses in sample L165 have a slight positive Eu anomaly, which is attributed to micro inclusions of plagioclase. Because most trace elements are orders of magnitude lower in plagioclase than in zircon (except Sr and LREE) these analyses are still considered valid for all other elements. All zircon also have a positive Ce anomaly (Fig. 4.7) originated from the Ce^{3+} oxidized to Ce^{4+}, which better fits the Zr site in zircon (Hinton and Upton 1991).

4.9 U-PB GEOCHRONOLOGY

U-Pb ages were obtained from 3 samples (L165, A91 and A71) for which the $^{206}Pb/^{238}U$ ages are discussed below (Tab. 4.4). Zircons analyses from **L165** (n=15 from 9 crystals) have a Th/U mainly between 0.34 and 0.65 with the exception of one analysis with a ratio of 3.25 due to very high Th contents. In this sample there is no apparent correlation between age and internal structure,

Table 4.3:Trace element compositions of zircons measured by LA-ICP-MS from ferro-gabbro samples (L165, A71 and A91).

L165	**P**	**Ti**	**Sr**	**Y**	**Nb**	**La**	**Ce**	**Pr**	**Nd**	**Sm**	**Eu**	**Gd**	**Tb**	**Dy**
19-L165b-1	402.9	15	4.6	906	0.63	0.21	4.3	0.09	1.0	2.1	1.0	13	5	74
20-L165b-2	527.6	16	4.2	1222	1.12	0.03	5.7	0.08	1.0	2.1	1.2	14	6	92
21-L165b-3.1	383.3	13	0.8	710	0.55	0.01	4.3	0.02	0.4	1.2	0.54	8	4	54
24-L165b-3.2	363.5	15	1.4	745	0.57	0.05	4.3	0.03	0.6	1.4	0.67	9	4	58
25-L165b-4.1	701.7	19	5.6	1719	1.87	0.04	7.5	0.10	1.4	3.1	1.7	20	8	128
26-L165b-4.2	477.5	12	2.7	1354	0.73	0.02	5.8	0.08	1.4	3.2	1.5	19	8	110
27-L165b-4.3	490.4	13	0.7	1253	0.98	bdl	6.2	0.03	0.9	2.1	0.92	15	6	95
28-L165b-4.4	466.5	17	7.5	978	1.18	0.06	5.9	0.13	1.5	2.2	1.7	13	5	76
29-L165b-4.5	506.4	12	0.7	1230	0.90	bdl	5.4	0.04	0.7	2.1	0.97	15	6	93
30-L165b-5	456.5	13	3.4	1503	0.50	0.01	5.2	0.10	1.7	4.4	2.0	26	10	131
31-L165b-6.1	662.8	14	1.2	2583	1.02	bdl	8.1	0.24	3.5	7.0	3.0	44	17	235
34-L165b-7.2	445.4	11	1.7	910	0.60	bdl	5.3	0.04	0.5	1.3	1.0	10	5	69
35-L165b-7.1	354.9	16	1.6	750	0.61	bdl	4.8	0.03	0.5	1.0	0.71	8	4	57
36-L165b-7.3	346.8	13	3.7	717	0.57	0.01	4.7	0.03	0.4	1.1	0.86	8	4	53
37-L165b-9	396.9	20	1.7	1470	0.42	bdl	3.8	0.16	2.5	5.1	2.3	30	10	138
Likely plagioclase inclusion														
38-L165b-10	296.3	15	4.3	491	0.44	0.06	2.6	0.05	0.6	0.8	1.1	6	3	37
41-L165b-15	425.9	16	53	1448	0.49	0.62	7.5	0.53	4.6	4.8	5.6	26	9	124

A71	**P**	**Ti**	**Sr**	**Y**	**Nb**	**La**	**Ce**	**Pr**	**Nd**	**Sm**	**Eu**	**Gd**	**Tb**	**Dy**
04-A71b-1	177	5	2.1	2681	2.2	bdl	5.3	0.08	1.1	2.3	0.88	21	10	173
06-A71b-3	321	8	1.4	1540	0.7	bdl	3.2	0.09	1.7	3.7	1.3	24	9	134
07-A71b-5	728	51	6.7	6650	2.8	bdl	58	0.48	8.5	21	3.7	128	49	626
08-A71b-7	1447	20	1.2	3731	1.9	0.02	29	0.19	3.4	8.5	1.3	59	25	340
09-A71b-10	676	5	1.9	3311	8.3	0.02	22	0.07	1.4	4.6	1.2	36	16	250
10-A71b-11	1083	31	2.4	5274	12	0.04	60	0.42	7.1	17	3.5	110	42	531
11-A71b-12	427	15	0.8	1982	0.8	0.01	3.8	0.21	3.4	7.1	2.2	41	15	189
14-A71b-14	389	15	0.7	997	1.1	bdl	3.2	0.03	0.7	1.9	0.63	13	5	76
17-A71b-15	167	5	1.2	1956	3.3	bdl	9.4	0.05	0.8	1.8	0.51	15	7	114
18-A71b-18	332	16	0.8	1900	2.5	bdl	15	0.14	2.5	5.7	0.85	33	13	169
15-A71b-19	2908	42	15	4008	18	0.14	25	0.36	5.2	9.3	1.7	47	19	280
16-A71b-19	2002	16	12	10056	11	5.35	100	4	40	55	8.8	249	86	1040

A91	**P**	**Ti**	**Sr**	**Y**	**Nb**	**La**	**Ce**	**Pr**	**Nd**	**Sm**	**Eu**	**Gd**	**Tb**	**Dy**
43-A91-1a	323	11	0.8	557	0.29	0.1	3.0	0.03	0.4	1.0	0.20	8	3	41
45-A91-1b	611	21	1.1	1131	0.36	0.1	9.2	0.10	1.3	2.7	0.40	19	7	91
46-A91-1c	443	16	0.6	740	0.44	0.0	5.5	0.03	0.5	1.1	0.29	9	4	56
47-A91-2	822	145	0.3	1024	0.56	bdl	7.4	0.14	2.7	4.9	1.3	24	8	99
48-A91-3	680	22	0.9	1812	0.50	0.0	6.7	0.07	1.7	4.7	1.9	31	12	160
49-A91-4.1	819	34	0.7	2058	0.91	0.1	6.5	0.27	3.7	6.7	5.5	42	15	197
50-A91-4.2	665	28	0.7	1682	0.59	0.0	4.8	0.15	2.5	4.9	2.3	29	11	144
51-A91-5	400	33	0.6	745	0.33	0.0	3.7	0.05	0.7	1.9	0.72	13	5	68
54-A91-15	508	22	1.1	825	0.48	0.2	5.3	0.06	0.8	1.5	0.89	11	4	64
55-A91-18	572	23	0.6	1328	0.49	0.0	5.8	0.08	1.4	3.6	1.6	22	8	114
56-A91-10	416	35	0.5	570	0.33	0.0	2.8	0.05	0.8	1.5	1.3	10	4	50

Table 4.3: continued.

L165	**Ho**	**Er**	**Tm**	**Yb**	**Lu**	**Hf**	**Ta**	**Th**	**U**	**Th\U**	**Eu/Eu***	**Ce/Ce***
19-L165b-1	30	157	40	403	73	8331	0.34	11	23	0.48	0.47	7
20-L165b-2	39	220	58	625	115	10630	0.77	125	286	0.44	0.51	19
21-L165b-3.1	23	126	33	347	63	9264	0.35	12	31	0.40	0.40	65
24-L165b-3.2	24	132	33	354	63	8565	0.33	10	19	0.53	0.45	24
25-L165b-4.1	55	315	82	897	161	9751	1.10	149	486	0.31	0.50	20
26-L165b-4.2	44	235	59	604	105	10334	0.54	110	220	0.50	0.44	20
27-L165b-4.3	41	223	58	610	110	10386	0.75	109	252	0.43	0.38	64
28-L165b-4.4	31	170	44	464	83	10639	0.54	99	209	0.48	0.77	12
29-L165b-4.5	39	220	57	605	109	10181	0.76	97	237	0.41	0.39	46
30-L165b-5	51	260	63	638	108	8806	0.36	21	37	0.57	0.45	15
31-L165b-6.1	88	433	101	981	151	9555	0.75	311	572	0.54	0.40	10
34-L165b-7.2	29	158	41	444	78	10516	0.49	82	193	0.43	0.58	46
35-L165b-7.1	24	133	35	381	68	10523	0.47	56	149	0.38	0.52	51
36-L165b-7.3	23	128	34	366	65	10546	0.39	54	143	0.38	0.64	37
37-L165b-9	50	247	56	542	90	6075	0.16	5	7	0.67	0.46	7
38-L165b-10	16	87	23	240	42	8410	0.23	3	7	0.35	1.13	10
41-L165b-15	48	246	61	601	99	8621	0.32	16	28	0.57	1.23	3

A71	**Ho**	**Er**	**Tm**	**Yb**	**Lu**	**Hf**	**Ta**	**Th**	**U**	**Th\U**	**Eu/Eu***	**Ce/Ce***
04-A71b-1	82	513	146	1692	350	10588	0.51	270	353	0.76	0.26	20
06-A71b-3	51	261	61	562	90	8794	0.56	22	47	0.48	0.32	11
07-A71b-5	221	947	189	1492	202	5874	1.84	159	78	2.04	0.17	36
08-A71b-7	128	620	142	1298	204	8868	1.82	236	146	1.62	0.13	45
09-A71b-10	107	595	151	1534	275	10229	9.55	591	423	1.40	0.21	82
10-A71b-11	188	844	178	1531	239	7539	3.94	140	112	1.25	0.19	42
11-A71b-12	69	327	73	654	106	8061	0.52	21	33	0.62	0.31	5
14-A71b-14	32	173	42	415	72	8006	0.63	11	29	0.38	0.29	36
17-A71b-15	56	360	108	1331	283	9910	0.62	186	264	0.71	0.21	62
18-A71b-18	63	303	68	624	100	7958	1.38	13	22	0.61	0.15	32
15-A71b-19	129	761	202	2059	367	7789	4.91	219	196	1.11	0.20	19
16-A71b-19	360	1608	342	2972	459	7121	2.53	131	120	1.09	0.19	5

A91	**Ho**	**Er**	**Tm**	**Yb**	**Lu**	**Hf**	**Ta**	**Th**	**U**	**Th\U**	**Eu/Eu***	**Ce/Ce***
43-A91-1a	17	90	23	249	50	11682	0.12	68	32	2.12	0.16	18.8
45-A91-1b	34	168	40	399	71	11900	0.21	149	76	1.95	0.12	19.7
46-A91-1c	24	129	34	360	69	11484	0.39	25	41	0.61	0.20	39.6
47-A91-2	34	151	32	271	41	7899	0.22	3	5	0.73	0.31	15.6
48-A91-3	60	292	69	653	105	10137	0.30	67	70	0.95	0.36	25.1
49-A91-4.1	71	309	66	580	86	9337	0.45	73	105	0.69	0.76	6.3
50-A91-4.2	57	277	65	633	110	9456	0.37	57	60	0.94	0.47	9.0
51-A91-5	25	117	26	246	40	7738	0.11	24	14	1.77	0.32	17.3
54-A91-15	27	139	36	372	67	9728	0.26	12	23	0.53	0.49	11.0
55-A91-18	44	215	52	528	93	9960	0.38	29	38	0.75	0.42	20.5
56-A91-10	19	93	22	213	37	7402	0.10	8	8	1.01	0.81	15.9

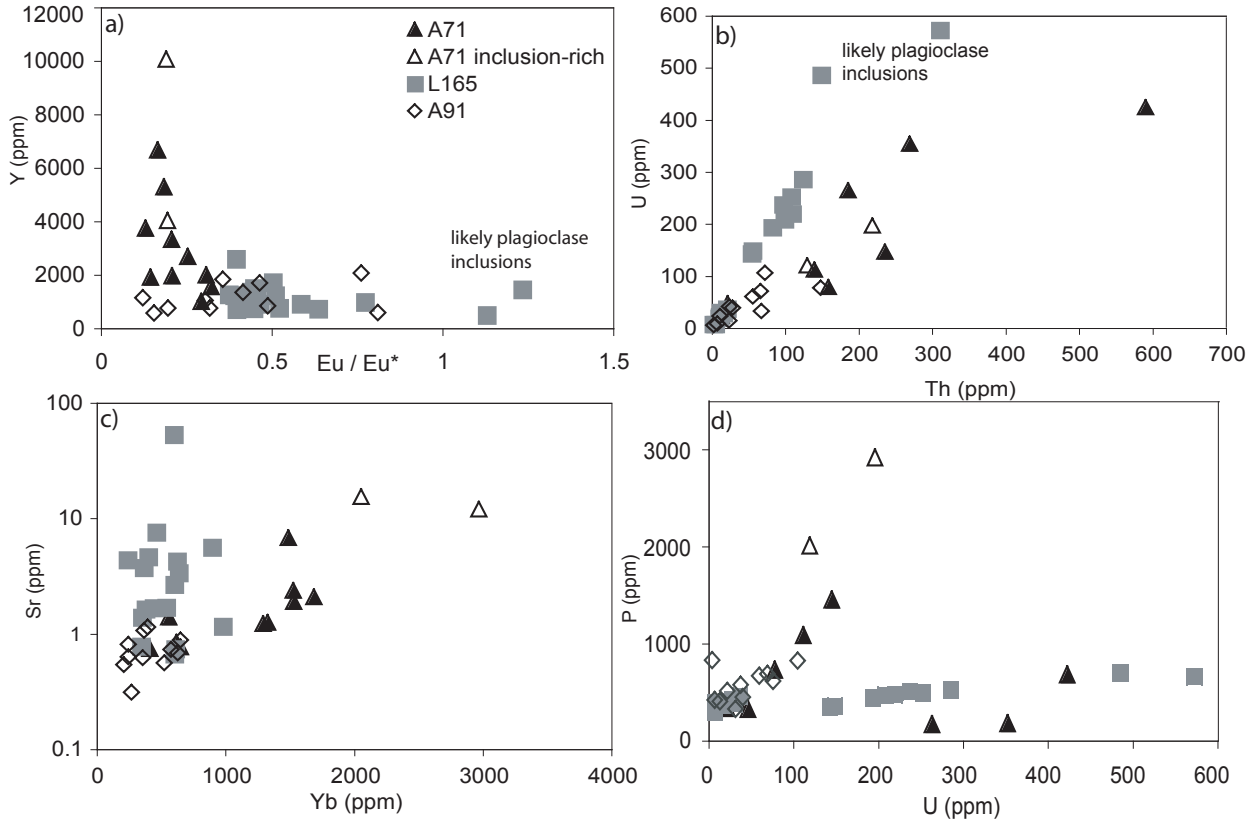

Fig. 4.8 Zircon trace element composition measured by LA-ICP-MS. (a) Eu/Eu vs Y. Zircons from A71 have substantially more negative Eu anomalies and tend to much higher Y contents with respect to the other samples. (b) Th vs U. Zircons from different samples show two different Th/U ratio trends, which are probably controlled by coexisting silicate liquids. (c) Sr vs Yb. (d) U vs P. Some analyses show Sr > 10ppm and P > 2000 ppm, which might be related to apatite micro-inclusions. See text for further discussion.*

with CL-dark zones along fractures yielding the same age as pristine magmatic zones (Fig. 4.6). The $^{206}Pb/^{238}U$ ages range from 151 ± 6 to 167 ± 4 Ma. Two analyses (L165-9.1 and L165-11.1) that contain a high percent of common Pb (12 and 39 %) and large analytical errors were excluded from the age calculation. Of the remaining analyses, 13 form a tight cluster with an intercept age of 162 ± 2 Ma (MSWD = 1.6, Fig. 4.9a). Two analyses, including the one with high Th, yielded significantly younger ages and are suspected of Pb loss. The intense fracturing of zircons and Alpine metamorphism could be the likely cause of Pb loss. At these young ages, even discordant analyses are close to Concordia and discordance cannot be necessarily identified with the present analytical errors. Therefore, analyses affected by Pb loss might still be analytically concordant, but their exclusion from average age calculations is justified on statistical and geological reasons.

A large number of analyses (n=24) were performed on zircon from metagabbro **A91** because of the complex texture observed. The chemistry of the dated domains is quite variable with U between 5-469 ppm, Th between 4-1480 ppm and Th/U from 0.04 to 3.15. The $^{206}Pb/^{238}U$ ages range between 136 ± 16 Ma and 173 ± 5 Ma, with large analytical errors and high common Pb (up to 44%) in domains with low U contents. Four analyses on unzoned rims (Fig. 4.6f) or bright domains yielded significantly younger ages and are excluded from the age calculation. The remaining analyses correspond to oscillatory-zoned domains as well as to unzoned or bright domains and define a regression line to common Pb with a lower intercept of 158 ± 2 Ma (MSWD = 1.7, Fig.9b).

Seventeen analyses on zircon from Fe-gabbro **A71** yielded variable U and Th composition (28-760 and 11-1051 ppm, respectively) with resulting Th/U between 0.4 and 3.2. Fifteen analyses range in age from 155 ± 2 to 166 ± 4 Ma and define an intercept age of 163 ± 1 Ma (MSWD = 1.2). Two analyses resulting in significantly younger ages are excluded from the age calculation.

A small number of analyses (n=3) were performed on zircons from the plagiogranite **V16**. $^{206}Pb/^{238}U$ ages of these oscillatory zones domains are between 161 ± 4 Ma and 167 ± 8 Ma (Tab. 4.4). These data are insufficient to define a robust regression in a Tera-Wasserburg diagram, but are sufficient to suggest that this rock type is within the same range of the Fe-gabbros.

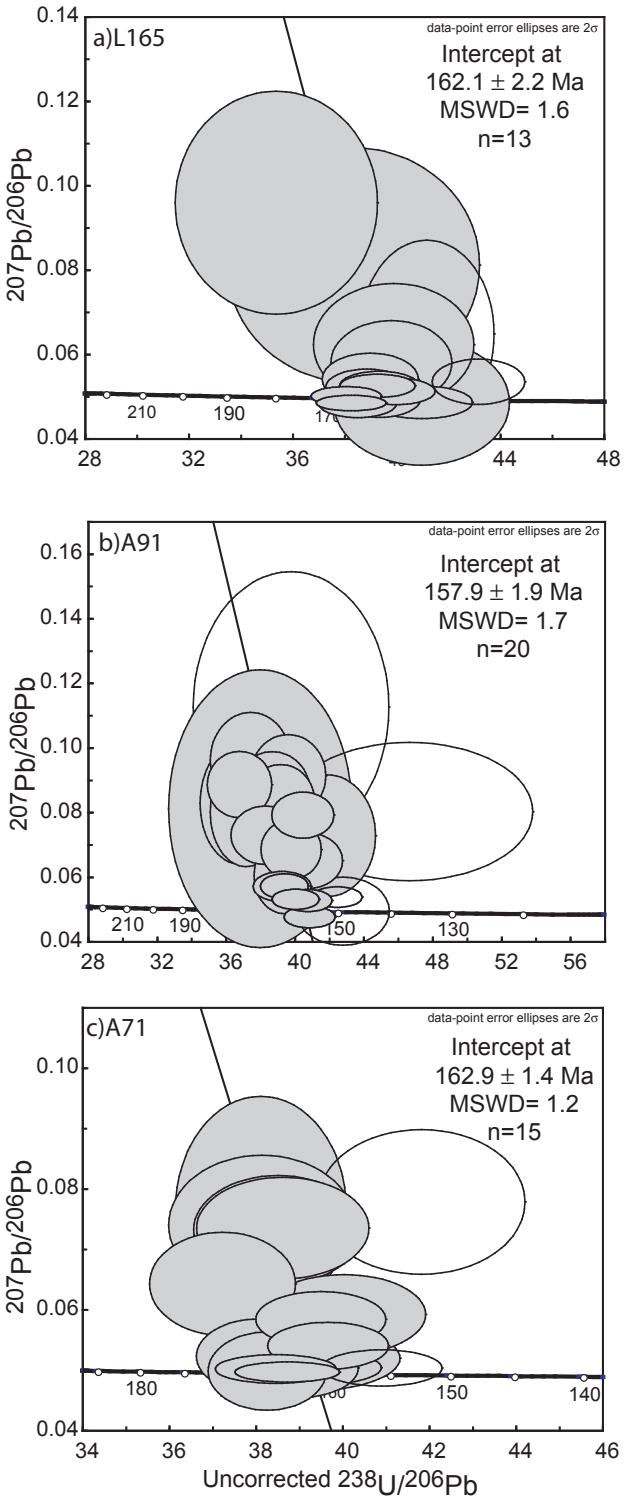

Fig. 4.9: Tera-Wasserburg diagram for uncorrected isotopic ratios for zircons of samples L165, A71 and A91. Ages are calculated as Concordia intercept at 95% c.l of a regression line anchored to the common Pb composition predicted by the Stacey and Kramers (1975) model. Empty ellipses are excluded from the average age calculation.

4.10 DISCUSSION

4.10.1 Chemical differentiation of mafic rocks

The Lanzo mafic rocks show a tholeiitic differentiation trend, covering the entire range of gabbroic rocks, from primitive plagioclase-rich troctolite and olivine-gabbros, to Fe-Ti gabbros and plagiogranite (e.g. Pognante et al. 1985). This range is typical for some other ophiolites from the Western, Eastern Alps and Northern Apennine (Costa and Caby 2001; Desmurs et al. 2002; Serri 1980; Tribuzio et al. 2004).

The large variation of Mg# (Fig. 4.4) indicates that most dikes record differentiation processes and only a few samples provide evidence of being crystallized from primitive liquids. The high Mg# (up to 0.9) and high Al_2O_3 contents in olivine-gabbros and troctolites are consistent with being cumulates crystallized from primitive basalts with Mg# ~0.7, taking olivine-liquid partition coefficients of ~0.3 (Roeder and Emslie 1970). However, basalts with Mg# of ~0.7 are extremely rare (Fig. 4.4) and the average Mg# of basalts recovered from various fragments of the Tethyan oceanic crust is around 0.6 (Fig. 4.4). Thus, there must be an important volume of plutonic rocks in the mantle to account for the differentiated composition of most basalt. The high Mg# troctolites and olivine gabbros are low in incompatible trace elements like Ti, Zr and P and would thus fulfill the criteria of being the complementary cumulates of evolved basalts.

The three zircon-bearing ferro-gabbros have substantially higher Zr compared to average Fe-Ti gabbros. The high Zr contents could be partly explained by migration of highly differentiated melts along shear zones from a cumulate pile beneath the actual level of crystallization.

The Eu anomaly in zircon-bearing Fe-Ti gabbros varies from positive to negative suggesting that these gabbros had a different genesis. The three-fold increase of whole rock REE element enrichment is related to differentiation. However,

Table 4.4: U/Pb Th, and SHRIMP analyses of the zircons.

Grain spot	U (ppm)	Th (ppm)	Th/U	Pb* (ppm)	Pb comm 206 %	uncorrected 207Pb/206Pb	uncorrected 238U/206Pb	206Pb/238U ± (1)	ages (Ma) 206Pb/238U 208 cor	CL structure
L165B.1.1	84	47	0.55	1.9	0.52	0.055 ±2	39.0 ± 0.8	0.0256 ± 5	**162 ± 3**	zoned
L165B.2.1	310	137	0.44	6.7	0.41	0.052 ± 1	40.0 ± 0.6	0.0250 ± 4	**159 ± 3**	patchy
L165B.3.1	33	12	0.38	0.7	2.02	0.066 ± 9	41.2 ± 1.1	0.0243 ± 6	**152 ± 4**	unzoned
L165B.3.2	19	9	0.50	0.4	2.76	0.063 ± 6	39.9 ± 1.3	0.0251 ± 8	**155 ± 6**	unzoned
L165B.4.1	385	132	0.34	8.4	0.26	0.054 ± 1	39.3 ± 0.6	0.0255 ± 4	**162 ± 3**	new zoning
L165B.4.2	199	113	0.57	4.2	0.12	0.050 ± 2	41.0 ± 0.8	0.0244 ± 5	**155 ± 3**	new zoning
L165B.4.3	240	94	0.39	5.3	0.16	0.050 ± 1	38.5 ± 0.6	0.0260 ± 4	**165 ± 3**	unzoned
L165B.4.4	228	103	0.45	5.0	0.29	0.054 ± 1	39.3 ± 0.6	0.0254 ± 4	**161 ± 3**	patchy
L165B.5.1	39	21	0.55	0.8	1.56	0.059 ± 4	39.8 ± 1.0	0.0251 ± 6	**157 ± 4**	unzoned
L165B.6.1	776	442	0.57	17.4	<0.01	0.050 ± 1	38.3 ± 0.6	0.0261 ± 4	**167 ± 3**	patchy
L165B.6.2	622	326	0.52	14.0	0.01	0.051 ± 1	38.1 ± 0.6	0.0263 ± 4	**167 ± 4**	patchy
L165B.7.1	157	58	0.37	3.5	0.25	0.053 ± 2	38.9 ± 0.7	0.0257 ± 4	**163 ± 3**	unzoned
L165B.7.2	194	78	0.40	4.2	<0.01	0.051 ± 2	39.4 ± 0.6	0.0254 ± 4	**162 ± 4**	on fracture
L165B.8.1	162	527	3.25	3.2	<0.01	0.055 ± 2	43.2 ± 0.7	0.0232 ± 4	**151 ± 6**	patchy
L165B.10.1	16	10	0.59	0.3	0.10	0.050 ± 6	41.0 ± 1.4	0.0244 ± 8	**155 ± 6**	patchy
A71.1.1	499	394	0.79	11.2	<0.01	0.051 ± 1	38.5 ± 0.6	0.0260 ± 4	**166 ± 3**	patchy
A71.2.1	436	881	2.02	9.5	<0.01	0.051 ± 1	39.2 ± 0.7	0.0255 ± 4	**166 ± 4**	unzoned
A71.3.1	61	28	0.47	1.4	4.01	0.074 ± 3	38.6 ± 0.8	0.0256 ± 5	**158 ± 4**	unzoned
A71.5.1	92	185	2.01	2.0	2.36	0.060 ± 3	40.0 ± 0.8	0.0250 ± 5	**155 ± 5**	patchy
A71-6.1	111	40	0.36	2.5	1.86	0.053 ± 2	38.1 ± 0.6	0.0263 ± 4	**166 ± 3**	unzoned
A71-7.1	109	139	1.27	2.4	0.98	0.051 ± 2	38.9 ± 0.6	0.0257 ± 4	**163 ± 3**	patchy
A71-8.1	174	94	0.54	3.9	0.00	0.051 ± 3	38.3 ± 0.6	0.0261 ± 4	**166 ± 3**	patchy
A71-9.1	85	45	0.53	1.9	6.48	0.053 ± 2	39.2 ± 0.9	0.0255 ± 6	**162 ± 4**	unzoned
A71-10.1	760	1051	1.38	16.9	0.49	0.051 ± 1	38.7 ± 0.5	0.0258 ± 3	**164 ± 3**	growth
A71-11.1	121	140	1.16	2.6	4.96	0.059 ± 2	39.5 ± 0.6	0.0253 ± 4	**161 ± 3**	patchy
A71-12.1	39	23	0.59	0.9	16.80	0.074 ± 4	38.5 ± 0.8	0.0260 ± 5	**163 ± 4**	unzoned
A71-13.1	28	11	0.38	0.6	22.69	0.074 ± 5	38.1 ± 0.9	0.0262 ± 6	**163 ± 4**	patchy
A71-14.1	37	13	0.35	0.8	21.05	0.077 ± 8	38.1 ± 0.8	0.0262 ± 6	**164 ± 4**	growth
A71-15.1	206	630	3.06	4.5	3.73	0.055 ± 2	39.7 ± 0.6	0.0252 ± 4	**162 ± 5**	patchy
A71-16.1	57	55	0.97	1.3	11.20	0.065 ± 3	37.2 ± 0.7	0.0269 ± 5	**166 ± 4**	growth
A71-17.1	273	268	0.98	5.7	1.95	0.051 ± 1	40.9 ± 0.6	0.0244 ± 3	**155 ± 3**	patchy
A71-18.1	30	19	0.61	0.6	20.14	0.078 ± 5	41.8 ± 1.0	0.0239 ± 6	**149 ± 4**	patchy
A91-1.1	36	33	0.91	0.7	<0.01	0.051 ± 4	42.8 ± 1.1	0.0234 ± 6	**151 ± 5**	rim
A91-1.2	469	1480	3.15	9.9	<0.01	0.049 ± 1	40.9 ± 0.6	0.0245 ± 4	**158 ± 5**	growth
A91-1.3	30	66	2.21	0.6	8.63	0.074 ± 8	41.9 ± 1.1	0.0239 ± 7	**159 ± 7**	rim
A91.1.4	13	35	2.63	0.2	15.54	0.081 ± 9	46.7 ± 2.9	0.0214 ± 13	**136 ± 16**	rim
A91.2.1	5	4	0.81	0.1	30.25	0.113 ± 17	39.8 ± 2.3	0.0251 ± 15	**150 ± 11**	patchy
A91.2.2	5	4	0.75	0.1	6.82	0.082 ± 17	38.0 ± 2.2	0.0263 ± 15	**156 ± 12**	unzoned
A91-3.1	68	58	0.85	1.5	13.73	0.070 ± 4	39.8 ± 0.7	0.0251 ± 5	**159 ± 3**	patchy
A91-4.1	123	87	0.71	2.7	1.36	0.059 ± 2	39.3 ± 0.7	0.0255 ± 4	**162 ± 3**	patchy
A91-4.2	62	58	0.93	1.4	6.02	0.062 ± 5	39.4 ± 0.7	0.0254 ± 5	**161 ± 4**	patchy
A91-5.1	22	42	1.93	0.5	23.09	0.084 ± 8	36.8 ± 1.0	0.0227 ± 7	**172 ± 7**	unzoned
A91-6.1	31	1	0.04	0.7	12.09	0.081 ± 7	37.2 ± 0.8	0.0269 ± 16	**167 ± 4**	patchy
A91-7.1	259	398	1.54	5.2	4.82	0.055 ± 1	42.5 ± 0.6	0.0235 ± 3	**151 ± 3**	patchy
A91-8.1	29	46	1.59	0.6	22.39	0.088 ± 5	38.7 ± 0.9	0.0258 ± 6	**163 ± 6**	unzoned
A91-9.1	48	32	0.67	1.0	5.65	0.067 ± 3	40.8 ± 0.8	0.0245 ± 5	**156 ± 4**	patchy
A91-11.1	244	176	0.72	5.2	4.65	0.055 ± 1	40.1 ± 0.6	0.0250 ± 3	**158 ± 2**	patchy
A91-12.1	212	372	1.76	4.5	1.88	0.054 ± 1	40.8 ± 0.6	0.0245 ± 3	**158 ± 3**	growth
A91-13.1	200	131	0.66	4.3	5.42	0.059 ± 2	39.4 ± 0.6	0.0254 ± 4	**161 ± 3**	patchy
A91-14.1	24	18	0.74	0.5	44.74	0.097 ± 6	37.4 ± 1.0	0.0627 ± 7	**165 ± 5**	patchy
A91-15.1	47	21	0.45	1.0	23.85	0.074 ± 4	38.3 ± 0.8	0.0261 ± 6	**164 ± 4**	unzoned
A91-16.1	42	43	1.02	0.9	22.69	0.085 ± 5	39.2 ± 0.8	0.0255 ± 5	**160 ± 4**	patchy
A91-17.1	42	46	1.09	0.9	13.30	0.081 ± 5	38.9 ± 0.8	0.0257 ± 5	**162 ± 4**	patchy
A91-18.1	40	42	1.03	0.9	20.22	0.090 ± 4	36.8 ± 0.8	0.0272 ± 6	**173 ± 5**	unzoned
A91-19.1	82	70	0.85	1.7	13.00	0.080 ± 3	40.5 ± 0.7	0.0247 ± 4	**155 ± 3**	patchy
A91-20.1	33	15	0.45	0.7	25.41	0.092 ± 5	39.6 ± 0.9	0.0252 ± 6	**159 ± 4**	unzoned
V16-1	17	10	0.45	0.4	0.40	0.053 ± 5	37.9 ± 1.7	0.0264 ± 12	**167 ± 8**	growth
V16-1A	59	73	1.24	1.3	0.06	0.050 ± 3	39.7 ± 0.7	0.0252 ± 5	**158 ± 4**	growth
V16-2	31	13	0.41	0.7	<0.01	0.049 ± 4	39.4 ± 1.0	0.0254 ± 6	**161 ± 4**	growth

the Eu concentrations remain almost constant (Fig. 4.5) and Eu anomalies change from being positive to negative. This suggests that the different zircon-bearing samples record different fractionation processes. While a positive Eu anomaly is indicative of plagioclase accumulation, the negative Eu anomaly of some samples indicates substantial plagioclase fractionation prior to the solidification of the gabbro. Surprisingly, the chemical features can be linked with the texture of individual gabbro samples. Zircon-bearing gabbroic dikes with a granular texture (A71) have a positive Eu anomalies indicate in-situ crystallization, with large amounts of trapped liquid, from which zircon (and other trace phases) crystallized in-situ. On the contrary, sample A91, which is highly sheared, has a negative Eu anomaly, indicating that substantial amounts of plagioclase fractionation occurred at depth, prior to the solidification of the gabbro. Zircons are concentrated in the middle of a highly sheared zone, suggesting that differentiated liquid moved from below, along shear zones. Gabbro L165, which has a central shear zone present an intermediate composition between the other two samples (A91 and A71). Assuming that the all Fe-Ti gabbros might be originated from a similar source, we propose that their chemical and textural differences most probably reflect different emplacement mechanisms, which evolved through time.

In contrast to most other gabbros, the plagiogranite shows a large negative Eu anomaly (Eu* = 0.30) suggesting substantial plagioclase fractionation prior to dike formation. This is consistent with crystal fractionation modeling for the genesis of plagiogranites (Aldiss 1981).

4.10.2 Age interpretation and zircon chemistry

The zircon dated present features indicative of a magmatic origin. They occasionally preserve euhedral crystal faces, display weak oscillatory zoning or are unzoned. They have high Th/U as often observed in magmatic zircon from mafic rock types (Corfu et al. 2003; Rubatto and Gebauer 2000). The steep REE pattern and the negative Eu-anomaly are in line with crystallization from a melt after substantial plagioclase fractionation. Therefore the U-Pb ages obtained are interpreted as crystallization ages at around ~160 Ma.

The application of the Ti-in-zircon thermometer (Watson et al. 2006) to the investigated samples returns temperatures of 775± 15°C for L165, 751 ± 61°C for A71 and 822 ± 37°C for A91 (Tab. 4.3). Assuming a TiO_2 activity of 0.5, as likely for these ilmenite-bearing gabbros, would increase the estimated temperature by ~50°C (Watson and Harrison 2005). Even with this correction, the temperatures obtained from zircon are much lower than what expected for the crystallization of ferro-gabbros and the variations within a single sample are large. This has been documented elsewhere and attributed to the fact that zircon is a late crystallizing phase and its Ti-content might represent local melt composition, rather than the original chemistry of the mafic magma (e.g. Coogan and Hinton 2006; Hiess et al. 2006).

Of particular interest is the network of apparent fractures observed in many crystals (Fig. 4.6). Similar features in zircon grains from mafic rocks have been recently studied in detail with Electron Back Scattered Diffraction (EBSD) techniques (Reddy et al. 2006; Timms et al. 2006). Their results show that these networks of apparent fractures correspond to dislocation structures, rather than open and resealed fractures. Timms et al. (2006) documented that deformed zones defining sub-grains correspond to zones of CL intensity decrease due to either structural or chemical changes during deformation. In the Lanzo samples, the zircon within the shear zones show the highest concentration of these apparent fractures, indicating that they are possibly related to dislocation zones. These dislocations have the same age within error and slightly lower REE concentrations when compared to pristine oscillatory zones (see in particular sample L165). This would suggest that, even though there was some chemical and possibly isotopic changes in the deformed zones, shearing must have occurred simultaneous to, or shortly after crystallization of the zircon, producing an irrelevant loss of radiogenic Pb. Strong syn-magmatic deformation is in fact reflected in the structure of the high-temperature shear zones. The dated samples later underwent variable degrees of HP metamorphic overprint during the Alpine orogeny; therefore it is not surprising that a few analyses, particularly on unzoned zircon rims (sample A91) yielded

substantially younger ages, which are attributed to Pb during Cenozoic metamorphism.
In summary, U-Pb dating constrain the intrusion of the gabbros at 161 ± 2, 158 ± 2 and 163 ± 1 Ma. The small age difference between the youngest and the oldest gabbro (5 ± 1.1 Ma, 1 sigma) suggests magmatism over a few millions of years, which is possibly linked to the chemical evolution of the magmatic system that ultimately formed the gabbro dikes. The youngest intrusion age (158 ± 2 Ma) corresponds to the most deformed dike (A91), which is also the most fractionated sample, with evidence of plagioclase fractionation prior to crystallization. The sample L165 shows an intermediate composition in terms of REE. The undeformed gabbro A71 crystallized at 163 ± 1 Ma and its chemistry suggests plagioclase accumulation, reflected by a positive whole rock Eu anomaly (Fig. 4.5a). We therefore suggest that zircon formation in this sample is related to in-situ crystallization of trapped interstitial liquid. The correlation between structure, geochemistry and age suggests the following scenario: (i) emplacement of gabbros and in-situ crystallization, followed by (ii) crystallization of zircon-bearing oxide gabbros along synmagmatic shear zones. This latter, fractionated magma was extracted from cumulate gabbros at depth. Such a scenario implies that the formation of a 'stratified' oceanic crust might be time progressive, with 'early magmatism' dominated by in-situ crystallization of individual magma batches and 'later magmatism' accompanied by syn-magmatic deformation, enhancing efficient extraction of highly differentiated liquid from a cumulus pile.

4.10.3 Tracking the thermal evolution of a nascent ultra-slow spreading system

The Lanzo massif was partly re-equilibrated during uplift from the spinel to the plagioclase facies (chapter 2, Sandrone et al. 1986), which was accompanied by cooling from > 1100°C to 850°C (chapter 2, Pognante et al. 1985) and by fracturing and intrusion of gabbroic dikes generated at greater depth. The gabbro dikes studied here indicate intrusions in a refertilized, brittle mantle along fractures. It is likely that magmatism composed of several pulses from a source close to N-MORB persisted for some millions of years.

Published radiometric ages suggest that mafic magmatism in the Piemont-Ligurian ophiolites lasted from ~170 to 150 Ma with different types of gabbroic rocks intruding is sequence. Gabbros from the Ligurian peridotite were dated by Sm-Nd mineral isochrons (plagioclase-clinopyroxene) and represent the earliest group of MORB-type gabbros (External Liguride gabbros: 179±9 and Tuscany gabbros: 170+/-13 and 173+/- 4.8 Ma), (Tribuzio et al. 2004). These gabbros are interpreted as representing early (syn-rift) melt intrusion in lithospheric mantle peridotite. U-Pb zircon ages on zircon-bearing Fe-Ti gabbros from the Piemont-Ligurian ocean show ages ranging between 166 and 156 Ma (Costa and Caby 2001; Ohnenstetter et al. 1981; Rubatto et al. 1998; Rubatto and Hermann 2003; Schaltegger et al. 2002) consistent with the new age determinations from Lanzo gabbros. Similar ages were obtained for Internal Liguride gabbros with Sm-Nd mineral isochrones at 164±14 Ma, (Rampone et al. 1998).
Plagiogranites from a number of localities in the Western Alps and the Apennine were found to be significantly younger than the corresponding mafic rocks : 150–153 Ma (Borsi et al. 1996), 148 ± 2 Ma (Costa and Caby 2001), 152 ± 2 Ma (Lombardo et al. 2002). The plagiogranites described by Costa and Caby (2001) cut across breccias and basaltic rocks and thus clearly postdate continental breakup. On the other hand, plagiogranites from the Platta nappe and those described in this paper show similar age as the zircon bearing gabbros. We conclude that the ~160 Ma plagiogranites are formed by differentiation whereas the younger ones are eventually formed by different processes, possibly hydrous melting (Koepke et al. 2005).

4.10.4 Paleogeographic consequences

The intrusion of mafic melts recorded in Piemont-Ligurian ophiolites of the Western Alps, Corsica and Northern Apennines lasted from 180 to 150 Ma with most gabbros intruding at 165-160 Ma. The spatial distribution of ages illustrated on figure 4.10 indicates a progressive younging of the first crystallization ages from the south (Tuscany and Northern Apennines) to the north (Platta nappe) of the Piemont Ligurian ocean. However, the different gabbroic rocks, albeit crystallized from MORB type melts, are found in different structural/paleogeographic domains. For example

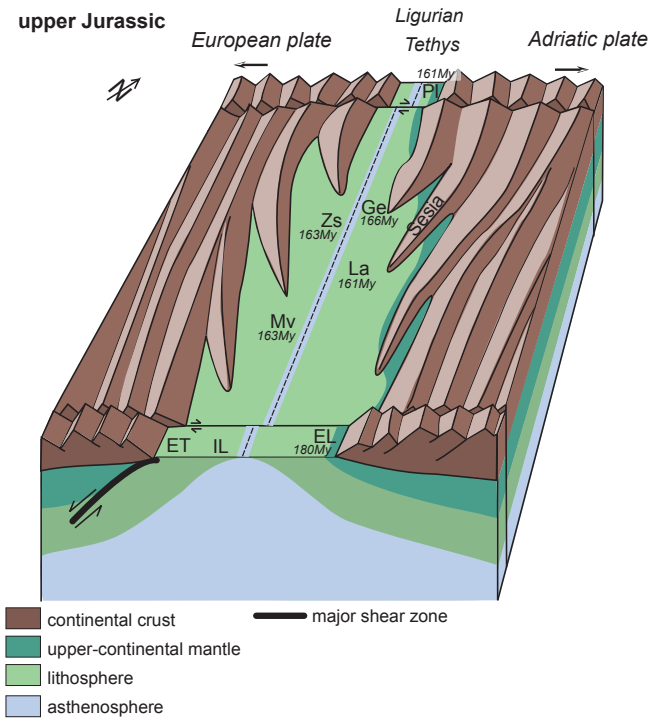

Fig. 4.10: Proposed schematic paleogeography for the Upper Jurassic with the location of the different remnants of oceanic crust, after Dal Piaz (1988), and Péron-Pinvidic (2007). Abbreviations are EL: External Liguride, ER: Erro-Tobbio, Ge: Gets nappe, IL: Internal Liguride, La: Lanzo, Mv: Monviso, Pl: Platta, Zs: Zermatt-Saas.

the Monviso gabbros are intruded in a 'mature' oceanic crust, related to important volumes of basaltic rocks, while the gabbros from the Nappe des Gets and the Platta gabbros are intruded into the ocean-continent transition zone. There is an age difference of ~5±2 my between the intrusion of the gabbros in the Gets nappe (166 ± 1 Ma, Bill et al. 1997) and those in the Platta nappe (161 ± 1 Ma, Schaltegger et al. 2002). Gabbros in both localities intruded into an ocean-continent transition zone, separated by approximately 250±100 km, by taking the paleogeographic reconstructions of Froitzheim et al. (1996). Assuming that the opening mechanism remains similar for both localities, an average rate of 5 cm/y (taking into account the errors: 2-12 cm/y) can be calculated for the northward propagation of the first MORB type magmatism in the ocean-continent transition zone. Despite the large uncertainties, this propagation velocity is remarkably similar to the 4.4 ± 0.3 cm/y obtained for the Iberia ocean-continent transition (Schärer et al. 2000).

If one considers the age difference of gabbroic intrusions within the Lanzo peridotite (163 ± 1 Ma, 158 ± 2 Ma), and assuming that the paleodistance distance between the different localities does not exceed 25 km, a much lower rate of ~0.5 cm/y (taking into account the errors: 0.3-0.8 cm/y) for the propagation of magmatism can be inferred. Although highly speculative, this slow rate is well within the range of ultra-slow spreading rates determined for the Gakkel ridge and the southwest Indian ridge (Dick et al. 2003). This has the interesting consequence that the northward propagation rate of ocean opening is apparently much higher than the inferred spreading velocity itself.

4.11 CONCLUSIONS

• The geochemistry of gabbroic dikes from the Lanzo massif indicates a typical MORB type evolution from primitive troctolitic cumulates to highly differentiated Fe-Ti gabbros and plagiogranites

•Zircon-bearing gabbros have different origins; some of them crystallized within synmagmatic shear zones, while others are virtually undeformed. The different textures correlate with chemistry: the undeformed gabbro represents a cumulate with crystallization of zircon from the intercumulus liquid, while zircon synmagmatic shear zones crystallized from evolved liquid that was expelled from a cumulus pile at depth.

•The trace element composition demonstrates that zircon crystallized after substantial plagioclase fractionation. Crystallization temperatures are estimated by Ti-in-zircon thermometry to about 800 to 850°C.

• U-Pb determinations of zircons provide ages between 158±2 to 163±1 Ma, consistent with magmatic activity during opening of the Piemont Ligurian ocean.

• A slow rate of ~0.5 cm/y is calculated for the propagation of magmatism in the Lanzo massif which is well within the range of ultra-slow spreading rates.

ACKNOWLEDGEMENTS

We thank V. Serneels for helping with the XRF analyses and A. Ulianov for LA-ICP-MS

analyses of whole rock glasses. Comments from two reviewers improved the final version of the manuscript. The Electron Microscopy Unit at the Australian National University provided for access to the CL facility. This research was financially supported by the Swiss National Foundation (Project 21-66923.01 and 200020-104636/1).

CHAPTER 5:

CONCLUSIONS AND OUTLOOKS

Monte Civrari from Monte Arpone

5.1 RESULTS AND CONCLUSIONS

The aim of this research was to better constrain the relationships between the deformation and the interplay with melt during exhumation of mantle peridotite through tectonic processes. This study has permitted to understand the "deep deformation" of oceanic-continent transition zones (OCT) and particularly in zones of exhumed continental mantle with focus on the high temperature processes. Results demonstrate that the shear zone between the Northern and the Central parts of the Lanzo massif was responsible for mantle exhumation during the Piemont-Ligurian ocean formation.

5.1.1 Principal results

Deformation in the peridotite

This study demonstrates:
- Parallelism of the layering and the foliation in the mylonite area and the lineation is sub-horizontal.
- A global sinistral sense of shear
- Shearing of the pyroxenite layering by high temperature deformation indicating that pyroxenite bands predate high temperature deformation.
- An asymmetric distribution of the deformation towards the shear zone: the northern part is mapped as CGSG rocks and the central part from south as CGSG rocks to north as ultra-mylonite rocks.
- Grain size reduction and localization of the deformation in a 200 m wide zone in the peridotite mylonite zone.
- Localization of the deformation at the thin section scale with formation of ultra fine-grained bands.
- The localization of the deformation can be associated to a thermal.

Minerals and peridotite geochemistry

The mineral composition coupled with the peridotite geochemistry highlight several important points:
- A rapid retrogression from spinel (~1070 ± 20°C) to plagioclase facies (~860 ± 40 °C).
- The hydrous-mylonite neoblasts indicate equilibration temperatures at 800 ± 25 °C.
- The chemical composition of minerals is influenced by local melt interaction (e.g. Cr enrichment in cpx, heterogeneous Al and Cr content in spinel).
- Homogenization of the spinel compositions in the deformed rocks.
- Coarse grained peridotite preserved high temperature interaction processes with migrating liquid, mylonite record cooling to ~800 °C.

- The plagioclase peridotite composition is close to the primitive mantle and enriched with respect to depleted MORB mantle (DMM).
- Major and trace elements show homogeneous composition in the deformed rocks.
- The deformed peridotite (mylonite) are the most enriched peridotite which emphasis that the mylonite act as a melt impermeability barrier.

- The northern and the central body are impregnated by melt.
- The Micro-textural evidences indicate that reactive porous flow of melt precedes high temperature deformation.
- The deformation and the melt migration are coupled in the mylonite zone.

Mafic dikes in the Lanzo peridotite

The study area recorded porous and focused melt flow in the peridotite, and melt/rock interaction:
- Repartition of mafic dikes: rare or absent in the northern body and numerous at the south of the shear zone.
- The mafic dikes intrusions postdate the high temperature foliation.
- Mafic dikes: from troctolite, ol-gabbro, to amph-gabbro, Fe-Ti gabbro and plagiogranite.
- The gabbros from the central body are smaller (from 5 to 40 cm thick) than in the southern body (from 10 cm thick to meter gabbroic bodies).
- The Fe-Ti gabbros are more abundant in the southern body of the Lanzo massif.
- Some Fe-Ti gabbros are sheared and contain numerous zircons in the shear zone.
- The timing of gabbros intrusion is at 161 ± 2, 158 ± 2 and 163 ± 1 Ma.

- The impregnating melt adds several types of basaltic components, from gabbroic microgranular

to gabbroic dikes with a MORB signature.
- The chemical composition indicates a tholeiitic trend from troctolite to Fe-Ti gabbros.
- The Fe-Ti gabbros are crystallized from highly differentiated melts.
- Gabbroic dikes originated from a similar source than basaltic dikes and the chemical and textural differences reflect different emplacement mechanisms.

5.1.2 What is new on the Lanzo massif ?

This study highlights the initial polarity of the shear zone: the central part is the footwall and the northern part is the hanging wall. The Lanzo shear zone is not considered as the major shear zone exhuming mantle on the seafloor but as a shear zone exhuming mantle from near asthenospheric to lithosphere conditions. Disequilibrium compositions of peridotite minerals indicate rapid exhumation. The model of this rapid mantle exhumation corresponds to an asymmetric structure toward the shear zone.

The plagioclase peridotite from the Lanzo massif corresponds to an exhumed part of sub-continental mantle with refertilization between 6 and 10% of N-MORB material. Moreover, the particular shear zone area, seems to be the most enriched part, clearly indicating the mutual relationships between melt accumulation and deformation. The shear zone act as a melt barrier to the upper part and most probably focuses melt flow.
What was mechanism of the shear zone initialization? The presence of melt allows the localization of the deformation or vice versa? The presence of porous melt flow in the entire massif, prior to the localized shearing suggests that the birth of the shear zone was influenced by the presence of melt. And following, the localization of deformation permits melt enrichment, as a positive feedback mechanism.

5.2 THE LANZO SHEAR ZONE IN RELATION TO OTHER MANTLE PERIDOTITES

The comparison of the Lanzo shear zone to orogenic and actual peridotite, highlights numerous similarities. The Lanzo massif was exhumed from spinel to plagioclase facies as observed in orogenic or actual ridges: Galicia margin, Iberia (Beslier et al., 1996), Erro-Tobbio (Hoogerduijn Strating et al., 1993; Lagabrielle and Cannat, 1990; Vissers et al., 1995), Turon de Técouère, (Newman et al., 1999; Vissers et al., 1997). The presence of melt in plagioclase lherzolite was observed in several ophiolites as for example Newfoundland, Othris and conjugate Iberia margin, South Western Indian Ridge (SWIR), the Lanzo massif. These margins are considered as magma-poor rifted margin, and defined melt associated. The Iberia margin show plagioclases lenses and dikelets (plagioclase-rich) parallel to the high temperature foliation (Beslier et al., 1996). The Erro-Tobbio plagioclase peridotite is impregnated by melt and crossed-cut by MORB-type gabbroic dikes (Vissers et al., 1995), similar to the Lanzo massif (Bodinier et al., 1991; Boudier and Nicolas, 1972; Kaczmarek et al., accepted; Müntener et al., 2004; Piccardo et al., 2004; Piccardo et al., 2007). The range of gabbros (from ol-gabbro, gabbro-norite to Fe-Ti gabbros and plagiogranite) found in the Lanzo massif is typical for some other ophiolites from the Western and Eastern Alps (Costa and Caby, 2001; Desmurs et al., 2002).

Localized shearing of peridotite is observed in mantle xenoliths (e.g. Kenya, Massif central), in orogenic peridotite (e.g. Lanzo, Lherz, Erro-Tobio), in OCT's (Iberia, Platta) or in actual ridges (SWIR). The shear zones vary in size from the hundred meters scale (Lanzo and Erro-Tobbio massifs), to meters scale (Turon de Técouère, Galicia margin) or centimeter scale (Turon de Técouère, Lherz massif). The shear zones are interpreted as localization of the deformation during cooling in an extensional context and demonstrate the lithosphere stretching before the break-up, but the quantitative estimates influence of the shear zone on mantle exhumation is poorly constrained. The parameters influencing the shearing and the localization of deformation are the presence of

melt, cooling, polyphase bands or weak minerals (Mainprice, 1997; Newman et al., 1999; Vissers et al., 1995; Warren and Hirth, 2006), and are difficult to estimate. The presence of plagioclase may favor mylonite development during subsolidus phase transformation from spinel facies (Beslier et al., 1996; Furusho and Kanagawa, 1999; Vissers et al., 1997), or alternatively, as proposed here, active deformation and melt focusing are juxtaposed. In this context, it is worth nothing that Newman et al. (1999) observed an increasing proportion of plagioclase with increasing deformation.

Numerous similarities between the Lanzo and Erro-Tobbio massifs, as spinel to plagioclase stability field retrogression, important melt impregnation with ascending MORB-type melt and large shear zones (around 200 meters), suggests important melt influence. The melt percolation decreases the resistance of the peridotite to stress and the deformation might take place at large scale.

In the two cases the Lanzo and Erro-Tobbio massifs suggest a lithospheric extension, reflected in the development of km-scale shear zone and a several 100 m scale mylonite zone. The high temperature foliation measured in the Erro-Tobbio is sub-vertical with a lineation sub-horizontal, has observed in the Lanzo massif. But contrary to the Lanzo massif, the initial polarity of the Erro-Tobbio massif is unknown.

The age of gabbros crystallization in the Lanzo massif is not different that previous ages found in other gabbros from Piemont-Ligurian ocean (~170 to 150 Ma). Dating of gabbros from Erro-Tobbio and External Liguride around 170-180Ma (Borghini et al., 2007; Tribuzio et al., 2004) represent the earliest group of MORB-type gabbros and the early syn-rift melt intrusion in the oceanic crust. This event is concordant to Fe-Ti gabbros from the Lanzo massif (~165Ma) and other Piemont-Ligurian dating (between 166 and 156 Ma, Costa and Caby, 2001; Rubatto et al., 1998; Rubatto and Hermann, 2003; Schaltegger et al., 2002). The gabbros correspond to the melt crystallization during the period of Jurassic rifting and development of the Piemonte-Ligurian oceanic basin. The SWIR seafloor spreading half rate is estimates at 0.85 cm/y (Dick et al., 1991) and presents gabbroic bodies crystallized in the cold lithospheric mantle (Schwartz et al., 2005). The velocity of the oceanic crust formation in the Piedmont-Ligurian ocean is estimates in this study as 0.5 cm/y, which present the ridge as slow-spreading center and close to ultra-slow spreading rates determined for the Gakkel ridge and the SWIR (Dick et al., 2003).

5.3 OUTLOOKS

The shearing is features of deformation mechanisms, which are important to understand mantle exhumation processes. Previous works (Boudier, 1972; Nicolas et al., 1971) indicate that olivine neoblasts from the Lanzo massif was results of recrystallized olivine by post-tectonic reheating. The Lanzo shear zone display localization of deformation illustrates at thin section scale by several domains with grain size reduction (from granular areas to ultra-mylonite bands). Details of the olivine recrystallization mechanisms should be studied by means of Electron Backscatter Diffraction (EBSD), to determine the relation between plastic deformation and melt migration.

The melt impregnation and the deformation are closely linked, and overprinted by cooling during mantle exhumation. The outcrop L187 located at the north of the shear zone, as illustrated in part 2.3, is a key to understanding these processes. The presence of gabbros rich in amphibole parallel to the high temperature foliation, and K-Ti-amphibole in the shear planes which cross-cut the high temperature foliation argue for hydrous melt and/or interaction with (crustally derived?) fluids. This type of gabbro dike and its interplay with the deformation, fluid and cooling was never described before. These gabbros might provide answers to the interplay between melt migration, deformation, cooling and fluid flow.

Finally, comparisons with other areas of the Piemont Ligurian ocean (Chenaillet, Platta, Liguria, Corsica) and in particular modern analogues (Atlantic) of magma poor margin are required to test and refine current models. The Malenco-Platta-Totalp peridotites, which formed part of a relatively well preserve fossil ocean-continent transition, contains high-temperature mantle shear zones and associated low-temperature

detachment faults. Basaltic dikes and detachment faults postdate high temperature deformation. It should be interesting to investigate the relationship between mantle shear zones, the detachment faults and the impact on the mantle exhumation.

APPENDIX

APPENDIX 1

ANALYTICAL METHODS (CD)

A1.1. ELECTRON MICROPROBE

Minerals composition was analyzed using a Cameca SX 50 at Bern, A Cameca SX100 with 5 crystals at Heidelberg and a Jeol with 5 crystals spectrometers at Bern. Samples were coated with carbon. Operating parameters include an acceleration potential of 15kV, a beam current at 20nA and a beam size of ~1μm. For amphibole, serpentine and chlorite the beam size has been enlarged (~5μm). Data collection on background positions on both sides of the peaks was half the time of data collection on the respective peak position. Natural and synthetic oxides and silicates were used as standards. A ZAF correction was applied to the data. More details on the data label acquisition are below for the CAMECA SX50 microprobe.

Table. A.1.1: Label from the Cameca SX50 at Bern

TA.1.1a: Label to silicates with Ni (olivine, orthopyroxene…)

Beam Conditions:	Accel. (KV)	Current (nA)
	15	20

Element	Standard		X-Ray position					Acquisition	
	Name	Group	Line	Crystal	Peak (sinθ)	+Bkgd offset	-Bkgd offset	Peak (sec)	Bkgd (sec)
Si	Woll	H10	Kα	TAP	27737	+500	-500	20	/2
Ti	Ruti	B11	Kα	PET	31425	+500	-500	30	/2
Al	Coru	B51	Kα	TAP	32461	+500	-500	30	/2
Cr	Esco	B43	Kα	LiF	56864	+500	-500	20	/2
Fe	Hema	B47	Kα	LiF	48082	+500	-500	20	/2
Mg	Fors	H15	Kα	TAP	38507	+500	-500	30	/2
Mn	Teph	H44	Kα	LiF	52197	+500	-1200	20	/2
Ca	Woll	H10	Kα	PET	38385	+500	-500	30	/2
Na	Albi	H3	Kα	TAP	46355	+500	-500	20	/2
K	Orth	H88	Kα	PET	42763	+500	-500	20	/2
Ni	Buns	B14	Kα	LiF	41175	+500	-500	20	/2

Spectrometer configuration								
SP1		SP2		SP3		SP4		SP5
LiF	PET	LiF	TAP	LiF	PET	TAP	PC1	EDS
Fe^{20}			Si^{20}		K^{20}	Na^{20}		
Cr^{20}			Mg^{30}		Ca^{20}	Al^{20}		
Mn^{20}					Ti^{20}			
Ni^{20}								

TA.1.1b: Label to silicates derived from genani by excluding Ni and changing some counting

Beam Conditions:	Accel. (KV)	Current (nA)
	15	20

Element	Standard		X-Ray position					Acquisition	
	Name	Group	Line	Crystal	Peak (sinθ)	+Bkgd offset	-Bkgd offset	Peak (sec)	Bkgd (sec)
Si	Woll	H10	Kα	TAP	27737	+500	-500	20	/2
Ti	Ruti	B11	Kα	PET	31425	+500	-500	20	/2
Al	Coru	B51	Kα	TAP	32461	+500	-500	30	/2
Cr	Esco	B43	Kα	LiF	56864	+500	-500	20	/2
Fe	Hema	B47	Kα	LiF	48082	+500	-500	20	/2
Mg	Fors	H15	Kα	TAP	38507	+500	-500	30	/2
Mn	Teph	H44	Kα	LiF	52197	+500	-1200	20	/2
Ca	Woll	H10	Kα	PET	38385	+500	-500	20	/2
Na	Albi	H3	Kα	TAP	46355	+500	-500	20	/2
K	Orth	H88	Kα	PET	42763	+500	-500	20	/2

Spectrometer configuration								
SP1		SP2		SP3		SP4		SP5
LiF	PET	LiF	TAP	LiF	PET	TAP	PC1	EDS
Fe^{20}			Si^{20}		K^{20}	Na^{20}		
Cr^{20}			Mg^{30}		Ca^{20}	Al^{30}		
Mn^{20}					Ti^{20}			

TA.1.1c: Label to spinel

Beam Conditions:	Accel. (KV)	Current (nA)
	15	20

Element	Standard		X-Ray position					Acquisition	
	Name	Group	Line	Crystal	Peak (sinθ)	+Bkgd offset	-Bkgd offset	Peak (sec)	Bkgd (sec)
Si	Woll	H10	Kα	TAP	27737	+500	-500	20	/2
Ti	Ruti	B11	Kα	PET	31425	+500	-500	30	/2
Al	Spin	B1	Kα	TAP	32461	+500	-500	20	/2
Cr	Esco	B43	Kα	LiF	56864	+500	-500	20	/2
Fe	Hema	B47	Kα	LiF	48082	+500	-500	20	/2
Mg	Spin	B1	Kα	TAP	38507	+500	-500	20	/2

Mn	Teph	H44	Kα	LiF	52197	+500	-1200	20	/2
Ca	Woll	H10	Kα	PET	38385	+500	-500	30	/2
Na	Albi	H3	Kα	TAP	46355	+500	-500	20	/2
Ni	Buns	B14	Kα	LiF	41175	+500	-500	20	/2
Zn	Gahn	B52	Kα	LiF	35642	+500	-500	20	/2

Spectrometer configuration								
SP1		SP2		SP3		SP4		SP5
LiF	PET	LiF	TAP	LiF	PET	TAP	PC1	EDS
Fe^{20}			Mg^{30}		Ti^{20}	Al^{30}		
Cr^{20}			Si^{20}		Ca^{20}			
Mn^{20}								
Ni^{20}								
Zn^{20}								

TA.1.1d: Label to feldspath

Beam Conditions:	Accel. (KV)	Current (nA)
	15	20

Element	Standard		X-Ray position					Acquisition	
	Name	Group	Line	Crystal	Peak (sinθ)	+Bkgd offset	-Bkgd offset	Peak (sec)	Bkgd (sec)
Si	Orth	H88	Kα	TAP	27737	+500	-500	20	/2
Al	Coru	B51	Kα	TAP	32461	+500	-500	20	/2
Fe	Hema	B47	Kα	LiF	48082	+500	-500	40	/2
Ca	Anor	H81	Kα	PET	38385	+500	-500	20	/2
Na	Albi	H3	Kα	TAP	46355	+500	-500	20	/2
K	Orth	H88	Kα	PET	42763	+500	-500	20	/2
Mn	Teph	H44	Kα	LiF	52197	+500	-1200	20	/2
Mg	Fost	H15	Kα	TAP	38507	+500	-500	20	/2
Ti	Rut	B11	Kα	PET	31425	+500	-500	30	/2

Spectrometer configuration								
SP1		SP2		SP3		SP4		SP5
LiF	PET	LiF	TAP	LiF	PET	TAP	PC1	EDS
Fe^{40}			Si^{20}		K^{20}	Na^{20}		
Mn^{20}			Mg^{20}		Ca^{20}	Al^{20}		
Ti^{30}								

TA.1.1e: Label to general mica (chlorite, talc, serpentine, amphibole…)

Beam Conditions:	Accel. (KV)	Current (nA)
10000	15	20

Element	Standard		X-Ray position					Acquisition	
	Name	Group	Line	Crystal	Peak (sinθ)	+Bkgd offset	-Bkgd offset	Peak (sec)	Bkgd (sec)
Na	Albi 3	H3	Kα	TAP	46355	+500	-600	20	/2
Ca	Woll	H10	Kα	PET	38385	+500	-700	30	/2
Al	Coru	B51	Kα	TAP	32461	+500	-600	30	/2
Si	Woll	H10	Kα	TAP	27737	+500	-500	20	/2
K	Orth	H88	Kα	PET	42763	+400	-500	20	/2
Fe	Hema	B47	Kα	LiF	48082	+500	-400	20	/2
Ti	Ruti	B11	Kα	PET	31425	+750	-500	30	/2
Mn	Teph	H44	Kα	LiF	52197	+500	-750	20	/2
Mg	Fors	H15	Kα	TAP	38507	+500	-700	30	/2
Cr	Esco	B43	Kα	LiF	56864	+350	-400	20	/2
F	Phlo		Kα	TAP	71159	+800	-1300	30	/2
Cl	Scap		Kα	PET	54032	+400	-500	30	/2
Ba	Bari 1	B14	Kα	PET	31725	+400	-800	30	/2

Spectrometer configuration								
SP1		SP2		SP3		SP4		SP5
LiF	PET	LiF	TAP	LiF	PET	TAP	PC1	EDS
Fe^{20}			Si^{20}		K^{20}	Na^{20}		
Mn^{20}			Mg^{20}		Cl^{30}	Al^{30}		
Cr^{20}					Ca^{30}	F^{30}		
					Ti^{30}			
					Ba^{30}			

A1.2. ZIRCON SEPARATION FOR U-PB DATING

Samples were crushed and sieved three fractions (250 / 160 μm, 160 / 80 μm and 160 / 80 μm) choose after preliminary zircon grain size determination by SEM. Samples was washed with water and ethanol, and a large quantity of magnetite was separated with a magnet. Zircons were separated with magnetic separator properties and density (denses liquor). The separate fraction was composed of apatite, titanite, garnet, amphibole and zircons. Zircons were finally selected by hand picking and mounted on a 25 mm epoxy discs and polished down to expose the grain centers coated with gold.

A1.3. SHRIMP II

U-Th-Pb analyses of zircons were performed with a Sensitive High Resolution Ion Microprobe (SHRIMP II) at the ANU using a beam size of ~25 μm. Analytical procedures were similar as described by Compston et al. (1984). The measured U-Pb ratios were corrected using the standard zircon TEM (417 Ma, (Black et al. 2003), which was analyzed each fourth analysis. A zircon of knows composition (SL13) has been used to determine the U content of zircon. The data were corrected for common Pb on the basis of the measured $^{207}Pb/^{206}Pb$ ratios as described in Compston et al. (1992) and assuming a common Pb composition according to the model of Stacey and Kramers (1975). The analytical uncertainty in the reproducibility of the U-Pb age of the standard was between 2.2 and 2.4 % (2σ). Age calculations were done using the software Isoplot/Ex (Ludwig 2003). Mean ages are intercept ages in uncorrected $^{207}Pb/^{206}Pb$ versus $^{238}U/^{206}Pb$ (Tera Wasserburg) diagrams and are given at 95% confidence level.

A1.4. X-RAY FLUORESCENCE

The bulk chemical composition of peridotite basalts and gabbros was determined by X-ray fluorescence (XRF) analyses with a sequential spectrometer (Philips PW 1404) using natural USGS reference rock samples for calibration at the Geological department of Fribourg (Switzerland). Rocks were crushed with an agate mill to reduce trace element contamination. Three samples were ground with a tungstene mill to compare the element composition (Table A1.3).
Whole rock glasses were prepared with the addition of Li-Tetraborate (dilution at 1:10). Major elements were determined using glass beads which were fused from ignited (at 1050°C) rocks powders mixed with Li2B4O7 in a 1/5 ratio in gold platinum pans at 1150°C.

Table A1.3: Element composition of 3 samples crusched with agata and tungstene mill.

	mylonite		**proto-mylonite**		**CGSG**	
sample	agata	tungstene	agata	tungstene	agata	tungstene
SiO2	44.74	44.72	43.55	43.84	44.65	44.11
TiO2	0.14	0.15	0.11	0.11	0.12	0.11
Al2O3	3.21	3.32	2.62	2.75	4.98	3.04
FeO tot	9.34	9.16	9.05	9.09	8.58	8.85
MnO	0.13	0.13	0.13	0.13	0.13	0.13
MgO	38.59	38.5	40.63	40.44	37.9	40.20
CaO	2.81	2.78	2.53	2.49	3.32	2.73
Na2O	0.61	0.25	0.20	0.43	0.59	0.25
K2O	0.03	0.01	0.01<	0.01<	0.01<	0.00<
P2O5	0.01<	0.01<	0.01<	0.03	0.01	0.01<
LOI	6.35	6.09	1.68	1.81	2.17	2.59
Cr	2395	2517	2421	2628	3093	2618

Ni	2130	2168	2192	2210	2327	2170
Cu	27	36	25	32	63	29
Zn	53	52	51	51	53	49
Rb	4	1<	-1<	-1<	1<	1<
Sr	16	19	8	6	14	10
Y	2<	2<	2<	2<	2<	2<
Zr	16	17	12	12	16	10
Nb	Bdl	Bdl	Bdl	Bdl	Bdl	Bdl
Pb	1<	7<	5<	6<	6<	6<

A1.5. ICP-MS LASER ABLATION

Whole rocks

The laser ablation whole rocks was realized on the glass beads prepared to the X-ray fluorescence.
Trace element precision is generally better than 5%. All major and trace element analyses for basalts and Fe-Ti gabbros were obtained by Laser Ablation ICP-MS on the glasses using a pulsed 193nm Excimer Laser system (Lambda Physik, Geolas 200M), coupled with an ICP-MS (Perkin Elmer DRC 6200), at the University of Lausanne, with operating conditions of 27kV, and 10Hz repetition rate, yielding a flux of ca 12J/cm2 on the ablation site. Helium was used as a carrier gas. The NIST 610 glass was chosen as an external standard, and Ca as the internal standard. BCR2 basaltic glass was used to monitor the reproducibility and accuracy of the system.
Conditions are:
Laser frequency: 10 Hz
Laser energy: 140 mJ
Laser diameter : 80-120 μm
The standard used was NIST612, for more details see Pearce et al., 1996.

Zircons

Trace element analyses on zircons were performed by Laser Ablation ICP-MS at the Research School of Earth Sciences (RSES) using a pulsed 193-nm ArF Excimer laser, with 100mJ energy at a repetition rate of a 5Hz, coupled to an Agilent 7500 quadrupole ICP-MS (Eggins et al. 1998). During the time-resolved analysis, the contamination from inclusions, fractures and zones of different composition was detected by monitoring several elements. Analysis spot size was 25 μm in diameter. External calibration was performed relative to NIST 612 glass using the concentration given in Pearce et al. (1996). Internal standard was Si.

A1.6. INDUCTIVELY COUPLED PLASMA MASS SPECTROMETER (ICP-MS)

The ICP-MS analyses were conducted at the Centre Géologique et Géophysique, Montpellier. The sample preparation and the data acquisition are describe in Ionov et al., 1992 and Godard et al., 2000.

Olivine gabbros and troctolite whole rock trace elements (REE, Cs, Rb, Th, U, Nb, Ta, Sr, Zr, Hf) were analyzed by a VG-PQ2 Turbo + Inductively Coupled Plasma-Mass Spectrometer (ICP-MS) at ISTEEM (Université Montpellier II, Montpellier, France) and are reported in Table 2. REE, Cs, Rb, Pb, Th, U, Sr, Zr, and Hf concentrations were determined by external calibration following the $HF/HClO_4$ dissolution and analytical procedure described in detail by Ionov et al. (1992). To avoid memory effects due to the intake of concentrated Nb–Ta solutions in the instrument, Nb and Ta concentrations were determined by using Zr and Hf, respectively, as internal standards. This technique is an implementation to ICP-MS analysis of the method described by Jochum et al. (1990). Detection limits obtained by long-term analyses of chemical blanks at ISTEEM can be found in Ionov et al. (1992).

APPENDIX 2

MAPS, TEXTURES AND MICROPROBE DATASET

A2.1 MICROTEXTURE DEFORMATION CLASSES

Coarse grained secondary granular from the central body

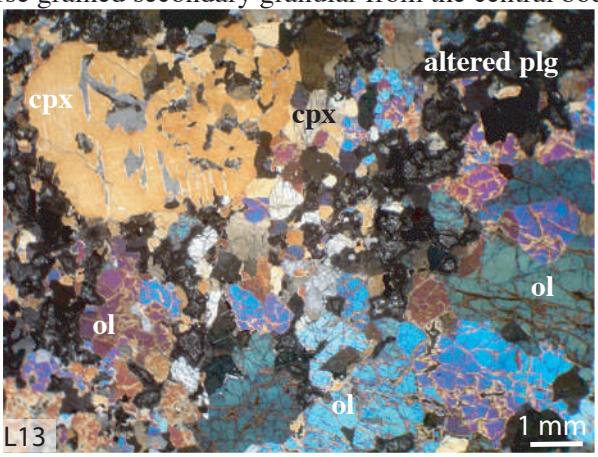

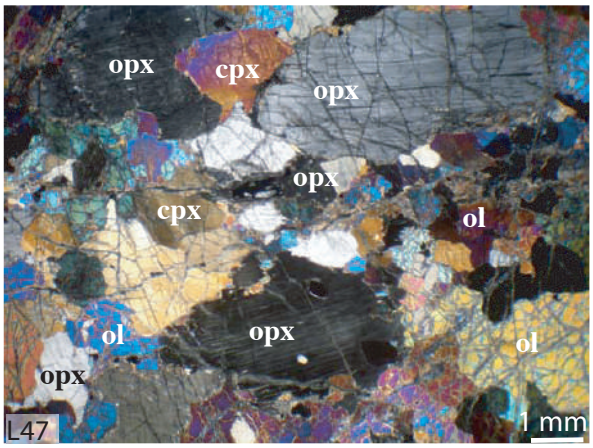

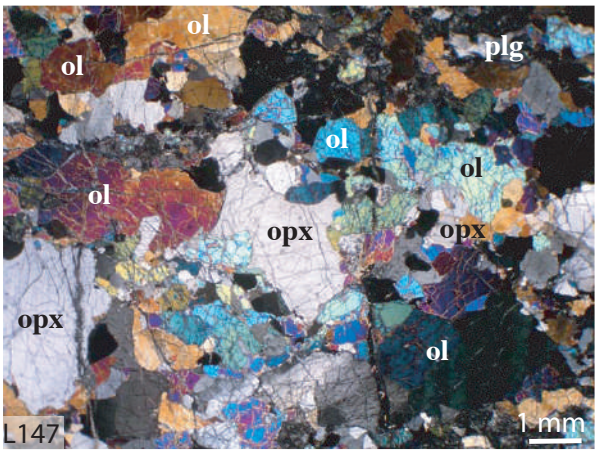

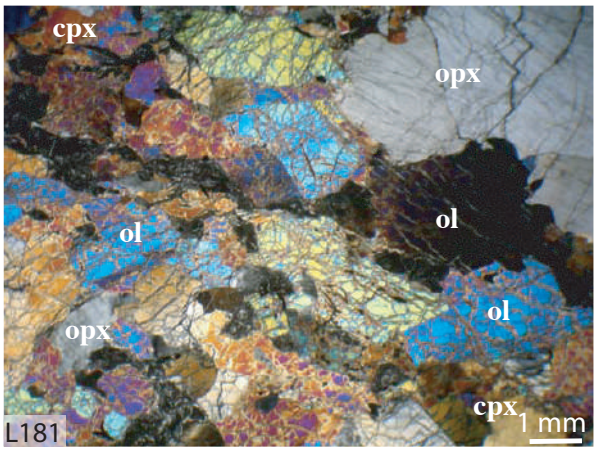

Coarse grained secondary granular from the northern body

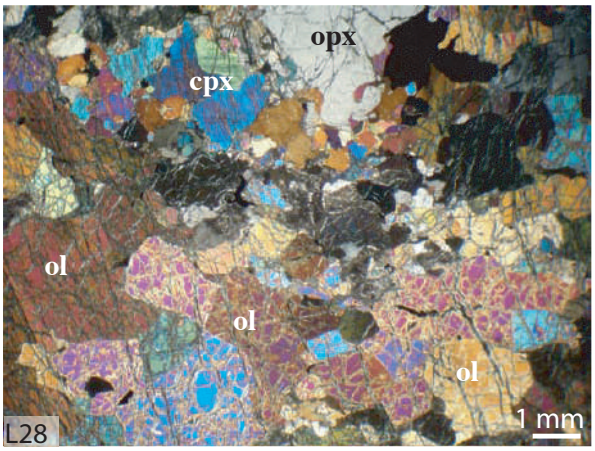

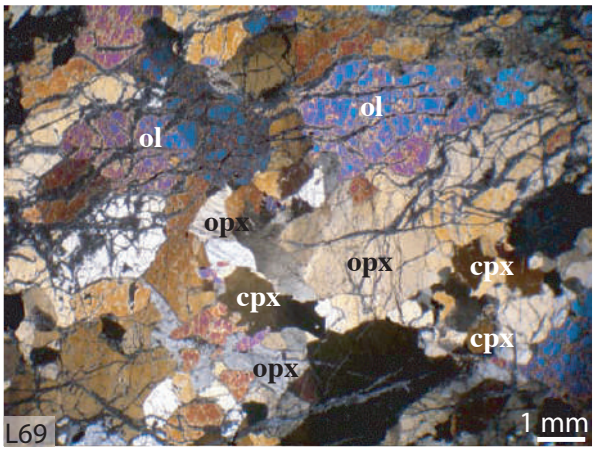

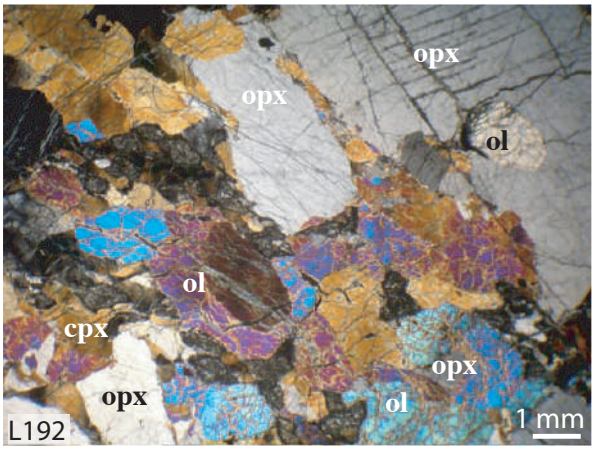

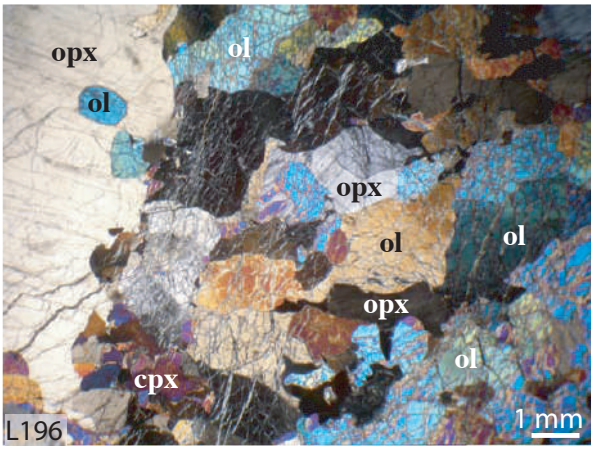

Fine grained secondary granular

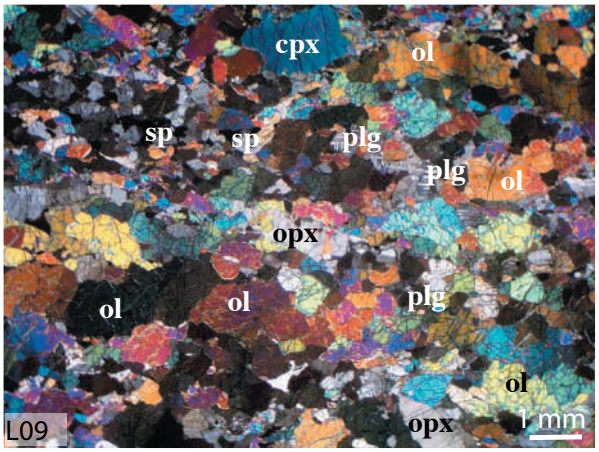

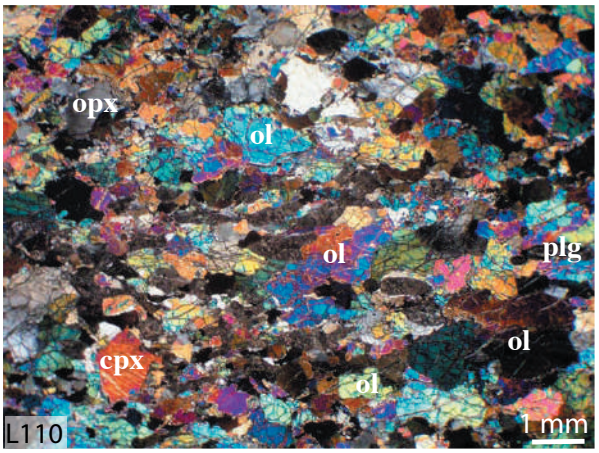

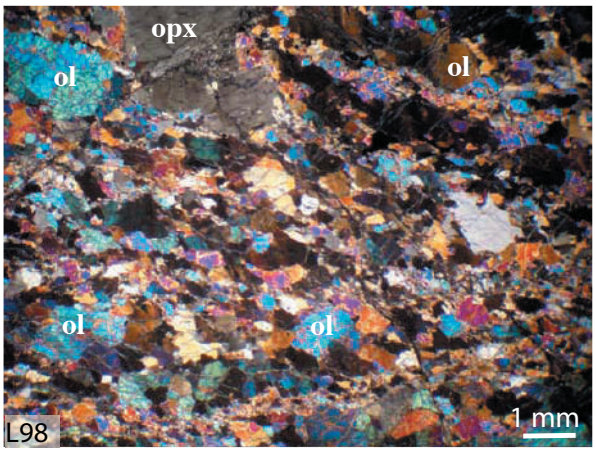

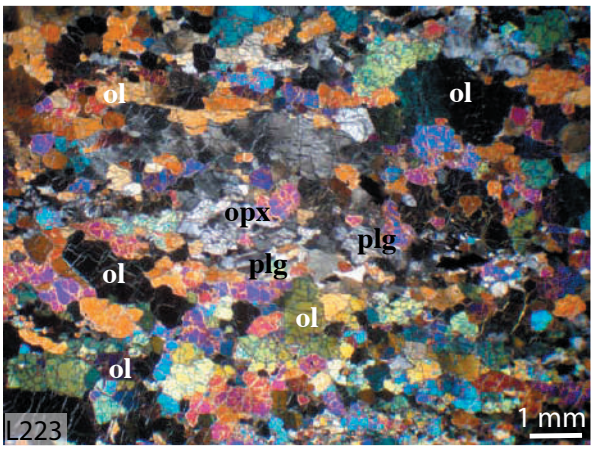

Proto-mylonite

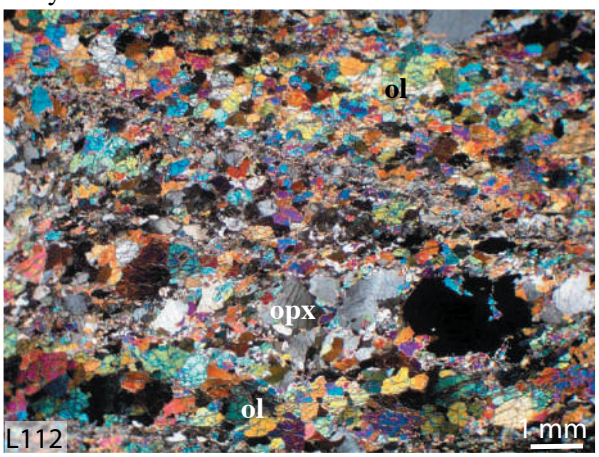

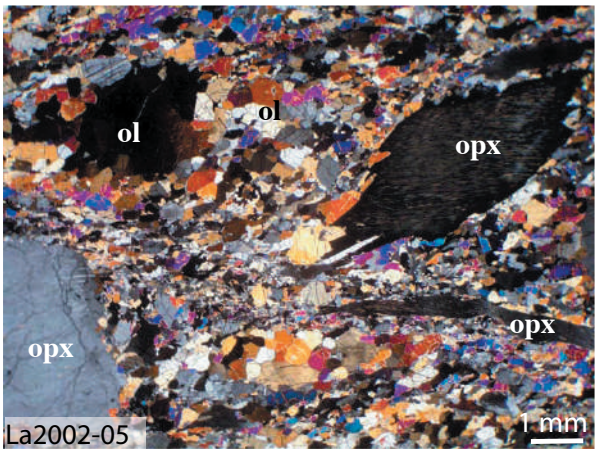

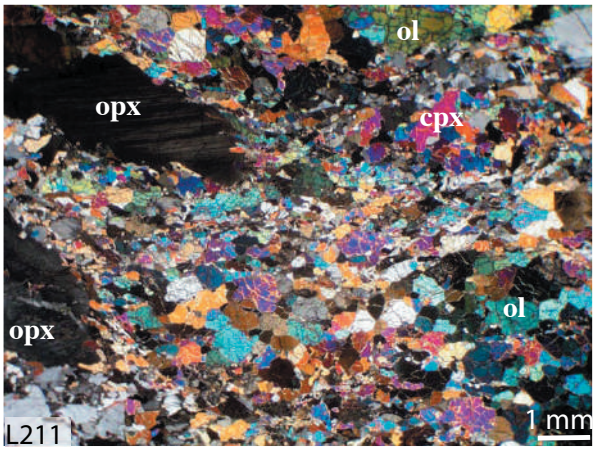

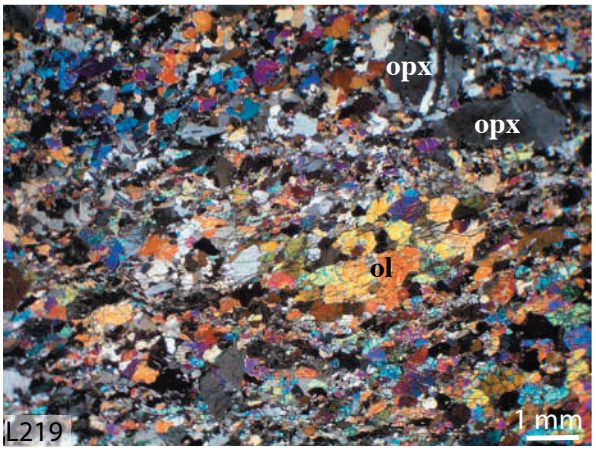

Mylonite

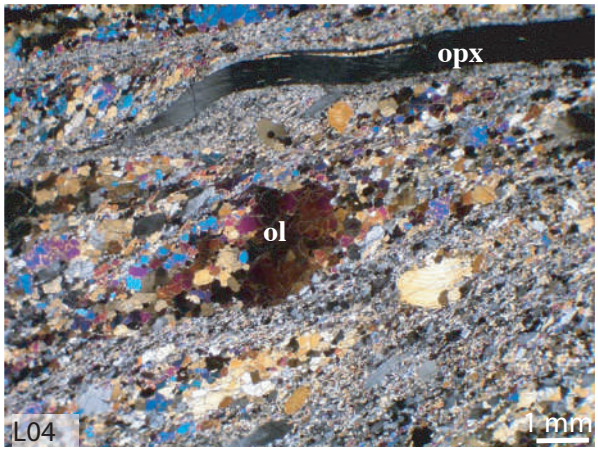

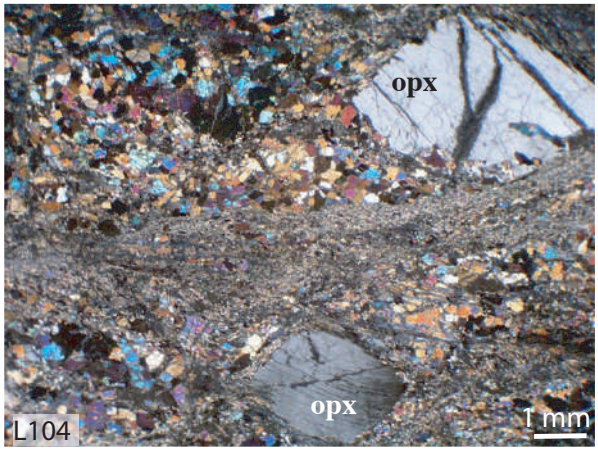

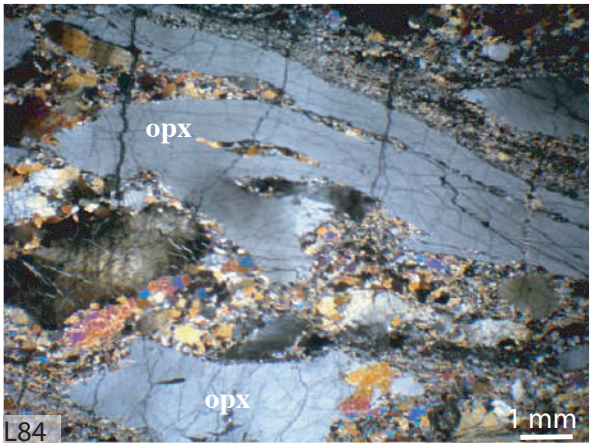

Hydrous-mylonite

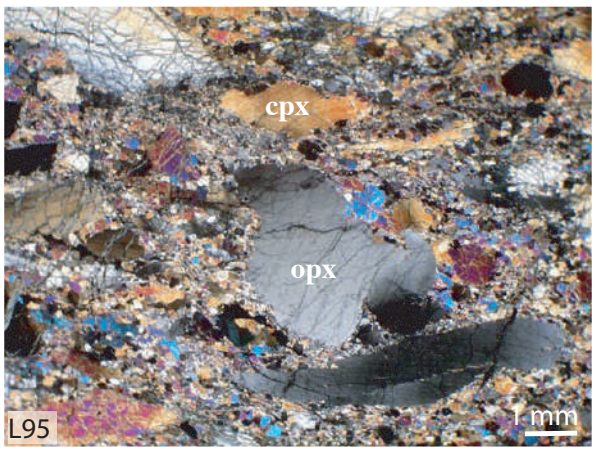

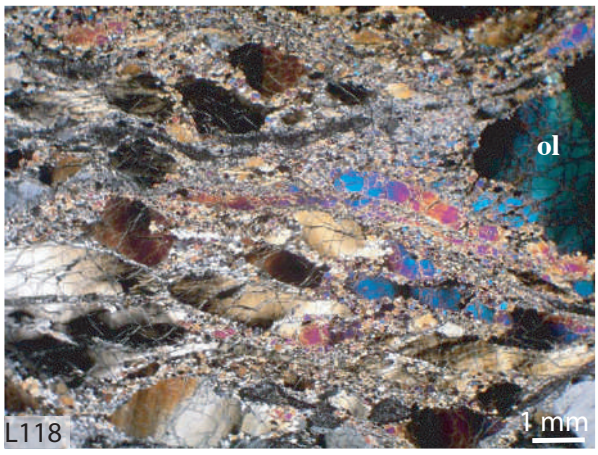

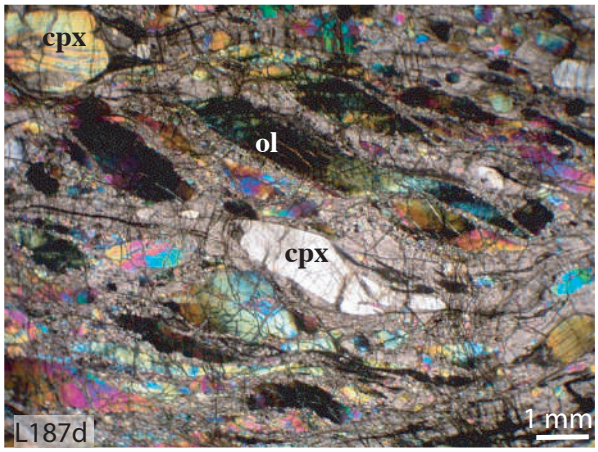

A2.2 LANZO MAPS AND SAMPLE LOCALIZATION

A2.2a Northern part

Outcrops and sample localization

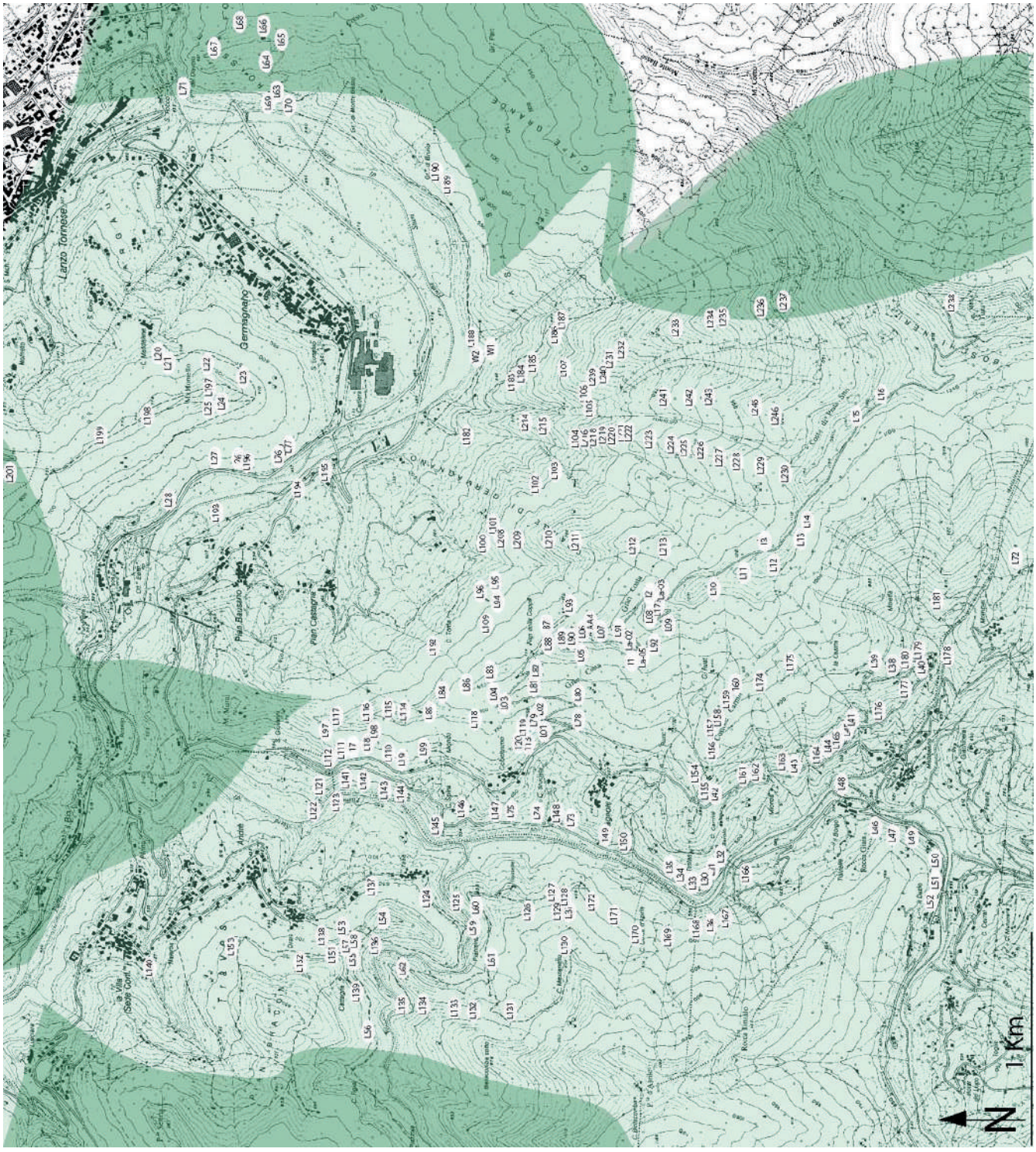

Sample and microtexture classes

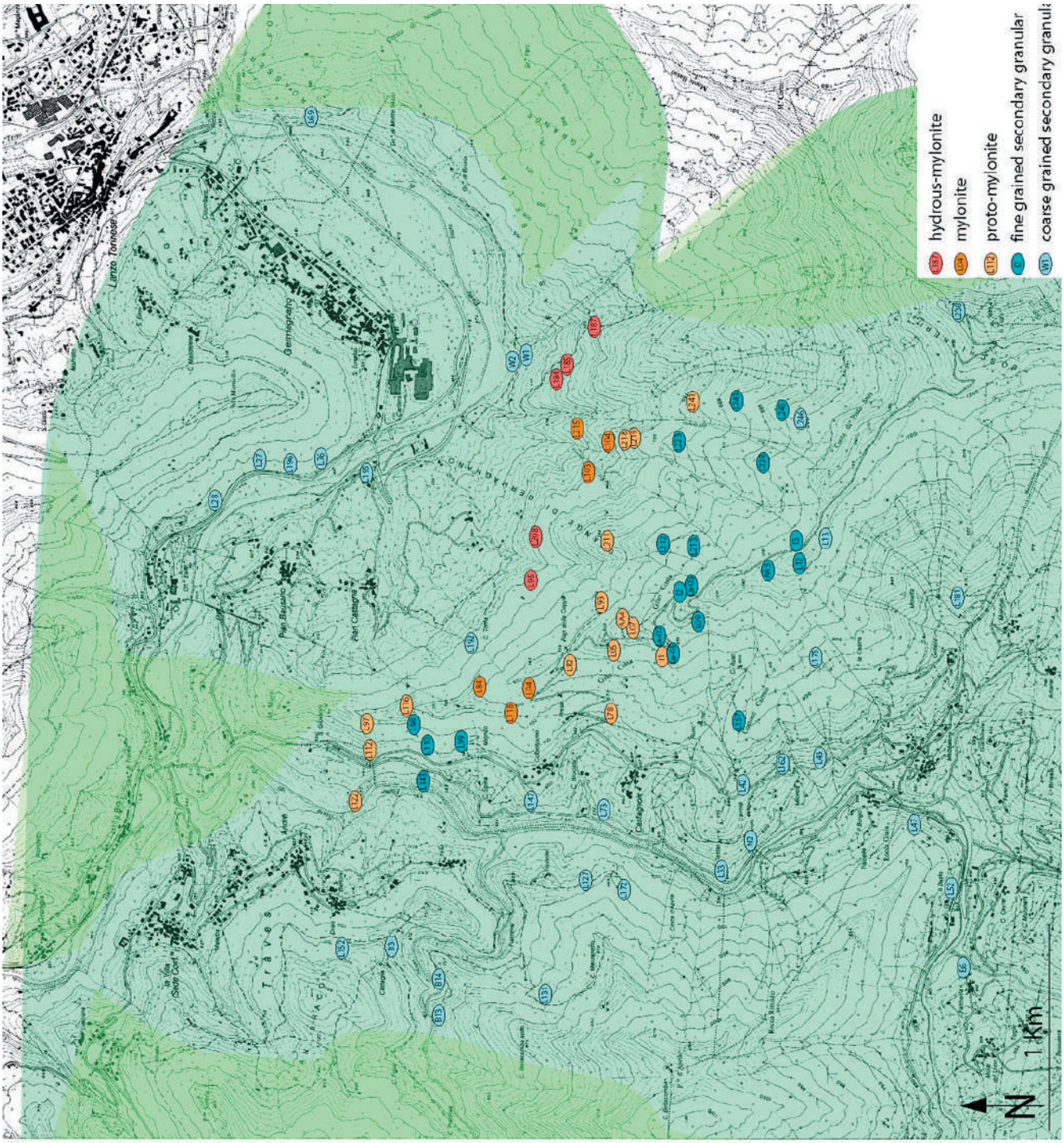

A2.2b Sample list from the northern part (by classes of deformation)

Hydrous-mylonite

L95
L184
L185
L187c
L187d
L208

Mylonite

L04
L84
L103
L104
L118

Proto-mylonite

L05
L07
L78
L82
L93
L97
L112
L122
L211
L215
L219
L218
La2002-5
AA4
I2
I1

Fine Grained Secondary Granular

L09
L98
L110
L212
L213
L223
L241
L243
La2002-2
La2002-03

Coarse Grained Secondary Granular Central

L12
L13
L30
L33
L42
L43
L47
L52
L73
L99
L127
L131
L147
L152
L157
L162
L172
L175
L181
L228
L238
L245
L246
AA3
B3
B13
B14
E6
I3
N2
OT1

Coarse grained Secondary Granular North

L28
L69
L76
L192
L195
L196
W1
W2

A2.2c Southern part

Sample localization in Lanzo south

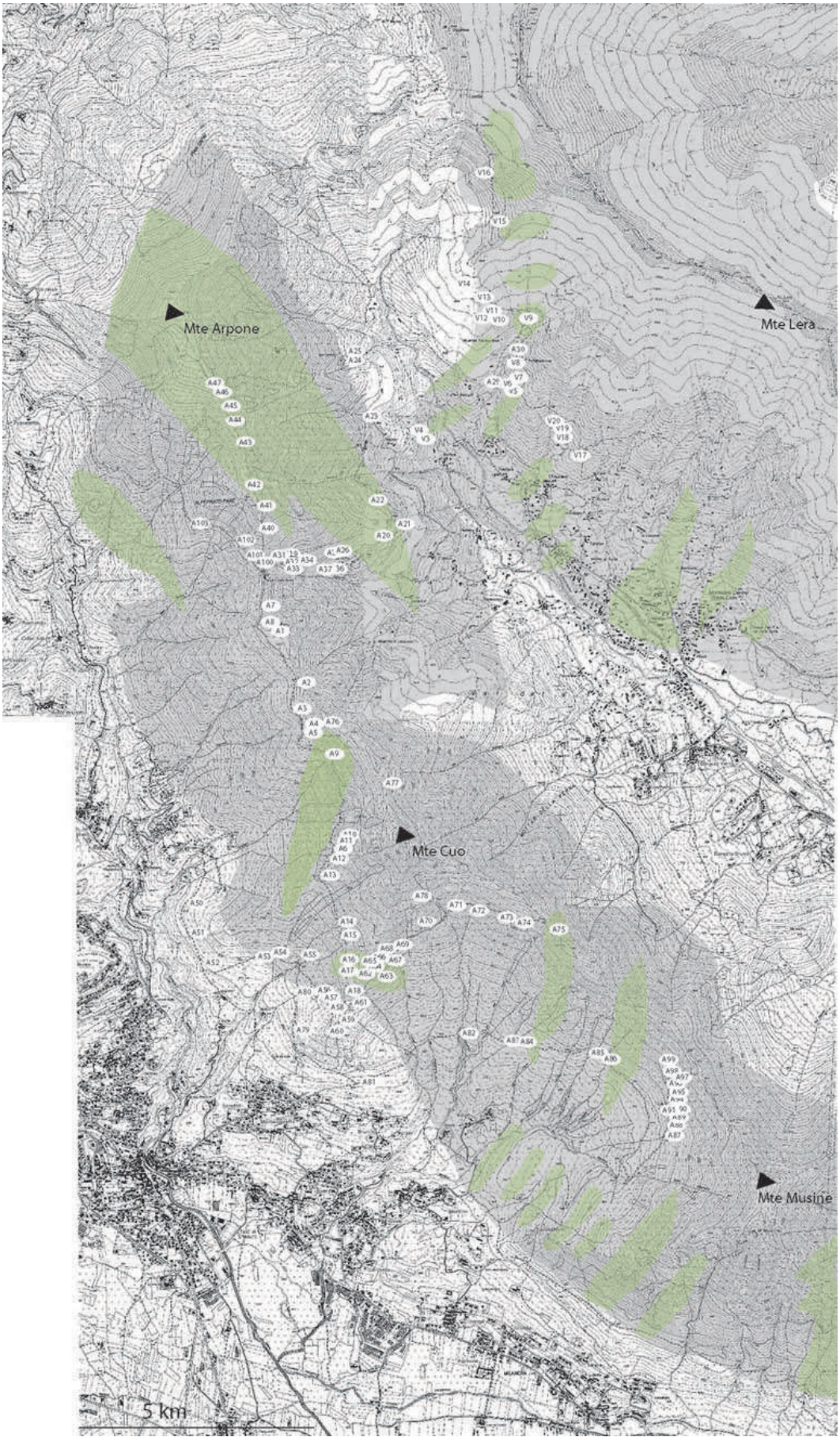

Foliation, layering and dike orientation

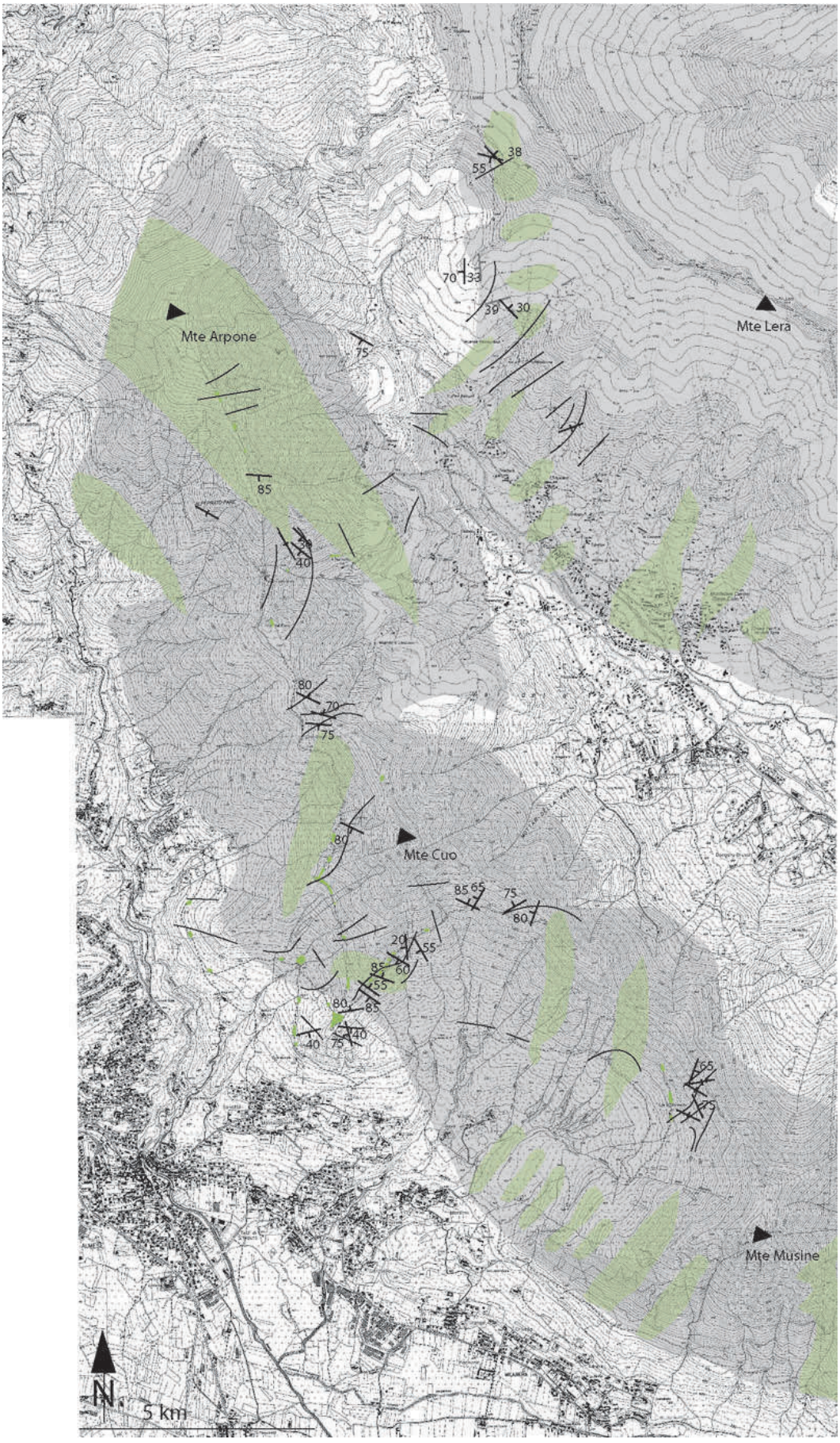

A2.3 L187 OUTCROP: HYDROUS- AND ULTRA-MYLONITE

The previous chapter was focused on the high temperature mantle shear zone between the northern and the central part of the Lanzo massif (SZ I). Five different micro-textures that highlighted deformation and temperature gradients from south to north were described (Fig. 2.7). The hydrous-mylonite rock type, located at the interface between the northern and the central part, is characterized by a retrograde overprint at lower temperatures in the presence of fluids (part 2.2.4). The presence of a hydrous-mylonite zone is a key to the mantle exhumation and will further be discussed here along a N-S profile, with special emphasis on a 50m long detailed section that is located about 500m south of Germagnano (L187 outcrop, Fig. A2.3.2).

A2.3.1 Microstructure of the hydrous-mylonite zone

The hydrous-mylonite is composed of elongate and stretched orthopyroxene, clinopyroxene and olivine porphyroclasts (~1cm size), embedded in a fine-grained matrix (Fig. A2.3.1, see detailed description in part 2.4). Olivine porphyroclasts show pressure shadows composed of recrystallized olivine (10 to 50 μm) oriented parallel to the foliation (Fig. A2.3.1b). Olivine porphyroclasts are elongated with pronounced deformation bands and kink bands. The fine-grained mylonitic matrix is composed of opx, cpx, spinel, Ti-hbl and plagioclase (mostly altered). Five hydrous-mylonite outcrops where studied during field investigations and present substantial textural variation (Fig. A2.3.1).

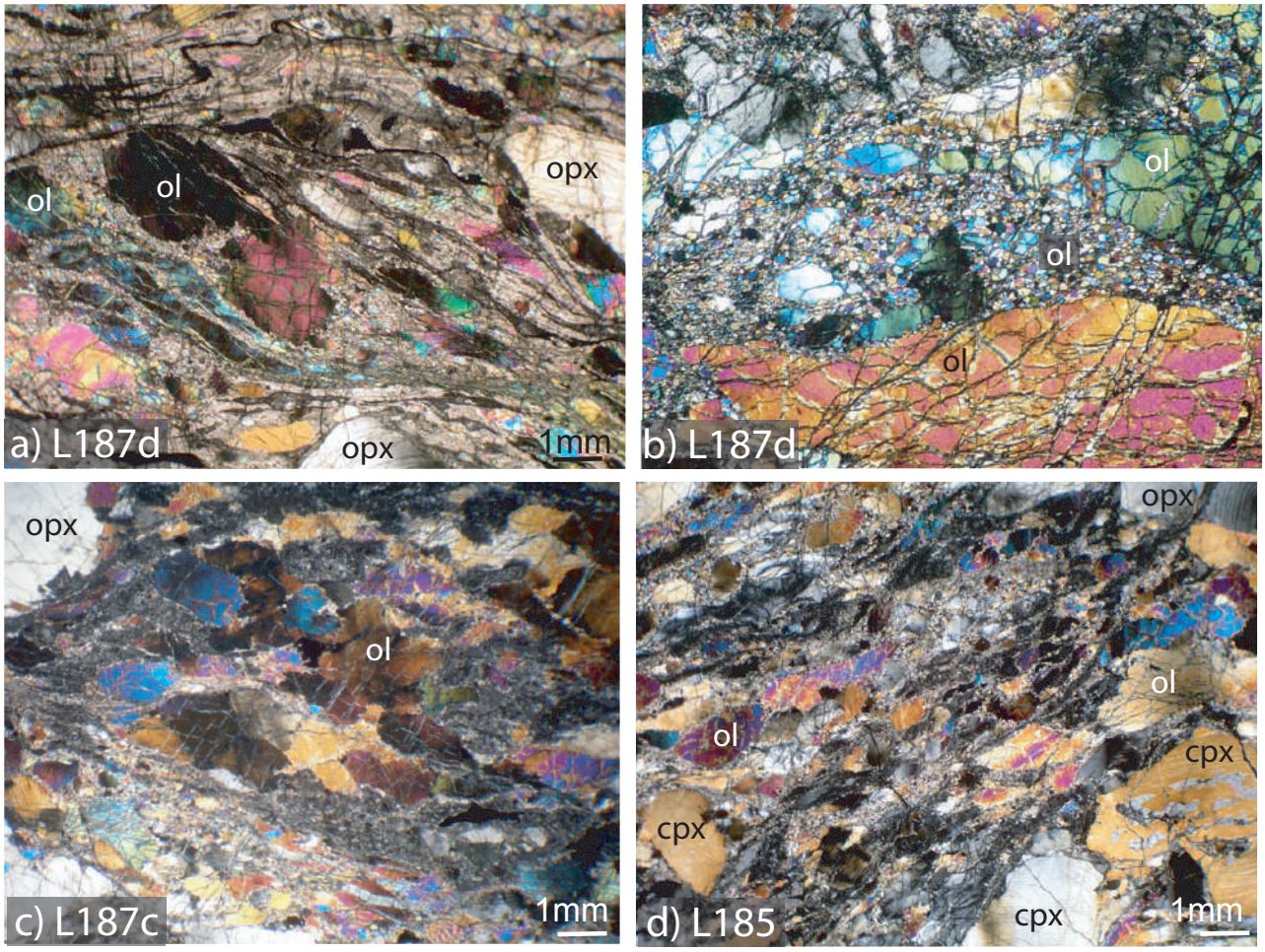

Fig. A2.3.1: Photomicrographs of hydrous peridotite mylonites. Note the overall elongate shape of olivine and pyroxene porphyroclasts and the dynamically recrystallized grains within the pressure shadows. (a) L187d, (b) L187d, zoom on recrystallized olivine elongated along the foliation, (c) L187c, (d) L118, (e) L185, (f) L95. opx: orthopyroxene, cpx: clinopyroxene, ol: olivine. Note that orthopyroxene porphyroclasts are folded and kinked, in contrast to (001) gliding observed in Fig. 2.5).

A2.3.2 Hydrous-mylonite foliation and shearing

The hydrous-mylonite zone mapped on the Figure A2.3.2 is represented by five samples. L187 outcrop permits detailed observations along a 50 m long cross section (Fig. A2.3.3). The main foliation shows important variations from N110 (general orientation of the mylonite) to N185 and is commonly parallel to the pyroxenite layering (≤ 2 cm thick). Along the outcrop four shear planes (P1 to P4) cut the main foliation. Along these shear planes dragging of the foliation indicates a sinistral the sense of shear (Fig. A2.3.3b-d). The hydrous-mylonite foliations and their relationships with the shear planes indicate a top to the SW sense of shear. In the southern part of the outcrop, the pyroxenite layering is discordant to the foliation by an angle of ~15° and at the north of the shear plan P4, by an angle of ~35° (Fig. A2.3.3), while in all other locations where pyroxenite layers could be distinguished, they are parallel to the main foliation. The orientation of the shear planes vary between N62 and N75 (P1 to P3) and P4 is orientated at 105N.

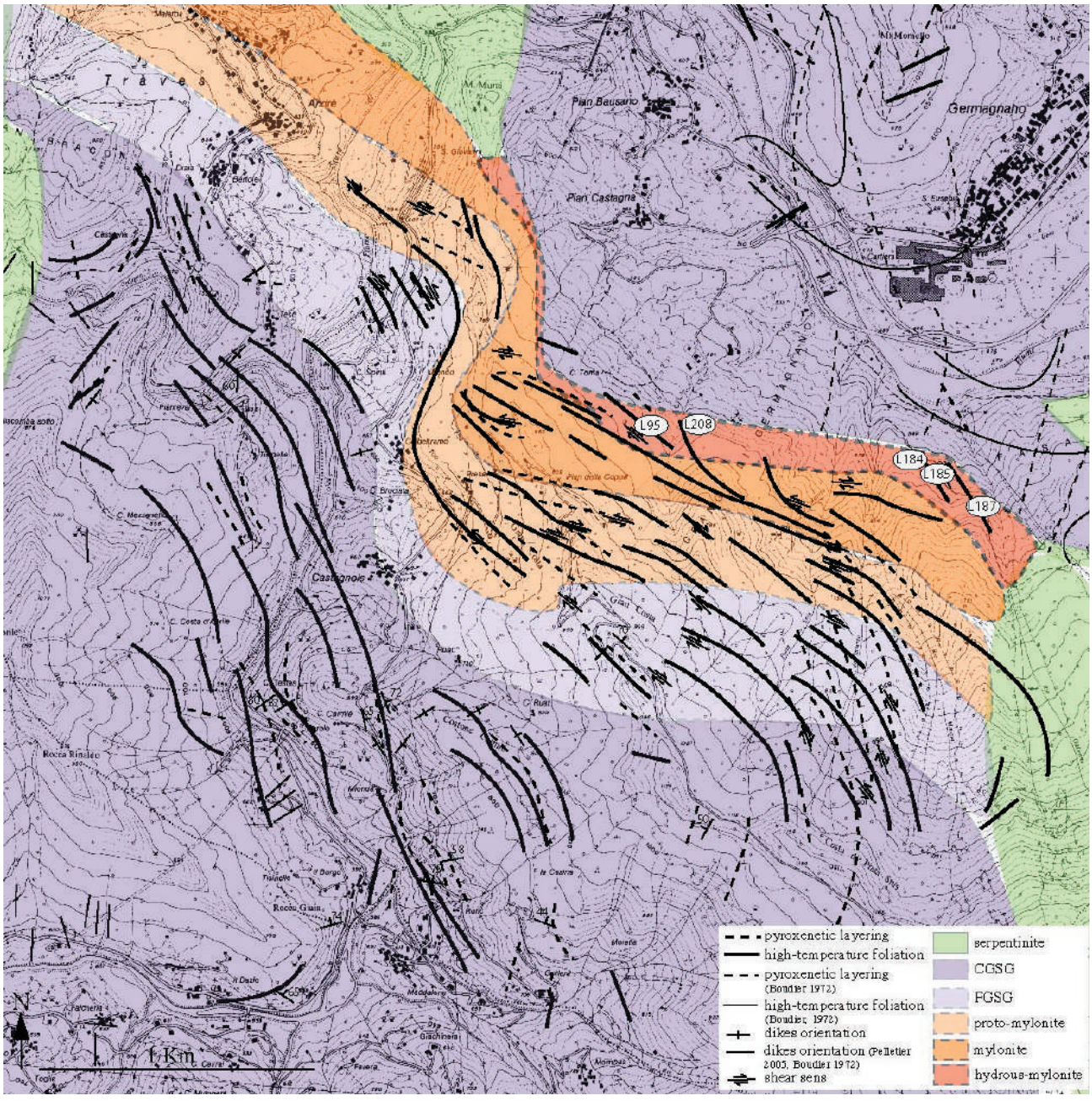

Fig. A2.3.2: Map of the shear zone between the northern and the central part of the Lanzo massif, with sampling locations of hydrous mylonite.

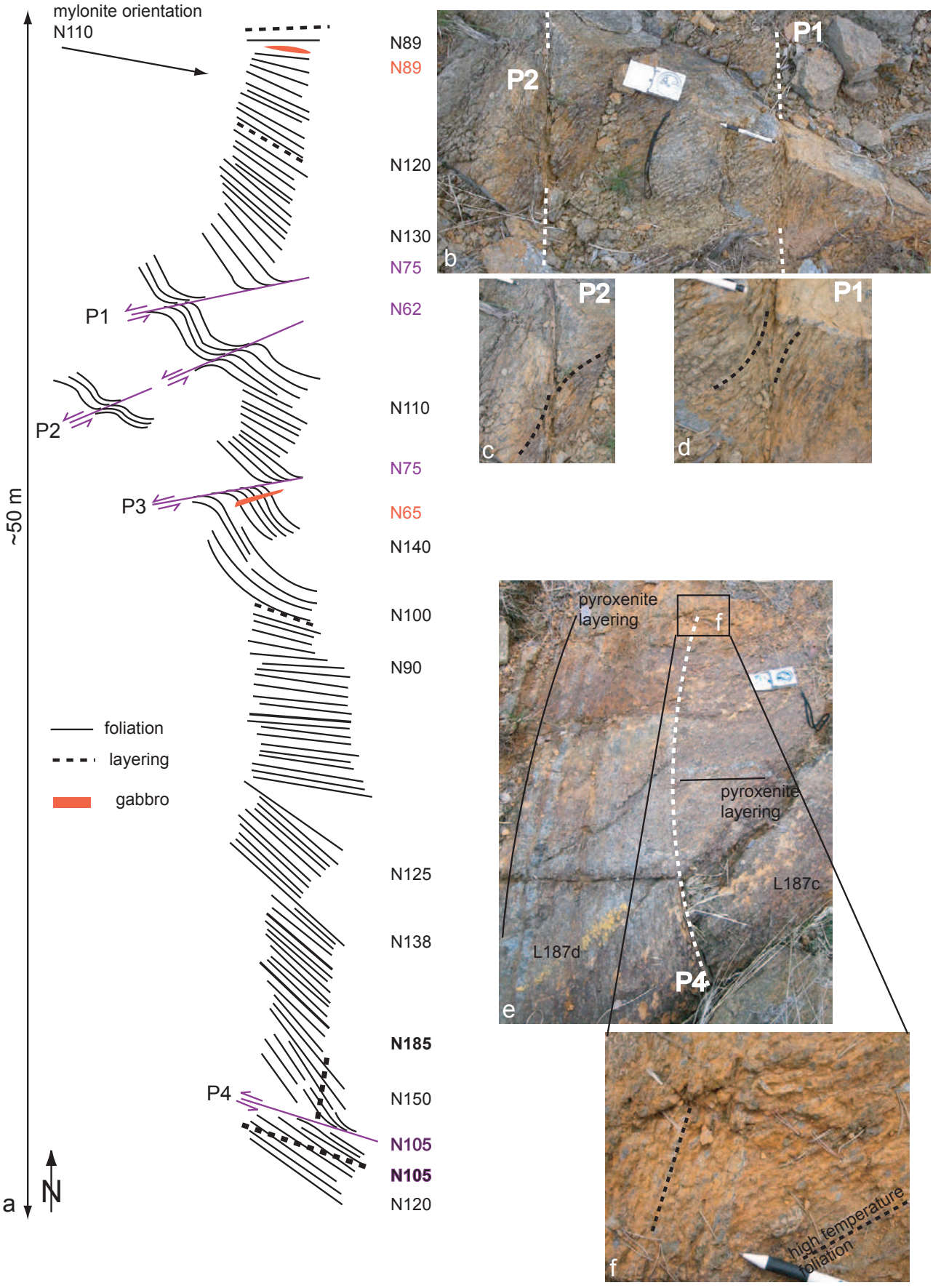

Fig. A2.3.3: L187 outcrop. (a) Sketch of the outcrop with representation of the main foliation, pyroxenite layering, gabbro dikes and the shear planes (P1-P4). (b) Shear planes P1 and P2, (c) Detail of (P2) with drag folds; (d) Detail of P1 with drag folds; (e) Shear plane P4, with locations of samples L187c, L187d and L187e; (f) Close up of P4 shear plane illustrating the discordance of high temperature foliation and pyroxenite layering.

A2.3.3 Mineralogy of shear plane P4

The petrographic study of the hydrous-mylonite (sample L187d, chapter 2) was completed by investigations of samples from the P4 shear plane (L187e, Fig. A2.3.3f). L187e is an ultra-mylonite composed of rounded prophyroclasts (olivine, clinopyroxene and orthopyroxene) embedded in a fine-grained matrix (<10 μm) (Fig. A2.3.4). The matrix is composed of cpx, opx, ol neoblasts, Ti-hbl and plg (sometimes altered to zoisite). The olivine porphyroclasts are elongated parallel to the foliation with grain size ranging from 1 several mm. The orthopyroxene porphyroclasts (2 - 8 mm) display clinopyroxene exsolutions, kink bands and internal folding. The porphyroclastic clinopyroxene (grain size 200 - 1000μm) displays orthopyroxene exsolution lamellae and that oriented subparallel to the foliation. Porphyroclastic Ti-hornblende (> 50 μm) are occasionally found, embedded in the fine-grained matrix. The amphibole is light brown colored and pleochroic, and show kaersutitic compositions (Table A2.3.1).

The principal minerals were analyzed with the microprobe (see condition in appendix 1) and results are reported in Table A2.3.1. The opx porphyroclastic cores display high Al_2O_3 (3.27 to 4.37 wt%) and Cr_2O_3 content (0.58 and 0.80 wt%). These compositions are similar to those of other porphyroclastic opx from the entire shear zone (Fig. A2.3.5a-b). The CaO content is very low (0.36 to 0.59, Fig. A2.3.5a), indicating substantial reequilibration with cpx. From core to rim, the Al_2O_3 and Cr_2O_3 content decreases, but much less than in illustrated in Fig. 2.12.

The chemical composition of clinopyroxene porphyroclasts shows an Al_2O_3 increase with Cr_2O_3 (Tab. 2.8). The rim and core compositions from the L187e ultra-mylonite displays core compositions that are enriched in TiO_2 and Al_2O_3 content (Fig. A2.3.5c-d). Several rims show a very low Cr_2O_3 content at high Al_2O_3 (Fig. A2.3.5d), and probably represent completely disaggregated pyroxenite layers.

Olivine Mg# varies between 0.89 and 0.91. The composition of cores, rims and neoblasts are homogeneous, and are similar to those measured in peridotites from the central and northern bodies.

The neoblastic plagioclase from the matrix is andesine, with 0.32 % An content. The porphyroclastic brown amphibole is Ti- and K-rich (~4.67 wt % and ~1.08 wt%, respectively) and can be classified as kearsutite (Tab. A2.3.1).

A2.3.4 Mylonite and gabbros

The occurrence of gabbros in the northern part of the massif is rare, and the majority of gabbros are found south of the shear zone (Fig. 2.7, part 2.2.3). However, at the outcrop L187 located at the northern of the shear zone, mylonite peridotite is intercalated with zones of plagioclase enrichment (size < 1cm), discontinuous and parallel to the foliation (Fig. A2.3.6a). The peridotite contains gabbroic dikelets of ~ 3cm thickness with smooth shapes (Fig. A2.3.6b-e). Gabbro dikelets are mostly

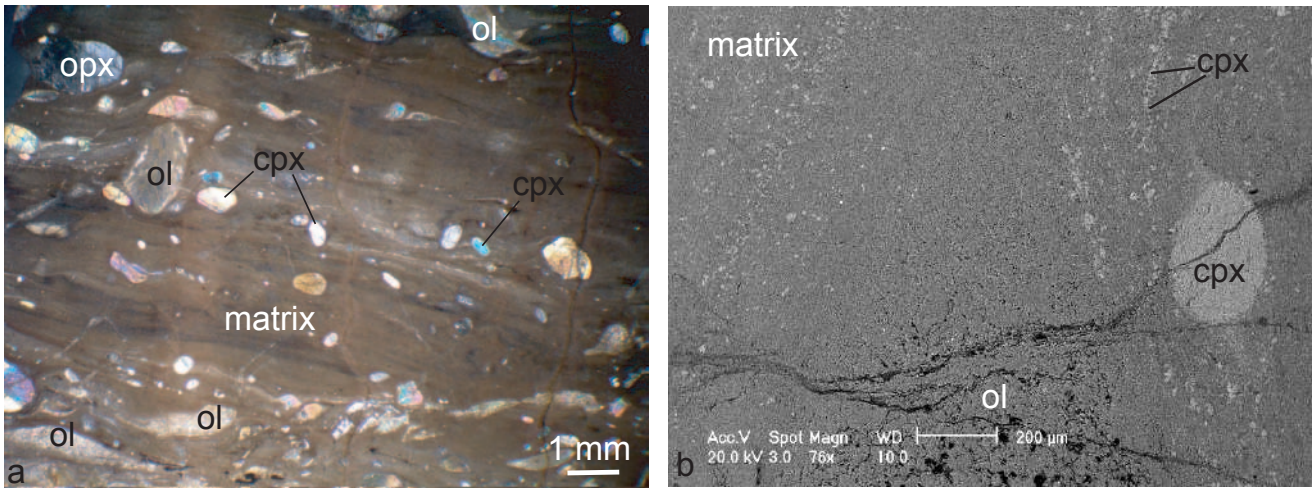

Fig. A2.3.4: Microphotographs of sample L187e from the P4 shear plane. (a) The porphyroclasts are rounded and embedded in a fine-grained matrix (transmitted light). (b) SEM picture of the matrix and rounded clinopyroxene.

Table A2.3.1: Orthopyroxene, clinopyroxene, olivine, feldspath and amphibole composition of neoblasts, porphyroclasts core (core) and porphyroclast rim (rim). (n= number of analyses). Mg# = (Mg / (Mg + Fe^{2+} + Fe^{3+})) and Cr# = (Cr/(Cr+Al)).

Minerals		olivine			orthopyroxene			clinopyroxene		amphibole	feldspath
		neoblasts	*rim*	*core*	*neoblast*	*rim*	*core*	*rim*	*core*		
		n=5	*n=5*	*n=5*	*n=3*	*n=4*	*n=4*	*n=5*	*n=4*	*n=4*	*n=1*
wt%	SiO2	40.7(5)	40.3(5)	40.6(3)	54.8(5)	55.6(1.4)	54.7(5)	51.0(7)	50.8(5)	42.2(5)	52.45
	TiO2	0.02(3)	0.02(2)	0.01(0)	0.58(10)	0.40(31)	0.65(10)	1.04(20)	1.10(18)	4.67(1)	0.03
	Al2O3	0.01(1)	0.01(1)	<0.01	0.22(2)	0.18(7)	0.20(3)	0.79(15)	0.80(13)	12.4(0)	0.03
	Cr2O3	<0.01	0.01(2)	<0.01	3.14(4)	2.17(1.2)	3.77(5)	5.0(8)	5.3(1.1)	1.15(7)	28.11
	Fe2O3	9.9(17)	9.74(27)	9.74(50)	0.45(5)	0.47(41)	0.72(18)	0.40(26)	0.50(6)	5.03(11)	0.84
	FeO	0.14(2)	0.14(1)	0.13(2)	6.31(5)	6.21(33)	6.27(8)	2.42(19)	2.40(8)	<0.01	<0.01
	MnO	0.40(2)	0.37(4)	0.40(4)	0.16(1)	0.16(2)	0.16(0)	0.09(2)	0.09(1)	0.05(1)	0.02
	NiO	0.02(1)	0.02(2)	0.02(1)	0.08(1)	0.09(3)	0.09(2)	0.03(2)	0.04(2)	0.09(2)	0.04
	MgO	48.7(4)	48.7(6)	49.1(5)	32.8(1)	33.4(8)	32.8(4)	15.4(7)	15.2(5)	15.7(3)	0.40
	CaO	<0.01	<0.01	<0.01	0.54(1)	0.43(1)	0.46(1)	22.1(1.0)	22.2(6)	11.4(2)	8.27
	Na2O	<0.01	<0.01	<0.01	0.02(1)	0.01(1)	0.01(1)	0.71(9)	0.71(1)	2.93(1)	9.60
	K2O	<0.01	<0.01	<0.01	<0.01	<0.01	<0.01	0.01(1)	<0.01	1.08(2)	0.02
	H2O	-	-	-	-	-	-	-	-	2.1(1)	-
	Total	99.9(4)	99.3(9)	100.0(4)	99.1(1)	99.2(5)	99.9(3)	99.0(3)	99.1(4)	98.9(4)	99.82
cation	Si	0.999(12)	0.995(5)	0.996(4)	1.92(2)	1.94(4)	1.90(1)	1.87(2)	1.87(1)	5.95(4)	2.292
	Ti	<0.001	<0.001	<0.001	0.016(13)	0.011(8)	0.018(3)	0.030(6)	0.032(5)	0.128(8)	0.001
	Al	<0.001	<0.001	<0.001	<0.001	0.005(2)	0.005(1)	0.022(4)	0.022(3)	0.494(2)	0.001
	Cr	<0.001	<0.001	<0.001	0.13(2)	0.09(5)	0.15(2)	0.22(4)	0.23(5)	2.06(1)	1.448
	Fe3+	0.205(4)	0.201(7)	0.200(11)	0.012(13)	0.012(11)	0.019(5)	0.011(7)	0.014(2)	0.534(15)	0.028
	Fe2+	0.003(0)	0.003(0)	0.003(0)	0.184(16)	0.181(8)	0.182(3)	0.074(6)	0.074(2)	<0.001	<0.001
	Mn	0.008(1)	0.007(1)	0.008(1)	0.005(0)	0.005(0)	0.005(0)	0.003(1)	0.003(0)	0.006(2)	0.001
	Ni	0.000	0.000	0.001(0)	0.002(0)	0.003(1)	0.002(1)	0.001(1)	0.001(1)	0.011(2)	0.001
	Mg	1.78(1)	1.792(8)	1.79(1)	1.708(6)	1.738(32)	1.697(17)	0.844(33)	0.833(23)	3.30(4)	0.026
	Ca	<0.001	<0.001	<0.001	0.020(3)	0.016(4)	0.017(4)	0.87(4)	0.87(2)	1.71(4)	0.387
	Na	<0.001	<0.001	<0.001	0.001(1)	0.001(1)	0.001(4)	0.051(6)	0.051(1)	0.800(1)	0.813
	K	<0.001	<0.001	<0.001	<0.001	<0.001	<0.001	0.000(1)	<0.001	0.193(5)	0.001
	H	-	-	-	-	-	-	-	-	2.000	-
	Total	3.000	3.000	3.000	4.000	4.000	4.000	4.000	4.000	15.00	5.000
	# Mg	0.897	0.899	0.900	0.897	0.900	0.895	0.909	0.906	0.873	An=32
	# Cr	-	-	-	0.110	0.110	0.104	0.121	0.123	0.058	Alb=68

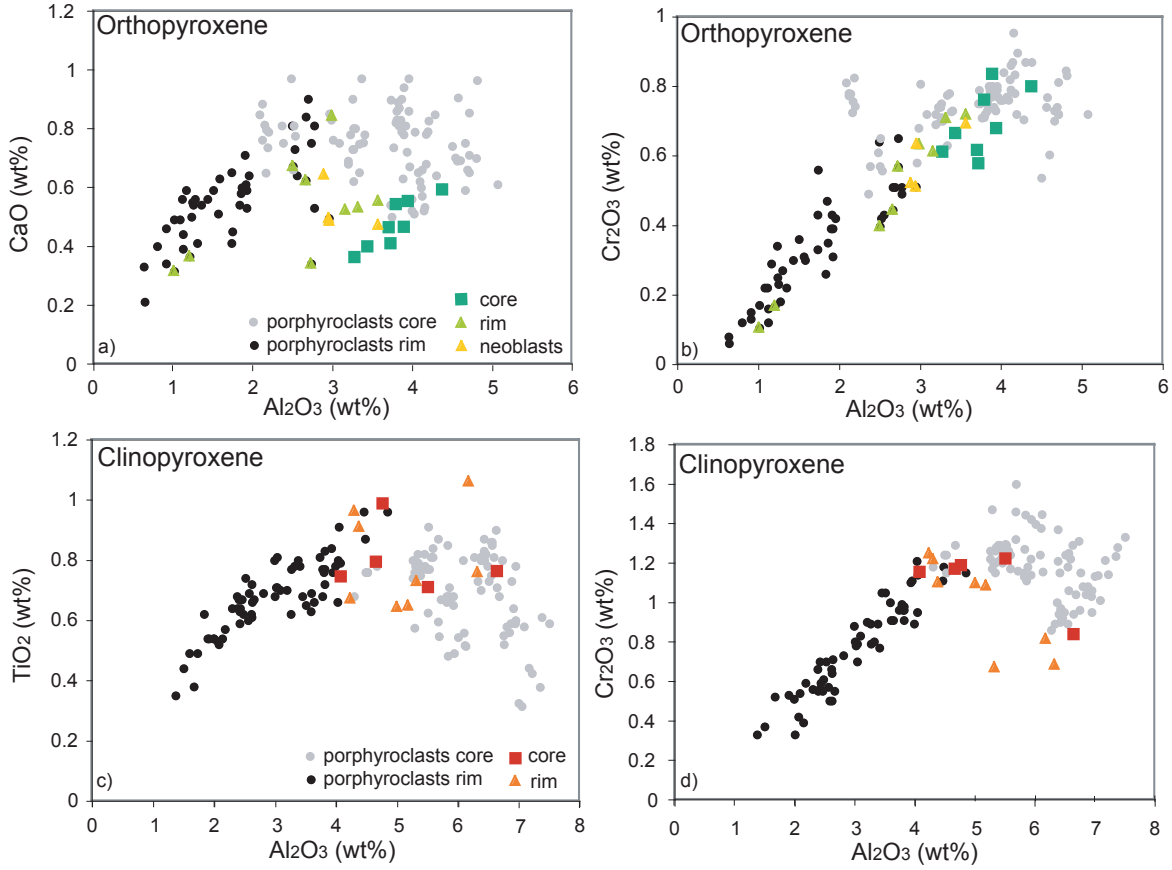

Fig. A2.3.5: Diagrams of orthopyroxene and clinopyroxene composition from porphyroclasts and neoblasts of ultra-mylonite sample L187e (a-b) Al2O3 vs. CaO and Cr2O3 (wt%) in orthopyroxene and (c-d) Al2O3 vs. TiO2 and Cr2O3 in clinopyroxene. Circles represent pyroxene compositions discussed in Fig. 2.8.

Fig. A2.3.6: Field aspects of gabbros from the L187 outcrop. (a) Plagioclase lenses oriented parallel to the main foliation. (b to e) Field aspect and polished surface of L187a (b,c) and L187b (d,e) gabbro dike with cm-scale elongate hornblende. (f-h) Microphotographs of amphibole-gabbro (crossed-polarized light). Note the consistent sense of shear in peridotite and gabbro in (h). Abbreviations are hbl: hornblende; plg: plagioclase.

parallel to the foliation with one exception, which is discontinuous and discordant to the foliation (Fig. A2.3.5). Gabbros are composed of altered plagioclase and hornblende (3 to 10 mm in size), which are organized as layers (Fig. A2.3.6b-g). The hornblende layers are internally boudinaged and the minerals show pressure shadows with dynamic recrystallization of hornblende (Fig. A2.3.6e-g). The transition from gabbro layer to peridotite mylonite is a fine-grained mylonite layer (from 50 μm to 1mm) composed essentially of hornblende and olivine aligned parallel to the foliation (Fig. A2.3.6g).

A2.3.5 Conclusions on the hydrous-mylonite zone

The L187 outcrop, localized at the northern part of the shear zone, in the hydrous-mylonite zone, provides important information about the shearing mechanisms during mantle exhumation and cooling. The late shear planes (P1 to P4) dissected and "tilted" the foliation at high temperature conditions. The top to S-W sense of shear is concordant to the shear sense determination obtained for the entire shear zone and is interpreted as secondary shear planes (C′, Fig. A2.3.7). C′-type shear band cleavage is developed during late shear zone activity after a strong mineral preferred orientation has already been accomplished, and probably represents flow partitioning in strongly anisotropic materials (Dennis and Secor, 1987; Passchier, 1991; Platt, 1984; Platt and Vissers, 1980). The feldspar enrichment lenses and thin amphibole-gabbro dikes parallel to the high temperature foliation, argue for the presence of melt in the mylonite zone during deformation. One gabbro dike orientation was discordant to the main foliation, but is close to the orientation of the others dikelets and parallel to the shear plan P3. This orientation is interpreted as melt accumulation continuous during formation of shear plans. The gabbros contacts with the host peridotite are no sharp indicating a small range of temperature between the peridotite and dikelets. The gabbro matrix is deformed and minerals are elongate and parallel to the peridotite mylonite and boudins of amphiboles. The presence of amphibole in the gabbro indicates H_2O-rich magma source with a solidus substantially lower than the peridotite. These observations suggest either syn-magmatic deformation in the crystallizing gabbroic dike and/or concomitant shearing of the peridotite.

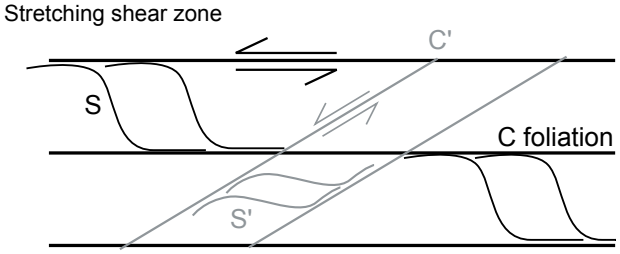

Fig. A2.3.7: Schematic diagram showing the development of C 'type shear bands. The regular fabric is composed of shear bands illustrated the main foliation (C) associated to an oblique passive foliation (S). C/S fabrics can be overprinted by C' type shear band cleavage (Berthé et al., 1979). C'-type shear band cleavage develops mainly in strongly foliated mylonites.

These preliminary observations indicate the presence of evolved magmas in the mylonite zone, which were most probably not completely solidified while the shear zone was active. The deformation plays an important role in focusing melt migration. The absence of gabbros in the hangingwall of the shear zone, the presence of plagioclase-rich lenses and amphibole-gabbros dikelets in the hydrous mylonite indicate that the actively deforming shear zone was "impermeable" for migrating gabbroic dikes.

A.2.3.6 Summary and conclusions on the shear zones

The detailed study of a high temperature shear zone, which separates the northern to the central bodies of the Lanzo massif, displays the relationship between melt/rock interaction and high temperature deformation.

The shear zone between the northern and the central bodies of the Lanzo massif is characterized by 5 classes of deformation: (1) coarse grained secondary granular texture (CGSG) progressively replaced by (2) fine grained secondary granular texture (FGSG), (3) proto-mylonite, (4) mylonite and (5) hydrous-mylonite. The CGSG rocks are composed of numerous centimeter grain size porphyroclast and recrystallize zone of clinopyroxene, orthopyroxene and olivine. The mylonite and hydrous-mylonite

are characterized by stretched porphyroclasts (10:1 aspect ratio) embedded in a fine-grained matrix of opx, cpx, sp and ol, in equilibrium with plagioclase (~50 μm grain size). The deformation is asymmetrical distributed toward the shear zones, increase from south to north and became localized at the northern part of the central body. The northern body is composed of CGSG rocks and is in sharp contact with the hydrous mylonite. The high temperature foliation and the layering are discordant in the CGSG zone (northern body and south of the central body) and tend to be parallel in the mylonite zone. The foliation, at the map scale indicates a top to N-W sense of shear (Fig. 2.7). The mylonite rocks contain orthopyroxene with pressure shadows and a "passive foliation", both indicate a top to N-W sense of shear. The presence of high temperature shear planes at the north of the central body, illustrates a continuous deformation and a progressive localization up to formation of mm-cm scale C′ shear planes. The localization of the deformation, the asymmetrical distribution of the deformation and the presence of late high temperature shear planes, collectively suggest that the central body of the Lanzo massif was the footwall of the shear zone, and the northern body was the hanging wall.

The chemical composition of orthopyroxene and clinopyroxene porphyroclast cores indicate a high Al_2O_3 content, which corresponds to calculated temperature of 1100°C and interpreted as remnants of spinel facies. From core to rim, the clinopyroxene and orthopyroxene porphyroclasts are zoned and display a continuous decrease in Al_2O_3. The neoblasts display low contents of Al_2O_3, TiO_2 and CaO and the calculated temperature indicates retrogression to 880°C in the mylonite, and 800°C in the hydrous-mylonite. The porphyroclast zoning and the decrease of temperature suggest a rapid exhumation of the footwall of the shear zone, which preserved a large chemical disequilibrium. The spinel chemical composition from the central part of the Lanzo massif recorded the entire range of abyssal peridotite composition (high TiO_2 and large Cr# variation). The spinels from granular rocks show a larger chemical variation than spinel from mylonites. This illustrates a faster equilibration and homogenization indiced by grain size reduction. Contrary to the central body, the northern body displays homogeneous spinel composition close to be totally equilibrated in the plagioclase facies. This suggests a relatively faster exhumation of the central body (the footwall) compared to the northern body (the hanging wall).

The melt impregnation microstructures were observed in the entire massif and were partially destroyed by the mylonitic deformation. The melt reacted with the peridotite before the deformation and/or during the deformation. The mafic dikes from the Lanzo massif are concentrated in the footwall of the shear zone and cross-cut the high temperature foliation. Gabbro dikes are rare or absent in the northern body, and few centimetric gabbroic dikes, parallel to the foliation are found within the hydrous peridotite mylonite. The concentration of dikes in the footwall of the shear zone and the presence of a few dikelets in the hydrous-mylonite suggest that the actively deforming shear zone was "impermeable" for migrating gabbroic dikes to the hanging-wall and was a melt accumulation.

The presence of pargasite in the recrystallized domains within the entire shear zone indicates hydrous component, crystallized from hydrous melt at ≤1050°C (Niida and Green, 1999). The increase of the modal abundance of Ti-pargasite towards the hydrous mylonite, indicates migration of hydrous liquid (or fluid) concentrated in the top part of the shear zone. It is concluded that the mylonite is a marker of important accumulation of melt in the system, probably as a consequence of high thermal gradients between the footwall and the hanging-wall of a mantle shear zone.

A2.4 MELT IMPREGNATION TEXTURES

A2.4a Clinopyroxene porphyroclastic replaced by oxp + plg

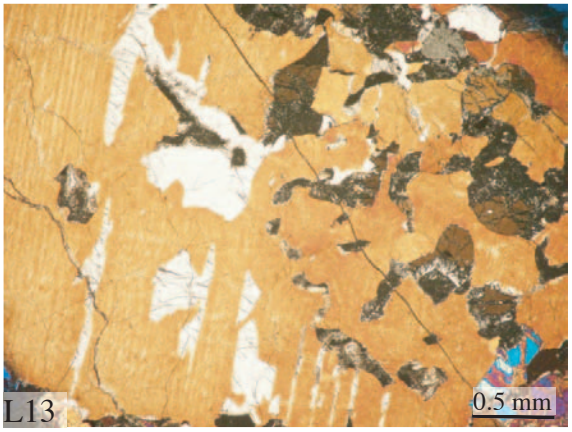

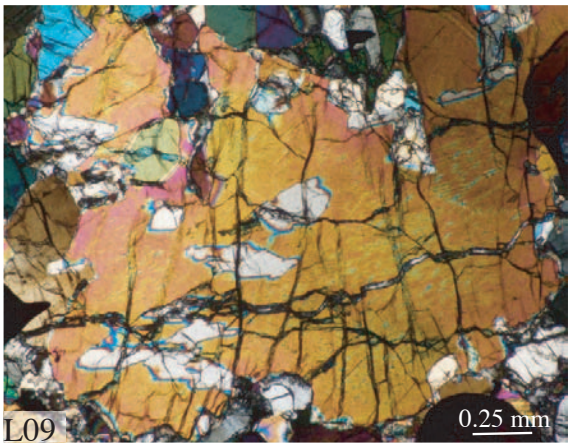

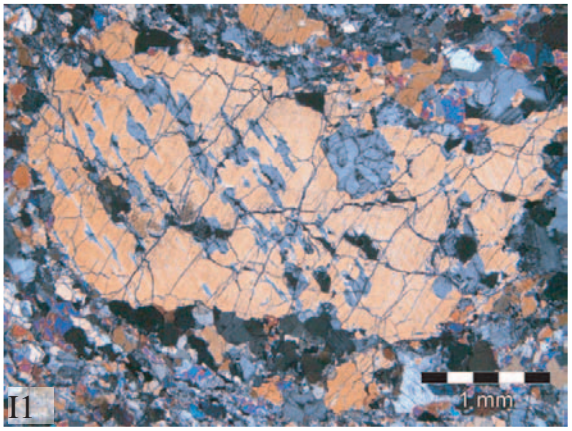

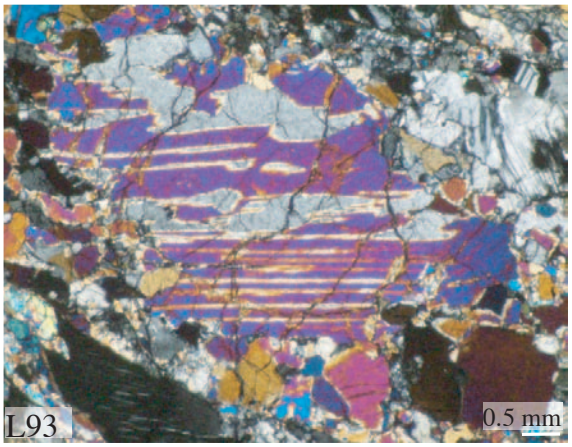

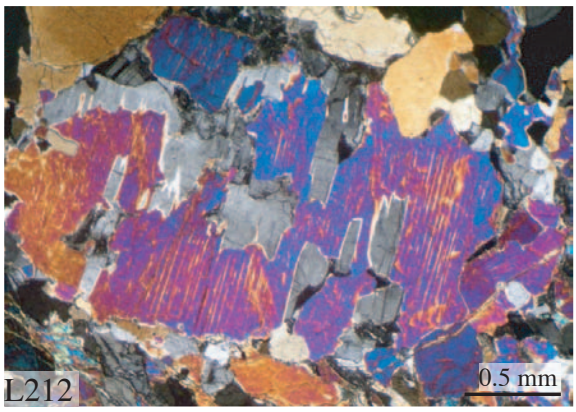

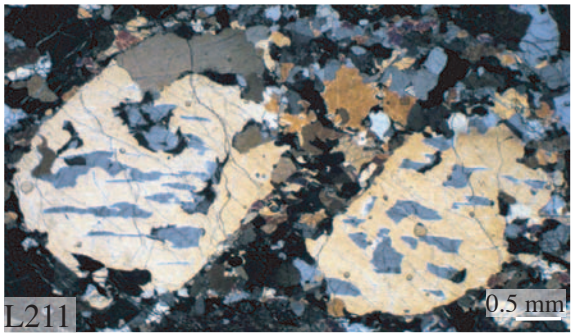

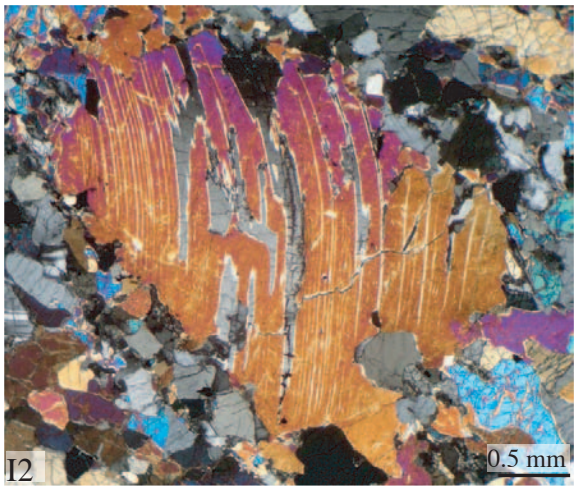

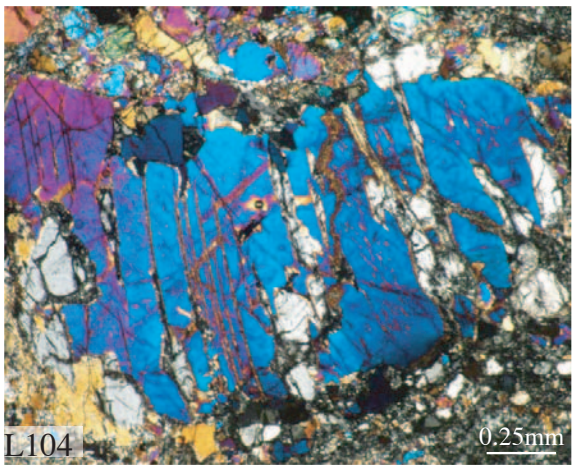

A2.4b Olivine porphyroclasts replaced by orthopyroxene

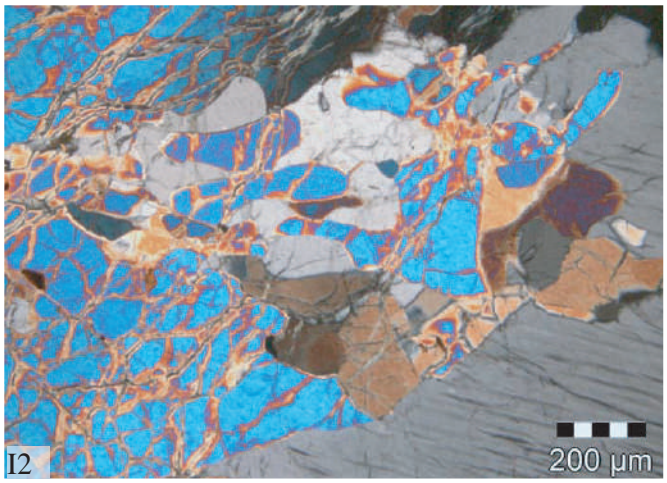

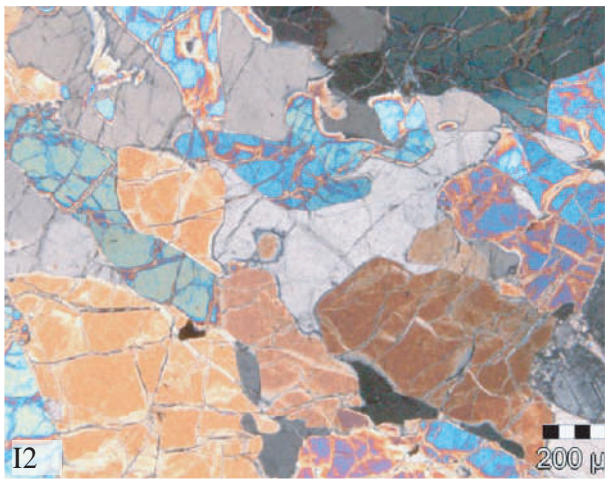

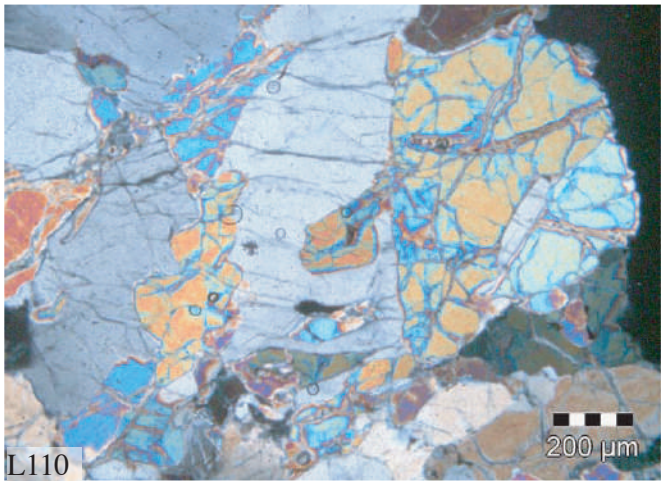

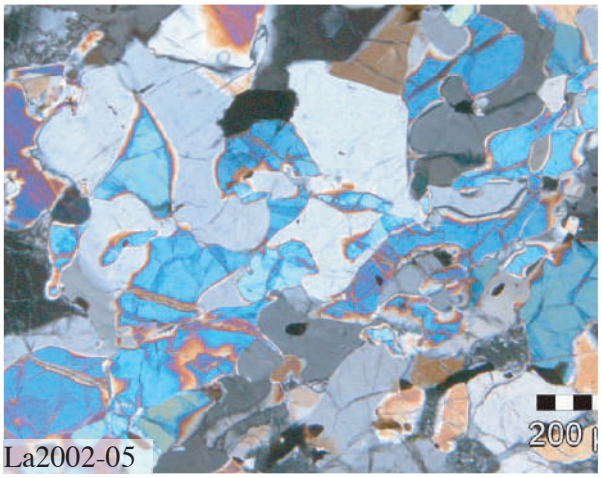

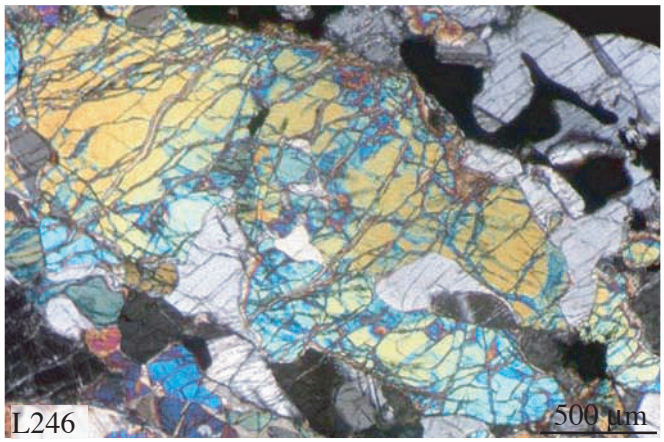

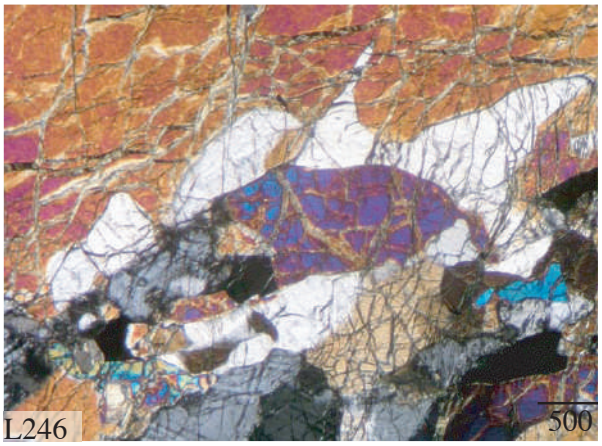

A2.4c Crystallization of feldspath close to spinel

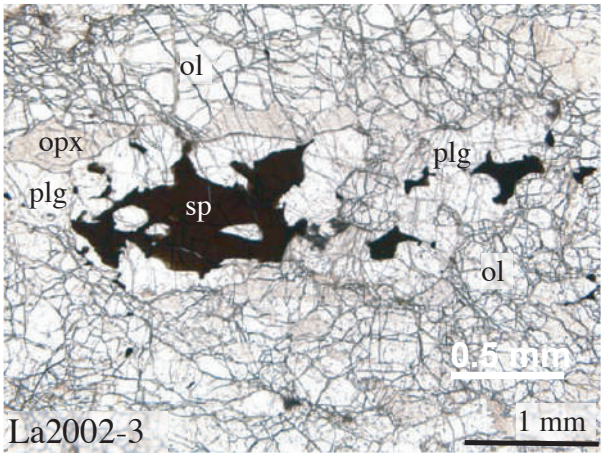

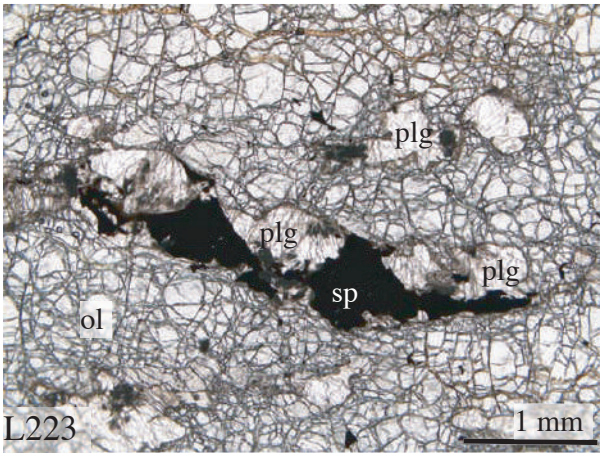

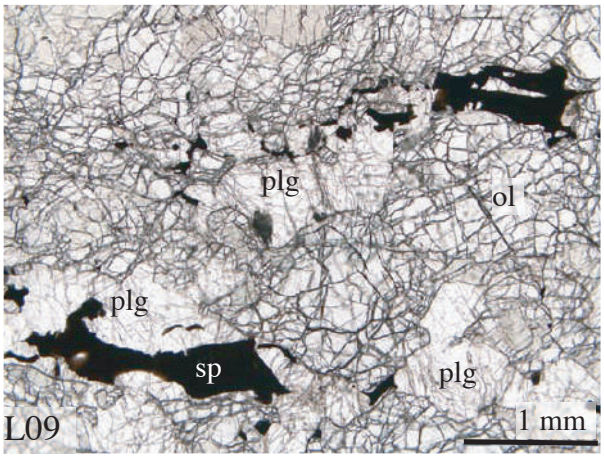

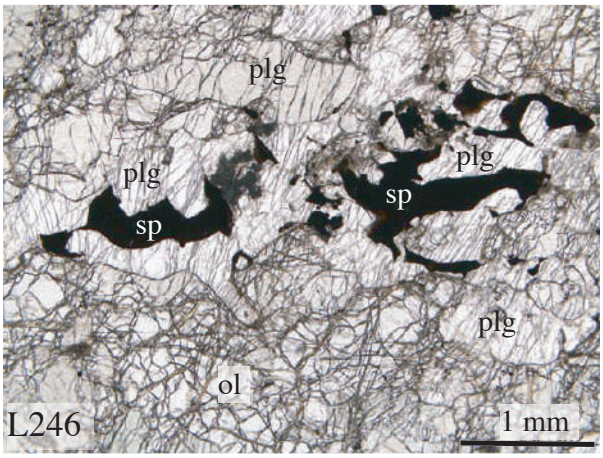

A2.4d Recrystallization of ol, cpx, opx

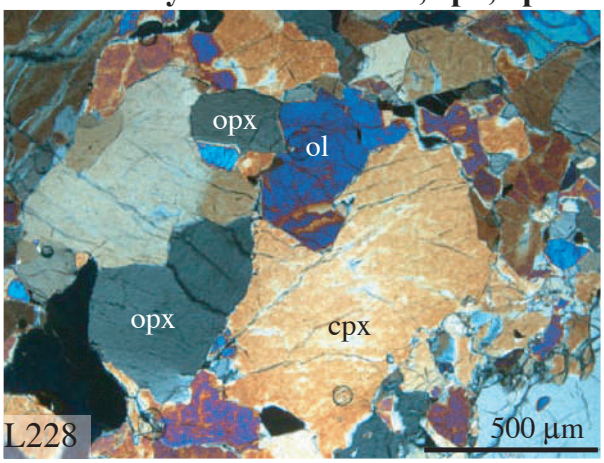

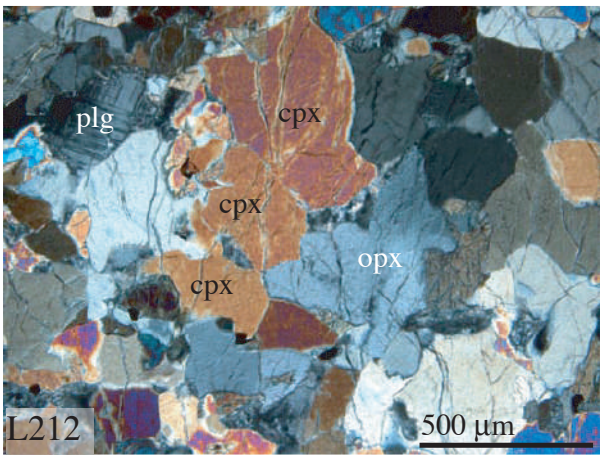

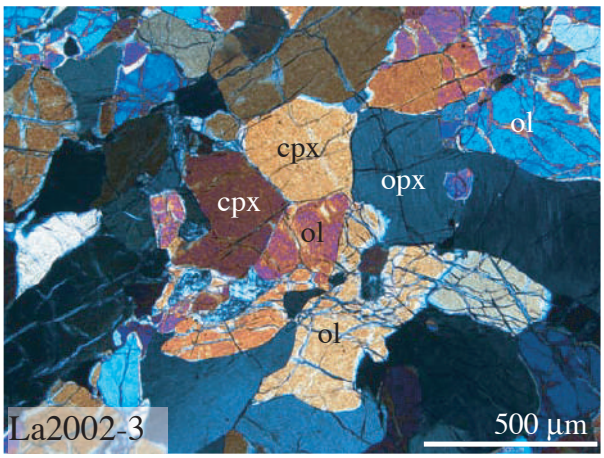

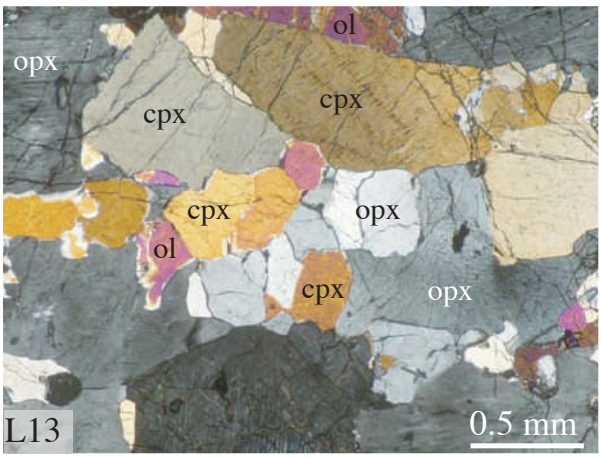

A2.5 MICROPROBE DATASET (SEE CD)

A2.5a Orthopyroxene

A2.5b Clinopyroxene

A2.5c Olivine

A2.5d Spinel

A2.5e Plagioclase

A2.5f Hornblende

A2.5a: Orthopyroxene dataset

opx neoblasts

	hydrous-mylonite				mylonite									
sample	L187d				L04					L104				
	1	2	3	4	1	2	3	4	5	1	2	3	4	5
SiO2	57.7	57.2	57.4	57.6	57.9	57.2	57.7	57.2	57.9	57.1	56.9	57.3	56.9	57.2
TiO2	0.13	0.16	0.14	0.08	0.15	0.21	0.19	0.21	0.15	0.23	0.26	0.20	0.21	0.23
Al2O3	0.80	1.12	1.12	0.63	0.91	1.58	1.08	1.43	0.91	1.92	1.92	1.25	1.73	1.86
Cr2O3	0.12	0.12	0.16	0.08	0.15	0.30	0.22	0.30	0.15	0.39	0.31	0.23	0.43	0.35
Fe2O3	0.89	0.70	1.44	1.18	0.90	1.73	1.43	1.59	0.90	0.83	1.55	1.36	1.08	0.47
FeO	6.07	6.03	5.68	5.86	5.63	5.01	5.40	5.51	5.63	5.91	5.54	6.17	5.73	6.32
MnO	0.15	0.22	0.22	0.20	0.13	0.16	0.18	0.17	0.13	0.17	0.18	0.18	0.16	0.17
NiO	0.10	0.05	0.05	0.02	0.06	0.02	0.09	0.03	0.06	0.08	0.09	0.09	0.08	0.11
MgO	34.9	34.6	35.0	35.0	35.4	35.1	35.2	34.8	35.4	34.6	34.5	34.5	34.5	34.3
CaO	0.40	0.39	0.44	0.33	0.34	0.63	0.49	0.56	0.34	0.53	0.59	0.54	0.65	0.60
Na2O	0.02	<0.01	<0.01	0.01	0.02	<0.01	0.02	0.02	0.02	<0.01	0.02	0.02	<0.01	0.03
K2O	<0.01	<0.01	<0.01	<0.01	<0.01	0.01	0.01	<0.01	<0.01	<0.01	0.03	<0.01	0.01	<0.01
Total	101.26	100.6	101.65	101.07	101.61	101.88	102.0	101.78	101.61	101.72	101.87	101.79	101.47	101.61
Si	1.9681	1.9625	1.9534	1.9693	1.965	1.937	1.953	1.942	1.965	1.940	1.9325	1.950	1.940	1.947
Ti	0.0033	0.0042	0.0035	0.0021	0.004	0.005	0.005	0.005	0.004	0.0058	0.0065	0.0051	0.0054	0.006
Al	0.0323	0.0453	0.0451	0.0254	0.036	0.063	0.043	0.057	0.036	0.077	0.0769	0.050	0.070	0.075
Cr	0.0032	0.0034	0.0042	0.0021	0.004	0.008	0.006	0.008	0.004	0.010	0.0082	0.0063	0.0116	0.009
Fe3+	0.0229	0.0182	0.0369	0.030	0.023	0.044	0.036	0.041	0.023	0.0212	0.040	0.0349	0.0278	0.012
Fe2+	0.1733	0.1732	0.1615	0.1675	0.160	0.142	0.153	0.157	0.160	0.168	0.1575	0.1757	0.1635	0.180
Mn	0.0044	0.0065	0.0062	0.0058	0.004	0.005	0.005	0.005	0.004	0.0048	0.0053	0.0051	0.0047	0.005
Ni	0.0028	0.0013	0.0014	0.0006	0.002	0.001	0.002	0.001	0.002	0.0021	0.0025	0.0023	0.0021	0.003
Mg	1.7738	1.7708	1.7717	1.7842	1.789	1.772	1.777	1.763	1.789	1.7516	1.7465	1.750	1.7511	1.739
Ca	0.0145	0.0144	0.0161	0.0122	0.012	0.023	0.018	0.020	0.012	0.0192	0.0216	0.020	0.0238	0.022
Na	0.001	<0.001	<0.001	<0.001	0.001	<0.001	0.001	0.001	0.001	<0.001	0.002	0.001	<0.001	0.002
K	<0.001	<0.001	<0.001	<0.001	<0.001	<0.001	<0.001	<0.001	<0.001	<0.001	0.001	<0.001	<0.001	<0.001
# Mg	0.90	0.90	0.90	0.90	0.91	0.91	0.91	0.90	0.91	0.90	0.90	0.89	0.90	0.90
# Cr	0.09	0.07	0.09	0.08	0.10	0.11	0.12	0.12	0.10	0.12	0.10	0.11	0.14	0.11

opx neoblasts **opx porphyro**

	proto-mylonite						FGSG						hydrous-myloni	
sample	L112		La2002-05				L09			L110			L187d	
	1	2	1	2	3	4	1	2	3	1	2	3	1	2
SiO2	56.4	56.9	56.4	56.7	57.3	57.7	56.2	56.3	56.1	56.7	56.8	56.7	55.1	54.9
TiO2	0.24	0.21	0.26	0.20	0.20	0.15	0.23	0.21	0.24	0.23	0.15	0.24	0.23	0.26
Al2O3	1.83	1.16	1.90	1.50	1.11	0.91	2.52	2.66	2.77	1.56	1.30	1.85	3.74	3.99
Cr2O3	0.26	0.29	0.39	0.36	0.22	0.13	0.42	0.51	0.51	0.31	0.27	0.47	0.75	0.76
Fe2O3	0.45	0.70	0.54	0.47	0.49	0.49	1.32	1.27	0.67	0.94	0.86	0.00	0.72	1.37
FeO	6.36	5.71	6.64	6.58	6.40	6.53	5.67	5.96	6.44	6.35	6.46	6.76	5.92	5.80
MnO	0.21	0.13	0.18	0.15	0.15	0.16	0.21	0.16	0.15	0.19	0.14	0.18	0.07	0.09
NiO	0.07	0.10	0.07	0.07	0.06	0.08	0.09	0.10	0.04	0.09	0.09	0.03	0.09	0.09
MgO	33.8	34.5	33.5	33.9	34.4	34.6	33.9	33.8	33.3	34.0	34.1	33.6	33.2	33.2
CaO	0.54	0.59	0.71	0.59	0.56	0.46	0.73	0.84	0.81	0.51	0.41	0.58	0.50	0.52
Na2O	0.02	0.02	0.02	0.02	0.01	<0.01	0.02	0.01	0.04	0.01	0.01	0.02	0.04	<0.01
K2O	0.01	<0.01	<0.01	<0.01	0.01	<0.01	<0.01	<0.01	0.01	0.04	0.01	<0.01	<0.01	<0.01
Total	100.12	100.3	100.7	100.5	101.0	101.2	101.3	101.8	101.1	100.9	100.67	100.48	100.4	101.0
Si	1.948	1.959	1.943	1.954	1.964	1.970	1.922	1.918	1.924	1.947	1.955	1.954	1.900	1.885
Ti	0.006	0.006	0.007	0.005	0.005	0.004	0.006	0.005	0.006	0.006	0.004	0.006	0.006	0.007
Al	0.075	0.047	0.077	0.061	0.045	0.037	0.101	0.107	0.112	0.063	0.053	0.075	0.152	0.161
Cr	0.007	0.008	0.011	0.010	0.006	0.004	0.011	0.014	0.014	0.009	0.007	0.013	0.021	0.021
Fe3+	0.012	0.018	0.014	0.012	0.013	0.013	0.034	0.033	0.017	0.024	0.022	<0.001	0.019	0.036
Fe2+	0.184	0.165	0.191	0.190	0.183	0.187	0.162	0.170	0.185	0.182	0.186	0.195	0.171	0.167
Mn	0.006	0.004	0.005	0.004	0.004	0.005	0.006	0.005	0.004	0.006	0.004	0.005	0.002	0.003
Ni	0.002	0.003	0.002	0.002	0.002	0.002	0.003	0.003	0.001	0.003	0.003	0.001	0.002	0.003
Mg	1.739	1.768	1.722	1.739	1.757	1.763	1.727	1.715	1.705	1.739	1.750	1.728	1.706	1.700
Ca	0.020	0.022	0.026	0.022	0.020	0.017	0.027	0.031	0.030	0.019	0.015	0.021	0.019	0.019
Na	0.001	0.002	0.001	0.001	0.001	0.000	0.002	0.001	0.002	0.001	<0.001	0.001	0.003	<0.001
K	0.001	<0.001	<0.001	<0.001	<0.001	<0.001	<0.001	<0.001	<0.001	0.002	<0.001	<0.001	<0.001	<0.001
# Mg	0.90	0.91	0.89	0.90	0.90	0.90	0.90	0.90	0.89	0.89	0.89	0.90	0.90	0.90
# Cr	0.09	0.14	0.12	0.14	0.12	0.09	0.10	0.11	0.11	0.12	0.12	0.15	0.12	0.11

A2.5a: Orthopyroxene dataset

opx porphyroclasts core

	hydrous-mylo		**mylonite**						**proto-mylonite**				
sample	**L187d**		**L04**			**L104**			**L112**			**La2002-05**	
	3	4	1	2	3	1	2	3	1	2	3	1	2
SiO2	55.0	54.9	54.4	54.0	54.2	54.7	54.5	54.7	54.8	54.7	55.1	54.8	54.9
TiO2	0.27	0.24	0.11	0.17	0.13	0.21	0.14	0.21	0.23	0.23	0.22	0.19	0.18
Al2O3	3.72	4.02	0.81	0.74	0.79	4.48	4.66	4.68	3.95	3.89	3.79	3.85	3.83
Cr2O3	0.75	0.76	4.89	4.95	5.05	0.91	0.78	0.82	0.80	0.80	0.71	0.80	0.75
Fe2O3	1.13	1.59	0.41	1.27	0.72	1.43	1.73	0.57	0.00	0.00	0.00	1.22	1.21
FeO	5.81	5.80	6.15	5.47	6.00	5.53	5.47	6.12	6.34	6.46	6.77	5.74	5.86
MnO	0.10	0.14	0.10	0.15	0.08	0.17	0.14	0.17	0.15	0.12	0.19	0.18	0.10
NiO	0.11	0.09	0.09	0.14	0.15	-	-	-	0.15	0.12	0.10	0.09	0.07
MgO	33.2	33.1	32.5	32.6	32.3	33.0	33.1	32.7	32.4	32.1	32.4	32.8	32.9
CaO	0.54	0.51	0.63	0.63	0.68	0.68	0.56	0.72	0.86	0.94	0.82	0.83	0.87
Na2O	0.01	0.01	0.02	0.02	0.05	0.04	0.02	0.03	0.02	0.03	0.02	0.02	0.01
K2O	<0.01	0.03	0.02	0.01	0.02	<0.01	<0.01	0.01	<0.01	<0.01	<0.01	<0.01	0.02
Total	100.6	101.2	100.1	100.2	100.2	101.2	101.1	100.7	99.6	99.4	100.2	100.5	100.7
Si	1.893	1.883	1.882	1.869	1.876	1.875	1.870	1.882	1.906	1.909	1.908	1.891	1.892
Ti	0.007	0.006	0.003	0.004	0.003	0.005	0.004	0.005	0.006	0.006	0.006	0.005	0.005
Al	0.151	0.163	0.022	0.020	0.022	0.181	0.188	0.190	0.162	0.160	0.155	0.156	0.155
Cr	0.021	0.021	0.200	0.202	0.206	0.025	0.021	0.022	0.022	0.022	0.020	0.022	0.021
Fe3+	0.029	0.041	0.011	0.033	0.019	0.037	0.045	0.015	0.000	0.000	0.000	0.032	0.032
Fe2+	0.167	0.167	0.178	0.158	0.174	0.158	0.157	0.176	0.184	0.189	0.196	0.166	0.169
Mn	0.003	0.004	0.003	0.004	0.002	0.005	0.004	0.005	0.005	0.003	0.006	0.005	0.003
Ni	0.003	0.002	0.002	0.004	0.004	-	-	-	0.004	0.004	0.003	0.003	0.002
Mg	1.706	1.694	1.674	1.680	1.666	1.686	1.690	1.676	1.678	1.670	1.675	1.689	1.688
Ca	0.020	0.019	0.023	0.023	0.025	0.025	0.021	0.027	0.032	0.035	0.031	0.031	0.032
Na	<0.001	0.001	0.001	0.001	0.003	0.003	0.001	0.002	0.002	0.002	0.001	0.001	0.001
K	<0.001	0.001	0.001	0.001	0.001	<0.001	<0.001	<0.001	<0.001	<0.001	<0.001	<0.001	0.001
# Mg	0.90	0.89	0.90	0.90	0.90	0.90	0.90	0.90	0.90	0.90	0.90	0.90	0.90
# Cr	0.12	0.11	0.90	0.91	0.91	0.12	0.10	0.11	0.12	0.12	0.11	0.12	0.12

opx porphyroclasts core

te	**proto-mylonite**		**FGSG**					FGSG				CGSGc	
sample	**La2002-05**		**L09**					**L110**				**L13**	
	3	4	1	2	3	4	5	1	2	3	4	1	2
SiO2	55.0	55.1	54.9	55.2	54.9	55.1	55.5	55.6	55.6	55.5	55.4	55.4	55.5
TiO2	0.20	0.20	0.22	0.21	0.20	0.27	0.21	0.23	0.27	0.22	0.27	0.22	0.24
Al2O3	3.86	3.82	4.33	3.95	4.11	4.26	3.95	3.06	3.20	3.12	3.18	3.20	3.31
Cr2O3	0.75	0.78	0.91	0.79	0.77	0.83	0.75	0.66	0.68	0.74	0.71	0.67	0.70
Fe2O3	0.70	0.98	0.69	0.43	0.92	0.29	0.00	0.00	0.00	0.00	0.00	0.57	0.08
FeO	6.10	5.74	6.08	6.30	6.23	6.27	6.70	5.22	5.44	5.42	5.38	6.87	6.88
MnO	0.12	0.16	0.16	0.21	0.12	0.13	0.12	0.17	0.09	0.17	0.10	0.13	0.17
NiO	0.12	0.10	0.07	0.08	0.07	-	-	0.07	0.10	0.08	0.06	0.06	0.08
MgO	32.8	33.0	32.7	33.1	32.9	33.1	32.9	32.6	32.7	32.8	32.7	32.8	32.8
CaO	0.84	0.84	0.95	0.52	0.62	0.53	0.59	0.78	0.88	0.66	0.80	0.66	0.67
Na2O	<0.01	0.01	0.01	<0.01	0.02	0.01	0.02	0.02	0.03	<0.01	0.01	0.02	0.04
K2O	<0.01	<0.01	<0.01	0.01	<0.01	<0.01	<0.01	<0.01	0.02	0.01	<0.01	0.01	0.01
Total	100.5	100.8	100.9	100.7	100.8	100.8	100.7	98.4	99.0	98.7	98.6	100.6	100.5
Si	1.897	1.895	1.886	1.899	1.890	1.892	1.908	1.952	1.943	1.943	1.941	1.913	1.917
Ti	0.005	0.005	0.006	0.005	0.005	0.007	0.006	0.006	0.007	0.006	0.007	0.006	0.006
Al	0.157	0.155	0.025	0.021	0.021	0.023	0.020	0.127	0.132	0.129	0.131	0.131	0.135
Cr	0.021	0.021	0.176	0.160	0.167	0.172	0.160	0.018	0.019	0.020	0.020	0.018	0.019
Fe3+	0.018	0.025	0.018	0.011	0.024	0.008	0.000	0.000	0.000	0.000	0.000	0.015	0.002
Fe2+	0.176	0.165	0.175	0.181	0.179	0.180	0.193	0.153	0.159	0.159	0.158	0.198	0.199
Mn	0.003	0.005	0.005	0.006	0.004	0.004	0.004	0.005	0.003	0.005	0.003	0.004	0.005
Ni	0.004	0.003	0.003	0.003	0.003	-	-	0.003	0.003	0.002	0.002	0.002	0.002
Mg	1.688	1.694	1.675	1.697	1.687	1.694	1.687	1.706	1.700	1.711	1.708	1.687	1.687
Ca	0.031	0.031	0.035	0.019	0.023	0.019	0.022	0.029	0.033	0.025	0.030	0.025	0.025
Na	<0.001	0.001	0.001	<0.001	0.001	0.001	0.001	0.002	0.002	<0.001	0.001	0.001	0.002
K	<0.001	<0.001	<0.001	<0.001	<0.001	<0.001	<0.001	<0.001	0.001	<0.001	<0.001	<0.001	0.001
# Mg	0.90	0.90	0.90	0.90	0.89	0.90	0.90	0.92	0.91	0.92	0.92	0.89	0.89
	0.12	0.12	0.88	0.88	0.89	0.88	0.89	0.13	0.12	0.14	0.13	0.12	0.12

A2.5a: Orthopyroxene dataset

opx porphyroclasts core

	CGSGc										CGSGn		
sample	L13		L42		L147		L241				L195		
	3	4	1	2	1	2	1	2	3	4	1	2	3
SiO2	55.6	55.2	54.3	53.8	55.7	55.7	54.8	55.1	54.7	55.0	55.2	54.5	54.9
TiO2	0.29	0.26	0.12	0.22	0.27	0.26	0.19	0.18	0.17	0.20	0.09	0.17	0.11
Al2O3	3.28	3.34	4.17	4.15	3.74	3.78	4.08	4.01	4.11	4.07	4.57	4.54	4.50
Cr2O3	0.71	0.71	0.83	0.95	0.85	0.75	0.81	0.75	0.82	0.77	0.77	2.41	0.54
Fe2O3	0.05	0.38	0.91	3.18	0.60	0.48	1.09	1.65	1.83	1.21	0.00	0.00	0.39
FeO	7.20	6.86	5.33	3.50	6.30	6.34	5.83	5.49	5.34	5.88	5.87	5.60	5.57
MnO	0.09	0.14	0.18	0.19	0.15	0.21	0.15	0.22	0.13	0.17	0.17	0.15	0.16
NiO	0.10	0.08	0.12	0.08	0.10	0.15	0.11	0.15	0.12	0.09	0.02	0.07	0.02
MgO	32.6	32.6	32.6	33.6	33.3	33.2	33.0	33.4	33.1	33.1	32.9	31.4	33.1
CaO	0.77	0.71	0.78	0.53	0.59	0.70	0.60	0.56	0.60	0.65	0.90	0.70	0.74
Na2O	0.04	0.02	0.03	0.03	0.03	0.01	0.01	0.01	0.02	0.02	<0.01	0.00	0.01
K2O	<0.01	<0.01	0.01	<0.01	0.04	<0.01	<0.01	<0.01	0.03	<0.01	<0.01	<0.01	<0.01
Total	100.7	100.3	99.4	100.2	101.7	101.6	100.6	101.4	100.9	101.1	100.6	99.6	100.0
Si	1.917	1.911	1.889	1.857	1.901	1.902	1.887	1.884	1.879	1.887	1.896	1.906	1.893
Ti	0.008	0.007	0.003	0.006	0.007	0.007	0.005	0.005	0.004	0.005	0.002	0.004	0.003
Al	0.133	0.136	0.171	0.169	0.150	0.152	0.166	0.161	0.167	0.165	0.185	0.187	0.183
Cr	0.019	0.020	0.023	0.026	0.023	0.020	0.022	0.020	0.022	0.021	0.021	0.067	0.015
Fe3+	0.001	0.010	0.024	0.083	0.016	0.012	0.028	0.042	0.047	0.031	0.000	0.000	0.010
Fe2+	0.208	0.199	0.155	0.101	0.180	0.181	0.168	0.157	0.153	0.169	0.169	0.164	0.161
Mn	0.003	0.004	0.005	0.006	0.004	0.006	0.004	0.007	0.004	0.005	0.005	0.005	0.005
Ni	0.003	0.002	0.003	0.002	0.003	0.004	0.003	0.004	0.003	0.002	0.001	0.002	0.001
Mg	1.678	1.684	1.694	1.729	1.692	1.690	1.693	1.700	1.695	1.690	1.686	1.636	1.700
Ca	0.029	0.026	0.029	0.020	0.022	0.025	0.022	0.020	0.022	0.024	0.033	0.026	0.027
Na	0.003	0.002	0.002	0.002	0.002	0.001	0.001	<0.001	0.001	0.001	<0.001	<0.001	<0.001
K	<0.001	<0.001	0.001	<0.001	0.002	<0.001	<0.001	<0.001	0.001	<0.001	<0.001	<0.001	<0.001
# Mg	0.89	0.89	0.91	0.91	0.90	0.90	0.90	0.90	0.90	0.90	0.91	0.91	0.91
# Cr	0.13	0.13	0.12	0.13	0.13	0.12	0.12	0.11	0.12	0.11	0.10	0.26	0.07

opx porphyroclasts core						**opx porphyroclasts rim**							
	CGSGn					hydrous-mylonit	mylonite						proto-m
sample	L195		W2			L187d	L04		L104				L112
	4	5	1	2	3	1	2	1	2	1	2	3	1
SiO2	54.6	55.2	53.9	54.1	54.2	56.2	56.7	56.8	57.0	56.7	56.5	57.1	56.7
TiO2	0.14	0.13	0.13	0.13	0.13	0.12	0.19	0.14	0.21	0.18	0.20	0.23	0.21
Al2O3	4.60	4.28	4.71	4.81	4.80	2.32	2.06	0.99	1.14	1.95	1.99	1.48	1.19
Cr2O3	0.60	0.70	0.81	0.83	0.85	0.39	0.30	0.17	0.19	0.42	0.50	0.27	0.20
Fe2O3	0.84	0.04	0.89	1.36	0.29	0.95	0.65	0.19	0.23	1.50	0.61	0.41	0.00
FeO	5.19	5.94	5.64	5.14	6.07	5.87	6.52	6.48	6.34	5.45	7.08	6.09	6.43
MnO	0.13	0.14	0.15	0.12	0.16	0.18	0.20	0.21	0.11	0.13	0.22	0.21	0.19
NiO	0.02	0.11	0.10	0.08	0.07	0.09	0.06	0.02	0.05	-	-	-	0.07
MgO	33.2	32.9	32.3	32.5	32.3	34.0	34.1	34.2	34.3	34.6	33.6	34.5	33.7
CaO	0.69	0.85	0.85	0.96	0.70	0.36	0.34	0.38	0.50	0.44	0.37	0.54	0.57
Na2O	<0.01	0.02	0.01	0.04	0.03	0.01	<0.01	<0.01	0.02	0.01	0.02	0.01	<0.01
K2O	<0.01	0.01	<0.01	<0.01	<0.01	0.01	<0.01	<0.01	<0.01	0.01	<0.01	<0.01	<0.01
Total	100.1	100.3	99.5	100.1	99.6	100.6	101.0	99.6	100.0	101.4	101.1	100.9	99.2
Si	1.884	1.900	1.878	1.871	1.884	1.933	1.941	1.972	1.966	1.932	1.941	1.956	1.974
Ti	0.004	0.003	0.004	0.003	0.003	0.003	0.005	0.004	0.006	0.005	0.005	0.006	0.005
Al	0.187	0.174	0.193	0.196	0.197	0.094	0.083	0.040	0.046	0.078	0.081	0.060	0.049
Cr	0.016	0.019	0.022	0.023	0.023	0.011	0.008	0.005	0.005	0.011	0.014	0.007	0.005
Fe3+	0.022	0.001	0.023	0.036	0.007	0.025	0.017	0.005	0.006	0.038	0.016	0.011	0.000
Fe2+	0.150	0.171	0.164	0.149	0.176	0.169	0.187	0.188	0.183	0.156	0.203	0.174	0.187
Mn	0.004	0.004	0.004	0.004	0.005	0.005	0.006	0.006	0.003	0.004	0.007	0.006	0.006
Ni	0.001	0.003	0.003	0.002	0.002	0.002	0.002	0.001	0.002	-	-	-	0.002
Mg	1.706	1.691	1.676	1.678	1.674	1.744	1.739	1.766	1.763	1.759	1.720	1.760	1.750
Ca	0.026	0.031	0.032	0.036	0.026	0.013	0.013	0.014	0.018	0.016	0.014	0.020	0.021
Na	<0.001	0.001	0.001	0.003	0.002	0.001	<0.001	<0.001	0.001	0.001	0.001	0.001	<0.001
K	<0.001	<0.001	<0.001	<0.001	<0.001	<0.001	<0.001	<0.001	<0.001	<0.001	<0.001	<0.001	<0.001
# Mg	0.91	0.91	0.90	0.90	0.90	0.901	0.896	0.902	0.904	0.902	0.888	0.905	0.903
# Cr	0.08	0.10	0.10	0.10	0.11	0.102	0.088	0.100	0.103	0.127	0.143	0.110	0.099

A2.5a: Orthopyroxene dataset

opx porphyroclasts rim

	proto-mylonite			**FGSG**		**CGSGc**								
sample	**L112**	**La2002-05**		**L110**		**L13**				**L42**		**L147**		
	2	1	2	1	2	1	2	3	1	2	1	2	3	4
SiO2	55.9	56.6	56.9	56.6	56.9	56.6	56.9	56.5	56.7	56.3	54.7	55.6	55.2	55.1
TiO2	0.23	0.23	0.23	0.25	0.22	0.32	0.28	0.32	0.24	0.20	0.24	0.24	0.25	0.23
Al2O3	2.04	1.48	1.63	1.82	1.73	2.18	1.89	2.20	1.73	1.10	1.31	1.25	1.37	1.31
Cr2O3	0.43	0.35	0.34	0.50	0.43	0.46	0.49	0.46	0.37	0.29	0.61	0.59	0.57	0.51
Fe2O3	0.00	1.86	0.15	0.00	0.00	0.00	0.00	0.00	0.00	0.96				
FeO	6.66	5.14	6.38	5.06	5.13	6.79	7.00	7.00	6.27	6.45	6.68	6.70	6.91	6.82
MnO	0.14	0.16	0.17	0.12	0.07	0.18	0.13	0.23	0.17	0.26	0.18	0.14	0.15	0.18
NiO	0.16	0.13	0.08	0.06	0.05	0.10	0.10	0.10	0.06	0.11	0.10	0.07	0.08	0.05
MgO	33.1	34.6	34.1	33.2	33.5	33.2	33.3	33.4	33.9	33.8	32.7	32.8	32.7	33.0
CaO	0.71	0.57	0.58	0.89	0.66	0.83	0.58	0.65	0.64	0.27	0.68	0.80	0.73	0.60
Na2O	0.04	0.01	<0.01	0.03	0.02	0.03	0.02	0.01	0.02	0.01	0.02	<0.01	0.03	<0.01
K2O	<0.01	<0.01	<0.01	0.02	<0.01	0.01	<0.01	<0.01	<0.01	0.02	0.02	<0.01	<0.01	0.01
Total	99.4	101.1	100.5	98.5	98.7	100.7	100.7	100.8	100.1	99.8	97.3	98.1	97.9	97.8
Si	1.948	1.936	1.954	1.981	1.987	1.949	1.959	1.944	1.956	1.956	1.952	1.963	1.956	1.953
Ti	0.006	0.006	0.006	0.007	0.006	0.008	0.007	0.008	0.006	0.005	0.006	0.006	0.007	0.006
Al	0.084	0.060	0.066	0.075	0.071	0.088	0.077	0.089	0.070	0.045	0.055	0.052	0.057	0.055
Cr	0.012	0.010	0.009	0.014	0.012	0.013	0.013	0.013	0.010	0.008	0.017	0.016	0.016	0.014
Fe3+	0.000	0.048	0.004	0.000	0.000	0.000	0.000	0.000	0.000	0.025	0.000	0.000	0.000	0.000
Fe2+	0.194	0.147	0.184	0.148	0.150	0.196	0.202	0.202	0.181	0.187	0.199	0.198	0.205	0.202
Mn	0.004	0.005	0.005	0.004	0.002	0.005	0.004	0.007	0.005	0.008	0.005	0.004	0.005	0.005
Ni	0.004	0.004	0.002	0.002	0.001	0.003	0.003	0.003	0.002	0.003	0.003	0.002	0.002	0.001
Mg	1.718	1.764	1.748	1.733	1.745	1.706	1.712	1.711	1.745	1.751	1.739	1.725	1.725	1.746
Ca	0.026	0.021	0.021	0.034	0.025	0.031	0.021	0.024	0.024	0.010	0.026	0.030	0.028	0.023
Na	0.003	0.001	<0.001	0.002	0.001	0.002	0.002	0.001	0.002	<0.001	0.001	<0.001	0.002	<0.001
K	<0.001	<0.001	<0.001	0.001	<0.001	<0.001	<0.001	<0.001	<0.001	0.001	0.001	<0.001	<0.001	0.001
# Mg	0.898	0.903	0.903	0.921	0.921	0.90	0.89	0.89	0.91	0.89	0.90	0.90	0.89	0.90
# Cr	0.125	0.137	0.122	0.155	0.144	0.13	0.15	0.12	0.13	0.15	0.24	0.24	0.22	0.21

opx porphyroclasts rim

	CGSGc			**CGSGn**								
sample	**L241**			**L195**					**W2**			
	1	2	3	1	2	3	4	5	1	2	3	4
SiO2	56.4	56.4	55.9	55.7	56.6	56.8	56.1	55.7	55.3	56.0	55.2	55.4
TiO2	0.21	0.14	0.21	0.16	0.08	0.09	0.13	0.16	0.16	0.20	0.19	0.22
Al2O3	2.24	2.27	2.56	2.71	2.24	2.34	2.54	2.89	2.44	2.06	2.51	2.68
Cr2O3	0.57	0.55	0.59	0.51	0.59	0.55	0.47	0.61	0.57	0.46	0.50	0.50
Fe2O3	0.75	1.09	1.18	0.14	0.00	0.00	0.00	0.04	0.82	0.50	0.99	0.23
FeO	6.25	6.02	5.94	5.77	5.62	5.70	5.93	5.98	5.55	6.25	5.98	6.37
MnO	0.16	0.13	0.15	0.16	0.16	0.17	0.15	0.16	0.15	0.13	0.15	0.15
NiO	0.10	0.08	0.09	0.10	0.02	0.07	0.05	0.07	0.09	0.06	0.09	0.09
MgO	34.0	33.9	33.7	33.5	34.0	34.0	33.7	33.4	33.2	33.5	33.2	33.0
CaO	0.49	0.56	0.56	0.86	0.58	0.71	0.66	0.69	0.87	0.67	0.55	0.71
Na2O	<0.01	<0.01	0.02	<0.01	<0.01	0.02	0.02	0.01	0.02	0.01	0.02	0.01
K2O	<0.01	0.03	<0.01	<0.01	<0.01	0.02	0.02	0.02	0.01	<0.01	<0.01	<0.01
Total	101.1	101.2	100.9	99.6	100.0	100.4	99.8	99.6	99.1	99.8	99.4	99.4
Si	1.932	1.930	1.920	1.932	1.952	1.949	1.941	1.929	1.928	1.940	1.924	1.930
Ti	0.006	0.004	0.006	0.004	0.002	0.002	0.003	0.004	0.004	0.005	0.005	0.006
Al	0.090	0.092	0.104	0.111	0.091	0.095	0.104	0.118	0.100	0.084	0.103	0.110
Cr	0.016	0.015	0.016	0.014	0.016	0.015	0.013	0.017	0.016	0.013	0.014	0.014
Fe3+	0.019	0.028	0.031	0.004	0.000	0.000	0.000	0.001	0.022	0.013	0.026	0.006
Fe2+	0.179	0.172	0.171	0.167	0.162	0.164	0.171	0.173	0.162	0.181	0.174	0.185
Mn	0.005	0.004	0.005	0.005	0.005	0.005	0.004	0.005	0.004	0.004	0.005	0.005
Ni	0.003	0.002	0.002	0.003	0.000	0.002	0.001	0.002	0.003	0.002	0.002	0.003
Mg	1.733	1.732	1.725	1.729	1.749	1.740	1.735	1.724	1.727	1.733	1.725	1.715
Ca	0.018	0.021	0.021	0.032	0.021	0.026	0.025	0.026	0.032	0.025	0.020	0.026
Na	<0.001	<0.001	0.001	<0.001	<0.001	0.001	0.001	0.001	0.001	0.001	0.001	0.001
K	0.000	0.001	<0.001	<0.001	<0.001	0.001	0.001	0.001	<0.001	<0.001	<0.001	<0.001
# Mg	0.90	0.90	0.90	0.91	0.92	0.91	0.91	0.91	0.90	0.90	0.90	0.90
# Cr	0.15	0.14	0.13	0.11	0.15	0.14	0.11	0.12	0.13	0.13	0.12	0.11

A2.5a: Orthopyroxene dataset

opx impregnation (ol + liq1 -> opx + liq2)

	mylonite											proto-mylonite		
sample	L04						L104					L112		
	1	2	3	4	5	6	1	2	3	4 (rim)	5 (rim)	1	2	3
SiO2	57.0	56.6	56.8	57.4	56.9	57.3	56.1	56.3	56.3	56.6	56.5	55.3	55.9	55.9
TiO2	0.18	0.18	0.18	0.16	0.17	0.19	0.27	0.30	0.25	0.26	0.20	0.22	0.25	0.26
Al2O3	1.44	1.54	1.46	1.37	1.09	1.39	2.43	2.36	2.55	1.89	2.04	2.98	2.17	2.54
Cr2O3	0.29	0.25	0.22	0.18	0.19	0.23	0.47	0.49	0.46	0.25	0.36	0.66	0.53	0.52
Fe2O3	0.00	0.69	0.00	0.00	0.07	0.00	1.30	1.37	1.24	1.38	1.83	0.00	0.45	0.12
FeO	6.35	5.65	6.43	6.44	6.32	6.46	5.53	5.61	5.86	5.79	5.32	6.36	6.65	6.60
MnO	0.17	0.19	0.18	0.18	0.20	0.17	0.15	0.13	0.15	0.15	0.14	0.15	0.18	0.16
NiO	0.08	0.06	0.08	0.10	0.04	0.08	0.08	0.11	0.06	0.09	0.04	0.05	0.11	0.11
MgO	33.99	34.34	34.06	34.30	34.22	34.11	34.04	34.10	34.02	34.32	34.44	32.76	33.34	33.4
CaO	0.48	0.52	0.42	0.41	0.43	0.42	0.63	0.63	0.58	0.55	0.52	0.61	0.54	0.59
Na2O	0.02	0.01	0.02	<0.01	0.01	0.02	0.01	0.03	0.01	<0.01	0.04	0.02	0.01	<0.01
K2O	0.01	0.01	<0.01	0.01	0.01	0.01	<0.01	<0.01	<0.01	<0.01	<0.01	<0.01	<0.01	<0.01
Total	100.0	100.0	99.9	100.6	99.6	100.4	101.0	101.4	101.5	101.3	101.5	99.2	100.1	100.2
Si	1.970	1.952	1.964	1.971	1.971	1.972	1.921	1.922	1.921	1.934	1.927	1.932	1.936	1.933
Ti	0.005	0.005	0.005	0.004	0.004	0.005	0.007	0.008	0.007	0.007	0.005	0.006	0.007	0.007
Al	0.058	0.063	0.059	0.055	0.045	0.056	0.098	0.095	0.102	0.076	0.082	0.123	0.088	0.103
Cr	0.008	0.007	0.006	0.005	0.005	0.006	0.013	0.013	0.012	0.007	0.010	0.018	0.014	0.014
Fe3+	0.000	0.018	0.000	0.000	0.002	0.000	0.034	0.035	0.032	0.036	0.047	0.000	0.012	0.003
Fe2+	0.183	0.163	0.186	0.185	0.183	0.186	0.159	0.160	0.167	0.165	0.152	0.186	0.193	0.191
Mn	0.005	0.006	0.005	0.005	0.006	0.005	0.004	0.004	0.004	0.004	0.004	0.005	0.005	0.005
Ni	0.002	0.002	0.002	0.003	0.001	0.002	0.002	0.003	0.002	0.003	0.001	0.001	0.003	0.003
Mg	1.749	1.766	1.755	1.756	1.767	1.750	1.738	1.735	1.731	1.749	1.750	1.705	1.721	1.719
Ca	0.018	0.019	0.016	0.015	0.016	0.016	0.023	0.023	0.021	0.020	0.019	0.023	0.020	0.022
Na	0.002	<0.001	0.001	<0.001	0.001	0.001	0.001	0.002	0.001	<0.001	0.003	0.002	0.001	<0.001
K	<0.001	<0.001	<0.001	<0.001	<0.001	<0.001	<0.001	<0.001	<0.001	<0.001	<0.001	<0.001	<0.001	<0.001
# Mg	0.91	0.91	0.90	0.90	0.91	0.90	0.90	0.90	0.90	0.90	0.90	0.90	0.89	0.90
# Cr	0.12	0.10	0.09	0.08	0.10	0.10	0.12	0.12	0.11	0.08	0.11	0.13	0.14	0.12

opx impregnation (ol + liq1 -> opx + liq2)

	proto-mylonite			FGSG					CGSGc					
sample	La2002-05			L110					L13					L42
	1	2	3	1	2	3	4	5	1	2	3	4	5	1
SiO2	56.0	55.8	56.1	54.7	55.7	55.7	56.0	55.6	56.7	56.6	56.1	55.9	56.0	55.3
TiO2	0.29	0.26	0.27	0.28	0.30	0.29	0.29	0.33	0.30	0.31	0.32	0.37	0.35	0.18
Al2O3	2.31	2.55	2.34	2.65	2.64	2.61	2.34	2.73	1.76	1.76	2.60	2.48	2.63	1.98
Cr2O3	0.48	0.52	0.45	0.62	0.62	0.57	0.55	0.59	0.50	0.52	0.55	0.61	0.54	0.42
Fe2O3	1.02	0.67	1.01	0.85	0.65	0.92	0.70	1.08	1.15	1.17	0.49	1.00	1.13	1.54
FeO	6.15	6.29	5.94	6.44	6.27	6.12	6.12	5.64	6.28	5.92	6.42	6.08	6.02	5.03
MnO	0.12	0.11	0.21	0.09	0.25	0.13	0.09	0.09	0.19	0.17	0.19	0.18	0.16	0.18
NiO	0.09	0.07	0.07	0.11	0.09	0.07	0.06	0.07	0.02	0.11	0.07	0.08	0.08	0.07
MgO	33.6	33.2	33.6	32.5	33.1	33.2	33.1	32.2	34.1	33.9	33.3	33.3	33.3	33.7
CaO	0.81	0.93	0.84	0.75	0.89	0.87	1.28	2.47	0.63	0.96	0.93	0.97	1.12	0.69
Na2O	<0.01	0.03	0.02	0.04	0.03	0.04	0.04	0.08	0.01	0.02	0.03	0.04	0.05	0.01
K2O	<0.01	<0.01	<0.01	0.01	<0.01	0.02	0.01	0.01	<0.01	0.02	0.02	0.02	0.02	<0.01
Total	100.8	100.5	100.9	99.0	100.5	100.6	100.6	100.8	101.6	101.5	101.1	101.1	101.3	99.1
Si	1.926	1.927	1.927	1.919	1.923	1.922	1.930	1.917	1.936	1.936	1.927	1.921	1.918	1.929
Ti	0.008	0.007	0.007	0.008	0.008	0.007	0.008	0.009	0.008	0.008	0.008	0.010	0.009	0.005
Al	0.093	0.104	0.095	0.109	0.108	0.106	0.095	0.111	0.071	0.071	0.105	0.101	0.106	0.081
Cr	0.013	0.014	0.012	0.017	0.017	0.016	0.015	0.016	0.014	0.014	0.015	0.017	0.015	0.012
Fe3+	0.026	0.018	0.026	0.023	0.017	0.024	0.018	0.028	0.030	0.030	0.013	0.026	0.029	0.040
Fe2+	0.177	0.182	0.171	0.189	0.181	0.177	0.177	0.163	0.179	0.169	0.184	0.175	0.173	0.147
Mn	0.004	0.003	0.006	0.003	0.007	0.004	0.003	0.003	0.006	0.005	0.006	0.005	0.005	0.005
Ni	0.002	0.002	0.002	0.003	0.003	0.002	0.002	0.002	0.001	0.003	0.002	0.002	0.002	0.002
Mg	1.721	1.709	1.722	1.698	1.702	1.707	1.703	1.655	1.734	1.727	1.704	1.706	1.699	1.753
Ca	0.030	0.034	0.031	0.028	0.033	0.032	0.047	0.091	0.023	0.035	0.034	0.036	0.041	0.026
Na	<0.001	0.002	0.001	0.003	0.002	0.003	0.003	0.006	<0.001	0.001	0.002	0.002	0.003	0.001
K	<0.001	<0.001	<0.001	<0.001	<0.001	0.001	<0.001	<0.001	<0.001	0.001	0.001	0.001	0.001	<0.001
# Mg	0.90	0.90	0.90	0.89	0.90	0.90	0.90	0.90	0.89	0.90	0.90	0.90	0.90	0.91
# Cr	0.12	0.12	0.11	0.14	0.14	0.13	0.14	0.13	0.16	0.17	0.12	0.14	0.12	0.13

A2.5a: Orthopyroxene dataset

opx impregnation (ol + liq1 -> opx + liq2)

	CGSGc													CGSGn
sample	L42			L147				L241						L195
	2	3	4	1	2	3	4	1	2	3	4	5	6	1
SiO2	56.3	55.2	54.3	55.5	55.3	55.5	55.6	55.9	56.5	56.4	57.0	56.0	57.5	57.0
TiO2	0.23	0.17	0.14	0.28	0.27	0.32	0.29	0.26	0.23	0.21	0.24	0.22	0.10	0.14
Al2O3	1.01	2.36	3.44	2.38	3.03	2.45	2.46	2.35	2.15	1.98	1.68	2.55	1.16	1.99
Cr2O3	0.38	0.72	0.89	0.56	0.67	0.63	0.50	0.46	0.40	0.48	0.33	0.50	0.13	0.41
Fe2O3	0.98	1.71	2.05	0.00	0.05	0.00	0.91	1.45	0.80	1.12	0.41	1.48	0.99	0.00
FeO	5.68	4.77	4.42	6.51	6.61	6.59	6.34	5.87	6.07	6.00	6.47	5.78	6.07	5.78
MnO	0.18	0.17	0.17	0.20	0.15	0.14	0.14	0.11	0.19	0.17	0.21	0.17	0.18	0.18
NiO	0.07	0.10	0.09	0.03	0.07	0.08	0.06	0.09	0.05	0.06	0.06	0.12	0.11	0.06
MgO	34.3	33.6	33.2	32.7	32.8	32.8	33.1	33.6	34.0	33.9	34.2	33.6	34.7	33.8
CaO	0.40	0.81	0.86	0.92	0.69	0.80	0.80	0.83	0.61	0.60	0.53	0.94	0.48	0.91
Na2O	0.01	0.03	0.01	0.01	0.04	0.03	0.04	0.02	0.02	0.03	<0.01	0.03	0.01	0.02
K2O	<0.01	0.01	0.01	<0.01	0.01	<0.01	<0.01	<0.01	0.02	<0.01	0.01	<0.01	<0.01	<0.01
Total	99.5	99.6	99.6	99.1	99.6	99.4	100.2	101.0	101.1	100.9	101.1	101.4	101.3	100.3
Si	1.956	1.916	1.888	1.942	1.922	1.937	1.925	1.922	1.936	1.935	1.950	1.918	1.960	1.961
Ti	0.006	0.004	0.004	0.007	0.007	0.008	0.008	0.007	0.006	0.005	0.006	0.006	0.003	0.004
Al	0.041	0.097	0.141	0.098	0.124	0.101	0.101	0.095	0.087	0.080	0.068	0.103	0.047	0.081
Cr	0.011	0.020	0.025	0.016	0.019	0.017	0.014	0.013	0.011	0.013	0.009	0.014	0.004	0.011
Fe3+	0.025	0.045	0.054	0.000	0.001	0.000	0.024	0.038	0.021	0.029	0.011	0.038	0.026	0.000
Fe2+	0.165	0.138	0.128	0.191	0.192	0.192	0.184	0.169	0.174	0.172	0.185	0.165	0.173	0.166
Mn	0.005	0.005	0.005	0.006	0.004	0.004	0.004	0.003	0.006	0.005	0.006	0.005	0.005	0.005
Ni	0.002	0.003	0.003	0.001	0.002	0.002	0.002	0.003	0.001	0.002	0.002	0.003	0.003	0.002
Mg	1.772	1.739	1.720	1.704	1.699	1.706	1.708	1.720	1.734	1.735	1.743	1.712	1.762	1.735
Ca	0.015	0.030	0.032	0.034	0.026	0.030	0.030	0.030	0.022	0.022	0.020	0.034	0.017	0.034
Na	0.001	0.002	0.001	0.001	0.002	0.002	0.003	0.002	0.001	0.002	<0.001	0.002	0.001	0.002
K	<0.001	<0.001	0.001	<0.001	0.001	<0.001	<0.001	<0.001	0.001	<0.001	<0.001	<0.001	<0.001	<0.001
# Mg	0.90	0.91	0.91	0.90	0.90	0.90	0.89	0.89	0.90	0.90	0.90	0.90	0.90	0.91
# Cr	0.20	0.17	0.15	0.14	0.13	0.15	0.12	0.12	0.11	0.14	0.12	0.12	0.07	0.12

opx impregnation (ol + liq1 -> opx + liq2) **opx impregnation (cpx + liq -> opx + feld)**

	CGSGn								hydrous-m		CGSGc			
sample	L195				W2				L187d		L13			
	2	3	4	5	1	2	3	4	1	2	1	2	3	4
SiO2	56.5	56.2	56.0	56.6	56.0	55.3	56.1	56.7	54.7	54.1	54.9	55.0	54.6	56.2
TiO2	0.17	0.15	0.15	0.15	0.19	0.24	0.20	0.12	0.18	0.20	0.28	0.30	0.22	0.27
Al2O3	2.15	2.92	3.07	2.29	2.28	2.72	1.89	1.33	4.32	5.60	4.03	3.57	4.53	2.66
Cr2O3	0.53	0.61	0.67	0.40	0.38	0.42	0.34	0.16	0.76	0.66	0.96	0.91	1.02	0.73
Fe2O3	0.00	0.00	0.00	0.00	0.00	0.34	0.00	0.31	1.32	0.49	1.94	1.31	1.19	1.20
FeO	5.85	5.86	5.85	5.88	6.45	6.46	6.83	6.35	5.68	6.52	5.74	6.00	6.29	6.33
MnO	0.16	0.15	0.16	0.16	0.15	0.17	0.17	0.16	0.18	0.18	0.20	0.15	0.20	0.18
NiO	0.09	0.10	0.11	0.06	0.08	0.06	0.07	0.08	0.13	0.08	0.07	0.00	0.08	0.05
MgO	33.9	33.4	33.7	33.8	33.1	32.8	33.4	34.0	33.0	32.2	32.9	32.8	32.4	33.7
CaO	0.85	0.67	0.60	0.71	0.85	0.87	0.44	0.52	0.46	0.48	0.84	0.93	0.79	0.67
Na2O	0.02	0.02	0.01	0.02	0.02	0.01	0.01	0.01	0.02	0.03	0.03	0.03	0.03	<0.01
K2O	<0.01	0.01	0.01	<0.01	<0.01	<0.01	<0.01	<0.01	<0.01	0.01	0.01	0.01	<0.01	<0.01
Total	100.2	100.1	100.3	100.1	99.5	99.4	99.4	99.7	100.8	100.5	101.9	101.0	101.4	101.9
Si	1.946	1.940	1.927	1.951	1.949	1.928	1.952	1.964	1.881	1.867	1.875	1.892	1.875	1.914
Ti	0.005	0.004	0.004	0.004	0.005	0.006	0.005	0.003	0.005	0.005	0.007	0.008	0.006	0.007
Al	0.087	0.119	0.124	0.093	0.093	0.112	0.077	0.054	0.175	0.228	0.162	0.145	0.183	0.107
Cr	0.014	0.017	0.018	0.011	0.010	0.012	0.009	0.004	0.021	0.018	0.026	0.025	0.028	0.020
Fe3+	0.000	0.000	0.000	0.000	0.000	0.009	0.000	0.008	0.034	0.013	0.050	0.034	0.031	0.031
Fe2+	0.169	0.169	0.168	0.169	0.188	0.188	0.199	0.184	0.163	0.188	0.164	0.173	0.181	0.180
Mn	0.005	0.004	0.005	0.005	0.004	0.005	0.005	0.005	0.005	0.005	0.006	0.004	0.006	0.005
Ni	0.003	0.003	0.003	0.002	0.002	0.002	0.002	0.002	0.004	0.002	0.002	0.000	0.002	0.002
Mg	1.738	1.718	1.727	1.738	1.715	1.705	1.734	1.756	1.693	1.654	1.675	1.683	1.658	1.710
Ca	0.031	0.025	0.022	0.026	0.032	0.032	0.016	0.019	0.017	0.018	0.031	0.034	0.029	0.024
Na	0.002	0.001	0.001	0.001	0.001	0.001	0.001	<0.001	0.001	0.002	0.002	0.002	0.002	<0.001
K	<0.001	<0.001	<0.001	<0.001	<0.001	<0.001	<0.001	<0.001	<0.001	0.001	<0.001	0.001	<0.001	<0.001
# Mg	0.91	0.91	0.91	0.91	0.90	0.90	0.90	0.90	0.90	0.89	0.89	0.89	0.89	0.89
# Cr	0.14	0.12	0.13	0.11	0.10	0.09	0.11	0.08	0.11	0.07	0.14	0.15	0.13	0.16

A2.5a: Orthopyroxene dataset
opx impregnation (cpx + liq -> opx + feld)

	CGSGc	**CGSGn**				
sample	**L13**	**L195**				
	5	1	2	3	4	5
SiO2	54.9	54.0	53.8	53.4	53.5	53.8
TiO2	0.23	0.10	0.06	0.05	0.07	0.05
Al2O3	4.24	6.20	6.22	6.85	6.30	5.99
Cr2O3	0.83	0.88	0.80	0.86	1.00	0.87
Fe2O3	1.18	0.00	0.00	0.04	0.65	0.72
FeO	6.56	6.26	6.19	6.49	5.54	5.46
MnO	0.18	0.16	0.14	0.17	0.17	0.17
NiO	0.02	0.09	0.10	0.11	0.12	0.11
MgO	32.5	31.8	32.0	31.6	32.2	32.5
CaO	0.86	0.73	0.52	0.54	0.60	0.49
Na2O	0.02	0.04	0.01	0.01	0.01	0.01
K2O	0.02	<0.01	0.01	0.01	0.01	<0.01
Total	101.5	100.3	99.8	100.1	100.1	100.2
Si	1.883	1.865	1.864	1.847	1.848	1.856
Ti	0.006	0.003	0.001	0.001	0.002	0.001
Al	0.171	0.252	0.254	0.280	0.257	0.244
Cr	0.023	0.024	0.022	0.023	0.027	0.024
Fe3+	0.030	0.000	0.000	0.001	0.017	0.019
Fe2+	0.188	0.181	0.179	0.188	0.160	0.158
Mn	0.005	0.005	0.004	0.005	0.005	0.005
Ni	0.001	0.002	0.003	0.003	0.003	0.003
Mg	1.660	1.638	1.652	1.631	1.658	1.672
Ca	0.032	0.027	0.019	0.020	0.022	0.018
Na	0.001	0.002	0.001	0.001	0.001	0.001
K	0.001	<0.001	<0.001	<0.001	0.001	<0.001
# Mg	0.89	0.90	0.90	0.90	0.90	0.91
# Cr	0.12	0.09	0.08	0.08	0.10	0.09

A2.5c: Clinopyroxene dataset

cpx neoblasts

	hydrous-mylonite				mylonite								proto-mylonite	
sample	L187d				L04				L104				L112	
	1	2	3	4	1	2	3	4	1	2	3	4	1	2
SiO2	53.6	53.4	53.8	54.0	53.4	53.5	53.1	52.8	52.0	52.2	51.7	52.9	52.9	52.8
TiO2	0.49	0.62	0.54	0.49	0.62	0.62	0.69	0.69	0.80	0.78	0.76	0.70	0.64	0.67
Al2O3	1.73	1.84	1.92	1.60	2.61	2.48	2.58	2.81	4.04	3.99	3.80	3.09	2.30	2.41
Cr2O3	0.33	0.40	0.44	0.38	0.66	0.61	0.50	0.73	0.95	0.89	0.96	0.83	0.56	0.56
Fe2O3	1.46	1.11	0.52	0.94	0.55	1.13	1.59	1.65	1.46	1.86	2.38	1.38	0.89	2.05
FeO	1.17	1.65	1.84	1.57	2.09	1.50	1.24	1.15	1.89	1.37	0.98	1.76	2.03	0.82
MnO	0.08	0.05	0.11	0.07	0.03	0.07	0.05	0.10	0.10	0.05	0.07	0.11	0.10	0.05
NiO	0.09	0.05	0.05	0.04	0.03	0.00	0.03	0.00	0.01	0.05	0.05	0.04	0.06	0.05
MgO	17.1	17.0	17.0	17.2	17.2	17.3	17.2	17.1	16.6	16.7	16.7	17.0	16.8	16.9
CaO	24.1	23.9	23.8	24.0	23.0	23.1	23.2	23.0	22.1	22.7	22.1	22.6	23.2	23.8
Na2O	0.40	0.36	0.42	0.40	0.48	0.53	0.51	0.56	0.64	0.63	0.70	0.60	0.40	0.50
K2O	<0.01	<0.01	0.01	<0.01	<0.01	<0.01	<0.01	<0.01	<0.01	<0.01	0.01	<0.01	0.01	<0.01
Total	100.6	100.4	100.5	100.7	100.6	100.8	100.6	100.6	100.6	101.1	100.3	100.9	99.9	100.6
Si	1.939	1.936	1.946	1.949	1.928	1.925	1.916	1.909	1.881	1.878	1.877	1.906	1.927	1.912
Ti	0.013	0.017	0.015	0.013	0.017	0.017	0.019	0.019	0.022	0.021	0.021	0.019	0.018	0.018
Al	0.074	0.079	0.082	0.068	0.111	0.105	0.110	0.120	0.172	0.169	0.163	0.131	0.099	0.103
Cr	0.010	0.012	0.013	0.011	0.019	0.017	0.014	0.021	0.027	0.025	0.027	0.024	0.016	0.016
Fe3+	0.040	0.030	0.014	0.026	0.015	0.031	0.043	0.045	0.040	0.050	0.065	0.037	0.025	0.056
Fe2+	0.035	0.050	0.056	0.047	0.063	0.045	0.037	0.035	0.057	0.041	0.030	0.053	0.062	0.025
Mn	0.002	0.002	0.003	0.002	0.001	0.002	0.002	0.003	0.003	0.002	0.002	0.003	0.003	0.002
Ni	0.003	0.002	0.002	0.001	0.001	0.000	0.001	0.000	0.000	0.001	0.001	0.001	0.002	0.001
Mg	0.923	0.920	0.917	0.927	0.924	0.930	0.926	0.919	0.895	0.894	0.905	0.913	0.912	0.912
Ca	0.933	0.929	0.924	0.928	0.888	0.891	0.897	0.891	0.857	0.874	0.860	0.871	0.908	0.921
Na	0.028	0.025	0.029	0.028	0.034	0.037	0.036	0.039	0.045	0.044	0.050	0.042	0.028	0.035
K	<0.001	<0.001	<0.001	<0.001	<0.001	<0.001	<0.001	<0.001	<0.001	<0.001	<0.001	<0.001	<0.001	<0.001
# Mg	0.93	0.92	0.93	0.93	0.92	0.93	0.92	0.92	0.91	0.91	0.91	0.91	0.92	0.92
# Cr	0.11	0.13	0.13	0.14	0.15	0.14	0.12	0.15	0.14	0.13	0.14	0.15	0.14	0.13

cpx neoblasts

	proto-mylonite				FGSG			FGSG			CGSGn			
	La2002-05				L09			L110			L13			
	1	2	3	4	1	2	3	1	2	3	1	2	3	4
SiO2	53.7	53.4	54.5	52.3	52.1	52.2	52.0	53.2	53.7	52.1	50.9	51.0	50.7	50.9
TiO2	0.54	0.57	0.35	0.81	0.68	0.66	0.66	0.64	0.38	0.78	1.03	0.96	1.03	1.00
Al2O3	1.99	2.18	1.37	3.04	3.78	3.64	4.03	2.43	1.67	3.32	5.00	4.94	4.83	4.81
Cr2O3	0.51	0.59	0.33	0.79	0.98	0.91	1.21	0.59	0.52	0.80	1.29	1.31	1.52	1.32
Fe2O3	0.93	0.49	0.00	1.34	1.39	1.39	1.30	0.61	0.60	1.47	1.50	1.76	1.77	1.83
FeO	1.98	2.18	2.58	1.66	1.64	1.68	1.93	2.16	2.14	1.76	1.95	1.71	1.56	1.61
MnO	0.07	0.07	0.11	0.11	0.12	0.10	0.04	0.06	0.05	0.11	0.07	0.13	0.14	0.07
NiO	0.03	0.04	0.07	0.06	0.03	0.04	0.01	0.02	0.09	0.07	0.06	0.04	0.08	0.11
MgO	17.2	16.8	17.7	16.5	16.7	16.9	17.0	16.7	17.3	16.4	15.5	15.6	16.0	15.9
CaO	23.5	23.4	23.0	23.0	22.7	22.3	21.9	23.5	23.1	22.9	22.4	22.5	22.1	22.5
Na2O	0.40	0.48	0.35	0.54	0.49	0.56	0.55	0.45	0.42	0.51	0.73	0.73	0.66	0.59
K2O	0.01	<0.01	0.01	0.02	<0.01	<0.01	<0.01	<0.01	<0.01	0.02	<0.01	0.02	0.02	0.01
Total	100.8	100.1	100.3	100.2	100.5	100.4	100.6	100.4	99.9	100.2	100.4	100.6	100.4	100.7
Si	1.937	1.939	1.970	1.903	1.885	1.892	1.881	1.929	1.953	1.894	1.851	1.851	1.846	1.850
Ti	0.015	0.016	0.009	0.022	0.018	0.018	0.018	0.018	0.010	0.021	0.028	0.026	0.028	0.029
Cr	0.085	0.094	0.058	0.130	0.161	0.155	0.172	0.104	0.072	0.142	0.215	0.212	0.207	0.201
Al	0.015	0.017	0.010	0.023	0.028	0.026	0.035	0.017	0.015	0.023	0.037	0.038	0.044	0.036
Fe3+	0.025	0.013	0.000	0.037	0.038	0.038	0.035	0.017	0.016	0.040	0.041	0.048	0.049	0.042
Fe2+	0.060	0.066	0.078	0.051	0.050	0.051	0.058	0.065	0.065	0.054	0.059	0.052	0.047	0.059
Mn	0.002	0.002	0.003	0.003	0.004	0.003	0.001	0.002	0.002	0.003	0.002	0.004	0.004	0.004
Ni	0.001	0.001	0.002	0.002	0.001	0.001	0.000	0.001	0.003	0.002	0.002	0.001	0.002	0.001
Mg	0.924	0.908	0.954	0.896	0.901	0.913	0.916	0.903	0.936	0.890	0.842	0.842	0.865	0.859
Ca	0.909	0.910	0.890	0.896	0.880	0.864	0.846	0.914	0.899	0.893	0.871	0.874	0.860	0.883
Na	0.028	0.034	0.025	0.038	0.035	0.039	0.038	0.031	0.030	0.036	0.051	0.052	0.046	0.036
K	<0.001	<0.001	0.001	0.001	<0.001	<0.001	<0.001	<0.001	<0.001	0.001	<0.001	0.001	0.001	0.001
# Mg	0.92	0.92	0.92	0.91	0.92	0.91	0.91	0.92	0.92	0.91	0.90	0.90	0.90	0.90
# Cr	0.15	0.15	0.14	0.15	0.15	0.14	0.17	0.14	0.17	0.14	0.15	0.15	0.17	0.15

A2.5c: Clinopyroxene dataset

cpx porphyroclasts core

	hydrous-mylonite				mylonite						proto-mylonite			
	L187d				L04			L104			L112			La2002-
	1	2	3	4	1	2	3	1	2	3	1	2	3	1
SiO2	50.2	50.2	50.1	49.9	50.1	49.8	50.4	50.3	50.1	49.8	50.5	50.6	50.1	51.2
TiO2	0.80	0.78	0.86	0.82	0.58	0.64	0.59	0.74	0.74	0.84	0.81	0.83	0.87	0.72
Al2O3	6.44	6.49	6.55	6.43	7.09	6.91	6.87	6.69	6.51	6.65	5.71	5.71	5.82	4.63
Cr2O3	0.92	0.95	0.89	0.90	1.01	1.05	1.07	1.08	1.13	1.08	1.23	1.27	1.27	1.28
Fe2O3	2.19	2.17	1.39	1.52	1.99	2.67	1.32	1.52	2.58	2.20	1.99	2.06	2.17	1.70
FeO	1.34	1.11	2.04	1.72	1.43	0.85	1.84	1.91	1.31	1.56	1.48	1.54	1.09	1.52
MnO	0.14	0.17	0.17	0.09	0.12	0.10	0.07				0.12	0.05	0.14	0.06
NiO	0.05	0.09	0.07	0.05	0.02	0.05	0.04	0.06	0.09	0.08	0.01	0.03	0.02	0.07
MgO	14.8	15.0	14.6	14.7	15.1	15.3	14.9	15.3	16.1	15.3	15.3	15.2	14.9	15.7
CaO	23.0	22.8	22.8	22.6	22.4	22.3	22.8	22.1	21.2	21.9	22.6	22.8	23.1	22.7
Na2O	0.74	0.75	0.69	0.72	0.71	0.70	0.67	0.71	0.70	0.73	0.68	0.70	0.72	0.66
K2O	0.01	<0.01	<0.01	<0.01	0.01	0.01	<0.01	<0.01	0.01	<0.01	0.02	<0.01	<0.01	0.02
Total	100.5	100.6	100.1	99.5	100.5	100.3	100.5	100.3	100.5	100.1	100.4	100.8	100.2	100.3
Si	1.823	1.823	1.828	1.830	1.816	1.808	1.827	1.825	1.814	1.815	1.835	1.834	1.828	1.863
Ti	0.022	0.021	0.024	0.023	0.016	0.017	0.016	0.020	0.020	0.023	0.022	0.023	0.024	0.020
Al	0.276	0.278	0.282	0.278	0.303	0.296	0.294	0.287	0.278	0.285	0.245	0.244	0.250	0.199
Cr	0.026	0.027	0.026	0.026	0.029	0.030	0.031	0.031	0.032	0.031	0.035	0.036	0.037	0.037
Fe3+	0.060	0.059	0.038	0.042	0.054	0.073	0.036	0.042	0.070	0.060	0.054	0.056	0.060	0.047
Fe2+	0.041	0.034	0.062	0.053	0.043	0.026	0.056	0.058	0.040	0.047	0.045	0.047	0.033	0.046
Mn	0.004	0.005	0.005	0.003	0.004	0.003	0.002	0.002	0.003	0.003	0.004	0.002	0.004	0.002
Ni	0.002	0.003	0.002	0.002	0.001	0.002	0.001				0.000	0.001	0.001	0.002
Mg	0.800	0.809	0.794	0.804	0.814	0.826	0.805	0.828	0.870	0.828	0.830	0.821	0.811	0.852
Ca	0.894	0.888	0.891	0.889	0.870	0.869	0.886	0.858	0.823	0.856	0.879	0.887	0.902	0.886
Na	0.052	0.053	0.049	0.051	0.050	0.050	0.047	0.050	0.049	0.051	0.048	0.050	0.051	0.046
K	0.001	0.000	0.000	0.000	0.000	0.000	0.000	0.000	0.001	0.000	0.001	0.000	0.000	0.001
# Mg	0.89	0.90	0.89	0.90	0.90	0.90	0.90	0.90	0.89	0.89	0.90	0.89	0.90	0.91
# Cr	0.09	0.09	0.08	0.09	0.09	0.09	0.09	0.10	0.10	0.10	0.13	0.13	0.13	0.16

cpx porphyroclasts core

	proto-mylonite			FGSG							CGSGc			
	La2002-05			L09				L110			L13			
	2	3	4	1	2	3	4	1	2	3	4	1	2	3
SiO2	51.4	51.3	51.5	49.8	49.6	50.1	49.4	50.2	50.0	49.9	50.0	50.3	50.2	49.9
TiO2	0.76	0.76	0.78	0.90	0.81	0.80	0.85	0.80	0.68	0.85	0.87	0.54	0.57	0.51
Al2O3	4.49	4.52	4.67	6.63	6.59	6.73	6.56	6.40	6.40	6.51	6.57	7.33	7.35	7.33
Cr2O3	1.24	1.15	1.29	1.29	1.22	1.31	1.25	0.94	0.99	1.00	0.97	1.15	1.27	1.22
Fe2O3	1.17	1.37	0.94	1.23	1.70	1.90	2.23	0.23	3.20	0.63	0.69	1.22	0.85	1.53
FeO	1.92	1.80	2.13	1.74	1.54	1.47	1.07	2.54	0.00	2.29	2.06	2.48	2.54	2.19
MnO	0.11	0.09	0.07	0.04	0.07	0.09	0.06	0.10	0.12	0.12	0.01	0.11	0.06	0.09
NiO	0.03	0.03	0.02	-	-	-	-	0.05	0.04	0.03	0.03	0.04	0.04	0.10
MgO	15.7	15.6	15.7	14.8	15.0	15.4	15.0	14.6	18.2	14.8	14.7	14.1	14.1	14.5
CaO	22.7	22.8	22.6	22.9	22.4	22.1	22.5	22.7	20.3	22.5	22.7	23.1	22.7	22.5
Na2O	0.63	0.66	0.65	0.61	0.66	0.71	0.70	0.65	0.45	0.61	0.71	0.70	0.79	0.69
K2O	0.01	<0.01	<0.01	<0.01	0.01	<0.01	<0.01	<0.01	0.02	0.01	<0.01	<0.01	0.01	<0.01
Total	100.1	100.1	100.4	100.0	99.6	100.5	99.5	99.2	100.4	99.2	99.3	101.2	100.5	100.5
Si	1.872	1.870	1.870	1.819	1.818	1.815	1.811	1.845	1.799	1.834	1.835	1.820	1.825	1.815
Ti	0.021	0.021	0.021	0.025	0.022	0.022	0.024	0.022	0.018	0.024	0.024	0.015	0.016	0.014
Cr	0.193	0.194	0.200	0.285	0.284	0.288	0.283	0.277	0.271	0.282	0.284	0.313	0.315	0.314
Al	0.036	0.033	0.037	0.037	0.035	0.038	0.036	0.027	0.028	0.029	0.028	0.033	0.037	0.035
Fe3+	0.032	0.038	0.026	0.034	0.047	0.052	0.062	0.007	0.087	0.017	0.019	0.033	0.023	0.042
Fe2+	0.059	0.055	0.065	0.053	0.047	0.045	0.033	0.078	0.000	0.070	0.063	0.075	0.077	0.067
Mn	0.003	0.003	0.002	0.001	0.002	0.003	0.002	0.003	0.004	0.004	0.000	0.003	0.002	0.003
Ni	0.001	0.001	0.001	-	-	-	-	0.002	0.001	0.001	0.001	0.001	0.001	0.003
Mg	0.855	0.848	0.852	0.807	0.817	0.831	0.818	0.801	0.978	0.808	0.802	0.762	0.764	0.784
Ca	0.885	0.890	0.881	0.896	0.880	0.857	0.883	0.892	0.781	0.887	0.893	0.896	0.884	0.875
Na	0.045	0.047	0.046	0.043	0.047	0.050	0.050	0.046	0.031	0.043	0.050	0.049	0.056	0.049
K	0.001	<0.001	<0.001	<0.001	0.001	<0.001	<0.001	<0.001	0.001	0.001	<0.001	<0.001	0.001	<0.001
# Mg	0.91	0.91	0.91	0.91	0.90	0.90	0.90	0.91	0.93	0.90	0.91	0.88	0.89	0.88
# Cr	0.16	0.15	0.16	0.12	0.11	0.12	0.11	0.09	0.09	0.09	0.09	0.10	0.10	0.10

A2.5c: Clinopyroxene dataset

cpx porphyroclasts core

	CGSGc													
-05	**L13**	**L42**					**L147**				**L241**			
	4	1	2	3	4	5	1	2	3	4	1	2	3	4
SiO2	49.8	49.3	49.9	49.6	49.7	49.3	50.9	50.6	50.8	50.7	50.5	50.4	50.3	50.5
TiO2	0.59	0.53	0.41	0.44	0.54	0.51	0.79	0.80	0.80	0.84	0.68	0.66	0.65	0.71
Al2O3	7.40	6.18	5.91	5.91	6.01	6.13	5.71	5.90	5.85	5.78	5.93	5.82	5.93	5.86
Cr2O3	1.22	1.47	1.44	1.46	1.40	1.16	1.21	1.21	1.27	1.17	1.22	1.13	1.14	1.11
Fe2O3	2.13	2.79	2.16	3.18	2.23	3.29	1.01	1.58	1.84	1.35	1.43	2.39	2.11	2.40
FeO	1.74	0.44	0.96	0.00	0.91	0.00	2.14	1.69	1.36	1.94	1.88	1.11	1.36	1.07
MnO	0.05	0.12	0.11	0.13	0.09	0.12	0.12	0.10	0.06	0.03	0.15	0.10	0.10	0.09
NiO	0.09	0.04	0.05	0.05	0.05	0.07	0.04	0.09	0.05	0.05	0.06	0.00	0.00	0.06
MgO	14.5	15.3	15.3	15.4	15.4	15.0	15.2	15.2	15.2	15.1	15.0	15.2	15.2	15.2
CaO	22.7	22.2	22.2	22.9	22.1	23.3	22.9	22.9	23.1	23.0	22.7	22.7	22.6	23.1
Na2O	0.68	0.67	0.69	0.68	0.65	0.66	0.62	0.61	0.72	0.62	0.68	0.74	0.68	0.68
K2O	0.01	0.01	<0.01	<0.01	0.01	<0.01	<0.01	<0.01	0.01	<0.01	<0.01	0.03	<0.01	<0.01
Total	100.9	99.0	99.1	99.7	99.1	99.5	100.7	100.8	100.9	100.6	100.1	100.3	100.2	100.7
Si	1.804	1.816	1.835	1.814	1.827	1.808	1.847	1.835	1.836	1.840	1.841	1.835	1.834	1.831
Ti	0.016	0.015	0.011	0.012	0.015	0.014	0.021	0.022	0.022	0.023	0.019	0.018	0.018	0.019
Al	0.316	0.268	0.256	0.255	0.260	0.265	0.244	0.252	0.249	0.247	0.255	0.250	0.255	0.251
Cr	0.035	0.043	0.042	0.042	0.041	0.033	0.035	0.035	0.036	0.034	0.035	0.033	0.033	0.032
Fe3+	0.058	0.077	0.060	0.088	0.062	0.091	0.028	0.043	0.050	0.037	0.039	0.065	0.058	0.066
Fe2+	0.053	0.013	0.029	0.000	0.028	0.000	0.065	0.051	0.041	0.059	0.057	0.034	0.042	0.033
Mn	0.001	0.004	0.003	0.004	0.003	0.004	0.004	0.003	0.002	0.001	0.005	0.003	0.003	0.003
Ni	0.003	0.001	0.001	0.001	0.002	0.002	0.001	0.003	0.002	0.001	0.002	<0.001	<0.001	0.002
Mg	0.785	0.840	0.838	0.839	0.845	0.821	0.820	0.823	0.817	0.818	0.813	0.823	0.828	0.822
Ca	0.881	0.875	0.874	0.896	0.871	0.915	0.891	0.891	0.895	0.896	0.887	0.887	0.883	0.896
Na	0.048	0.048	0.050	0.048	0.047	0.047	0.044	0.043	0.051	0.044	0.048	0.052	0.048	0.048
K	<0.001	0.001	<0.001	<0.001	<0.001	<0.001	<0.001	<0.001	<0.001	<0.001	<0.001	0.001	<0.001	<0.001
# Mg	0.88	0.91	0.91	0.91	0.91	0.91	0.90	0.90	0.90	0.90	0.90	0.90	0.90	0.90
# Cr	0.10	0.14	0.14	0.14	0.13	0.11	0.12	0.12	0.13	0.12	0.12	0.12	0.11	0.11

cpx porphyroclasts core **cpx porphyroclasts rim**

	CGSGn							hydrous-m		mylonite				
	L195					**W2**		**L187d**		**L04**				**L104**
	1	2	3	4	5	1	2	1	2	1	2	3	4	1
SiO2	50.4	50.4	50.4	50.1	50.6	50.4	50.5	52.3	51.8	52.2	52.5	52.2	51.8	51.5
TiO2	0.33	0.32	0.42	0.44	0.38	0.62	0.57	0.80	0.90	0.68	0.60	0.72	0.73	0.79
Al2O3	7.00	7.05	7.22	7.17	7.35	1.29	1.47	3.30	3.79	3.43	3.33	3.20	3.22	4.11
Cr2O3	1.13	1.14	1.14	1.21	1.23	5.51	5.29	1.02	1.07	0.94	0.91	1.20	0.97	1.07
Fe2O3	0.12	0.17	0.00	0.53	0.00	1.85	2.74	0.96	1.45	1.89	1.94	1.52	1.61	2.54
FeO	2.61	2.84	2.69	2.06	2.80	1.23	0.42	1.67	1.37	1.06	1.03	1.29	1.24	0.54
MnO	0.13	0.12	0.11	0.06	0.09	0.13	0.08	0.09	0.10	0.09	0.13	0.13	0.07	0.11
NiO	0.05	0.05	0.02	0.03	0.06	0.05	0.05	0.02	0.06	0.01	0.04	-	-	-
MgO	14.4	14.7	14.7	14.5	14.9	14.9	15.2	16.2	15.9	17.0	17.2	16.6	16.5	16.3
CaO	22.6	22.2	22.4	23.0	21.6	23.0	23.4	23.3	23.3	22.5	22.5	22.9	22.8	22.7
Na2O	0.67	0.62	0.62	0.58	0.74	0.71	0.73	0.58	0.66	0.58	0.55	0.60	0.55	0.75
K2O	<0.01	0.01	0.01	0.01	0.01	0.01	<0.01	0.00	0.00	0.00	0.02	0.00	0.00	0.00
Total	99.4	99.6	99.7	99.8	99.8	99.7	100.4	100.28	100.3	100.38	100.77	100.35	99.55	100.5
Si	1.846	1.843	1.840	1.830	1.834	1.845	1.838	1.900	1.882	1.890	1.894	1.895	1.894	1.867
Ti	0.009	0.009	0.012	0.012	0.012	0.017	0.016	0.022	0.025	0.019	0.016	0.020	0.020	0.022
Cr	0.033	0.033	0.033	0.035	0.038	0.037	0.042	0.141	0.162	0.147	0.141	0.137	0.139	0.176
Al	0.302	0.304	0.311	0.309	0.319	0.238	0.227	0.029	0.031	0.027	0.026	0.034	0.028	0.031
Fe3+	0.003	0.005	0.000	0.015	0.000	0.051	0.075	0.026	0.040	0.051	0.053	0.042	0.044	0.069
Fe2+	0.080	0.087	0.082	0.063	0.080	0.038	0.013	0.051	0.042	0.032	0.031	0.039	0.038	0.017
Mn	0.004	0.004	0.003	0.002	0.003	0.004	0.003	0.003	0.003	0.003	0.004	0.004	0.002	0.003
Ni	0.001	0.001	0.001	0.001	0.001	0.001	0.002	0.001	0.002	0.000	0.001	-	-	-
Mg	0.786	0.802	0.799	0.791	0.791	0.814	0.822	0.878	0.861	0.919	0.923	0.898	0.902	0.881
Ca	0.888	0.868	0.875	0.901	0.880	0.903	0.911	0.908	0.906	0.873	0.871	0.889	0.894	0.883
Na	0.047	0.044	0.044	0.041	0.042	0.050	0.052	0.041	0.046	0.041	0.039	0.042	0.039	0.053
K	<0.001	0.001	<0.001	<0.001	<0.001	<0.001	<0.001	<0.001	<0.001	<0.001	0.001	<0.001	<0.001	<0.001
# Mg	0.90	0.90	0.91	0.91	0.91	0.91	0.91	0.92	0.92	0.92	0.92	0.92	0.92	0.92
# Cr	0.90	0.90	0.90	0.90	0.89	0.86	0.84	0.17	0.16	0.16	0.16	0.20	0.17	0.15

A2.5c: Clinopyroxene dataset

cpx porphyroclasts rim

	mylonit proto-mylonite						FGSG					CGSGc		
	L104	L112	La2002-05				L09		L110			L13	L42	
	2	1	2	1	2	3	1	2	1	2	3	1	2	1
SiO2	51.7	52.3	52.3	52.7	52.3	51.9	52.2	51.8	51.8	51.6	51.8	52.4	52.3	50.9
TiO2	0.79	0.79	0.78	0.65	0.67	0.72	0.72	0.73	0.86	0.94	0.93	0.97	0.99	0.69
Al2O3	4.06	3.07	3.51	3.26	3.78	3.77	3.20	3.22	3.69	3.81	3.78	3.19	3.69	4.07
Cr2O3	1.01	0.79	0.87	0.92	1.06	1.05	1.20	0.97	1.05	1.09	1.17	0.92	1.06	1.27
Fe2O3	1.98	0.99	1.01	0.71	0.61	0.63	1.52	1.61	0.98	0.53	0.45	1.24	0.77	2.75
FeO	0.87	2.00	1.94	2.23	2.29	2.21	1.29	1.24	1.74	1.59	2.01	1.88	2.50	0.19
MnO	0.08	0.08	0.12	0.04	0.01	0.07	0.13	0.07	0.13	0.07	0.01	0.17	0.10	0.13
NiO	-	0.03	0.06	0.07	0.07	0.02	-	-	0.04	<0.01	<0.01	0.05	0.05	0.06
MgO	16.3	16.3	16.4	16.5	16.4	16.1	16.6	16.5	15.9	15.7	15.8	16.4	16.6	16.0
CaO	23.3	23.1	22.8	22.9	22.6	22.8	22.9	22.8	23.3	23.5	23.3	23.1	22.3	23.2
Na2O	0.59	0.53	0.56	0.55	0.57	0.55	0.60	0.55	0.58	0.57	0.58	0.55	0.57	0.61
K2O	<0.01	<0.01	<0.01	<0.01	<0.01	<0.01	<0.01	<0.01	0.02	0.02	<0.01	0.01	<0.01	<0.01
Total	100.7	100.0	100.4	100.5	100.3	99.7	100.4	99.6	100.0	99.5	99.9	100.9	101.0	99.8
Si	1.871	1.906	1.897	1.909	1.897	1.895	1.895	1.894	1.889	1.890	1.891	1.895	1.889	1.859
Ti	0.021	0.022	0.021	0.018	0.018	0.020	0.020	0.020	0.024	0.026	0.026	0.026	0.027	0.019
Al	0.173	0.132	0.150	0.139	0.162	0.163	0.137	0.139	0.159	0.164	0.162	0.136	0.157	0.175
Cr	0.029	0.023	0.025	0.027	0.031	0.030	0.034	0.028	0.030	0.032	0.034	0.026	0.030	0.037
Fe3+	0.054	0.027	0.028	0.019	0.017	0.017	0.042	0.044	0.027	0.015	0.012	0.034	0.021	0.076
Fe2+	0.026	0.061	0.059	0.068	0.070	0.067	0.039	0.038	0.053	0.049	0.061	0.057	0.075	0.006
Mn	0.003	0.003	0.004	0.001	<0.001	0.002	-	-	0.004	0.002	0.000	0.005	0.003	0.004
Ni	-	0.001	0.002	0.002	0.002	0.001	0.004	0.002	0.001	<0.001	<0.001	0.001	0.002	0.002
Mg	0.880	0.887	0.887	0.891	0.886	0.875	0.898	0.902	0.862	0.858	0.861	0.883	0.893	0.873
Ca	0.902	0.902	0.887	0.887	0.878	0.892	0.889	0.894	0.909	0.923	0.912	0.896	0.863	0.907
Na	0.041	0.037	0.040	0.039	0.040	0.039	0.042	0.039	0.041	0.041	0.041	0.039	0.040	0.043
K	<0.001	0.000	0.000	0.000	0.000	<0.001	<0.001	<0.001	0.001	0.001	<0.001	0.001	<0.001	<0.001
# Mg	0.92	0.91	0.91	0.91	0.91	0.91	0.92	0.92	0.92	0.93	0.92	0.91	0.90	0.92
# Cr	0.14	0.15	0.14	0.16	0.16	0.16	0.20	0.17	0.16	0.16	0.17	0.16	0.16	0.17

cpx porphyroclasts rim

	CGSCc								CGSGn		
	L42		L147			L241			L195	W2	
	2	3	1	2	3	1	2	3	1	1	2
SiO2	51.1	51.0	52.2	51.9	52.0	51.2	51.7	51.4	52.6	52.0	51.2
TiO2	0.62	0.63	0.87	0.91	0.94	0.73	0.82	0.78	0.45	0.66	0.78
Al2O3	4.19	4.15	3.67	4.37	4.05	4.03	3.86	3.95	1.06	1.17	1.25
Cr2O3	1.17	1.29	0.94	1.19	1.12	1.02	0.91	0.97	3.79	3.42	4.03
Fe2O3	0.88	2.12	1.26	0.44	0.73	1.91	1.45	1.68	<0.01	1.74	2.53
FeO	1.85	0.73	1.57	2.34	1.89	1.36	1.62	1.49	2.49	0.94	0.18
MnO	0.11	0.12	0.08	0.02	0.08	0.07	0.08	0.08	0.09	0.10	0.10
NiO	0.01	0.08	0.05	0.03	0.07	0.02	0.02	0.02	0.06	0.05	<0.01
MgO	15.9	16.0	16.1	15.7	15.8	16.1	16.0	16.0	16.0	15.9	15.6
CaO	22.0	22.5	24.1	23.3	23.5	22.7	23.4	23.1	22.3	23.6	24.4
Na2O	0.65	0.69	0.41	0.56	0.56	0.57	0.51	0.54	0.52	0.66	0.59
K2O	<0.01	0.01	0.02	0.02	<0.01	<0.01	<0.01	<0.01	0.01	<0.01	0.01
Total	98.5	99.4	101.2	100.8	100.8	99.7	100.3	100.0	99.4	100.3	100.6
Si	1.886	1.870	1.883	1.879	1.882	1.872	1.880	1.876	1.928	1.892	1.861
Ti	0.017	0.017	0.024	0.025	0.026	0.020	0.022	0.021	0.012	0.018	0.021
Al	0.182	0.179	0.156	0.186	0.173	0.174	0.166	0.170	0.031	0.034	0.036
Cr	0.034	0.037	0.027	0.034	0.032	0.030	0.026	0.028	0.164	0.147	0.173
Fe3+	0.024	0.058	0.034	0.012	0.020	0.053	0.040	0.046	<0.001	0.048	0.069
Fe2+	0.057	0.022	0.047	0.071	0.057	0.042	0.049	0.046	0.076	0.028	0.005
Mn	0.004	0.004	0.002	0.001	0.002	0.002	0.002	0.002	0.003	0.003	0.003
Ni	<0.001	0.002	0.002	0.001	0.002	0.001	<0.001	0.001	0.002	0.002	0.000
Mg	0.877	0.876	0.866	0.849	0.854	0.877	0.866	0.872	0.872	0.863	0.842
Ca	0.872	0.885	0.930	0.902	0.913	0.890	0.912	0.901	0.875	0.920	0.948
Na	0.047	0.049	0.029	0.039	0.039	0.040	0.036	0.038	0.037	0.047	0.041
K	<0.001	<0.001	0.001	0.001	<0.001	<0.001	<0.001	<0.001	<0.001	<0.001	<0.001
# Mg	0.92	0.92	0.92	0.91	0.92	0.91	0.91	0.91	0.92	0.92	0.93
# Cr	0.16	0.17	0.15	0.15	0.16	0.15	0.14	0.14	0.84	0.81	0.83

A2.5c: olivine dataset

Olivine neoblasts

	hydrous-mylonite							**mylonite**						
sample	**L187d**				round grain			**L04**					**L104**	
	1	2	3	4	5	6	7	1	2	3	4	5	1	2
SiO2	41.4	41.5	41.6	41.4	40.8	40.8	40.7	41.5	41.2	41.3	41.8	41.5	41.2	40.9
TiO2	0.02	0.03	0.01	<0.01	<0.01	0.01	0.01	0.01	0.02	0.01	0.00	0.03	<0.01	<0.01
Al2O3	0.00	0.01	0.01	<0.01	0.01	<0.01	0.01	<0.01	<0.01	0.01	1.83	0.07	<0.01	<0.01
Cr2O3	0.02	0.02	0.04	<0.01	<0.01	0.03	<0.01	0.04	0.01	0.04	0.01	0.07	<0.01	<0.01
FeO	8.58	8.34	7.78	7.97	10.25	9.82	9.86	9.12	9.59	9.33	9.35	9.68	10.56	11.03
MnO	0.05	0.04	0.04	0.07	0.12	0.17	0.16	0.18	0.09	0.11	0.15	0.16	0.19	0.22
NiO	0.39	0.42	0.43	0.35	0.38	0.39	0.35	0.33	0.40	0.45	0.34	0.39	0.35	0.33
MgO	50.9	51.0	51.6	51.3	49.3	49.6	49.4	50.5	50.0	50.2	48.5	50.2	49.1	48.6
CaO	0.06	0.10	0.11	0.11	0.00	0.00	0.00	0.18	0.07	0.05	0.70	0.05	0.03	0.01
Na2O	<0.01	0.01	0.01	0.03	0.02	<0.01	<0.01	<0.01	<0.01	0.02	0.06	0.01	0.02	<0.01
K2O	<0.01	<0.01	<0.01	<0.01	0.01	0.01	<0.01	0.01	0.01	<0.01	0.01	0.01	<0.01	<0.01
Total	101.5	101.5	101.7	101.2	100.9	100.8	100.5	101.9	101.4	101.5	102.7	102.2	101.4	101.1
Si	0.995	0.996	0.994	0.994	0.993	0.992	0.993	0.996	0.995	0.995	1.000	0.995	0.998	0.999
Ti	<0.001	0.001	<0.001	<0.001	<0.001	<0.001	<0.001	<0.001	<0.001	<0.001	<0.001	0.001	<0.001	<0.001
Al	<0.001	<0.001	<0.001	<0.001	<0.001	<0.001	<0.001	<0.001	<0.001	<0.001	0.052	0.002	<0.001	<0.001
Cr	<0.001	<0.001	0.001	<0.001	<0.001	0.001	<0.001	0.001	<0.001	0.001	<0.001	0.001	<0.001	<0.001
Fe2	0.172	0.167	0.155	0.160	0.209	0.200	0.201	0.183	0.194	0.188	0.187	0.194	0.214	0.225
Mn	0.001	0.001	0.001	0.001	0.002	0.004	0.003	0.004	0.002	0.002	0.003	0.003	0.004	0.005
Ni	0.008	0.008	0.008	0.007	0.008	0.008	0.007	0.006	0.008	0.009	0.007	0.008	0.007	0.006
Mg	1.822	1.824	1.837	1.834	1.787	1.797	1.796	1.805	1.799	1.802	1.730	1.795	1.775	1.765
Ca	0.002	0.003	0.003	0.003	<0.001	<0.001	<0.001	0.005	0.002	0.001	0.018	0.001	0.001	<0.001
Na	<0.001	0.001	0.001	0.001	0.001	<0.001	<0.001	<0.001	<0.001	0.001	0.003	0.001	0.001	<0.001
K	<0.001	<0.001	<0.001	<0.001	<0.001	<0.001	0.000	<0.001	<0.001	<0.001	<0.001	<0.001	<0.001	<0.001
# Mg	0.91	0.92	0.92	0.92	0.90	0.90	0.90	0.91	0.90	0.91	0.90	0.90	0.89	0.89

Olivine neoblasts

	mylonite		proto-mylonite							**FGSG**				
sample	**L104**		**L112**				**La2002-05**			**L09**				**L110**
	3	4	1	2	3	4	1	2	3	1	2	3	4	1
SiO2	40.7	40.9	40.9	41.0	40.8	40.9	41.4	40.9	41.1	41.5	41.2	41.2	41.3	41.2
TiO2	0.00	0.02	0.02	<0.01	<0.01	<0.01	0.01	0.01	<0.01	<0.01	0.02	0.04	0.02	0.02
Cr2O3	0.03	0.01	<0.01	<0.01	<0.01	<0.01	0.01	0.01	<0.01	<0.01	<0.01	0.01	<0.01	<0.01
Al2O3	0.01	<0.01	0.02	0.06	<0.01	0.09	0.04	<0.01	0.18	0.07	0.10	<0.01	0.06	<0.01
FeO	12.06	12.18	9.91	9.51	9.59	9.65	9.56	9.88	9.31	9.91	9.85	9.51	9.76	9.85
MnO	0.30	0.33	0.18	0.16	0.22	0.12	0.16	0.14	0.13	0.18	0.12	0.16	0.15	0.07
NiO	0.15	0.20	0.37	0.36	0.39	0.39	0.35	0.41	0.33	0.37	0.36	0.38	0.37	0.38
MgO	47.9	47.7	49.2	49.0	48.8	49.2	50.0	49.5	50.1	49.7	50.0	49.7	49.8	49.4
CaO	0.00	0.00	0.02	0.03	0.03	0.01	0.00	0.01	0.00	0.02	0.01	0.03	0.02	0.09
Na2O	0.01	0.01	<0.01	<0.01	0.02	<0.01	<0.01	<0.01	0.02	0.01	0.01	<0.01	0.01	0.03
K2O	<0.01	<0.01	<0.01	0.01	<0.01	<0.01	0.01	<0.01	<0.01	0.01	<0.01	<0.01	<0.01	0.01
Total	101.2	101.3	100.6	100.1	99.9	100.3	101.5	100.8	101.2	101.7	101.6	101.1	101.4	101.0
Si	0.995	1.000	0.998	1.004	1.002	0.999	0.998	0.994	0.993	1.001	0.993	0.998	0.997	1.000
Ti	<0.001	<0.001	<0.001	<0.001	<0.001	<0.001	<0.001	<0.001	<0.001	<0.001	<0.001	0.001	<0.001	<0.001
Cr	0.001	<0.001	<0.001	<0.001	<0.001	<0.001	<0.001	<0.001	<0.001	<0.001	<0.001	<0.001	<0.001	<0.001
Al	<0.001	<0.001	0.001	0.001	<0.001	0.002	0.001	<0.001	0.003	0.001	0.002	<0.001	0.001	<0.001
Fe2+	0.247	0.249	0.202	0.195	0.197	0.197	0.193	0.201	0.188	0.200	0.199	0.193	0.197	0.200
Mn	0.006	0.007	0.004	0.003	0.005	0.003	0.003	0.003	0.003	0.004	0.002	0.003	0.003	0.002
Ni	0.003	0.004	0.007	0.007	0.008	0.008	0.007	0.008	0.007	0.007	0.007	0.008	0.007	0.008
Mg	1.748	1.739	1.787	1.788	1.787	1.791	1.797	1.794	1.805	1.786	1.796	1.796	1.793	1.787
Ca	<0.001	<0.001	0.001	0.001	0.001	<0.001	<0.001	<0.001	<0.001	<0.001	<0.001	0.001	0.001	0.002
Na	<0.001	0.001	<0.001	<0.001	0.001	<0.001	<0.001	<0.001	0.001	<0.001	<0.001	<0.001	<0.001	0.001
K	<0.001	<0.001	<0.001	<0.001	<0.001	<0.001	<0.001	<0.001	<0.001	<0.001	<0.001	<0.001	<0.001	<0.001
# Mg	0.88	0.87	0.90	0.90	0.90	0.90	0.90	0.90	0.91	0.90	0.90	0.90	0.90	0.90

A2.5c: Olivine dataset

Olivine neob Olivine porphyroclasts core

	FGSG	hydrous-m		mylonite										
	L110	L187d		L04		L104			L112 proto-mylonite				La2002-05	
	2	1	2	1	2	1	2	3	1	2	3	4	1	2
SiO2	40.8	41.0	40.8	40.6	41.2	41.1	41.2	41.1	40.9	41.0	41.0	41.0	40.8	41.0
TiO2	0.01	0.03	<0.01	<0.01	<0.01	<0.01	0.01	0.01	0.02	0.01	0.01	0.00	0.03	<0.01
Al2O3	0.02	0.02	<0.01	<0.01	0.02	<0.01	0.02	0.01	<0.01	<0.01	<0.01	<0.01	<0.01	0.01
Cr2O3	0.04	<0.01	0.01	<0.01	<0.01	0.03	<0.01	<0.01	0.02	<0.01	0.02	0.06	0.02	0.02
FeO	10.64	10.10	10.39	10.09	9.29	11.28	10.89	10.64	9.91	9.91	9.56	9.51	10.29	10.05
MnO	0.17	0.12	0.25	0.19	0.15	0.22	0.18	0.21	0.18	0.24	0.21	0.16	0.10	0.11
NiO	0.38	0.41	0.37	0.32	0.38	0.33	0.37	0.36	0.37	0.38	0.39	0.36	0.34	0.42
MgO	48.9	49.5	49.7	49.0	49.8	48.4	49.0	49.0	49.2	48.8	48.9	49.0	49.3	49.1
CaO	0.04	0.03	0.02	0.01	0.04	0.00	0.00	0.02	0.02	0.01	0.03	0.03	0.04	0.05
Na2O	<0.01	<0.01	0.01	0.01	<0.01	<0.01	<0.01	0.01	<0.01	<0.01	0.01	<0.01	<0.01	0.01
K2O	<0.01	0.02	<0.01	<0.01	<0.01	<0.01	<0.01	<0.01	<0.01	<0.01	0.01	0.01	0.02	0.01
Total	101.0	101.2	101.6	100.2	100.9	101.4	101.6	101.4	100.6	100.4	100.1	100.1	101.0	100.8
Si	0.995	0.994	0.986	0.995	0.998	1.001	0.998	0.997	0.998	1.003	1.004	1.004	0.993	0.999
Ti	<0.001	0.001	<0.001	<0.001	<0.001	<0.001	<0.001	<0.001	<0.001	<0.001	<0.001	<0.001	0.001	<0.001
Al	<0.001	<0.001	<0.001	<0.001	<0.001	<0.001	<0.001	<0.001	<0.001	<0.001	<0.001	<0.001	<0.001	<0.001
Cr	0.001	<0.001	<0.001	<0.001	<0.001	0.001	<0.001	<0.001	0.001	<0.001	0.001	0.001	<0.001	0.001
Fe2	0.217	0.205	0.210	0.207	0.188	0.230	0.221	0.216	0.202	0.203	0.196	0.195	0.209	0.205
Mn	0.004	0.002	0.005	0.004	0.003	0.004	0.004	0.004	0.004	0.005	0.004	0.003	0.002	0.002
Ni	0.007	0.008	0.007	0.006	0.007	0.006	0.007	0.007	0.007	0.008	0.008	0.007	0.007	0.008
Mg	1.775	1.788	1.790	1.787	1.801	1.758	1.770	1.774	1.787	1.781	1.787	1.788	1.786	1.783
Ca	0.001	0.001	0.001	<0.001	0.001	<0.001	<0.001	0.001	0.001	<0.001	0.001	0.001	0.001	0.001
Na	<0.001	<0.001	0.001	0.001	<0.001	<0.001	<0.001	<0.001	<0.001	<0.001	0.001	<0.001	<0.001	<0.001
K	<0.001	0.001	<0.001	<0.001	<0.001	<0.001	<0.001	<0.001	<0.001	<0.001	<0.001	<0.001	0.001	<0.001
# Mg	0.89	0.90	0.90	0.90	0.91	0.88	0.89	0.89	0.90	0.90	0.90	0.90	0.90	0.90

Olivine porphyroclasts core

	FGSG										CGSGc			
	L09						L110				L13		L42	
	1	2	3	4	5	6	1	2	3	4	1	2	1	2
SiO2	40.2	40.8	40.7	40.7	40.7	40.5	40.8	40.7	41.1	40.9	41.2	41.1	41.0	41.1
TiO2	0.02	<0.01	<0.01	<0.01	0.01	<0.01	0.02	0.01	0.02	<0.01	0.02	<0.01	0.01	0.01
Cr2O3	<0.01	<0.01	<0.01	<0.01	<0.01	<0.01	0.01	0.01	<0.01	<0.01	0.02	<0.01	<0.01	<0.01
Al2O3	0.00	0.04	0.04	0.02	0.05	<0.01	0.03	<0.01	<0.01	<0.01	0.00	<0.01	0.01	<0.01
FeO	9.99	9.67	9.46	9.85	9.85	9.45	10.17	10.37	10.13	10.27	10.77	11.04	9.13	9.24
MnO	0.15	0.17	0.15	0.15	0.16	0.16	0.14	0.18	0.15	0.22	0.17	0.21	0.16	0.17
NiO	0.40	0.39	0.41	0.36	0.36	0.39	0.35	0.38	0.34	0.40	0.36	0.34	0.38	0.42
MgO	49.2	48.8	49.1	49.0	49.1	49.2	49.1	49.4	48.9	49.2	49.2	49.0	50.0	50.2
CaO	0.06	0.03	0.05	0.05	0.03	0.03	0.02	0.03	0.03	0.03	0.02	0.03	0.02	0.03
Na2O	0.01	<0.01	<0.01	<0.01	0.01	<0.01	0.01	<0.01	<0.01	0.01	0.02	<0.01	<0.01	0.02
K2O	<0.01	<0.01	<0.01	<0.01	0.00	<0.01	<0.01	<0.01	0.01	0.01	<0.01	<0.01	<0.01	0.01
Total	100.0	100.0	99.9	100.2	100.2	99.8	100.7	101.1	100.7	101.1	101.7	101.8	100.7	101.2
Si	0.986	1.002	0.998	0.995	0.994	0.999	0.995	0.988	1.003	0.995	0.996	0.995	0.996	0.992
Ti	<0.001	<0.001	<0.001	<0.001	<0.001	<0.001	<0.001	<0.001	<0.001	<0.001	<0.001	<0.001	<0.001	<0.001
Cr	<0.001	<0.001	<0.001	<0.001	<0.001	<0.001	<0.001	0.000	0.000	<0.001	0.001	0.000	0.000	0.000
Al	<0.001	0.001	<0.001	0.001	<0.001	0.001	0.001	<0.001	<0.001	<0.001	<0.001	<0.001	<0.001	<0.001
Fe2+	0.205	0.198	0.202	0.202	0.194	0.194	0.208	0.211	0.207	0.209	0.218	0.224	0.185	0.187
Mn	0.003	0.004	0.003	0.003	0.003	0.003	0.003	0.004	0.003	0.005	0.004	0.004	0.003	0.004
Ni	0.008	0.008	0.007	0.007	0.008	0.008	0.007	0.008	0.007	0.008	0.007	0.007	0.007	0.008
Mg	1.796	1.787	1.788	1.791	1.801	1.794	1.785	1.789	1.779	1.782	1.773	1.770	1.808	1.808
Ca	0.001	0.001	0.001	0.001	0.001	0.001	<0.001	0.001	0.001	0.001	0.001	0.001	<0.001	0.001
Na	0.001	<0.001	<0.001	<0.001	<0.001	<0.001	0.001	<0.001	<0.001	0.001	0.001	<0.001	<0.001	0.001
K	<0.001	<0.001	<0.001	<0.001	<0.001	<0.001	<0.001	<0.001	<0.001	<0.001	<0.001	<0.001	<0.001	<0.001
# Mg	0.90	0.90	0.90	0.90	0.90	0.90	0.90	0.89	0.90	0.90	0.89	0.89	0.91	0.91

A2.5c: Olivine dataset

Olivine porphyroclasts core

	CGSGc							CGSGn						
	L42	L147			L241			L195						W2
	3	1	2	3	1	2	3	1	2	3	4	5	6	1
SiO2	41.1	40.7	40.7	40.7	40.9	40.9	41.2	41.0	40.8	41.1	41.1	41.0	41.1	40.5
TiO2	0.00	<0.01	<0.01	0.01	<0.01	<0.01	<0.01	<0.01	0.02	0.01	0.01	0.01	<0.01	0.01
Al2O3	0.11	<0.01	<0.01	<0.01	0.02	0.01	0.01	0.02	0.01	<0.01	<0.01	<0.01	<0.01	0.03
Cr2O3	0.02	0.02	0.01	<0.01	0.02	0.01	<0.01	0.03	0.04	0.02	<0.01	<0.01	<0.01	0.00
FeO	9.09	9.95	10.27	9.71	10.51	10.20	10.27	8.77	8.70	8.48	8.59	8.50	8.50	9.51
MnO	0.14	0.16	0.15	0.12	0.18	0.14	0.14	0.16	0.15	0.13	0.13	0.13	0.14	0.13
NiO	0.35	0.35	0.33	0.37	0.42	0.40	0.37	0.40	0.34	0.39	0.40	0.41	0.38	0.39
MgO	50.1	48.6	49.5	48.7	48.6	48.8	49.0	49.4	49.8	49.9	50.2	50.5	49.9	49.1
CaO	0.09	0.01	0.03	0.01	0.06	0.03	0.03	0.03	0.04	0.03	0.01	0.03	0.03	0.00
Na2O	0.01	<0.01	<0.01	<0.01	0.01	<0.01	0.01	0.01	0.01	<0.01	0.02	0.02	<0.01	<0.01
K2O	0.01	<0.01	<0.01	0.01	0.01	0.01	<0.01	0.01	<0.01	<0.01	<0.01	<0.01	0.01	<0.01
Total	101.0	99.8	101.0	99.7	100.68	100.43	100.91	99.876	99.905	100.1	100.5	100.58	100.1	99.7
Si	0.993	1.003	0.988	1.002	0.999	1.001	1.002	1.004	0.996	1.003	0.997	0.994	1.002	0.994
Ti	<0.001	<0.001	<0.001	<0.001	<0.001	<0.001	<0.001	<0.001	<0.001	<0.001	<0.001	<0.001	<0.001	<0.001
Al	0.003	<0.001	<0.001	<0.001	<0.001	<0.001	<0.001	<0.001	0.001	<0.001	<0.001	<0.001	<0.001	<0.001
Cr	<0.001	<0.001	<0.001	<0.001	<0.001	<0.001	<0.001	0.001	<0.001	<0.001	<0.001	<0.001	<0.001	0.001
Fe2	0.184	0.205	0.209	0.200	0.215	0.209	0.209	0.179	0.178	0.173	0.174	0.172	0.173	0.195
Mn	0.003	0.003	0.003	0.002	0.004	0.003	0.003	0.003	0.003	0.003	0.003	0.003	0.003	0.003
Ni	0.007	0.007	0.006	0.007	0.008	0.008	0.007	0.008	0.007	0.008	0.008	0.008	0.008	0.008
Mg	1.807	1.781	1.792	1.788	1.771	1.779	1.777	1.803	1.814	1.812	1.817	1.821	1.813	1.799
Ca	0.002	<0.001	0.001	<0.001	0.002	0.001	0.001	0.001	0.001	0.001	<0.001	0.001	0.001	0.000
Na	<0.001	<0.001	<0.001	<0.001	<0.001	<0.001	<0.001	<0.001	<0.001	<0.001	0.001	0.001	<0.001	<0.001
K	<0.001	<0.001	<0.001	<0.001	<0.001	<0.001	<0.001	<0.001	<0.001	<0.001	<0.001	<0.001	<0.001	<0.001
# Mg	0.91	0.90	0.90	0.90	0.89	0.89	0.89	0.91	0.91	0.91	0.91	0.91	0.91	0.90

Olivine porphyroclasts core

	CGSGn		
	W2		
	2	3	4
SiO2	40.5	40.7	40.6
TiO2	0.01	<0.01	<0.01
Cr2O3	0.01	<0.01	<0.01
Al2O3	<0.01	<0.01	0.07
FeO	9.56	9.64	9.55
MnO	0.14	0.14	0.16
NiO	0.43	0.39	0.37
MgO	49.2	49.1	49.2
CaO	0.01	0.04	0.02
Na2O	<0.01	<0.01	<0.01
K2O	<0.01	0.01	0.01
Total	99.9	99.9	100.0
Si	0.994	0.997	0.995
Ti	<0.001	<0.001	<0.001
Cr	<0.001	<0.001	0.001
Al	<0.001	<0.001	0.000
Fe2+	0.196	0.198	0.196
Mn	0.003	0.003	0.003
Ni	0.008	0.008	0.007
Mg	1.798	1.794	1.797
Ca	<0.001	0.001	0.001
Na	<0.001	<0.001	<0.001
K	<0.001	<0.001	<0.001
# Mg	0.90	0.90	0.90

A2.5d: spinel dataset

Spinel neoblasts

	hydrous-mylonite				mylonite				proto-mylonite					
sample	L187d				L04				L112			La2002-05		
	1	2	3	4	1	2	3	4	1	2	3	1	2	3
SiO2	0.02	0.04	0.03	0.01	0.10	0.04	0.03	0.06	<0.01	<0.01	0.02	0.02	0.02	<0.01
TiO2	0.18	0.09	0.34	0.14	0.57	0.38	0.41	0.18	0.35	0.58	0.79	0.54	0.55	0.41
Al2O3	30.2	34.9	33.7	33.8	29.0	34.5	36.8	42.2	31.4	22.5	28.1	28.6	28.3	24.6
Cr2O3	31.2	28.1	28.2	29.5	33.5	28.0	25.9	19.6	25.6	32.9	30.0	31.0	32.0	36.3
Fe2O3	6.94	5.97	5.57	6.41	6.19	5.58	5.98	6.05	9.51	11.57	9.50	7.19	7.13	6.57
FeO	20.4	18.2	18.9	18.3	17.4	21.2	18.2	16.7	22.8	25.4	20.9	19.4	19.2	19.9
MnO	0.21	0.12	0.05	0.00	0.24	0.28	0.29	0.25	0.24	0.33	0.15	0.16	0.13	0.18
NiO	0.17	0.19	0.15	0.14	0.20	0.16	0.27	0.28	0.19	0.21	0.17	0.21	0.21	0.11
MgO	10.3	12.4	11.8	12.5	12.5	9.8	12.7	13.9	8.6	6.3	10.3	10.6	11.0	9.9
CaO	0.03	0.01	0.03	0.03	0.09	0.01	<0.01	0.01	<0.01	0.02	<0.01	0.02	<0.01	<0.01
Na2O	0.02	0.01	<0.01	<0.01	-	-	-	-	0.04	0.03	<0.01	0.02	<0.01	0.01
ZnO	0.21	0.22	0.11	0.26	0.19	0.25	0.30	0.22	0.48	0.31	0.31	0.32	0.28	0.36
Total	99.8	100.2	98.8	101.1	100.0	100.2	100.8	99.4	99.17	100.15	100.25	98.07	98.72	98.27
Si	0.001	0.001	0.001	<0.001	0.003	0.001	0.001	0.002	<0.001	<0.001	0.001	0.001	0.001	<0.001
Ti	0.004	0.002	0.008	0.003	0.013	0.009	0.009	0.004	0.008	0.014	0.018	0.013	0.013	0.010
Al	1.083	1.208	1.189	1.168	1.030	1.013	1.257	1.418	1.142	0.854	1.016	1.047	1.029	0.916
Cr	0.750	0.654	0.668	0.684	0.797	0.838	0.593	0.442	0.623	0.839	0.727	0.761	0.779	0.909
Fe3	0.159	0.132	0.126	0.141	0.140	0.129	0.130	0.130	0.221	0.281	0.219	0.168	0.165	0.157
Fe2	0.520	0.448	0.474	0.449	0.437	0.543	0.440	0.398	0.587	0.683	0.535	0.505	0.494	0.526
Mn	0.006	0.003	0.001	0.000	0.006	0.007	0.007	0.006	0.006	0.009	0.004	0.004	0.003	0.005
Ni	0.004	0.005	0.004	0.003	0.005	0.004	0.006	0.006	0.005	0.006	0.004	0.005	0.005	0.003
Mg	0.467	0.542	0.527	0.544	0.561	0.449	0.549	0.590	0.395	0.304	0.468	0.488	0.505	0.467
Ca	0.001	<0.001	0.001	0.001	0.003	<0.001	<0.001	<0.001	<0.001	0.001	<0.001	0.001	<0.001	<0.001
Na	0.001	<0.001	<0.001	<0.001	-	-	-	-	0.002	0.002	<0.001	0.001	<0.001	0.001
Zn	0.005	0.005	0.003	0.006	0.004	0.006	0.007	0.005	0.011	0.007	0.007	0.007	0.006	0.009
# Mg	0.41	0.49	0.47	0.49	0.50	0.41	0.50	0.53	0.33	0.25	0.39	0.43	0.44	0.41
# Cr	0.41	0.35	0.36	0.37	0.44	0.45	0.32	0.24	0.35	0.50	0.42	0.42	0.43	0.50

Spinel neoblasts **Spinel porphyroclasts core**

	FGSG								CGSGc		hydrous-m		mylonite	
sample	L09						L110		L42		L187d		L04	
	1	2	3	4	5	6	1	2	1	2	1	2	1	2
SiO2	0.02	0.04	0.05	0.02	0.03	0.03	0.03	0.01	0.04	0.03	<0.01	0.03	0.04	0.00
TiO2	0.57	0.39	0.50	0.20	0.44	0.30	0.42	0.65	0.67	0.64	0.56	0.32	0.60	0.53
Al2O3	30.5	31.0	25.7	44.9	28.6	35.5	28.5	31.9	28.7	29.1	34.1	36.1	32.3	32.2
Cr2O3	31.2	29.7	34.1	17.3	30.1	25.8	32.5	29.4	33.8	32.1	28.1	26.3	29.1	29.6
Fe2O3	6.21	6.73	7.32	5.00	7.80	5.94	5.63	5.99	6.06	6.20	6.07	6.37	7.14	7.00
FeO	17.9	18.8	21.8	15.1	21.6	18.7	18.8	15.9	16.8	17.1	17.4	16.4	14.5	14.6
MnO	0.22	0.21	0.32	0.14	0.30	0.21	0.23	0.18	0.71	0.74	0.10	0.11	0.07	0.13
NiO	0.18	0.26	0.16	0.27	0.20	0.20	0.12	0.18	0.15	0.20	0.25	0.24	0.23	0.24
MgO	12.1	11.3	8.8	14.9	9.1	11.7	10.9	13.3	12.5	12.0	12.9	13.7	14.4	14.4
CaO	<0.01	<0.01	0.01	<0.01	0.01	0.01	<0.01	0.02	<0.01	0.02	<0.01	<0.01	0.02	<0.01
Na2O	-	-	-	-	-	-	-	-	<0.01	<0.01	0.02	0.01	0.03	<0.01
ZnO	0.33	0.28	0.51	0.53	0.41	0.44	0.37	0.23	0.43	0.35	0.26	0.23	0.25	0.09
Total	99.2	98.7	99.3	98.2	98.6	98.8	97.5	97.8	99.8	98.5	99.8	99.8	98.6	98.9
Si	0.001	0.001	0.002	0.001	0.001	0.001	0.001	<0.001	0.001	0.001	<0.001	0.001	<0.001	<0.001
Ti	0.013	0.009	0.012	0.004	0.010	0.007	0.010	0.015	0.015	0.015	0.012	0.007	0.014	0.012
Al	1.086	1.111	0.952	1.497	1.052	1.245	1.046	1.132	1.022	1.050	1.186	1.240	1.112	1.126
Cr	0.746	0.715	0.848	0.387	0.742	0.607	0.801	0.702	0.807	0.776	0.656	0.606	0.694	0.694
Fe3	0.141	0.154	0.173	0.107	0.183	0.133	0.132	0.136	0.138	0.143	0.135	0.140	0.166	0.156
Fe2	0.452	0.478	0.575	0.357	0.564	0.466	0.489	0.402	0.425	0.437	0.430	0.399	0.353	0.363
Mn	0.006	0.006	0.008	0.003	0.008	0.005	0.006	0.005	0.018	0.019	0.002	0.003	0.002	0.003
Ni	0.004	0.006	0.004	0.006	0.005	0.005	0.003	0.004	0.004	0.005	0.006	0.006	0.005	0.006
Mg	0.544	0.515	0.414	0.627	0.425	0.522	0.504	0.599	0.561	0.546	0.566	0.595	0.648	0.637
Ca	<0.001	<0.001	0.001	<0.001	<0.001	<0.001	<0.001	0.001	<0.001	0.001	<0.001	<0.001	<0.001	<0.001
Na	-	-	-	-	-	-	-	-	<0.001	<0.001	0.001	<0.001	0.002	<0.001
Zn	0.007	0.006	0.012	0.011	0.010	0.010	0.009	0.005	0.010	0.008	0.006	0.005	0.002	0.002
# Mg	0.48	0.46	0.36	0.58	0.37	0.47	0.45	0.53	0.51	0.49	0.51	0.53	0.56	0.56
# Cr	0.41	0.39	0.47	0.21	0.41	0.33	0.43	0.38	0.44	0.42	0.36	0.33	0.38	0.38

A2.5d: spinel dataset

Spinel porphyroclasts core

	mylonite							proto-mylonite						FGSG
sample	L04		L104					L112		La2002-05				L09
	3	4	1	2	3	4	5	1	2	1	2	3	4	1
SiO2	0.01	0.01	0.03	0.35	0.02	<0.01	0.02	<0.01	<0.01	<0.01	<0.01	<0.01	0.01	0.02
TiO2	0.64	0.59	0.25	0.18	0.19	0.21	0.55	1.66	0.63	0.52	0.57	0.55	0.51	0.47
Al2O3	31.8	31.5	30.0	28.2	29.9	29.1	25.5	31.2	32.0	31.4	31.1	31.3	31.3	36.6
Cr2O3	29.6	29.8	29.1	30.6	29.7	30.3	33.3	31.2	31.4	30.9	30.9	31.1	31.2	27.7
Fe2O3	6.88	7.03	7.62	7.15	7.06	7.96	7.75	5.15	6.13	6.14	6.19	6.07	6.16	5.16
FeO	14.9	14.7	23.1	24.3	23.7	21.8	23.8	17.3	16.0	14.8	14.9	14.8	14.6	15.1
MnO	0.15	0.16	0.43	0.54	0.48	0.44	0.43	0.17	0.16	0.17	0.14	0.14	0.14	0.11
NiO	0.24	0.24	0.16	0.15	0.18	0.24	0.18	0.20	0.17	0.26	0.21	0.21	0.19	0.25
MgO	14.0	14.2	8.3	7.4	7.9	8.9	7.6	13.5	13.9	14.0	14.1	14.2	14.3	14.8
CaO	<0.01	<0.01	0.01	<0.01	<0.01	<0.01	0.01	<0.01	<0.01	<0.01	0.02	0.01	0.02	<0.01
NaO	0.04	<0.01	-	-	-	-	-	0.03	0.01	-	-	-	-	-
ZnO	0.17	0.13	0.41	0.65	0.27	0.43	0.39	0.16	0.17	0.23	0.01	0.09	0.19	0.23
Total	98.5	98.3	99.4	99.4	99.4	99.3	99.6	100.5	100.5	98.6	98.0	98.4	98.6	100.4
Si	0.001	<0.001	0.001	0.011	0.001	<0.001	0.001	<0.001	<0.001	<0.001	<0.001	<0.001	<0.001	0.001
Ti	0.013	0.013	0.006	0.004	0.005	0.005	0.013	0.037	0.014	0.012	0.013	0.012	0.011	0.010
Al	1.045	1.111	1.095	1.041	1.094	1.063	0.953	1.085	1.107	1.107	1.100	1.103	1.102	1.239
Cr	0.754	0.704	0.714	0.759	0.731	0.742	0.835	0.728	0.730	0.731	0.734	0.735	0.736	0.628
Fe3	0.173	0.158	0.178	0.169	0.165	0.186	0.185	0.114	0.136	0.138	0.140	0.137	0.138	0.112
Fe2	0.382	0.369	0.599	0.638	0.614	0.564	0.630	0.426	0.394	0.371	0.374	0.369	0.364	0.363
Mn	0.005	0.004	0.011	0.014	0.013	0.012	0.012	0.004	0.004	0.004	0.004	0.004	0.004	0.003
Ni	0.006	0.006	0.004	0.004	0.005	0.006	0.005	0.005	0.004	0.006	0.005	0.005	0.005	0.006
Mg	0.617	0.631	0.383	0.344	0.367	0.413	0.359	0.595	0.608	0.625	0.629	0.632	0.635	0.635
Ca	<0.001	<0.001	<0.001	<0.001	<0.001	<0.001	<0.001	<0.001	<0.001	<0.001	0.001	<0.001	0.001	<0.001
Na	<0.001	<0.001	-	-	-	-	-	0.002	<0.001	-	-	-	-	-
Zn	0.004	0.003	0.009	0.015	0.006	0.010	0.009	0.004	0.004	0.005	<0.001	0.002	0.004	0.005
# Mg	0.53	0.55	0.34	0.30	0.32	0.36	0.31	0.53	0.54	0.56	0.56	0.56	0.57	0.58
# Cr	0.42	0.39	0.39	0.42	0.40	0.41	0.47	0.40	0.40	0.40	0.40	0.40	0.40	0.34

Spinel porphyroclasts core

	FGSG							CGSGc						
sample	L09				L110			L13		L42			L147	
	2	3	4	5	1	2	3	1		1	2	3	1	2
SiO2	0.01	0.01	0.01	0.01	<0.01	<0.01	0.01	0.03	0	0.01	0.03	0.02	0.05	0.04
TiO2	0.38	0.37	0.39	0.39	0.63	0.87	1.42	0.65	0.62	0.58	0.62	0.66	0.51	0.59
Al2O3	36.8	36.8	36.8	36.8	31.3	31.1	30.6	25.8	25.81	29.3	28.2	28.1	30.5	30.8
Cr2O3	27.1	27.8	27.5	27.8	31.0	30.4	30.0	32.0	31.09	32.7	35.0	34.5	30.8	31.4
Fe2O3	5.26	4.95	4.82	4.68	6.19	6.30	6.00	9.06	9.88	7.30	6.40	5.88	6.71	6.41
FeO	14.9	14.5	14.5	14.6	15.5	15.8	16.2	23.4	22.57	16.9	17.8	19.3	18.6	18.0
MnO	0.23	0.21	0.17	0.10	0.00	0.13	0.19	0.15	0.12	0.69	0.70	0.64	0.21	0.13
NiO	0.21	0.28	0.23	0.13	0.22	0.16	0.30	0.17	0.22	0.18	0.21	0.21	0.18	0.22
MgO	14.8	15.1	15.0	15.1	13.9	13.7	13.5	8.07	8.35	12.6	12.0	11.1	11.6	12.3
CaO	<0.01	0.01	<0.01	<0.01	<0.01	0.01	<0.01	-	0.01	0.02	0.01	<0.01	0.01	0.02
Na2O								<0.01	0.04	<0.01	<0.01	<0.01	0.03	<0.01
ZnO	0.26	0.13	0.17	0.09	0.21	0.16	0.24	-	-	0.15	0.41	0.01	0.24	0.22
Total	99.8	100.2	99.5	99.7	98.9	98.5	98.5	99.7	99.1	100.4	101.3	100.5	99.5	100.2
Si	<0.001	<0.001	<0.001	<0.001	<0.001	<0.001	<0.001	0.001	<0.001	<0.001	0.001	0.001	0.002	0.001
Ti	0.008	0.008	0.008	0.008	0.014	0.020	0.032	0.015	0.015	0.013	0.014	0.015	0.012	0.013
Al	1.251	1.246	1.251	1.249	1.103	1.098	1.086	0.958	0.962	1.033	0.996	1.006	1.087	1.085
Cr	0.617	0.631	0.627	0.633	0.730	0.720	0.713	0.797	0.777	0.776	0.829	0.828	0.736	0.742
Fe3	0.114	0.107	0.105	0.101	0.139	0.142	0.136	0.215	0.235	0.165	0.144	0.134	0.153	0.144
Fe2	0.358	0.347	0.349	0.352	0.387	0.397	0.409	0.616	0.597	0.425	0.445	0.490	0.471	0.451
Mn	0.006	0.005	0.004	0.003	0.000	0.003	0.005	0.004	0.003	0.018	0.018	0.016	0.005	0.003
Ni	0.005	0.007	0.005	0.003	0.005	0.004	0.007	0.004	0.006	0.004	0.005	0.005	0.005	0.005
Mg	0.634	0.647	0.646	0.649	0.617	0.612	0.606	0.379	0.009	0.563	0.537	0.503	0.523	0.550
Ca	<0.001	<0.001	<0.001	<0.001	<0.001	<0.001	<0.001	<0.001	0.394	0.001	<0.001	<0.001	<0.001	0.001
Na	-	-	-	-	-	-	-	0.001	<0.001	<0.001	<0.001	<0.001	0.002	<0.001
Zn	0.006	0.003	0.004	0.002	0.005	0.004	0.005	-	-	0.003	0.009	0.000	0.005	0.005
# Mg	0.58	0.59	0.59	0.59	0.55	0.54	0.53	0.32	0.01	0.50	0.48	0.45	0.46	0.49
# Cr	0.33	0.34	0.33	0.34	0.40	0.40	0.40	0.45	0.45	0.43	0.45	0.45	0.40	0.41

A2.5d: spinel dataset

Spinel porphyroclasts core

	CGSGc			**CGSGn**							
sample	**L241**			**L195**				**W2**			
	1	2	3	1	2	3	4	1	2	3	4
SiO2	0.05	0.02	0.02	0.02	0.02	0.04	0.01	0.02	0.01	0.03	0.01
TiO2	0.42	0.50	0.74	0.28	0.39	0.44	0.40	0.76	0.20	0.38	0.39
Al2O3	33.6	33.8	33.0	32.7	33.3	32.5	32.7	28.1	27.9	29.8	28.1
Cr2O3	29.0	29.1	29.8	28.9	31.1	30.7	30.8	33.5	32.3	32.9	32.5
Fe2O3	7.22	7.19	6.95	6.24	5.36	6.33	5.64	6.56	8.31	6.69	7.86
FeO	15.3	15.2	15.4	20.8	16.4	14.3	16.9	21.8	23.2	20.6	22.5
MnO	0.17	0.05	0.10	0.77	0.65	0.66	0.64	0.73	0.78	0.74	0.83
NiO	0.29	0.29	0.25	0.20	0.22	0.16	0.22	0.15	0.17	0.13	0.22
MgO	14.3	14.6	14.5	10.2	13.3	14.5	12.9	9.3	7.2	10.1	8.2
CaO	<0.01	0.01	<0.01	<0.01	<0.01	<0.01	<0.01	0.03	<0.01	<0.01	0.01
NaO	0.02	<0.01	0.02	<0.01	<0.01	<0.01	<0.01	<0.01	<0.01	<0.01	<0.01
ZnO	0.17	0.19	0.24	0.18	0.28	0.27	0.08	0.87	2.34	0.98	1.43
Total	100.6	100.9	101.0	100.3	101.0	100.0	100.2	101.8	102.4	102.4	102.0
Si	0.001	0.001	0.001	<0.001	0.001	0.001	<0.001	<0.001	<0.001	0.001	<0.001
Ti	0.009	0.011	0.016	0.006	0.009	0.010	0.009	0.017	0.005	0.009	0.009
Al	1.154	1.155	1.131	1.158	1.146	1.125	1.138	1.008	1.012	1.053	1.013
Cr	0.668	0.666	0.685	0.687	0.718	0.713	0.719	0.806	0.785	0.777	0.787
Fe3	0.158	0.157	0.152	0.141	0.118	0.140	0.125	0.150	0.192	0.151	0.181
Fe2	0.372	0.369	0.373	0.522	0.402	0.351	0.416	0.554	0.597	0.516	0.575
Mn	0.004	0.001	0.002	0.019	0.016	0.016	0.016	0.019	0.020	0.019	0.022
Ni	0.007	0.007	0.006	0.005	0.005	0.004	0.005	0.004	0.004	0.003	0.005
Mg	0.622	0.630	0.626	0.456	0.580	0.634	0.570	0.019	0.053	0.022	0.032
Ca	<0.001	<0.001	<0.001	<0.001	<0.001	<0.001	<0.001	0.421	0.331	0.450	0.374
Na	0.001	<0.001	0.001	<0.001	<0.001	<0.001	<0.001	0.001	<0.001	<0.001	<0.001
Zn	0.004	0.004	0.005	0.004	0.006	0.006	0.002	<0.001	<0.001	<0.001	<0.001
# Mg	0.55	0.55	0.55	0.41	0.53	0.57	0.52	0.03	0.06	0.03	0.04
# Cr	0.37	0.37	0.38	0.37	0.39	0.39	0.39	0.44	0.44	0.42	0.44

A2.5e: plagioclase

	mylonite						proto-mylonite							
sample	L04						L112						La2002-05	
	1	2	3	4	5	6	1	2	3	4	5	6	1	2
SiO2	50.0	50.2	50.4	50.4	50.5	50.6	50.0	50.2	50.5	49.8	49.6	50.0	49.2	48.5
Al2O3	33.3	33.2	33.2	33.3	33.2	33.1	32.6	32.8	32.3	32.8	33.4	32.6	32.9	33.3
Fe2O3	0.16	0.11	0.07	0.06	0.13	0.08	0.11	0.00	0.09	0.00	0.04	0.16	0.11	0.09
FeO	<0.01	<0.01	<0.01	<0.01	<0.01	<0.01	0.04	0.16	<0.01	0.12	<0.01	<0.01	<0.01	<0.01
CaO	15.6	15.4	15.2	15.4	15.2	15.2	14.2	14.6	14.3	14.9	15.1	14.5	15.5	15.8
Na2O	3.00	3.12	3.12	3.12	3.16	3.12	3.29	3.16	3.40	2.99	2.98	3.43	2.76	2.58
K2O	<0.01	0.01	0.01	<0.01	0.02	<0.01	<0.01	<0.01	<0.01	<0.01	0.01	<0.01	0.01	0.03
Total	102.0	102.1	102.0	102.3	102.2	102.1	100.2	100.9	100.6	100.6	101.0	100.7	100.5	100.3
Si	2.236	2.242	2.250	2.244	2.252	2.259	2.271	2.268	2.284	2.258	2.236	2.257	2.238	2.209
Al	1.753	1.746	1.749	1.748	1.744	1.739	1.745	1.744	1.724	1.750	1.774	1.734	1.760	1.787
Fe3	0.006	0.004	0.002	0.002	0.004	0.003	0.004	<0.001	0.003	<0.001	0.001	0.005	0.004	0.003
Fe2	<0.001	<0.001	<0.001	<0.001	<0.001	<0.001	0.002	0.006	<0.001	0.005	<0.001	<0.001	<0.001	<0.001
Ca	0.745	0.736	0.727	0.735	0.724	0.728	0.689	0.705	0.691	0.725	0.728	0.703	0.755	0.772
Na	0.260	0.270	0.271	0.269	0.273	0.270	0.290	0.277	0.299	0.263	0.261	0.300	0.244	0.227
K	<0.001	<0.001	0.001	<0.001	0.001	<0.001	<0.001	<0.001	<0.001	<0.001	<0.001	<0.001	0.001	0.002
An	0.741	0.731	0.728	0.732	0.725	0.730	0.704	0.718	0.698	0.734	0.736	0.701	0.756	0.771
Alb	0.259	0.268	0.271	0.268	0.274	0.270	0.296	0.282	0.302	0.266	0.264	0.299	0.244	0.227

	proto-mylonite			FGSG						CGSGc				
	La2002-05			L09						L241				
	3	4	5	1	2	3	4	5	6	1	2	3	4	5
SiO2	48.3	48.4	49.2	50.3	49.5	48.6	48.7	49.2	50.0	48.3	48.1	48.7	47.5	49.1
Al2O3	33.4	33.2	32.6	33.1	33.2	33.5	33.7	33.7	32.7	34.1	34.1	32.9	34.1	33.2
Fe2O3	0.09	0.05	0.17	0.00	0.17	0.51	0.16	0.14	0.13	0.13	0.21	0.16	0.16	0.17
FeO	<0.01	<0.01	<0.01	0.11	<0.01	<0.01	<0.01	<0.01	<0.01	<0.01	<0.01	<0.01	<0.01	<0.01
CaO	16.2	16.0	15.3	14.4	15.0	15.4	15.6	15.4	14.6	16.0	16.1	15.3	16.2	15.5
Na2O	2.49	2.62	2.95	3.22	3.01	2.68	2.64	2.80	3.33	2.49	2.36	2.87	2.32	2.86
K2O	<0.01	<0.01	<0.01	<0.01	0.05	0.01	<0.01	<0.01	<0.01	0.02	<0.01	0.03	<0.01	0.02
Total	100.5	100.3	100.2	101.1	100.9	100.6	100.7	101.2	100.7	101.0	100.9	100.0	100.3	100.8
Si	2.199	2.205	2.240	2.264	2.235	2.205	2.205	2.217	2.257	2.184	2.181	2.222	2.167	2.220
Al	1.790	1.782	1.746	1.756	1.768	1.792	1.802	1.791	1.742	1.815	1.821	1.769	1.832	1.771
Fe3	0.003	0.002	0.006	<0.001	0.006	0.017	0.006	0.005	0.005	0.004	0.007	0.006	0.006	0.006
Fe2	<0.001	<0.001	<0.001	0.004	<0.001	<0.001	<0.001	<0.001	<0.001	<0.001	<0.001	<0.001	<0.001	<0.001
Ca	0.788	0.780	0.748	0.695	0.724	0.749	0.755	0.742	0.706	0.777	0.783	0.747	0.791	0.751
Na	0.220	0.232	0.260	0.281	0.264	0.236	0.232	0.244	0.291	0.218	0.208	0.254	0.205	0.251
K	<0.001	<0.001	<0.001	<0.001	0.003	0.001	<0.001	<0.001	<0.001	0.001	<0.001	0.002	<0.001	0.001
An	0.782	0.771	0.742	0.712	0.731	0.760	0.765	0.752	0.708	0.780	0.790	0.745	0.794	0.749
Alb	0.218	0.229	0.258	0.288	0.266	0.239	0.235	0.248	0.292	0.219	0.210	0.253	0.206	0.250

A2.5f: hornblende

	hydrous-mylonite				mylonite			proto-mylonite						
	L187d				L04			L112					La2002-05	
	1	2	3	4	1	2	3	1	2	3	4	5	1	2
SiO2	44.7	44.2	44.4	44.1	42.2	43.2	43.4	42.8	42.2	42.0	42.4	42.0	43.2	43.4
TiO2	2.62	2.82	3.10	3.27	4.52	4.53	3.70	4.12	4.17	4.04	4.28	4.42	3.72	3.86
Al2O3	12.2	12.5	11.9	11.8	13.0	12.5	14.1	11.6	11.6	11.1	11.4	11.8	11.1	11.4
Cr2O3	1.18	1.27	1.04	1.46	1.45	1.73	1.43	1.25	1.45	1.55	1.68	1.52	2.26	1.68
Fe2O3	<0.01	<0.01	<0.01	<0.01	<0.01	<0.01	<0.01	<0.01	<0.01	<0.01	<0.01	<0.01	<0.01	<0.01
FeO	3.49	3.69	4.06	3.79	4.92	4.13	3.92	4.33	4.38	4.19	4.43	4.42	3.95	4.30
MnO	0.06	0.10	0.04	0.07	0.05	0.05	0.02	0.09	0.02	0.01	0.07	0.03	0.08	0.07
NiO	0.07	0.08	0.09	0.10	-	-	-	0.13	0.06	0.08	0.08	0.14	0.11	0.09
MgO	17.5	17.4	17.2	17.2	17.0	16.8	17.0	16.7	16.6	16.7	16.6	16.4	16.6	17.0
CaO	12.0	12.6	12.5	12.0	12.0	12.0	12.2	12.2	12.6	12.5	12.3	12.3	12.4	12.2
Na2O	3.21	3.57	3.66	3.50	3.56	3.71	3.79	3.42	3.28	3.45	3.31	3.48	3.40	3.44
K2O	<0.01	0.02	0.02	0.01	0.03	<0.01	<0.01	0.04	<0.01	0.01	<0.01	<0.01	<0.01	<0.01
H2O	2.08	2.09	2.08	2.07	2.09	2.08	2.11	1.95	1.96	1.92	1.94	1.96	2.05	2.06
total	99.3	100.3	100.1	99.3	100.9	100.6	101.8	98.7	98.5	97.7	98.7	98.5	98.9	99.5
Si	6.44	6.33	6.39	6.41	6.06	6.23	6.16	6.28	6.20	6.22	6.23	6.18	6.33	6.32
Ti	0.284	0.304	0.336	0.357	0.487	0.491	0.395	0.455	0.460	0.450	0.472	0.490	0.410	0.422
Al	2.078	2.115	2.025	2.018	2.206	2.117	2.364	2.010	2.011	1.935	1.977	2.044	1.919	1.945
Cr	0.134	0.143	0.119	0.168	0.164	0.198	0.161	0.144	0.169	0.181	0.195	0.178	0.261	0.194
Fe3	<0.001	<0.001	<0.001	<0.001	<0.001	<0.001	<0.001	<0.001	<0.001	<0.001	<0.001	<0.001	<0.001	<0.001
Fe2	0.420	0.442	0.489	0.460	0.590	0.499	0.465	0.531	0.538	0.519	0.544	0.545	0.485	0.523
Mn	0.007	0.012	0.005	0.008	0.007	0.006	0.002	0.012	0.002	0.002	0.009	0.004	0.010	0.008
Ni	0.008	0.009	0.010	0.011	-	-	-	0.015	0.007	0.009	0.009	0.017	0.013	0.010
Mg	3.766	3.723	3.694	3.713	3.645	3.608	3.600	3.640	3.628	3.696	3.633	3.591	3.626	3.681
Ca	1.858	1.927	1.935	1.859	1.842	1.853	1.855	1.910	1.986	1.986	1.934	1.947	1.945	1.902
Na	0.896	0.991	1.022	0.985	0.989	1.037	1.041	0.972	0.932	0.992	0.941	0.995	0.966	0.970
K	<0.001	0.004	0.003	0.002	0.006	<0.001	<0.001	0.007	0.001	0.001	0.001	0.001	<0.001	0.001
H	2.000	2.000	2.000	2.000	2.000	2.000	2.000	1.910	1.914	1.896	1.898	1.922	2.000	2.000
# Mg	0.90	0.89	0.88	0.89	0.86	0.88	0.89	0.87	0.87	0.88	0.87	0.87	0.88	0.88

	Proto-m	FGSG									CGSGc			
sample	La2002	L09					L110				L13			L147
	3	1	2	3	4	5	1	2	3	4	1	2	3	1
SiO2	43.4	43.1	43.2	42.9	43.2	43.7	42.1	42.9	42.9	42.8	43.8	43.4	44.4	41.3
TiO2	3.20	2.92	2.59	3.02	2.69	2.43	4.37	3.97	3.90	4.24	4.19	3.10	2.96	4.19
Al2O3	11.9	12.0	11.7	12.2	11.8	11.2	12.1	11.8	11.8	11.6	12.3	12.5	11.7	14.4
Cr2O3	1.41	1.84	1.59	2.08	1.81	1.67	1.43	1.90	1.54	1.64	1.52	1.45	1.38	1.58
Fe2O3	<0.01	<0.01	<0.01	<0.01	<0.01	<0.01	<0.01	<0.01	<0.01	<0.01	<0.01	<0.01	<0.01	<0.01
FeO	4.26	4.82	4.99	4.62	5.06	5.00	4.70	4.56	4.48	4.17	4.62	5.42	5.32	4.11
MnO	0.14	0.08	0.03	0.07	0.03	0.06	0.05	0.08	0.06	0.03	0.03	0.06	0.10	0.09
NiO	0.09	0.14	0.10	0.10	0.11	0.07	0.07	0.08	0.10	0.11	-	-	-	0.08
MgO	17.1	16.9	17.3	16.8	17.0	17.3	16.3	16.6	16.8	16.7	16.8	16.9	17.0	15.5
CaO	12.2	12.2	12.4	12.3	12.3	12.4	12.5	12.2	11.9	12.5	12.8	12.4	13.0	12.2
Na2O	3.46	3.33	3.26	3.21	3.35	3.25	3.21	3.30	3.52	3.58	3.20	3.47	3.34	3.50
K2O	<0.01	0.02	<0.01	<0.01	<0.01	<0.01	0.01	<0.01	0.01	0.04	0.04	0.05	0.06	0.01
H2O	2.07	2.07	2.07	2.07	2.07	2.07	2.05	2.06	2.05	2.05	2.10	2.09	2.11	2.05
total	99.3	99.4	99.2	99.3	99.4	99.2	98.9	99.4	99.0	99.4	101.3	100.7	101.4	99.0
Si	6.294	6.250	6.258	6.227	6.272	6.343	6.170	6.250	6.267	6.252	6.243	6.224	6.322	6.047
Ti	0.350	0.319	0.283	0.330	0.293	0.265	0.481	0.434	0.429	0.466	0.449	0.335	0.317	0.461
Al	2.042	2.045	2.000	2.090	2.014	1.914	2.090	2.020	2.025	1.988	2.060	2.108	1.971	2.483
Cr	0.162	0.211	0.182	0.239	0.208	0.191	0.165	0.218	0.178	0.189	0.171	0.165	0.155	0.183
Fe3	<0.001	<0.001	<0.001	<0.001	<0.001	<0.001	<0.001	<0.001	<0.001	<0.001	<0.001	<0.001	<0.001	<0.001
Fe2	0.517	0.585	0.604	0.561	0.615	0.607	0.576	0.555	0.548	0.510	0.551	0.650	0.633	0.503
Mn	0.017	0.010	0.004	0.008	0.004	0.007	0.007	0.009	0.008	0.004	0.004	0.007	0.012	0.011
Ni	0.010	0.016	0.012	0.012	0.013	0.008	0.008	0.009	0.011	0.013	-	-	-	0.009
Mg	3.706	3.663	3.740	3.623	3.673	3.737	3.551	3.608	3.668	3.626	3.563	3.612	3.617	3.389
Ca	1.902	1.901	1.918	1.912	1.908	1.928	1.952	1.896	1.865	1.951	1.959	1.899	1.975	1.914
Na	0.973	0.936	0.915	0.903	0.943	0.914	0.911	0.932	0.998	1.013	0.885	0.966	0.922	0.993
K	<0.001	0.004	<0.001	<0.001	<0.001	<0.001	0.002	<0.001	0.002	0.007	0.007	0.010	0.010	0.001
H	2.000	2.000	2.000	2.000	2.000	2.000	2.000	2.000	2.000	2.000	2.000	2.000	2.000	2.000
# Mg	0.88	0.86	0.86	0.87	0.86	0.86	0.86	0.87	0.87	0.88	0.87	0.85	0.85	0.87

A2.5f: hornblende

	CGSGc									
	L147					**L241**				
	2	3	4	5	6	1	2	3	4	5
SiO2	42.7	42.8	42.6	42.6	42.7	42.2	42.7	42.8	43.4	41.6
TiO2	3.32	3.35	3.53	3.49	2.91	3.51	3.80	2.45	2.77	3.85
Al2O3	13.8	13.4	13.2	13.2	13.0	12.2	11.7	12.6	11.5	12.0
Cr2O3	1.71	1.33	1.20	1.37	1.38	1.43	1.33	1.26	1.04	1.68
Fe2O3	<0.01	<0.01	<0.01	<0.01	<0.01	<0.01	<0.01	<0.01	<0.01	<0.01
FeO	4.03	4.19	4.18	4.08	4.29	4.88	4.64	5.05	5.26	5.09
MnO	0.08	0.07	0.06	0.07	0.07	0.07	0.02	0.02	0.10	0.06
NiO	0.09	0.06	0.11	0.09	0.10	0.07	0.13	0.08	0.09	0.12
MgO	16.2	16.6	16.6	16.6	16.7	16.8	17.0	17.6	17.7	17.8
CaO	12.6	12.2	12.5	12.6	12.6	12.4	12.5	12.2	12.4	11.8
Na2O	3.61	3.72	3.63	3.54	3.77	3.37	3.35	3.11	3.28	3.15
K2O	0.01	0.02	0.01	0.01	<0.01	<0.01	<0.01	0.02	<0.01	<0.01
H2O	2.08	2.07	2.07	2.07	2.07	2.06	2.06	2.08	2.08	2.07
total	100.2	99.8	99.8	99.6	99.5	99.0	99.2	99.3	99.7	99.2
Si	6.166	6.203	6.171	6.170	6.192	6.149	6.212	6.165	6.244	6.035
Ti	0.360	0.365	0.384	0.380	0.318	0.385	0.416	0.265	0.301	0.420
Al	2.353	2.290	2.256	2.247	2.218	2.093	2.008	2.144	1.955	2.045
Cr	0.195	0.153	0.138	0.157	0.158	0.165	0.153	0.143	0.118	0.193
Fe3	<0.001	<0.001	<0.001	<0.001	<0.001	<0.001	<0.001	<0.001	<0.001	<0.001
Fe2	0.486	0.508	0.506	0.494	0.521	0.595	0.565	0.609	0.634	0.617
Mn	0.009	0.009	0.008	0.009	0.008	0.009	0.003	0.002	0.012	0.008
Ni	0.011	0.007	0.013	0.011	0.012	0.008	0.015	0.009	0.010	0.014
Mg	3.476	3.575	3.581	3.585	3.612	3.653	3.677	3.781	3.808	3.838
Ca	1.944	1.892	1.943	1.947	1.962	1.943	1.951	1.882	1.918	1.831
Na	1.010	1.045	1.019	0.994	1.061	0.951	0.946	0.869	0.916	0.886
K	0.001	0.003	0.002	0.001	0.001	0.001	0.001	0.004	0.001	<0.001
H	2.000	2.000	2.000	2.000	2.000	2.000	2.000	2.000	2.000	2.000
# Mg	0.88	0.88	0.88	0.88	0.87	0.86	0.87	0.86	0.86	0.86

A2.6: profiles of minerals (data set associated on CD)

A2.6a: orthopyroxene profiles

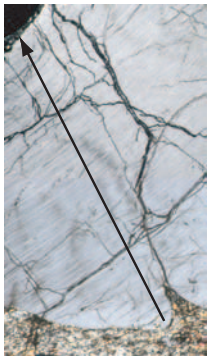

Sample L04, mylonite
distance: 2580 µm

Sample L104, mylonite
distance: 2468 µm

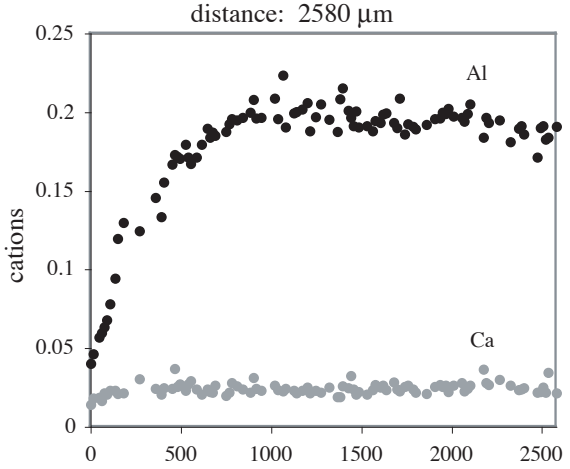

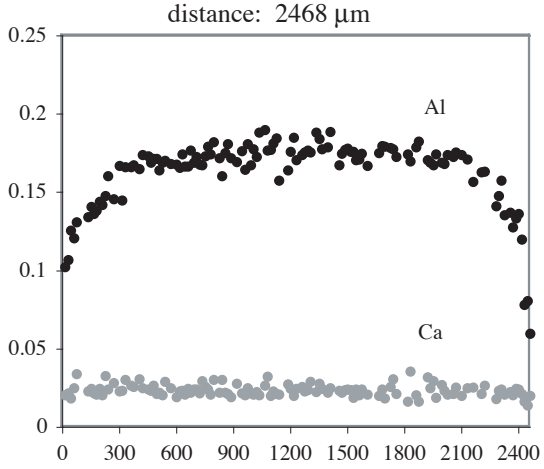

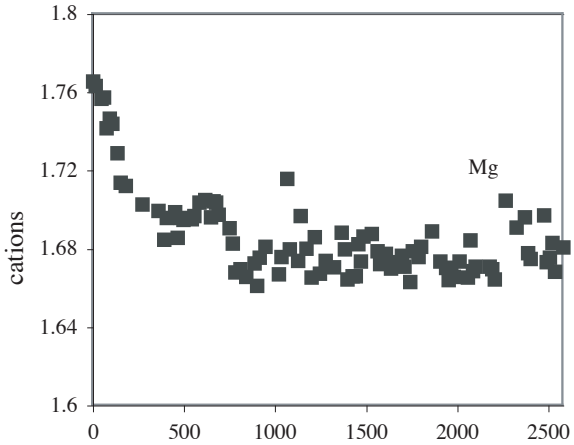

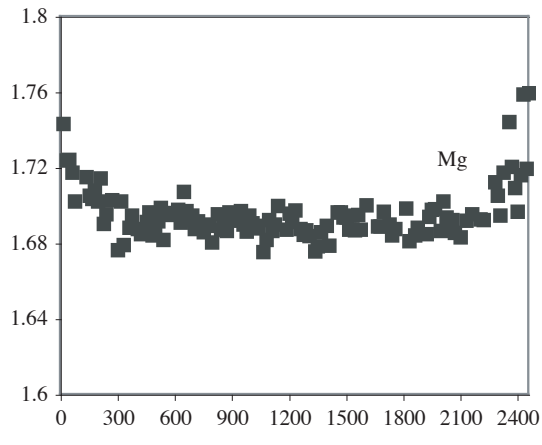

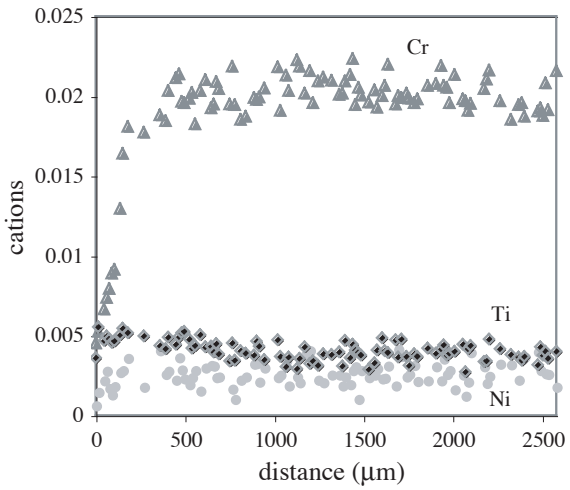

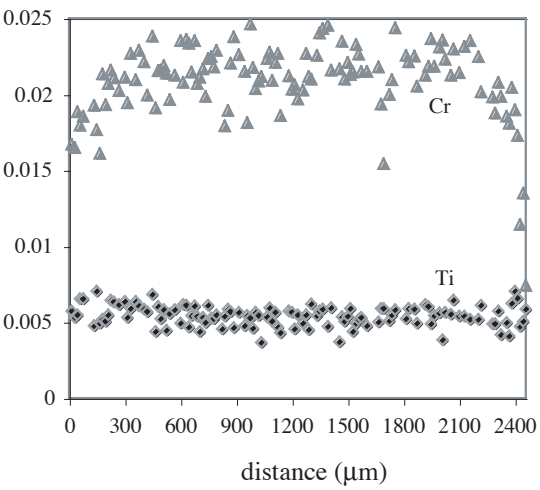

A2.6: profiles of minerals (data set associated on CD)

A2.6a: orthopyroxene profiles

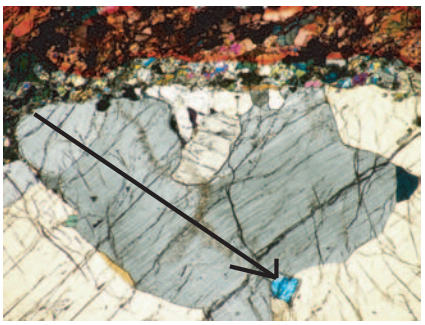

Sample L112, proto-mylonite
distance: 2520 µm

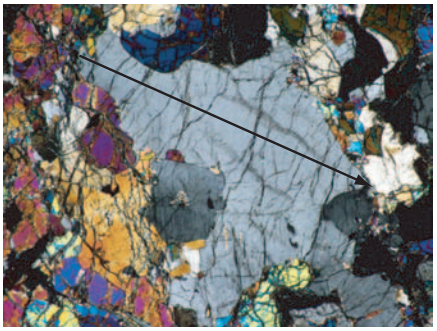

Sample L110, FGSG
distance: 2265 µm

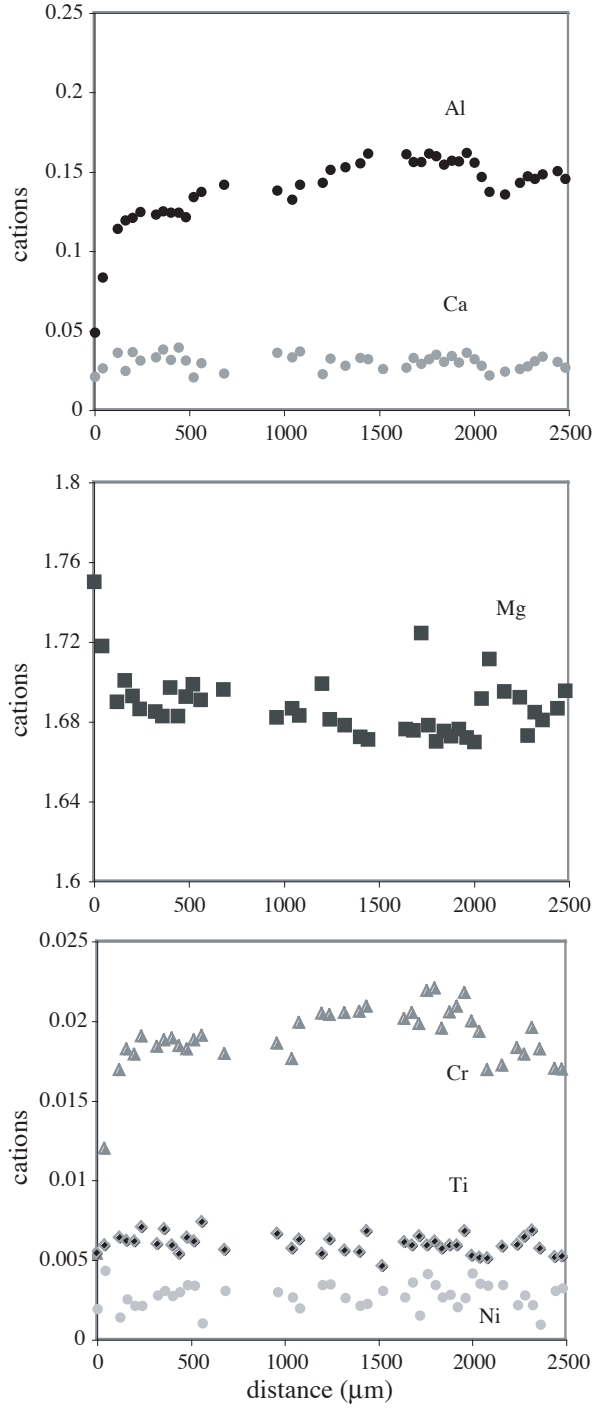

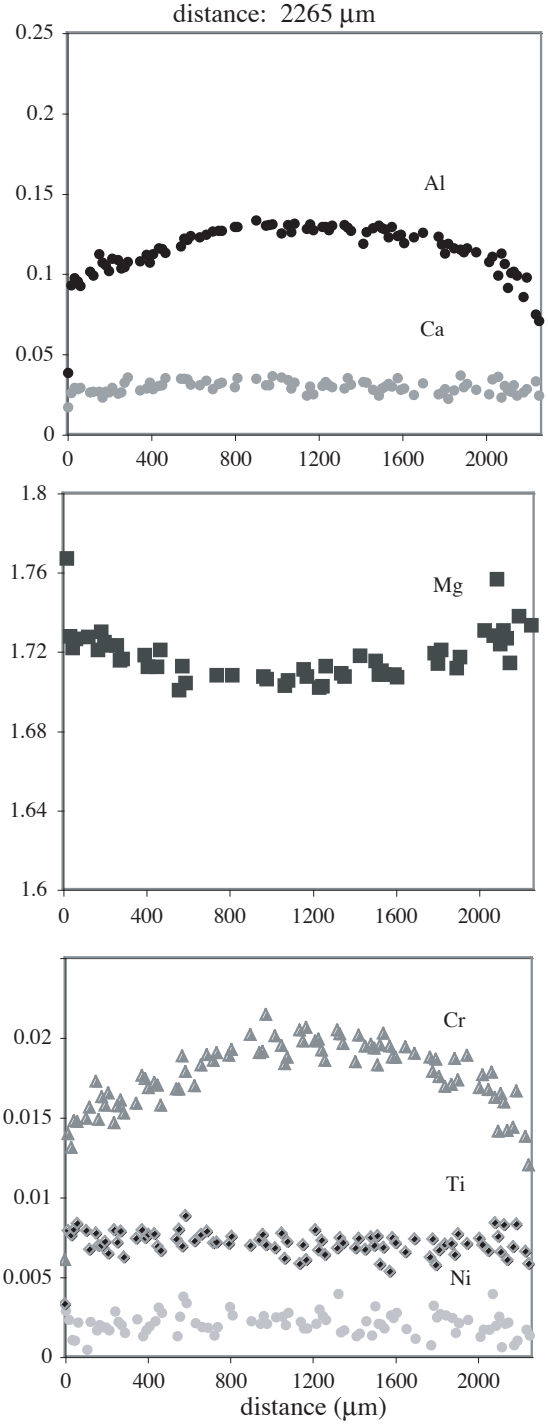

A2.6: profiles of minerals (data set associated on CD)

A2.6a: orthopyroxene profiles

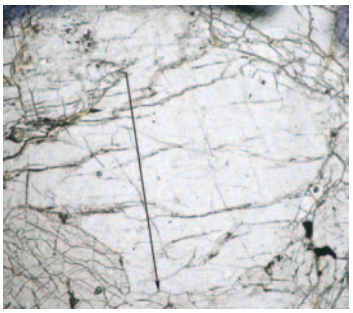

Sample L13, CGSG
distance: 2215 µm

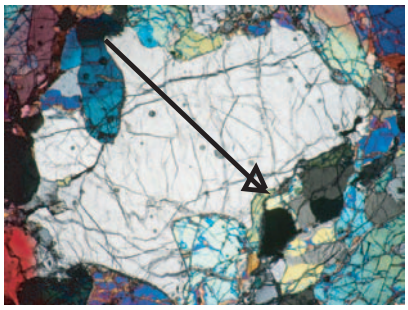

Sample L147, CGSG
distance: 1479 µm

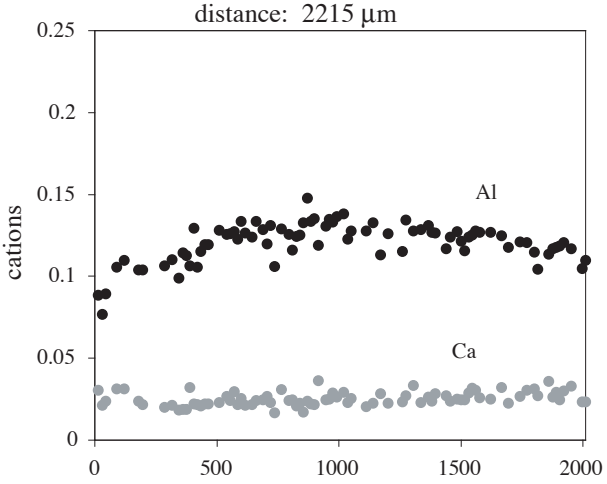

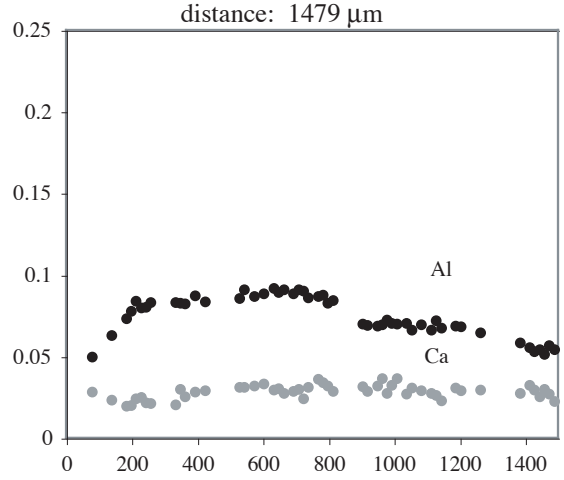

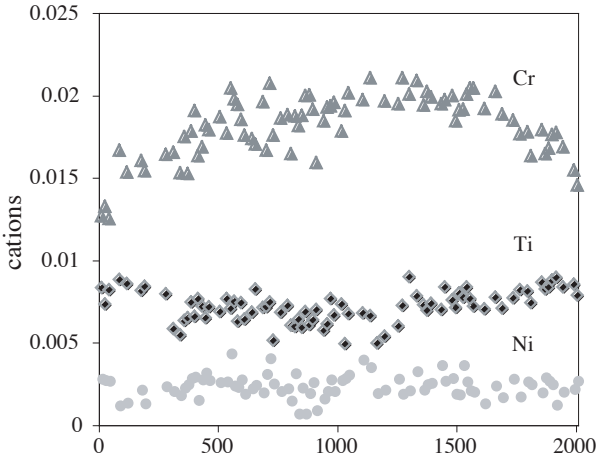

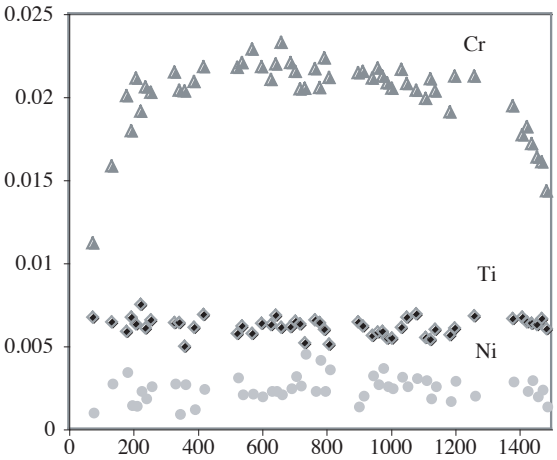

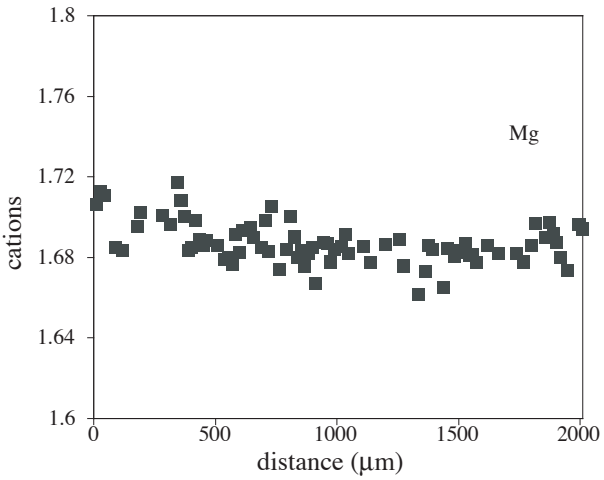

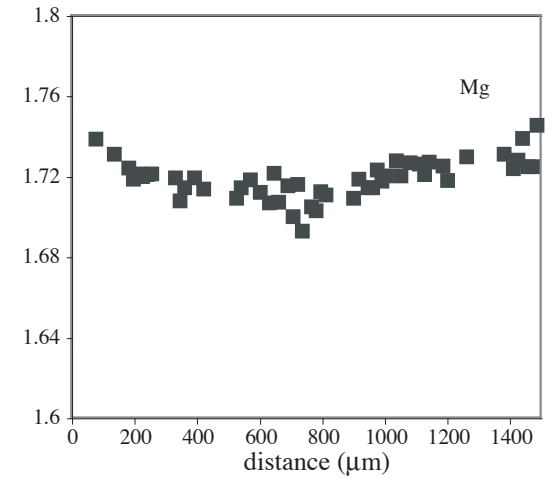

A2.6: profiles of minerals (data set associated on CD)

A2.6a: orthopyroxene profiles

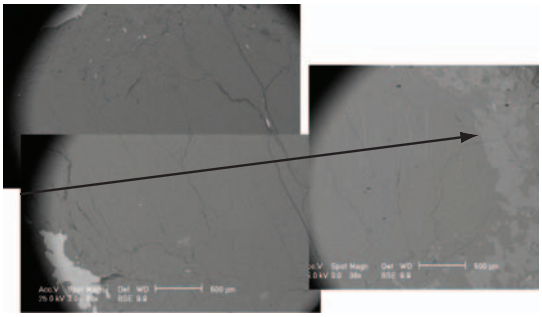

Sample L241, CGSG
distance: 5028 µm

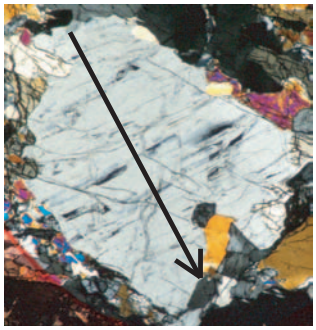

Sample La2002-02, FGSG
distance: 1540 µm

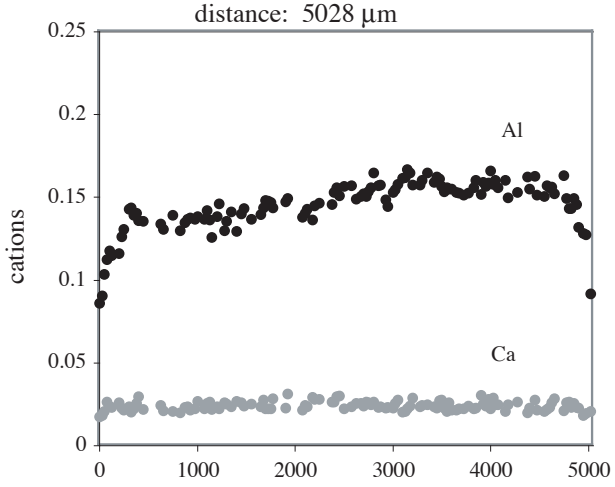

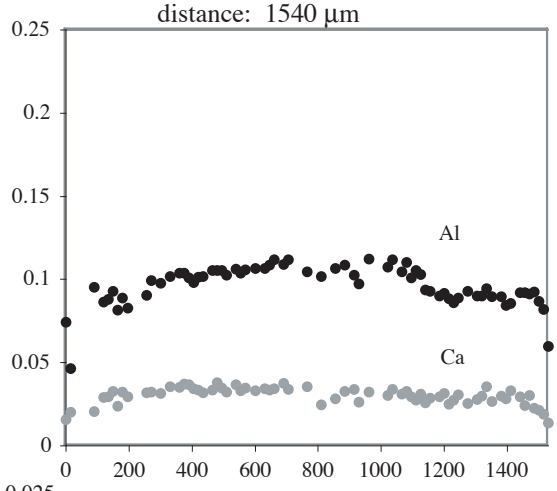

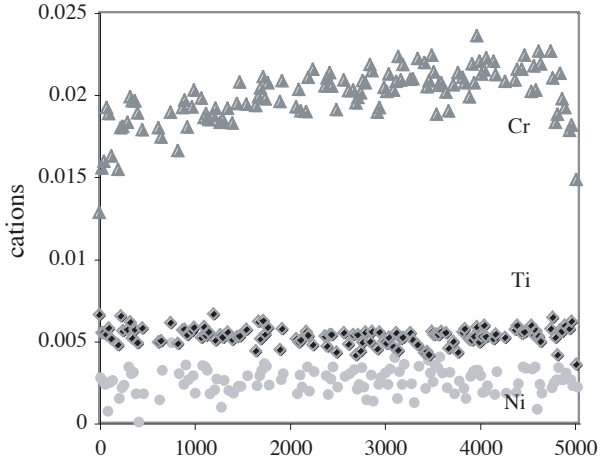

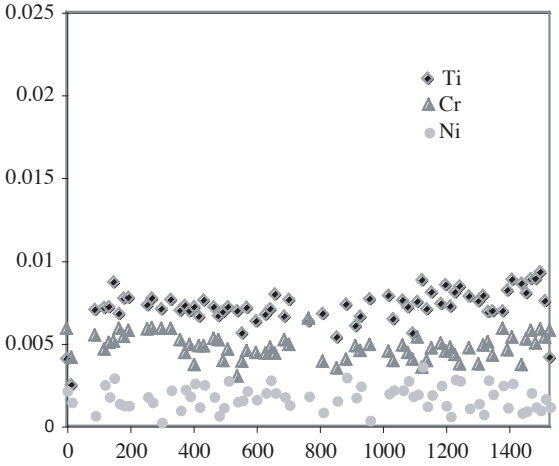

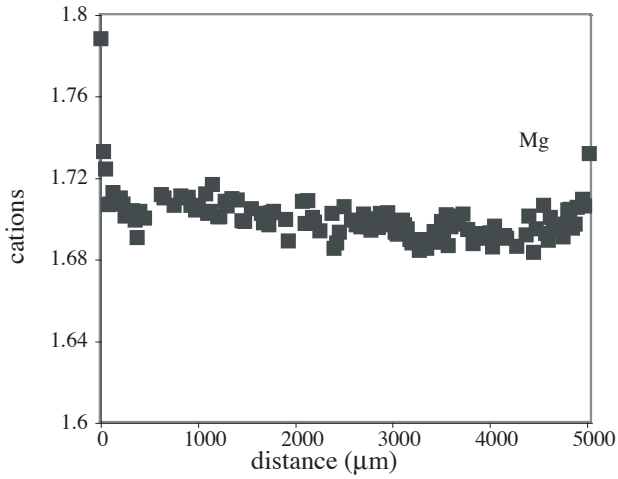

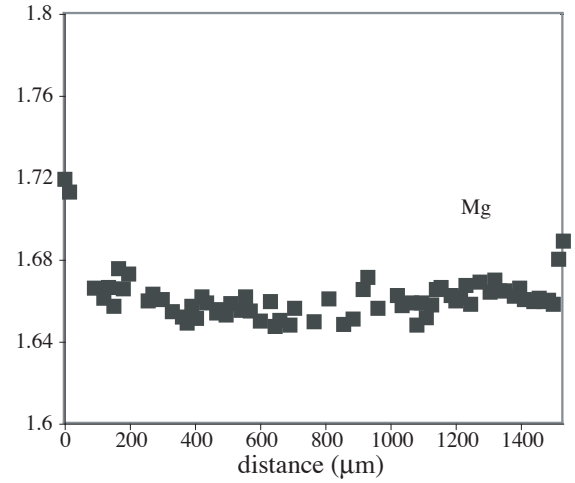

A2.6: profiles of minerals (data set associated on CD)

A2.6a: orthopyroxene profiles (impregnated opx)

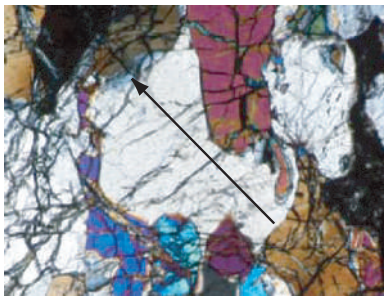

Sample L110, FGSG
distance: 595 µm

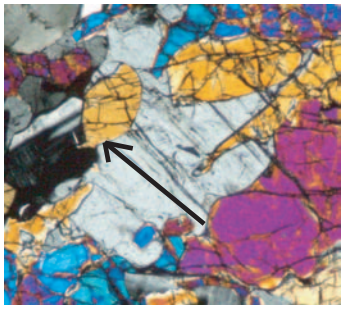

Sample La2002_02, FGSG
distance: 360 µm

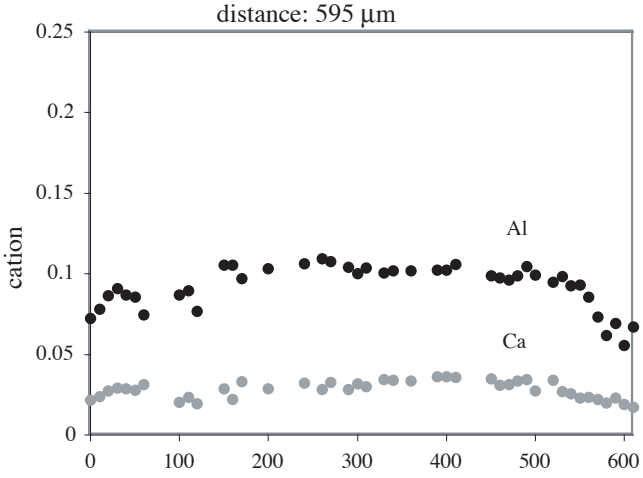

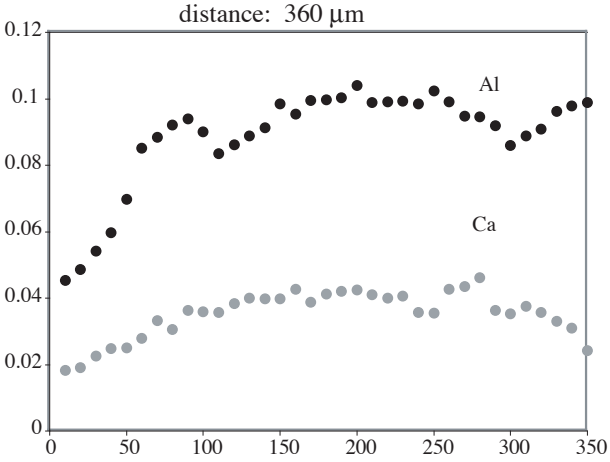

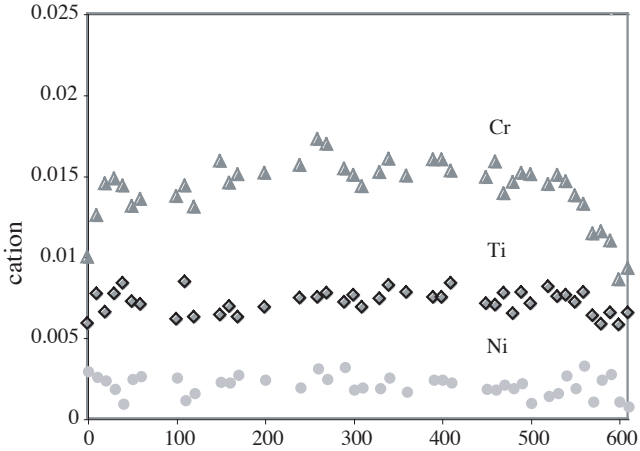

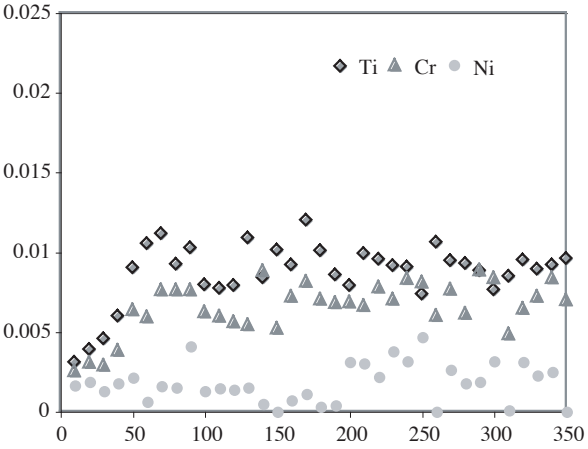

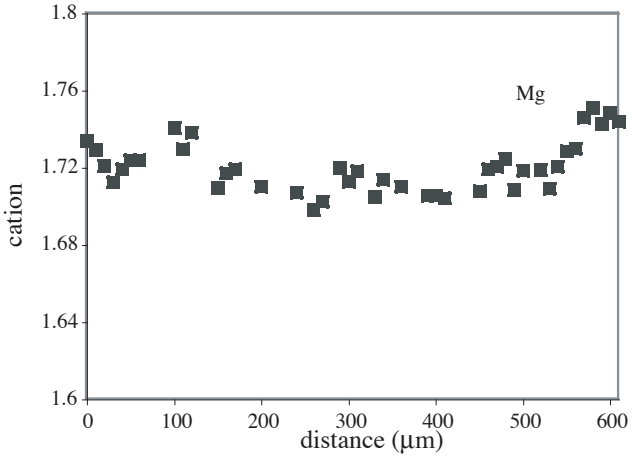

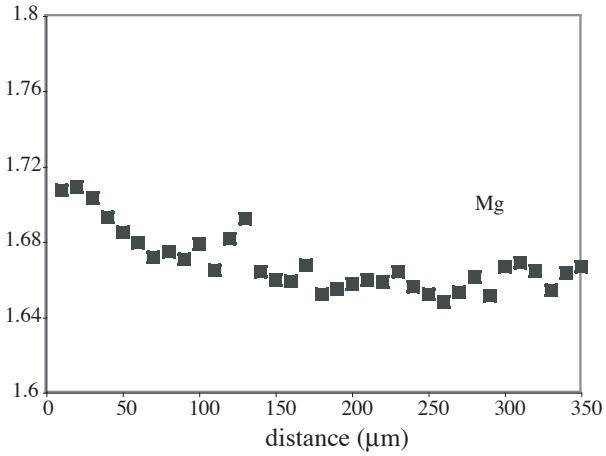

A2.6a: Orthopyroxene profils

Sample L04														
distanc	**0**	**15**	**45**	**60**	**75**	**90**	**105**	**135**	**150**	**180**	**270**	**360**	**390**	**405**
SiO2	56.8	57.0	57.1	57.0	56.8	57.1	56.7	56.5	55.9	55.6	55.7	55.2	54.3	55.0
TiO2	0.14	0.21	0.18	0.19	0.18	0.18	0.18	0.20	0.21	0.20	0.19	0.17	0.16	0.19
Al2O3	0.99	1.14	1.40	1.48	1.56	1.68	1.93	2.33	2.95	3.20	3.06	3.60	3.18	3.83
Cr2O3	0.17	0.19	0.25	0.27	0.29	0.33	0.34	0.48	0.60	0.67	0.65	0.69	0.65	0.75
Fe2O3	0.19	0.23	0.23	0.23	<0.01	<0.01	<0.01	<0.01	0.11	0.47	0.16	1.07	<0.01	0.90
FeO	6.5	6.3	6.2	6.3	6.5	6.4	6.3	6.2	6.5	6.2	6.4	5.8	6.4	5.8
MnO	0.21	0.11	0.21	0.14	0.15	0.17	0.10	0.17	0.19	0.15	0.11	0.16	0.15	0.19
NiO	0.02	0.05	0.08	0.10	0.06	0.05	0.07	0.10	0.10	0.13	0.06	0.15	0.09	0.10
MgO	34.2	34.3	34.3	34.3	33.8	34.1	34.0	33.7	33.4	33.4	33.1	33.2	31.7	33.0
CaO	0.38	0.50	0.51	0.45	0.58	0.57	0.63	0.63	0.58	0.58	0.83	0.67	0.54	0.68
Na2O	<0.01	0.02	0.02	0.01	0.03	<0.01	0.02	0.01	<0.01	<0.01	0.03	0.03	0.06	0.01
K2O	<0.01	<0.01	0.02	<0.01	0.01	<0.01	0.02	0.01	<0.01	<0.01	<0.01	<0.01	<0.01	0.02
Total	99.6	100.0	100.6	100.5	100.0	100.5	100.3	100.3	100.6	100.6	100.3	100.8	97.1	100.5
Si	1.97	1.97	1.96	1.96	1.96	1.96	1.95	1.95	1.93	1.91	1.92	1.90	1.94	1.90
Ti	0.004	0.006	0.005	0.005	0.005	0.005	0.005	0.005	0.005	0.005	0.005	0.004	0.004	0.005
Al	0.040	0.046	0.057	0.060	0.064	0.068	0.078	0.095	0.120	0.130	0.125	0.146	0.134	0.156
Cr	0.005	0.005	0.007	0.007	0.008	0.009	0.009	0.013	0.016	0.018	0.018	0.019	0.018	0.020
Fe3	0.005	0.006	0.006	0.006	<0.001	<0.001	<0.001	<0.001	0.003	0.012	0.004	0.028	0.000	0.024
Fe2	0.19	0.18	0.18	0.18	0.19	0.18	0.18	0.18	0.19	0.18	0.19	0.17	0.19	0.17
Mn	0.006	0.003	0.006	0.004	0.005	0.005	0.003	0.005	0.006	0.004	0.003	0.005	0.004	0.006
Ni	0.001	0.002	0.002	0.003	0.002	0.001	0.002	0.003	0.003	0.004	0.002	0.004	0.003	0.003
Mg	1.77	1.76	1.76	1.76	1.74	1.75	1.74	1.73	1.71	1.71	1.70	1.70	1.68	1.70
Ca	0.014	0.018	0.019	0.017	0.022	0.021	0.023	0.023	0.021	0.022	0.031	0.025	0.021	0.025
Na	<0.001	0.001	0.001	0.001	0.002	<0.001	0.001	0.001	<0.001	<0.001	0.002	0.002	0.004	0.001
K	<0.001	<0.001	0.001	<0.001	<0.001	<0.001	0.001	0.001	<0.001	<0.001	<0.001	<0.001	<0.001	0.001

Sample L04														
distanc	**450**	**465**	**480**	**495**	**525**	**540**	**555**	**585**	**615**	**645**	**660**	**675**	**690**	**750**
SiO2	54.3	54.0	54.1	54.3	53.9	54.0	54.1	53.6	53.5	53.2	53.9	53.5	53.8	54.3
TiO2	0.17	0.19	0.20	0.20	0.18	0.16	0.17	0.19	0.16	0.17	0.15	0.17	0.15	0.13
Al2O3	4.06	4.24	4.19	4.18	4.40	4.19	4.08	4.17	4.37	4.61	4.51	4.57	4.50	4.6
Cr2O3	0.77	0.78	0.71	0.71	0.72	0.74	0.66	0.74	0.76	0.70	0.71	0.76	0.74	0.71
Fe2O3	0.94	2.10	1.59	1.51	2.21	2.18	1.51	2.49	2.67	2.63	2.44	2.54	1.30	0.87
FeO	5.6	4.9	5.2	5.3	5.0	4.8	5.2	4.5	4.4	4.5	4.5	4.4	5.1	5.62
MnO	0.14	0.18	0.10	0.10	0.13	0.18	0.15	0.15	0.21	0.16	0.15	0.15	0.14	0.17
NiO	0.08	0.13	0.10	0.08	0.07	0.09	0.10	0.06	0.11	0.11	0.11	0.09	0.09	0.12
MgO	32.7	32.7	32.7	32.8	32.8	32.8	32.7	32.8	32.9	32.6	33.1	32.9	32.6	32.7
CaO	0.65	0.99	0.69	0.73	0.63	0.74	0.78	0.64	0.56	0.64	0.60	0.59	0.71	0.53
Na2O	0.00	0.02	0.03	0.04	0.01	0.03	0.04	0.06	0.02	0.02	0.01	0.02	0.01	0.02
K2O	0.02	<0.01	0.03	0.02	0.01	0.02	<0.01	<0.01	<0.01	<0.01	<0.01	<0.01	<0.01	0.01
Total	99.4	100.2	99.6	100.0	100.1	99.9	99.3	99.5	99.6	99.4	100.1	99.7	99.2	99.7
Si	1.89	1.87	1.88	1.88	1.87	1.87	1.88	1.87	1.86	1.86	1.86	1.86	1.88	1.88
Ti	0.005	0.005	0.005	0.005	0.005	0.004	0.004	0.005	0.004	0.004	0.004	0.005	0.004	0.003
Al	0.167	0.173	0.172	0.171	0.180	0.171	0.168	0.171	0.179	0.190	0.184	0.187	0.185	0.188
Cr	0.021	0.021	0.020	0.020	0.020	0.020	0.018	0.020	0.021	0.019	0.020	0.021	0.021	0.020
Fe3	0.025	0.055	0.042	0.039	0.058	0.057	0.040	0.065	0.070	0.069	0.064	0.066	0.034	0.023
Fe2	0.16	0.14	0.15	0.15	0.15	0.14	0.15	0.13	0.13	0.13	0.13	0.13	0.15	0.16
Mn	0.004	0.005	0.003	0.003	0.004	0.005	0.004	0.005	0.006	0.005	0.005	0.004	0.004	0.005
Ni	0.002	0.004	0.003	0.002	0.002	0.002	0.003	0.002	0.003	0.003	0.003	0.002	0.002	0.003
Mg	1.70	1.69	1.70	1.69	1.70	1.70	1.70	1.70	1.71	1.70	1.70	1.70	1.70	1.69
Ca	0.024	0.037	0.026	0.027	0.023	0.027	0.029	0.024	0.021	0.024	0.022	0.022	0.027	0.020
Na	<0.001	0.001	0.002	0.003	0.001	0.002	0.003	0.004	0.002	0.002	0.001	0.002	0.001	0.002
K	0.001	<0.001	0.001	0.001	<0.001	0.001	<0.001	<0.001	<0.001	<0.001	<0.001	<0.001	<0.001	0.001

A2.6a: Orthopyroxene profils

Sample L04

distanc	765	780	810	840	885	900	915	945	1020	1035	1065	1080	1125	1140
SiO2	54.4	54.4	54.4	54.7	54.3	54.3	54.5	54.2	54.2	54.6	51.3	54.3	54.4	50.3
TiO2	0.17	0.13	0.16	0.15	0.15	0.18	0.17	0.13	0.18	0.14	0.11	0.14	0.11	0.13
Al2O3	4.7	4.8	4.8	4.8	4.9	5.1	4.8	4.8	5.1	4.8	5.3	4.7	4.9	4.6
Cr2O3	0.80	0.71	0.68	0.69	0.73	0.72	0.73	0.75	0.80	0.70	0.76	0.74	0.81	0.75
Fe2O3	0.64	0.31	0.84	0.00	0.97	0.06	0.14	0.64	0.46	0.17	4.23	1.19	0.41	1.72
FeO	5.90	6.39	6.11	6.57	5.95	6.32	6.29	5.91	6.17	6.36	2.43	5.71	6.15	4.2
MnO	0.12	0.10	0.12	0.21	0.16	0.13	0.15	0.07	0.13	0.15	0.13	0.22	0.10	0.15
NiO	0.06	0.04	0.08	0.09	0.12	0.12	0.08	0.11	0.09	0.09	0.12	0.07	0.09	0.07
MgO	32.6	32.3	32.4	32.3	32.5	32.2	32.5	32.5	32.3	32.6	32.4	32.6	32.5	30.7
CaO	0.59	0.76	0.70	0.65	0.59	0.85	0.66	0.63	0.71	0.63	0.60	0.66	0.63	0.55
Na2O	0.04	0.02	0.04	0.03	0.03	0.02	0.02	0.02	<0.01	<0.01	0.03	0.01	0.02	0.06
K2O	<0.01	0.01	0.01	<0.01	<0.01	<0.01	<0.01	<0.01	<0.01	<0.01	<0.01	<0.01	0.02	0.04
Total	100.0	99.9	100.4	100.2	100.5	100.0	100.1	99.8	100.1	100.2	97.4	100.3	100.1	93.2
Si	1.88	1.89	1.88	1.89	1.87	1.88	1.89	1.88	1.87	1.89	1.82	1.88	1.88	1.86
Ti	0.005	0.003	0.004	0.004	0.004	0.005	0.004	0.004	0.005	0.004	0.003	0.004	0.003	0.004
Al	0.193	0.196	0.195	0.197	0.200	0.208	0.196	0.197	0.209	0.196	0.223	0.190	0.200	0.20
Cr	0.022	0.020	0.019	0.019	0.020	0.020	0.020	0.021	0.022	0.019	0.021	0.020	0.022	0.022
Fe3	0.017	0.008	0.022	0.000	0.025	0.002	0.004	0.017	0.012	0.004	0.113	0.031	0.011	0.048
Fe2	0.17	0.19	0.18	0.19	0.17	0.18	0.18	0.17	0.18	0.18	0.07	0.17	0.18	0.13
Mn	0.003	0.003	0.003	0.006	0.005	0.004	0.004	0.002	0.004	0.005	0.004	0.007	0.003	0.005
Ni	0.002	0.001	0.002	0.002	0.003	0.003	0.002	0.003	0.002	0.003	0.004	0.002	0.002	0.002
Mg	1.68	1.67	1.67	1.67	1.67	1.66	1.68	1.68	1.67	1.68	1.72	1.68	1.67	1.70
Ca	0.022	0.028	0.026	0.024	0.022	0.032	0.024	0.023	0.026	0.024	0.023	0.025	0.023	0.022
Na	0.002	0.001	0.002	0.002	0.002	0.001	0.001	0.001	<0.001	<0.001	0.002	0.001	0.001	0.005
K	<0.001	<0.001	0.001	<0.001	<0.001	<0.001	<0.001	<0.001	<0.001	<0.001	<0.001	<0.001	0.001	0.002

Sample L04

distanc	1170	1200	1215	1245	1275	1320	1365	1380	1395	1425	1440	1455	1470	1485
SiO2	54.0	54.2	54.7	54.6	54.4	54.5	54.6	54.1	54.1	54.6	54.3	54.3	54.3	54.2
TiO2	0.17	0.13	0.13	0.12	0.15	0.15	0.15	0.12	0.18	0.14	0.17	0.16	0.15	0.15
Al2O3	5.0	5.1	4.6	4.8	5.0	4.8	4.6	5.1	5.3	5.0	4.8	4.7	4.9	4.7
Cr2O3	0.74	0.79	0.72	0.77	0.77	0.77	0.74	0.74	0.76	0.78	0.82	0.71	0.75	0.73
Fe2O3	1.27	0.72	0.23	<0.01	<0.01	0.35	0.48	1.40	0.39	0.34	0.67	0.97	0.20	1.09
FeO	5.5	6.0	6.1	6.6	6.2	6.4	6.1	5.6	6.2	6.5	6.0	5.7	6.4	5.5
MnO	0.15	0.08	0.13	0.14	0.10	0.09	0.08	0.12	0.13	0.11	0.15	0.17	0.11	0.18
NiO	0.14	0.15	0.12	0.08	0.08	0.09	0.09	0.07	0.09	0.07	0.10	0.11	0.04	0.10
MgO	32.6	32.3	32.7	32.3	32.4	32.4	32.8	32.7	32.2	32.5	32.3	32.6	32.4	32.7
CaO	0.63	0.68	0.58	0.63	0.59	0.69	0.52	0.52	0.71	0.67	0.87	0.65	0.56	0.60
Na2O	0.02	0.05	0.02	0.03	0.01	0.01	<0.01	0.02	0.02	0.02	0.03	0.02	0.02	0.03
K2O	0.01	0.02	0.01	<0.01	0.02	<0.01	<0.01	<0.01	<0.01	<0.01	<0.01	0.01	<0.01	<0.01
Total	100.2	100.2	100.0	100.1	99.7	100.3	100.1	100.5	100.0	100.6	100.2	100.1	99.8	100.0
Si	1.87	1.88	1.89	1.89	1.89	1.88	1.89	1.86	1.87	1.88	1.88	1.88	1.88	1.88
Ti	0.004	0.003	0.003	0.003	0.004	0.004	0.004	0.003	0.005	0.004	0.005	0.004	0.004	0.004
Al	0.20	0.21	0.19	0.20	0.21	0.20	0.19	0.21	0.22	0.20	0.20	0.19	0.20	0.19
Cr	0.020	0.022	0.020	0.021	0.021	0.021	0.020	0.020	0.021	0.021	0.022	0.020	0.021	0.020
Fe3	0.033	0.019	0.006	<0.001	<0.001	0.009	0.013	0.036	0.010	0.009	0.017	0.025	0.005	0.028
Fe2	0.16	0.17	0.18	0.19	0.18	0.18	0.18	0.16	0.18	0.19	0.17	0.16	0.19	0.16
Mn	0.004	0.002	0.004	0.004	0.003	0.003	0.002	0.004	0.004	0.003	0.004	0.005	0.003	0.005
Ni	0.004	0.004	0.004	0.002	0.002	0.003	0.003	0.002	0.002	0.002	0.003	0.003	0.001	0.003
Mg	1.68	1.67	1.69	1.67	1.67	1.67	1.69	1.68	1.66	1.67	1.67	1.68	1.67	1.69
Ca	0.023	0.025	0.022	0.023	0.022	0.025	0.019	0.019	0.026	0.025	0.032	0.024	0.021	0.022
Na	0.001	0.003	0.001	0.002	0.001	0.001	<0.001	0.001	0.001	0.002	0.002	0.001	0.001	0.002
K	0.001	0.001	0.001	<0.001	0.001	<0.001	<0.001	<0.001	<0.001	<0.001	<0.001	0.001	<0.001	<0.001

A2.6a: Orthopyroxene profils

Sample L04

distanc	1530	1560	1575	1605	1620	1635	1680	1695	1710	1740	1755	1785	1800	1860
SiO2	54.5	54.8	54.4	54.4	54.3	54.3	53.6	54.8	53.6	54.9	54.2	54.8	54.7	54.4
TiO2	0.11	0.13	0.16	0.19	0.16	0.15	0.18	0.14	0.18	0.14	0.12	0.15	0.14	0.16
Al2O3	4.7	4.6	4.8	4.8	4.9	4.9	4.7	4.7	5.1	4.6	4.7	4.7	4.7	4.7
Cr2O3	0.72	0.75	0.70	0.73	0.75	0.80	0.70	0.74	0.72	0.74	0.72	0.72	0.73	0.76
Fe2O3	0.43	0.21	0.22	0.72	0.58	0.80	0.10	0.76	0.81	<0.01	0.95	0.46	0.38	1.02
FeO	5.9	6.3	6.2	5.9	6.0	5.9	6.3	6.1	5.9	6.5	5.7	6.2	6.2	5.6
MnO	0.17	0.08	0.14	0.20	0.11	0.18	0.16	0.10	0.14	0.13	0.12	0.12	0.14	0.12
NiO	0.09	0.09	0.11	0.08	0.09	0.11	0.07	0.15	0.13	0.09	0.09	0.11	0.08	0.08
MgO	32.7	32.7	32.3	32.6	32.4	32.4	31.8	32.7	32.1	32.2	32.5	32.7	32.7	32.9
CaO	0.56	0.64	0.73	0.69	0.71	0.64	0.75	0.66	0.61	0.69	0.71	0.65	0.59	0.57
Na2O	0.02	0.03	0.02	0.03	0.03	0.04	<0.01	0.03	0.01	0.04	0.03	0.03	0.02	0.03
K2O	0.01	<0.01	0.02	<0.01	0.02	0.02	<0.01	<0.01	0.02	0.01	<0.01	<0.01	<0.01	<0.01
Total	99.8	100.4	99.8	100.3	100.0	100.3	98.3	100.8	99.2	100.0	99.9	100.6	100.4	100.4
Si	1.89	1.89	1.89	1.88	1.88	1.88	1.89	1.88	1.87	1.90	1.88	1.89	1.89	1.88
Ti	0.003	0.003	0.004	0.005	0.004	0.004	0.005	0.004	0.005	0.004	0.003	0.004	0.004	0.004
Al	0.19	0.19	0.19	0.19	0.20	0.20	0.19	0.19	0.21	0.19	0.19	0.19	0.19	0.19
Cr	0.020	0.020	0.019	0.020	0.021	0.022	0.020	0.020	0.020	0.020	0.020	0.020	0.020	0.021
Fe3	0.011	0.006	0.006	0.019	0.015	0.021	0.003	0.020	0.021	<0.001	0.025	0.012	0.010	0.026
Fe2	0.17	0.18	0.18	0.17	0.17	0.17	0.19	0.17	0.17	0.19	0.17	0.18	0.18	0.16
Mn	0.005	0.002	0.004	0.006	0.003	0.005	0.005	0.003	0.004	0.004	0.004	0.004	0.004	0.004
Ni	0.002	0.003	0.003	0.002	0.002	0.003	0.002	0.004	0.004	0.002	0.003	0.003	0.002	0.002
Mg	1.69	1.68	1.67	1.68	1.67	1.67	1.67	1.68	1.67	1.66	1.68	1.68	1.68	1.69
Ca	0.021	0.024	0.027	0.025	0.027	0.024	0.028	0.024	0.023	0.026	0.026	0.024	0.022	0.021
Na	0.001	0.002	0.002	0.002	0.002	0.003	<0.001	0.002	0.001	0.003	0.002	0.002	0.002	0.002
K	<0.001	<0.001	0.001	<0.001	0.001	0.001	<0.001	<0.001	0.001	<0.001	<0.001	<0.001	<0.001	<0.001

Sample L04

distanc	1905	1935	1950	1965	1980	2010	2055	2070	2085	2100	2175	2190	2205	2265
SiO2	54.1	54.5	55.2	54.7	54.0	54.4	54.9	54.7	55.5	54.3	54.6	54.4	54.6	52.2
TiO2	0.15	0.16	0.17	0.15	0.15	0.16	0.17	0.11	0.16	0.17	0.13	0.13	0.18	0.16
Al2O3	4.8	4.8	5.0	4.9	4.9	4.9	4.9	4.8	5.0	5.0	4.5	4.8	4.7	4.7
Cr2O3	0.76	0.80	0.77	0.76	0.71	0.78	0.73	0.73	0.71	0.72	0.75	0.77	0.79	0.70
Fe2O3	1.39	0.02	0.50	0.47	<0.01	0.65	0.47	1.01	0.42	0.77	0.42	0.41	<0.01	2.97
FeO	5.7	6.4	6.5	6.1	6.4	5.9	6.3	5.7	6.5	5.9	6.0	6.2	6.6	3.6
MnO	0.12	0.12	0.09	0.19	0.17	0.19	0.12	0.09	0.12	0.10	0.20	0.15	0.14	0.12
NiO	0.11	0.08	0.13	0.09	0.10	0.06	0.09	0.04	0.08	0.14	0.11	0.07	0.09	0.11
MgO	32.5	32.4	32.8	32.6	32.0	32.5	32.6	32.9	33.0	32.5	32.4	32.4	32.2	32.3
CaO	0.69	0.72	0.70	0.72	0.60	0.72	0.76	0.62	0.68	0.71	0.99	0.76	0.72	0.80
Na2O	0.02	0.01	0.03	0.03	0.03	0.02	0.04	0.04	0.03	0.03	0.03	0.03	0.04	0.03
K2O	<0.01	0.01	<0.01	<0.01	0.01	0.01	<0.01	<0.01	0.01	<0.01	<0.01	<0.01	<0.01	0.01
Total	100.3	100.0	101.8	100.8	99.1	100.4	101.1	100.9	102.2	100.3	100.1	100.2	100.0	97.7
Si	1.87	1.89	1.88	1.88	1.89	1.88	1.88	1.88	1.88	1.87	1.89	1.88	1.89	1.85
Ti	0.004	0.004	0.004	0.004	0.004	0.004	0.005	0.003	0.004	0.004	0.003	0.003	0.005	0.004
Al	0.20	0.20	0.20	0.20	0.20	0.20	0.20	0.19	0.20	0.21	0.18	0.20	0.19	0.20
Cr	0.021	0.022	0.021	0.021	0.020	0.021	0.020	0.020	0.019	0.020	0.021	0.021	0.022	0.020
Fe3	0.036	0.001	0.013	0.012	<0.001	0.017	0.012	0.026	0.011	0.020	0.011	0.011	<0.001	0.079
Fe2	0.17	0.19	0.18	0.18	0.19	0.17	0.18	0.16	0.18	0.17	0.17	0.18	0.19	0.11
Mn	0.004	0.004	0.003	0.006	0.005	0.006	0.003	0.003	0.004	0.003	0.006	0.005	0.004	0.004
Ni	0.003	0.002	0.004	0.003	0.003	0.002	0.003	0.001	0.002	0.004	0.003	0.002	0.003	0.003
Mg	1.67	1.67	1.66	1.67	1.67	1.67	1.67	1.68	1.67	1.67	1.67	1.67	1.66	1.70
Ca	0.026	0.027	0.026	0.027	0.022	0.027	0.028	0.023	0.025	0.026	0.037	0.028	0.027	0.030
Na	0.001	0.001	0.002	0.002	0.002	0.001	0.003	0.003	0.002	0.002	0.002	0.002	0.003	0.002
K	<0.001	<0.001	<0.001	<0.001	0.001	0.001	<0.001	<0.001	<0.001	<0.001	<0.001	<0.001	<0.001	<0.001

A2.6a: Orthopyroxene profils

Sample L04											**Sample L104**			
distanc	**2325**	**2370**	**2385**	**2400**	**2475**	**2490**	**2505**	**2520**	**2535**	**2580**	**distance**	**15**	**30**	**45**
SiO2	53.6	53.4	54.8	54.9	54.6	54.8	54.6	54.9	54.7	54.3	SiO2	55.9	56.4	55.8
TiO2	0.15	0.14	0.13	0.14	0.12	0.17	0.15	0.16	0.14	0.15	TiO2	0.22	0.21	0.21
Al2O3	4.4	4.6	4.7	4.6	4.2	4.7	4.7	4.5	4.5	4.7	Al2O3	2.5	2.7	3.1
Cr2O3	0.67	0.70	0.72	0.69	0.70	0.71	0.69	0.77	0.70	0.79	Cr2O3	0.62	0.61	0.70
Fe2O3	2.06	2.04	0.66	0.74	0.87	<0.01	0.35	0.59	0.00	0.51	Fe2O3	1.67	0.71	0.97
FeO	5.0	4.7	6.1	6.2	5.6	6.5	6.2	6.1	6.3	6.1	FeO	5.2	6.1	5.6
MnO	0.12	0.15	0.10	0.18	0.17	0.16	0.15	0.11	0.18	0.09	MnO	0.12	0.15	0.24
NiO	0.11	0.08	0.13	0.13	0.14	0.10	0.14	0.10	0.09	0.06	MgO	34.1	33.9	33.8
MgO	32.5	32.6	32.7	32.8	32.9	32.5	32.6	32.8	32.2	32.5	CaO	0.55	0.59	0.50
CaO	0.71	0.63	0.65	0.68	0.59	0.61	0.68	0.60	0.93	0.58	Na2O	0.04	0.04	0.04
Na2O	0.03	0.04	0.02	0.01	0.03	0.01	0.01	0.04	0.02	0.01	K2O	<0.01	0.01	<0.01
K2O	0.01	<0.01	<0.01	<0.01	<0.01	0.02	<0.01	<0.01	<0.01	0.01				
											Total	101.0	101.3	101.1
Total	99.4	99.1	100.7	101.1	99.9	100.2	100.3	100.7	99.8	99.8				
Si	1.87	1.87	1.88	1.88	1.89	1.89	1.89	1.89	1.90	1.88	Si	1.91	1.93	1.91
Ti	0.004	0.004	0.004	0.004	0.003	0.004	0.004	0.004	0.004	0.004	Ti	0.006	0.005	0.006
Al	0.18	0.19	0.19	0.19	0.17	0.19	0.19	0.18	0.18	0.19	Al	0.10	0.11	0.13
Cr	0.019	0.020	0.020	0.019	0.019	0.019	0.019	0.021	0.019	0.022	Cr	0.017	0.017	0.019
Fe3	0.054	0.054	0.017	0.019	0.023	<0.001	0.009	0.015	0.000	0.013	Fe3	0.043	0.018	0.025
Fe2	0.14	0.14	0.18	0.18	0.16	0.19	0.18	0.18	0.18	0.18	Fe2	0.15	0.17	0.16
Mn	0.004	0.004	0.003	0.005	0.005	0.005	0.004	0.003	0.005	0.003	Mn	0.003	0.005	0.007
Ni	0.003	0.002	0.004	0.004	0.004	0.003	0.004	0.003	0.003	0.002	Mg	1.74	1.72	1.72
Mg	1.69	1.70	1.68	1.68	1.70	1.67	1.68	1.68	1.67	1.68	Ca	0.020	0.022	0.018
Ca	0.026	0.024	0.024	0.025	0.022	0.023	0.025	0.022	0.035	0.022	Na	0.002	0.003	0.003
Na	0.002	0.003	0.002	0.001	0.002	0.001	0.001	0.002	0.002	0.001	K	<0.001	<0.001	<0.001
K	<0.001	<0.001	<0.001	<0.001	<0.001	0.001	<0.001	<0.001	<0.001	0.001				

Sample L104														
distanc	**60**	**75**	**135**	**150**	**165**	**180**	**195**	**210**	**225**	**240**	**270**	**300**	**315**	**330**
SiO2	55.9	55.9	56.0	55.6	55.7	55.7	55.5	55.7	55.6	55.1	55.3	54.8	55.6	55.1
TiO2	0.25	0.25	0.19	0.27	0.19	0.20	0.20	0.21	0.25	0.25	0.24	0.25	0.20	0.20
Al2O3	3.0	3.3	3.3	3.5	3.4	3.4	3.6	3.5	3.7	4.0	3.6	4.1	3.6	4.1
Cr2O3	0.66	0.69	0.71	0.65	0.59	0.79	0.71	0.77	0.80	0.78	0.75	0.78	0.70	0.80
Fe2O3	0.47	0.65	0.58	0.87	0.06	0.74	1.05	0.55	0.48	0.97	1.21	1.16	0.66	1.04
FeO	6.2	6.2	6.0	6.1	6.6	6.1	5.9	6.0	6.1	5.9	5.7	6.3	6.1	6.0
MnO	0.13	0.12	0.12	0.12	0.14	0.19	0.14	0.17	0.16	0.17	0.13	0.23	0.16	0.17
MgO	33.6	33.4	33.7	33.4	33.2	33.5	33.4	33.6	33.1	33.1	33.3	32.7	33.3	32.9
CaO	0.68	0.93	0.63	0.67	0.59	0.57	0.67	0.56	0.89	0.66	0.76	0.62	0.60	0.80
Na2O	0.02	0.01	0.02	0.03	0.03	0.01	0.04	<0.01	0.06	0.01	0.03	0.04	<0.01	<0.01
K2O	<0.01	<0.01	<0.01	<0.01	<0.01	0.01	<0.01	<0.01	<0.01	0.02	0.01	0.01	0.01	0.01
Total	100.9	101.4	101.3	101.2	100.5	101.2	101.2	101.1	101.2	100.9	101.0	100.9	101.0	101.3
Si	1.92	1.91	1.91	1.90	1.92	1.91	1.90	1.91	1.90	1.89	1.90	1.89	1.91	1.89
Ti	0.007	0.007	0.005	0.007	0.005	0.005	0.005	0.006	0.006	0.006	0.006	0.006	0.005	0.006
Al	0.12	0.13	0.13	0.14	0.14	0.14	0.14	0.14	0.15	0.16	0.15	0.17	0.15	0.17
Cr	0.018	0.019	0.019	0.018	0.016	0.021	0.019	0.021	0.022	0.021	0.020	0.021	0.019	0.023
Fe3	0.012	0.017	0.015	0.022	0.002	0.019	0.027	0.014	0.012	0.025	0.031	0.030	0.017	0.027
Fe2	0.18	0.18	0.17	0.17	0.19	0.17	0.17	0.17	0.18	0.17	0.16	0.18	0.18	0.17
Mn	0.004	0.004	0.004	0.004	0.004	0.005	0.004	0.005	0.005	0.005	0.004	0.007	0.005	0.005
Mg	1.72	1.70	1.72	1.71	1.70	1.71	1.70	1.71	1.69	1.70	1.70	1.68	1.70	1.68
Ca	0.025	0.034	0.023	0.025	0.022	0.021	0.025	0.020	0.033	0.024	0.028	0.023	0.020	0.030
Na	0.001	0.001	0.001	0.002	0.002	0.001	0.002	<0.001	0.004	0.001	0.002	0.002	0.002	0.003
K	<0.001	<0.001	<0.001	<0.001	<0.001	0.001	<0.001	<0.001	<0.001	0.001	<0.001	0.001	0.001	0.001

A2.6a: Orthopyroxene profils

Sample L104

distance	360	375	405	420	450	465	480	495	510	525	540	570	600	615
SiO2	55.1	55.0	54.9	55.2	54.8	54.8	55.2	55.3	55.2	55.1	54.9	55.2	55.0	54.8
TiO2	0.25	0.24	0.23	0.22	0.27	0.17	0.23	0.20	0.23	0.17	0.22	0.23	0.19	0.24
Al2O3	4.1	4.2	4.1	4.3	4.3	4.2	4.2	4.3	4.1	4.2	4.2	4.2	4.1	4.1
Cr2O3	0.77	0.84	0.81	0.74	0.88	0.70	0.80	0.80	0.81	0.79	0.72	0.78	0.87	0.76
Fe2O3	1.14	1.29	1.07	0.72	1.17	0.84	0.61	0.62	0.67	1.09	0.71	0.65	0.55	1.22
FeO	5.9	5.6	5.7	6.1	5.8	5.9	6.1	6.3	6.1	5.8	6.1	5.9	6.2	5.7
MnO	0.13	0.17	0.16	0.15	0.10	0.17	0.15	0.15	0.19	0.17	0.15	0.19	0.15	0.17
MgO	33.1	33.2	32.9	33.1	33.1	33.0	33.0	33.1	33.1	33.3	32.8	33.2	33.1	33.1
CaO	0.73	0.70	0.83	0.68	0.65	0.63	0.72	0.58	0.60	0.55	0.79	0.68	0.52	0.62
Na2O	0.04	0.03	0.05	0.03	0.02	0.01	0.04	<0.01	0.04	0.01	0.06	0.02	0.00	0.02
K2O	0.01	<0.01	0.02	0.02	0.01	<0.01	<0.01	<0.01	<0.01	<0.01	<0.01	<0.01	<0.01	<0.01
Total	101.2	101.1	100.8	101.3	101.0	100.4	101.2	101.3	101.0	101.1	100.6	101.1	100.6	100.7
Si	1.89	1.88	1.89	1.89	1.88	1.89	1.89	1.89	1.89	1.89	1.89	1.89	1.89	1.89
Ti	0.006	0.006	0.006	0.006	0.007	0.004	0.006	0.005	0.006	0.005	0.006	0.006	0.005	0.006
Al	0.17	0.17	0.17	0.17	0.17	0.17	0.17	0.17	0.16	0.17	0.17	0.17	0.17	0.17
Cr	0.021	0.023	0.022	0.020	0.024	0.019	0.022	0.022	0.022	0.021	0.020	0.021	0.024	0.021
Fe3	0.029	0.033	0.028	0.019	0.030	0.022	0.016	0.016	0.017	0.028	0.018	0.017	0.014	0.032
Fe2	0.17	0.16	0.16	0.18	0.17	0.17	0.18	0.18	0.17	0.17	0.17	0.17	0.18	0.16
Mn	0.004	0.005	0.005	0.004	0.003	0.005	0.004	0.004	0.006	0.005	0.005	0.006	0.004	0.005
Mg	1.69	1.70	1.69	1.69	1.69	1.70	1.68	1.69	1.69	1.70	1.68	1.70	1.70	1.70
Ca	0.027	0.026	0.031	0.025	0.024	0.023	0.027	0.021	0.022	0.020	0.029	0.025	0.019	0.023
Na	0.002	0.002	0.003	0.002	0.001	0.001	0.003	<0.001	0.003	<0.001	0.004	0.001	<0.001	0.001
K	0.001	<0.001	0.001	0.001	<0.001	<0.001	<0.001	<0.001	<0.001	<0.001	<0.001	<0.001	<0.001	<0.001

Sample L104

distance	630	645	660	675	690	705	720	735	750	765	780	795	825	840
SiO2	54.8	54.8	55.1	54.9	55.0	55.0	55.0	55.0	54.9	54.8	54.9	54.5	54.9	55.1
TiO2	0.24	0.18	0.21	0.24	0.21	0.17	0.21	0.19	0.24	0.21	0.20	0.21	0.18	0.21
Al2O3	4.3	4.1	4.1	4.4	4.2	4.3	4.1	4.1	4.3	4.4	4.3	4.5	4.3	4.0
Cr2O3	0.87	0.86	0.79	0.87	0.76	0.78	0.80	0.73	0.82	0.83	0.80	0.84	0.95	0.66
Fe2O3	0.64	1.84	0.57	1.26	1.13	0.76	0.89	1.10	1.23	1.39	0.74	1.33	1.74	0.91
FeO	6.0	5.0	6.0	5.6	5.7	6.1	6.0	5.8	5.8	5.6	6.1	5.6	5.2	5.9
MnO	0.14	0.17	0.14	0.10	0.16	0.15	0.12	0.07	0.15	0.20	0.15	0.14	0.17	0.17
MgO	33.0	33.4	33.1	33.2	33.2	33.0	33.0	33.0	33.0	33.1	33.0	32.7	33.3	32.9
CaO	0.64	0.57	0.66	0.60	0.66	0.66	0.59	0.80	0.70	0.65	0.57	0.82	0.60	0.83
Na2O	<0.01	0.04	0.01	0.03	0.03	0.03	0.03	0.06	0.05	0.01	0.03	0.04	0.06	0.07
K2O	<0.01	<0.01	<0.01	0.02	<0.01	<0.01	<0.01	<0.01	<0.01	<0.01	<0.01	0.01	<0.01	<0.01
Total	100.7	101.1	100.7	101.2	101.0	100.9	100.8	100.9	101.2	101.2	100.8	100.7	101.4	100.6
Si	1.89	1.88	1.89	1.88	1.89	1.89	1.89	1.89	1.88	1.88	1.89	1.88	1.88	1.90
Ti	0.006	0.005	0.005	0.006	0.005	0.004	0.005	0.005	0.006	0.005	0.005	0.006	0.005	0.005
Al	0.17	0.17	0.17	0.18	0.17	0.17	0.17	0.17	0.17	0.18	0.17	0.18	0.17	0.16
Cr	0.024	0.023	0.021	0.024	0.021	0.021	0.022	0.020	0.022	0.023	0.022	0.023	0.026	0.018
Fe3	0.017	0.047	0.015	0.033	0.029	0.020	0.023	0.028	0.032	0.036	0.019	0.034	0.045	0.024
Fe2	0.17	0.14	0.17	0.16	0.16	0.17	0.17	0.17	0.17	0.16	0.17	0.16	0.15	0.17
Mn	0.004	0.005	0.004	0.003	0.005	0.004	0.003	0.002	0.005	0.006	0.004	0.004	0.005	0.005
Mg	1.69	1.71	1.70	1.69	1.70	1.69	1.69	1.69	1.69	1.69	1.69	1.68	1.70	1.69
Ca	0.023	0.021	0.024	0.022	0.024	0.024	0.022	0.030	0.026	0.024	0.021	0.030	0.022	0.031
Na	<0.001	0.003	0.001	0.002	0.002	0.002	0.002	0.004	0.003	0.001	0.002	0.002	0.004	0.005
K	<0.001	<0.001	<0.001	<0.001	<0.001	<0.001	<0.001	<0.001	<0.001	<0.001	<0.001	<0.001	<0.001	<0.001

A2.6a: Orthopyroxene profils

Sample L104

distance	855	870	885	915	945	960	975	990	1005	1020	1035	1065	1080	1095
SiO2	54.8	54.6	55.1	54.8	54.8	55.4	54.7	55.0	54.9	55.1	54.5	54.7	55.0	54.8
TiO2	0.23	0.22	0.18	0.22	0.19	0.21	0.21	0.18	0.22	0.21	0.14	0.21	0.23	0.20
Al2O3	4.3	4.5	4.3	4.2	4.4	4.1	4.5	4.1	4.4	4.3	4.7	4.7	4.4	4.4
Cr2O3	0.70	0.81	0.88	0.83	0.79	0.67	0.91	0.80	0.75	0.77	0.78	0.82	0.84	0.77
Fe2O3	1.05	1.21	0.80	1.02	1.59	0.29	1.43	1.02	1.23	0.78	1.73	0.57	1.30	0.97
FeO	5.8	5.9	5.9	5.7	5.4	6.6	5.5	5.9	5.8	6.2	5.5	6.1	5.6	5.8
MnO	0.16	0.11	0.17	0.12	0.12	0.16	0.17	0.11	0.17	0.09	0.14	0.17	0.14	0.13
MgO	33.0	32.9	33.2	33.0	33.2	33.0	33.0	33.1	33.1	33.0	33.1	32.7	33.0	33.0
CaO	0.59	0.58	0.53	0.75	0.60	0.55	0.68	0.59	0.57	0.62	0.56	0.72	0.88	0.54
Na2O	0.03	0.02	0.02	0.05	0.03	0.01	0.04	0.04	0.02	0.02	0.02	0.03	0.03	0.03
K2O	<0.01	0.01	<0.01	<0.01	0.01	0.01	<0.01	<0.01	<0.01	<0.01	<0.01	0.01	0.01	0.02
Total	100.7	100.9	101.0	100.6	101.1	100.9	101.2	100.9	101.2	101.0	101.1	100.7	101.5	100.7
Si	1.88	1.88	1.89	1.89	1.88	1.90	1.88	1.89	1.88	1.89	1.87	1.88	1.88	1.88
Ti	0.006	0.006	0.005	0.006	0.005	0.005	0.005	0.005	0.006	0.005	0.004	0.005	0.006	0.005
Al	0.18	0.18	0.17	0.17	0.18	0.16	0.18	0.17	0.18	0.17	0.19	0.19	0.18	0.18
Cr	0.019	0.022	0.024	0.023	0.022	0.018	0.025	0.022	0.020	0.021	0.021	0.022	0.023	0.021
Fe3	0.027	0.031	0.021	0.026	0.041	0.008	0.037	0.026	0.032	0.020	0.045	0.015	0.033	0.025
Fe2	0.17	0.17	0.17	0.16	0.15	0.19	0.16	0.17	0.17	0.18	0.16	0.18	0.16	0.17
Mn	0.005	0.003	0.005	0.004	0.004	0.005	0.005	0.003	0.005	0.003	0.004	0.005	0.004	0.004
Mg	1.69	1.69	1.70	1.69	1.70	1.69	1.69	1.70	1.69	1.69	1.69	1.68	1.68	1.69
Ca	0.022	0.021	0.019	0.028	0.022	0.020	0.025	0.022	0.021	0.023	0.021	0.027	0.032	0.020
Na	0.002	0.001	0.001	0.003	0.002	0.001	0.003	0.003	0.002	0.002	0.001	0.002	0.002	0.002
K	<0.001	<0.001	<0.001	<0.001	0.001	<0.001	<0.001	<0.001	<0.001	<0.001	<0.001	<0.001	0.001	0.001

Sample L104

distance	1110	1125	1140	1185	1200	1215	1230	1260	1275	1290	1305	1335	1350	1365
SiO2	54.6	54.7	55.3	55.1	54.9	54.7	54.8	55.0	54.9	55.1	54.9	54.72	54.48	54.8
TiO2	0.22	0.18	0.17	0.22	0.22	0.18	0.21	0.19	0.21	0.18	0.24	0.21	0.22	0.23
Al2O3	4.5	4.6	3.9	4.1	4.4	4.6	4.2	4.3	4.4	4.4	4.4	4.7	4.5	4.4
Cr2O3	0.81	0.84	0.69	0.78	0.75	0.76	0.72	0.75	0.84	0.78	0.77	0.83	0.88	0.90
Fe2O3	1.09	1.29	0.86	0.93	1.06	1.03	1.59	1.30	1.34	1.18	1.16	0.90	1.14	1.32
FeO	5.8	5.6	5.9	6.0	5.6	5.8	5.3	5.7	5.9	5.8	5.8	6.0	5.7	5.7
MnO	0.16	0.17	0.21	0.09	0.13	0.16	0.18	0.18	0.15	0.16	0.13	0.16	0.15	0.18
MgO	32.9	33.1	33.2	33.0	33.2	33.0	33.2	33.1	33.0	33.1	33.0	32.7	32.7	33.0
CaO	0.62	0.58	0.57	0.74	0.67	0.54	0.67	0.70	0.62	0.65	0.79	0.61	0.76	0.67
Na2O	0.04	0.01	0.02	0.05	0.03	0.00	0.04	0.04	0.04	0.06	0.05	0.06	0.04	0.03
K2O	<0.01	<0.01	0.02	0.01	<0.01	<0.01	0.01	<0.01	<0.01	<0.01	<0.01	<0.01	0.02	<0.01
Total	100.6	101.0	100.8	101.0	100.9	100.8	100.9	101.2	101.3	101.4	101.2	100.9	100.6	101.2
Si	1.88	1.88	1.90	1.89	1.88	1.88	1.88	1.88	1.88	1.88	1.88	1.88	1.88	1.88
Ti	0.006	0.005	0.004	0.006	0.006	0.005	0.006	0.005	0.006	0.005	0.006	0.005	0.006	0.006
Al	0.18	0.18	0.16	0.16	0.18	0.19	0.17	0.17	0.18	0.18	0.18	0.19	0.18	0.18
Cr	0.022	0.023	0.019	0.021	0.020	0.021	0.020	0.020	0.023	0.021	0.021	0.023	0.024	0.024
Fe3	0.028	0.033	0.022	0.024	0.027	0.027	0.041	0.034	0.035	0.030	0.030	0.023	0.029	0.034
Fe2	0.17	0.16	0.17	0.17	0.16	0.17	0.15	0.16	0.17	0.16	0.16	0.17	0.16	0.16
Mn	0.005	0.005	0.006	0.003	0.004	0.005	0.005	0.005	0.004	0.005	0.004	0.005	0.004	0.005
Mg	1.69	1.69	1.70	1.69	1.70	1.69	1.70	1.69	1.68	1.69	1.68	1.68	1.68	1.69
Ca	0.023	0.021	0.021	0.027	0.025	0.020	0.025	0.026	0.023	0.024	0.029	0.02	0.03	0.02
Na	0.003	0.001	0.002	0.003	0.002	0.000	0.003	0.003	0.003	0.004	0.003	0.004	0.003	0.002
K	<0.001	<0.001	0.001	0.001	<0.001	<0.001	0.001	<0.001	<0.001	<0.001	<0.001	<0.001	0.001	<0.001

A2.6a: Orthopyroxene profils

Sample L104

distance	**1395**	**1410**	**1455**	**1470**	**1485**	**1500**	**1515**	**1530**	**1545**	**1560**	**1575**	**1605**	**1665**	**1680**
SiO2	54.84	54.79	55.24	54.78	54.75	54.69	54.74	55.12	55.0	55.0	55.08	55.1	54.6	54.9
TiO2	0.18	0.23	0.15	0.21	0.20	0.21	0.23	0.17	0.19	0.20	0.21	0.19	0.19	0.23
Al2O3	4.4	4.7	4.2	4.3	4.4	4.4	4.4	4.4	4.2	4.2	4.3	4.1	4.3	4.4
Cr2O3	0.91	0.80	0.80	0.87	0.77	0.82	0.78	0.79	0.86	0.83	0.79	0.79	0.80	0.71
Fe2O3	1.17	0.67	1.11	1.19	1.14	1.89	1.41	0.74	1.21	0.59	0.72	1.1	0.8	0.8
FeO	5.8	6.1	5.7	5.6	5.6	5.2	5.6	6.0	5.7	6.0	6.0	5.69	6.12	5.99
MnO	0.18	0.17	0.12	0.16	0.22	0.14	0.14	0.14	0.22	0.14	0.11	0.14	0.13	0.11
MgO	33.1	32.8	33.3	33.2	33.1	33.2	33.0	33.2	33.0	33.1	33.0	33.3	32.8	33.0
CaO	0.61	0.68	0.64	0.60	0.65	0.66	0.65	0.51	0.66	0.56	0.65	0.57	0.54	0.65
Na2O	<0.01	0.02	0.05	0.01	0.01	0.04	0.06	0.01	0.05	0.02	0.04	0.03	0.01	0.02
K2O	<0.01	<0.01	<0.01	<0.01	0.02	<0.01	0.01	<0.01	<0.01	<0.01	0.01	0.01	<0.01	<0.01
Total	101.2	101.0	101.2	100.9	100.7	101.3	100.9	101.1	101.1	100.8	101.0	100.9	100.4	100.8
Si	1.88	1.88	1.89	1.88	1.88	1.87	1.88	1.89	1.88	1.89	1.89	1.89	1.89	1.89
Ti	0.005	0.006	0.004	0.005	0.005	0.005	0.006	0.004	0.005	0.005	0.005	0.005	0.005	0.006
Al	0.18	0.19	0.17	0.17	0.18	0.18	0.18	0.18	0.17	0.17	0.17	0.17	0.18	0.18
Cr	0.025	0.022	0.022	0.024	0.021	0.022	0.021	0.021	0.023	0.023	0.022	0.022	0.022	0.019
Fe3	0.030	0.017	0.029	0.031	0.029	0.049	0.036	0.019	0.031	0.015	0.019	0.028	0.022	0.021
Fe2	0.17	0.18	0.16	0.16	0.16	0.15	0.16	0.17	0.16	0.17	0.17	0.16	0.18	0.17
Mn	0.005	0.005	0.004	0.005	0.006	0.004	0.004	0.004	0.007	0.004	0.003	0.004	0.004	0.003
Mg	1.69	1.68	1.70	1.70	1.69	1.69	1.69	1.70	1.69	1.70	1.69	1.70	1.69	1.69
Ca	0.02	0.02	0.02	0.02	0.02	0.02	0.02	0.02	0.02	0.02	0.02	0.021	0.020	0.024
Na	<0.001	0.001	0.004	0.001	0.001	0.003	0.004	0.001	0.003	0.002	0.002	0.002	0.001	0.001
K	<0.001	<0.001	<0.001	<0.001	0.001	<0.001	0.001	<0.001	<0.001	<0.001	0.001	0.001	<0.001	<0.001

Sample L104

distance	**1695**	**1725**	**1740**	**1755**	**1815**	**1830**	**1860**	**1875**	**1920**	**1935**	**1950**	**1965**	**1995**	**2010**
SiO2	54.7	54.5	54.4	55.1	54.8	54.9	55.0	54.7	55.0	54.9	54.8	54.65	54.72	54.68
TiO2	0.23	0.20	0.21	0.23	0.20	0.23	0.23	0.19	0.24	0.23	0.19	0.21	0.22	0.15
Al2O3	4.4	4.4	4.4	4.3	4.3	4.2	4.4	4.5	4.2	4.2	4.1	4.3	4.2	4.2
Cr2O3	0.57	0.74	0.77	0.90	0.83	0.81	0.83	0.75	0.78	0.81	0.87	0.80	0.85	0.87
Fe2O3	1.6	1.9	1.3	0.5	1.0	0.9	0.8	1.0	0.9	1.4	1.6	1.16	0.98	1.53
FeO	5.49	5.22	5.65	6.34	5.89	5.82	6.21	5.91	5.90	5.54	5.15	5.6	5.9	5.4
MnO	0.19	0.18	0.21	0.08	0.17	0.14	0.16	0.15	0.15	0.14	0.14	0.17	0.22	0.11
MgO	33.2	33.0	32.7	33.0	33.2	32.8	33.0	32.9	32.9	33.2	33.2	33.1	32.8	33.2
CaO	0.50	0.70	0.83	0.58	0.44	0.96	0.55	0.44	0.86	0.68	0.80	0.51	0.73	0.64
Na2O	0.03	0.04	<0.01	0.01	<0.01	0.04	0.02	0.05	0.02	0.04	0.04	0.02	0.01	0.01
K2O	<0.01	0.01	<0.01	0.01	<0.01	0.01	<0.01	0.01	<0.01	<0.01	<0.01	0.01	<0.01	<0.01
Total	101.0	100.9	100.5	101.0	100.8	100.7	101.3	100.6	101.0	101.2	100.9	100.5	100.6	100.7
Si	1.88	1.87	1.88	1.89	1.88	1.89	1.88	1.88	1.89	1.88	1.88	1.88	1.89	1.88
Ti	0.006	0.005	0.006	0.006	0.005	0.006	0.006	0.005	0.006	0.006	0.005	0.005	0.006	0.004
Al	0.18	0.18	0.18	0.17	0.17	0.17	0.18	0.18	0.17	0.17	0.17	0.17	0.17	0.17
Cr	0.015	0.020	0.021	0.024	0.023	0.022	0.023	0.021	0.021	0.022	0.024	0.022	0.023	0.024
Fe3	0.042	0.050	0.033	0.014	0.025	0.022	0.021	0.026	0.024	0.036	0.042	0.030	0.026	0.040
Fe2	0.16	0.15	0.16	0.18	0.17	0.17	0.18	0.17	0.17	0.16	0.15	0.16	0.17	0.15
Mn	0.006	0.005	0.006	0.002	0.005	0.004	0.005	0.004	0.004	0.004	0.004	0.005	0.007	0.003
Mg	1.70	1.69	1.68	1.69	1.70	1.68	1.68	1.69	1.69	1.69	1.70	1.70	1.69	1.70
Ca	0.019	0.026	0.031	0.021	0.016	0.036	0.020	0.016	0.032	0.025	0.029	0.019	0.027	0.023
Na	0.002	0.003	<0.001	0.001	<0.001	0.002	0.001	0.004	0.001	0.003	0.002	0.002	0.001	<0.001
K	<0.001	<0.001	<0.001	<0.001	<0.001	0.001	<0.001	<0.001	<0.001	<0.001	<0.001	0.001	<0.001	<0.001

A2.6a: Orthopyroxene profils

Sample L104

distance	2025	2055	2070	2100	2130	2160	2205	2220	2280	2295	2310	2325	2355	2370
SiO2	54.92	54.75	55.22	54.61	54.6	55.22	55.22	55.0	55.55	55.45	55.28	54.9	54.7	55.8
TiO2	0.22	0.21	0.25	0.21	0.21	0.20	0.20	0.24	0.19	0.19	0.22	0.16	0.19	0.16
Al2O3	4.3	4.3	4.4	4.3	4.2	3.9	4.0	4.0	3.5	3.7	3.9	3.3	3.4	3.2
Cr2O3	0.82	0.78	0.85	0.78	0.85	0.87	0.83	0.74	0.73	0.69	0.77	0.73	0.69	0.67
Fe2O3	1.20	1.03	0.76	1.10	1.06	1.28	0.85	1.37	1.00	0.93	0.67	1.84	3.56	0.84
FeO	5.7	5.9	6.1	6.1	5.8	5.7	6.1	5.6	5.8	5.9	6.1	5.4	3.6	5.9
MnO	0.16	0.17	0.15	0.16	0.11	0.14	0.15	0.18	0.17	0.13	0.17	0.17	0.17	0.12
MgO	33.2	33.0	33.1	32.7	32.9	33.2	33.2	33.1	33.5	33.4	33.1	33.4	34.2	33.7
CaO	0.57	0.58	0.70	0.54	0.67	0.69	0.58	0.72	0.49	0.63	0.65	0.56	0.61	0.55
Na2O	0.03	0.02	0.01	0.04	0.02	0.06	0.02	0.05	0.04	0.03	0.03	0.00	0.02	0.03
K2O	<0.01	<0.01	<0.01	<0.01	0.01	<0.01	<0.01	0.01	0.01	<0.01	<0.01	<0.01	<0.01	0.01
Total	101.1	100.7	101.5	100.5	100.4	101.3	101.2	101.0	101.0	101.0	100.9	100.5	101.2	100.8
Si	1.88	1.88	1.89	1.88	1.88	1.89	1.89	1.89	1.90	1.90	1.90	1.89	1.87	1.91
Ti	0.006	0.006	0.007	0.005	0.005	0.005	0.005	0.006	0.005	0.005	0.006	0.004	0.005	0.004
Al	0.17	0.17	0.18	0.17	0.17	0.16	0.16	0.16	0.14	0.15	0.16	0.14	0.14	0.13
Cr	0.022	0.021	0.023	0.021	0.023	0.024	0.022	0.020	0.020	0.019	0.021	0.020	0.019	0.018
Fe3	0.031	0.027	0.020	0.029	0.028	0.033	0.022	0.036	0.026	0.024	0.017	0.048	0.092	0.022
Fe2	0.16	0.17	0.17	0.18	0.17	0.16	0.18	0.16	0.17	0.17	0.18	0.16	0.10	0.17
Mn	0.005	0.005	0.004	0.005	0.003	0.004	0.004	0.005	0.005	0.004	0.005	0.005	0.005	0.004
Mg	1.69	1.69	1.69	1.68	1.69	1.70	1.69	1.69	1.71	1.71	1.70	1.72	1.74	1.72
Ca	0.021	0.021	0.026	0.020	0.025	0.025	0.021	0.027	0.018	0.023	0.024	0.021	0.023	0.020
Na	0.002	0.001	0.001	0.003	0.001	0.004	0.001	0.003	0.003	0.002	0.002	<0.001	0.001	0.002
K	<0.001	<0.001	<0.001	<0.001	<0.001	<0.001	<0.001	<0.001	<0.001	<0.001	<0.001	<0.001	<0.001	0.001

Sample L104

distance	2385	2400	2415	2430	2445	2460
SiO2	55.6	55.1	55.8	56.7	56.5	57.1
TiO2	0.24	0.27	0.25	0.18	0.20	0.23
Al2O3	3.3	3.4	3.0	2.0	2.0	1.5
Cr2O3	0.75	0.70	0.63	0.42	0.50	0.27
Fe2O3	1.00	1.29	0.33	1.50	0.61	0.41
FeO	5.9	6.0	6.3	5.5	7.1	6.1
MnO	0.10	0.16	0.17	0.13	0.22	0.21
MgO	33.5	33.0	33.4	34.6	33.6	34.5
CaO	0.67	0.65	0.58	0.44	0.37	0.54
Na2O	0.05	0.05	0.02	0.01	0.02	0.01
K2O	<0.01	0.01	<0.01	0.01	<0.01	<0.01
Total	101.1	100.7	100.5	101.4	101.1	100.9
Si	1.91	1.90	1.92	1.93	1.94	1.96
Ti	0.006	0.007	0.007	0.005	0.005	0.006
Al	0.13	0.14	0.12	0.08	0.08	0.06
Cr	0.020	0.019	0.017	0.011	0.014	0.007
Fe3	0.026	0.034	0.009	0.038	0.016	0.011
Fe2	0.17	0.17	0.18	0.16	0.20	0.17
Mn	0.003	0.005	0.005	0.004	0.007	0.006
Mg	1.71	1.70	1.72	1.76	1.72	1.76
Ca	0.025	0.024	0.021	0.016	0.014	0.020
Na	0.003	0.004	0.002	0.001	0.001	0.001
K	<0.001	<0.001	<0.001	<0.001	<0.001	<0.001

Sample L112

distance	0	40	120	160	200	240	320
SiO2	56.7	55.9	55.3	55.3	55.2	55.1	55.2
TiO2	0.21	0.23	0.24	0.24	0.24	0.27	0.23
Al2O3	1.2	2.0	2.8	2.9	3.0	3.0	3.0
Cr2O3	0.20	0.43	0.61	0.66	0.65	0.69	0.67
Fe2O3	<0.01	<0.01	<0.01	0.06	0.44	0.00	0.00
FeO	6.4	6.7	6.6	6.7	6.3	6.6	6.7
MnO	0.19	0.14	0.11	0.17	0.16	0.14	0.14
NiO	0.07	0.16	0.05	0.09	0.08	0.08	0.10
MgO	33.7	33.1	32.4	32.8	32.7	32.3	32.4
CaO	0.57	0.71	0.97	0.66	0.99	0.84	0.90
Na2O	<0.01	0.04	0.01	0.01	0.03	0.02	0.04
K2O	<0.01	<0.01	0.01	<0.01	0.01	<0.01	<0.01
Total	99.2	99.4	99.1	99.6	99.7	99.0	99.4
Si	1.97	1.95	1.94	1.92	1.92	1.93	1.93
Ti	0.005	0.006	0.006	0.006	0.006	0.007	0.006
Al	0.05	0.08	0.11	0.12	0.12	0.13	0.12
Cr	0.005	0.012	0.017	0.018	0.018	0.019	0.018
Fe3	<0.001	<0.001	<0.001	0.002	0.012	0.000	0.000
Fe2	0.19	0.19	0.19	0.20	0.18	0.19	0.20
Mn	0.006	0.004	0.003	0.005	0.005	0.004	0.004
Ni	0.002	0.004	0.001	0.003	0.002	0.002	0.003
Mg	1.75	1.72	1.69	1.70	1.69	1.69	1.69
Ca	0.021	0.026	0.036	0.025	0.037	0.032	0.034
Na	<0.001	0.003	0.001	0.001	0.002	0.001	0.003
K	<0.001	<0.001	<0.001	<0.001	0.001	<0.001	<0.001

A2.6a: Orthopyroxene profils

Sample L112

distance	360	400	440	480	520	560	680	960	1040	1080	1200	1240	1320	1400
SiO2	55.0	55.1	55.1	55.1	54.7	54.7	54.6	54.7	54.9	54.5	54.8	54.4	54.7	54.6
TiO2	0.26	0.23	0.21	0.24	0.23	0.28	0.21	0.25	0.22	0.24	0.21	0.24	0.21	0.21
Al2O3	3.0	3.0	3.0	3.0	3.3	3.3	3.5	3.4	3.2	3.5	3.5	3.7	3.7	3.8
Cr2O3	0.68	0.69	0.67	0.66	0.68	0.69	0.65	0.67	0.63	0.72	0.74	0.74	0.74	0.74
Fe2O3	0.03	0.51	0.03	0.18	0.64	0.02	0.44	0.75	0.00	0.51	0.40	0.18	0.46	0.00
FeO	6.6	6.2	6.7	6.6	6.4	6.5	6.4	6.2	6.5	6.2	6.1	6.4	6.5	6.9
MnO	0.22	0.17	0.19	0.13	0.12	0.14	0.13	0.15	0.12	0.17	0.14	0.13	0.17	0.09
NiO	0.11	0.10	0.11	0.12	0.12	0.04	0.11	0.11	0.10	0.07	0.12	0.12	0.09	0.08
MgO	32.3	32.7	32.3	32.5	32.6	32.4	32.6	32.4	32.3	32.3	32.7	32.2	32.3	32.1
CaO	1.03	0.85	1.05	0.84	0.56	0.79	0.62	0.98	0.89	0.99	0.61	0.88	0.76	0.89
Na2O	0.02	0.02	0.03	0.04	0.02	0.04	0.01	0.04	0.05	0.02	0.04	0.03	0.03	0.01
K2O	0.02	0.02	<0.01	0.01	<0.01	0.01	<0.01	0.01	<0.01	0.01	0.02	0.01	<0.01	<0.01
Total	99.3	99.6	99.3	99.3	99.3	99.0	99.2	99.6	98.8	99.2	99.3	99.0	99.7	99.3
Si	1.92	1.92	1.92	1.92	1.91	1.92	1.91	1.91	1.92	1.91	1.91	1.91	1.90	1.91
Ti	0.007	0.006	0.005	0.006	0.006	0.007	0.006	0.007	0.006	0.006	0.005	0.006	0.006	0.006
Al	0.13	0.12	0.12	0.12	0.13	0.14	0.14	0.14	0.13	0.14	0.14	0.15	0.15	0.16
Cr	0.019	0.019	0.018	0.018	0.019	0.019	0.018	0.019	0.018	0.020	0.020	0.020	0.021	0.021
Fe3	0.001	0.013	0.001	0.005	0.017	0.001	0.012	0.020	0.000	0.013	0.010	0.005	0.012	0.000
Fe2	0.19	0.18	0.19	0.19	0.19	0.19	0.19	0.18	0.19	0.18	0.18	0.19	0.19	0.20
Mn	0.007	0.005	0.006	0.004	0.004	0.004	0.004	0.004	0.004	0.005	0.004	0.004	0.005	0.003
Ni	0.003	0.003	0.003	0.004	0.003	0.001	0.003	0.003	0.003	0.002	0.004	0.004	0.003	0.002
Mg	1.68	1.70	1.68	1.69	1.70	1.69	1.70	1.68	1.69	1.68	1.70	1.68	1.68	1.67
Ca	0.038	0.032	0.040	0.032	0.021	0.030	0.023	0.036	0.034	0.037	0.023	0.033	0.028	0.033
Na	0.002	0.001	0.002	0.003	0.001	0.003	0.001	0.003	0.003	0.002	0.003	0.002	0.002	0.001
K	0.001	0.001	<0.001	<0.001	<0.001	<0.001	<0.001	<0.001	<0.001	<0.001	0.001	0.001	<0.001	<0.001

Sample L112

distance	1440	1520	1640	1680	1720	1760	1800	1840	1880	1920	1960	2000	2040	2080
SiO2	54.3	56.2	54.7	54.9	55.2	54.8	54.7	55.1	54.6	54.7	54.3	54.8	54.6	56.3
TiO2	0.26	0.18	0.23	0.23	0.25	0.23	0.23	0.22	0.23	0.23	0.26	0.20	0.20	0.20
Al2O3	3.9	3.4	3.9	3.8	3.9	4.0	3.9	3.8	3.8	3.8	4.0	3.8	3.6	3.4
Cr2O3	0.75	0.60	0.73	0.75	0.74	0.80	0.80	0.71	0.75	0.76	0.79	0.72	0.70	0.63
Fe2O3	0.04	0.05	<0.01	0.00	2.66	<0.01	<0.01	<0.01	0.49	0.22	0.89	<0.01	0.65	0.73
FeO	6.7	6.7	6.5	6.5	4.0	6.3	6.5	6.8	6.4	6.6	6.0	6.7	6.1	6.0
MnO	0.10	0.13	0.22	0.14	0.14	0.15	0.12	0.19	0.24	0.14	0.14	0.14	0.15	0.22
NiO	0.08	0.11	0.10	0.13	0.06	0.15	0.12	0.10	0.10	0.07	0.09	0.15	0.13	0.13
MgO	32.0	33.3	32.3	32.3	34.1	32.4	32.1	32.4	32.3	32.3	32.2	32.2	32.5	33.9
CaO	0.86	0.71	0.72	0.89	0.81	0.86	0.94	0.82	0.93	0.81	0.97	0.86	0.75	0.61
Na2O	0.02	0.03	0.03	0.03	0.04	0.02	0.03	0.02	0.02	0.03	0.07	0.03	0.03	0.01
K2O	<0.01	<0.01	<0.01	<0.01	0.03	<0.01	<0.01	<0.01	<0.01	<0.01	<0.01	0.01	0.01	0.01
Total	99.1	101.3	99.5	99.7	101.9	99.6	99.4	100.2	99.9	99.7	99.6	99.6	99.3	102.1
Si	1.90	1.92	1.91	1.91	1.87	1.91	1.91	1.91	1.90	1.90	1.89	1.910	1.904	1.909
Ti	0.007	0.005	0.006	0.006	0.007	0.006	0.006	0.006	0.006	0.006	0.007	0.005	0.005	0.005
Al	0.16	0.14	0.16	0.16	0.16	0.16	0.16	0.15	0.16	0.16	0.16	0.156	0.147	0.138
Cr	0.021	0.016	0.020	0.021	0.020	0.022	0.022	0.020	0.021	0.021	0.022	0.020	0.019	0.017
Fe3	0.001	0.001	<0.001	<0.001	0.068	<0.001	<0.001	<0.001	0.013	0.006	0.023	0.000	0.017	0.019
Fe2	0.20	0.19	0.19	0.19	0.11	0.18	0.19	0.20	0.19	0.19	0.17	0.196	0.177	0.169
Mn	0.003	0.004	0.007	0.004	0.004	0.005	0.003	0.006	0.007	0.004	0.004	0.004	0.004	0.007
Ni	0.002	0.003	0.003	0.004	0.002	0.004	0.004	0.003	0.003	0.002	0.003	0.004	0.004	0.003
Mg	1.67	1.70	1.68	1.68	1.72	1.68	1.67	1.68	1.67	1.68	1.67	1.670	1.692	1.711
Ca	0.032	0.026	0.027	0.033	0.030	0.032	0.035	0.031	0.035	0.030	0.036	0.032	0.028	0.022
Na	0.002	0.002	0.002	0.002	0.003	0.002	0.002	0.001	0.002	0.002	0.005	0.002	0.002	<0.001
K	<0.001	<0.001	<0.001	<0.001	0.001	<0.001	<0.001	<0.001	<0.001	<0.001	<0.001	0.001	0.001	0.001

Sample L112								**Sample L110**						
distance	**2160**	**2240**	**2280**	**2320**	**2360**	**2440**	**2480**	**distance**	**0**	**15**	**30**	**45**	**60**	**105**
SiO2	54.6	54.8	54.9	54.7	55.0	54.8	55.1	SiO2	57.5	56.1	56.0	56.0	56.3	56.0
TiO2	0.22	0.23	0.25	0.26	0.22	0.20	0.20	TiO2	0.13	0.30	0.29	0.30	0.32	0.30
Al2O3	3.3	3.5	3.6	3.5	3.6	3.7	3.6	Al2O3	1.0	2.3	2.4	2.3	2.3	2.5
Cr2O3	0.62	0.67	0.65	0.70	0.66	0.62	0.62	Cr2O3	0.22	0.50	0.47	0.53	0.53	0.54
Fe2O3	0.05	0.48	<0.01	<0.01	0.35	0.63	0.27	Fe2O3	<0.01	<0.01	<0.01	<0.01	<0.01	<0.01
FeO	6.6	6.4	6.9	6.4	6.4	6.3	6.4	FeO	5.8	5.4	5.5	5.6	5.5	5.5
MnO	0.17	0.15	0.16	0.12	0.20	0.10	0.13	MnO	0.15	0.13	0.11	0.12	0.14	0.14
NiO	0.12	0.08	0.10	0.08	0.04	0.11	0.12	NiO	0.11	0.08	0.04	0.04	0.08	0.02
MgO	32.4	32.6	32.2	32.2	32.5	32.6	32.8	MgO	34.2	33.1	33.0	33.2	33.2	33.2
CaO	0.65	0.70	0.75	0.82	0.92	0.82	0.73	CaO	0.47	0.70	0.78	0.76	0.79	0.72
Na2O	0.01	0.03	0.02	0.01	0.03	0.02	<0.01	Na2O	0.01	0.03	<0.01	0.01	0.04	0.01
K2O	<0.01	<0.01	<0.01	<0.01	<0.01	0.02	<0.01	K2O	0.01	<0.01	0.01	0.02	0.01	<0.01
Total	98.8	99.6	99.5	98.9	100.0	99.8	100.0	Total	99.5	98.6	98.5	98.9	99.1	98.9
Si	1.918	1.908	1.917	1.919	1.907	1.904	1.910	Si	1.992	1.965	1.965	1.96	1.96	1.95
Ti	0.006	0.006	0.006	0.007	0.006	0.005	0.005	Ti	0.003	0.008	0.008	0.008	0.008	0.008
Al	0.136	0.144	0.147	0.146	0.149	0.151	0.146	Al	0.039	0.093	0.098	0.10	0.09	0.10
Cr	0.017	0.018	0.018	0.020	0.018	0.017	0.017	Cr	0.006	0.014	0.013	0.015	0.015	0.015
Fe3	0.001	0.013	<0.001	<0.001	0.009	0.017	0.007	Fe3	<0.001	<0.001	<0.001	<0.001	<0.001	<0.001
Fe2	0.193	0.185	0.202	0.187	0.187	0.182	0.185	Fe2	0.167	0.157	0.161	0.16	0.16	0.16
Mn	0.005	0.004	0.005	0.004	0.006	0.003	0.004	Mn	0.004	0.004	0.003	0.003	0.004	0.004
Ni	0.004	0.002	0.003	0.002	0.001	0.003	0.003	Ni	0.003	0.002	0.001	0.001	0.002	0.001
Mg	1.695	1.692	1.673	1.685	1.681	1.687	1.696	Mg	1.767	1.728	1.722	1.73	1.72	1.73
Ca	0.024	0.026	0.028	0.031	0.034	0.031	0.027	Ca	0.018	0.026	0.029	0.029	0.030	0.027
Na	0.001	0.002	0.001	0.001	0.002	0.001	<0.001	Na	0.001	0.002	<0.001	0.001	0.003	0.001
K	<0.001	<0.001	<0.001	<0.001	<0.001	0.001	<0.001	K	<0.001	<0.001	0.001	0.001	0.001	<0.001

Sample L110														
distance	**120**	**150**	**165**	**180**	**195**	**210**	**240**	**255**	**270**	**285**	**345**	**375**	**390**	**405**
SiO2	56.3	55.9	55.9	56.0	56.0	55.9	55.8	56.1	56.0	56.1	56.0	55.9	56.2	55.9
TiO2	0.26	0.30	0.27	0.27	0.27	0.25	0.30	0.27	0.30	0.24	0.28	0.30	0.28	0.29
Al2O3	2.5	2.8	2.6	2.6	2.5	2.7	2.7	2.5	2.5	2.6	2.6	2.7	2.6	2.7
Cr2O3	0.58	0.63	0.54	0.59	0.57	0.60	0.53	0.57	0.58	0.56	0.57	0.64	0.63	0.61
Fe2O3	1.57	<0.01	<0.01	<0.01	<0.01	<0.01	<0.01	<0.01	<0.01	<0.01	<0.01	<0.01	<0.01	<0.01
FeO	4.1	5.6	5.3	5.4	5.4	5.6	5.6	5.6	5.4	5.4	5.2	5.2	5.5	5.2
MnO	0.12	0.18	0.20	0.11	0.14	0.18	0.14	0.14	0.10	0.11	0.11	0.11	0.10	0.18
NiO	0.08	0.06	0.07	0.07	0.07	0.06	0.10	0.08	0.07	0.05	0.09	0.05	0.06	0.07
MgO	34.7	33.2	33.2	33.1	33.1	33.0	33.1	32.9	33.0	33.3	32.8	32.9	33.0	32.9
CaO	0.74	0.72	0.63	0.72	0.72	0.79	0.69	0.71	0.88	0.97	0.74	0.77	0.88	0.76
Na2O	0.06	0.01	0.02	0.03	0.01	0.01	0.02	<0.01	0.03	0.06	0.01	<0.01	0.02	0.03
K2O	0.03	0.01	0.01	<0.01	<0.01	0.01	<0.01	<0.01	<0.01	0.02	0.01	<0.01	0.02	0.01
Total	101.0	99.3	98.7	98.9	98.8	99.1	98.9	98.9	98.9	99.4	98.4	98.6	99.3	98.7
Si	1.92	1.94	1.95	1.95	1.96	1.95	1.95	1.96	1.96	1.95	1.96	1.96	1.96	1.96
Ti	0.007	0.008	0.007	0.007	0.007	0.007	0.008	0.007	0.008	0.006	0.007	0.008	0.007	0.008
Al	0.10	0.11	0.11	0.11	0.10	0.11	0.11	0.10	0.10	0.11	0.11	0.11	0.11	0.11
Cr	0.016	0.017	0.015	0.016	0.016	0.017	0.015	0.016	0.016	0.015	0.016	0.018	0.017	0.017
Fe3	0.040	<0.001	<0.001	<0.001	<0.001	<0.001	<0.001	<0.001	<0.001	<0.001	<0.001	<0.001	<0.001	<0.001
Fe2	0.12	0.16	0.15	0.16	0.16	0.16	0.16	0.16	0.16	0.16	0.15	0.15	0.16	0.15
Mn	0.004	0.005	0.006	0.003	0.004	0.005	0.004	0.004	0.003	0.003	0.003	0.003	0.003	0.005
Ni	0.002	0.002	0.002	0.002	0.002	0.002	0.003	0.002	0.002	0.002	0.002	0.001	0.002	0.002
Mg	1.77	1.72	1.73	1.72	1.72	1.72	1.72	1.72	1.72	1.72	1.72	1.72	1.71	1.72
Ca	0.027	0.027	0.024	0.027	0.027	0.030	0.026	0.027	0.033	0.036	0.028	0.029	0.033	0.029
Na	0.004	0.001	0.002	0.002	0.001	<0.001	0.001	0.000	0.002	0.004	0.001	<0.001	0.001	0.002
K	0.001	<0.001	<0.001	<0.001	<0.001	<0.001	<0.001	<0.001	<0.001	0.001	0.001	<0.001	0.001	0.001

A2.6a: Orthopyroxene profils

Sample L110

distance	435	450	465	540	555	570	585	630	660	690	720	735	795	810
SiO2	55.7	55.6	55.9	56.0	55.5	55.8	55.7	55.5	55.6	55.7	55.8	55.7	55.5	55.7
TiO2	0.29	0.26	0.25	0.28	0.30	0.26	0.33	0.28	0.29	0.30	0.27	0.27	0.27	0.29
Al2O3	2.8	2.8	2.7	2.9	3.0	3.0	3.0	3.0	3.0	3.1	3.1	3.1	3.1	3.1
Cr2O3	0.62	0.61	0.57	0.61	0.61	0.68	0.64	0.61	0.66	0.68	0.67	0.69	0.68	0.70
Fe2O3	<0.01	<0.01	<0.01	<0.01	<0.01	<0.01	<0.01	<0.01	<0.01	<0.01	<0.01	<0.01	<0.01	<0.01
FeO	5.5	4.9	5.1	5.2	5.2	5.2	5.2	5.1	4.9	5.5	5.2	5.4	5.2	5.3
MnO	0.09	0.14	0.08	0.20	0.09	0.10	0.09	0.19	0.11	0.10	0.15	0.14	0.16	0.14
NiO	0.08	0.11	0.10	0.05	0.09	0.14	0.12	0.08	0.07	0.07	0.05	0.07	0.11	0.09
MgO	32.8	32.9	32.6	32.6	32.8	32.6	31.6	32.9	32.5	32.7	32.8	32.8	32.8	32.6
CaO	0.82	0.82	0.94	0.94	0.93	0.92	0.83	0.82	0.90	0.76	0.85	0.88	0.79	0.94
Na2O	0.03	0.03	0.01	0.03	0.02	<0.01	0.10	0.01	0.04	0.02	0.01	0.01	0.04	0.02
K2O	<0.01	<0.01	<0.01	0.01	0.01	<0.01	0.01	0.03	0.02	<0.01	0.01	0.02	0.02	<0.01
Total	98.7	98.1	98.4	98.8	98.6	98.6	97.5	98.5	98.1	98.8	98.9	99.0	98.8	98.9
Si	1.95	1.95	1.96	1.96	1.94	1.96	1.98	1.94	1.96	1.95	1.95	1.95	1.94	1.95
Ti	0.008	0.007	0.007	0.007	0.008	0.007	0.009	0.007	0.008	0.008	0.007	0.007	0.007	0.008
Al	0.12	0.12	0.11	0.12	0.12	0.12	0.12	0.12	0.12	0.13	0.13	0.13	0.13	0.13
Cr	0.017	0.017	0.016	0.017	0.017	0.019	0.018	0.017	0.018	0.019	0.019	0.019	0.019	0.019
Fe3	<0.001	<0.001	<0.001	<0.001	<0.001	<0.001	<0.001	<0.001	<0.001	<0.001	<0.001	<0.001	<0.001	<0.001
Fe2	0.16	0.14	0.15	0.15	0.15	0.15	0.15	0.15	0.14	0.16	0.15	0.16	0.15	0.16
Mn	0.003	0.004	0.003	0.006	0.003	0.003	0.003	0.006	0.003	0.003	0.005	0.004	0.005	0.004
Ni	0.002	0.003	0.003	0.001	0.003	0.004	0.003	0.002	0.002	0.002	0.001	0.002	0.003	0.003
Mg	1.71	1.72	1.71	1.70	1.71	1.70	1.67	1.72	1.70	1.70	1.71	1.71	1.71	1.70
Ca	0.031	0.031	0.035	0.035	0.035	0.035	0.032	0.031	0.034	0.029	0.032	0.033	0.030	0.035
Na	0.002	0.002	0.001	0.002	0.001	0.000	0.007	0.001	0.003	0.001	0.001	<0.001	0.003	0.002
K	<0.001	<0.001	<0.001	<0.001	<0.001	<0.001	<0.001	0.001	0.001	<0.001	<0.001	0.001	0.001	<0.001

Sample L110

distance	900	945	960	975	1020	1050	1065	1080	1140	1155	1170	1215	1230	1245
SiO2	55.3	55.4	55.3	55.3	55.5	55.6	55.6	55.6	55.5	55.4	55.8	55.6	55.6	55.5
TiO2	0.26	0.28	0.29	0.27	0.26	0.29	0.23	0.27	0.22	0.27	0.23	0.30	0.25	0.28
Al2O3	3.2	3.2	3.2	3.2	3.0	3.2	3.1	3.2	3.1	3.2	3.1	3.1	3.1	3.1
Cr2O3	0.73	0.69	0.69	0.77	0.72	0.70	0.66	0.68	0.74	0.71	0.74	0.71	0.72	0.69
Fe2O3	<0.01	<0.01	<0.01	<0.01	<0.01	<0.01	<0.01	<0.01	<0.01	<0.01	<0.01	<0.01	<0.01	<0.01
FeO	5.5	5.3	5.2	5.4	4.9	5.0	5.2	5.4	5.4	5.4	5.0	5.3	5.3	5.3
MnO	0.13	0.10	0.07	0.12	0.09	0.12	0.17	0.09	0.17	0.10	0.16	0.13	0.09	0.09
NiO	0.08	0.08	0.09	0.08	0.09	0.09	0.07	0.10	0.08	0.06	0.06	0.08	0.11	0.09
MgO	32.5	32.7	32.6	32.6	32.4	32.6	32.6	32.7	32.8	32.7	32.7	32.6	32.7	32.9
CaO	0.94	0.83	0.82	0.98	0.95	0.91	0.78	0.88	0.66	0.80	0.68	0.81	0.88	0.83
Na2O	<0.01	0.02	0.05	0.01	0.03	0.01	0.02	0.03	<0.01	0.01	0.02	<0.01	0.02	0.01
K2O	<0.01	<0.01	<0.01	0.01	<0.01	0.02	<0.01	0.02	0.01	<0.01	<0.01	<0.01	0.01	<0.01
Total	98.6	98.5	98.2	98.7	97.9	98.6	98.4	99.0	98.7	98.6	98.5	98.6	98.8	98.8
Si	1.94	1.94	1.94	1.94	1.96	1.95	1.95	1.94	1.94	1.94	1.96	1.95	1.95	1.94
Ti	0.007	0.007	0.008	0.007	0.007	0.008	0.006	0.007	0.006	0.007	0.006	0.008	0.007	0.007
Al	0.13	0.13	0.13	0.13	0.13	0.13	0.13	0.13	0.13	0.13	0.13	0.13	0.13	0.13
Cr	0.020	0.019	0.019	0.021	0.020	0.020	0.018	0.019	0.020	0.020	0.021	0.020	0.020	0.019
Fe3	<0.001	<0.001	<0.001	<0.001	<0.001	<0.001	<0.001	<0.001	<0.001	<0.001	<0.001	<0.001	<0.001	<0.001
Fe2	0.16	0.16	0.15	0.16	0.14	0.15	0.15	0.16	0.16	0.16	0.15	0.15	0.16	0.15
Mn	0.004	0.003	0.002	0.004	0.003	0.004	0.005	0.003	0.005	0.003	0.005	0.004	0.003	0.003
Ni	0.002	0.002	0.003	0.002	0.003	0.003	0.002	0.003	0.002	0.002	0.002	0.002	0.003	0.003
Mg	1.70	1.71	1.71	1.70	1.70	1.70	1.71	1.70	1.71	1.71	1.71	1.70	1.70	1.71
Ca	0.035	0.031	0.031	0.037	0.036	0.034	0.029	0.033	0.025	0.030	0.026	0.031	0.033	0.031
Na	<0.001	0.001	0.003	0.001	0.002	0.001	0.002	0.002	<0.001	0.001	0.001	<0.001	0.002	0.001
K	<0.001	<0.001	<0.001	<0.001	<0.001	0.001	<0.001	0.001	<0.001	<0.001	<0.001	<0.001	0.001	<0.001

A2.6a: Orthopyroxene profils

Sample L110

distance	1260	1320	1335	1350	1410	1425	1455	1485	1500	1515	1530	1545	1575	1590
SiO2	55.5	55.5	54.9	55.6	57.5	55.3	55.4	55.8	55.6	55.6	55.9	55.9	55.5	55.8
TiO2	0.24	0.26	0.28	0.27	0.27	0.28	0.25	0.28	0.27	0.29	0.22	0.26	0.20	0.28
Al2O3	3.2	3.2	3.1	3.1	3.0	3.1	3.1	3.2	3.1	3.1	3.0	3.2	3.0	3.0
Cr2O3	0.67	0.74	0.72	0.71	0.69	0.72	0.70	0.71	0.70	0.66	0.71	0.73	0.70	0.68
Fe2O3	<0.01	<0.01	<0.01	<0.01	<0.01	<0.01	<0.01	<0.01	<0.01	<0.01	<0.01	<0.01	<0.01	<0.01
FeO	5.7	5.2	5.2	5.3	5.4	5.2	5.0	4.9	5.3	5.0	5.1	5.1	5.1	5.2
MnO	0.17	0.14	0.12	0.06	0.17	0.22	0.10	0.13	0.19	0.12	0.22	0.04	0.12	0.14
NiO	0.08	0.14	0.06	0.06	0.05	0.05	0.08	0.05	0.11	0.08	0.07	0.06	0.09	0.09
MgO	32.7	32.8	32.4	32.8	34.1	32.6	32.7	32.9	32.9	32.7	32.8	32.9	32.6	32.7
CaO	0.80	0.78	0.94	0.84	0.91	0.87	0.75	0.66	0.78	0.80	0.85	0.82	0.95	0.75
Na2O	0.01	0.02	0.03	0.04	0.03	0.02	0.03	0.03	0.03	0.02	0.02	0.03	0.02	0.02
K2O	<0.01	0.01	0.01	<0.01	<0.01	0.01	<0.01	<0.01	0.01	<0.01	<0.01	0.01	0.03	<0.01
Total	99.0	98.7	97.7	98.7	102.2	98.3	98.1	98.6	99.0	98.4	98.8	98.9	98.2	98.7
Si	1.94	1.94	1.94	1.94	1.94	1.94	1.95	1.95	1.94	1.95	1.95	1.95	1.95	1.95
Ti	0.006	0.007	0.007	0.007	0.007	0.007	0.007	0.008	0.007	0.008	0.006	0.007	0.005	0.007
Al	0.13	0.13	0.13	0.13	0.12	0.13	0.13	0.13	0.13	0.13	0.12	0.13	0.12	0.13
Cr	0.019	0.021	0.020	0.020	0.019	0.020	0.019	0.020	0.019	0.018	0.020	0.020	0.019	0.019
Fe3	<0.001	<0.001	<0.001	<0.001	<0.001	<0.001	<0.001	<0.001	<0.001	<0.001	<0.001	<0.001	<0.001	<0.001
Fe2	0.17	0.15	0.15	0.15	0.15	0.15	0.15	0.14	0.15	0.15	0.15	0.15	0.15	0.15
Mn	0.005	0.004	0.004	0.002	0.005	0.006	0.003	0.004	0.006	0.004	0.007	0.001	0.004	0.004
Ni	0.002	0.004	0.002	0.002	0.001	0.002	0.002	0.001	0.003	0.002	0.002	0.002	0.003	0.003
Mg	1.70	1.71	1.71	1.71	1.72	1.71	1.71	1.72	1.71	1.71	1.71	1.71	1.71	1.71
Ca	0.030	0.029	0.036	0.032	0.033	0.033	0.028	0.025	0.029	0.030	0.032	0.031	0.036	0.028
Na	0.001	0.001	0.002	0.003	0.002	0.001	0.002	0.002	0.002	0.002	0.002	0.002	0.001	0.002
K	<0.001	0.001	<0.001	<0.001	<0.001	<0.001	<0.001	<0.001	0.001	<0.001	<0.001	0.001	0.001	<0.001

Sample L110

distance	1605	1650	1665	1680	1695	1770	1785	1800	1815	1845	1875	1890	1905	1950
SiO2	55.8	55.6	55.6	55.6	55.5	55.8	55.7	55.8	56.0	55.6	55.8	55.8	55.7	56.0
TiO2	0.27	0.25	0.46	0.31	0.28	0.24	0.28	0.22	0.26	0.27	0.27	0.24	0.29	0.27
Al2O3	2.9	3.0	3.0	3.0	3.0	3.0	2.9	2.7	2.9	2.8	2.8	2.8	2.8	2.8
Cr2O3	0.68	0.70	0.69	0.65	0.68	0.68	0.64	0.67	0.64	0.61	0.61	0.67	0.62	0.68
Fe2O3	<0.01	<0.01	<0.01	<0.01	<0.01	<0.01	<0.01	<0.01	<0.01	<0.01	<0.01	<0.01	<0.01	<0.01
FeO	5.1	5.5	5.4	5.0	5.0	5.0	5.3	5.0	5.1	5.0	4.9	5.2	5.3	4.8
MnO	0.09	0.10	0.15	0.12	0.16	0.12	0.11	0.05	0.14	0.18	0.09	0.11	0.13	0.13
NiO	0.10	0.06	0.06	0.05	0.04	0.03	0.12	0.09	0.10	0.09	0.09	0.05	0.08	0.08
MgO	32.9	32.8	30.7	32.7	32.8	33.0	32.8	32.9	33.4	32.5	32.7	32.9	32.8	32.9
CaO	0.77	0.67	0.73	0.84	0.86	0.68	0.69	0.77	0.60	0.74	0.98	0.79	0.85	0.75
Na2O	<0.01	0.03	0.14	0.04	0.04	0.03	0.02	<0.01	0.01	0.05	0.00	0.01	<0.01	0.02
K2O	<0.01	<0.01	<0.01	0.01	<0.01	<0.01	<0.01	<0.01	<0.01	<0.01	0.01	0.01	<0.01	<0.01
Total	98.6	98.7	96.9	98.3	98.3	98.6	98.6	98.2	99.2	97.9	98.2	98.5	98.6	98.5
Si	1.95	1.94	1.99	1.95	1.95	1.95	1.95	1.96	1.95	1.96	1.96	1.96	1.95	1.96
Ti	0.007	0.007	0.012	0.008	0.007	0.006	0.007	0.006	0.007	0.007	0.007	0.006	0.008	0.007
Al	0.12	0.12	0.13	0.13	0.13	0.12	0.12	0.11	0.12	0.12	0.12	0.11	0.12	0.11
Cr	0.019	0.019	0.020	0.018	0.019	0.019	0.018	0.019	0.018	0.017	0.017	0.019	0.017	0.019
Fe3	<0.001	<0.001	<0.001	<0.001	<0.001	<0.001	<0.001	<0.001	<0.001	<0.001	<0.001	<0.001	<0.001	<0.001
Fe2	0.15	0.16	0.16	0.15	0.15	0.15	0.15	0.15	0.15	0.15	0.15	0.15	0.16	0.14
Mn	0.003	0.003	0.005	0.004	0.005	0.004	0.003	0.001	0.004	0.006	0.003	0.003	0.004	0.004
Ni	0.003	0.002	0.002	0.001	0.001	0.001	0.003	0.003	0.003	0.003	0.003	0.002	0.002	0.002
Mg	1.72	1.71	1.64	1.71	1.71	1.72	1.71	1.72	1.73	1.71	1.71	1.72	1.71	1.72
Ca	0.029	0.025	0.028	0.031	0.032	0.026	0.026	0.029	0.023	0.028	0.037	0.030	0.032	0.028
Na	<0.001	0.002	0.010	0.003	0.003	0.002	0.002	<0.001	0.001	0.004	<0.001	0.001	<0.001	0.001
K	<0.001	<0.001	<0.001	0.001	<0.001	<0.001	<0.001	<0.001	<0.001	<0.001	<0.001	<0.001	<0.001	<0.001

A2.6a: Orthopyroxene profils

Sample L110

distance	2010	2025	2055	2070	2085	2100	2115	2130	2145	2175	2190	2205	2235	2250
SiO2	56.1	56.0	56.2	52.9	55.8	56.1	56.4	56.2	54.2	56.3	55.5	56.3	56.6	56.9
TiO2	0.28	0.27	0.25	1.41	0.32	0.29	0.25	0.31	0.23	0.26	0.30	0.28	0.25	0.22
Al2O3	2.6	2.7	2.4	2.7	2.6	2.2	2.5	2.5	2.4	2.1	2.3	2.2	1.8	1.7
Cr2O3	0.61	0.64	0.60	0.63	0.58	0.51	0.60	0.58	0.50	0.52	0.58	0.51	0.50	0.43
Fe2O3	<0.01	<0.01	<0.01	<0.01	<0.01	<0.01	<0.01	<0.01	<0.01	<0.01	<0.01	<0.01	<0.01	<0.01
FeO	5.0	5.0	4.8	4.7	5.1	5.2	5.1	5.3	5.5	5.1	5.1	5.6	5.1	5.1
MnO	0.13	0.17	0.06	0.11	0.09	0.14	0.13	0.07	0.16	0.10	0.17	0.09	0.12	0.07
NiO	0.05	0.06	0.06	0.14	0.07	0.09	0.02	0.08	0.08	0.03	0.04	0.03	0.06	0.05
MgO	33.2	32.9	33.1	33.0	32.9	33.1	33.2	32.9	32.6	33.3	31.0	33.1	33.2	33.5
CaO	0.68	0.93	0.96	0.61	0.81	0.74	0.72	0.83	0.65	0.71	0.74	0.83	0.89	0.66
Na2O	0.01	0.02	<0.01	0.01	0.03	0.02	0.02	0.02	0.02	0.02	0.03	0.01	0.03	0.02
K2O	0.01	<0.01	0.01	0.01	<0.01	<0.01	0.01	0.02	0.02	<0.01	0.02	<0.01	0.02	<0.01
Total	98.7	98.6	98.5	96.5	98.3	98.5	98.9	98.7	96.3	98.4	95.7	99.0	98.5	98.7
Si	1.96	1.96	1.97	1.89	1.96	1.97	1.97	1.97	1.94	1.97	2.01	1.96	1.98	1.99
Ti	0.007	0.007	0.007	0.038	0.008	0.008	0.007	0.008	0.006	0.007	0.008	0.007	0.007	0.006
Al	0.11	0.11	0.10	0.11	0.11	0.09	0.10	0.10	0.10	0.09	0.10	0.09	0.08	0.07
Cr	0.017	0.018	0.017	0.018	0.016	0.014	0.016	0.016	0.014	0.014	0.017	0.014	0.014	0.012
Fe3	<0.001	<0.001	<0.001	<0.001	<0.001	<0.001	<0.001	<0.001	<0.001	<0.001	<0.001	<0.001	<0.001	<0.001
Fe2	0.15	0.15	0.14	0.14	0.15	0.15	0.15	0.16	0.17	0.15	0.15	0.16	0.15	0.15
Mn	0.004	0.005	0.002	0.003	0.003	0.004	0.004	0.002	0.005	0.003	0.005	0.003	0.004	0.002
Ni	0.001	0.002	0.002	0.004	0.002	0.003	0.001	0.002	0.002	0.001	0.001	0.001	0.002	0.001
Mg	1.73	1.72	1.73	1.76	1.72	1.73	1.73	1.71	1.74	1.74	1.67	1.72	1.73	1.75
Ca	0.025	0.035	0.036	0.023	0.031	0.028	0.027	0.031	0.025	0.027	0.029	0.031	0.034	0.025
Na	<0.001	0.002	<0.001	<0.001	0.002	0.002	0.001	0.001	0.002	0.001	0.002	0.001	0.002	0.001
K	0.001	<0.001	<0.001	<0.001	<0.001	<0.001	<0.001	0.001	0.001	<0.001	0.001	<0.001	0.001	<0.001

Sample L13

distance	15	30	45	90	120	180	195	285	315	345	360	375	390	405
SiO2	56.6	56.9	56.5	56.2	56.0	56.2	55.9	56.0	56.0	55.9	56.5	56.1	56.5	55.8
TiO2	0.32	0.28	0.32	0.34	0.33	0.32	0.32	0.31	0.22	0.21	0.25	0.25	0.29	0.25
Al2O3	2.2	1.9	2.2	2.6	2.7	2.6	2.6	2.6	2.7	2.4	2.8	2.8	2.6	3.2
Cr2O3	0.46	0.49	0.46	0.61	0.56	0.59	0.56	0.60	0.61	0.56	0.64	0.56	0.65	0.70
Fe2O3	<0.01	<0.01	<0.01	<0.01	<0.01	0.17	0.08	<0.01	0.20	0.27	<0.01	<0.01	<0.01	<0.01
FeO	6.8	7.0	7.0	7.4	7.1	7.2	7.1	7.0	7.2	6.8	6.8	7.2	6.9	7.0
MnO	0.18	0.13	0.23	0.20	0.18	0.22	0.21	0.17	0.22	0.15	0.14	0.12	0.17	0.11
NiO	0.10	0.10	0.10	0.04	0.05	0.08	0.05	0.09	0.08	0.07	0.08	0.09	0.10	0.11
MgO	33.2	33.3	33.4	32.9	32.6	33.1	33.0	33.0	33.1	33.3	33.5	33.1	32.9	32.8
CaO	0.83	0.58	0.65	0.85	0.84	0.64	0.59	0.54	0.58	0.49	0.52	0.51	0.87	0.60
Na2O	0.03	0.02	0.01	0.03	0.02	0.02	0.02	0.04	0.01	0.01	0.02	0.01	0.04	0.04
K2O	0.01	<0.01	<0.01	<0.01	<0.01	0.01	<0.01	0.01	<0.01	<0.01	<0.01	<0.01	0.02	0.01
Total	100.7	100.7	100.8	101.1	100.3	101.2	100.4	100.4	100.9	100.1	101.3	100.7	101.1	100.6
Si	1.95	1.96	1.94	1.93	1.94	1.93	1.93	1.94	1.93	1.93	1.93	1.93	1.94	1.93
Ti	0.008	0.007	0.008	0.009	0.009	0.008	0.008	0.008	0.006	0.005	0.006	0.007	0.007	0.007
Al	0.09	0.08	0.09	0.11	0.11	0.10	0.10	0.11	0.11	0.10	0.11	0.11	0.11	0.13
Cr	0.013	0.013	0.013	0.017	0.015	0.016	0.015	0.016	0.017	0.015	0.017	0.015	0.018	0.019
Fe3	<0.001	<0.001	<0.001	<0.001	<0.001	0.005	0.002	<0.001	0.005	0.007	<0.001	<0.001	<0.001	<0.001
Fe2	0.20	0.20	0.20	0.21	0.21	0.21	0.21	0.20	0.21	0.20	0.19	0.21	0.20	0.20
Mn	0.005	0.004	0.007	0.006	0.005	0.007	0.006	0.005	0.006	0.004	0.004	0.004	0.005	0.003
Ni	0.003	0.003	0.003	0.001	0.001	0.002	0.001	0.002	0.002	0.002	0.002	0.003	0.003	0.003
Mg	1.71	1.71	1.71	1.68	1.68	1.70	1.70	1.70	1.70	1.72	1.71	1.70	1.68	1.68
Ca	0.031	0.021	0.024	0.031	0.031	0.024	0.022	0.020	0.021	0.018	0.019	0.019	0.032	0.022
Na	0.002	0.002	0.001	0.002	0.001	0.001	0.001	0.003	0.001	0.001	0.001	0.001	0.002	0.003
K	<0.001	<0.001	<0.001	<0.001	<0.001	<0.001	<0.001	0.001	<0.001	<0.001	<0.001	<0.001	0.001	0.001

A2.6a: Orthopyroxene profils

Sample L13

distance	**420**	**435**	**450**	**465**	**510**	**540**	**555**	**570**	**585**	**600**	**615**	**645**	**660**	**690**
SiO2	56.2	56.1	56.0	56.0	55.7	55.9	55.9	55.8	55.8	55.5	55.3	55.5	55.2	55.3
TiO2	0.30	0.28	0.25	0.28	0.26	0.29	0.27	0.29	0.24	0.28	0.25	0.26	0.32	0.27
Al2O3	2.6	2.8	3.0	2.9	3.2	3.1	3.1	3.1	3.0	3.3	3.1	3.0	3.3	3.2
Cr2O3	0.60	0.62	0.67	0.66	0.68	0.65	0.75	0.72	0.71	0.68	0.64	0.63	0.62	0.72
Fe2O3	<0.01	<0.01	<0.01	<0.01	<0.01	<0.01	<0.01	<0.01	<0.01	0.14	0.62	<0.01	0.53	0.67
FeO	7.3	7.4	7.5	7.2	7.1	6.9	7.1	7.1	7.0	7.1	6.7	7.0	6.8	6.8
MnO	0.14	0.22	0.12	0.18	0.22	0.21	0.16	0.23	0.14	0.17	0.16	0.19	0.18	0.23
NiO	0.06	0.10	0.12	0.10	0.09	0.10	0.16	0.09	0.08	0.10	0.07	0.08	0.09	0.07
MgO	33.1	33.0	32.9	32.9	32.8	32.6	32.7	32.6	32.9	32.7	32.8	32.8	32.8	32.7
CaO	0.59	0.57	0.60	0.60	0.62	0.72	0.65	0.80	0.59	0.68	0.58	0.58	0.65	0.67
Na2O	0.01	0.04	0.01	0.01	0.01	0.05	0.02	0.01	0.03	0.01	0.03	0.02	<0.01	0.03
K2O	<0.01	<0.01	<0.01	<0.01	<0.01	<0.01	0.01	0.01	<0.01	0.01	<0.01	<0.01	<0.01	<0.01
Total	100.9	101.2	101.1	100.8	100.7	100.5	100.9	100.7	100.5	100.7	100.3	100.0	100.4	100.6
Si	1.93	1.93	1.93	1.93	1.92	1.93	1.93	1.93	1.93	1.92	1.91	1.92	1.91	1.91
Ti	0.008	0.007	0.007	0.007	0.007	0.008	0.007	0.007	0.006	0.007	0.006	0.007	0.008	0.007
Al	0.11	0.12	0.12	0.12	0.13	0.13	0.13	0.13	0.12	0.13	0.13	0.12	0.13	0.13
Cr	0.016	0.017	0.018	0.018	0.019	0.018	0.020	0.020	0.019	0.019	0.018	0.017	0.017	0.020
Fe3	<0.001	<0.001	<0.001	<0.001	<0.001	<0.001	<0.001	<0.001	<0.001	0.004	0.016	<0.001	0.014	0.018
Fe2	0.21	0.21	0.21	0.21	0.20	0.20	0.21	0.20	0.20	0.21	0.20	0.20	0.20	0.20
Mn	0.004	0.006	0.004	0.005	0.006	0.006	0.005	0.007	0.004	0.005	0.005	0.006	0.005	0.007
Ni	0.002	0.003	0.003	0.003	0.003	0.003	0.004	0.002	0.002	0.003	0.002	0.002	0.002	0.002
Mg	1.70	1.69	1.69	1.69	1.69	1.68	1.68	1.68	1.69	1.68	1.69	1.69	1.69	1.69
Ca	0.022	0.021	0.022	0.022	0.023	0.027	0.024	0.029	0.022	0.025	0.021	0.022	0.024	0.025
Na	0.001	0.003	0.001	0.001	0.001	0.003	0.001	0.000	0.002	0.001	0.002	0.002	<0.001	0.002
K	<0.001	<0.001	<0.001	<0.001	<0.001	<0.001	<0.001	<0.001	<0.001	0.001	<0.001	<0.001	<0.001	<0.001

Sample L13

distance	**705**	**720**	**735**	**765**	**795**	**810**	**825**	**840**	**855**	**870**	**885**	**900**	**915**	**945**
SiO2	55.3	55.4	56.4	55.8	55.7	54.3	55.8	55.8	56.0	55.4	55.6	55.0	55.6	55.4
TiO2	0.27	0.29	0.20	0.26	0.28	0.23	0.23	0.25	0.23	0.26	0.23	0.24	0.27	0.22
Al2O3	2.9	3.2	2.6	3.2	3.1	2.8	3.0	3.1	3.3	3.6	3.3	3.3	2.9	3.2
Cr2O3	0.61	0.76	0.64	0.68	0.69	0.59	0.68	0.66	0.69	0.73	0.73	0.70	0.58	0.67
Fe2O3	0.65	0.03	<0.01	<0.01	0.39	0.69	<0.01	<0.01	<0.01	<0.01	<0.01	0.73	<0.01	0.57
FeO	6.5	7.2	7.0	7.3	7.2	6.4	6.8	7.3	7.4	7.0	7.2	6.8	7.5	6.9
MnO	0.14	0.17	0.15	0.12	0.17	0.19	0.18	0.20	0.16	0.15	0.19	0.22	0.23	0.13
NiO	0.11	0.15	0.09	0.08	0.08	0.05	0.11	0.03	0.08	0.03	0.07	0.09	0.03	0.06
MgO	32.9	32.6	33.2	32.6	32.9	32.3	32.7	32.6	32.9	32.5	32.7	32.6	32.2	32.8
CaO	0.72	0.62	0.46	0.83	0.65	0.65	0.56	0.60	0.46	0.65	0.59	0.58	0.98	0.66
Na2O	0.01	0.02	0.02	0.03	0.00	0.02	0.03	0.01	0.02	0.03	<0.01	0.02	0.04	0.02
K2O	0.01	<0.01	<0.01	<0.01	0.01	0.02	<0.01	0.01	0.01	0.02	<0.01	<0.01	<0.01	0.01
Total	100.1	100.4	100.7	100.9	101.1	98.2	100.2	100.5	101.2	100.4	100.7	100.2	100.3	100.6
Si	1.92	1.92	1.94	1.92	1.92	1.92	1.93	1.93	1.92	1.92	1.92	1.91	1.93	1.91
Ti	0.007	0.007	0.005	0.007	0.007	0.006	0.006	0.006	0.006	0.007	0.006	0.006	0.007	0.006
Al	0.12	0.13	0.11	0.13	0.13	0.12	0.12	0.13	0.13	0.15	0.13	0.14	0.12	0.13
Cr	0.017	0.021	0.018	0.019	0.019	0.016	0.019	0.018	0.019	0.020	0.020	0.019	0.016	0.018
Fe3	0.017	0.001	<0.001	<0.001	0.010	0.018	<0.001	<0.001	<0.001	<0.001	<0.001	0.019	<0.001	0.015
Fe2	0.19	0.21	0.20	0.21	0.21	0.19	0.20	0.21	0.21	0.20	0.21	0.20	0.22	0.20
Mn	0.004	0.005	0.004	0.004	0.005	0.006	0.005	0.006	0.005	0.005	0.006	0.006	0.007	0.004
Ni	0.003	0.004	0.003	0.002	0.002	0.002	0.003	0.001	0.002	0.001	0.002	0.003	0.001	0.002
Mg	1.70	1.68	1.70	1.67	1.68	1.70	1.69	1.68	1.68	1.68	1.68	1.68	1.67	1.69
Ca	0.027	0.023	0.017	0.031	0.024	0.025	0.021	0.022	0.017	0.024	0.022	0.022	0.036	0.025
Na	0.001	0.001	0.001	0.002	<0.001	0.002	0.002	0.001	0.002	0.002	<0.001	0.001	0.003	0.001
K	<0.001	<0.001	<0.001	<0.001	0.001	0.001	<0.001	<0.001	<0.001	0.001	<0.001	<0.001	<0.001	<0.001

A2.6a: Orthopyroxene profils

Sample L13

distance	960	975	990	1020	1035	1050	1110	1140	1200	1260	1275	1305	1335	1365
SiO2	55.5	55.6	55.2	55.1	55.7	55.8	55.7	55.4	55.7	55.7	55.4	55.9	55.7	55.5
TiO2	0.24	0.29	0.26	0.28	0.19	0.26	0.26	0.25	0.21	0.23	0.28	0.34	0.30	0.28
Al2O3	3.3	3.3	3.3	3.4	3.0	3.1	3.1	3.3	3.1	2.8	3.3	3.1	3.1	3.2
Cr2O3	0.70	0.71	0.71	0.65	0.70	0.74	0.72	0.77	0.72	0.71	0.77	0.73	0.76	0.71
Fe2O3	0.08	0.05	0.38	0.48	<0.01	<0.01	<0.01	<0.01	<0.01	<0.01	<0.01	<0.01	<0.01	<0.01
FeO	6.9	7.2	6.9	6.7	6.9	6.9	7.2	7.2	7.1	7.2	7.1	7.2	7.2	7.3
MnO	0.17	0.09	0.14	0.12	0.24	0.21	0.09	0.18	0.24	0.20	0.15	0.20	0.12	0.20
NiO	0.08	0.10	0.08	0.10	0.10	0.11	0.14	0.13	0.08	0.10	0.07	0.08	0.12	0.08
MgO	32.8	32.6	32.6	32.7	32.8	32.6	32.7	32.5	32.8	32.7	32.5	31.4	32.0	32.4
CaO	0.67	0.77	0.71	0.79	0.61	0.69	0.55	0.61	0.60	0.63	0.73	0.89	0.61	0.71
Na2O	0.04	0.04	0.02	0.01	0.01	0.03	0.01	0.03	0.03	0.01	0.03	0.11	0.05	0.03
K2O	0.01	<0.01	<0.01	<0.01	0.01	<0.01	<0.01	0.02	<0.01	<0.01	<0.01	<0.01	<0.01	<0.01
Total	100.5	100.7	100.3	100.3	100.2	100.5	100.4	100.3	100.6	100.4	100.3	100.0	100.0	100.3
Si	1.92	1.92	1.91	1.91	1.93	1.93	1.93	1.92	1.92	1.93	1.92	1.95	1.94	1.92
Ti	0.006	0.008	0.007	0.007	0.005	0.007	0.007	0.007	0.005	0.006	0.007	0.009	0.008	0.007
Al	0.13	0.13	0.14	0.14	0.12	0.13	0.13	0.13	0.13	0.12	0.13	0.13	0.13	0.13
Cr	0.019	0.019	0.020	0.018	0.019	0.020	0.020	0.021	0.020	0.019	0.021	0.020	0.021	0.019
Fe3	0.002	0.001	0.010	0.013	<0.001	<0.001	<0.001	<0.001	<0.001	<0.001	<0.001	<0.001	<0.001	<0.001
Fe2	0.20	0.21	0.20	0.19	0.20	0.20	0.21	0.21	0.21	0.21	0.21	0.21	0.21	0.21
Mn	0.005	0.003	0.004	0.004	0.007	0.006	0.003	0.005	0.007	0.006	0.004	0.006	0.004	0.006
Ni	0.002	0.003	0.002	0.003	0.003	0.003	0.004	0.004	0.002	0.003	0.002	0.002	0.003	0.002
Mg	1.69	1.68	1.68	1.69	1.69	1.68	1.69	1.68	1.69	1.69	1.68	1.63	1.66	1.67
Ca	0.025	0.029	0.026	0.029	0.023	0.025	0.020	0.023	0.022	0.024	0.027	0.033	0.023	0.026
Na	0.002	0.003	0.002	0.001	0.001	0.002	0.001	0.002	0.002	0.001	0.002	0.008	0.003	0.002
K	0.001	<0.001	<0.001	<0.001	<0.001	<0.001	<0.001	0.001	<0.001	<0.001	<0.001	<0.001	<0.001	<0.001

Sample L13

distance	1380	1395	1440	1455	1485	1500	1515	1530	1545	1560	1575	1620	1665	1695
SiO2	55.8	55.4	55.6	55.7	55.8	56.0	56.2	55.6	55.7	55.6	55.6	55.3	55.5	57.1
TiO2	0.27	0.28	0.27	0.32	0.29	0.27	0.31	0.30	0.32	0.29	0.28	0.27	0.30	0.28
Al2O3	3.1	3.1	2.8	3.1	3.1	3.0	2.9	3.1	3.1	3.1	3.1	3.1	3.1	3.0
Cr2O3	0.74	0.72	0.70	0.72	0.73	0.68	0.70	0.70	0.73	0.75	0.74	0.70	0.74	0.71
Fe2O3	<0.01	0.17	<0.01	0.19	<0.01	<0.01	<0.01	0.05	<0.01	<0.01	<0.01	0.86	0.42	0.76
FeO	7.2	7.0	7.1	7.3	7.2	7.2	7.3	7.0	6.7	7.0	7.1	6.8	6.8	6.3
MnO	0.17	0.15	0.19	0.15	0.09	0.18	0.15	0.13	0.10	0.14	0.13	0.19	0.20	0.17
NiO	0.09	0.09	0.13	0.10	0.10	0.07	0.07	0.13	0.10	0.08	0.07	0.05	0.09	0.06
MgO	32.9	32.6	31.9	32.8	32.7	32.8	32.8	32.8	32.5	32.7	32.4	32.8	32.7	34.2
CaO	0.64	0.76	0.73	0.65	0.67	0.67	0.67	0.78	0.85	0.82	0.69	0.67	0.87	0.63
Na2O	0.01	0.02	0.06	0.02	0.02	<0.01	0.02	0.04	0.02	0.05	0.03	0.01	0.03	0.03
K2O	0.02	<0.01	0.01	<0.01	<0.01	<0.01	0.01	<0.01	0.01	<0.01	<0.01	0.01	0.02	0.01
Total	100.9	100.3	99.5	100.9	100.7	100.8	101.0	100.5	100.2	100.6	100.2	100.8	100.7	103.2
Si	1.92	1.92	1.94	1.92	1.92	1.93	1.93	1.92	1.93	1.92	1.93	1.91	1.92	1.92
Ti	0.007	0.007	0.007	0.008	0.008	0.007	0.008	0.008	0.008	0.008	0.007	0.007	0.008	0.007
Al	0.13	0.13	0.12	0.12	0.13	0.12	0.12	0.12	0.13	0.13	0.13	0.13	0.12	0.12
Cr	0.020	0.020	0.019	0.020	0.020	0.018	0.019	0.019	0.020	0.020	0.020	0.019	0.020	0.019
Fe3	<0.001	0.004	<0.001	0.005	<0.001	<0.001	<0.001	0.001	<0.001	<0.001	<0.001	0.022	0.011	0.019
Fe2	0.21	0.20	0.21	0.21	0.21	0.21	0.21	0.20	0.19	0.20	0.21	0.20	0.20	0.18
Mn	0.005	0.004	0.006	0.004	0.003	0.005	0.004	0.004	0.003	0.004	0.004	0.006	0.006	0.005
Ni	0.003	0.003	0.004	0.003	0.003	0.002	0.002	0.004	0.003	0.002	0.002	0.001	0.002	0.002
Mg	1.69	1.68	1.66	1.68	1.68	1.68	1.68	1.69	1.68	1.68	1.68	1.69	1.68	1.71
Ca	0.024	0.028	0.027	0.024	0.025	0.025	0.025	0.029	0.032	0.031	0.026	0.025	0.032	0.023
Na	0.001	0.001	0.004	0.001	0.001	<0.001	0.001	0.003	0.001	0.003	0.002	0.001	0.002	0.002
K	0.001	<0.001	0.001	<0.001	<0.001	<0.001	<0.001	<0.001	<0.001	<0.001	<0.001	<0.001	0.001	<0.001

A2.6a: Orthopyroxene profils

Sample L13

distance	**1740**	**1770**	**1800**	**1815**	**1860**	**1875**	**1890**	**1905**	**1920**	**1950**	**1995**	**2010**
SiO2	55.9	55.8	55.8	56.1	55.6	55.4	55.6	55.8	55.7	56.1	56.3	56.1
TiO2	0.30	0.32	0.31	0.28	0.33	0.32	0.32	0.34	0.34	0.32	0.33	0.30
Al2O3	3.0	3.0	2.8	2.6	2.8	2.9	2.9	2.9	3.0	2.9	2.6	2.7
Cr2O3	0.68	0.65	0.65	0.59	0.65	0.60	0.61	0.65	0.65	0.62	0.57	0.53
Fe2O3	<0.01	0.03	0.18	<0.01	0.31	0.71	0.67	0.20	<0.01	<0.01	0.06	0.08
FeO	7.2	7.3	7.1	6.8	6.8	6.5	6.7	7.3	7.3	7.1	7.2	7.2
MnO	0.15	0.20	0.18	0.17	0.18	0.20	0.18	0.20	0.15	0.20	0.20	0.16
NiO	0.10	0.06	0.10	0.09	0.07	0.10	0.10	0.09	0.04	0.07	0.08	0.10
MgO	32.7	32.6	32.8	32.9	32.8	32.9	32.9	32.9	32.6	32.5	33.2	33.0
CaO	0.72	0.83	0.84	0.73	0.98	0.71	0.79	0.66	0.81	0.89	0.63	0.63
Na2O	0.03	0.03	0.03	0.01	0.02	0.03	0.01	<0.01	0.02	0.01	0.04	0.04
K2O	<0.01	<0.01	<0.01	<0.01	<0.01	0.01	0.01	<0.01	0.01	<0.01	0.02	0.01
Total	100.8	100.8	100.7	100.3	100.5	100.5	100.8	100.9	100.6	100.7	101.2	100.8
Si	1.93	1.92	1.92	1.94	1.92	1.92	1.92	1.92	1.92	1.94	1.93	1.93
Ti	0.008	0.008	0.008	0.007	0.009	0.008	0.008	0.009	0.009	0.008	0.009	0.008
Al	0.12	0.12	0.11	0.10	0.11	0.12	0.12	0.12	0.12	0.12	0.10	0.11
Cr	0.018	0.018	0.018	0.016	0.018	0.016	0.017	0.018	0.018	0.017	0.015	0.015
Fe3	<0.001	0.001	0.005	<0.001	0.008	0.019	0.017	0.005	<0.001	<0.001	0.001	0.002
Fe2	0.21	0.21	0.20	0.20	0.20	0.19	0.19	0.21	0.21	0.20	0.21	0.21
Mn	0.004	0.006	0.005	0.005	0.005	0.006	0.005	0.006	0.004	0.006	0.006	0.005
Ni	0.003	0.002	0.003	0.003	0.002	0.003	0.003	0.003	0.001	0.002	0.002	0.003
Mg	1.68	1.68	1.69	1.70	1.69	1.70	1.69	1.69	1.68	1.67	1.70	1.69
Ca	0.027	0.031	0.031	0.027	0.036	0.026	0.029	0.025	0.030	0.033	0.023	0.023
Na	0.002	0.002	0.002	0.001	0.001	0.002	0.001	<0.001	0.001	0.001	0.003	0.003
K	<0.001	<0.001	<0.001	<0.001	<0.001	<0.001	0.001	<0.001	0.001	<0.001	0.001	<0.001

Sample L147

distance	**75**	**135**	**180**	**195**	**210**	**225**	**240**	**255**	**330**	**345**	**360**	**390**	**420**	**525**
SiO2	55.7	55.1	54.8	54.8	54.5	54.6	54.4	54.5	54.5	54.4	54.5	54.3	54.4	54.7
TiO2	0.25	0.24	0.22	0.25	0.24	0.28	0.23	0.25	0.24	0.24	0.19	0.23	0.26	0.22
Al2O3	1.2	1.5	1.8	1.9	2.0	1.9	1.9	2.0	2.0	2.0	2.0	2.1	2.0	2.1
Cr2O3	0.40	0.57	0.71	0.64	0.75	0.68	0.73	0.72	0.76	0.72	0.72	0.74	0.78	0.78
Fe2O3	0.50	0.47	<0.01	0.56	0.36	0.02	<0.01	0.21	<0.01	<0.01	<0.01	<0.01	<0.01	<0.01
FeO	6.4	6.4	6.7	6.6	6.3	6.7	6.5	6.4	6.8	6.8	6.9	6.6	6.9	6.7
MnO	0.18	0.14	0.18	0.12	0.14	0.12	0.17	0.19	0.13	0.16	0.07	0.15	0.12	0.12
NiO	0.04	0.10	0.12	0.05	0.05	0.08	0.06	0.09	0.10	0.03	0.10	0.04	0.09	0.11
MgO	33.2	32.8	32.5	32.6	32.5	32.5	32.3	32.5	32.4	32.1	32.3	32.4	32.3	32.3
CaO	0.77	0.63	0.53	0.54	0.65	0.68	0.58	0.57	0.55	0.80	0.68	0.76	0.78	0.84
Na2O	0.00	0.02	0.01	0.02	0.02	<0.01	0.03	<0.01	0.01	<0.01	0.02	0.02	0.03	<0.01
K2O	0.02	0.02	<0.01	0.02	<0.01	<0.01	<0.01	0.02	0.03	0.01	0.01	<0.01	0.01	0.02
Total	98.7	98.0	97.5	98.1	97.6	97.5	96.8	97.4	97.5	97.2	97.4	97.3	97.7	97.8
Si	1.96	1.95	1.95	1.94	1.94	1.94	1.95	1.94	1.94	1.94	1.9421	1.9359	1.9354	1.9394
Ti	0.007	0.006	0.006	0.007	0.006	0.008	0.006	0.007	0.006	0.006	0.005	0.006	0.007	0.006
Al	0.05	0.06	0.07	0.08	0.08	0.08	0.08	0.08	0.08	0.08	0.08	0.09	0.08	0.09
Cr	0.011	0.016	0.020	0.018	0.021	0.019	0.021	0.020	0.021	0.020	0.020	0.021	0.022	0.022
Fe3	0.013	0.013	<0.001	0.015	0.010	0.001	<0.001	0.006	<0.001	<0.001	<0.001	<0.001	<0.001	<0.001
Fe2	0.19	0.19	0.20	0.20	0.19	0.20	0.19	0.19	0.20	0.20	0.20	0.20	0.21	0.20
Mn	0.006	0.004	0.005	0.004	0.004	0.004	0.005	0.006	0.004	0.005	0.002	0.005	0.004	0.003
Ni	0.001	0.003	0.004	0.002	0.001	0.002	0.002	0.003	0.003	0.001	0.003	0.001	0.002	0.003
Mg	1.74	1.73	1.72	1.72	1.72	1.72	1.72	1.72	1.72	1.71	1.71	1.72	1.71	1.71
Ca	0.029	0.024	0.020	0.020	0.025	0.026	0.022	0.022	0.021	0.031	0.026	0.029	0.030	0.032
Na	0.000	0.001	0.001	0.002	0.001	<0.001	0.002	<0.001	0.001	<0.001	0.001	0.002	0.002	<0.001
K	0.001	0.001	<0.001	0.001	<0.001	<0.001	<0.001	0.001	0.001	<0.001	0.001	<0.001	<0.001	0.001

A2.6a: Orthopyroxene profils

Sample L147

distance	540	570	600	630	645	660	690	705	720	735	765	780	795	810
SiO2	54.0	54.2	54.2	54.0	54.1	54.3	54.2	54.0	54.2	54.5	54.2	54.3	54.2	54.1
TiO2	0.23	0.21	0.24	0.23	0.25	0.23	0.23	0.24	0.23	0.19	0.24	0.24	0.22	0.19
Al2O3	2.2	2.1	2.1	2.2	2.1	2.2	2.1	2.2	2.2	2.1	2.1	2.1	2.0	2.0
Cr2O3	0.78	0.81	0.77	0.74	0.78	0.82	0.78	0.76	0.73	0.73	0.77	0.73	0.79	0.75
Fe2O3	<0.01	<0.01	<0.01	<0.01	<0.01	<0.01	<0.01	<0.01	<0.01	<0.01	0.52	0.52	0.53	0.46
FeO	6.6	6.6	6.7	6.9	6.6	6.7	6.8	6.6	6.6	6.8	6.3	6.4	6.3	6.3
MnO	0.20	0.19	0.14	0.13	0.16	0.16	0.10	0.11	0.16	0.14	0.15	0.08	0.15	0.16
NiO	0.07	0.08	0.07	0.08	0.08	0.07	0.09	0.11	0.09	0.16	0.08	0.15	0.08	0.13
MgO	32.1	32.3	32.2	32.0	32.4	32.1	32.2	31.8	32.2	31.8	32.1	32.1	32.2	32.1
CaO	0.83	0.85	0.88	0.79	0.81	0.74	0.76	0.80	0.65	0.83	0.96	0.91	0.85	0.77
Na2O	0.02	<0.01	0.02	0.03	0.02	<0.01	0.01	0.01	<0.01	<0.01	0.01	0.03	<0.01	0.02
K2O	0.00	0.01	<0.01	0.01	0.01	<0.01	0.01	0.01	<0.01	0.01	0.01	0.03	<0.01	0.01
Total	96.9	97.3	97.4	97.1	97.3	97.3	97.3	96.6	97.1	97.3	97.4	97.6	97.4	97.1
Si	1.9325	1.9334	1.9337	1.933	1.9303	1.9365	1.9338	1.94	1.9371	1.9458	1.93	1.93	1.93	1.94
Ti	0.006	0.006	0.006	0.006	0.007	0.006	0.006	0.006	0.006	0.005	0.007	0.006	0.006	0.005
Al	0.09	0.09	0.09	0.09	0.09	0.09	0.09	0.09	0.09	0.09	0.09	0.09	0.08	0.09
Cr	0.022	0.023	0.022	0.021	0.022	0.023	0.022	0.021	0.020	0.020	0.022	0.021	0.022	0.021
Fe3	<0.001	<0.001	<0.001	<0.001	<0.001	<0.001	<0.001	<0.001	<0.001	<0.001	0.014	0.014	0.014	0.013
Fe2	0.20	0.20	0.20	0.21	0.20	0.20	0.20	0.20	0.20	0.20	0.19	0.19	0.19	0.19
Mn	0.006	0.006	0.004	0.004	0.005	0.005	0.003	0.003	0.005	0.004	0.005	0.002	0.004	0.005
NiO	0.002	0.002	0.002	0.002	0.002	0.002	0.002	0.003	0.003	0.005	0.002	0.004	0.002	0.004
Mg	1.71	1.72	1.71	1.71	1.72	1.71	1.72	1.70	1.72	1.69	1.71	1.70	1.71	1.71
Ca	0.032	0.032	0.034	0.030	0.031	0.028	0.029	0.031	0.025	0.032	0.037	0.035	0.033	0.030
Na	0.002	<0.001	0.002	0.002	0.001	<0.001	0.001	0.001	<0.001	<0.001	<0.001	0.002	<0.001	0.001
K	<0.001	<0.001	<0.001	0.001	0.001	<0.001	<0.001	<0.001	<0.001	<0.001	0.001	0.001	<0.001	0.001

Sample L147

distance	900	915	945	960	975	990	1005	1035	1050	1080	1110	1125	1140	1185
SiO2	54.4	54.4	54.4	54.5	54.0	54.4	54.1	54.4	54.6	54.5	54.7	54.3	54.4	54.6
TiO2	0.24	0.23	0.21	0.22	0.22	0.20	0.20	0.23	0.25	0.26	0.21	0.20	0.22	0.21
Al2O3	1.7	1.7	1.7	1.7	1.7	1.7	1.7	1.7	1.6	1.7	1.6	1.7	1.6	1.6
Cr2O3	0.75	0.76	0.75	0.77	0.75	0.74	0.72	0.77	0.74	0.72	0.71	0.75	0.72	0.68
Fe2O3	<0.01	0.11	0.33	0.51	0.92	0.28	0.77	0.80	0.30	1.04	0.40	1.23	0.99	<0.01
FeO	6.7	6.5	6.5	6.2	6.0	6.4	5.9	6.0	6.5	6.0	6.4	6.0	6.1	6.5
MnO	0.14	0.20	0.17	0.14	0.13	0.16	0.14	0.10	0.10	0.13	0.13	0.14	0.20	0.11
NiO	0.05	0.07	0.11	0.10	0.13	0.09	0.09	0.11	0.09	0.11	0.10	0.06	0.09	0.06
MgO	31.9	32.2	32.2	32.3	32.3	32.2	32.2	32.5	32.4	32.6	32.6	32.5	32.6	32.4
CaO	0.84	0.76	0.85	0.97	0.73	0.87	0.97	0.72	0.82	0.78	0.73	0.71	0.62	0.82
Na2O	<0.01	<0.01	<0.01	0.02	0.01	0.01	0.01	0.01	0.02	<0.01	0.01	0.04	0.01	0.03
K2O	<0.01	0.01	0.03	0.01	<0.01	<0.01	<0.01	0.01	<0.01	<0.01	<0.01	<0.01	0.01	0.01
Total	96.7	96.9	97.2	97.5	96.9	97.1	96.9	97.3	97.4	97.8	97.5	97.7	97.5	97.0
Si	1.95	1.95	1.95	1.94	1.94	1.95	1.94	1.94	1.95	1.93	1.95	1.93	1.94	1.95
Ti	0.006	0.006	0.006	0.006	0.006	0.005	0.005	0.006	0.007	0.007	0.006	0.005	0.006	0.006
Al	0.07	0.07	0.07	0.07	0.07	0.07	0.07	0.07	0.07	0.07	0.07	0.07	0.07	0.07
Cr	0.021	0.022	0.021	0.022	0.021	0.021	0.021	0.022	0.021	0.020	0.020	0.021	0.020	0.019
Fe3	<0.001	0.003	0.009	0.014	0.025	0.008	0.021	0.021	0.008	0.028	0.011	0.033	0.026	<0.001
Fe2	0.20	0.20	0.19	0.19	0.18	0.19	0.18	0.18	0.19	0.18	0.19	0.18	0.18	0.19
Mn	0.004	0.006	0.005	0.004	0.004	0.005	0.004	0.003	0.003	0.004	0.004	0.004	0.006	0.003
Ni	0.001	0.002	0.003	0.003	0.004	0.003	0.003	0.003	0.003	0.003	0.003	0.002	0.003	0.002
Mg	1.71	1.72	1.71	1.71	1.72	1.72	1.72	1.73	1.72	1.73	1.73	1.72	1.73	1.73
Ca	0.032	0.029	0.033	0.037	0.028	0.033	0.037	0.028	0.031	0.030	0.028	0.027	0.024	0.031
Na	<0.001	<0.001	<0.001	0.001	0.001	0.001	0.001	0.001	0.001	<0.001	0.001	0.003	0.001	0.002
K	<0.001	0.001	0.001	0.001	<0.001	<0.001	<0.001	<0.001	<0.001	<0.001	<0.001	<0.001	<0.001	0.001

Sample L147										Sample L241				
distance	**1200**	**1260**	**1380**	**1410**	**1425**	**1440**	**1455**	**1470**	**1485**	**distance**	**0**	**25**	**50**	**75**
SiO2	54.3	54.5	54.5	55.0	54.9	54.7	55.6	55.2	55.1	SiO2	52.5	56.4	55.9	55.8
TiO2	0.22	0.25	0.25	0.25	0.24	0.24	0.24	0.25	0.23	TiO2	0.25	0.21	0.21	0.21
Al2O3	1.6	1.5	1.4	1.3	1.3	1.3	1.2	1.4	1.3	Al2O3	2.1	2.2	2.6	2.8
Cr2O3	0.75	0.75	0.69	0.63	0.65	0.61	0.59	0.57	0.51	Cr2O3	0.45	0.57	0.59	0.70
Fe2O3	<0.01	<0.01	<0.01	<0.01	<0.01	<0.01	<0.01	<0.01	<0.01	Fe2O3	5.30	0.75	1.18	0.28
FeO	6.7	6.5	6.9	7.0	6.7	6.7	6.7	6.9	6.8	FeO	2.1	6.3	5.9	6.5
MnO	0.13	0.12	0.16	0.15	0.14	0.18	0.14	0.15	0.18	MnO	0.15	0.16	0.15	0.19
NiO	0.10	0.07	0.10	<0.01	0.08	0.10	0.07	0.08	0.05	NiO	0.10	0.10	0.09	0.03
MgO	32.1	32.5	32.5	32.6	32.5	32.7	32.8	32.7	33.0	MgO	33.6	34.0	33.7	33.2
CaO	0.78	0.79	0.73	0.87	0.79	0.68	0.80	0.73	0.60	CaO	0.46	0.49	0.56	0.72
Na2O	0.02	0.02	0.02	0.02	0.01	0.02	<0.01	0.03	<0.01	Na2O	0.03	<0.01	0.02	0.02
K2O	<0.01	0.01	0.01	0.02	0.01	0.02	<0.01	<0.01	0.01	K2O	<0.01	<0.01	<0.01	<0.01
Total	96.8	97.0	97.2	97.9	97.2	97.3	98.1	97.9	97.8	Total	97.1	101.1	100.9	100.5
Si	1.95	1.95	1.95	1.95	1.96	1.95	1.96	1.96	1.95	Si	1.87	1.93	1.92	1.93
Ti	0.006	0.007	0.007	0.007	0.006	0.006	0.006	0.007	0.006	Ti	0.007	0.006	0.006	0.005
Al	0.07	0.07	0.06	0.06	0.05	0.05	0.05	0.06	0.05	Al	0.09	0.09	0.10	0.11
Cr	0.021	0.021	0.019	0.018	0.018	0.017	0.016	0.016	0.014	Cr	0.013	0.016	0.016	0.019
Fe3	<0.001	<0.001	<0.001	<0.001	<0.001	<0.001	<0.001	<0.001	<0.001	Fe3	0.142	0.019	0.031	0.007
Fe2	0.20	0.19	0.20	0.21	0.20	0.20	0.20	0.20	0.20	Fe2	0.06	0.18	0.17	0.19
Mn	0.004	0.004	0.005	0.005	0.004	0.005	0.004	0.005	0.005	Mn	0.005	0.005	0.005	0.006
Ni	0.003	0.002	0.003	<0.001	0.002	0.003	0.002	0.002	0.001	Ni	0.003	0.003	0.002	0.001
Mg	1.72	1.73	1.73	1.72	1.73	1.74	1.73	1.73	1.75	Mg	1.79	1.73	1.72	1.71
Ca	0.030	0.030	0.028	0.033	0.030	0.026	0.030	0.028	0.023	Ca	0.018	0.018	0.021	0.027
Na	0.002	0.002	0.002	0.001	0.001	0.001	<0.001	0.002	<0.001	Na	0.002	<0.001	0.001	0.001
K	<0.001	0.001	0.001	0.001	<0.001	0.001	<0.001	<0.001	0.001	K	<0.001	<0.001	<0.001	<0.001

Sample L241														
distance	**100**	**125**	**200**	**225**	**250**	**300**	**325**	**350**	**375**	**400**	**450**	**625**	**650**	**750**
SiO2	55.9	55.7	55.8	55.6	55.7	55.3	55.2	55.4	55.5	55.4	55.5	55.5	55.6	55.2
TiO2	0.22	0.20	0.18	0.25	0.22	0.22	0.24	0.20	0.22	0.19	0.22	0.19	0.19	0.24
Al2O3	2.9	2.8	2.9	3.1	3.2	3.5	3.6	3.4	3.5	3.4	3.4	3.3	3.2	3.4
Cr2O3	0.69	0.60	0.57	0.66	0.66	0.67	0.73	0.72	0.72	0.69	0.66	0.67	0.64	0.69
Fe2O3	1.01	0.77	0.62	0.68	0.43	0.83	1.24	0.78	0.19	1.24	0.94	1.82	1.32	1.12
FeO	6.2	6.2	6.3	6.3	6.5	6.0	5.8	6.1	6.7	5.8	6.4	5.4	5.8	5.9
MnO	0.11	0.17	0.20	0.12	0.21	0.14	0.14	0.20	0.12	0.09	0.09	0.14	0.14	0.13
NiO	0.09	0.10	0.06	0.08	0.09	0.13	0.11	0.11	0.07	0.00	0.07	0.05	0.12	0.18
MgO	33.4	33.4	33.3	33.3	33.2	33.2	33.3	33.1	32.9	33.3	33.2	33.6	33.5	33.2
CaO	0.65	0.62	0.70	0.61	0.58	0.63	0.55	0.61	0.70	0.80	0.60	0.66	0.58	0.56
Na2O	0.03	0.03	0.01	0.02	0.01	0.02	0.04	0.03	0.02	0.03	<0.01	0.04	0.03	0.01
K2O	0.03	0.01	0.02	<0.01	<0.01	<0.01	0.01	<0.01	0.01	<0.01	<0.01	0.02	<0.01	<0.01
Total	101.2	100.6	100.5	100.7	100.9	100.6	100.9	100.8	100.7	100.9	101.1	101.3	101.1	100.7
Si	1.91	1.92	1.92	1.91	1.91	1.90	1.90	1.91	1.91	1.90	1.91	1.90	1.90	1.90
Ti	0.006	0.005	0.005	0.007	0.006	0.006	0.006	0.005	0.006	0.005	0.006	0.005	0.005	0.006
Al	0.12	0.11	0.12	0.13	0.13	0.14	0.14	0.14	0.14	0.14	0.14	0.13	0.13	0.14
Cr	0.019	0.016	0.015	0.018	0.018	0.018	0.020	0.020	0.020	0.019	0.018	0.018	0.017	0.019
Fe3	0.026	0.020	0.016	0.018	0.011	0.022	0.032	0.020	0.005	0.032	0.024	0.047	0.034	0.029
Fe2	0.18	0.18	0.18	0.18	0.19	0.17	0.17	0.18	0.19	0.17	0.18	0.15	0.17	0.17
Mn	0.003	0.005	0.006	0.004	0.006	0.004	0.004	0.006	0.004	0.003	0.003	0.004	0.004	0.004
Ni	0.003	0.003	0.002	0.002	0.002	0.004	0.003	0.003	0.002	0.000	0.002	0.002	0.003	0.005
Mg	1.71	1.71	1.71	1.71	1.70	1.70	1.70	1.70	1.69	1.70	1.70	1.71	1.71	1.71
Ca	0.024	0.023	0.026	0.023	0.021	0.023	0.020	0.022	0.026	0.030	0.022	0.024	0.021	0.021
Na	0.002	0.002	0.001	0.001	<0.001	0.001	0.002	0.002	0.001	0.002	<0.001	0.003	0.002	0.001
K	0.001	<0.001	0.001	<0.001	<0.001	<0.001	0.001	<0.001	<0.001	<0.001	<0.001	0.001	<0.001	<0.001

A2.6a: Orthopyroxene profils

Sample L241

distance	825	875	900	925	975	1000	1075	1100	1125	1150	1200	1225	1275	1300
SiO2	55.7	55.4	55.3	55.4	55.5	55.3	55.3	55.1	55.4	55.5	55.3	55.3	55.6	55.4
TiO2	0.19	0.22	0.22	0.21	0.22	0.23	0.20	0.23	0.21	0.21	0.26	0.20	0.21	0.20
Al2O3	3.2	3.3	3.4	3.4	3.4	3.4	3.4	3.5	3.4	3.1	3.4	3.6	3.2	3.4
Cr2O3	0.61	0.71	0.72	0.66	0.71	0.75	0.73	0.68	0.69	0.68	0.69	0.70	0.67	0.68
Fe2O3	0.49	1.13	1.20	0.56	1.25	1.67	1.63	1.51	1.51	1.34	0.88	1.03	1.01	1.30
FeO	6.2	5.9	5.7	6.1	5.9	5.5	5.4	5.7	5.7	5.7	6.2	5.9	5.9	5.8
MnO	0.14	0.06	0.17	0.17	0.20	0.17	0.13	0.14	0.14	0.19	0.15	0.19	0.15	0.16
NiO	0.11	0.09	0.13	0.10	0.11	0.07	0.13	0.13	0.12	0.07	0.08	0.10	0.04	0.10
MgO	33.4	33.4	33.4	33.2	33.4	33.5	33.5	33.2	33.4	33.6	33.2	33.2	33.4	33.4
CaO	0.54	0.63	0.63	0.58	0.61	0.73	0.61	0.69	0.71	0.60	0.64	0.61	0.71	0.69
Na2O	0.03	0.03	<0.01	0.02	0.01	0.01	0.03	0.02	0.03	0.01	0.01	0.01	0.03	<0.01
K2O	0.02	<0.01	<0.01	<0.01	<0.01	0.02	<0.01	<0.01	<0.01	<0.01	0.01	<0.01	0.01	<0.01
Total	100.5	100.7	100.8	100.5	101.4	101.4	101.0	100.8	101.2	100.9	100.7	100.9	100.9	101.1
Si	1.92	1.90	1.90	1.91	1.90	1.89	1.90	1.89	1.90	1.91	1.90	1.90	1.91	1.90
Ti	0.005	0.006	0.006	0.005	0.006	0.006	0.005	0.006	0.005	0.006	0.007	0.005	0.005	0.005
Al	0.13	0.13	0.14	0.14	0.14	0.14	0.14	0.14	0.14	0.13	0.14	0.15	0.13	0.14
Cr	0.017	0.019	0.020	0.018	0.019	0.020	0.020	0.019	0.019	0.019	0.019	0.019	0.018	0.019
Fe3	0.013	0.029	0.031	0.014	0.032	0.043	0.042	0.039	0.039	0.035	0.023	0.027	0.026	0.034
Fe2	0.18	0.17	0.16	0.18	0.17	0.16	0.16	0.16	0.16	0.16	0.18	0.17	0.17	0.17
Mn	0.004	0.002	0.005	0.005	0.006	0.005	0.004	0.004	0.004	0.005	0.004	0.006	0.005	0.005
Ni	0.003	0.002	0.004	0.003	0.003	0.002	0.004	0.004	0.003	0.002	0.002	0.003	0.001	0.003
Mg	1.71	1.71	1.71	1.71	1.70	1.71	1.71	1.70	1.70	1.72	1.70	1.70	1.71	1.71
Ca	0.020	0.023	0.023	0.022	0.022	0.027	0.023	0.025	0.026	0.022	0.024	0.022	0.026	0.025
Na	0.002	0.002	<0.001	0.002	0.001	0.001	0.002	0.001	0.002	<0.001	0.001	0.001	0.002	<0.001
K	0.001	<0.001	<0.001	<0.001	<0.001	0.001	<0.001	<0.001	<0.001	<0.001	<0.001	<0.001	<0.001	<0.001

Sample L241

distance	1350	1400	1450	1475	1550	1650	1675	1700	1725	1750	1775	1900	1925	2075
SiO2	55.3	55.2	55.5	55.5	55.3	55.3	55.3	55.0	55.0	55.0	55.1	55.2	55.2	55.4
TiO2	0.21	0.20	0.20	0.21	0.22	0.17	0.24	0.20	0.24	0.21	0.22	0.17	0.22	0.20
Al2O3	3.5	3.2	3.5	3.5	3.4	3.5	3.6	3.7	3.6	3.6	3.5	3.6	3.7	3.4
Cr2O3	0.71	0.67	0.72	0.76	0.71	0.71	0.73	0.75	0.77	0.72	0.76	0.72	0.76	0.71
Fe2O3	1.36	1.29	1.44	0.66	1.28	1.35	1.47	1.74	0.69	1.33	1.34	0.39	0.68	1.00
FeO	5.7	5.7	5.8	6.2	5.7	5.9	5.7	5.5	6.2	5.7	5.5	6.2	6.0	5.9
MnO	0.14	0.17	0.15	0.16	0.22	0.18	0.14	0.15	0.09	0.14	0.20	0.17	0.23	0.20
NiO	0.07	0.07	0.08	0.08	0.11	0.09	0.11	0.12	0.13	0.13	0.09	0.10	0.11	0.07
MgO	33.5	33.2	33.3	33.2	33.3	33.3	33.2	33.2	32.9	33.2	33.2	33.0	32.9	33.3
CaO	0.64	0.73	0.71	0.65	0.69	0.64	0.75	0.60	0.60	0.60	0.77	0.61	0.85	0.58
Na2O	<0.01	0.01	0.02	0.01	0.03	0.01	0.04	0.03	0.02	0.01	0.02	<0.01	0.02	0.02
K2O	0.01	<0.01	0.02	<0.01	<0.01	<0.01	0.01	0.01	<0.01	<0.01	0.01	0.02	<0.01	<0.01
Total	101.1	100.5	101.4	101.1	100.9	101.1	101.2	101.0	100.2	100.7	100.7	100.2	100.6	100.7
Si	1.90	1.90	1.90	1.90	1.90	1.90	1.89	1.89	1.90	1.89	1.90	1.91	1.90	1.90
Ti	0.006	0.005	0.005	0.005	0.006	0.004	0.006	0.005	0.006	0.005	0.006	0.005	0.006	0.005
Al	0.14	0.13	0.14	0.14	0.14	0.14	0.14	0.15	0.15	0.15	0.14	0.15	0.15	0.14
Cr	0.019	0.018	0.019	0.021	0.019	0.019	0.020	0.020	0.021	0.020	0.021	0.020	0.021	0.019
Fe3	0.035	0.033	0.037	0.017	0.033	0.035	0.038	0.045	0.018	0.034	0.035	0.010	0.018	0.026
Fe2	0.16	0.17	0.17	0.18	0.16	0.17	0.16	0.16	0.18	0.17	0.16	0.18	0.17	0.17
Mn	0.004	0.005	0.005	0.005	0.006	0.005	0.004	0.004	0.003	0.004	0.006	0.005	0.007	0.006
Ni	0.002	0.002	0.002	0.002	0.003	0.002	0.003	0.003	0.004	0.004	0.002	0.003	0.003	0.002
Mg	1.71	1.71	1.70	1.70	1.71	1.70	1.70	1.70	1.70	1.70	1.70	1.70	1.69	1.71
Ca	0.024	0.027	0.026	0.024	0.025	0.024	0.028	0.022	0.022	0.022	0.028	0.023	0.031	0.022
Na	<0.001	0.001	0.001	<0.001	0.002	<0.001	0.002	0.002	0.001	0.001	0.001	<0.001	0.002	0.001
K	<0.001	<0.001	0.001	<0.001	<0.001	<0.001	0.001	<0.001	<0.001	<0.001	<0.001	0.001	<0.001	<0.001

A2.6a: Orthopyroxene profils

Sample L241

distance	2100	2125	2175	2200	2250	2375	2400	2425	2450	2500	2575	2625	2675	2700
SiO2	55.6	55.3	55.5	55.3	55.0	55.1	55.4	54.9	54.9	56.2	55.1	55.3	55.2	55.2
TiO2	0.19	0.19	0.22	0.21	0.18	0.20	0.18	0.21	0.21	0.17	0.21	0.19	0.21	0.16
Al2O3	3.5	3.5	3.4	3.6	3.6	3.6	3.8	3.8	3.7	4.0	3.9	3.7	3.7	3.8
Cr2O3	0.75	0.70	0.70	0.77	0.79	0.75	0.77	0.78	0.75	0.72	0.77	0.74	0.74	0.72
Fe2O3	0.62	0.50	1.02	1.08	1.10	1.08	0.59	0.88	1.40	1.69	0.76	0.70	0.82	0.91
FeO	6.1	6.1	5.9	5.9	5.8	5.8	6.3	6.0	5.6	5.4	5.8	6.1	6.0	5.8
MnO	0.24	0.10	0.10	0.08	0.20	0.08	0.21	0.18	0.17	0.13	0.19	0.14	0.10	0.19
NiO	0.11	0.08	0.13	0.07	0.12	0.11	0.06	0.10	0.12	0.08	0.11	0.11	0.12	0.08
MgO	33.2	33.3	33.2	33.2	33.0	33.2	32.9	32.8	33.0	34.0	33.1	33.1	33.1	33.2
CaO	0.66	0.64	0.80	0.76	0.76	0.71	0.72	0.80	0.82	0.62	0.63	0.70	0.69	0.65
Na2O	0.03	<0.01	0.02	0.02	0.04	<0.01	0.04	<0.01	0.02	0.03	0.03	<0.01	0.02	0.01
K2O	<0.01	<0.01	0.02	0.02	<0.01	0.02	<0.01	<0.01	<0.01	0.04	<0.01	0.02	<0.01	<0.01
Total	101.1	100.4	101.0	101.0	100.6	100.6	101.0	100.6	100.6	103.0	100.6	100.7	100.7	100.7
Si	1.91	1.91	1.90	1.90	1.90	1.90	1.90	1.89	1.89	1.89	1.90	1.90	1.90	1.90
Ti	0.005	0.005	0.006	0.005	0.005	0.005	0.005	0.005	0.005	0.004	0.006	0.005	0.005	0.004
Al	0.14	0.14	0.14	0.14	0.15	0.15	0.15	0.16	0.15	0.16	0.16	0.15	0.15	0.15
Cr	0.020	0.019	0.019	0.021	0.022	0.021	0.021	0.021	0.021	0.019	0.021	0.020	0.020	0.020
Fe3	0.016	0.013	0.026	0.028	0.028	0.028	0.015	0.023	0.037	0.043	0.020	0.018	0.021	0.024
Fe2	0.18	0.17	0.17	0.17	0.17	0.17	0.18	0.17	0.16	0.15	0.17	0.18	0.17	0.17
Mn	0.007	0.003	0.003	0.002	0.006	0.002	0.006	0.005	0.005	0.004	0.005	0.004	0.003	0.006
Ni	0.003	0.002	0.004	0.002	0.003	0.003	0.002	0.003	0.004	0.002	0.003	0.003	0.003	0.002
Mg	1.70	1.71	1.70	1.70	1.69	1.70	1.69	1.69	1.69	1.71	1.70	1.70	1.70	1.70
Ca	0.024	0.024	0.029	0.028	0.028	0.026	0.027	0.030	0.030	0.023	0.023	0.026	0.026	0.024
Na	0.002	<0.001	0.001	0.001	0.003	<0.001	0.003	<0.001	0.001	0.002	0.002	<0.001	0.002	0.001
K	<0.001	<0.001	0.001	0.001	<0.001	0.001	<0.001	<0.001	<0.001	0.002	<0.001	0.001	<0.001	<0.001

Sample L241

distance	2725	2750	2775	2800	2850	2875	2925	2950	3000	3025	3050	3100	3125	3150
SiO2	55.2	55.1	54.9	54.5	54.9	54.8	55.4	54.9	55.1	55.1	54.9	55.1	55.0	54.7
TiO2	0.21	0.17	0.19	0.21	0.19	0.22	0.18	0.21	0.19	0.19	0.20	0.18	0.21	0.17
Al2O3	3.7	3.8	3.8	4.1	3.9	3.9	3.7	3.5	3.8	3.8	3.9	4.0	4.0	4.1
Cr2O3	0.73	0.74	0.76	0.76	0.80	0.79	0.70	0.70	0.75	0.74	0.78	0.75	0.76	0.82
Fe2O3	0.74	0.90	1.11	1.70	1.50	1.38	1.05	0.66	0.89	0.98	0.91	1.65	1.10	1.83
FeO	6.1	5.9	5.7	5.2	5.6	5.6	5.8	6.0	6.0	6.0	5.8	5.5	5.8	5.3
MnO	0.11	0.09	0.24	0.13	0.18	0.14	0.24	0.21	0.16	0.12	0.15	0.22	0.17	0.13
NiO	0.09	0.12	0.08	0.05	0.11	0.05	0.09	0.10	0.11	0.09	0.12	0.15	0.06	0.12
MgO	33.1	33.0	33.0	33.0	33.1	33.2	33.3	32.9	33.1	33.0	32.9	33.4	33.1	33.1
CaO	0.71	0.70	0.67	0.72	0.62	0.64	0.62	0.63	0.61	0.70	0.75	0.56	0.56	0.60
Na2O	0.01	0.04	0.03	0.03	0.02	0.01	0.01	0.01	<0.01	0.01	0.03	0.01	0.01	0.02
K2O	<0.01	0.01	0.02	0.02	0.01	<0.01	<0.01	<0.01	0.02	0.01	<0.01	<0.01	0.01	0.03
Total	100.8	100.5	100.6	100.3	100.9	100.7	101.0	99.9	100.6	100.8	100.5	101.4	100.8	100.9
Si	1.90	1.90	1.89	1.88	1.89	1.89	1.90	1.90	1.90	1.90	1.89	1.88	1.89	1.88
Ti	0.005	0.004	0.005	0.006	0.005	0.006	0.005	0.006	0.005	0.005	0.005	0.005	0.006	0.004
Al	0.15	0.15	0.16	0.16	0.16	0.16	0.15	0.14	0.15	0.15	0.16	0.16	0.16	0.17
Cr	0.020	0.020	0.021	0.021	0.022	0.021	0.019	0.019	0.020	0.020	0.021	0.020	0.021	0.022
Fe3	0.019	0.023	0.029	0.044	0.039	0.036	0.027	0.017	0.023	0.026	0.024	0.042	0.028	0.047
Fe2	0.18	0.17	0.16	0.15	0.16	0.16	0.17	0.17	0.17	0.17	0.17	0.16	0.17	0.15
Mn	0.003	0.003	0.007	0.004	0.005	0.004	0.007	0.006	0.005	0.004	0.004	0.007	0.005	0.004
Ni	0.002	0.003	0.002	0.002	0.003	0.001	0.002	0.003	0.003	0.002	0.003	0.004	0.002	0.003
Mg	1.70	1.70	1.69	1.70	1.70	1.70	1.70	1.70	1.70	1.69	1.69	1.70	1.70	1.70
Ca	0.026	0.026	0.025	0.027	0.023	0.024	0.023	0.023	0.023	0.026	0.028	0.020	0.021	0.022
Na	<0.001	0.003	0.002	0.002	0.001	0.001	0.001	0.001	<0.001	0.001	0.002	<0.001	0.001	0.001
K	<0.001	<0.001	0.001	0.001	0.001	<0.001	<0.001	<0.001	0.001	<0.001	<0.001	<0.001	0.001	0.001

A2.6a: Orthopyroxene profils

Sample L241

distance	3175	3200	3275	3300	3350	3425	3450	3475	3500	3525	3550	3575	3600	3650
SiO2	55.0	54.9	55.2	54.8	54.7	55.1	55.1	54.7	54.7	55.1	55.0	55.2	55.1	55.1
TiO2	0.20	0.20	0.21	0.20	0.18	0.17	0.17	0.16	0.22	0.21	0.21	0.21	0.22	0.21
Al2O3	4.1	3.9	3.9	4.0	4.1	3.9	4.0	4.0	3.9	3.8	3.8	3.8	3.8	3.8
Cr2O3	0.77	0.80	0.77	0.77	0.81	0.81	0.75	0.76	0.82	0.79	0.69	0.76	0.76	0.74
Fe2O3	1.21	1.44	0.61	1.50	1.12	1.19	0.54	1.11	1.48	1.63	0.94	0.68	0.95	1.23
FeO	5.9	5.8	6.5	5.8	6.0	5.9	6.4	5.8	5.4	5.7	5.8	6.2	6.0	5.9
MnO	0.17	0.11	0.13	0.16	0.17	0.18	0.12	0.16	0.16	0.14	0.13	0.22	0.15	0.14
NiO	0.09	0.13	0.09	0.05	0.13	0.08	0.14	0.11	0.09	0.13	0.12	0.15	0.11	0.08
MgO	33.1	33.0	32.9	33.0	32.8	33.1	32.9	32.8	33.1	33.1	33.1	32.9	33.1	33.2
CaO	0.65	0.78	0.63	0.67	0.67	0.64	0.61	0.74	0.74	0.62	0.56	0.70	0.58	0.59
Na2O	0.02	0.01	0.02	0.03	<0.01	0.01	<0.01	0.01	0.01	0.04	0.02	0.01	0.01	<0.01
K2O	<0.01	<0.01	<0.01	<0.01	0.02	<0.01	<0.01	0.02	0.01	0.02	0.02	<0.01	0.02	<0.01
Total	101.1	101.1	101.0	100.9	100.6	101.0	100.6	100.4	100.6	101.2	100.5	100.8	100.7	100.9
Si	1.89	1.89	1.90	1.89	1.89	1.89	1.90	1.89	1.89	1.89	1.90	1.90	1.90	1.89
Ti	0.005	0.005	0.006	0.005	0.005	0.004	0.004	0.004	0.006	0.005	0.005	0.005	0.006	0.006
Al	0.16	0.16	0.16	0.16	0.16	0.16	0.16	0.16	0.16	0.15	0.16	0.16	0.15	0.15
Cr	0.021	0.022	0.021	0.021	0.022	0.022	0.021	0.021	0.022	0.021	0.019	0.021	0.021	0.020
Fe3	0.031	0.037	0.016	0.039	0.029	0.031	0.014	0.029	0.038	0.042	0.024	0.018	0.025	0.032
Fe2	0.17	0.17	0.19	0.17	0.17	0.17	0.18	0.17	0.16	0.16	0.17	0.18	0.17	0.17
Mn	0.005	0.003	0.004	0.005	0.005	0.005	0.004	0.005	0.005	0.004	0.004	0.007	0.004	0.004
Ni	0.002	0.004	0.003	0.001	0.004	0.002	0.004	0.003	0.003	0.004	0.003	0.004	0.003	0.002
Mg	1.69	1.69	1.68	1.69	1.69	1.69	1.69	1.69	1.70	1.69	1.70	1.69	1.70	1.70
Ca	0.024	0.029	0.023	0.025	0.025	0.024	0.023	0.027	0.028	0.023	0.021	0.026	0.022	0.022
Na	0.001	<0.001	0.001	0.002	<0.001	0.001	<0.001	0.001	0.001	0.002	0.002	<0.001	0.001	<0.001
K	<0.001	<0.001	<0.001	<0.001	0.001	<0.001	<0.001	0.001	<0.001	0.001	0.001	<0.001	0.001	<0.001

Sample L241

distance	3675	3725	3775	3825	3850	3900	3925	3950	3975	4000	4025	4050	4075	4150
SiO2	55.1	55.1	55.2	55.2	55.2	55.2	55.0	55.1	54.9	54.8	54.9	55.4	55.0	54.9
TiO2	0.18	0.19	0.17	0.21	0.22	0.20	0.19	0.21	0.23	0.19	0.20	0.23	0.20	0.20
Al2O3	3.8	3.7	3.8	3.9	4.0	3.8	3.9	3.9	3.9	4.1	3.9	4.0	3.8	4.0
Cr2O3	0.70	0.76	0.78	0.77	0.76	0.73	0.80	0.76	0.87	0.81	0.78	0.80	0.82	0.81
Fe2O3	1.15	1.34	0.68	0.87	1.00	1.24	0.62	1.19	1.61	1.09	1.30	1.49	0.94	1.43
FeO	6.0	5.8	6.2	6.2	6.2	5.7	6.1	5.9	5.5	5.8	5.8	5.5	5.9	5.8
MnO	0.11	0.17	0.17	0.23	0.09	0.14	0.18	0.16	0.09	0.15	0.17	0.19	0.19	0.15
NiO	0.11	0.07	0.09	0.08	0.06	0.11	0.11	0.12	0.12	0.11	0.07	0.07	0.08	0.06
MgO	33.1	33.3	33.0	33.0	33.1	33.1	32.9	33.1	33.1	33.0	32.9	33.4	32.9	33.0
CaO	0.61	0.60	0.64	0.61	0.62	0.82	0.68	0.66	0.76	0.60	0.79	0.67	0.67	0.56
Na2O	<0.01	<0.01	0.01	0.02	<0.01	0.04	0.01	0.01	0.05	0.01	0.04	0.02	0.02	0.04
K2O	0.02	<0.01	<0.01	0.01	<0.01	<0.01	0.03	<0.01	<0.01	<0.01	<0.01	0.03	0.03	<0.01
Total	100.7	101.0	100.7	101.0	101.2	101.0	100.5	101.1	101.1	100.6	100.9	101.8	100.6	101.0
Si	1.90	1.89	1.90	1.90	1.89	1.89	1.90	1.89	1.88	1.89	1.89	1.89	1.89	1.89
Ti	0.005	0.005	0.004	0.006	0.006	0.005	0.005	0.005	0.006	0.005	0.005	0.006	0.005	0.005
Al	0.15	0.15	0.15	0.16	0.16	0.15	0.16	0.16	0.16	0.17	0.16	0.16	0.16	0.16
Cr	0.019	0.021	0.021	0.021	0.021	0.020	0.022	0.021	0.024	0.022	0.021	0.022	0.022	0.022
Fe3	0.030	0.035	0.018	0.023	0.026	0.032	0.016	0.031	0.042	0.028	0.034	0.038	0.024	0.037
Fe2	0.17	0.17	0.18	0.18	0.18	0.16	0.17	0.17	0.16	0.17	0.17	0.16	0.17	0.17
Mn	0.003	0.005	0.005	0.007	0.003	0.004	0.005	0.005	0.003	0.004	0.005	0.005	0.006	0.004
Ni	0.003	0.002	0.003	0.002	0.002	0.003	0.003	0.003	0.003	0.003	0.002	0.002	0.002	0.002
Mg	1.70	1.70	1.69	1.69	1.69	1.69	1.69	1.69	1.69	1.69	1.69	1.70	1.69	1.69
Ca	0.022	0.022	0.024	0.023	0.023	0.030	0.025	0.024	0.028	0.022	0.029	0.025	0.025	0.021
Na	<0.001	<0.001	<0.001	0.001	<0.001	0.003	0.001	<0.001	0.003	0.001	0.003	0.002	0.002	0.003
K	0.001	<0.001	<0.001	<0.001	<0.001	<0.001	0.001	<0.001	<0.001	<0.001	<0.001	0.001	0.001	<0.001

A2.6a: Orthopyroxene profils

Sample L241

distance	**4175**	**4275**	**4375**	**4400**	**4450**	**4475**	**4550**	**4575**	**4600**	**4625**	**4650**	**4750**	**4775**	**4800**
SiO2	55.3	55.2	54.9	55.1	55.0	55.0	55.1	55.1	55.2	54.9	55.2	54.9	55.1	55.0
TiO2	0.21	0.20	0.22	0.23	0.21	0.21	0.23	0.21	0.22	0.20	0.19	0.22	0.25	0.20
Al2O3	3.7	3.8	4.0	3.8	4.0	3.7	3.7	3.9	3.8	3.9	3.8	4.0	3.7	3.5
Cr2O3	0.78	0.76	0.77	0.79	0.79	0.82	0.74	0.80	0.74	0.83	0.80	0.83	0.77	0.67
Fe2O3	0.41	0.84	1.17	1.25	0.85	1.14	1.56	0.91	0.67	1.16	1.15	0.68	1.27	1.26
FeO	6.4	6.3	6.0	5.8	6.1	5.9	5.5	6.0	6.3	5.5	5.7	6.2	5.8	5.8
MnO	0.10	0.17	0.14	0.08	0.11	0.18	0.10	0.14	0.18	0.18	0.19	0.13	0.13	0.10
NiO	0.12	0.07	0.07	0.09	0.13	0.12	0.12	0.13	0.03	0.09	0.07	0.08	0.09	0.10
MgO	32.9	32.9	33.0	33.3	32.8	33.0	33.4	33.0	32.9	33.1	33.1	32.9	33.2	33.1
CaO	0.67	0.71	0.54	0.61	0.75	0.58	0.56	0.59	0.63	0.70	0.77	0.57	0.71	0.71
Na2O	0.03	0.02	0.02	<0.01	0.03	0.03	0.02	0.03	0.04	0.03	0.01	0.01	0.02	<0.01
K2O	0.01	<0.01	0.01	0.01	<0.01	0.02	0.01	<0.01	<0.01	<0.01	0.01	<0.01	0.01	<0.01
Total	100.5	100.9	100.9	101.0	100.8	100.8	101.1	100.8	100.8	100.6	101.0	100.5	101.0	100.4
Si	1.90	1.90	1.89	1.89	1.89	1.89	1.89	1.89	1.90	1.89	1.89	1.89	1.89	1.90
Ti	0.005	0.005	0.006	0.006	0.005	0.006	0.006	0.005	0.006	0.005	0.005	0.006	0.006	0.005
Al	0.15	0.15	0.16	0.16	0.16	0.15	0.15	0.16	0.16	0.16	0.15	0.16	0.15	0.14
Cr	0.021	0.021	0.021	0.022	0.022	0.022	0.020	0.022	0.020	0.023	0.022	0.023	0.021	0.018
Fe3	0.011	0.022	0.030	0.032	0.022	0.030	0.040	0.024	0.017	0.030	0.030	0.018	0.033	0.033
Fe2	0.18	0.18	0.17	0.17	0.18	0.17	0.16	0.17	0.18	0.16	0.16	0.18	0.17	0.17
Mn	0.003	0.005	0.004	0.002	0.003	0.005	0.003	0.004	0.005	0.005	0.005	0.004	0.004	0.003
Ni	0.003	0.002	0.002	0.003	0.004	0.003	0.003	0.004	0.001	0.002	0.002	0.002	0.003	0.003
Mg	1.69	1.69	1.69	1.70	1.68	1.70	1.71	1.69	1.69	1.70	1.70	1.69	1.70	1.70
Ca	0.025	0.026	0.020	0.023	0.028	0.022	0.021	0.022	0.023	0.026	0.028	0.021	0.026	0.026
Na	0.002	0.001	0.002	<0.001	0.002	0.002	0.001	0.002	0.003	0.002	0.001	0.001	0.002	<0.001
K	0.001	<0.001	<0.001	<0.001	<0.001	0.001	0.001	<0.001	<0.001	<0.001	0.001	<0.001	<0.001	<0.001

Sample L241								**Sample La2002-02**						
distance	**4825**	**4850**	**4875**	**4900**	**4950**	**4975**	**5025**	**distanc**	**0**	**15**	**90**	**120**	**135**	**150**
SiO2	55.3	55.2	55.2	55.5	55.7	55.8	56.4	SiO2	55.76	55.9	55.1	55.2	55.1	54.8
TiO2	0.16	0.22	0.22	0.23	0.22	0.24	0.14	TiO2	0.15	0.09	0.27	0.27	0.27	0.33
Al2O3	3.5	3.7	3.6	3.3	3.2	3.2	2.3	Al2O3	1.79	1.12	2.3	2.1	2.1	2.2
Cr2O3	0.69	0.78	0.72	0.71	0.66	0.67	0.55	Cr2O3	0.21	0.15	0.20	0.17	0.18	0.18
Fe2O3	0.86	1.14	1.19	0.94	1.00	0.83	1.09	Fe2O3	0	0.47	<0.01	<0.01	<0.01	<0.01
FeO	5.9	5.9	5.8	6.0	6.2	6.3	6.0	FeO	7.08	7.56	8.5	8.5	8.2	8.3
MnO	0.19	0.17	0.18	0.11	0.09	0.19	0.13	MnO	0.26	0.32	0.25	0.26	0.25	0.19
NiO	0.12	0.10	0.10	0.11	0.10	0.09	0.08	NiO	0.08	0.05	0.02	0.09	0.06	0.10
MgO	33.3	33.1	33.1	33.3	33.4	33.4	33.9	MgO	32.78	32.67	31.7	31.6	31.6	31.3
CaO	0.63	0.70	0.63	0.62	0.50	0.53	0.56	CaO	0.42	0.54	0.55	0.77	0.78	0.86
Na2O	<0.01	0.03	0.06	0.03	0.03	0.03	<0.01	Na2O	0.01	0.01	0.01	0.01	0.03	0.05
K2O	<0.01	0.01	<0.01	0.02	0.02	<0.01	0.03	K2O	0	0	<0.01	0.01	<0.01	0.01
Total	100.7	101.0	100.7	100.9	101.0	101.2	101.2	Total	98.54	98.9	98.8	98.9	98.6	98.4
Si	1.90	1.90	1.90	1.91	1.91	1.91	1.93	Si	1.96	1.97	1.95	1.95	1.95	1.95
Ti	0.004	0.006	0.006	0.006	0.006	0.006	0.004	Ti	0.004	0.003	0.007	0.007	0.007	0.009
Al	0.14	0.15	0.15	0.13	0.13	0.13	0.09	Al	0.07	0.05	0.10	0.09	0.09	0.09
Cr	0.019	0.021	0.020	0.019	0.018	0.018	0.015	Cr	0.006	0.004	0.006	0.005	0.005	0.005
Fe3	0.022	0.029	0.031	0.024	0.026	0.021	0.028	Fe3	0.000	0.013	<0.001	<0.001	<0.001	<0.001
Fe2	0.17	0.17	0.17	0.17	0.18	0.18	0.17	Fe2	0.21	0.22	0.25	0.25	0.24	0.25
Mn	0.006	0.005	0.005	0.003	0.003	0.006	0.004	Mn	0.008	0.010	0.008	0.008	0.008	0.006
Ni	0.004	0.003	0.003	0.003	0.003	0.002	0.002	Ni	0.002	0.002	0.001	0.003	0.002	0.003
Mg	1.70	1.70	1.70	1.71	1.71	1.71	1.73	Mg	1.72	1.71	1.67	1.66	1.67	1.66
Ca	0.023	0.026	0.023	0.023	0.018	0.019	0.021	Ca	0.016	0.020	0.021	0.029	0.029	0.033
Na	<0.001	0.002	0.004	0.002	0.002	0.002	<0.001	Na	0.001	0.001	<0.001	0.001	0.002	0.003
K	<0.001	<0.001	<0.001	0.001	0.001	<0.001	0.001	K	<0.001	<0.001	<0.001	<0.001	<0.001	<0.001

A2.6a: Orthopyroxene profils

Sample La2002-02

distance	**165**	**180**	**195**	**255**	**270**	**300**	**330**	**345**	**360**	**375**	**390**	**405**	**420**	**435**
SiO2	55.1	54.6	54.6	56.1	55.0	54.8	54.7	54.4	54.5	54.5	54.8	54.7	54.7	54.7
TiO2	0.26	0.29	0.29	0.28	0.29	0.27	0.29	0.29	0.26	0.27	0.26	0.27	0.25	0.29
Al2O3	2.0	2.1	2.0	2.2	2.4	2.3	2.4	2.6	2.5	2.5	2.4	2.3	2.4	2.4
Cr2O3	0.21	0.19	0.20	0.21	0.21	0.21	0.21	0.18	0.18	0.16	0.18	0.13	0.17	0.17
Fe2O3	0.36	0.59	0.53	<0.01	<0.01	<0.01	0.21	0.02	0.29	0.37	0.18	0.00	0.61	0.25
FeO	8.1	8.0	7.8	8.3	8.1	8.2	8.1	8.1	8.2	8.1	8.2	8.3	7.9	8.1
MnO	0.36	0.25	0.39	0.31	0.30	0.27	0.27	0.25	0.29	0.34	0.25	0.31	0.26	0.32
NiO	0.05	0.04	0.04	0.06	0.05	0.01	0.08	0.06	0.03	0.08	0.06	0.09	0.04	0.09
MgO	31.8	31.5	31.6	32.0	31.6	31.4	31.3	31.0	31.2	31.2	31.5	31.1	31.6	31.5
CaO	0.63	0.85	0.78	0.86	0.86	0.83	0.94	1.39	0.92	0.98	0.97	0.90	0.89	0.85
Na2O	0.01	0.01	<0.01	<0.01	<0.01	0.03	0.02	<0.01	0.01	0.02	<0.01	0.03	0.01	0.02
K2O	0.01	<0.01	0.01	<0.01	<0.01	<0.01	<0.01	<0.01	0.01	0.00	0.01	<0.01	0.01	<0.01
Total	98.8	98.4	98.2	100.3	98.8	98.4	98.6	98.2	98.3	98.4	98.8	98.2	98.9	98.7
Si	1.95	1.94	1.94	1.95	1.94	1.94	1.94	1.94	1.94	1.93	1.94	1.94	1.93	1.94
Ti	0.007	0.008	0.008	0.007	0.008	0.007	0.008	0.008	0.007	0.007	0.007	0.007	0.007	0.008
Al	0.08	0.09	0.08	0.09	0.10	0.10	0.10	0.11	0.10	0.10	0.10	0.10	0.10	0.10
Cr	0.006	0.005	0.006	0.006	0.006	0.006	0.006	0.005	0.005	0.004	0.005	0.004	0.005	0.005
Fe3	0.010	0.016	0.014	<0.001	<0.001	<0.001	0.006	0.001	0.008	0.010	0.005	0.000	0.016	0.007
Fe2	0.24	0.24	0.23	0.24	0.24	0.24	0.24	0.24	0.24	0.24	0.24	0.25	0.23	0.24
Mn	0.011	0.008	0.012	0.009	0.009	0.008	0.008	0.008	0.009	0.010	0.007	0.010	0.008	0.010
Ni	0.001	0.001	0.001	0.002	0.001	<0.001	0.002	0.002	0.001	0.002	0.002	0.003	0.001	0.003
Mg	1.68	1.67	1.67	1.66	1.66	1.66	1.65	1.64	1.65	1.65	1.66	1.65	1.66	1.66
Ca	0.024	0.032	0.030	0.032	0.033	0.032	0.036	0.053	0.035	0.037	0.037	0.034	0.034	0.032
Na	0.001	0.001	<0.001	<0.001	<0.001	0.002	0.002	<0.001	<0.001	0.002	<0.001	0.002	<0.001	0.001
K	<0.001	<0.001	<0.001	<0.001	<0.001	<0.001	<0.001	<0.001	0.001	<0.001	<0.001	<0.001	<0.001	<0.001

Sample La2002-02

distance	**465**	**480**	**495**	**510**	**540**	**555**	**570**	**600**	**630**	**645**	**660**	**690**	**705**	**765**
SiO2	54.7	54.6	55.0	54.8	54.7	54.9	54.7	54.8	54.4	54.5	54.2	54.8	54.6	53.2
TiO2	0.27	0.25	0.26	0.27	0.26	0.21	0.27	0.24	0.25	0.27	0.30	0.25	0.29	0.23
Al2O3	2.5	2.5	2.5	2.5	2.6	2.5	2.5	2.6	2.6	2.6	2.7	2.6	2.7	2.4
Cr2O3	0.19	0.19	0.14	0.17	0.11	0.14	0.16	0.16	0.16	0.17	0.16	0.19	0.18	0.23
Fe2O3	0.00	0.89	0.00	0.42	0.50	0.00	0.04	0.69	0.77	0.92	0.36	0.17	0.46	0.26
FeO	8.2	7.6	8.0	8.1	7.9	8.1	8.2	8.1	7.8	7.9	8.0	8.2	7.9	7.9
MnO	0.30	0.31	0.28	0.32	0.29	0.23	0.25	0.32	0.27	0.25	0.25	0.34	0.28	0.32
NiO	0.06	0.02	0.04	0.10	0.05	0.06	0.08	0.06	0.07	0.10	0.07	0.06	0.05	0.06
MgO	31.3	31.5	31.3	31.6	31.4	31.5	31.4	31.5	31.4	31.3	31.1	31.3	31.5	30.4
CaO	0.88	1.00	0.92	0.85	0.97	0.88	0.92	0.88	0.90	0.88	0.90	0.99	0.89	0.92
Na2O	0.01	0.03	0.03	<0.01	0.02	<0.01	0.02	0.03	<0.01	0.05	0.03	0.01	0.02	0.03
K2O	<0.01	0.01	<0.01	<0.01	<0.01	0.01	<0.01	<0.01	<0.01	0.01	0.01	<0.01	<0.01	0.01
Total	98.3	98.9	98.5	99.0	98.9	98.4	98.6	99.3	98.5	98.9	98.1	98.8	98.9	96.0
Si	1.94	1.93	1.95	1.93	1.93	1.94	1.94	1.93	1.93	1.93	1.93	1.93	1.93	1.94
Ti	0.007	0.007	0.007	0.007	0.007	0.006	0.007	0.006	0.007	0.007	0.008	0.007	0.008	0.006
Al	0.11	0.11	0.11	0.10	0.11	0.10	0.11	0.11	0.11	0.11	0.11	0.11	0.11	0.10
Cr	0.005	0.005	0.004	0.005	0.003	0.004	0.005	0.004	0.004	0.005	0.004	0.005	0.005	0.007
Fe3	0.000	0.024	0.000	0.011	0.013	0.000	0.001	0.018	0.021	0.025	0.010	0.005	0.012	0.007
Fe2	0.24	0.23	0.24	0.24	0.23	0.24	0.24	0.24	0.23	0.23	0.24	0.24	0.23	0.24
Mn	0.009	0.009	0.008	0.010	0.009	0.007	0.007	0.010	0.008	0.008	0.008	0.010	0.008	0.010
Ni	0.002	0.001	0.001	0.003	0.002	0.002	0.002	0.002	0.002	0.003	0.002	0.002	0.001	0.002
Mg	1.65	1.66	1.65	1.66	1.66	1.66	1.66	1.65	1.66	1.65	1.65	1.65	1.66	1.65
Ca	0.034	0.038	0.035	0.032	0.037	0.033	0.035	0.033	0.034	0.034	0.034	0.037	0.034	0.036
Na	0.001	0.002	0.002	<0.001	0.001	<0.001	0.001	0.002	<0.001	0.004	0.002	0.001	0.001	0.002
K	<0.001	0.001	<0.001	<0.001	<0.001	0.001	<0.001	<0.001	<0.001	0.001	<0.001	<0.001	<0.001	<0.001

A2.6a: Orthopyroxene profils

Sample La2002-02

distance	**810**	**855**	**885**	**915**	**930**	**960**	**1020**	**1035**	**1065**	**1080**	**1095**	**1110**	**1125**	**1140**
SiO2	55.2	55.2	55.0	54.9	54.8	54.8	55.9	54.5	54.6	54.6	54.9	54.8	54.6	54.9
TiO2	0.26	0.20	0.28	0.23	0.25	0.29	0.30	0.24	0.29	0.27	0.21	0.28	0.33	0.27
Al2O3	2.5	2.6	2.6	2.5	2.3	2.7	2.6	2.7	2.5	2.6	2.4	2.5	2.5	2.3
Cr2O3	0.14	0.13	0.14	0.17	0.16	0.18	0.16	0.14	0.17	0.16	0.14	0.19	0.13	0.14
Fe2O3	<0.01	<0.01	0.19	0.28	0.52	0.13	0.04	1.42	0.32	<0.01	0.05	0.28	<0.01	0.11
FeO	8.4	8.7	8.3	7.9	7.8	8.2	8.2	7.3	8.0	8.3	8.3	8.4	8.3	8.3
MnO	0.26	0.23	0.31	0.30	0.32	0.25	0.26	0.38	0.30	0.30	0.28	0.30	0.25	0.29
NiO	0.03	0.05	0.10	0.06	0.09	0.01	0.07	0.08	0.08	0.10	0.06	0.07	0.13	0.04
MgO	31.6	31.4	31.5	31.7	31.8	31.5	32.2	31.6	31.4	31.2	31.5	31.4	31.3	31.6
CaO	0.65	0.74	0.87	0.90	0.69	0.86	0.82	0.90	0.82	0.86	0.78	0.73	0.82	0.68
Na2O	0.01	0.01	<0.01	0.01	0.01	0.02	0.02	0.03	0.01	<0.01	0.01	0.03	<0.01	0.02
K2O	0.01	<0.01	0.01	<0.01	<0.01	<0.01	<0.01	<0.01	0.01	0.01	0.01	0.01	<0.01	0.01
Total	99.0	99.3	99.3	98.9	98.8	98.8	100.6	99.2	98.6	98.4	98.7	98.9	98.3	98.6
Si	1.95	1.94	1.93	1.94	1.94	1.93	1.94	1.92	1.93	1.94	1.94	1.93	1.94	1.94
Ti	0.007	0.005	0.007	0.006	0.007	0.008	0.008	0.006	0.008	0.007	0.006	0.008	0.009	0.007
Al	0.10	0.11	0.11	0.10	0.10	0.11	0.11	0.11	0.10	0.11	0.10	0.11	0.10	0.09
Cr	0.004	0.004	0.004	0.005	0.005	0.005	0.005	0.004	0.005	0.004	0.004	0.005	0.004	0.004
Fe3	<0.001	<0.001	0.005	0.007	0.014	0.003	0.001	0.038	0.009	<0.001	0.001	0.008	<0.001	0.003
Fe2	0.25	0.26	0.24	0.23	0.23	0.24	0.24	0.21	0.24	0.25	0.25	0.25	0.25	0.25
Mn	0.008	0.007	0.009	0.009	0.010	0.007	0.008	0.011	0.009	0.009	0.008	0.009	0.008	0.009
Ni	0.001	0.002	0.003	0.002	0.002	0.000	0.002	0.002	0.002	0.003	0.002	0.002	0.004	0.001
Mg	1.66	1.65	1.65	1.67	1.67	1.66	1.66	1.66	1.66	1.65	1.66	1.65	1.66	1.67
Ca	0.025	0.028	0.033	0.034	0.026	0.033	0.031	0.034	0.031	0.033	0.030	0.028	0.031	0.026
Na	0.001	0.001	<0.001	0.001	0.001	0.002	0.001	0.002	0.001	<0.001	0.001	0.002	<0.001	0.002
K	<0.001	<0.001	0.001	<0.001	<0.001	<0.001	<0.001	<0.001	<0.001	0.001	0.001	0.001	<0.001	0.001

Sample La2002-02

distance	**1155**	**1185**	**1200**	**1215**	**1230**	**1245**	**1275**	**1305**	**1320**	**1335**	**1350**	**1380**	**1395**	**1410**
SiO2	55.2	55.4	55.2	55.5	55.3	55.4	56.3	55.6	55.3	55.4	55.5	55.5	55.5	55.4
TiO2	0.31	0.28	0.32	0.27	0.31	0.32	0.30	0.29	0.30	0.26	0.26	0.26	0.31	0.34
Al2O3	2.2	2.2	2.2	2.1	2.1	2.2	2.3	2.2	2.2	2.3	2.2	2.2	2.0	2.1
Cr2O3	0.17	0.18	0.16	0.17	0.15	0.13	0.17	0.13	0.18	0.18	0.15	0.21	0.17	0.19
Fe2O3	<0.01	0.06	0.29	<0.01	0.70	0.15	0.16	<0.01	0.82	0.93	0.19	<0.01	0.28	0.05
FeO	8.2	8.3	8.2	8.7	8.1	8.5	8.4	8.4	7.9	7.7	8.5	8.5	8.5	8.3
MnO	0.35	0.33	0.36	0.37	0.32	0.29	0.32	0.29	0.29	0.35	0.30	0.28	0.25	0.29
NiO	0.07	0.09	0.04	0.02	0.10	0.10	0.04	0.05	0.03	0.10	0.07	0.09	0.04	0.09
MgO	31.7	31.8	31.7	31.8	31.9	31.7	32.5	31.9	32.0	32.0	31.9	31.8	31.9	31.7
CaO	0.76	0.79	0.84	0.67	0.74	0.81	0.68	0.74	0.80	0.95	0.71	0.80	0.76	0.88
Na2O	0.01	0.03	0.02	<0.01	<0.01	0.01	0.02	0.03	0.01	<0.01	0.01	<0.01	<0.01	0.04
K2O	0.01	<0.01	0.01	0.01	<0.01	<0.01	<0.01	<0.01	<0.01	<0.01	<0.01	<0.01	<0.01	<0.01
Total	99.0	99.5	99.3	99.6	99.7	99.6	101.1	99.6	99.8	100.1	99.8	99.6	99.8	99.3
Si	1.95	1.95	1.94	1.95	1.94	1.94	1.94	1.95	1.93	1.93	1.94	1.95	1.94	1.95
Ti	0.008	0.007	0.009	0.007	0.008	0.008	0.008	0.008	0.008	0.007	0.007	0.007	0.008	0.009
Al	0.09	0.09	0.09	0.09	0.09	0.09	0.09	0.09	0.09	0.09	0.09	0.09	0.08	0.09
Cr	0.005	0.005	0.005	0.005	0.004	0.004	0.005	0.004	0.005	0.005	0.004	0.006	0.005	0.005
Fe3	<0.001	0.002	0.008	<0.001	0.018	0.004	0.004	<0.001	0.022	0.024	0.005	<0.001	0.007	0.001
Fe2	0.24	0.24	0.24	0.25	0.24	0.25	0.24	0.25	0.23	0.22	0.25	0.25	0.25	0.24
Mn	0.010	0.010	0.011	0.011	0.010	0.009	0.009	0.009	0.009	0.010	0.009	0.008	0.007	0.009
Ni	0.002	0.003	0.001	0.001	0.003	0.003	0.001	0.001	0.001	0.003	0.002	0.003	0.001	0.003
Mg	1.67	1.66	1.66	1.66	1.67	1.66	1.67	1.66	1.67	1.67	1.66	1.66	1.67	1.66
Ca	0.029	0.030	0.032	0.025	0.028	0.031	0.025	0.028	0.030	0.035	0.027	0.030	0.028	0.033
Na	0.001	0.002	0.002	<0.001	<0.001	<0.001	0.001	0.002	0.001	<0.001	0.001	<0.001	<0.001	0.003
K	<0.001	<0.001	0.001	<0.001	<0.001	<0.001	<0.001	<0.001	<0.001	<0.001	<0.001	<0.001	<0.001	<0.001

A2.6a: Orthopyroxene profils

Sample La2002-02								**Sample L110**						
distance	**1440**	**1455**	**1470**	**1485**	**1500**	**1515**	**1530**	**distance**	**0**	**10**	**20**	**30**	**40**	**50**
SiO2	55.5	55.5	55.1	55.1	55.4	55.2	55.8	SiO2	56.8	56.5	56.3	56.0	56.3	56.2
TiO2	0.33	0.31	0.34	0.34	0.35	0.28	0.16	TiO2	0.23	0.30	0.26	0.30	0.32	0.28
Al2O3	2.2	2.2	2.2	2.2	2.1	2.0	1.4	Al2O3	1.8	1.9	2.1	2.2	2.1	2.1
Cr2O3	0.13	0.19	0.21	0.18	0.21	0.19	0.21	Cr2O3	0.37	0.46	0.53	0.54	0.53	0.48
Fe2O3	0.06	0.12	0.21	<0.01	<0.01	<0.01	<0.01	Fe2O3	0.58	0.47	0.69	0.81	0.60	0.50
FeO	8.6	8.6	8.4	8.7	8.7	8.2	8.4	FeO	6.5	6.6	6.3	6.4	6.4	6.4
MnO	0.29	0.29	0.33	0.28	0.31	0.27	0.33	MnO	0.11	0.15	0.18	0.19	0.19	0.18
NiO	0.03	0.03	0.07	0.04	0.03	0.06	0.04	NiO	0.11	0.09	0.09	0.07	0.03	0.09
MgO	31.8	31.9	31.6	31.6	31.6	31.9	32.1	MgO	34.0	33.8	33.6	33.3	33.6	33.5
CaO	0.78	0.64	0.81	0.60	0.56	0.50	0.36	CaO	0.59	0.65	0.75	0.79	0.77	0.75
Na2O	<0.01	0.01	<0.01	0.02	0.04	0.01	<0.01	Na2O	0.02	0.01	0.03	0.02	0.04	0.01
K2O	0.02	0.02	<0.01	<0.01	<0.01	0.01	<0.01	K2O	<0.01	<0.01	0.01	<0.01	<0.01	<0.01
Total	99.8	99.9	99.2	99.0	99.4	98.6	98.8	Total	101.1	100.9	100.9	100.7	100.9	100.5
Si	1.94	1.94	1.94	1.94	1.95	1.95	1.97	Si	1.95	1.94	1.94	1.93	1.93	1.94
Ti	0.009	0.008	0.009	0.009	0.009	0.008	0.004	Ti	0.006	0.008	0.007	0.008	0.008	0.007
Al	0.09	0.09	0.09	0.09	0.09	0.08	0.06	Al	0.07	0.08	0.09	0.09	0.09	0.09
Cr	0.004	0.005	0.006	0.005	0.006	0.005	0.006	Cr	0.010	0.013	0.015	0.015	0.014	0.013
Fe3	0.002	0.003	0.006	<0.001	<0.001	<0.001	<0.001	Fe3	0.015	0.012	0.018	0.021	0.016	0.013
Fe2	0.25	0.25	0.25	0.26	0.26	0.24	0.25	Fe2	0.19	0.19	0.18	0.19	0.18	0.18
Mn	0.009	0.009	0.010	0.008	0.009	0.008	0.010	Mn	0.003	0.004	0.005	0.006	0.005	0.005
Ni	0.001	0.001	0.002	0.001	0.001	0.002	0.001	Ni	0.003	0.003	0.002	0.002	0.001	0.003
Mg	1.66	1.66	1.66	1.66	1.66	1.68	1.69	Mg	1.73	1.73	1.72	1.71	1.72	1.72
Ca	0.029	0.024	0.031	0.023	0.021	0.019	0.014	Ca	0.022	0.024	0.027	0.029	0.028	0.028
Na	<0.001	0.001	<0.001	0.001	0.003	0.001	<0.001	Na	0.002	<0.001	0.002	0.001	0.002	0.001
K	0.001	0.001	<0.001	<0.001	<0.001	0.001	<0.001	K	<0.001	<0.001	<0.001	<0.001	<0.001	<0.001

Sample L110														
distance	**60**	**100**	**110**	**120**	**150**	**160**	**170**	**200**	**240**	**260**	**270**	**290**	**300**	**310**
SiO2	56.3	56.4	56.2	56.6	55.9	56.1	55.9	56.0	55.7	54.7	55.7	55.6	55.9	55.8
TiO2	0.27	0.24	0.33	0.24	0.25	0.27	0.24	0.27	0.29	0.28	0.30	0.28	0.29	0.27
Al2O3	1.8	2.2	2.2	1.9	2.6	2.6	2.4	2.6	2.6	2.7	2.6	2.6	2.5	2.5
Cr2O3	0.50	0.51	0.53	0.48	0.58	0.53	0.55	0.56	0.57	0.62	0.62	0.56	0.55	0.52
Fe2O3	0.38	1.18	0.68	0.86	0.64	0.63	0.98	0.95	0.92	0.85	0.65	0.94	0.64	0.77
FeO	6.5	5.8	6.1	6.2	6.4	6.4	5.8	6.2	6.1	6.4	6.3	5.8	6.3	6.1
MnO	0.09	0.21	0.17	0.20	0.13	0.14	0.16	0.21	0.13	0.09	0.25	0.22	0.16	0.11
NiO	0.10	0.09	0.04	0.06	0.08	0.08	0.10	0.09	0.07	0.11	0.09	0.12	0.07	0.07
MgO	33.5	34.2	33.8	34.1	33.3	33.5	33.5	33.4	33.2	32.5	33.1	33.4	33.3	33.4
CaO	0.84	0.55	0.63	0.53	0.78	0.60	0.89	0.78	0.87	0.75	0.89	0.77	0.86	0.81
Na2O	0.04	<0.01	0.03	0.01	0.01	0.02	0.05	0.03	0.04	0.04	0.03	0.02	<0.01	0.01
K2O	<0.01	0.01	0.02	<0.01	<0.01	0.02	<0.01	0.01	0.02	0.01	<0.01	0.01	0.01	0.02
Total	100.3	101.2	100.7	101.2	100.7	100.9	100.6	101.0	100.6	99.0	100.5	100.3	100.5	100.3
Si	1.95	1.93	1.93	1.94	1.93	1.93	1.93	1.92	1.92	1.92	1.92	1.92	1.93	1.93
Ti	0.007	0.006	0.009	0.006	0.006	0.007	0.006	0.007	0.007	0.008	0.008	0.007	0.008	0.007
Al	0.07	0.09	0.09	0.08	0.11	0.11	0.10	0.10	0.11	0.11	0.11	0.10	0.10	0.10
Cr	0.014	0.014	0.014	0.013	0.016	0.015	0.015	0.015	0.016	0.017	0.017	0.015	0.015	0.014
Fe3	0.010	0.030	0.018	0.022	0.017	0.016	0.025	0.025	0.024	0.023	0.017	0.025	0.017	0.020
Fe2	0.19	0.16	0.18	0.18	0.19	0.18	0.17	0.18	0.18	0.19	0.18	0.17	0.18	0.17
Mn	0.003	0.006	0.005	0.006	0.004	0.004	0.005	0.006	0.004	0.003	0.007	0.006	0.005	0.003
Ni	0.003	0.003	0.001	0.002	0.002	0.002	0.003	0.002	0.002	0.003	0.003	0.003	0.002	0.002
Mg	1.72	1.74	1.73	1.74	1.71	1.72	1.72	1.71	1.71	1.70	1.70	1.72	1.71	1.72
Ca	0.031	0.020	0.023	0.019	0.029	0.022	0.033	0.029	0.032	0.028	0.033	0.028	0.032	0.030
Na	0.002	<0.001	0.002	0.001	0.001	0.001	0.003	0.002	0.003	0.003	0.002	0.001	<0.001	0.001
K	<0.001	<0.001	0.001	<0.001	<0.001	0.001	<0.001	0.001	0.001	<0.001	<0.001	<0.001	<0.001	0.001

A2.6a: Orthopyroxene profils

Sample L110

distance	320	330	340	360	390	400	410	450	460	470	480	490	500	520
SiO2	50.1	55.3	55.9	55.8	56.0	56.0	55.8	56.0	55.9	56.0	55.5	55.9	56.1	55.9
TiO2	0.31	0.28	0.32	0.30	0.29	0.29	0.32	0.27	0.27	0.30	0.25	0.30	0.27	0.31
Al2O3	2.1	2.4	2.5	2.5	2.5	2.5	2.6	2.4	2.4	2.4	2.4	2.6	2.4	2.3
Cr2O3	0.56	0.55	0.59	0.55	0.58	0.58	0.56	0.55	0.58	0.51	0.53	0.55	0.55	0.53
Fe2O3	<0.01	<0.01	0.21	<0.01	<0.01	<0.01	<0.01	0.31	0.23	0.62	0.82	<0.01	<0.01	<0.01
FeO	6.6	6.6	6.4	6.5	6.6	6.6	6.7	6.5	6.3	6.0	5.6	6.4	6.5	6.3
MnO	0.13	0.18	0.09	0.20	0.14	0.14	0.08	0.11	0.14	0.23	0.21	0.14	0.16	0.15
NiO	0.12	0.07	0.09	0.06	0.09	0.09	0.08	0.07	0.07	0.08	0.07	0.08	0.04	0.05
MgO	27.9	32.7	33.3	33.1	33.1	33.1	33.1	33.2	33.3	33.5	33.3	33.1	33.4	33.2
CaO	0.75	0.92	0.92	0.90	0.97	0.97	0.97	0.94	0.84	0.85	0.90	0.92	0.74	0.91
Na2O	0.04	0.01	0.01	0.03	<0.01	<0.01	<0.01	0.02	0.03	0.04	0.03	0.03	0.02	0.02
K2O	0.02	0.02	0.01	<0.01	0.01	0.01	0.01	0.01	<0.01	0.01	<0.01	0.01	0.02	<0.01
Total	88.7	99.1	100.2	99.9	100.2	100.2	100.2	100.4	100.1	100.5	99.6	100.0	100.2	99.7
Si	1.98	1.94	1.93	1.93	1.94	1.94	1.93	1.93	1.93	1.93	1.93	1.94	1.94	1.94
Ti	0.009	0.007	0.008	0.008	0.008	0.008	0.008	0.007	0.007	0.008	0.007	0.008	0.007	0.008
Al	0.10	0.10	0.10	0.10	0.10	0.10	0.11	0.10	0.10	0.10	0.10	0.10	0.10	0.09
Cr	0.018	0.015	0.016	0.015	0.016	0.016	0.015	0.015	0.016	0.014	0.015	0.015	0.015	0.015
Fe3	<0.001	<0.001	0.006	<0.001	<0.001	<0.001	<0.001	0.008	0.006	0.016	0.021	<0.001	<0.001	<0.001
Fe2	0.22	0.19	0.18	0.19	0.19	0.19	0.19	0.19	0.18	0.17	0.16	0.19	0.19	0.18
Mn	0.004	0.005	0.003	0.006	0.004	0.004	0.002	0.003	0.004	0.007	0.006	0.004	0.005	0.004
Ni	0.004	0.002	0.003	0.002	0.002	0.002	0.002	0.002	0.002	0.002	0.002	0.002	0.001	0.001
Mg	1.64	1.71	1.71	1.71	1.71	1.71	1.70	1.71	1.72	1.72	1.72	1.71	1.72	1.72
Ca	0.032	0.034	0.034	0.033	0.036	0.036	0.036	0.035	0.031	0.031	0.034	0.034	0.027	0.034
Na	0.003	0.001	<0.001	0.002	<0.001	<0.001	<0.001	0.001	0.002	0.002	0.002	0.002	0.001	0.001
K	0.001	0.001	0.001	<0.001	<0.001	<0.001	0.001	<0.001	<0.001	<0.001	<0.001	<0.001	0.001	<0.001

Sample L110 opx impregnation										**Sample La2002-02**				
distance	**530**	**540**	**550**	**560**	**570**	**580**	**590**	**600**	**610**	**distance**	**10**	**20**	**30**	**40**
SiO2	56.1	56.0	56.5	56.2	56.6	56.8	56.3	57.0	56.7	SiO2	56.7	56.6	56.2	56.5
TiO2	0.29	0.29	0.28	0.30	0.25	0.23	0.25	0.22	0.25	TiO2	0.12	0.15	0.17	0.23
Al2O3	2.4	2.3	2.3	2.1	1.8	1.5	1.7	1.4	1.7	Al2O3	1.1	1.2	1.3	1.5
Cr2O3	0.55	0.53	0.50	0.49	0.42	0.42	0.40	0.31	0.34	Cr2O3	0.09	0.11	0.11	0.14
Fe2O3	<0.01	0.20	<0.01	0.31	<0.01	0.05	0.45	<0.01	0.14	Fe2O3	0.90	0.76	0.93	<0.01
FeO	6.5	6.5	6.1	6.2	6.2	6.3	6.2	6.6	6.8	FeO	7.9	7.8	7.7	8.2
MnO	0.15	0.19	0.10	0.25	0.17	0.15	0.16	0.14	0.10	MnO	0.29	0.29	0.21	0.20
NiO	0.06	0.10	0.07	0.12	0.04	0.09	0.10	0.04	0.03	NiO	0.06	0.07	0.05	0.06
MgO	33.1	33.4	33.5	33.6	33.9	34.1	33.8	34.0	34.0	MgO	33.1	33.1	32.8	32.7
CaO	0.72	0.69	0.62	0.63	0.60	0.54	0.62	0.51	0.46	CaO	0.49	0.52	0.60	0.66
Na2O	0.04	0.01	<0.01	0.04	0.02	0.03	<0.01	0.00	0.00	Na2O	0.01	<0.01	0.03	0.01
K2O	0.01	<0.01	<0.01	<0.01	<0.01	<0.01	<0.01	0.02	0.01	K2O	<0.01	<0.01	<0.01	0.01
Total	99.8	100.1	100.0	100.2	100.0	100.2	100.0	100.3	100.5	Total	100.7	100.7	100.1	100.2
Si	1.95	1.94	1.95	1.94	1.95	1.96	1.95	1.97	1.9538	Si	1.96	1.96	1.96	1.96
Ti	0.008	0.008	0.007	0.008	0.006	0.006	0.007	0.006	0.0065	Ti	0.003	0.004	0.005	0.006
Al	0.10	0.09	0.09	0.09	0.07	0.06	0.07	0.06	0.0669	Al	0.05	0.05	0.05	0.06
Cr	0.015	0.015	0.014	0.013	0.011	0.012	0.011	0.009	0.0093	Cr	0.003	0.003	0.003	0.004
Fe3	<0.001	0.005	<0.001	0.008	<0.001	0.001	0.012	<0.001	0.0038	Fe3	0.024	0.020	0.024	<0.001
Fe2	0.19	0.19	0.18	0.18	0.18	0.18	0.18	0.19	0.1945	Fe2	0.23	0.23	0.22	0.24
Mn	0.004	0.006	0.003	0.007	0.005	0.004	0.005	0.004	0.003	Mn	0.008	0.008	0.006	0.006
Ni	0.002	0.003	0.002	0.003	0.001	0.002	0.003	0.001	0.0008	Ni	0.002	0.002	0.001	0.002
Mg	1.71	1.72	1.73	1.73	1.75	1.75	1.74	1.75	1.744	Mg	1.71	1.71	1.70	1.69
Ca	0.027	0.026	0.023	0.023	0.022	0.020	0.023	0.019	0.017	Ca	0.018	0.019	0.023	0.025
Na	0.002	<0.001	<0.001	0.002	0.001	0.002	<0.001	<0.001	0.0001	Na	0.001	<0.001	0.002	0.001
K	<0.001	<0.001	<0.001	<0.001	<0.001	<0.001	<0.001	0.001	0.0004	K	<0.001	<0.001	<0.001	<0.001

A2.6a: Orthopyroxene profils

Sample La2002-02

distance	**50**	**60**	**70**	**80**	**90**	**100**	**110**	**120**	**130**	**140**	**150**	**160**	**170**	**180**
SiO2	55.9	55.5	55.5	54.5	55.4	55.3	56.1	55.6	54.1	55.8	55.1	54.9	55.0	55.6
TiO2	0.35	0.40	0.43	0.35	0.39	0.30	0.30	0.30	0.41	0.32	0.39	0.35	0.45	0.38
Al2O3	1.7	2.1	2.2	2.2	2.3	2.2	2.1	2.1	2.1	2.2	2.4	2.3	2.4	2.4
Cr2O3	0.23	0.21	0.28	0.28	0.28	0.23	0.22	0.20	0.20	0.32	0.19	0.26	0.29	0.26
Fe2O3	1.35	1.06	1.83	2.79	0.44	2.17	0.66	1.66	2.69	1.03	1.67	0.58	0.56	<0.01
FeO	7.4	7.6	7.3	6.6	7.7	6.7	8.1	6.9	5.9	7.7	7.5	7.6	7.4	8.2
MnO	0.35	0.28	0.27	0.36	0.20	0.26	0.24	0.33	0.27	0.18	0.17	0.41	0.29	0.21
NiO	0.08	0.02	0.06	0.05	0.15	0.05	0.05	0.05	0.05	0.02	0.00	0.03	0.04	0.01
MgO	32.6	32.4	32.5	32.2	32.1	32.5	32.3	32.6	32.2	32.3	32.0	31.6	31.9	31.8
CaO	0.67	0.75	0.90	0.82	0.97	0.96	0.96	1.03	1.06	1.07	1.07	1.13	1.03	1.10
Na2O	0.06	0.02	0.02	0.04	<0.01	0.05	0.03	<0.01	<0.01	0.04	0.03	<0.01	0.05	0.04
K2O	0.02	<0.01	0.01	<0.01	0.01	<0.01	<0.01	<0.01	0.03	<0.01	0.01	0.01	<0.01	<0.01
Total	100.7	100.4	101.2	100.2	100.0	100.8	101.0	100.7	99.1	101.0	100.5	99.2	99.4	100.0
Si	1.94	1.93	1.92	1.91	1.93	1.92	1.94	1.92	1.91	1.93	1.92	1.93	1.93	1.94
Ti	0.009	0.011	0.011	0.009	0.010	0.008	0.008	0.008	0.011	0.008	0.010	0.009	0.012	0.010
Al	0.07	0.09	0.09	0.09	0.09	0.09	0.08	0.09	0.09	0.09	0.10	0.10	0.10	0.10
Cr	0.006	0.006	0.008	0.008	0.008	0.006	0.006	0.006	0.006	0.009	0.005	0.007	0.008	0.007
Fe3	0.035	0.028	0.048	0.073	0.012	0.057	0.017	0.043	0.071	0.027	0.044	0.016	0.015	<0.001
Fe2	0.21	0.22	0.21	0.19	0.23	0.20	0.23	0.20	0.17	0.22	0.22	0.22	0.22	0.24
Mn	0.010	0.008	0.008	0.011	0.006	0.008	0.007	0.010	0.008	0.005	0.005	0.012	0.009	0.006
Ni	0.002	0.001	0.002	0.002	0.004	0.001	0.002	0.001	0.002	0.001	0.000	0.001	0.001	0.000
Mg	1.69	1.68	1.67	1.67	1.67	1.68	1.66	1.68	1.69	1.66	1.66	1.66	1.67	1.65
Ca	0.025	0.028	0.033	0.031	0.036	0.036	0.036	0.038	0.040	0.040	0.040	0.043	0.039	0.041
Na	0.004	0.001	0.002	0.002	<0.001	0.003	0.002	<0.001	<0.001	0.002	0.002	<0.001	0.004	0.003
K	0.001	<0.001	<0.001	<0.001	0.001	<0.001	<0.001	<0.001	0.001	<0.001	<0.001	0.001	<0.001	<0.001

Sample La2002-02

distance	**190**	**200**	**210**	**220**	**230**	**240**	**250**	**260**	**270**	**280**	**290**	**300**	**310**	**320**
SiO2	55.1	55.0	55.0	55.4	55.5	55.5	55.5	55.8	55.5	55.7	55.8	55.8	55.6	55.8
TiO2	0.33	0.30	0.38	0.36	0.35	0.35	0.28	0.41	0.36	0.36	0.34	0.29	0.32	0.37
Al2O3	2.4	2.5	2.4	2.4	2.4	2.4	2.5	2.4	2.3	2.3	2.3	2.1	2.2	2.2
Cr2O3	0.25	0.25	0.24	0.28	0.26	0.30	0.30	0.22	0.28	0.23	0.32	0.30	0.18	0.24
Fe2O3	0.69	0.62	1.06	0.33	0.59	0.70	0.49	0.00	0.13	0.65	0.62	0.03	0.54	1.49
FeO	7.8	7.6	7.4	8.0	7.6	7.8	7.9	8.4	7.9	7.7	8.3	8.1	7.9	7.5
MnO	0.35	0.19	0.34	0.16	0.25	0.40	0.35	0.19	0.29	0.19	0.37	0.28	0.30	0.26
NiO	0.01	0.11	0.11	0.08	0.13	0.11	0.17	0.00	0.09	0.06	0.07	0.11	0.00	0.11
MgO	31.7	31.7	31.9	31.9	32.1	32.0	31.8	31.8	31.7	32.1	32.0	32.1	32.1	32.4
CaO	1.12	1.13	1.09	1.07	1.09	0.96	0.95	1.14	1.16	1.24	0.98	0.94	1.00	0.97
Na2O	0.00	0.02	0.01	0.02	<0.01	<0.01	0.04	0.03	0.08	0.03	0.01	<0.01	<0.01	0.04
K2O	0.02	0.04	0.01	0.01	0.05	0.06	0.01	0.01	<0.01	<0.01	<0.01	0.02	<0.01	<0.01
Total	99.8	99.4	100.0	100.1	100.2	100.5	100.3	100.4	99.9	100.6	101.1	100.1	100.2	101.4
Si	1.93	1.93	1.92	1.93	1.93	1.93	1.93	1.94	1.94	1.93	1.93	1.95	1.94	1.92
Ti	0.009	0.008	0.010	0.010	0.009	0.009	0.007	0.011	0.009	0.009	0.009	0.008	0.009	0.010
Al	0.10	0.10	0.10	0.10	0.10	0.10	0.10	0.10	0.09	0.09	0.09	0.09	0.09	0.09
Cr	0.007	0.007	0.007	0.008	0.007	0.008	0.008	0.006	0.008	0.006	0.009	0.008	0.005	0.007
Fe3	0.018	0.017	0.028	0.009	0.016	0.018	0.013	0.000	0.003	0.017	0.016	0.001	0.014	0.039
Fe2	0.23	0.22	0.22	0.23	0.22	0.23	0.23	0.25	0.23	0.22	0.24	0.24	0.23	0.22
Mn	0.010	0.006	0.010	0.005	0.007	0.012	0.010	0.006	0.009	0.006	0.011	0.008	0.009	0.008
Ni	0.000	0.003	0.003	0.002	0.004	0.003	0.005	0.000	0.003	0.002	0.002	0.003	0.000	0.003
Mg	1.66	1.66	1.66	1.66	1.66	1.66	1.65	1.65	1.65	1.66	1.65	1.67	1.67	1.66
Ca	0.042	0.043	0.041	0.040	0.041	0.036	0.035	0.043	0.044	0.046	0.036	0.035	0.038	0.036
Na	0.000	0.001	0.001	0.001	<0.001	<0.001	0.003	0.002	0.005	0.002	0.001	<0.001	<0.001	0.003
K	0.001	0.002	0.001	<0.001	0.002	0.003	<0.001	0.001	<0.001	<0.001	<0.001	0.001	<0.001	<0.001

A2.6a: Orthopyroxene profils
Sample La2002-02

distance	**330**	**340**	**350**
SiO2	55.3	55.2	55.2
TiO2	0.34	0.35	0.37
Al2O3	2.33	2.39	2.40
Cr2O3	0.26	0.30	0.25
Fe2O3	0.49	1.50	0.65
FeO	8.2	7.5	8.1
MnO	0.20	0.17	0.29
NiO	0.08	0.09	<0.01
MgO	31.7	32.1	32.0
CaO	0.88	0.83	0.65
Na2O	0.06	0.07	0.02
K2O	<0.01	0.01	<0.01
Total	99.8	100.5	99.9
Si	1.94	1.92	1.93
Ti	0.009	0.009	0.010
Al	0.10	0.10	0.10
Cr	0.007	0.008	0.007
Fe3	0.013	0.039	0.017
Fe2	0.24	0.22	0.24
Mn	0.006	0.005	0.009
Ni	0.002	0.003	<0.001
Mg	1.65	1.66	1.67
Ca	0.033	0.031	0.024
Na	0.004	0.005	0.002
K	<0.001	0.001	<0.001

Annexe A2.6: profiles of minerals (data set associated on CD)

A2.6b: clinopyroxene profiles

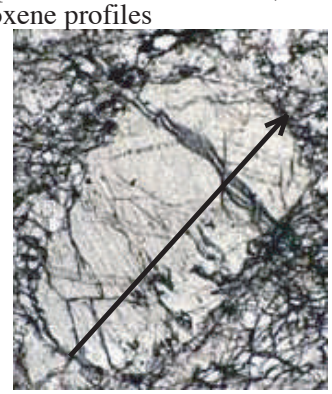

Sample L04: mylonite
distance: 1130µm

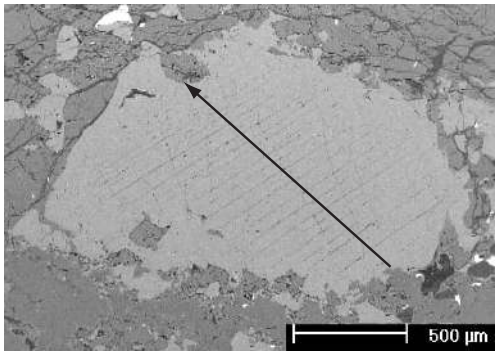

Sample L112, proto-mylonite
distance: 861 µm

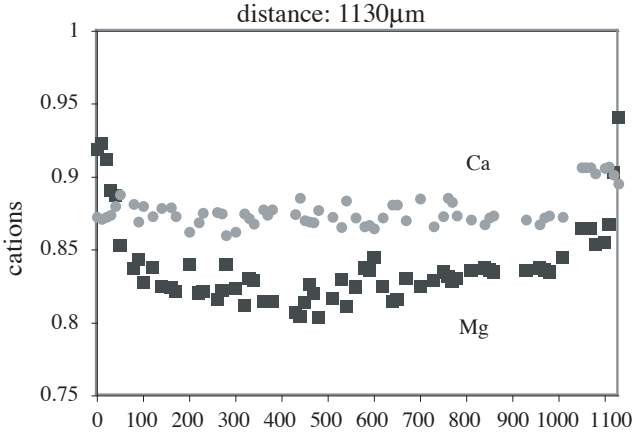

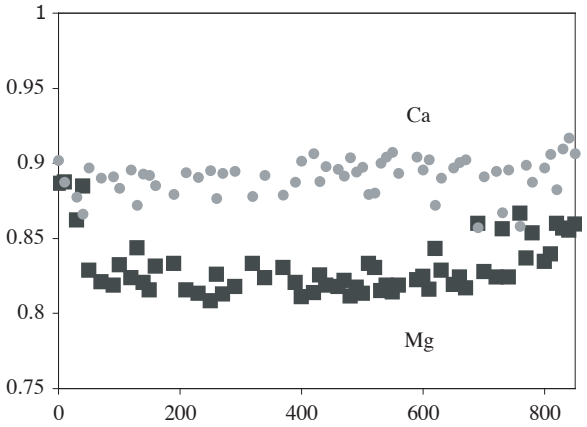

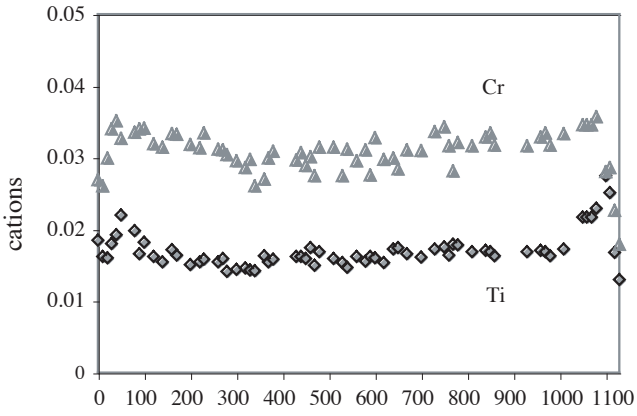

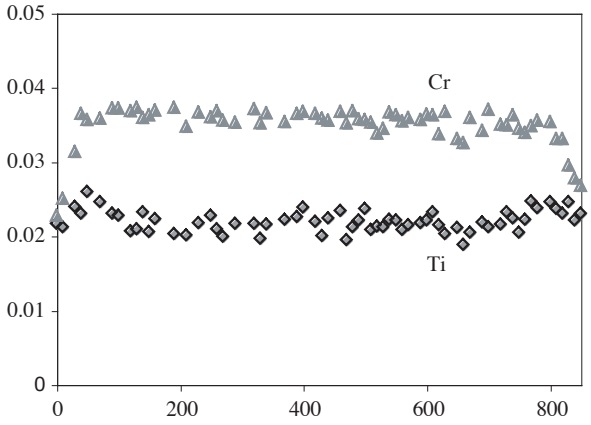

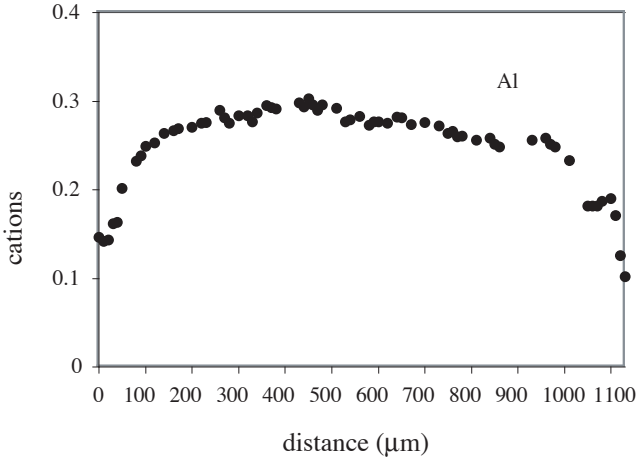

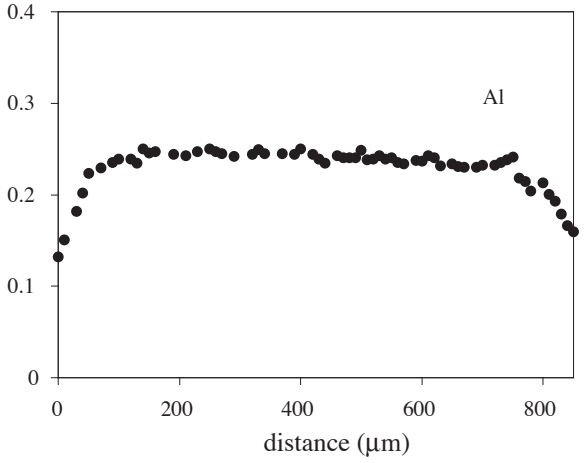

Annexe A2.6: profiles of minerals (data set associated on CD)

A2.6b: clinopyroxene profiles

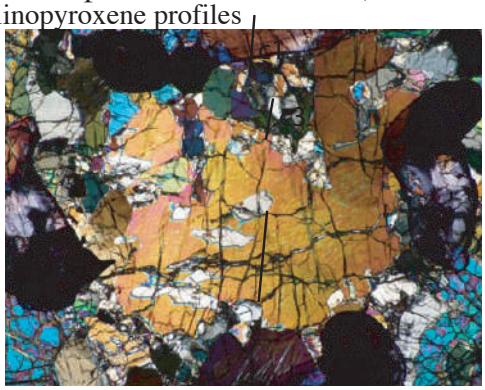

Sample L09, FGSG
distance: 2477 µm

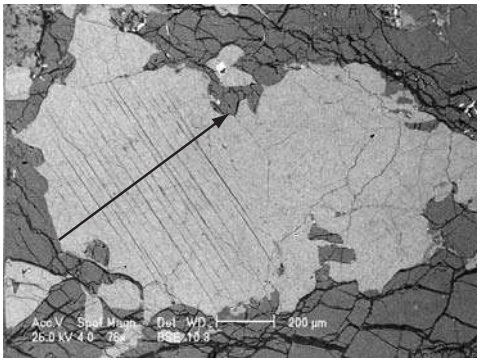

Sample L110, FGSG
distance: 731 µm

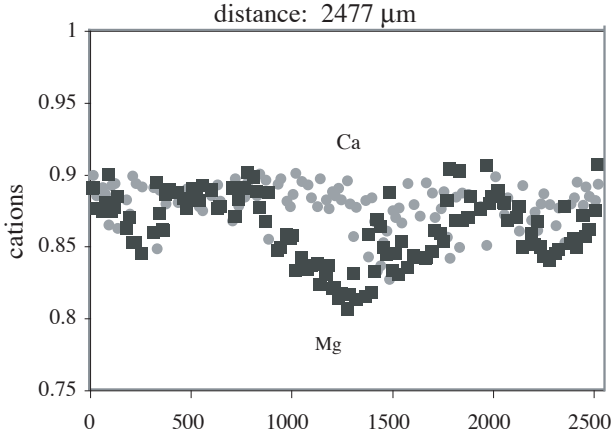

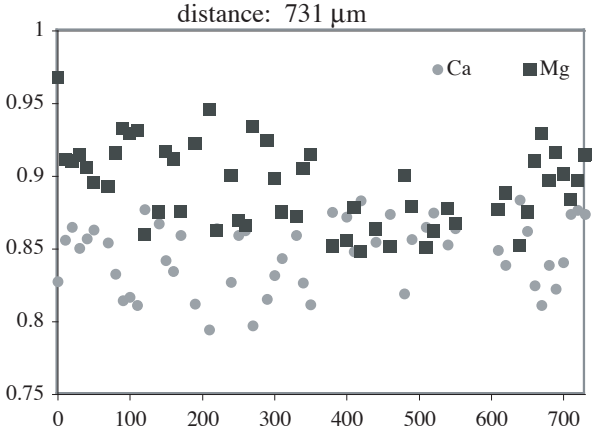

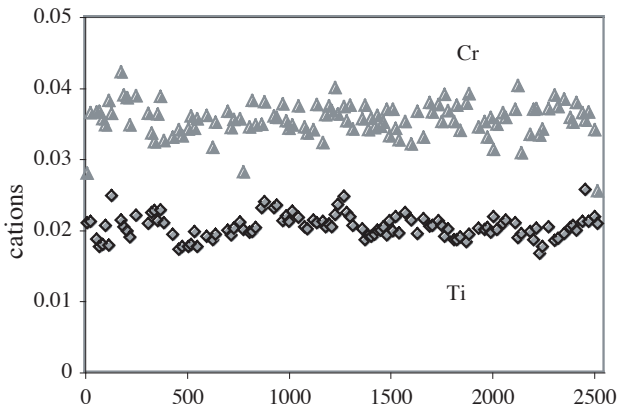

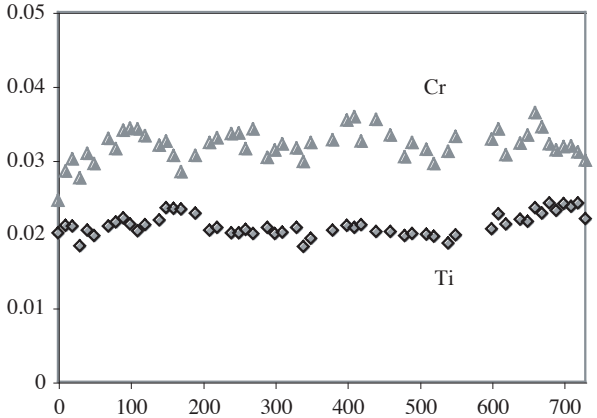

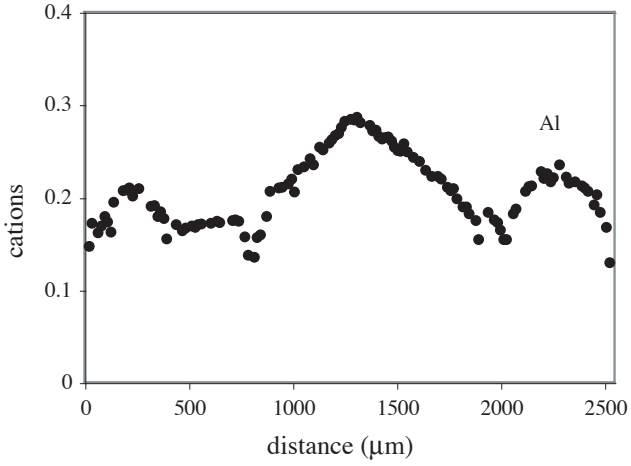

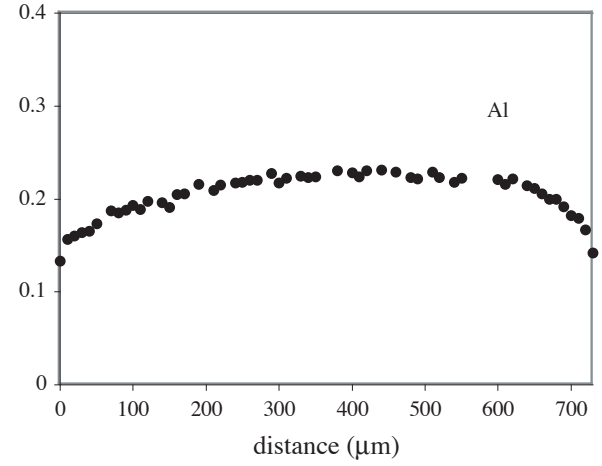

Annexe A2.6: profiles of minerals (data set associated on CD)

A2.6b: clinopyroxene profiles

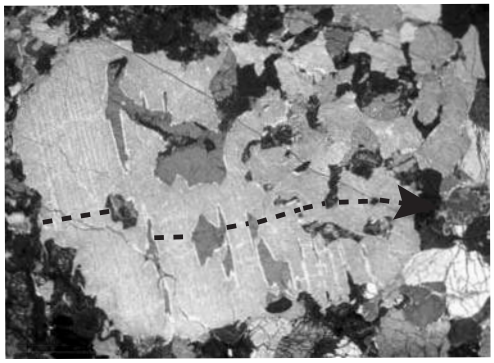

Sample L13: CGSG central
distance: 2755 µm

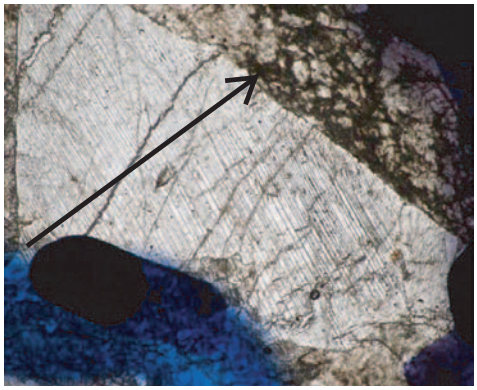

Sample L13, CGSG central
distance: 900 µm

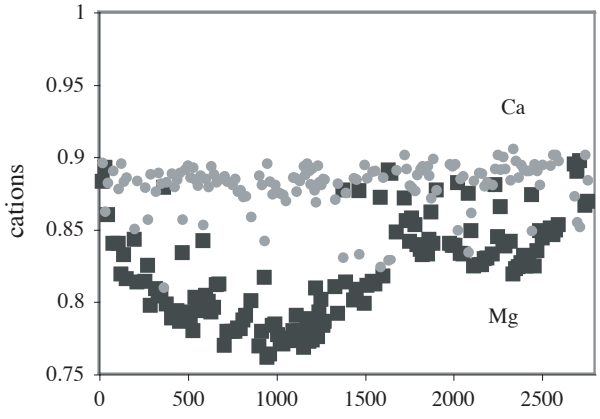

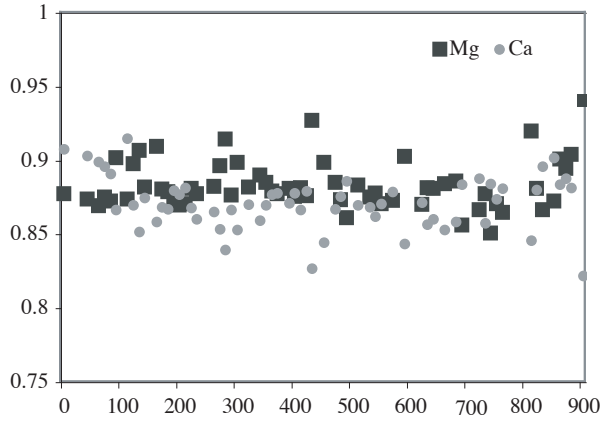

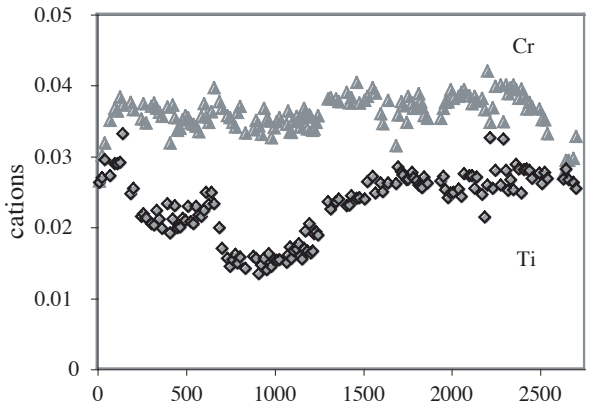

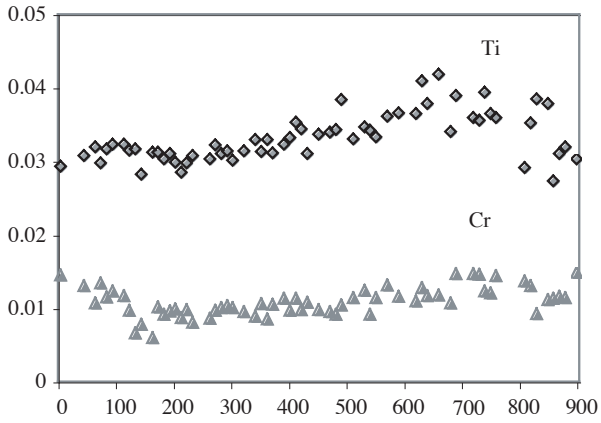

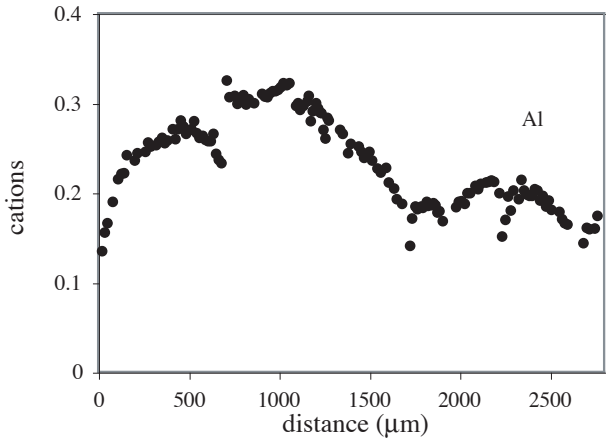

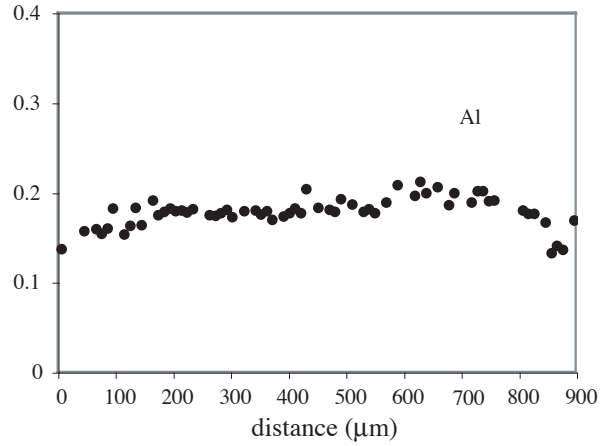

Annexe A2.6: profiles of minerals (data set associated on CI

A2.6b: clinopyroxene profiles

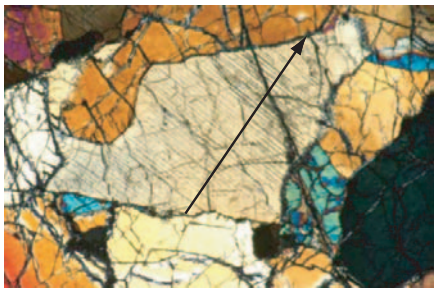

Sample L147, CGSG central
distance: 1001 µm

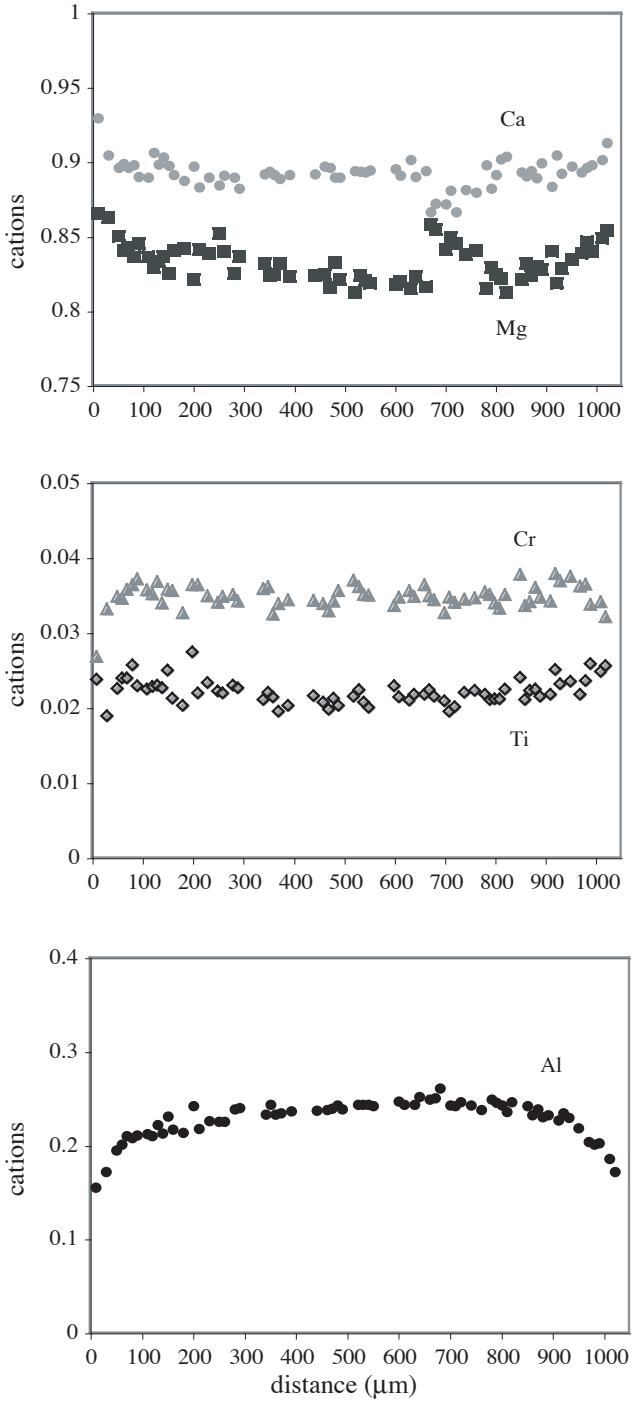

A2.6b: Clinopyroxene profils

Sample L04

distance	**0**	**10**	**20**	**30**	**40**	**50**	**70**	**80**	**90**	**100**	**120**	**130**	**140**	**160**
SiO2	52.2	52.5	53.0	52.6	52.7	51.7	50.9	51.6	51.5	51.2	51.1	51.1	51.1	50.9
TiO2	0.68	0.60	0.59	0.67	0.71	0.81	0.76	0.73	0.61	0.67	0.60	0.67	0.57	0.63
Al2O3	3.4	3.3	3.4	3.8	3.9	4.7	5.7	5.5	5.6	5.9	5.9	6.3	6.2	6.3
Cr2O3	0.94	0.91	1.05	1.20	1.24	1.15	1.26	1.18	1.19	1.20	1.12	1.18	1.10	1.17
Fe2O3	1.89	1.94	1.41	1.42	0.95	1.49	2.02	1.66	1.81	1.84	1.29	1.49	1.85	1.88
FeO	1.06	1.03	1.56	1.58	1.79	1.34	0.91	1.26	1.17	1.09	1.65	1.68	1.23	1.15
MnO	0.09	0.13	0.11	0.12	0.07	0.11	0.08	0.03	0.07	0.14	0.11	0.03	0.06	0.08
NiO	0.01	0.04	<0.01	0.09	0.08	0.04	0.07	0.09	<0.01	0.07	<0.01	0.01	0.08	0.06
MgO	17.0	17.2	17.1	16.7	16.6	15.9	15.5	15.6	15.7	15.4	15.5	15.9	15.4	15.3
CaO	22.5	22.5	22.7	22.7	22.9	23.0	22.7	22.9	22.5	22.8	22.5	22.0	22.8	22.8
Na2O	0.58	0.55	0.57	0.63	0.60	0.74	0.81	0.81	0.84	0.82	0.72	0.70	0.79	0.79
K2O	<0.01	0.02	0.01	<0.01	0.01	<0.01	0.02	<0.01	0.02	0.02	0.01	0.02	<0.01	<0.01
Total	100.4	100.8	101.5	101.5	101.5	101.0	100.8	101.3	101.0	101.1	100.5	101.1	101.1	101.02
Si	1.89	1.89	1.90	1.89	1.89	1.87	1.84	1.85	1.85	1.84	1.85	1.84	1.84	1.84
Ti	0.019	0.016	0.016	0.018	0.019	0.022	0.021	0.020	0.017	0.018	0.016	0.018	0.015	0.017
Al	0.15	0.14	0.14	0.16	0.16	0.20	0.24	0.23	0.24	0.25	0.25	0.27	0.26	0.27
Cr	0.027	0.026	0.030	0.034	0.035	0.033	0.036	0.034	0.034	0.034	0.032	0.034	0.031	0.033
Fe3	0.051	0.053	0.038	0.038	0.026	0.041	0.055	0.045	0.049	0.050	0.035	0.041	0.050	0.051
Fe2	0.032	0.031	0.047	0.047	0.054	0.040	0.028	0.038	0.035	0.033	0.050	0.051	0.037	0.035
Mn	0.003	0.004	0.004	0.004	0.002	0.003	0.003	0.001	0.002	0.004	0.003	0.001	0.002	0.003
Ni	<0.001	0.001	<0.001	0.003	0.002	0.001	0.002	0.003	<0.001	0.002	<0.001	<0.001	0.002	0.002
Mg	0.92	0.92	0.91	0.89	0.89	0.85	0.83	0.84	0.84	0.83	0.84	0.85	0.83	0.82
Ca	0.87	0.87	0.87	0.87	0.88	0.89	0.88	0.88	0.87	0.88	0.87	0.85	0.88	0.88
Na	0.041	0.039	0.040	0.044	0.041	0.052	0.057	0.057	0.058	0.057	0.050	0.049	0.055	0.055
K	<0.001	0.001	<0.001	<0.001	<0.001	<0.001	0.001	<0.001	0.001	0.001	<0.001	0.001	<0.001	<0.001

Sample L04

distance	**170**	**200**	**210**	**220**	**230**	**240**	**260**	**270**	**280**	**300**	**310**	**320**	**330**	**340**
SiO2	51.1	50.9	51.0	51.0	50.8	50.7	50.6	50.6	50.9	50.6	50.6	50.9	50.4	50.3
TiO2	0.60	0.56	0.56	0.57	0.58	0.54	0.57	0.59	0.52	0.53	0.54	0.54	0.52	0.52
Al2O3	6.3	6.4	6.3	6.5	6.5	6.6	6.8	6.6	6.5	6.6	6.6	6.7	6.5	6.7
Cr2O3	1.17	1.11	1.06	1.10	1.17	1.12	1.09	1.09	1.07	1.03	1.05	1.00	1.03	0.91
Fe2O3	1.28	1.64	2.16	1.70	1.66	2.18	2.20	2.00	1.76	1.49	2.28	1.52	1.72	2.35
FeO	1.74	1.63	1.22	1.56	1.41	1.27	1.03	1.22	1.39	1.85	1.16	1.82	1.49	1.19
MnO	0.06	0.07	0.08	0.06	0.03	0.10	0.10	0.10	0.08	0.08	0.10	0.11	0.06	0.12
NiO	0.09	0.03	0.06	0.11	0.02	0.05	0.08	<0.01	0.07	0.04	0.03	0.07	0.01	0.03
MgO	15.3	15.6	16.0	15.3	15.3	16.0	15.2	15.3	15.6	15.2	15.7	15.1	15.3	15.3
CaO	22.6	22.3	22.0	22.5	22.6	21.6	22.7	22.6	22.2	22.2	22.2	22.7	22.4	22.3
Na2O	0.77	0.69	0.73	0.78	0.76	0.72	0.78	0.75	0.73	0.73	0.71	0.72	0.69	0.71
K2O	<0.01	0.01	0.01	0.01	0.03	0.02	<0.01	0.01	<0.01	0.01	0.01	0.01	0.01	<0.01
Total	101.1	100.8	101.1	101.1	100.9	100.9	101.2	100.8	100.8	100.4	100.9	101.1	100.1	100.5
Si	1.84	1.84	1.83	1.84	1.83	1.83	1.82	1.83	1.83	1.83	1.83	1.83	1.83	1.82
Ti	0.016	0.015	0.015	0.015	0.016	0.015	0.015	0.016	0.014	0.014	0.015	0.015	0.014	0.014
Al	0.27	0.27	0.27	0.28	0.28	0.28	0.29	0.28	0.28	0.28	0.28	0.28	0.28	0.29
Cr	0.033	0.032	0.030	0.031	0.033	0.032	0.031	0.031	0.030	0.030	0.030	0.029	0.030	0.026
Fe3	0.035	0.045	0.059	0.046	0.045	0.059	0.060	0.054	0.048	0.041	0.062	0.041	0.047	0.064
Fe2	0.052	0.049	0.037	0.047	0.043	0.038	0.031	0.037	0.042	0.056	0.035	0.055	0.045	0.036
Mn	0.002	0.002	0.003	0.002	0.001	0.003	0.003	0.003	0.002	0.003	0.003	0.003	0.002	0.004
Ni	0.003	0.001	0.002	0.003	0.001	0.001	0.002	0.000	0.002	0.001	0.001	0.002	0.000	0.001
Mg	0.82	0.84	0.86	0.82	0.82	0.86	0.82	0.82	0.84	0.82	0.85	0.81	0.83	0.83
Ca	0.87	0.86	0.85	0.87	0.88	0.83	0.88	0.87	0.86	0.86	0.86	0.88	0.87	0.87
Na	0.054	0.048	0.051	0.055	0.054	0.050	0.055	0.053	0.051	0.051	0.049	0.051	0.049	0.050
K	<0.001	<0.001	<0.001	<0.001	0.001	0.001	<0.001	0.001	<0.001	0.001	0.001	<0.001	0.001	<0.001

A2.6b: Clinopyroxene profils

Sample L04

distance	**360**	**370**	**380**	**430**	**440**	**450**	**460**	**470**	**480**	**500**	**510**	**530**	**540**	**560**
SiO2	50.37	50.26	50.28	50.13	50.36	50.08	49.76	50.36	50.35	50.29	50.36	50.51	50.5	50.39
TiO2	0.60	0.56	0.58	0.59	0.59	0.58	0.64	0.55	0.62	0.58	0.59	0.56	0.54	0.60
Al2O3	7.0	6.9	6.8	6.9	6.9	7.1	6.9	6.8	6.9	6.8	6.9	6.5	6.5	6.6
Cr2O3	0.95	1.04	1.08	1.03	1.07	1.01	1.05	0.96	1.10	1.13	1.10	0.96	1.09	1.03
Fe2O3	2.39	1.75	1.82	1.41	1.32	1.99	2.67	1.64	1.94	1.95	1.80	1.69	1.83	2.14
FeO	1.00	1.62	1.36	1.74	1.84	1.43	0.85	1.62	1.45	1.13	1.48	1.60	1.44	1.16
MnO	0.09	0.09	0.08	0.08	0.07	0.12	0.10	0.10	0.10	0.07	0.11	0.10	0.10	0.05
NiO	0.05	0.09	0.04	0.05	0.04	0.02	0.05	0.06	0.01	<0.01	0.01	<0.01	0.08	0.05
MgO	15.2	15.1	15.1	14.9	14.9	15.1	15.3	15.1	14.9	15.0	15.1	15.3	15.0	15.3
CaO	22.7	22.5	22.6	22.4	22.8	22.4	22.3	22.3	22.6	22.8	22.5	22.2	22.8	22.5
Na2O	0.77	0.68	0.73	0.73	0.67	0.71	0.70	0.71	0.78	0.77	0.72	0.72	0.72	0.75
K2O	0.00	<0.01	0.01	0.02	<0.01	0.01	0.01	0.02	<0.01	0.01	0.01	0.02	0.01	<0.01
Total	101.0	100.5	100.4	100.0	100.5	100.5	100.3	100.2	100.8	100.5	100.6	100.2	100.6	100.6
Si	1.82	1.82	1.82	1.83	1.83	1.82	1.81	1.83	1.82	1.82	1.82	1.84	1.83	1.83
Ti	0.016	0.015	0.016	0.016	0.016	0.016	0.017	0.015	0.017	0.016	0.016	0.015	0.015	0.016
Al	0.30	0.29	0.29	0.30	0.29	0.30	0.30	0.29	0.30	0.29	0.29	0.28	0.28	0.28
Cr	0.027	0.030	0.031	0.030	0.031	0.029	0.030	0.028	0.031	0.032	0.031	0.028	0.031	0.030
Fe3	0.065	0.048	0.050	0.039	0.036	0.054	0.073	0.045	0.053	0.053	0.049	0.046	0.050	0.058
Fe2	0.030	0.049	0.041	0.053	0.056	0.043	0.026	0.049	0.044	0.034	0.045	0.049	0.044	0.035
Mn	0.003	0.003	0.003	0.002	0.002	0.004	0.003	0.003	0.003	0.002	0.003	0.003	0.003	0.002
Ni	0.001	0.003	0.001	0.002	0.001	0.001	0.002	0.002	<0.001	<0.001	<0.001	<0.001	0.002	0.001
Mg	0.81	0.81	0.81	0.81	0.80	0.81	0.83	0.82	0.80	0.81	0.82	0.83	0.81	0.82
Ca	0.88	0.87	0.88	0.87	0.89	0.87	0.87	0.87	0.88	0.88	0.87	0.87	0.88	0.87
Na	0.054	0.048	0.051	0.052	0.047	0.050	0.050	0.050	0.055	0.054	0.050	0.051	0.050	0.053
K	<0.001	<0.001	0.001	0.001	<0.001	<0.001	<0.001	0.001	<0.001	0.001	<0.001	0.001	<0.001	<0.001

Sample L04

distance	**580**	**590**	**600**	**620**	**630**	**640**	**650**	**670**	**700**	**710**	**730**	**750**	**760**	**770**
SiO2	50.29	50.21	50.02	50.46	49.56	50.15	50.26	50.26	50.03	50.4	50.77	50.41	50.33	50.71
TiO2	0.57	0.59	0.59	0.56	0.67	0.63	0.64	0.61	0.59	0.57	0.64	0.64	0.60	0.66
Al2O3	6.4	6.5	6.5	6.4	6.9	6.6	6.6	6.4	6.4	6.3	6.4	6.2	6.2	6.1
Cr2O3	1.09	0.96	1.14	1.03	1.08	1.04	0.99	1.08	1.08	1.10	1.18	1.20	1.10	0.98
Fe2O3	2.45	2.29	2.62	2.07	3.03	2.26	2.14	2.38	2.64	2.75	2.49	2.53	2.77	2.09
FeO	0.99	1.06	0.74	1.16	0.42	0.98	1.14	0.99	0.62	0.64	0.96	0.71	0.56	1.08
MnO	0.11	0.06	0.13	0.08	0.05	0.15	0.13	0.12	0.07	0.11	0.13	0.10	0.06	0.07
NiO	0.06	0.05	0.06	0.04	0.07	0.01	0.03	0.04	0.08	0.01	0.01	0.03	0.04	0.02
MgO	15.5	15.4	15.6	15.3	15.0	15.0	15.1	15.3	15.2	16.1	15.5	15.5	15.4	15.3
CaO	22.3	22.2	22.2	22.4	22.5	22.6	22.6	22.4	22.7	21.7	22.5	22.5	22.8	22.8
Na2O	0.72	0.74	0.68	0.78	0.80	0.78	0.76	0.75	0.73	0.75	0.82	0.79	0.73	0.77
K2O	<0.01	<0.01	<0.01	0.01	0.03	0.02	<0.01	<0.01	0.01	0.02	<0.01	<0.01	<0.01	<0.01
Total	100.4	100.1	100.2	100.3	100.1	100.2	100.4	100.3	100.2	100.4	101.4	100.5	100.7	100.6
Si	1.8243	1.8262	1.8175	1.8316	1.8058	1.8238	1.8251	1.8253	1.8199	1.8241	1.8252	1.8269	1.8225	1.8368
Ti	0.016	0.016	0.016	0.015	0.018	0.017	0.017	0.017	0.016	0.015	0.017	0.018	0.016	0.018
Al	0.27	0.28	0.28	0.28	0.30	0.28	0.28	0.27	0.28	0.27	0.27	0.26	0.27	0.26
Cr	0.031	0.028	0.033	0.030	0.031	0.030	0.028	0.031	0.031	0.031	0.034	0.034	0.032	0.028
Fe3	0.067	0.063	0.072	0.057	0.083	0.062	0.059	0.065	0.072	0.075	0.067	0.069	0.075	0.057
Fe2	0.030	0.032	0.022	0.035	0.013	0.030	0.035	0.030	0.019	0.020	0.029	0.021	0.017	0.033
Mn	0.004	0.002	0.004	0.002	0.001	0.005	0.004	0.004	0.002	0.003	0.004	0.003	0.002	0.002
Ni	0.002	0.002	0.002	0.001	0.002	<0.001	0.001	0.001	0.002	<0.001	<0.001	0.001	0.001	0.001
Mg	0.84	0.84	0.84	0.83	0.81	0.81	0.82	0.83	0.83	0.87	0.83	0.83	0.83	0.83
Ca	0.87	0.87	0.86	0.87	0.88	0.88	0.88	0.87	0.88	0.84	0.87	0.87	0.89	0.88
Na	0.050	0.052	0.048	0.055	0.056	0.055	0.053	0.053	0.051	0.053	0.057	0.056	0.051	0.054
K	<0.001	<0.001	<0.001	<0.001	0.001	0.001	<0.001	<0.001	<0.001	0.001	<0.001	<0.001	<0.001	<0.001

A2.6b: Clinopyroxene profils

Sample L04

distance	**780**	**810**	**840**	**850**	**860**	**870**	**880**	**890**	**930**	**960**	**970**	**980**	**990**	**1000**
SiO2	51	51.14	51	51.07	51.25	50.37	50.6	51.44	51.14	51	51.07	51.25	50.37	50.6
TiO2	0.66	0.62	0.63	0.62	0.60	0.56	0.66	0.64	0.62	0.63	0.62	0.60	0.56	0.66
Al2O3	6.2	6.1	6.1	5.9	5.9	6.0	6.0	5.5	6.1	6.1	5.9	5.9	6.0	6.0
Cr2O3	1.13	1.11	1.15	1.17	1.12	1.16	1.16	1.17	1.11	1.15	1.17	1.12	1.16	1.16
Fe2O3	2.02	1.94	1.71	1.62	2.06	2.51	2.06	1.76	1.94	1.71	1.62	2.06	2.51	2.06
FeO	1.21	1.33	1.49	1.48	1.28	0.48	1.00	1.35	1.33	1.49	1.48	1.28	0.48	1.00
MnO	0.09	0.09	0.08	0.11	0.09	0.06	0.08	0.05	0.09	0.08	0.11	0.09	0.06	0.08
NiO	0.06	0.07	0.04	<0.01	0.07	0.11	0.10	0.12	0.07	0.04	<0.01	0.07	0.11	0.10
MgO	15.5	15.6	15.6	15.5	15.6	16.5	16.1	15.7	15.6	15.6	15.5	15.6	16.5	16.1
CaO	22.6	22.6	22.4	22.5	22.7	21.5	21.8	22.6	22.6	22.4	22.5	22.7	21.5	21.8
Na2O	0.78	0.75	0.73	0.76	0.76	0.67	0.69	0.77	0.75	0.73	0.76	0.76	0.67	0.69
K2O	<0.01	<0.01	0.02	<0.01	0.01	0.01	0.02	0.01	<0.01	0.02	<0.01	0.01	0.01	0.02
Total	101.2	101.3	100.9	100.8	101.4	99.9	100.3	101.1	101.3	100.9	100.8	101.4	99.9	100.3
Si	1.84	1.84	1.84	1.85	1.84	1.83	1.83	1.85	1.84	1.84	1.85	1.84	1.83	1.83
Ti	0.018	0.017	0.017	0.017	0.016	0.015	0.018	0.017	0.017	0.017	0.017	0.016	0.015	0.018
Al	0.26	0.26	0.26	0.25	0.25	0.26	0.25	0.23	0.26	0.26	0.25	0.25	0.26	0.25
Cr	0.032	0.032	0.033	0.033	0.032	0.033	0.033	0.033	0.032	0.033	0.033	0.032	0.033	0.033
Fe3	0.055	0.053	0.046	0.044	0.056	0.069	0.056	0.048	0.053	0.046	0.044	0.056	0.069	0.056
Fe2	0.036	0.040	0.045	0.045	0.038	0.015	0.031	0.041	0.040	0.045	0.045	0.038	0.015	0.031
Mn	0.003	0.003	0.002	0.003	0.003	0.002	0.003	0.001	0.003	0.002	0.003	0.003	0.002	0.003
Ni	0.002	0.002	0.001	0.000	0.002	0.003	0.003	0.003	0.002	0.001	<0.001	0.002	0.003	0.003
Mg	0.83	0.84	0.84	0.84	0.83	0.89	0.87	0.84	0.84	0.84	0.84	0.83	0.89	0.87
Ca	0.87	0.87	0.87	0.87	0.87	0.84	0.85	0.87	0.87	0.87	0.87	0.87	0.84	0.85
Na	0.054	0.052	0.051	0.053	0.053	0.047	0.049	0.054	0.052	0.051	0.053	0.053	0.047	0.049
K	<0.001	<0.001	0.001	<0.001	0.001	0.001	0.001	<0.001	<0.001	0.001	<0.001	0.001	0.001	0.001

Sample L04

distance	**1010**	**1050**	**1060**	**1070**	**1080**	**1100**	**1110**	**1120**	**1130**	**1140**	**1150**	**1160**	**1170**	**1180**
SiO2	51.4	51.5	51.5	51.5	51.6	51.0	51.0	51.7	53.1	52.9	53.7	53.1	51.6	52.0
TiO2	0.64	0.80	0.80	0.80	0.84	1.00	0.92	0.92	0.62	0.48	0.51	0.61	0.86	0.82
Al2O3	5.5	4.3	4.3	4.3	4.4	4.4	4.5	4.0	3.0	2.4	2.2	2.4	3.9	3.7
Cr2O3	1.17	1.21	1.21	1.21	1.25	0.97	1.08	1.00	0.80	0.63	0.54	0.66	1.04	1.04
Fe2O3	1.76	2.20	2.20	2.20	1.84	2.36	3.04	2.15	2.10	2.21	1.45	1.62	2.10	1.68
FeO	1.35	0.66	0.66	0.66	0.97	0.61	0.03	0.77	0.67	0.57	0.92	0.93	0.89	1.16
MnO	0.05	0.02	0.02	0.02	0.09	0.07	0.12	0.06	0.06	0.08	0.08	0.05	0.10	0.10
NiO	0.12	<0.01	<0.01	<0.01	0.05	0.05	0.05	0.00	0.03	0.05	0.06	0.05	0.04	0.01
MgO	15.7	16.0	16.0	16.0	15.8	15.8	16.4	16.1	16.9	17.5	17.4	17.1	16.5	16.3
CaO	22.6	23.4	23.4	23.4	23.3	23.2	22.6	23.4	23.4	23.1	23.6	23.6	22.7	23.2
Na2O	0.77	0.65	0.65	0.65	0.70	0.70	0.70	0.67	0.67	0.50	0.54	0.49	0.63	0.61
K2O	0.01	0.03	0.03	0.03	0.01	0.02	0.01	0.01	<0.01	<0.01	<0.01	0.02	0.03	0.00
Total	101.1	100.8	100.8	100.8	100.8	100.2	100.4	100.9	101.3	100.4	101.0	100.6	100.3	100.7
Si	1.85	1.86	1.86	1.86	1.87	1.86	1.85	1.87	1.90	1.91	1.93	1.92	1.87	1.88
Ti	0.017	0.022	0.022	0.022	0.023	0.028	0.025	0.025	0.017	0.013	0.014	0.017	0.023	0.022
Al	0.23	0.18	0.18	0.18	0.19	0.19	0.19	0.17	0.13	0.10	0.09	0.10	0.16	0.16
Cr	0.033	0.035	0.035	0.035	0.036	0.028	0.031	0.029	0.023	0.018	0.015	0.019	0.030	0.030
Fe3	0.048	0.060	0.060	0.060	0.050	0.065	0.083	0.059	0.057	0.060	0.039	0.044	0.057	0.046
Fe2	0.041	0.020	0.020	0.020	0.029	0.019	0.001	0.023	0.020	0.017	0.028	0.028	0.027	0.035
Mn	0.001	0.001	0.001	0.001	0.003	0.002	0.004	0.002	0.002	0.003	0.003	0.002	0.003	0.003
Ni	0.003	<0.001	<0.001	<0.001	0.001	0.001	0.001	<0.001	0.001	0.002	0.002	0.002	0.001	<0.001
Mg	0.84	0.86	0.86	0.86	0.85	0.85	0.89	0.87	0.90	0.94	0.93	0.92	0.89	0.88
Ca	0.87	0.91	0.91	0.91	0.90	0.91	0.88	0.91	0.90	0.90	0.91	0.91	0.88	0.90
Na	0.054	0.046	0.046	0.046	0.049	0.050	0.050	0.047	0.047	0.035	0.038	0.034	0.044	0.043
K	<0.001	0.002	0.002	0.002	0.001	0.001	<0.001	0.001	<0.001	<0.001	<0.001	0.001	0.001	0.000

A2.6b: Clinopyroxene profils

Sample L04

distance	**1190**	**1200**	**1210**	**1220**	**1230**	**1240**	**1250**	**1260**	**1270**
SiO2	50.5	53.4	52.7	51.0	53.6	51.9	52.9	52.9	52.9
TiO2	0.47	0.48	0.60	0.60	0.46	0.89	0.64	0.63	0.64
Al2O3	5.0	2.4	3.2	5.9	2.2	3.6	3.0	2.9	2.8
Cr2O3	0.74	0.90	0.92	0.88	0.71	1.02	1.00	0.84	0.78
Fe2O3	0.96	1.30	1.44	0.32	0.96	1.68	1.63	1.61	2.37
FeO	1.28	1.24	1.20	2.18	1.52	1.18	1.09	1.09	0.58
MnO	0.05	0.07	0.04	0.05	0.15	0.06	0.07	0.04	0.10
NiO	0.03	0.03	0.07	0.05	0.03	0.02	0.01	0.01	0.09
MgO	16.1	17.3	16.5	15.4	17.3	16.4	17.0	17.0	17.1
CaO	21.7	23.1	23.2	21.9	23.0	23.0	23.1	23.0	23.2
Na2O	0.62	0.55	0.68	0.79	0.52	0.60	0.61	0.61	0.61
K2O	0.01	<0.01	<0.01	0.01	<0.01	0.01	0.01	0.01	<0.01
Total	97.4	100.8	100.5	99.0	100.5	100.4	100.9	100.8	101.3
Si	1.88	1.92	1.91	1.87	1.94	1.88	1.91	1.91	1.90
Ti	0.013	0.013	0.016	0.016	0.013	0.024	0.017	0.017	0.017
Al	0.22	0.10	0.14	0.25	0.09	0.15	0.13	0.12	0.12
Cr	0.022	0.026	0.026	0.025	0.020	0.029	0.029	0.024	0.022
Fe3	0.027	0.035	0.039	0.009	0.026	0.046	0.044	0.044	0.064
Fe2	0.040	0.037	0.036	0.067	0.046	0.036	0.033	0.033	0.018
Mn	0.002	0.002	0.001	0.002	0.005	0.002	0.002	0.001	0.003
Ni	0.001	0.001	0.002	0.002	0.001	0.001	<0.001	<0.001	0.003
Mg	0.89	0.93	0.89	0.84	0.93	0.89	0.91	0.92	0.92
Ca	0.87	0.89	0.90	0.86	0.89	0.90	0.89	0.89	0.89
Na	0.045	0.038	0.048	0.056	0.037	0.042	0.043	0.043	0.042
K	<0.001	<0.001	<0.001	<0.001	<0.001	<0.001	0.001	<0.001	<0.001

Sample L112

distance	**0**	**10**	**30**	**40**	**50**	**70**	**90**	**100**	**120**	**130**	**140**	**150**	**160**	**180**
SiO2	52.3	52.3	50.7	50.8	50.5	50.7	50.7	50.3	50.4	50.7	50.1	50.2	50.1	50.4
TiO2	0.79	0.78	0.86	0.84	0.95	0.90	0.84	0.83	0.75	0.77	0.85	0.75	0.81	0.75
Al2O3	3.1	3.5	4.2	4.7	5.2	5.3	5.5	5.6	5.6	5.5	5.8	5.7	5.8	5.6
Cr2O3	0.79	0.87	1.07	1.27	1.24	1.24	1.29	1.29	1.28	1.30	1.24	1.26	1.28	1.25
Fe2O3	0.99	1.01	1.42	2.30	2.02	1.63	1.70	1.89	1.92	1.85	1.96	2.07	2.29	2.12
FeO	2.00	1.94	1.71	0.98	1.20	1.71	1.76	1.44	1.44	1.64	1.34	1.26	1.19	1.38
MnO	0.08	0.12	0.11	0.05	0.04	0.11	0.09	0.13	0.09	0.10	0.06	0.18	0.11	0.14
NiO	0.03	0.06	<0.01	0.05	0.02	0.03	0.02	0.05	0.04	<0.01	<0.01	0.05	0.03	0.05
MgO	16.3	16.4	15.7	16.3	15.2	15.1	15.1	15.3	15.2	15.6	15.1	15.0	15.3	15.8
CaO	23.1	22.8	22.2	22.2	23.0	22.8	22.9	22.6	22.9	22.4	22.8	22.8	22.7	22.0
Na2O	0.53	0.56	0.68	0.61	0.74	0.73	0.70	0.66	0.64	0.67	0.69	0.73	0.65	0.65
K2O	<0.01	<0.01	0.06	0.01	<0.01	<0.01	0.01	<0.01	0.01	<0.01	0.01	0.01	<0.01	0.01
Total	100.0	100.4	98.6	100.2	100.1	100.3	100.6	100.1	100.2	100.5	99.9	100.0	100.2	100.2
Si	1.91	1.90	1.88	1.85	1.84	1.85	1.84	1.84	1.84	1.84	1.83	1.84	1.83	1.83
Ti	0.022	0.021	0.024	0.023	0.026	0.025	0.023	0.023	0.021	0.021	0.023	0.021	0.022	0.021
Al	0.13	0.15	0.18	0.20	0.22	0.23	0.23	0.24	0.24	0.23	0.25	0.25	0.25	0.24
Cr	0.023	0.025	0.031	0.036	0.036	0.036	0.037	0.037	0.037	0.037	0.036	0.036	0.037	0.036
Fe3	0.027	0.028	0.040	0.063	0.056	0.045	0.047	0.052	0.053	0.051	0.054	0.057	0.063	0.058
Fe2	0.061	0.059	0.053	0.030	0.037	0.052	0.053	0.044	0.044	0.050	0.041	0.038	0.036	0.042
Mn	0.003	0.004	0.003	0.002	0.001	0.003	0.003	0.004	0.003	0.003	0.002	0.006	0.004	0.004
Ni	0.001	0.002	<0.001	0.001	<0.001	0.001	0.001	0.002	0.001	<0.001	<0.001	0.001	0.001	0.002
Mg	0.89	0.89	0.86	0.88	0.83	0.82	0.82	0.83	0.82	0.84	0.82	0.82	0.83	0.86
Ca	0.90	0.89	0.88	0.87	0.90	0.89	0.89	0.88	0.90	0.87	0.89	0.89	0.89	0.86
Na	0.037	0.040	0.049	0.043	0.053	0.051	0.049	0.047	0.045	0.047	0.049	0.052	0.046	0.046
K	<0.001	<0.001	0.003	<0.001	<0.001	<0.001	0.001	<0.001	<0.001	<0.001	<0.001	<0.001	<0.001	<0.001

A2.6b: Clinopyroxene profils

Sample L112

distance	**190**	**210**	**230**	**250**	**260**	**270**	**290**	**310**	**320**	**330**	**340**	**370**	**390**	**400**
SiO2	50.6	50.8	50.6	50.6	50.7	50.7	50.6	50.5	50.5	50.4	50.4	50.5	50.6	50.1
TiO2	0.75	0.74	0.80	0.84	0.76	0.73	0.79	0.80	0.79	0.72	0.79	0.81	0.83	0.87
Al2O3	5.7	5.7	5.8	5.8	5.8	5.7	5.6	5.7	5.7	5.8	5.7	5.7	5.7	5.8
Cr2O3	1.30	1.21	1.28	1.26	1.28	1.24	1.23	1.25	1.29	1.22	1.27	1.23	1.27	1.27
Fe2O3	2.09	1.72	1.84	1.82	1.30	1.39	1.54	2.88	2.35	2.06	2.03	1.99	2.06	2.17
FeO	1.48	1.67	1.64	1.51	2.05	1.92	1.72	0.61	1.22	1.33	1.34	1.48	1.54	1.09
MnO	0.10	0.06	0.12	0.13	0.10	0.09	0.13	0.12	0.02	0.10	0.12	0.12	0.05	0.14
NiO	0.02	0.08	0.05	0.04	0.03	0.02	0.03	0.04	<0.01	0.04	0.03	0.01	0.03	0.02
MgO	15.4	15.1	15.0	15.0	15.2	15.0	15.1	16.1	15.4	15.8	15.2	15.3	15.2	14.9
CaO	22.7	23.0	22.9	23.0	22.5	22.9	22.9	22.2	22.6	22.2	22.9	22.6	22.8	23.1
Na2O	0.66	0.69	0.70	0.73	0.67	0.67	0.66	0.70	0.73	0.60	0.66	0.68	0.70	0.72
K2O	0.01	<0.01	<0.01	<0.01	0.01	0.02	<0.01	<0.01	0.02	0.02	0.02	0.02	<0.01	<0.01
Total	100.8	100.7	100.7	100.8	100.3	100.4	100.3	100.8	100.6	100.3	100.4	100.4	100.8	100.2
Si	1.83	1.84	1.84	1.84	1.84	1.85	1.84	1.83	1.83	1.83	1.83	1.84	1.83	1.83
Ti	0.020	0.020	0.022	0.023	0.021	0.020	0.022	0.022	0.022	0.020	0.022	0.022	0.023	0.024
Al	0.24	0.24	0.25	0.25	0.25	0.25	0.24	0.24	0.24	0.25	0.24	0.24	0.24	0.25
Cr	0.037	0.035	0.037	0.036	0.037	0.036	0.035	0.036	0.037	0.035	0.037	0.035	0.036	0.037
Fe3	0.057	0.047	0.050	0.050	0.036	0.038	0.042	0.079	0.064	0.056	0.056	0.054	0.056	0.060
Fe2	0.045	0.051	0.050	0.046	0.062	0.058	0.053	0.018	0.037	0.041	0.041	0.045	0.047	0.033
Mn	0.003	0.002	0.004	0.004	0.003	0.003	0.004	0.004	0.001	0.003	0.004	0.004	0.002	0.004
Ni	0.001	0.002	0.002	0.001	0.001	0.001	0.001	0.001	<0.001	0.001	0.001	<0.001	0.001	0.001
Mg	0.83	0.82	0.81	0.81	0.83	0.81	0.82	0.87	0.83	0.86	0.82	0.83	0.82	0.81
Ca	0.88	0.89	0.89	0.90	0.88	0.89	0.89	0.86	0.88	0.86	0.89	0.88	0.89	0.90
Na	0.046	0.049	0.049	0.052	0.047	0.048	0.047	0.049	0.051	0.042	0.047	0.048	0.050	0.051
K	<0.001	<0.001	<0.001	<0.001	<0.001	0.001	<0.001	<0.001	0.001	0.001	0.001	0.001	<0.001	<0.001

Sample L112

distance	**420**	**430**	**440**	**460**	**470**	**480**	**490**	**500**	**510**	**520**	**530**	**540**	**550**	**560**
SiO2	50.08	50.65	50.55	50.21	50.53	50.42	50.63	50.26	50.58	50.71	50.5	50.35	50.0	50.72
TiO2	0.80	0.73	0.82	0.85	0.71	0.77	0.81	0.86	0.76	0.78	0.77	0.81	0.80	0.76
Al2O3	5.7	5.6	5.5	5.6	5.6	5.6	5.6	5.8	5.6	5.6	5.6	5.6	5.6	5.5
Cr2O3	1.26	1.25	1.23	1.27	1.22	1.28	1.24	1.24	1.23	1.18	1.19	1.27	1.25	1.23
Fe2O3	2.41	1.61	1.68	1.85	1.93	1.72	1.60	1.73	1.80	1.60	1.45	1.67	2.12	1.58
FeO	0.97	1.66	1.58	1.48	1.41	1.60	1.64	1.64	1.68	1.78	1.73	1.47	1.16	1.65
MnO	0.12	0.10	0.12	0.10	0.11	0.05	0.06	0.11	0.04	0.06	0.10	0.09	0.06	0.07
NiO	0.05	0.08	0.06	0.03	0.07	0.04	0.06	0.00	0.06	0.03	0.03	0.07	0.05	0.03
MgO	15.0	15.2	15.1	15.0	15.1	14.9	15.1	15.0	15.4	15.3	15.0	15.0	14.9	15.1
CaO	23.2	22.8	23.0	22.9	22.8	23.1	22.9	23.0	22.5	22.6	23.0	23.1	23.1	22.9
Na2O	0.67	0.67	0.67	0.67	0.70	0.66	0.70	0.66	0.68	0.69	0.65	0.62	0.68	0.72
K2O	0.01	<0.01	0.01	0.01	<0.01	0.01	<0.01	<0.01	<0.01	0.01	<0.01	0.01	<0.01	0.02
Total	100.2	100.3	100.2	100.0	100.2	100.2	100.4	100.2	100.3	100.3	100.1	100.1	99.7	100.2
Si	1.83	1.84	1.84	1.84	1.84	1.84	1.84	1.83	1.84	1.85	1.84	1.84	1.83	1.85
Ti	0.022	0.020	0.022	0.023	0.019	0.021	0.022	0.024	0.021	0.021	0.021	0.022	0.022	0.021
Al	0.24	0.24	0.23	0.24	0.24	0.24	0.24	0.25	0.24	0.24	0.24	0.24	0.24	0.24
Cr	0.037	0.036	0.036	0.037	0.035	0.037	0.036	0.036	0.035	0.034	0.035	0.037	0.036	0.036
Fe3	0.066	0.044	0.046	0.051	0.053	0.047	0.044	0.048	0.049	0.044	0.040	0.046	0.059	0.043
Fe2	0.030	0.051	0.048	0.045	0.043	0.049	0.050	0.050	0.051	0.054	0.053	0.045	0.036	0.050
Mn	0.004	0.003	0.004	0.003	0.004	0.002	0.002	0.003	0.001	0.002	0.003	0.003	0.002	0.002
Ni	0.001	0.002	0.002	0.001	0.002	0.001	0.002	<0.001	0.002	0.001	0.001	0.002	0.002	0.001
Mg	0.81	0.83	0.82	0.82	0.82	0.81	0.82	0.81	0.83	0.83	0.82	0.82	0.81	0.82
Ca	0.91	0.89	0.90	0.90	0.89	0.90	0.89	0.90	0.88	0.88	0.90	0.90	0.91	0.89
Na	0.048	0.048	0.047	0.048	0.049	0.047	0.050	0.047	0.048	0.049	0.046	0.044	0.048	0.051
K	<0.001	<0.001	0.001	<0.001	<0.001	0.001	<0.001	<0.001	<0.001	0.001	<0.001	<0.001	<0.001	0.001

A2.6b: Clinopyroxene profils

Sample L112

distance	**570**	**590**	**600**	**610**	**620**	**630**	**650**	**660**	**670**	**690**	**700**	**720**	**730**	**740**
SiO2	50.8	50.1	50.4	50.2	50.7	51.1	50.7	50.7	50.7	50.8	50.7	50.6	50.5	50.7
TiO2	0.79	0.79	0.81	0.85	0.79	0.75	0.77	0.69	0.74	0.80	0.78	0.79	0.85	0.82
Al2O3	5.5	5.5	5.5	5.7	5.6	5.4	5.5	5.4	5.3	5.4	5.4	5.4	5.5	5.6
Cr2O3	1.26	1.23	1.26	1.26	1.18	1.28	1.15	1.13	1.24	1.19	1.29	1.22	1.21	1.26
Fe2O3	2.38	2.03	2.38	2.71	1.82	1.58	1.43	1.93	1.33	1.56	1.82	2.28	2.07	1.43
FeO	1.25	1.05	1.01	0.70	1.77	1.68	1.85	1.34	1.76	1.86	1.48	1.22	1.26	1.63
MnO	0.04	0.03	0.09	0.15	0.06	0.12	0.10	0.03	0.12	0.14	0.10	0.16	0.08	0.04
NiO	0.11	0.04	0.03	0.05	0.08	0.03	0.05	0.03	0.02	0.07	0.07	0.06	0.02	0.03
MgO	16.1	15.0	15.2	15.1	15.6	15.4	15.1	15.2	15.0	15.9	15.3	15.2	15.8	15.2
CaO	22.2	23.0	23.0	23.2	22.4	23.0	23.0	23.1	23.0	22.0	22.9	23.0	22.2	23.0
Na2O	0.64	0.70	0.69	0.73	0.62	0.66	0.64	0.69	0.67	0.61	0.68	0.68	0.67	0.66
K2O	<0.01	<0.01	0.04	<0.01	<0.01	0.01	0.02	0.02	<0.01	0.03	<0.01	0.02	0.01	0.02
Total	101.0	99.5	100.3	100.5	100.6	101.0	100.2	100.1	99.9	100.2	100.5	100.7	100.1	100.4
Si	1.83	1.84	1.83	1.83	1.84	1.85	1.85	1.85	1.85	1.85	1.84	1.84	1.84	1.84
Ti	0.022	0.022	0.022	0.023	0.021	0.020	0.021	0.019	0.021	0.022	0.021	0.022	0.023	0.022
Al	0.23	0.24	0.24	0.24	0.24	0.23	0.23	0.23	0.23	0.23	0.23	0.23	0.24	0.24
Cr	0.036	0.036	0.036	0.036	0.034	0.037	0.033	0.033	0.036	0.034	0.037	0.035	0.035	0.036
Fe3	0.065	0.056	0.065	0.074	0.050	0.043	0.039	0.053	0.037	0.043	0.050	0.062	0.057	0.039
Fe2	0.038	0.032	0.031	0.022	0.054	0.051	0.057	0.041	0.054	0.057	0.045	0.037	0.038	0.050
Mn	0.001	0.001	0.003	0.005	0.002	0.004	0.003	0.001	0.004	0.004	0.003	0.005	0.002	0.001
Ni	0.003	0.001	0.001	0.001	0.002	0.001	0.001	0.001	0.001	0.002	0.002	0.002	0.001	0.001
Mg	0.87	0.82	0.82	0.82	0.84	0.83	0.82	0.82	0.82	0.86	0.83	0.82	0.86	0.82
Ca	0.86	0.90	0.90	0.90	0.87	0.89	0.90	0.90	0.90	0.86	0.89	0.89	0.87	0.90
Na	0.045	0.050	0.049	0.051	0.044	0.046	0.045	0.049	0.047	0.043	0.048	0.048	0.048	0.047
K	<0.001	<0.001	0.002	<0.001	<0.001	<0.001	0.001	0.001	<0.001	0.002	<0.001	0.001	<0.001	0.001

Sample L112

distance	**750**	**760**	**770**	**780**	**800**	**810**	**820**	**830**	**840**	**850**
SiO2	50.6	50.9	50.6	50.6	50.8	51.1	51.8	51.4	52.1	52.3
TiO2	0.75	0.81	0.90	0.87	0.90	0.87	0.85	0.90	0.81	0.85
Al2O3	5.7	5.1	5.0	4.8	5.0	4.7	4.5	4.2	3.9	3.7
Cr2O3	1.20	1.18	1.20	1.23	1.23	1.15	1.16	1.03	0.97	0.94
Fe2O3	2.61	1.69	1.78	2.27	2.34	2.11	0.88	1.87	1.19	0.85
FeO	0.91	1.84	1.41	1.12	1.03	0.95	2.25	1.22	1.59	2.17
MnO	0.10	0.10	0.06	0.12	0.06	0.14	0.04	0.08	0.03	0.03
NiO	0.07	0.06	0.06	0.05	0.05	0.04	0.05	0.10	0.03	0.05
MgO	16.5	16.0	15.4	15.7	15.4	15.5	15.9	15.8	15.8	15.9
CaO	21.6	22.0	23.0	22.7	23.1	23.3	22.8	23.4	23.6	23.4
Na2O	0.66	0.61	0.64	0.64	0.73	0.70	0.59	0.58	0.61	0.59
K2O	0.02	<0.01	<0.01	<0.01	0.01	0.02	<0.01	0.01	<0.01	<0.01
Total	100.7	100.3	100.0	100.1	100.7	100.6	100.8	100.6	100.6	100.7
Si	1.83	1.85	1.85	1.85	1.85	1.86	1.87	1.87	1.89	1.89
Ti	0.021	0.022	0.025	0.024	0.025	0.024	0.023	0.025	0.022	0.023
Al	0.24	0.22	0.21	0.20	0.21	0.20	0.19	0.18	0.17	0.16
Cr	0.034	0.034	0.035	0.036	0.035	0.033	0.033	0.030	0.028	0.027
Fe3	0.071	0.046	0.049	0.062	0.064	0.058	0.024	0.051	0.033	0.023
Fe2	0.027	0.056	0.043	0.034	0.031	0.029	0.068	0.037	0.048	0.066
Mn	0.003	0.003	0.002	0.004	0.002	0.004	0.001	0.003	0.001	0.001
Ni	0.002	0.002	0.002	0.002	0.002	0.001	0.001	0.003	0.001	0.001
Mg	0.89	0.87	0.84	0.85	0.83	0.84	0.86	0.86	0.86	0.86
Ca	0.83	0.86	0.90	0.89	0.90	0.91	0.88	0.91	0.92	0.91
Na	0.046	0.043	0.046	0.046	0.052	0.049	0.041	0.041	0.043	0.041
K	0.001	<0.001	<0.001	<0.001	<0.001	0.001	<0.001	<0.001	<0.001	<0.001

A2.6b: Clinopyroxene profils

Sample L09

distance	**15**	**30**	**60**	**75**	**90**	**105**	**120**	**135**	**180**	**195**	**210**	**225**	**255**	**315**
SiO2	51.94	51.88	51.94	51.47	51.23	51.31	51.47	51.08	51.21	50.81	50.88	51.13	50.75	51.25
TiO2	0.76	0.78	0.68	0.64	0.65	0.75	0.65	0.91	0.79	0.74	0.73	0.69	0.80	0.76
Al2O3	3.5	4.1	3.8	4.0	4.2	4.1	3.8	4.6	4.9	4.9	4.9	4.7	4.9	4.5
Cr2O3	0.97	1.27	1.27	1.27	1.24	1.20	1.33	1.27	1.48	1.35	1.34	1.21	1.35	1.26
Fe2O3	1.37	1.20	1.05	1.79	2.41	1.79	1.99	2.34	1.73	1.95	2.07	1.58	2.09	1.76
FeO	1.41	1.74	1.90	1.32	0.86	1.31	1.21	0.81	1.26	1.09	0.98	1.54	1.16	1.29
MnO	0.10	0.13	0.05	0.12	0.10	0.11	0.12	0.08	0.09	0.08	0.09	0.10	0.03	0.03
MgO	16.4	16.3	16.1	16.2	16.6	16.1	16.2	16.4	16.0	16.0	15.8	15.7	15.6	15.9
CaO	23.1	22.8	22.9	22.7	22.2	22.9	22.9	22.2	22.8	22.3	23.1	22.9	22.8	22.9
Na2O	0.54	0.56	0.57	0.57	0.60	0.57	0.57	0.72	0.61	0.66	0.59	0.59	0.69	0.66
K2O	<0.01	0.01	0.01	<0.01	0.01	<0.01	<0.01	0.02	0.01	0.01	<0.01	<0.01	<0.01	<0.01
Total	100.0	100.7	100.3	100.1	100.2	100.1	100.2	100.4	100.9	99.9	100.5	100.2	100.2	100.2
Si	1.89	1.88	1.89	1.87	1.86	1.87	1.87	1.85	1.85	1.85	1.85	1.86	1.85	1.86
Ti	0.021	0.021	0.019	0.018	0.018	0.021	0.018	0.025	0.021	0.020	0.020	0.019	0.022	0.021
Al	0.15	0.17	0.16	0.17	0.18	0.17	0.16	0.20	0.21	0.21	0.21	0.20	0.21	0.19
Cr	0.028	0.036	0.037	0.037	0.036	0.035	0.038	0.036	0.042	0.039	0.039	0.035	0.039	0.036
Fe3	0.038	0.033	0.029	0.049	0.066	0.049	0.055	0.064	0.047	0.053	0.057	0.043	0.057	0.048
Fe2	0.043	0.053	0.058	0.040	0.026	0.040	0.037	0.025	0.038	0.033	0.030	0.047	0.035	0.039
Mn	0.003	0.004	0.002	0.004	0.003	0.003	0.004	0.002	0.003	0.003	0.003	0.003	0.001	0.001
Mg	0.89	0.88	0.87	0.88	0.90	0.87	0.88	0.88	0.86	0.87	0.85	0.85	0.85	0.86
Ca	0.90	0.89	0.89	0.89	0.87	0.89	0.89	0.86	0.88	0.87	0.90	0.89	0.89	0.89
Na	0.038	0.039	0.040	0.040	0.042	0.040	0.040	0.051	0.043	0.046	0.042	0.042	0.049	0.047
K	<0.001	0.001	0.001	<0.001	<0.001	<0.001	<0.001	0.001	<0.001	0.001	<0.001	<0.001	<0.001	<0.001

Sample L09

distance	**330**	**345**	**360**	**375**	**390**	**420**	**435**	**450**	**465**	**480**	**510**	**525**	**540**	**555**
SiO2	51.5	51.4	51.5	51.4	51.8	51.5	51.2	52.0	51.4	51.4	51.2	51.4	51.3	51.4
TiO2	0.82	0.83	0.78	0.83	0.77	0.64	0.70	0.64	0.62	0.64	0.64	0.65	0.72	0.64
Al2O3	4.5	4.2	4.3	4.2	3.7	4.0	4.0	3.9	3.8	3.9	4.0	3.9	4.0	4.0
Cr2O3	1.17	1.12	1.26	1.35	1.13	1.14	1.14	1.24	1.18	1.15	1.19	1.25	1.19	1.23
Fe2O3	0.97	1.43	1.58	1.76	1.93	2.05	1.67	1.34	1.67	2.02	2.33	1.84	2.49	1.98
FeO	2.17	1.47	1.47	1.24	1.07	1.36	1.34	1.91	1.30	1.03	0.94	1.38	0.78	1.27
MnO	0.05	0.09	0.07	0.04	0.07	0.12	0.12	0.08	0.07	0.08	0.09	0.09	0.06	0.11
MgO	16.5	16.1	15.9	16.4	16.4	17.2	16.3	17.3	16.2	16.1	16.4	16.3	16.3	16.4
CaO	21.8	22.8	22.9	22.6	22.9	21.3	22.5	21.3	22.6	22.7	22.6	22.7	22.5	22.4
Na2O	0.59	0.60	0.66	0.59	0.61	0.59	0.57	0.56	0.63	0.65	0.56	0.51	0.70	0.55
K2O	0.01	<0.01	<0.01	0.01	0.01	<0.01	<0.01	<0.01	0.01	0.02	<0.01	<0.01	0.04	0.01
Total	100.0	100.1	100.4	100.4	100.4	99.9	99.5	100.3	99.5	99.7	100.0	100.0	100.0	100.0
Si	1.8724	1.8725	1.8696	1.8655	1.88	1.8732	1.8759	1.8826	1.8828	1.8777	1.8682	1.8727	1.869	1.871
Ti	0.022	0.023	0.021	0.023	0.021	0.018	0.019	0.018	0.017	0.018	0.018	0.018	0.020	0.018
Al	0.19	0.18	0.19	0.18	0.16	0.17	0.17	0.17	0.17	0.17	0.17	0.17	0.17	0.17
Cr	0.034	0.032	0.036	0.039	0.033	0.033	0.033	0.035	0.034	0.033	0.034	0.036	0.034	0.036
Fe3	0.027	0.039	0.043	0.048	0.053	0.056	0.046	0.037	0.046	0.056	0.064	0.051	0.068	0.054
Fe2	0.066	0.045	0.045	0.038	0.033	0.042	0.041	0.058	0.040	0.031	0.029	0.042	0.024	0.039
Mn	0.001	0.003	0.002	0.001	0.002	0.004	0.004	0.002	0.002	0.003	0.003	0.003	0.002	0.003
Mg	0.89	0.87	0.86	0.89	0.89	0.93	0.89	0.93	0.88	0.88	0.89	0.88	0.88	0.89
Ca	0.85	0.89	0.89	0.88	0.89	0.83	0.88	0.83	0.88	0.89	0.88	0.89	0.88	0.88
Na	0.042	0.042	0.047	0.041	0.043	0.042	0.041	0.039	0.045	0.046	0.040	0.036	0.050	0.039
K	<0.001	<0.001	<0.001	0.001	<0.001	<0.001	<0.001	<0.001	<0.001	0.001	<0.001	<0.001	0.002	<0.001

A2.6b: Clinopyroxene profils

Sample L09

distance	**585**	**600**	**630**	**645**	**675**	**690**	**705**	**720**	**735**	**765**	**780**	**810**	**825**	**840**
SiO2	51.0	51.1	51.1	51.3	51.7	51.4	51.4	51.1	51.6	51.6	51.8	52.2	51.7	51.5
TiO2	0.72	0.69	0.67	0.70	0.67	0.71	0.73	0.70	0.74	0.77	0.73	0.72	0.72	0.74
Al2O3	3.9	4.0	4.1	4.0	4.1	4.1	4.1	4.1	4.1	3.7	3.2	3.2	3.7	3.7
Cr2O3	1.19	1.25	1.09	1.21	1.12	1.28	1.27	1.19	1.24	1.24	0.97	1.20	1.33	1.20
Fe2O3	2.63	2.20	2.41	2.04	1.59	1.86	1.76	1.99	1.64	1.82	1.61	1.52	1.92	1.78
FeO	0.70	0.97	0.83	1.14	1.80	1.45	1.43	1.10	1.59	1.26	1.24	1.29	0.92	0.93
MnO	0.11	0.05	0.15	0.07	0.09	0.10	0.11	0.09	0.08	0.08	0.07	0.13	0.14	0.09
MgO	16.9	16.3	16.1	16.1	17.3	17.1	16.4	16.0	16.3	16.4	16.5	16.6	16.4	16.1
CaO	22.1	22.6	22.8	22.5	21.1	21.3	22.3	22.9	22.6	22.7	22.8	22.9	22.8	23.0
Na2O	0.51	0.56	0.59	0.66	0.57	0.61	0.60	0.58	0.57	0.58	0.55	0.60	0.65	0.65
K2O	<0.01	<0.01	0.01	<0.01	<0.01	0.01	0.01	<0.01	<0.01	<0.01	<0.01	<0.01	<0.01	<0.01
Total	99.9	99.8	99.9	99.8	100.0	99.9	100.1	99.8	100.4	100.2	99.6	100.4	100.2	99.8
Si	1.86	1.87	1.87	1.87	1.88	1.87	1.87	1.87	1.87	1.88	1.89	1.90	1.88	1.88
Ti	0.020	0.019	0.019	0.019	0.018	0.020	0.020	0.019	0.020	0.021	0.020	0.020	0.020	0.020
Al	0.17	0.17	0.18	0.17	0.17	0.17	0.18	0.18	0.18	0.16	0.14	0.14	0.16	0.16
Cr	0.034	0.036	0.032	0.035	0.032	0.037	0.037	0.034	0.036	0.036	0.028	0.034	0.038	0.035
Fe3	0.072	0.060	0.066	0.056	0.044	0.051	0.048	0.055	0.045	0.050	0.044	0.042	0.053	0.049
Fe2	0.021	0.030	0.025	0.035	0.055	0.044	0.043	0.034	0.048	0.038	0.038	0.039	0.028	0.028
Mn	0.004	0.002	0.005	0.002	0.003	0.003	0.003	0.003	0.002	0.003	0.002	0.004	0.005	0.003
Mg	0.92	0.89	0.88	0.88	0.94	0.93	0.89	0.87	0.88	0.89	0.90	0.90	0.89	0.88
Ca	0.86	0.89	0.89	0.88	0.82	0.83	0.87	0.90	0.88	0.88	0.89	0.89	0.89	0.90
Na	0.036	0.039	0.042	0.047	0.040	0.043	0.042	0.041	0.040	0.041	0.039	0.042	0.046	0.046
K	<0.001	<0.001	0.001	<0.001	<0.001	0.001	<0.001	<0.001	<0.001	<0.001	<0.001	<0.001	<0.001	<0.001

Sample L09

distance	**870**	**885**	**900**	**930**	**945**	**975**	**990**	**1005**	**1020**	**1050**	**1080**	**1095**	**1125**	**1140**
SiO2	51.4	50.8	51.3	50.7	50.7	51.0	50.7	50.9	50.6	50.2	50.3	50.6	50.0	50.0
TiO2	0.84	0.87	0.79	0.84	0.85	0.78	0.80	0.77	0.82	0.79	0.74	0.73	0.77	0.76
Al2O3	4.2	4.8	4.5	4.9	4.9	5.0	5.2	4.8	5.4	5.5	5.7	5.5	5.9	5.9
Cr2O3	1.21	1.32	1.23	1.24	1.24	1.31	1.23	1.18	1.20	1.30	1.20	1.16	1.17	1.30
Fe2O3	1.51	1.94	1.94	1.79	2.27	1.45	1.87	1.44	1.76	2.77	2.34	1.38	1.73	2.45
FeO	1.30	1.23	1.42	1.23	0.83	1.62	1.35	1.52	1.42	0.50	0.94	1.76	1.47	0.78
MnO	0.05	0.06	0.07	0.05	0.11	0.08	0.06	0.10	0.11	0.11	0.12	0.06	0.06	0.09
MgO	16.0	16.4	17.2	15.5	15.6	15.8	15.8	15.7	15.4	15.5	15.4	15.4	15.3	15.1
CaO	23.0	21.9	21.1	22.8	23.0	22.7	22.5	22.6	23.1	23.0	22.9	22.6	22.3	22.9
Na2O	0.63	0.64	0.62	0.67	0.65	0.59	0.65	0.62	0.58	0.66	0.66	0.65	0.65	0.69
K2O	<0.01	0.01	<0.01	<0.01	0.02	<0.01	0.01	0.01	0.01	<0.01	<0.01	<0.01	<0.01	<0.01
Total	100.1	99.9	100.2	99.7	100.2	100.4	100.1	99.7	100.3	100.3	100.3	99.8	99.4	100.0
Si	1.87	1.85	1.86	1.85	1.84	1.85	1.85	1.86	1.84	1.83	1.83	1.85	1.83	1.82
Ti	0.023	0.024	0.022	0.023	0.023	0.021	0.022	0.021	0.023	0.022	0.020	0.020	0.021	0.021
Al	0.18	0.21	0.19	0.21	0.21	0.22	0.22	0.21	0.23	0.23	0.24	0.24	0.26	0.25
Cr	0.035	0.038	0.035	0.036	0.036	0.038	0.035	0.034	0.035	0.037	0.034	0.034	0.034	0.038
Fe3	0.042	0.053	0.053	0.049	0.062	0.040	0.051	0.040	0.048	0.076	0.064	0.038	0.048	0.067
Fe2	0.040	0.037	0.043	0.038	0.025	0.049	0.041	0.047	0.043	0.015	0.029	0.054	0.045	0.024
Mn	0.001	0.002	0.002	0.002	0.003	0.002	0.002	0.003	0.004	0.004	0.004	0.002	0.002	0.003
Mg	0.87	0.89	0.93	0.85	0.85	0.86	0.86	0.86	0.83	0.84	0.83	0.84	0.84	0.82
Ca	0.90	0.86	0.82	0.89	0.90	0.88	0.88	0.89	0.90	0.90	0.89	0.88	0.88	0.90
Na	0.044	0.045	0.044	0.048	0.046	0.041	0.046	0.044	0.041	0.047	0.046	0.046	0.046	0.049
K	<0.001	<0.001	<0.001	<0.001	0.001	<0.001	<0.001	<0.001	<0.001	<0.001	<0.001	<0.001	<0.001	<0.001

A2.6b: Clinopyroxene profils

Sample L09

distance	1170	1185	1200	1215	1230	1245	1275	1290	1305	1320	1365	1380	1395	1410
SiO2	50.0	50.0	50.0	49.7	49.4	49.4	49.8	49.6	50.1	50.1	50.1	50.2	50.1	50.28
TiO2	0.77	0.74	0.76	0.74	0.80	0.85	0.90	0.81	0.80	0.75	0.73	0.68	0.70	0.69
Al2O3	6.1	6.1	6.2	6.3	6.4	6.6	6.6	6.6	6.7	6.6	6.5	6.4	6.4	6.2
Cr2O3	1.12	1.25	1.30	1.27	1.37	1.25	1.29	1.22	1.31	1.18	1.24	1.30	1.18	1.24
Fe2O3	2.79	2.43	2.33	2.67	1.73	2.23	1.23	1.70	1.90	1.16	1.52	1.38	1.55	1.63
FeO	0.74	0.98	0.88	0.76	1.41	1.07	1.74	1.54	1.47	2.02	1.81	1.98	1.54	1.52
MnO	0.08	0.07	0.11	0.11	0.09	0.06	0.04	0.07	0.09	0.06	0.09	0.09	0.11	0.13
MgO	15.3	15.4	15.1	15.1	14.9	15.0	14.8	15.0	15.4	14.9	15.0	15.8	15.0	15.3
CaO	22.6	22.5	22.8	22.6	22.6	22.5	22.9	22.4	22.1	22.4	22.6	21.6	22.6	22.2
Na2O	0.72	0.67	0.71	0.71	0.61	0.70	0.61	0.66	0.71	0.66	0.63	0.57	0.68	0.71
K2O	0.01	<0.01	0.01	<0.01	<0.01	<0.01	<0.01	0.01	<0.01	0.01	<0.01	<0.01	<0.01	<0.01
Total	100.2	100.1	100.2	100.0	99.2	99.5	100.0	99.6	100.5	99.8	100.3	99.9	99.9	100.0
Si	1.82	1.82	1.82	1.81	1.82	1.81	1.82	1.82	1.81	1.83	1.82	1.83	1.83	1.83
Ti	0.021	0.020	0.021	0.020	0.022	0.024	0.025	0.022	0.022	0.021	0.020	0.019	0.019	0.019
Al	0.26	0.26	0.27	0.27	0.28	0.28	0.29	0.28	0.29	0.28	0.28	0.27	0.27	0.27
Cr	0.032	0.036	0.037	0.037	0.040	0.036	0.037	0.035	0.038	0.034	0.036	0.038	0.034	0.036
Fe3	0.076	0.067	0.064	0.073	0.048	0.062	0.034	0.047	0.052	0.032	0.042	0.038	0.043	0.045
Fe2	0.022	0.030	0.027	0.023	0.043	0.033	0.053	0.047	0.045	0.062	0.055	0.060	0.047	0.047
Mn	0.002	0.002	0.003	0.003	0.003	0.002	0.001	0.002	0.003	0.002	0.003	0.003	0.003	0.004
Mg	0.83	0.84	0.82	0.82	0.81	0.82	0.81	0.82	0.83	0.81	0.82	0.86	0.82	0.83
Ca	0.88	0.88	0.89	0.89	0.89	0.88	0.90	0.88	0.86	0.88	0.88	0.84	0.88	0.87
Na	0.051	0.047	0.050	0.051	0.044	0.050	0.043	0.047	0.050	0.047	0.044	0.040	0.048	0.050
K	0.001	<0.001	<0.001	<0.001	<0.001	<0.001	<0.001	0.001	<0.001	0.001	<0.001	<0.001	<0.001	<0.001

Sample L09

distance	1425	1440	1455	1470	1485	1500	1515	1530	1545	1575	1590	1605	1635	1665
SiO2	50.3	50.4	50.2	50.2	50.1	50.5	50.3	50.3	50.6	50.1	49.8	50.3	50.6	50.7
TiO2	0.71	0.73	0.73	0.74	0.70	0.77	0.72	0.79	0.71	0.82	0.83	0.78	0.71	0.78
Al2O3	6.2	6.2	6.2	6.1	5.9	5.9	5.9	6.0	5.8	5.7	5.8	5.6	5.4	5.2
Cr2O3	1.19	1.26	1.20	1.22	1.28	1.15	1.28	1.19	1.13	1.22	1.13	1.11	1.27	1.14
Fe2O3	1.57	2.22	2.35	1.77	2.30	1.57	2.06	1.62	1.38	2.58	1.66	2.03	2.24	1.39
FeO	1.82	1.45	1.13	1.52	1.11	1.72	1.26	1.52	1.79	0.80	1.33	1.34	1.09	1.63
MnO	0.09	0.08	0.17	0.11	0.10	0.11	0.11	0.07	0.12	0.09	0.05	0.02	0.09	0.16
MgO	16.0	16.0	15.7	15.5	16.3	15.4	15.6	15.3	15.8	15.4	14.2	15.5	15.5	15.5
CaO	21.3	21.6	21.9	22.0	21.2	22.4	22.3	22.5	22.3	22.9	24.2	22.5	22.3	22.9
Na2O	0.64	0.68	0.71	0.68	0.66	0.67	0.66	0.70	0.58	0.64	0.56	0.67	0.77	0.58
K2O	0.01	0.01	0.01	<0.01	<0.01	0.01	0.01	<0.01	<0.01	<0.01	<0.01	<0.01	0.05	<0.01
Total	99.8	100.7	100.4	99.9	99.6	100.1	100.1	100.0	100.2	100.3	99.6	99.9	99.9	100.0
Si	1.83	1.82	1.82	1.83	1.83	1.84	1.83	1.83	1.84	1.83	1.83	1.84	1.84	1.85
Ti	0.019	0.020	0.020	0.020	0.019	0.021	0.020	0.022	0.020	0.022	0.023	0.021	0.019	0.022
Al	0.26	0.27	0.27	0.26	0.26	0.25	0.25	0.26	0.25	0.24	0.25	0.24	0.23	0.22
Cr	0.034	0.036	0.035	0.035	0.037	0.033	0.037	0.034	0.033	0.035	0.033	0.032	0.037	0.033
Fe3	0.043	0.061	0.064	0.049	0.063	0.043	0.057	0.044	0.038	0.071	0.046	0.056	0.061	0.038
Fe2	0.056	0.044	0.034	0.047	0.034	0.052	0.038	0.046	0.055	0.024	0.041	0.041	0.033	0.050
Mn	0.003	0.003	0.005	0.003	0.003	0.003	0.004	0.002	0.004	0.003	0.001	0.001	0.003	0.005
Mg	0.87	0.86	0.85	0.84	0.89	0.83	0.85	0.83	0.85	0.84	0.78	0.84	0.84	0.84
Ca	0.83	0.84	0.85	0.86	0.83	0.88	0.87	0.88	0.87	0.89	0.96	0.88	0.87	0.89
Na	0.046	0.048	0.050	0.048	0.047	0.048	0.046	0.050	0.041	0.045	0.040	0.047	0.054	0.041
K	0.001	<0.001	<0.001	<0.001	<0.001	<0.001	<0.001	<0.001	<0.001	<0.001	<0.001	<0.001	0.003	<0.001

A2.6b: Clinopyroxene profils

Sample L09

distance	**1695**	**1710**	**1740**	**1755**	**1770**	**1785**	**1815**	**1830**	**1845**	**1860**	**1875**	**1890**	**1920**	**1935**
SiO2	51.0	50.9	51.0	51.0	51.0	51.2	51.4	51.3	51.3	52.0	51.6	52.0	51.8	51.5
TiO2	0.75	0.75	0.78	0.75	0.70	0.74	0.68	0.68	0.69	0.74	0.67	0.71	0.70	0.74
Al2O3	5.2	5.2	5.0	4.9	4.9	4.7	4.5	4.5	4.3	4.1	4.1	3.6	4.1	4.3
Cr2O3	1.32	1.27	1.31	1.22	1.36	1.28	1.22	1.31	1.18	1.38	1.31	1.36	1.27	1.20
Fe2O3	1.53	1.69	1.65	1.48	1.87	1.91	1.74	1.96	1.57	1.19	1.32	1.22	2.16	1.61
FeO	1.66	1.39	1.51	1.55	1.38	1.40	1.37	1.43	1.41	1.96	1.53	1.60	1.54	1.65
MnO	0.06	0.05	0.11	0.06	0.09	0.09	0.10	0.09	0.11	0.11	0.06	0.09	0.10	0.06
MgO	15.66	15.89	15.85	15.69	16.3	16.72	16.0	16.71	15.94	17.35	16.0	16.34	17.29	16.2
CaO	22.83	22.35	22.49	22.73	22.03	21.67	22.72	21.88	22.66	21.07	22.73	22.73	21.43	22.58
Na2O	0.58	0.68	0.64	0.63	0.63	0.61	0.61	0.57	0.63	0.61	0.66	0.62	0.57	0.59
K2O	<0.01	<0.01	<0.01	<0.01	<0.01	<0.01	0.01	<0.01	0.01	<0.01	<0.01	<0.01	<0.01	<0.01
Total	100.6	100.2	100.3	99.9	100.3	100.3	100.3	100.4	99.7	100.5	100.1	100.3	101.0	100.4
Si	1.8484	1.8517	1.8537	1.8595	1.8528	1.8571	1.8667	1.8607	1.8735	1.8786	1.8798	1.8885	1.8657	1.8688
Ti	0.021	0.021	0.021	0.021	0.019	0.020	0.019	0.019	0.019	0.020	0.018	0.019	0.019	0.020
Al	0.22	0.22	0.21	0.21	0.21	0.20	0.19	0.19	0.18	0.17	0.18	0.16	0.18	0.19
Cr	0.038	0.037	0.038	0.035	0.039	0.037	0.035	0.038	0.034	0.040	0.038	0.039	0.036	0.034
Fe3	0.042	0.046	0.045	0.041	0.051	0.052	0.048	0.053	0.043	0.032	0.036	0.033	0.059	0.044
Fe2	0.051	0.042	0.046	0.047	0.042	0.043	0.042	0.044	0.043	0.059	0.047	0.049	0.046	0.050
Mn	0.002	0.002	0.003	0.002	0.003	0.003	0.003	0.003	0.003	0.003	0.002	0.003	0.003	0.002
Mg	0.85	0.86	0.86	0.85	0.88	0.90	0.87	0.90	0.87	0.93	0.87	0.89	0.93	0.88
Ca	0.89	0.87	0.88	0.89	0.86	0.84	0.88	0.85	0.89	0.82	0.89	0.88	0.83	0.88
Na	0.041	0.048	0.045	0.044	0.044	0.043	0.043	0.040	0.045	0.043	0.046	0.044	0.040	0.041
K	<0.001	<0.001	<0.001	<0.001	<0.001	<0.001	0.001	<0.001	0.001	<0.001	<0.001	<0.001	<0.001	<0.001

Sample L09

distance	**1965**	**1980**	**1995**	**2010**	**2025**	**2040**	**2055**	**2070**	**2115**	**2130**	**2145**	**2190**	**2205**	**2220**
SiO2	51.8	51.6	51.7	51.9	51.9	52.0	51.4	51.3	51.0	50.7	50.7	50.7	51.0	50.9
TiO2	0.73	0.74	0.72	0.80	0.73	0.77	0.76	0.78	0.77	0.69	0.71	0.72	0.68	0.74
Al2O3	4.2	4.1	3.9	3.6	3.7	4.1	4.3	4.4	4.8	5.0	5.0	5.3	5.2	5.3
Cr2O3	1.23	1.15	1.24	1.09	1.22	1.19	1.27	1.24	1.28	1.40	1.07	1.16	1.28	1.29
Fe2O3	1.37	1.69	1.68	1.51	1.71	0.75	2.41	1.64	1.63	2.96	2.07	1.81	1.32	1.87
FeO	1.80	1.34	1.25	1.41	1.36	2.58	1.11	1.50	1.53	0.47	1.13	1.54	1.78	1.47
MnO	0.09	0.10	0.10	0.08	0.06	0.09	0.07	0.15	0.08	0.06	0.09	0.10	0.10	0.13
MgO	16.8	16.3	16.3	16.4	16.5	17.4	16.3	16.0	16.0	16.2	15.6	15.8	15.7	16.1
CaO	21.9	22.7	22.7	23.1	22.9	21.0	22.5	22.7	22.3	22.1	22.8	22.3	22.4	22.2
Na2O	0.57	0.64	0.63	0.53	0.56	0.50	0.65	0.59	0.62	0.72	0.65	0.63	0.66	0.61
K2O	0.01	<0.01	<0.01	0.01	0.01	0.01	0.01	<0.01	<0.01	0.03	<0.01	<0.01	<0.01	<0.01
Total	100.5	100.3	100.2	100.4	100.6	100.4	100.7	100.4	100.1	100.4	99.7	100.2	100.1	100.5
Si	1.88	1.88	1.88	1.88	1.88	1.88	1.86	1.87	1.86	1.84	1.85	1.85	1.86	1.84
Ti	0.020	0.020	0.020	0.022	0.020	0.021	0.021	0.021	0.021	0.019	0.019	0.020	0.019	0.020
Al	0.18	0.17	0.17	0.16	0.16	0.17	0.18	0.19	0.21	0.21	0.21	0.23	0.22	0.23
Cr	0.035	0.033	0.036	0.031	0.035	0.034	0.036	0.036	0.037	0.040	0.031	0.033	0.037	0.037
Fe3	0.037	0.046	0.046	0.041	0.047	0.020	0.066	0.045	0.045	0.081	0.057	0.050	0.036	0.051
Fe2	0.054	0.041	0.038	0.043	0.041	0.078	0.034	0.046	0.047	0.014	0.035	0.047	0.054	0.045
Mn	0.003	0.003	0.003	0.003	0.002	0.003	0.002	0.005	0.002	0.002	0.003	0.003	0.003	0.004
Mg	0.91	0.88	0.88	0.88	0.89	0.94	0.88	0.87	0.87	0.88	0.85	0.86	0.85	0.87
Ca	0.85	0.88	0.88	0.90	0.89	0.82	0.87	0.88	0.87	0.86	0.89	0.87	0.87	0.86
Na	0.040	0.045	0.044	0.038	0.040	0.035	0.045	0.042	0.044	0.051	0.046	0.044	0.046	0.043
K	0.001	<0.001	<0.001	0.001	0.001	0.001	<0.001	<0.001	<0.001	0.001	<0.001	<0.001	<0.001	<0.001

A2.6b: Clinopyroxene profils

Sample L09

distance	**2235**	**2250**	**2280**	**2310**	**2325**	**2340**	**2355**	**2385**	**2400**	**2415**	**2445**	**2460**	**2475**	**2490**
SiO2	51.1	50.83	50.48	51.28	51.06	51.17	51.17	51.18	51.18	51.12	51.4	50.82	51.5	51.71
TiO2	0.61	0.64	0.74	0.68	0.69	0.75	0.71	0.74	0.75	0.73	0.78	0.93	0.77	0.78
Al2O3	5.1	5.2	5.5	5.2	5.1	5.2	5.1	5.0	4.9	4.8	4.5	4.8	4.3	4.2
Cr2O3	1.15	1.19	1.28	1.35	1.30	1.34	1.34	1.24	1.22	1.32	1.27	1.23	1.27	1.18
Fe2O3	1.02	2.37	1.48	1.04	1.32	1.22	1.69	1.02	1.31	1.57	1.85	1.87	1.75	0.94
FeO	1.96	0.99	1.64	2.24	1.85	2.14	1.63	1.95	1.54	1.34	1.39	1.20	1.31	2.24
MnO	0.06	0.06	0.10	0.10	0.12	0.07	0.09	0.06	0.08	0.04	0.07	0.10	0.09	0.09
MgO	15.6	15.6	15.4	15.6	15.6	16.6	16.3	15.7	15.8	15.7	16.2	15.8	15.9	16.7
CaO	22.5	22.8	22.5	22.3	22.5	21.3	22.0	22.5	22.7	23.0	22.7	22.9	22.8	21.4
Na2O	0.65	0.73	0.65	0.69	0.66	0.62	0.63	0.65	0.65	0.65	0.62	0.62	0.71	0.63
K2O	<0.01	0.01	<0.01	<0.01	<0.01	<0.01	<0.01	<0.01	0.02	0.01	<0.01	<0.01	<0.01	<0.01
Total	99.7	100.4	99.8	100.5	100.1	100.4	100.7	100.0	100.1	100.3	100.7	100.2	100.4	100.0
Si	1.8668	1.8476	1.8456	1.8606	1.8595	1.8542	1.8515	1.8641	1.8617	1.859	1.8605	1.851	1.8694	1.8803
Ti	0.017	0.018	0.020	0.018	0.019	0.020	0.019	0.020	0.021	0.020	0.021	0.026	0.021	0.021
Al	0.22	0.22	0.24	0.22	0.22	0.22	0.22	0.21	0.21	0.21	0.19	0.20	0.18	0.18
Cr	0.033	0.034	0.037	0.039	0.037	0.038	0.038	0.036	0.035	0.038	0.037	0.035	0.037	0.034
Fe3	0.028	0.065	0.041	0.029	0.036	0.033	0.046	0.028	0.036	0.043	0.050	0.051	0.048	0.026
Fe2	0.060	0.030	0.050	0.068	0.056	0.065	0.049	0.060	0.047	0.041	0.042	0.037	0.040	0.068
Mn	0.002	0.002	0.003	0.003	0.004	0.002	0.003	0.002	0.002	0.001	0.002	0.003	0.003	0.003
Mg	0.85	0.84	0.84	0.85	0.85	0.89	0.88	0.85	0.86	0.85	0.87	0.86	0.86	0.91
Ca	0.88	0.89	0.88	0.86	0.88	0.83	0.85	0.88	0.88	0.90	0.88	0.89	0.89	0.83
Na	0.046	0.051	0.046	0.049	0.047	0.044	0.044	0.046	0.046	0.046	0.043	0.044	0.050	0.045
K	<0.001	<0.001	<0.001	<0.001	<0.001	<0.001	<0.001	<0.001	0.001	<0.001	<0.001	<0.001	<0.001	<0.001

Sample L09			**Sample L110**									
distance	**2505**	**2520**		**0**	**10**	**20**	**30**	**40**	**50**	**60**	**70**	**80**	**90**
SiO2	51.9	52.3	SiO2	51.7	51.5	51.3	51.3	51.5	51.1	51.3	51.0	51.0	50.9
TiO2	0.80	0.76	TiO2	0.73	0.77	0.76	0.66	0.74	0.71	0.7	0.76	0.78	0.8
Al2O3	4.0	3.1	Al2O3	3.1	3.6	3.7	3.8	3.8	4.0	4.1	4.3	4.3	4.4
Cr2O3	1.19	0.88	Cr2O3	0.85	0.98	1.04	0.95	1.07	1.01	1.16	1.13	1.09	1.18
Fe2O3	1.45	1.05	Fe2O3	1.99	1.20	1.44	1.31	1.32	1.07	<0.01	1.09	1.44	1.70
FeO	1.48	1.69	FeO	1.43	1.99	1.62	1.74	1.81	2.07	0.12	2.10	1.81	1.69
MnO	0.10	0.07	MnO	0.10	0.07	0.07	0.13	0.14	0.09	0.06	0.07	0.16	0.09
MgO	16.2	16.7	NiO	0.03	0.02	0.10	0.03	0.11	0.05	0.00	0.04	0.02	0.07
CaO	22.7	22.9	MgO	17.7	16.7	16.7	16.7	16.6	16.3	16.7	16.3	16.8	17.1
Na2O	0.69	0.50	CaO	21.1	21.8	22.0	21.6	21.9	21.9	21.5	21.7	21.2	20.7
K2O	<0.01	<0.01	Na2O	0.48	0.56	0.51	0.59	0.55	0.53	0.55	0.56	0.58	0.58
			K2O	<0.01	<0.01	<0.01	<0.01	<0.01	<0.01	<0.01	<0.01	<0.01	<0.01
Total	100.4	99.9											
			Total	99.2	99.1	99.2	98.7	99.5	98.9	96.1	99.0	99.1	99.1
			Si	1.89	1.89	1.88	1.89	1.88	1.88	1.92	1.87	1.87	1.86
Si	1.8814	1.9042	Ti	0.020	0.021	0.021	0.018	0.021	0.020	0.020	0.021	0.022	0.022
Ti	0.0218	0.0208	Al	0.13	0.16	0.16	0.16	0.17	0.17	0.18	0.19	0.18	0.19
Al	0.1688	0.1308	Cr	0.025	0.029	0.030	0.028	0.031	0.030	0.034	0.033	0.032	0.034
Cr	0.034	0.0254	Fe3	0.055	0.033	0.040	0.036	0.036	0.030	0.000	0.030	0.040	0.047
Fe3	0.0395	0.0288	Fe2	0.044	0.061	0.050	0.054	0.056	0.064	0.004	0.065	0.056	0.052
Fe2	0.0449	0.0515	Mn	0.003	0.002	0.002	0.004	0.004	0.003	0.002	0.002	0.005	0.003
Mn	0.003	0.0023	Ni	0.001	0.001	0.003	0.001	0.003	0.002	0.000	0.001	0.001	0.002
Mg	0.8754	0.9075	Mg	0.97	0.91	0.91	0.91	0.91	0.90	0.93	0.89	0.92	0.93
Ca	0.8824	0.8936	Ca	0.83	0.86	0.86	0.85	0.86	0.86	0.86	0.85	0.83	0.81
Na	0.0487	0.0351	Na	0.034	0.040	0.036	0.042	0.039	0.038	0.040	0.040	0.042	0.041
K	0	0	K	<0.001	<0.001	<0.001	<0.001	<0.001	<0.001	<0.001	<0.001	<0.001	<0.001

A2.6b: Clinopyroxene profils

Sample L110

distance	**100**	**110**	**120**	**140**	**150**	**160**	**170**	**190**	**210**	**220**	**240**	**250**	**260**	**270**
SiO2	50.8	51.1	51.1	50.6	50.2	50.3	51.0	50.4	50.8	50.4	50.4	50.3	50.4	50.5
TiO2	0.77	0.74	0.77	0.79	0.85	0.84	0.85	0.83	0.75	0.75	0.72	0.73	0.74	0.73
Al2O3	4.5	4.4	4.6	4.5	4.4	4.7	4.8	5.0	4.9	5.0	5.0	5.0	5.1	5.1
Cr2O3	1.18	1.18	1.15	1.09	1.11	1.05	0.98	1.06	1.12	1.13	1.15	1.15	1.08	1.18
Fe2O3	1.45	1.23	0.65	0.99	2.13	1.48	1.32	1.73	1.85	1.31	1.03	1.73	1.42	1.74
FeO	1.86	2.06	2.35	2.07	1.07	1.55	1.76	1.79	1.68	1.87	2.19	1.60	1.79	1.88
MnO	0.07	0.14	0.11	0.10	0.07	0.14	0.06	0.13	0.06	0.15	0.09	0.10	0.11	0.06
NiO	0.05	0.01	0.04	0.05	<0.01	0.04	0.07	0.05	0.06	0.04	0.03	0.04	0.02	0.04
MgO	17.0	17.1	15.7	15.9	16.6	16.5	16.1	16.9	17.4	15.7	16.4	15.8	15.8	17.1
CaO	20.8	20.7	22.3	21.9	21.3	21.1	21.9	20.7	20.3	21.9	20.9	21.8	21.9	20.3
Na2O	0.55	0.57	0.58	0.57	0.60	0.57	0.67	0.54	0.56	0.63	0.56	0.63	0.63	0.53
K2O	0.01	0.01	<0.01	<0.01	<0.01	0.01	0.01	0.01	<0.01	<0.01	0.01	0.01	<0.01	0.01
Total	99.0	99.2	99.4	98.5	98.3	98.3	99.5	99.1	99.4	98.8	98.4	99.0	98.9	99.3
Si	1.87	1.87	1.88	1.87	1.86	1.86	1.87	1.85	1.85	1.86	1.86	1.85	1.86	1.85
Ti	0.021	0.020	0.021	0.022	0.024	0.024	0.023	0.023	0.021	0.021	0.020	0.020	0.021	0.020
Al	0.19	0.19	0.20	0.20	0.19	0.20	0.21	0.22	0.21	0.22	0.22	0.22	0.22	0.22
Cr	0.034	0.034	0.033	0.032	0.033	0.031	0.028	0.031	0.032	0.033	0.034	0.034	0.032	0.034
Fe3	0.040	0.034	0.018	0.028	0.059	0.041	0.036	0.048	0.051	0.036	0.029	0.048	0.039	0.048
Fe2	0.057	0.063	0.072	0.064	0.033	0.048	0.054	0.055	0.051	0.058	0.068	0.049	0.055	0.058
Mn	0.002	0.004	0.003	0.003	0.002	0.004	0.002	0.004	0.002	0.005	0.003	0.003	0.003	0.002
Ni	0.001	<0.001	0.001	0.002	<0.001	0.001	0.002	0.002	0.002	0.001	0.001	0.001	0.001	0.001
Mg	0.93	0.93	0.86	0.88	0.92	0.91	0.88	0.92	0.95	0.86	0.90	0.87	0.87	0.93
Ca	0.82	0.81	0.88	0.87	0.84	0.83	0.86	0.81	0.79	0.86	0.83	0.86	0.86	0.80
Na	0.039	0.041	0.041	0.041	0.043	0.041	0.047	0.038	0.039	0.045	0.041	0.045	0.045	0.038
K	0.001	<0.001	<0.001	<0.001	<0.001	0.001	0.001	0.001	<0.001	<0.001	<0.001	0.001	<0.001	<0.001

Sample L110

distance	**290**	**300**	**310**	**330**	**340**	**350**	**380**	**400**	**410**	**420**	**440**	**460**	**480**	**490**
SiO2	50.0	51.4	51.7	51.2	51.4	51.5	51.3	50.9	50.9	50.7	50.9	50.5	51.2	50.6
TiO2	0.76	0.74	0.75	0.77	0.68	0.72	0.76	0.78	0.77	0.77	0.74	0.74	0.72	0.73
Al2O3	5.3	5.1	5.3	5.3	5.3	5.3	5.4	5.3	5.2	5.4	5.4	5.3	5.2	5.1
Cr2O3	1.05	1.10	1.14	1.10	1.05	1.14	1.15	1.24	1.25	1.13	1.24	1.15	1.06	1.12
Fe2O3	2.92	1.77	1.72	1.42	2.43	1.79	1.51	1.80	1.95	1.72	1.56	1.56	1.47	1.83
FeO	0.60	1.83	1.83	1.72	1.24	1.81	1.72	1.41	1.53	1.50	1.86	1.79	2.17	1.48
MnO	0.10	0.10	0.14	0.11	0.09	0.16	0.09	0.11	0.09	0.09	0.06	0.06	0.13	0.10
NiO	0.06	0.01	0.04	0.13	0.04	0.05	0.04	0.06	0.02	0.03	0.05	0.05	0.01	0.01
MgO	16.9	16.7	16.4	16.2	16.9	17.1	15.8	15.8	16.3	15.6	16.0	15.6	16.7	16.2
CaO	20.8	21.5	22.0	22.1	21.5	21.1	22.7	22.4	21.8	22.6	22.0	22.3	21.1	21.9
Na2O	0.63	0.60	0.68	0.59	0.65	0.58	0.61	0.64	0.64	0.61	0.63	0.60	0.60	0.60
K2O	0.01	<0.01	<0.01	<0.01	<0.01	<0.01	0.01	<0.01	<0.01	<0.01	<0.01	<0.01	<0.01	<0.01
Total	99.1	100.9	101.7	100.5	101.3	101.3	101.1	100.5	100.4	100.1	100.4	99.7	100.3	99.7
Si	1.83	1.85	1.85	1.85	1.84	1.85	1.85	1.85	1.84	1.85	1.85	1.85	1.85	1.85
Ti	0.021	0.020	0.020	0.021	0.018	0.019	0.021	0.021	0.021	0.021	0.020	0.020	0.020	0.020
Al	0.23	0.22	0.22	0.22	0.22	0.22	0.23	0.23	0.22	0.23	0.23	0.23	0.22	0.22
Cr	0.030	0.031	0.032	0.032	0.030	0.032	0.033	0.035	0.036	0.033	0.035	0.033	0.031	0.032
Fe3	0.081	0.048	0.046	0.039	0.066	0.048	0.041	0.049	0.053	0.047	0.043	0.043	0.040	0.050
Fe2	0.018	0.055	0.055	0.052	0.037	0.054	0.052	0.043	0.046	0.046	0.056	0.055	0.066	0.045
Mn	0.003	0.003	0.004	0.004	0.003	0.005	0.003	0.003	0.003	0.003	0.002	0.002	0.004	0.003
Ni	0.002	<0.001	0.001	0.004	0.001	0.002	0.001	0.002	0.001	0.001	0.002	0.002	0.000	0.000
Mg	0.92	0.90	0.88	0.87	0.91	0.91	0.85	0.86	0.88	0.85	0.86	0.85	0.90	0.88
Ca	0.82	0.83	0.84	0.86	0.83	0.81	0.88	0.87	0.85	0.88	0.85	0.87	0.82	0.86
Na	0.045	0.042	0.047	0.041	0.045	0.040	0.043	0.045	0.045	0.043	0.045	0.043	0.042	0.043
K	0.001	<0.001	<0.001	<0.001	<0.001	<0.001	<0.001	<0.001	<0.001	<0.001	<0.001	<0.001	<0.001	<0.001

A2.6b: Clinopyroxene profils

Sample L110

distance	**510**	**520**	**540**	**550**	**600**	**610**	**620**	**640**	**650**	**660**	**670**	**680**	**690**	**700**
SiO2	50.6	50.4	50.6	50.3	49.8	50.5	50.6	50.6	50.6	50.8	51.1	51.1	51.1	51.4
TiO2	0.72	0.71	0.68	0.72	0.75	0.82	0.77	0.80	0.79	0.86	0.83	0.88	0.84	0.88
Al2O3	5.3	5.2	5.0	5.1	5.1	5.0	5.1	5.0	4.9	4.8	4.6	4.6	4.4	4.2
Cr2O3	1.08	1.02	1.07	1.14	1.13	1.18	1.06	1.11	1.15	1.26	1.20	1.11	1.08	1.10
Fe2O3	1.07	1.78	0.99	2.17	2.74	1.85	1.61	1.39	1.77	1.71	1.30	1.06	1.07	0.80
FeO	2.20	1.43	2.22	1.22	0.70	1.58	1.65	1.79	1.56	1.69	2.03	2.19	2.33	2.44
MnO	0.13	0.15	0.09	0.09	0.13	0.16	0.10	0.12	0.09	0.09	0.06	0.11	0.09	0.11
NiO	0.03	0.01	0.05	0.02	0.05	0.06	0.12	0.03	0.01	0.03	0.08	0.06	0.03	0.11
MgO	15.6	15.8	16.0	15.9	17.6	16.1	16.3	15.6	16.0	16.8	17.1	16.5	16.8	16.6
CaO	22.0	22.2	21.6	22.0	20.0	21.6	21.4	22.5	22.0	21.1	20.8	21.4	21.0	21.5
Na2O	0.63	0.59	0.55	0.65	0.51	0.64	0.63	0.58	0.61	0.62	0.55	0.58	0.56	0.56
K2O	<0.01	0.01	<0.01	0.01	0.01	<0.01	<0.01	0.01	<0.01	<0.01	0.01	0.02	0.01	<0.01
Total	99.3	99.2	98.8	99.4	98.5	99.4	99.3	99.4	99.6	99.7	99.6	99.6	99.4	99.7
Si	1.86	1.85	1.86	1.85	1.83	1.85	1.85	1.86	1.85	1.85	1.86	1.87	1.87	1.88
Ti	0.020	0.020	0.019	0.020	0.021	0.023	0.021	0.022	0.022	0.024	0.023	0.024	0.023	0.024
Al	0.23	0.22	0.22	0.22	0.22	0.22	0.22	0.21	0.21	0.21	0.20	0.20	0.19	0.18
Cr	0.03	0.03	0.03	0.03	0.03	0.03	0.03	0.03	0.03	0.04	0.03	0.03	0.03	0.03
Fe3	0.030	0.049	0.027	0.060	0.076	0.051	0.044	0.039	0.049	0.047	0.036	0.029	0.030	0.022
Fe2	0.067	0.044	0.068	0.038	0.022	0.048	0.051	0.055	0.048	0.051	0.062	0.067	0.071	0.075
Mn	0.004	0.005	0.003	0.003	0.004	0.005	0.003	0.004	0.003	0.003	0.002	0.004	0.003	0.003
NiO	0.001	0.000	0.002	0.001	0.001	0.002	0.004	0.001	0.000	0.001	0.002	0.002	0.001	0.003
Mg	0.85	0.86	0.88	0.87	0.96	0.88	0.89	0.85	0.88	0.91	0.93	0.90	0.92	0.90
Ca	0.86	0.87	0.85	0.86	0.79	0.85	0.84	0.88	0.86	0.82	0.81	0.84	0.82	0.84
Na	0.045	0.042	0.039	0.046	0.037	0.045	0.045	0.041	0.043	0.044	0.039	0.041	0.040	0.040
K	<0.001	0.001	<0.001	<0.001	<0.001	<0.001	<0.001	<0.001	<0.001	<0.001	<0.001	0.001	0.001	<0.001

Sample L110				**Sample L13**										
distance	**710**	**720**	**730**		**15**	**30**	**45**	**75**	**105**	**120**	**135**	**150**	**195**	**210**
SiO2	51.4	51.4	51.9	SiO2	52.4	52.3	52.1	51.5	51.0	50.9	50.9	50.4	51.0	50.4
TiO2	0.86	0.88	0.80	TiO2	0.97	0.99	1.08	0.99	1.06	1.06	1.06	1.21	0.90	0.93
Al2O3	4.2	3.9	3.3	Al2O3	3.2	3.7	3.9	4.5	5.1	5.2	5.2	5.7	5.6	5.7
Cr2O3	1.10	1.08	1.04	Cr2O3	0.92	1.06	1.11	1.22	1.28	1.26	1.33	1.30	1.31	1.27
Fe2O3	0.87	1.45	1.18	Fe2O3	1.24	0.77	0.70	0.94	2.03	1.26	1.05	1.78	1.26	1.70
FeO	2.08	1.51	1.77	FeO	1.88	2.50	2.69	2.29	1.63	2.12	2.26	1.86	2.59	1.88
MnO	0.08	0.04	0.07	MnO	0.17	0.10	0.14	0.11	0.09	0.06	0.03	0.08	0.13	0.08
NiO	0.07	0.01	0.05	NiO	0.05	0.05	<0.01	0.08	0.05	<0.01	0.04	0.06	0.02	0.04
MgO	16.2	16.5	16.8	MgO	16.4	16.6	16.0	15.5	15.6	15.1	15.4	15.1	15.6	15.0
CaO	22.4	22.4	22.4	CaO	23.1	22.3	22.8	22.9	22.7	23.0	22.7	22.8	22.0	22.7
Na2O	0.54	0.56	0.49	Na2O	0.55	0.57	0.58	0.63	0.70	0.68	0.64	0.69	0.65	0.73
K2O	<0.01	<0.01	<0.01	K2O	0.01	<0.01	0.02	0.01	<0.01	<0.01	<0.01	<0.01	<0.01	<0.01
Total	99.8	99.8	99.7	Total	100.9	101.0	101.1	100.6	101.2	100.7	100.5	101.0	101.0	100.4
Si	1.88	1.88	1.89	Si	1.90	1.89	1.88	1.87	1.84	1.85	1.85	1.83	1.84	1.84
Ti	0.024	0.024	0.022	Ti	0.026	0.027	0.029	0.027	0.029	0.029	0.029	0.033	0.025	0.025
Al	0.18	0.17	0.14	Al	0.14	0.16	0.17	0.19	0.22	0.22	0.22	0.24	0.24	0.25
Cr	0.032	0.031	0.030	Cr	0.026	0.030	0.032	0.035	0.037	0.036	0.038	0.037	0.038	0.036
Fe3	0.024	0.040	0.033	Fe3	0.034	0.021	0.019	0.026	0.055	0.034	0.029	0.049	0.034	0.047
Fe2	0.064	0.046	0.054	Fe2	0.057	0.075	0.081	0.070	0.049	0.064	0.069	0.056	0.078	0.057
Mn	0.002	0.001	0.002	Mn	0.005	0.003	0.004	0.003	0.003	0.002	0.001	0.002	0.004	0.002
Ni	0.002	<0.001	0.001	Ni	0.001	0.002	0.000	0.002	0.002	<0.001	0.001	0.002	0.001	0.001
Mg	0.88	0.90	0.91	Mg	0.88	0.89	0.86	0.84	0.84	0.82	0.83	0.82	0.84	0.81
Ca	0.87	0.88	0.87	Ca	0.90	0.86	0.88	0.89	0.88	0.90	0.88	0.89	0.85	0.88
Na	0.038	0.040	0.035	Na	0.039	0.040	0.041	0.045	0.049	0.048	0.045	0.048	0.046	0.052
K	<0.001	<0.001	<0.001	K	0.001	<0.001	0.001	0.001	<0.001	<0.001	<0.001	<0.001	<0.001	<0.001

A2.6b: Clinopyroxene profils

Sample L13

distance	**255**	**270**	**285**	**315**	**330**	**345**	**360**	**375**	**405**	**420**	**435**	**450**	**465**	**480**
SiO2	50.4	50.6	50.8	50.7	50.4	50.3	51.0	50.8	50.7	50.8	50.4	50.3	50.2	50.2
TiO2	0.78	0.80	0.78	0.75	0.74	0.81	0.78	0.72	0.85	0.70	0.77	0.84	0.73	0.73
Al2O3	5.8	6.0	5.9	6.0	6.0	6.1	6.1	6.1	6.4	6.1	6.4	6.6	6.5	6.2
Cr2O3	1.22	1.30	1.21	1.29	1.30	1.28	1.27	1.24	1.29	1.11	1.30	1.23	1.17	1.17
Fe2O3	2.07	1.35	1.32	1.35	2.08	1.77	1.58	1.34	0.96	1.81	1.74	1.40	2.56	1.66
FeO	1.68	2.26	2.45	2.46	1.58	2.05	2.52	2.46	2.58	2.33	1.92	2.15	1.32	2.07
MnO	0.05	0.11	0.05	0.11	0.15	0.14	0.07	0.09	0.05	0.17	0.16	0.10	0.08	0.06
NiO	0.05	0.03	0.03	0.05	0.02	0.06	0.04	<0.01	0.10	0.07	0.03	<0.01	0.04	0.03
MgO	15.0	15.2	14.8	15.0	14.9	14.9	16.4	14.8	14.6	14.7	14.7	14.5	15.5	14.6
CaO	22.5	22.0	22.9	22.6	22.9	22.7	21.1	22.8	23.0	22.7	22.8	22.9	22.1	22.8
Na2O	0.78	0.73	0.70	0.66	0.71	0.67	0.61	0.71	0.68	0.78	0.74	0.72	0.71	0.70
K2O	<0.01	0.01	0.02	<0.01	0.01	0.01	<0.01	<0.01	<0.01	<0.01	<0.01	0.02	0.01	0.01
Total	100.4	100.5	101.0	100.8	100.9	100.8	101.4	101.0	101.2	101.3	100.9	100.7	100.8	100.2
Si	1.84	1.84	1.84	1.84	1.83	1.83	1.83	1.84	1.83	1.84	1.83	1.83	1.82	1.83
Ti	0.021	0.022	0.021	0.020	0.020	0.022	0.021	0.020	0.023	0.019	0.021	0.023	0.020	0.020
Al	0.25	0.26	0.25	0.25	0.26	0.26	0.26	0.26	0.27	0.26	0.27	0.28	0.28	0.27
Cr	0.035	0.037	0.035	0.037	0.037	0.037	0.036	0.036	0.037	0.032	0.037	0.035	0.034	0.034
Fe3	0.057	0.037	0.036	0.037	0.057	0.048	0.043	0.037	0.026	0.049	0.048	0.038	0.070	0.046
Fe2	0.051	0.069	0.074	0.075	0.048	0.062	0.076	0.075	0.078	0.070	0.058	0.065	0.040	0.063
Mn	0.002	0.003	0.002	0.004	0.005	0.004	0.002	0.003	0.002	0.005	0.005	0.003	0.003	0.002
Ni	0.002	0.001	0.001	0.002	0.001	0.002	0.001	<0.001	0.003	0.002	0.001	<0.001	0.001	0.001
Mg	0.81	0.83	0.80	0.81	0.81	0.80	0.88	0.80	0.79	0.79	0.79	0.79	0.83	0.79
Ca	0.88	0.86	0.89	0.88	0.89	0.88	0.81	0.88	0.89	0.88	0.88	0.89	0.86	0.89
Na	0.055	0.052	0.049	0.047	0.050	0.047	0.043	0.050	0.048	0.055	0.052	0.051	0.050	0.050
K	<0.001	0.001	0.001	<0.001	<0.001	0.001	<0.001	<0.001	<0.001	<0.001	<0.001	0.001	0.001	0.001

Sample L13

distance	**495**	**510**	**525**	**540**	**555**	**570**	**585**	**600**	**615**	**630**	**645**	**660**	**675**	**705**
SiO2	50.5	50.4	50.2	50.5	50.8	50.5	50.2	50.5	50.7	50.3	50.7	50.8	50.9	49.5
TiO2	0.78	0.77	0.84	0.76	0.75	0.84	0.79	0.79	0.82	0.91	0.85	0.91	0.85	0.73
Al2O3	6.4	6.4	6.6	6.3	6.1	6.2	6.1	6.1	6.0	6.2	5.7	5.6	5.5	7.6
Cr2O3	1.22	1.24	1.23	1.21	1.20	1.19	1.16	1.24	1.30	1.23	1.21	1.26	1.38	1.31
Fe2O3	1.76	1.85	1.88	1.67	1.06	1.69	2.22	2.03	1.23	1.72	1.66	1.24	1.17	1.77
FeO	1.94	2.06	1.86	2.08	2.66	2.10	1.58	1.72	2.49	1.81	2.23	2.34	2.28	1.96
MnO	0.12	0.11	0.16	0.07	0.06	0.10	0.11	0.14	0.06	0.08	0.17	0.03	0.06	0.16
NiO	0.06	0.01	0.03	0.01	0.06	0.03	0.02	0.01	0.01	0.04	0.04	0.02	0.02	<0.01
MgO	14.6	14.6	14.4	14.9	14.7	14.7	15.5	14.9	14.8	14.7	14.7	15.0	15.0	14.2
CaO	23.1	22.8	23.0	22.8	22.7	22.9	21.9	22.8	22.6	23.0	22.8	22.7	22.7	22.8
Na2O	0.72	0.74	0.76	0.68	0.73	0.74	0.70	0.74	0.73	0.75	0.74	0.73	0.74	0.69
K2O	0.01	<0.01	<0.01	0.01	<0.01	<0.01	0.01	<0.01	<0.01	<0.01	0.01	0.02	<0.01	<0.01
Total	101.2	101.0	100.9	100.8	100.8	100.9	100.2	100.9	100.8	100.7	100.9	100.5	100.7	100.8
Si	1.83	1.83	1.82	1.83	1.84	1.83	1.83	1.83	1.84	1.83	1.84	1.85	1.85	1.80
Ti	0.021	0.021	0.023	0.021	0.020	0.023	0.022	0.021	0.022	0.025	0.023	0.025	0.023	0.020
Al	0.27	0.27	0.28	0.27	0.26	0.26	0.26	0.26	0.26	0.27	0.24	0.24	0.23	0.33
Cr	0.035	0.036	0.035	0.035	0.034	0.034	0.033	0.036	0.037	0.035	0.035	0.036	0.040	0.038
Fe3	0.048	0.051	0.051	0.045	0.029	0.046	0.061	0.055	0.034	0.047	0.045	0.034	0.032	0.048
Fe2	0.059	0.062	0.057	0.063	0.081	0.064	0.048	0.052	0.076	0.055	0.068	0.071	0.069	0.059
Mn	0.004	0.004	0.005	0.002	0.002	0.003	0.003	0.004	0.002	0.003	0.005	0.001	0.002	0.005
Ni	0.002	<0.001	0.001	<0.001	0.002	0.001	0.001	<0.001	<0.001	0.001	0.001	0.001	0.001	<0.001
Mg	0.79	0.79	0.78	0.80	0.79	0.79	0.84	0.80	0.80	0.79	0.80	0.81	0.81	0.77
Ca	0.89	0.89	0.89	0.88	0.88	0.89	0.85	0.89	0.88	0.89	0.89	0.88	0.88	0.89
Na	0.050	0.052	0.053	0.048	0.052	0.052	0.050	0.052	0.051	0.053	0.052	0.051	0.052	0.048
K	<0.001	<0.001	<0.001	0.001	<0.001	<0.001	<0.001	<0.001	<0.001	<0.001	<0.001	0.001	<0.001	<0.001

A2.6b: Clinopyroxene profils

Sample L13

distance	**720**	**750**	**765**	**780**	**795**	**810**	**825**	**855**	**900**	**915**	**930**	**945**	**960**	**975**
SiO2	50.3	50.0	50.2	50.2	49.7	50.2	50.3	50.5	50.2	50.0	50.2	50.3	50.2	49.9
TiO2	0.62	0.57	0.53	0.56	0.59	0.55	0.58	0.52	0.58	0.57	0.49	0.54	0.57	0.51
Al2O3	7.2	7.2	7.0	7.1	7.2	7.0	7.2	7.1	7.3	7.2	7.2	7.3	7.4	7.3
Cr2O3	1.28	1.24	1.23	1.21	1.18	1.26	1.29	1.16	1.18	1.22	1.19	1.15	1.27	1.22
Fe2O3	0.87	1.78	1.52	0.95	1.99	1.64	1.43	1.29	1.67	1.89	1.30	1.22	0.85	1.53
FeO	2.39	1.80	2.16	2.57	1.80	2.21	2.10	2.35	2.09	1.99	2.50	2.48	2.54	2.19
MnO	0.12	0.11	0.02	0.07	0.07	0.06	0.11	0.10	0.12	0.05	0.14	0.11	0.06	0.09
NiO	0.06	0.01	0.02	0.03	0.03	0.04	0.01	0.04	0.09	0.04	<0.01	0.04	0.04	0.10
MgO	14.4	14.4	14.4	14.4	14.4	14.6	14.7	14.8	14.3	14.4	15.1	14.1	14.1	14.5
CaO	22.7	22.7	22.7	22.5	22.5	22.5	22.5	22.1	22.9	22.7	21.7	23.1	22.7	22.5
Na2O	0.71	0.79	0.75	0.72	0.78	0.74	0.74	0.75	0.74	0.74	0.68	0.70	0.79	0.69
K2O	<0.01	0.01	<0.01	<0.01	0.01	0.01	<0.01	<0.01	<0.01	<0.01	<0.01	<0.01	0.01	<0.01
Total	100.7	100.6	100.6	100.4	100.3	100.8	100.9	100.7	101.3	100.8	100.4	101.2	100.5	100.5
Si	1.82	1.82	1.82	1.83	1.81	1.82	1.82	1.83	1.81	1.81	1.82	1.82	1.83	1.82
Ti	0.017	0.016	0.014	0.015	0.016	0.015	0.016	0.014	0.016	0.016	0.013	0.015	0.016	0.014
Al	0.31	0.31	0.30	0.31	0.31	0.30	0.31	0.30	0.31	0.31	0.31	0.31	0.31	0.31
Cr	0.037	0.036	0.035	0.035	0.034	0.036	0.037	0.033	0.034	0.035	0.034	0.033	0.037	0.035
Fe3	0.024	0.049	0.042	0.026	0.055	0.045	0.039	0.035	0.045	0.052	0.036	0.033	0.023	0.042
Fe2	0.072	0.055	0.066	0.078	0.055	0.067	0.064	0.071	0.063	0.060	0.076	0.075	0.077	0.067
Mn	0.004	0.003	0.001	0.002	0.002	0.002	0.003	0.003	0.004	0.002	0.004	0.003	0.002	0.003
Ni	0.002	<0.001	0.001	0.001	0.001	0.001	<0.001	0.001	0.003	0.001	<0.001	0.001	0.001	0.003
Mg	0.78	0.78	0.78	0.78	0.78	0.79	0.79	0.80	0.77	0.78	0.82	0.76	0.76	0.78
Ca	0.88	0.88	0.89	0.88	0.88	0.87	0.87	0.86	0.89	0.88	0.84	0.90	0.88	0.87
Na	0.050	0.056	0.053	0.051	0.055	0.052	0.052	0.053	0.052	0.052	0.048	0.049	0.056	0.049
K	<0.001	<0.001	<0.001	<0.001	0.001	0.001	<0.001	<0.001	<0.001	<0.001	<0.001	<0.001	0.001	<0.001

Sample L13

distance	**990**	**1005**	**1020**	**1035**	**1050**	**1090**	**1100**	**1110**	**1120**	**1130**	**1150**	**1160**	**1170**	**1180**
SiO2	49.8	49.9	49.8	49.8	49.7	49.9	50.2	50.2	50.2	50.3	50.1	50.0	50.5	50.5
TiO2	0.59	0.53	0.56	0.56	0.56	0.55	0.59	0.63	0.57	0.61	0.62	0.64	0.58	0.57
Al2O3	7.4	7.5	7.6	7.5	7.6	6.9	7.1	6.9	6.9	7.0	7.1	7.2	6.6	6.8
Cr2O3	1.22	1.13	1.18	1.21	1.23	1.19	1.27	1.16	1.15	1.22	1.24	1.21	1.19	1.23
Fe2O3	2.13	1.75	1.86	1.52	2.16	1.95	1.95	2.20	1.34	1.12	1.29	1.55	1.89	1.32
FeO	1.74	2.23	1.89	2.42	1.82	1.75	1.91	1.94	2.36	2.39	2.27	2.06	1.77	2.43
MnO	0.05	0.02	0.17	0.20	0.12	0.19	0.03	0.19	0.10	0.08	0.04	0.04	0.17	0.06
NiO	0.09	0.06	0.07	0.02	0.03	0.06	0.03	0.06	0.05	0.04	0.06	0.06	<0.01	0.00
MgO	14.5	14.4	14.3	14.2	14.3	14.4	14.3	14.7	14.3	14.4	14.2	14.3	14.6	14.3
CaO	22.7	22.5	22.5	22.5	22.4	22.7	22.8	22.6	22.7	22.7	22.9	22.8	23.1	22.9
Na2O	0.68	0.72	0.79	0.71	0.80	0.75	0.80	0.69	0.74	0.73	0.73	0.74	0.69	0.75
K2O	0.01	<0.01	<0.01	<0.01	<0.01	<0.01	0.01	<0.01	0.01	<0.01	<0.01	<0.01	0.02	<0.01
Total	100.9	100.7	100.6	100.6	100.6	100.4	101.0	101.3	100.5	100.6	100.5	100.7	101.2	100.9
Si	1.80	1.81	1.81	1.81	1.80	1.82	1.82	1.81	1.83	1.83	1.82	1.82	1.83	1.83
Ti	0.016	0.014	0.015	0.015	0.015	0.015	0.016	0.017	0.016	0.017	0.017	0.018	0.016	0.015
Al	0.32	0.32	0.32	0.32	0.32	0.30	0.30	0.29	0.30	0.30	0.30	0.31	0.28	0.29
Cr	0.035	0.033	0.034	0.035	0.035	0.034	0.036	0.033	0.033	0.035	0.036	0.035	0.034	0.035
Fe3	0.058	0.048	0.051	0.042	0.059	0.054	0.053	0.060	0.037	0.031	0.035	0.042	0.052	0.036
Fe2	0.053	0.068	0.057	0.074	0.055	0.053	0.058	0.059	0.072	0.073	0.069	0.063	0.054	0.074
Mn	0.001	0.001	0.005	0.006	0.004	0.006	0.001	0.006	0.003	0.003	0.001	0.001	0.005	0.002
Ni	0.003	0.002	0.002	<0.001	0.001	0.002	0.001	0.002	0.002	0.001	0.002	0.002	<0.001	<0.001
Mg	0.79	0.78	0.77	0.77	0.78	0.78	0.77	0.79	0.78	0.78	0.77	0.77	0.79	0.77
Ca	0.88	0.88	0.88	0.87	0.87	0.89	0.89	0.88	0.88	0.88	0.89	0.89	0.90	0.89
Na	0.048	0.051	0.056	0.050	0.057	0.053	0.056	0.049	0.052	0.052	0.052	0.052	0.048	0.053
K	<0.001	<0.001	<0.001	<0.001	<0.001	<0.001	<0.001	<0.001	0.001	<0.001	<0.001	<0.001	0.001	<0.001

A2.6b: Clinopyroxene profils

Sample L13

distance	1190	1200	1210	1220	1230	1240	1250	1260	1270	1330	1345	1375	1390	1435
SiO2	50.4	50.1	50.3	50.4	50.3	50.8	51.1	50.3	50.3	50.2	50.3	51.8	50.6	50.5
TiO2	0.62	0.71	0.61	0.75	0.60	0.61	0.70	0.71	0.69	0.86	0.82	0.88	0.88	0.84
Al2O3	6.9	7.0	6.9	6.8	6.8	6.4	6.2	6.7	6.6	6.4	6.2	5.9	6.0	5.9
Cr2O3	1.28	1.26	1.18	1.25	1.24	1.17	1.19	1.21	1.24	1.32	1.32	1.35	1.32	1.35
Fe2O3	0.84	1.37	1.62	1.69	1.78	1.32	1.31	1.50	1.17	2.03	1.40	1.54	1.93	1.84
FeO	2.83	2.31	2.11	1.73	1.81	2.41	2.32	2.30	2.41	1.67	2.34	2.00	1.70	1.79
MnO	0.11	0.06	0.12	0.13	0.06	0.11	0.09	0.09	0.13	0.11	0.10	0.10	0.12	0.22
NiO	0.04	<0.01	0.04	0.05	0.04	0.04	0.03	0.04	0.04	0.05	0.06	0.04	0.05	0.01
MgO	14.4	14.3	14.6	15.0	14.4	14.7	14.9	14.5	14.5	15.0	14.6	16.6	15.1	14.8
CaO	22.7	23.0	22.6	22.5	23.0	22.8	22.8	22.8	22.7	22.4	22.6	21.9	22.6	22.8
Na2O	0.70	0.69	0.77	0.72	0.80	0.73	0.73	0.73	0.71	0.74	0.73	0.64	0.76	0.75
K2O	0.01	0.02	<0.01	0.02	<0.01	<0.01	0.01	<0.01	<0.01	0.03	<0.01	<0.01	0.02	0.02
Total	100.8	100.8	100.9	101.0	100.8	101.1	101.4	100.9	100.5	100.8	100.5	102.7	101.1	100.7
Si	1.83	1.82	1.82	1.82	1.82	1.84	1.84	1.83	1.83	1.82	1.83	1.84	1.83	1.83
Ti	0.017	0.019	0.017	0.020	0.016	0.017	0.019	0.019	0.019	0.024	0.022	0.024	0.024	0.023
Al	0.29	0.30	0.30	0.29	0.29	0.27	0.26	0.28	0.28	0.27	0.27	0.25	0.26	0.25
Cr	0.037	0.036	0.034	0.036	0.036	0.034	0.034	0.035	0.036	0.038	0.038	0.038	0.038	0.039
Fe3	0.023	0.037	0.044	0.046	0.049	0.036	0.036	0.041	0.032	0.055	0.038	0.041	0.053	0.050
Fe2	0.086	0.070	0.064	0.052	0.055	0.073	0.070	0.070	0.073	0.051	0.071	0.059	0.051	0.054
Mn	0.003	0.002	0.004	0.004	0.002	0.003	0.003	0.003	0.004	0.003	0.003	0.003	0.004	0.007
Ni	0.001	<0.001	0.001	0.001	0.001	0.001	0.001	0.001	0.001	0.002	0.002	0.001	0.001	<0.001
Mg	0.78	0.77	0.79	0.81	0.78	0.79	0.80	0.78	0.79	0.81	0.79	0.88	0.81	0.80
Ca	0.88	0.89	0.88	0.87	0.89	0.88	0.88	0.89	0.88	0.87	0.88	0.83	0.88	0.89
Na	0.049	0.048	0.054	0.051	0.056	0.051	0.051	0.051	0.050	0.052	0.052	0.044	0.053	0.053
K	0.001	0.001	<0.001	0.001	<0.001	<0.001	0.001	<0.001	<0.001	0.001	<0.001	<0.001	0.001	0.001

Sample L13

distance	1450	1465	1495	1510	1540	1555	1585	1600	1630	1645	1660	1675	1720	1730
SiO2	50.4	50.7	50.6	50.7	50.8	50.9	50.7	51.5	51.2	51.7	51.5	51.2	52.4	51.8
TiO2	0.84	0.90	0.88	0.88	0.88	0.97	0.99	0.91	0.96	0.92	0.94	0.95	0.96	1.04
Al2O3	5.8	5.7	5.7	5.6	5.4	5.2	5.3	5.0	4.8	4.6	4.6	4.4	3.3	4.1
Cr2O3	1.30	1.34	1.40	1.30	1.32	1.33	1.38	1.36	1.26	1.21	1.30	1.32	1.10	1.25
Fe2O3	2.09	2.30	1.14	1.93	2.12	1.54	1.20	0.76	2.04	1.17	0.98	1.57	0.66	1.16
FeO	1.67	1.69	2.14	1.56	1.58	1.96	2.53	2.52	1.92	2.76	2.86	1.88	2.25	1.94
MnO	0.15	0.06	0.11	0.18	0.10	0.12	0.10	0.08	0.12	0.09	0.11	0.05	0.09	0.07
NiO	0.05	<0.01	0.06	0.02	0.06	0.05	0.06	0.07	0.05	0.04	0.08	0.03	0.01	0.02
MgO	14.9	16.3	14.7	15.0	15.1	15.0	16.1	15.2	16.6	16.5	16.5	15.7	16.1	15.9
CaO	22.7	21.6	22.9	22.8	22.9	22.9	21.2	22.8	21.5	21.4	21.0	22.9	23.2	23.0
Na2O	0.74	0.62	0.72	0.80	0.75	0.75	0.67	0.74	0.65	0.60	0.65	0.62	0.56	0.66
K2O	0.01	0.02	<0.01	<0.01	0.01	<0.01	<0.01	<0.01	<0.01	0.01	<0.01	<0.01	<0.01	<0.01
Total	100.7	101.1	100.4	100.6	101.0	100.8	100.2	100.9	101.1	101.0	100.5	100.5	100.7	100.9
Si	1.83	1.83	1.84	1.84	1.84	1.85	1.85	1.87	1.85	1.87	1.87	1.86	1.90	1.87
Ti	0.023	0.024	0.024	0.024	0.024	0.026	0.027	0.025	0.026	0.025	0.026	0.026	0.026	0.028
Al	0.25	0.24	0.25	0.24	0.23	0.22	0.23	0.21	0.21	0.19	0.20	0.19	0.14	0.17
Cr	0.037	0.038	0.040	0.037	0.038	0.038	0.040	0.039	0.036	0.035	0.037	0.038	0.031	0.036
Fe3	0.057	0.063	0.031	0.053	0.058	0.042	0.033	0.021	0.055	0.032	0.027	0.043	0.018	0.032
Fe2	0.051	0.051	0.065	0.048	0.048	0.060	0.077	0.076	0.058	0.083	0.087	0.057	0.068	0.059
Mn	0.005	0.002	0.004	0.006	0.003	0.004	0.003	0.003	0.004	0.003	0.004	0.002	0.003	0.002
Ni	0.001	0.000	0.002	0.001	0.002	0.002	0.002	0.002	0.002	0.001	0.003	0.001	0.000	0.001
Mg	0.81	0.88	0.80	0.81	0.81	0.81	0.87	0.82	0.89	0.89	0.89	0.85	0.87	0.86
Ca	0.88	0.83	0.90	0.89	0.89	0.89	0.82	0.89	0.83	0.83	0.81	0.89	0.90	0.89
Na	0.052	0.043	0.051	0.057	0.053	0.053	0.047	0.052	0.045	0.042	0.046	0.044	0.040	0.047
K	0.001	0.001	<0.001	<0.001	0.001	<0.001	<0.001	<0.001	<0.001	<0.001	<0.001	<0.001	<0.001	<0.001

A2.6b: Clinopyroxene profils

Sample L13

distance	**1750**	**1760**	**1780**	**1790**	**1810**	**1840**	**1850**	**1860**	**1870**	**1880**	**1900**	**1975**	**1990**	**2005**
SiO2	51.7	51.5	51.7	51.6	51.6	51.4	51.4	51.6	51.7	51.4	51.5	51.4	51.4	51.2
TiO2	1.02	1.00	0.97	0.98	1.01	0.97	0.95	0.94	0.94	0.98	0.96	0.97	1.00	0.92
Al2O3	4.4	4.3	4.3	4.3	4.5	4.4	4.4	4.4	4.2	4.2	4.0	4.3	4.5	4.5
Cr2O3	1.31	1.29	1.21	1.34	1.30	1.28	1.34	1.31	1.29	1.24	1.23	1.23	1.28	1.30
Fe2O3	0.52	1.80	0.83	1.09	0.58	1.21	1.05	1.21	1.50	0.96	1.48	1.66	1.83	1.39
FeO	2.79	1.67	2.37	2.04	2.45	2.18	2.15	2.13	2.18	2.19	1.84	1.81	1.74	1.93
MnO	0.07	0.10	0.14	0.19	0.05	0.06	0.14	0.07	0.11	0.09	0.14	0.21	0.09	0.12
NiO	0.08	0.03	0.04	0.05	0.06	0.04	0.01	0.04	0.09	0.06	0.02	0.08	0.08	0.04
MgO	15.6	15.9	15.8	15.5	15.5	15.4	15.4	15.6	16.0	15.5	16.2	15.6	15.6	15.5
CaO	22.6	22.7	22.6	22.9	22.9	22.9	22.9	22.9	22.5	23.0	22.5	23.1	23.1	23.0
Na2O	0.65	0.70	0.67	0.73	0.68	0.69	0.69	0.67	0.62	0.63	0.58	0.64	0.66	0.65
K2O	<0.01	<0.01	<0.01	<0.01	<0.01	0.02	0.01	0.01	0.01	<0.01	<0.01	<0.01	0.01	<0.01
Total	100.7	101.0	100.7	100.7	100.5	100.6	100.5	100.8	101.1	100.2	100.5	101.0	101.3	100.5
Si	1.88	1.86	1.88	1.87	1.87	1.87	1.87	1.87	1.87	1.87	1.87	1.86	1.86	1.86
Ti	0.028	0.027	0.027	0.027	0.028	0.027	0.026	0.026	0.026	0.027	0.026	0.026	0.027	0.025
Al	0.19	0.18	0.19	0.18	0.19	0.19	0.19	0.19	0.18	0.18	0.17	0.19	0.19	0.19
Cr	0.038	0.037	0.035	0.038	0.037	0.037	0.039	0.038	0.037	0.036	0.035	0.035	0.037	0.038
Fe3	0.014	0.049	0.023	0.030	0.016	0.033	0.029	0.033	0.041	0.026	0.041	0.045	0.050	0.038
Fe2	0.085	0.051	0.072	0.062	0.074	0.066	0.065	0.065	0.066	0.067	0.056	0.055	0.053	0.059
Mn	0.002	0.003	0.004	0.006	0.001	0.002	0.004	0.002	0.003	0.003	0.004	0.007	0.003	0.004
NiO	0.002	0.001	0.001	0.001	0.002	0.001	<0.001	0.001	0.003	0.002	0.001	0.002	0.002	0.001
Mg	0.84	0.86	0.85	0.84	0.84	0.84	0.83	0.84	0.86	0.84	0.88	0.84	0.84	0.84
Ca	0.88	0.88	0.88	0.89	0.89	0.89	0.89	0.89	0.87	0.90	0.88	0.90	0.89	0.90
Na	0.046	0.049	0.047	0.051	0.048	0.049	0.049	0.047	0.043	0.045	0.041	0.045	0.046	0.046
K	<0.001	<0.001	<0.001	<0.001	<0.001	0.001	<0.001	0.001	0.001	<0.001	<0.001	<0.001	0.001	<0.001

Sample L13

distance	**2020**	**2035**	**2050**	**2080**	**2095**	**2110**	**2140**	**2155**	**2170**	**2185**	**2215**	**2230**	**2245**	**2260**
SiO2	51.7	51.1	51.4	51.2	51.3	51.0	51.0	50.9	51.0	51.0	51.3	52.4	51.6	50.6
TiO2	0.89	0.90	0.91	0.93	0.89	1.00	0.99	0.99	0.93	0.99	0.90	0.79	0.95	1.19
Al2O3	4.4	4.7	4.7	4.9	4.8	4.9	5.0	5.0	5.0	5.0	4.7	3.6	4.0	4.6
Cr2O3	1.32	1.37	1.33	1.34	1.36	1.37	1.34	1.29	1.33	1.32	1.33	1.28	1.46	1.21
Fe2O3	1.48	1.66	1.13	1.94	1.66	1.56	1.01	1.57	1.53	1.86	1.21	1.04	1.56	2.50
FeO	2.32	1.99	2.28	1.93	2.11	2.04	2.38	1.90	2.07	1.69	2.09	1.87	1.75	1.10
MnO	0.06	0.14	0.08	0.13	0.13	0.13	0.10	0.12	0.14	0.17	0.10	0.05	0.10	0.10
NiO	0.03	0.04	0.03	0.07	0.05	0.06	<0.01	0.03	0.06	0.05	0.08	0.01	0.06	0.05
MgO	16.4	15.4	15.4	16.3	15.7	15.3	15.2	15.2	15.3	15.4	15.4	16.4	15.7	16.0
CaO	22.0	22.7	22.8	21.6	22.2	22.7	22.8	22.8	22.6	22.8	22.6	23.1	23.3	23.0
Na2O	0.59	0.68	0.68	0.71	0.71	0.72	0.66	0.71	0.69	0.73	0.75	0.57	0.64	0.51
K2O	<0.01	0.01	<0.01	0.02	<0.01	<0.01	<0.01	<0.01	<0.01	0.01	0.02	<0.01	<0.01	<0.01
Total	101.2	100.6	100.7	101.0	101.0	100.8	100.5	100.5	100.7	101.0	100.5	101.0	101.1	100.9
Si	1.86	1.86	1.86	1.85	1.86	1.85	1.86	1.85	1.85	1.85	1.87	1.89	1.87	1.84
Ti	0.024	0.025	0.025	0.025	0.024	0.027	0.027	0.027	0.025	0.027	0.025	0.021	0.026	0.033
Al	0.19	0.20	0.20	0.21	0.21	0.21	0.21	0.21	0.22	0.21	0.20	0.15	0.17	0.20
Cr	0.038	0.039	0.038	0.038	0.039	0.039	0.038	0.037	0.038	0.038	0.038	0.036	0.042	0.035
Fe3	0.040	0.045	0.031	0.053	0.045	0.043	0.028	0.043	0.042	0.051	0.033	0.028	0.042	0.068
Fe2	0.070	0.061	0.069	0.058	0.064	0.062	0.072	0.058	0.063	0.051	0.063	0.057	0.053	0.033
Mn	0.002	0.004	0.003	0.004	0.004	0.004	0.003	0.004	0.004	0.005	0.003	0.002	0.003	0.003
Ni	0.001	0.001	0.001	0.002	0.001	0.002	<0.001	0.001	0.002	0.002	0.002	<0.001	0.002	0.002
Mg	0.88	0.83	0.83	0.88	0.85	0.83	0.83	0.83	0.83	0.83	0.83	0.88	0.85	0.87
Ca	0.85	0.89	0.89	0.83	0.86	0.88	0.89	0.89	0.88	0.88	0.88	0.89	0.90	0.89
Na	0.041	0.048	0.048	0.050	0.050	0.051	0.046	0.050	0.049	0.051	0.053	0.040	0.045	0.036
K	<0.001	<0.001	<0.001	0.001	<0.001	<0.001	<0.001	<0.001	<0.001	<0.001	0.001	<0.001	<0.001	<0.001

A2.6b: Clinopyroxene profils

Sample L13

distance	2275	2290	2320	2335	2350	2365	2380	2395	2410	2425	2440	2455	2470	2485
SiO2	51.4	50.8	51.2	50.8	51.0	51.5	51.4	51.4	51.1	51.1	51.5	51.1	51.4	51.0
TiO2	0.93	1.02	0.95	1.18	1.02	0.92	0.98	0.92	1.05	1.03	0.91	1.02	1.03	1.02
Al2O3	4.2	4.8	4.5	5.0	4.7	4.7	4.6	4.6	4.8	4.8	4.5	4.6	4.3	4.5
Cr2O3	1.28	1.38	1.39	1.21	1.39	1.35	1.39	1.39	1.37	1.33	1.38	1.34	1.27	1.30
Fe2O3	1.45	1.97	1.64	1.36	1.10	0.84	1.62	1.10	1.22	1.23	1.59	1.52	1.50	1.72
FeO	1.80	1.48	1.87	1.97	2.15	2.62	1.94	2.31	2.28	2.24	2.15	2.08	2.02	1.83
MnO	0.16	0.06	0.15	0.07	0.12	0.11	0.14	0.05	0.06	0.11	0.09	0.07	0.13	0.06
NiO	0.08	0.03	0.02	0.06	0.04	0.08	0.03	0.04	0.05	0.05	0.02	0.03	0.04	0.04
MgO	15.5	15.5	15.6	15.1	15.2	15.3	15.4	15.4	15.2	15.3	16.2	15.2	15.4	15.7
CaO	23.1	22.9	22.7	23.3	23.0	22.8	23.1	22.9	22.9	22.9	21.9	23.0	22.9	22.6
Na2O	0.63	0.68	0.67	0.62	0.67	0.69	0.68	0.65	0.67	0.66	0.67	0.70	0.70	0.68
K2O	0.01	<0.01	0.02	0.02	0.01	<0.01	0.03	<0.01	0.02	<0.01	<0.01	<0.01	0.01	0.01
Total	100.6	100.6	100.7	100.8	100.4	100.9	101.4	100.8	100.7	100.7	101.0	100.7	100.7	100.4
Si	1.87	1.85	1.86	1.85	1.86	1.87	1.86	1.86	1.86	1.86	1.86	1.86	1.87	1.86
Ti	0.025	0.028	0.026	0.032	0.028	0.025	0.027	0.025	0.029	0.028	0.025	0.028	0.028	0.028
Al	0.18	0.20	0.19	0.22	0.20	0.20	0.20	0.20	0.21	0.20	0.19	0.20	0.19	0.19
Cr	0.037	0.040	0.040	0.035	0.040	0.039	0.040	0.040	0.039	0.038	0.039	0.039	0.037	0.038
Fe3	0.040	0.054	0.045	0.037	0.030	0.023	0.044	0.030	0.033	0.034	0.043	0.042	0.041	0.047
Fe2	0.055	0.045	0.057	0.060	0.066	0.079	0.059	0.070	0.069	0.068	0.065	0.063	0.061	0.056
Mn	0.005	0.002	0.005	0.002	0.004	0.004	0.004	0.002	0.002	0.003	0.003	0.002	0.004	0.002
Ni	0.002	0.001	0.001	0.002	0.001	0.002	0.001	0.001	0.002	0.002	0.001	0.001	0.001	0.001
Mg	0.84	0.84	0.84	0.82	0.82	0.82	0.83	0.83	0.82	0.83	0.87	0.83	0.84	0.85
Ca	0.90	0.89	0.88	0.91	0.90	0.89	0.90	0.89	0.89	0.89	0.85	0.90	0.89	0.88
Na	0.045	0.048	0.047	0.044	0.048	0.049	0.048	0.046	0.047	0.046	0.047	0.049	0.050	0.048
K	<0.001	<0.001	0.001	0.001	<0.001	<0.001	0.001	<0.001	0.001	<0.001	<0.001	<0.001	0.001	<0.001

										Sample L13 profil 2				
distance	**2500**	**2545**	**2560**	**2575**	**2680**	**2695**	**2710**	**2740**	**2755**	**distanc**	**0**	**40**	**60**	**70**
SiO2	51.3	51.2	51.4	51.4	52.5	52.2	51.9	51.8	51.5	SiO2	52.5	51.9	52.1	52.2
TiO2	0.98	1.00	0.95	1.01	0.99	1.04	0.98	0.97	0.93	TiO2	1.08	1.13	1.17	1.10
Al2O3	4.3	4.2	4.0	3.9	3.4	3.8	3.8	3.8	4.1	Al2O3	3.2	3.7	3.8	3.6
Cr2O3	1.28	1.27	1.22	1.22	0.96	1.03	1.03	1.04	1.14	Cr2O3	0.51	0.46	0.37	0.47
Fe2O3	1.97	1.65	1.51	1.41	1.36	1.23	1.73	2.11	2.13	Fe2O3	1.14	1.85	1.23	1.41
FeO	1.44	1.56	1.81	1.87	2.20	2.52	2.15	1.31	1.27	FeO	2.07	1.73	2.13	1.91
MnO	0.10	0.10	0.10	0.14	0.07	0.09	0.12	0.05	0.12	MnO	0.11	0.08	0.10	0.07
NiO	0.08	0.04	0.02	0.05	<0.01	0.05	0.07	0.06	0.02	NiO	0.05	<0.01	<0.01	0.01
MgO	15.6	15.7	15.6	15.7	16.7	16.6	16.7	16.1	16.1	MgO	16.3	16.2	16.1	16.2
CaO	23.0	22.9	23.1	23.1	22.7	22.1	22.0	23.3	22.8	CaO	23.4	23.3	23.2	23.1
Na2O	0.71	0.67	0.63	0.62	0.54	0.59	0.58	0.61	0.67	Na2O	0.53	0.54	0.56	0.60
K2O	<0.01	0.02	0.02	<0.01	0.02	0.01	<0.01	<0.01	<0.01	K2O	<0.01	<0.01	0.03	0.02
Total	100.7	100.3	100.4	100.4	101.4	101.2	101.0	101.1	100.7	Total	100.9	101.0	100.7	100.8
Si	1.86	1.87	1.87	1.87	1.89	1.88	1.88	1.87	1.87	Si	1.90	1.88	1.89	1.89
Ti	0.027	0.028	0.026	0.028	0.027	0.028	0.027	0.026	0.025	Ti	0.029	0.031	0.032	0.030
Al	0.18	0.18	0.17	0.17	0.14	0.16	0.16	0.16	0.18	Al	0.14	0.16	0.16	0.16
Cr	0.037	0.037	0.035	0.035	0.027	0.029	0.029	0.030	0.033	Cr	0.015	0.013	0.011	0.013
Fe3	0.054	0.045	0.041	0.039	0.037	0.033	0.047	0.057	0.058	Fe3	0.031	0.050	0.034	0.038
Fe2	0.044	0.048	0.055	0.057	0.066	0.076	0.065	0.040	0.039	Fe2	0.063	0.052	0.065	0.058
Mn	0.003	0.003	0.003	0.004	0.002	0.003	0.004	0.002	0.004	Mn	0.003	0.002	0.003	0.002
Ni	0.003	0.001	0.001	0.001	<0.001	0.001	0.002	0.002	<0.001	Ni	0.002	<0.001	<0.001	0.000
Mg	0.84	0.85	0.85	0.85	0.90	0.89	0.90	0.87	0.87	Mg	0.88	0.87	0.87	0.88
Ca	0.90	0.89	0.90	0.90	0.87	0.86	0.85	0.90	0.88	Ca	0.91	0.90	0.90	0.90
Na	0.050	0.047	0.045	0.044	0.038	0.041	0.041	0.043	0.047	Na	0.037	0.038	0.039	0.042
K	<0.001	0.001	0.001	<0.001	0.001	<0.001	<0.001	<0.001	<0.001	K	<0.001	<0.001	0.001	0.001

A2.6b: Clinopyroxene profils

Sample L13

distance	**80**	**90**	**100**	**110**	**120**	**130**	**140**	**160**	**170**	**180**	**190**	**200**	**210**	**260**
SiO2	52.1	51.1	54.1	51.6	52.0	51.8	52.4	51.1	52.1	51.8	52.0	52.2	51.9	52.0
TiO2	1.16	1.18	0.50	1.19	1.16	1.17	1.04	1.14	1.15	1.11	1.14	1.11	1.05	1.11
Al2O3	3.8	4.3	1.8	3.6	3.9	4.3	3.9	4.5	4.1	4.2	4.3	4.3	4.3	4.1
Cr2O3	0.40	0.43	0.36	0.41	0.34	0.23	0.27	0.21	0.36	0.32	0.34	0.35	0.31	0.30
Fe2O3	1.44	2.94	0.98	2.21	1.52	1.67	1.55	2.83	1.75	1.54	1.84	1.57	2.13	1.25
FeO	2.03	0.75	2.09	1.34	2.09	1.90	1.90	0.73	1.89	2.11	1.66	2.16	1.57	2.33
MnO	0.14	0.12	0.12	0.13	0.13	0.14	0.09	0.15	0.09	0.08	0.13	0.09	0.11	0.15
NiO	0.00	0.01	<0.01	0.05	0.02	0.07	0.01	0.05	0.05	0.03	0.08	0.05	0.11	0.02
MgO	16.2	16.7	17.3	16.2	16.7	16.9	16.4	16.8	16.4	16.3	16.2	16.2	16.2	16.3
CaO	23.0	22.3	23.4	23.6	22.5	22.0	22.6	22.1	22.5	22.3	22.8	22.8	22.8	22.3
Na2O	0.61	0.63	0.47	0.48	0.54	0.56	0.72	0.61	0.69	0.67	0.69	0.65	0.66	0.63
K2O	<0.01	<0.01	0.01	0.02	<0.01	0.01	<0.01	<0.01	0.01	<0.01	<0.01	<0.01	0.01	<0.01
Total	100.8	100.4	101.1	100.8	100.9	100.7	100.8	100.2	101.1	100.5	101.2	101.4	101.2	100.5
Si	1.88	1.85	1.95	1.87	1.88	1.87	1.89	1.85	1.88	1.88	1.87	1.88	1.87	1.88
Ti	0.032	0.032	0.014	0.032	0.032	0.032	0.028	0.031	0.031	0.030	0.031	0.030	0.029	0.030
Al	0.16	0.18	0.07	0.15	0.16	0.18	0.16	0.19	0.18	0.18	0.18	0.18	0.18	0.18
Cr	0.012	0.012	0.010	0.012	0.010	0.007	0.008	0.006	0.010	0.009	0.010	0.010	0.009	0.009
Fe3	0.039	0.080	0.027	0.060	0.041	0.045	0.042	0.077	0.048	0.042	0.050	0.042	0.058	0.034
Fe2	0.062	0.023	0.063	0.041	0.063	0.058	0.057	0.022	0.057	0.064	0.050	0.065	0.047	0.071
Mn	0.004	0.004	0.004	0.004	0.004	0.004	0.003	0.005	0.003	0.003	0.004	0.003	0.003	0.005
Ni	<0.001	<0.001	<0.001	0.001	0.001	0.002	<0.001	0.002	0.002	0.001	0.002	0.001	0.003	0.001
Mg	0.87	0.90	0.93	0.87	0.90	0.91	0.88	0.91	0.88	0.88	0.87	0.87	0.87	0.88
Ca	0.89	0.87	0.90	0.92	0.87	0.85	0.88	0.86	0.87	0.87	0.88	0.88	0.88	0.87
Na	0.043	0.044	0.032	0.034	0.038	0.039	0.050	0.043	0.048	0.047	0.048	0.045	0.046	0.044
K	<0.001	<0.001	<0.001	0.001	<0.001	<0.001	<0.001	<0.001	0.001	<0.001	<0.001	<0.001	<0.001	<0.001

Sample L13 profil 2

distance	**270**	**280**	**290**	**300**	**320**	**330**	**340**	**350**	**360**	**370**	**390**	**400**	**410**	**420**
SiO2	52.1	51.7	52.1	52.0	51.8	51.9	51.7	51.8	51.7	52.1	51.6	51.9	51.7	51.7
TiO2	1.19	1.14	1.16	1.11	1.16	1.18	1.21	1.15	1.21	1.14	1.18	1.22	1.30	1.27
Al2O3	4.1	4.2	4.3	4.1	4.2	4.2	4.3	4.1	4.3	4.0	4.1	4.2	4.3	4.2
Cr2O3	0.34	0.35	0.36	0.35	0.33	0.27	0.31	0.37	0.30	0.37	0.39	0.34	0.39	0.34
Fe2O3	1.28	2.15	1.82	1.64	1.92	1.80	1.74	1.64	2.32	1.35	2.07	1.44	1.87	1.95
FeO	2.19	1.81	1.94	2.10	1.79	2.35	1.90	1.92	1.36	2.13	1.61	2.09	1.69	1.62
MnO	0.10	0.07	0.11	0.10	0.11	0.10	0.17	0.13	0.15	0.06	0.17	0.11	0.14	0.14
NiO	0.06	0.03	0.02	0.02	0.04	0.03	0.11	0.04	0.04	<0.01	0.02	<0.01	0.03	0.05
MgO	16.7	17.0	16.4	16.7	16.4	17.4	16.5	16.4	16.4	16.3	16.3	16.3	16.4	16.3
CaO	22.1	21.7	22.5	22.0	22.5	20.8	22.2	22.5	22.7	22.7	22.4	22.7	22.4	22.7
Na2O	0.66	0.61	0.70	0.63	0.64	0.62	0.62	0.62	0.67	0.66	0.67	0.62	0.68	0.65
K2O	<0.01	0.01	<0.01	<0.01	0.01	0.01	<0.01	<0.01	<0.01	<0.01	0.01	0.01	0.02	<0.01
Total	100.8	100.8	101.3	100.7	101.0	100.7	100.7	100.7	101.1	100.8	100.5	100.8	100.9	100.8
Si	1.88	1.87	1.87	1.88	1.87	1.87	1.87	1.87	1.86	1.88	1.87	1.88	1.87	1.87
Ti	0.032	0.031	0.031	0.030	0.031	0.032	0.033	0.031	0.033	0.031	0.032	0.033	0.035	0.034
Al	0.17	0.18	0.18	0.17	0.18	0.18	0.18	0.18	0.18	0.17	0.17	0.18	0.18	0.18
Cr	0.010	0.010	0.010	0.010	0.010	0.008	0.009	0.011	0.009	0.011	0.011	0.010	0.011	0.010
Fe3	0.035	0.059	0.049	0.045	0.052	0.049	0.047	0.045	0.063	0.037	0.057	0.039	0.051	0.053
Fe2	0.066	0.055	0.059	0.064	0.054	0.071	0.058	0.058	0.041	0.064	0.049	0.063	0.051	0.049
Mn	0.003	0.002	0.003	0.003	0.003	0.003	0.005	0.004	0.005	0.002	0.005	0.003	0.004	0.004
Ni	0.002	0.001	0.001	0.001	0.001	0.001	0.003	0.001	0.001	<0.001	0.001	<0.001	0.001	0.002
Mg	0.90	0.91	0.88	0.90	0.88	0.94	0.89	0.89	0.88	0.88	0.88	0.88	0.88	0.88
Ca	0.85	0.84	0.87	0.85	0.87	0.80	0.86	0.87	0.88	0.88	0.87	0.88	0.87	0.88
Na	0.046	0.043	0.049	0.044	0.045	0.044	0.044	0.044	0.047	0.046	0.047	0.044	0.047	0.046
K	<0.001	0.001	<0.001	<0.001	0.001	<0.001	<0.001	<0.001	<0.001	<0.001	<0.001	<0.001	0.001	<0.001

A2.6b: Clinopyroxene profils

Sample L13 profil 2

distance è	**430**	**450**	**470**	**480**	**490**	**510**	**530**	**540**	**550**	**560**	**570**	**590**	**600**	**620**
SiO2	50.6	51.7	52.3	51.9	51.1	51.4	51.6	51.9	52.1	52.0	51.6	50.9	51.5	51.3
TiO2	1.13	1.24	1.26	1.26	1.41	1.21	1.27	1.26	1.23	1.34	1.33	1.35	1.33	1.34
Al2O3	4.8	4.3	4.3	4.2	4.5	4.4	4.2	4.3	4.2	4.4	4.5	4.9	4.4	4.6
Cr2O3	0.38	0.34	0.33	0.32	0.36	0.40	0.43	0.32	0.40	0.45	0.46	0.41	0.46	0.38
Fe2O3	3.03	2.05	1.62	1.25	2.31	2.38	1.55	1.63	1.19	1.55	1.93	2.79	1.63	1.55
FeO	0.72	1.80	1.81	2.19	1.22	1.38	2.03	2.07	2.32	2.21	1.41	0.86	1.91	2.15
MnO	0.15	0.06	0.15	0.12	0.11	0.14	0.18	0.10	0.10	0.13	0.11	0.12	0.12	0.12
NiO	0.09	0.07	<0.01	0.02	0.04	<0.01	<0.01	0.06	0.02	0.07	0.01	<0.01	0.02	0.02
MgO	17.1	16.7	16.6	16.2	15.9	16.4	16.2	16.3	16.2	17.1	16.3	16.8	16.0	16.1
CaO	21.2	21.8	22.6	22.6	22.8	22.5	22.4	22.3	22.5	21.3	22.8	21.8	22.6	22.5
Na2O	0.61	0.69	0.67	0.65	0.71	0.65	0.68	0.70	0.70	0.69	0.70	0.70	0.69	0.59
K2O	0.03	0.01	0.02	<0.01	0.03	<0.01	<0.01	<0.01	0.01	<0.01	0.01	0.01	<0.01	0.02
Total	99.9	100.8	101.6	100.6	100.6	100.8	100.6	101.0	100.9	101.2	101.1	100.6	100.7	100.7
Si	1.84	1.87	1.87	1.88	1.85	1.86	1.87	1.87	1.88	1.87	1.86	1.84	1.87	1.86
Ti	0.031	0.034	0.034	0.034	0.038	0.033	0.035	0.034	0.033	0.036	0.036	0.037	0.036	0.037
Al	0.21	0.18	0.18	0.18	0.19	0.19	0.18	0.18	0.18	0.19	0.19	0.21	0.19	0.20
Cr	0.011	0.010	0.010	0.009	0.010	0.011	0.012	0.009	0.011	0.013	0.013	0.012	0.013	0.011
Fe3	0.083	0.056	0.044	0.034	0.063	0.065	0.042	0.044	0.032	0.042	0.053	0.076	0.045	0.042
Fe2	0.022	0.054	0.054	0.066	0.037	0.042	0.062	0.062	0.070	0.066	0.043	0.026	0.058	0.065
Mn	0.005	0.002	0.005	0.004	0.003	0.004	0.005	0.003	0.003	0.004	0.003	0.004	0.004	0.004
Ni	0.003	0.002	<0.001	0.001	0.001	<0.001	<0.001	0.002	0.001	0.002	<0.001	<0.001	0.001	0.001
Mg	0.93	0.90	0.89	0.87	0.86	0.88	0.88	0.88	0.87	0.91	0.87	0.90	0.87	0.87
Ca	0.83	0.84	0.87	0.88	0.89	0.87	0.87	0.86	0.87	0.82	0.88	0.84	0.88	0.87
Na	0.043	0.049	0.046	0.046	0.050	0.045	0.048	0.049	0.049	0.048	0.049	0.049	0.049	0.041
K	0.001	0.001	0.001	<0.001	0.001	<0.001	<0.001	<0.001	<0.001	<0.001	<0.001	0.001	<0.001	0.001

Sample L13 profil 2

distance	**630**	**640**	**660**	**680**	**690**	**720**	**730**	**740**	**750**	**760**	**810**	**820**	**830**	**850**
SiO2	50.8	50.9	51.2	51.8	51.1	51.3	51.3	51.3	51.3	51.4	51.4	51.8	51.5	51.7
TiO2	1.50	1.38	1.54	1.25	1.42	1.32	1.31	1.44	1.34	1.32	1.07	1.30	1.41	1.39
Al2O3	5.0	4.7	4.9	4.4	4.7	4.5	4.8	4.7	4.5	4.5	4.2	4.2	4.1	3.9
Cr2O3	0.45	0.41	0.41	0.38	0.51	0.51	0.51	0.43	0.42	0.50	0.48	0.46	0.33	0.39
Fe2O3	2.06	2.31	1.86	1.36	1.38	1.80	1.65	1.48	2.18	1.79	2.52	1.35	1.60	1.49
FeO	1.60	1.42	1.67	2.02	2.09	1.72	1.81	1.93	1.38	1.63	0.97	1.91	1.82	1.82
MnO	0.17	0.11	0.12	0.13	0.11	0.11	0.09	0.10	0.12	0.11	0.10	0.09	0.12	0.00
NiO	0.03	0.02	0.01	0.01	<0.01	0.04	0.10	0.01	0.09	0.05	0.09	<0.01	<0.01	0.02
MgO	16.3	16.3	16.4	16.4	15.8	16.1	16.3	15.8	16.1	16.0	17.0	16.4	16.0	16.2
CaO	22.1	22.1	22.1	22.2	22.7	22.9	22.1	22.8	22.5	22.7	21.8	22.8	23.1	23.2
Na2O	0.61	0.68	0.68	0.67	0.63	0.58	0.68	0.71	0.71	0.67	0.63	0.61	0.59	0.56
K2O	0.02	0.02	0.02	0.03	<0.01	<0.01	0.02	<0.01	0.01	0.01	0.01	0.01	<0.01	0.02
Total	100.7	100.3	100.8	100.6	100.5	100.8	100.6	100.6	100.7	100.7	100.3	100.8	100.6	100.7
Si	1.84	1.85	1.85	1.87	1.86	1.86	1.86	1.86	1.86	1.86	1.86	1.87	1.87	1.87
Ti	0.041	0.038	0.042	0.034	0.039	0.036	0.036	0.039	0.037	0.036	0.029	0.035	0.039	0.038
Al	0.21	0.20	0.21	0.19	0.20	0.19	0.20	0.20	0.19	0.19	0.18	0.18	0.18	0.17
Cr	0.013	0.012	0.012	0.011	0.015	0.015	0.015	0.012	0.012	0.014	0.014	0.013	0.009	0.011
Fe3	0.056	0.063	0.051	0.037	0.038	0.049	0.045	0.041	0.059	0.049	0.069	0.037	0.044	0.041
Fe2	0.048	0.043	0.050	0.061	0.064	0.052	0.055	0.059	0.042	0.049	0.030	0.058	0.055	0.055
Mn	0.005	0.004	0.004	0.004	0.003	0.003	0.003	0.003	0.004	0.003	0.003	0.003	0.004	0.000
Ni	0.001	0.001	<0.001	<0.001	<0.001	0.001	0.003	<0.001	0.003	0.001	0.003	<0.001	<0.001	0.001
Mg	0.88	0.88	0.88	0.89	0.86	0.87	0.88	0.85	0.87	0.87	0.92	0.88	0.87	0.87
Ca	0.86	0.86	0.85	0.86	0.88	0.89	0.86	0.88	0.87	0.88	0.85	0.88	0.90	0.90
Na	0.043	0.048	0.048	0.047	0.044	0.041	0.048	0.050	0.050	0.047	0.044	0.043	0.042	0.039
K	0.001	0.001	0.001	0.002	<0.001	<0.001	0.001	<0.001	<0.001	0.001	<0.001	<0.001	<0.001	0.001

A2.6b: Clinopyroxene profils

Sample L13 profil 2

distanc	**860**	**870**	**880**	**900**
SiO2	52.7	52.5	52.3	51.9
TiO2	1.00	1.15	1.17	1.12
Al2O3	3.1	3.3	3.2	4.0
Cr2O3	0.39	0.41	0.40	0.52
Fe2O3	1.09	1.62	1.88	1.98
FeO	2.09	1.86	1.63	1.65
MnO	0.11	0.07	0.09	0.11
NiO	0.05	0.02	0.03	0.03
MgO	16.7	16.7	16.8	17.5
CaO	22.8	23.0	22.8	21.3
Na2O	0.57	0.56	0.58	0.59
K2O	0.01	0.02	<0.01	0.01
Total	100.7	101.2	100.9	100.8
Si	1.91	1.89	1.89	1.87
Ti	0.027	0.031	0.032	0.030
Al	0.13	0.14	0.14	0.17
Cr	0.011	0.012	0.011	0.015
Fe3	0.030	0.044	0.051	0.054
Fe2	0.063	0.056	0.049	0.050
Mn	0.003	0.002	0.003	0.004
Ni	0.001	0.001	0.001	0.001
Mg	0.90	0.89	0.90	0.94
Ca	0.88	0.89	0.88	0.82
Na	0.040	0.039	0.041	0.041
K	<0.001	0.001	<0.001	0.001

Annexe A2.6: profiles of minerals (data set associated on CD)

A2.6c: spinel profiles

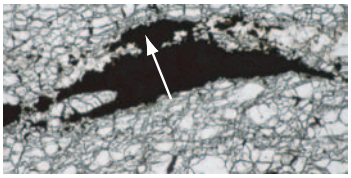

Sample L04: mylonite
distance: 340 µm

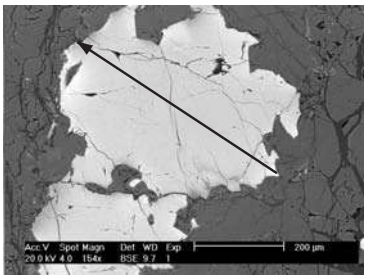

Sample L112:proto- mylonite
distance: 446 µm

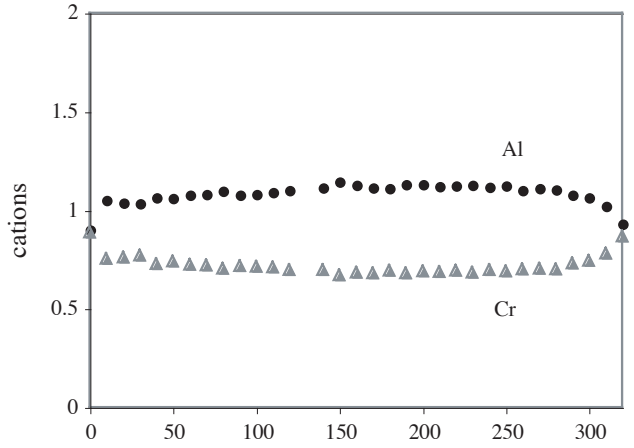

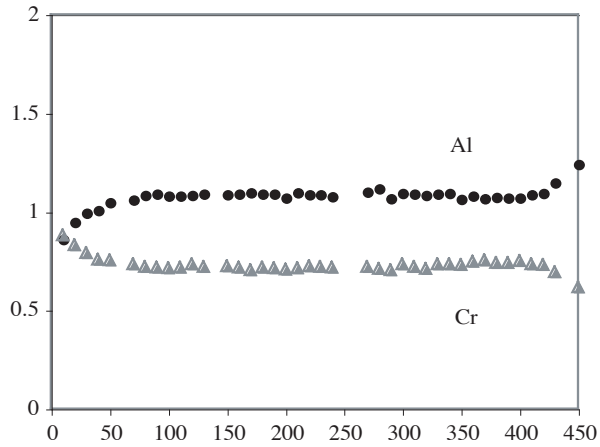

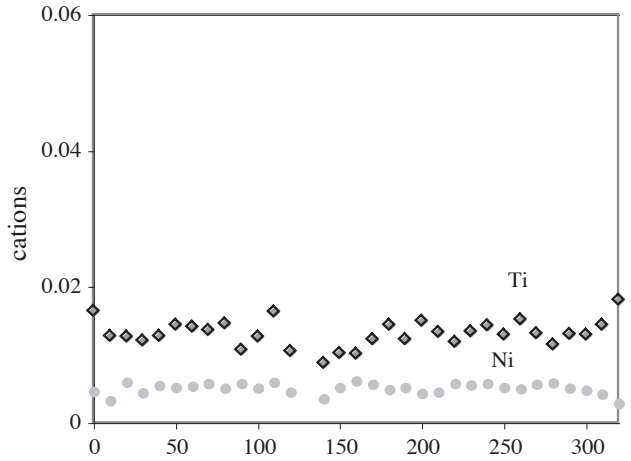

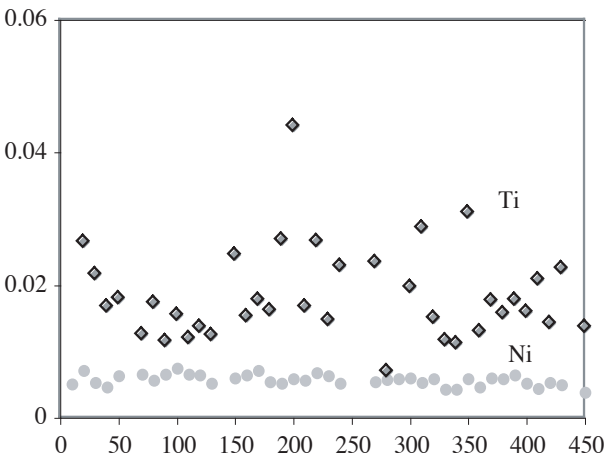

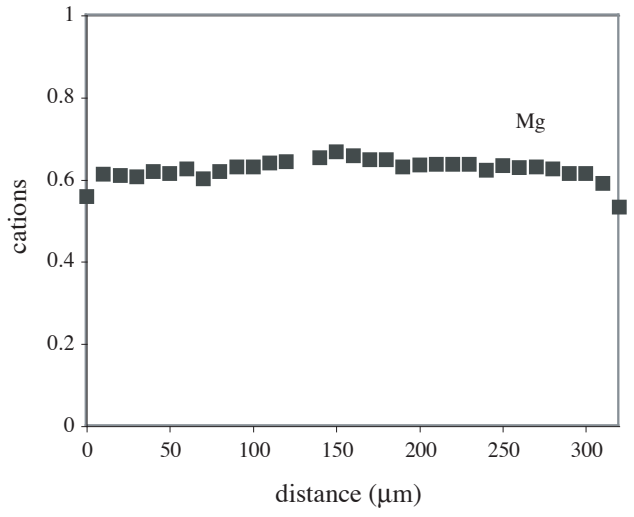

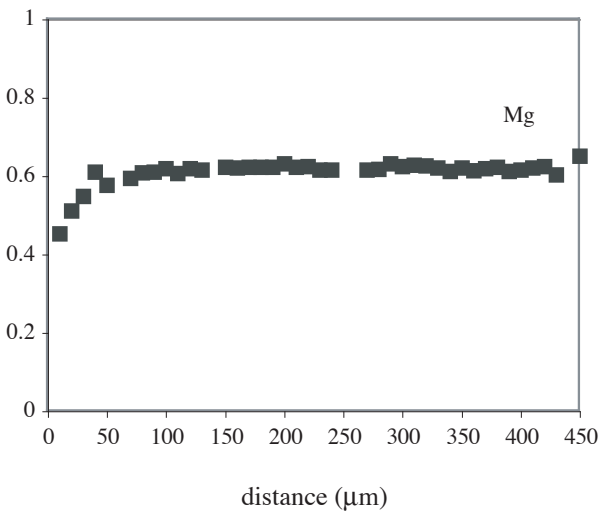

Annexe A2.6: profiles of minerals (data set associated on CD)

A2.6c: spinel profiles

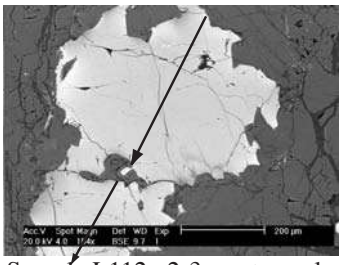

Sample L112 p2-3: proto-mylonite
distance: 386 + 207 µm

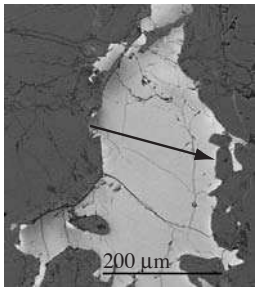

Sample L112 p4: proto-mylonite
distance: 213 µm

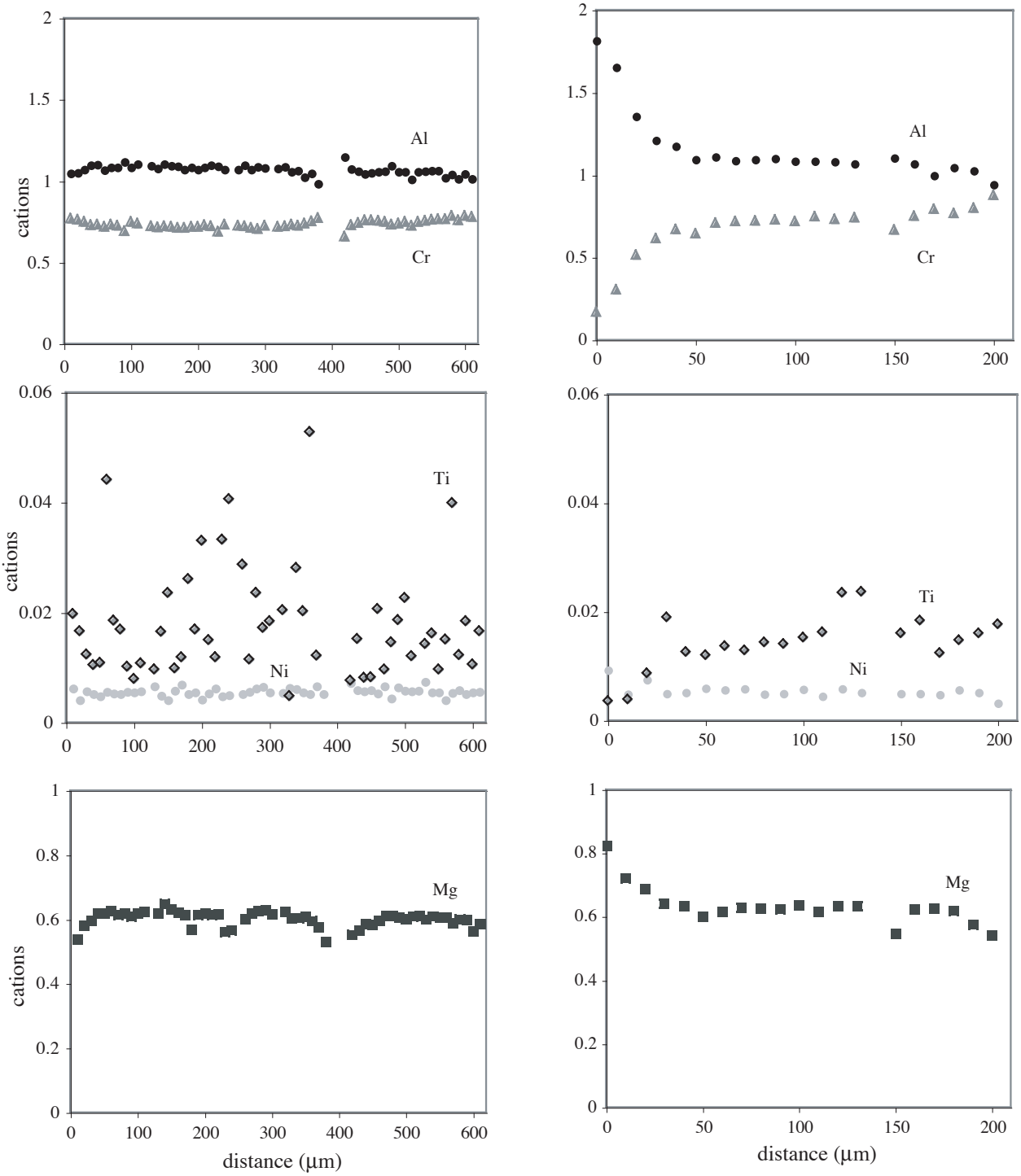

Annexe A2.6: profiles of minerals (data set associated on CD)

A2.6c: spinel profiles

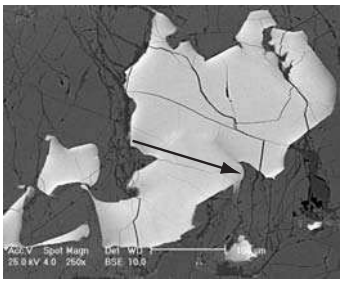

Sample La2002-05 p3: proto-mylonite
distance: 157 µm

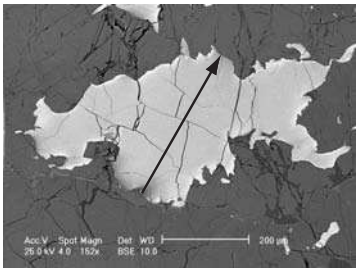

Sample La2002-05 p4: proto-mylonite
distance: 370 µm

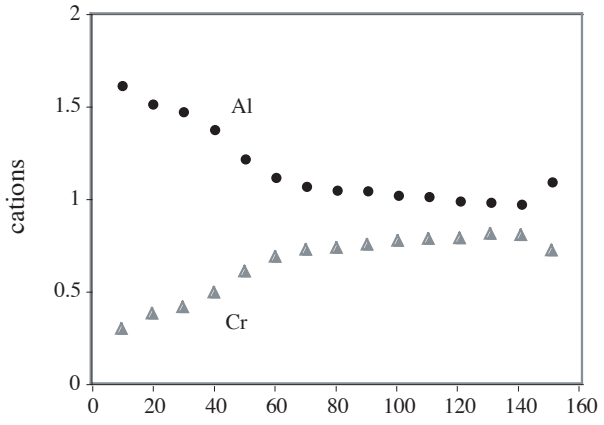

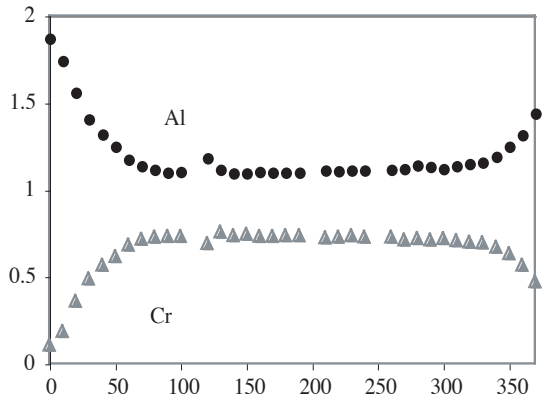

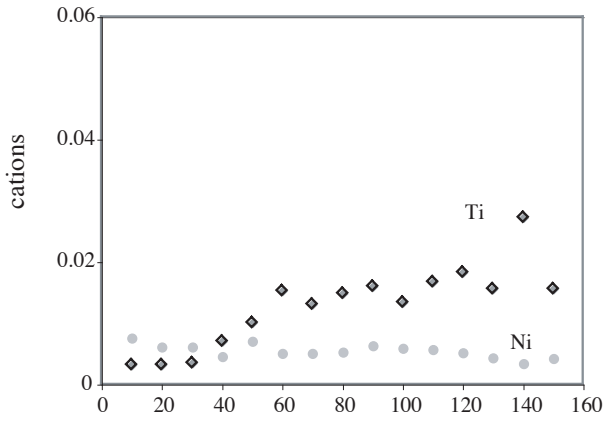

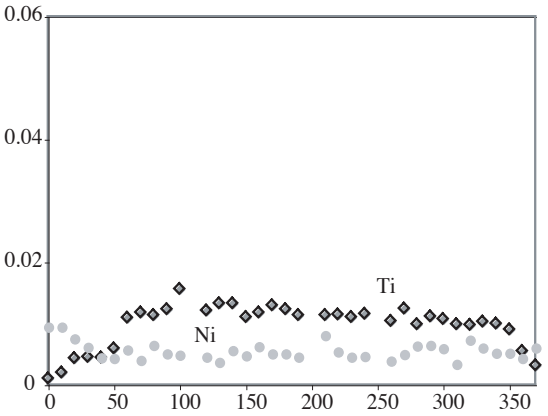

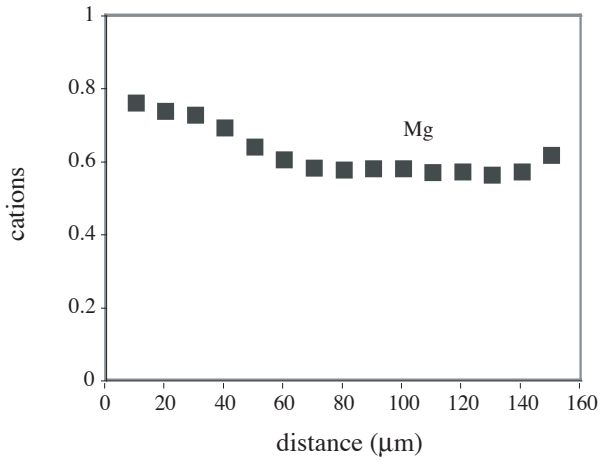

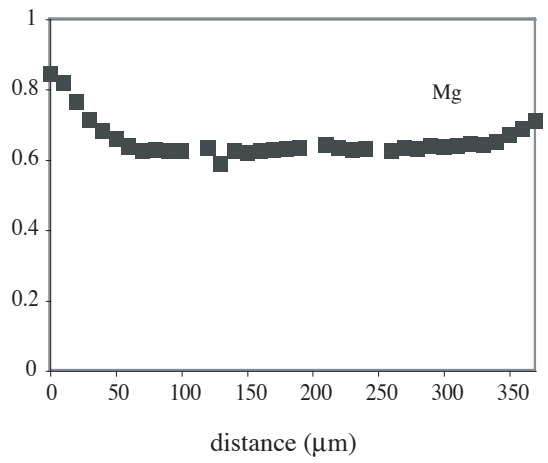

Annexe A2.6: profiles of minerals (data set associated on CD)

A2.6c: spinel profiles

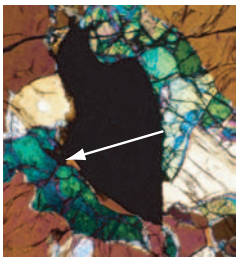

Sample L09 p1:FGSG
distance: 422 µm

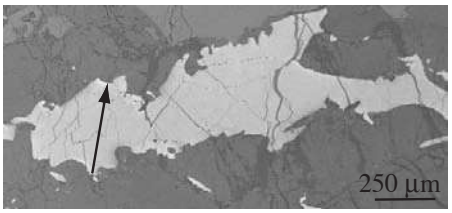

Sample L09 p2: FGSG
distance: 392 µm

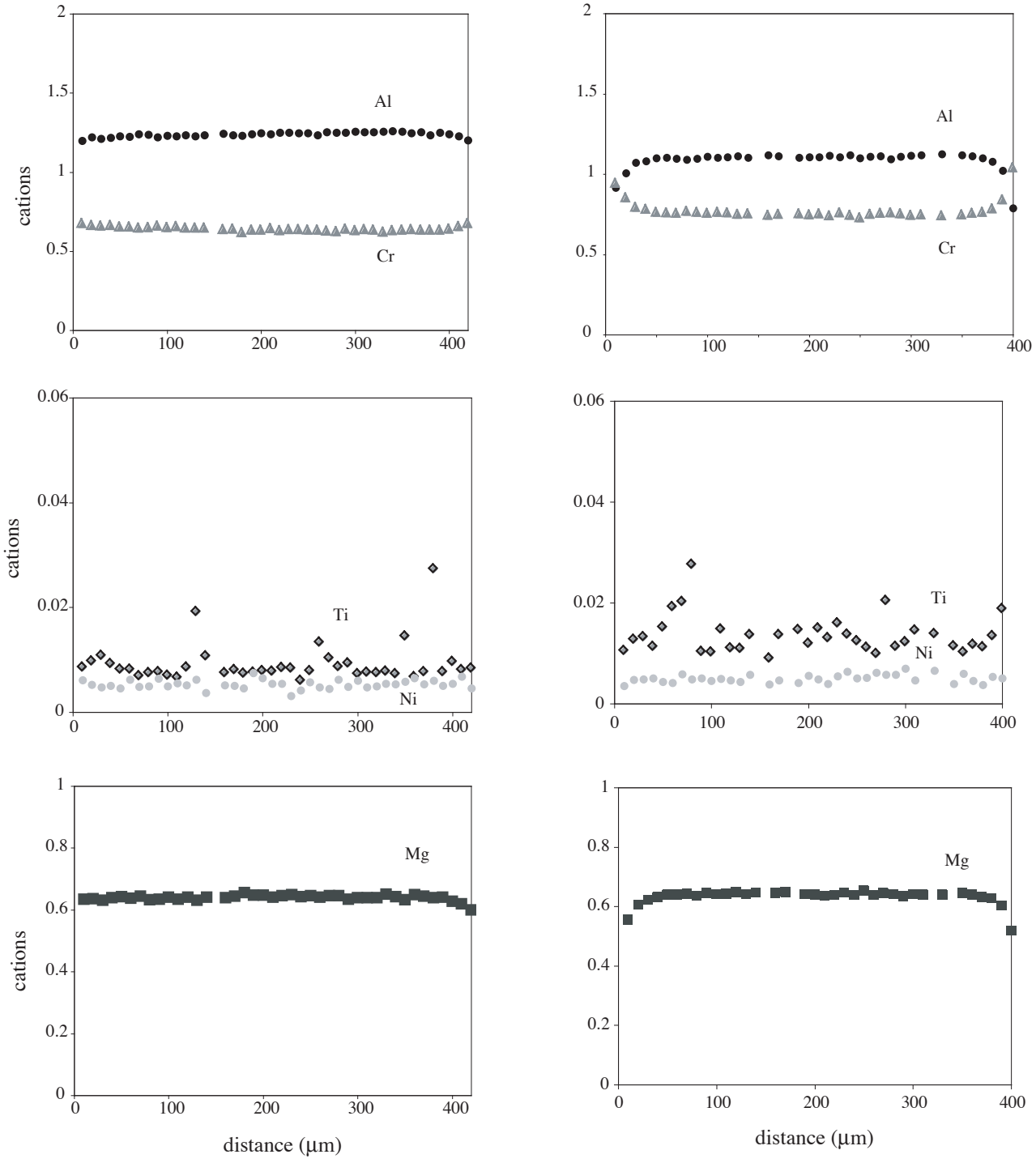

Annexe A2.6: profiles of minerals (data set associated on CD

A2.6c: spinel profiles

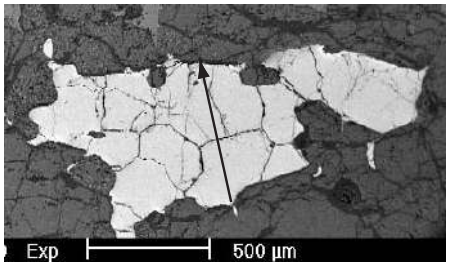

Sample L09 p3:FGSG
distance: 607 µm

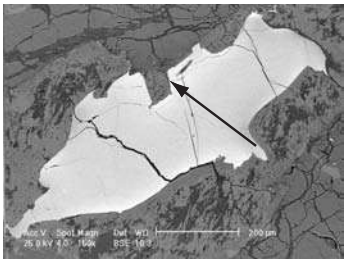

Sample L110 p2: FGSG
distance: 228 µm

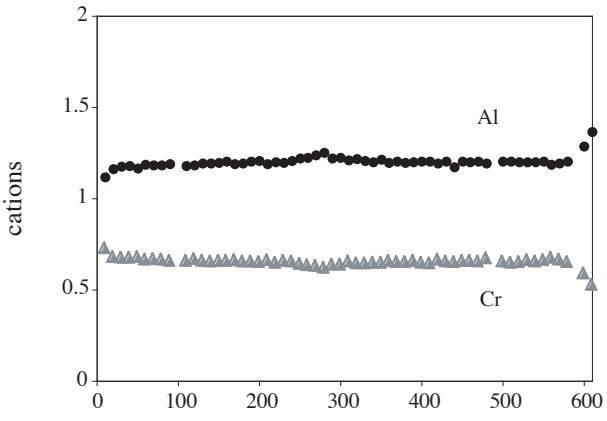

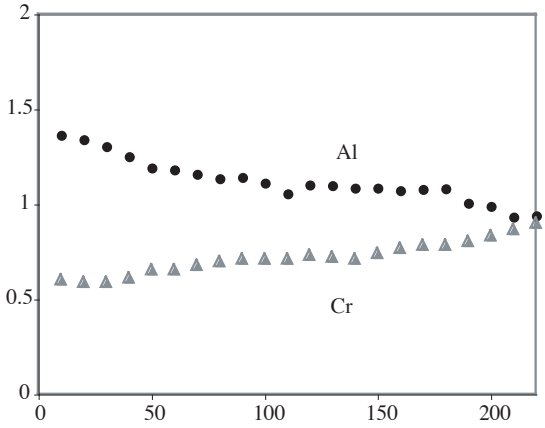

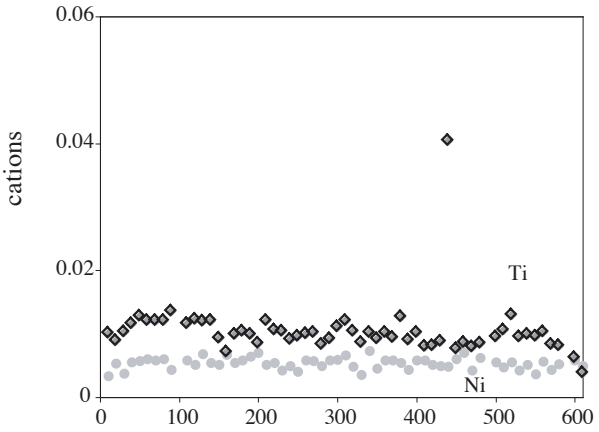

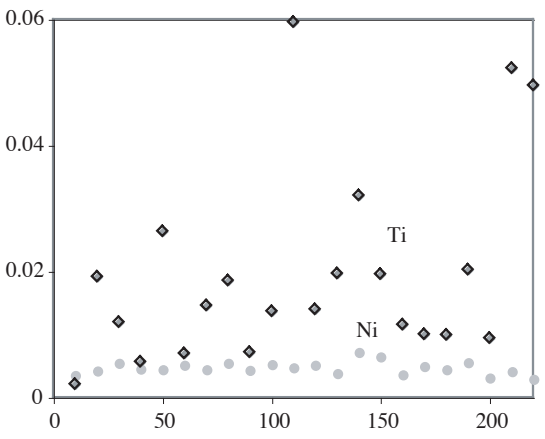

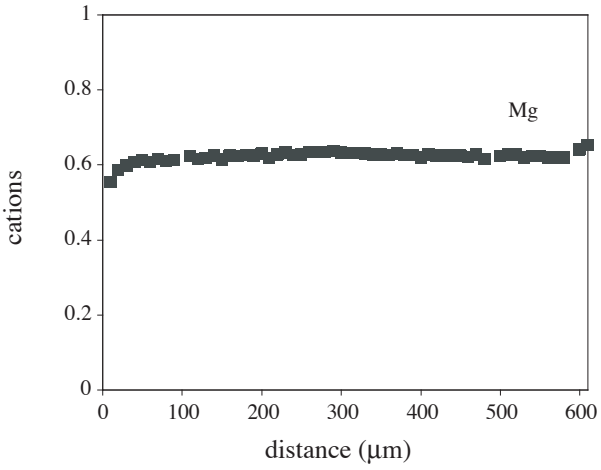

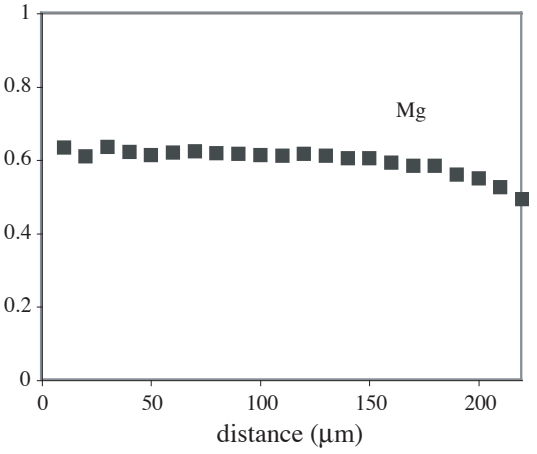

Annexe A2.6: profiles of minerals (data set associated on CD)

A2.6c: spinel profiles

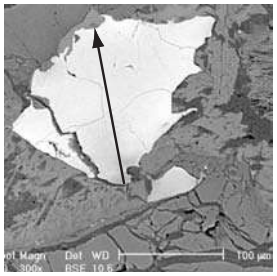

Sample L110 p3:FGSG
distance: 144 µm

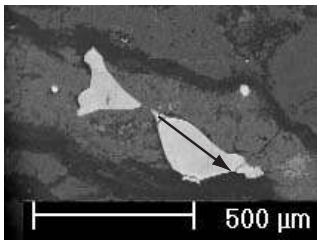

Sample L147 p4: CGSGn
distance: 183 µm

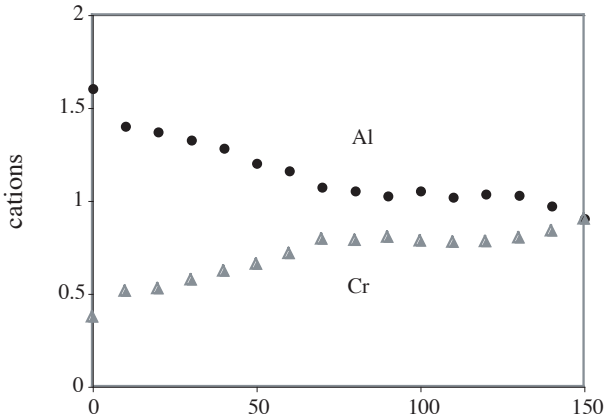

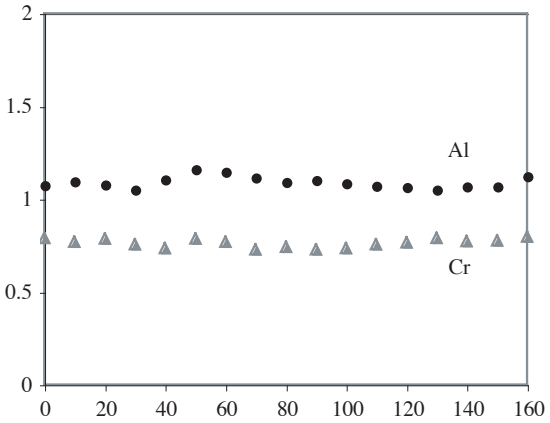

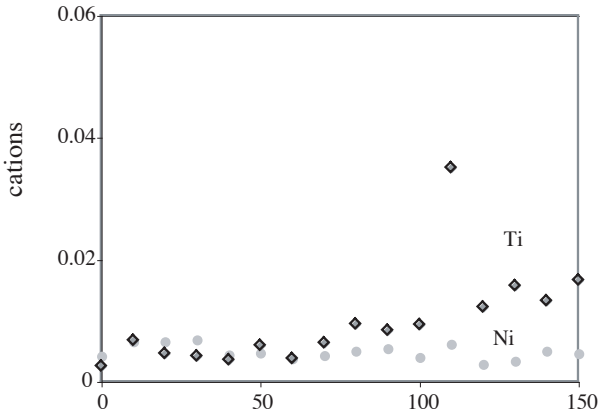

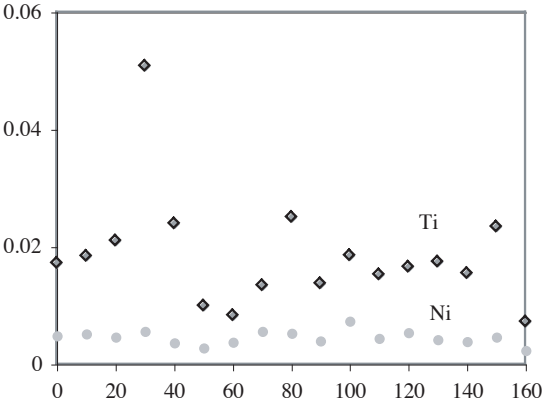

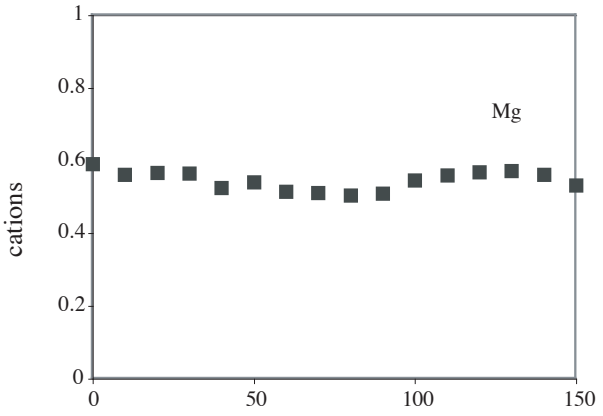

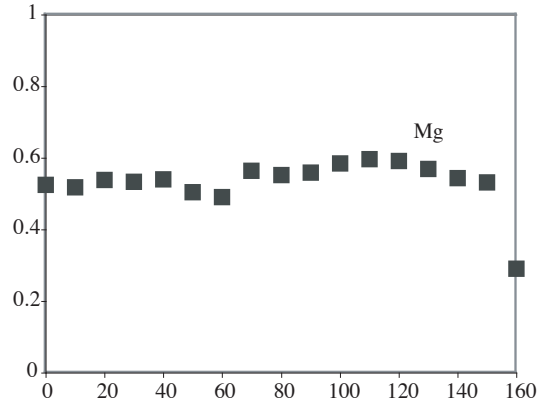

Annexe A2.6: profiles of minerals (data set associated on CD)

A2.6c: spinel profiles

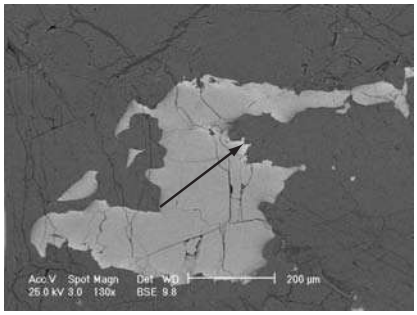

Sample L241 p1: CGSGc
distance: 193 µm

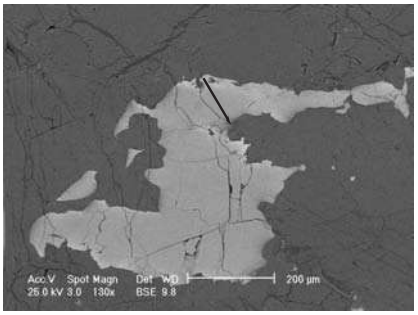

Sample L241 p2: CGSGc
distance: 103 µm

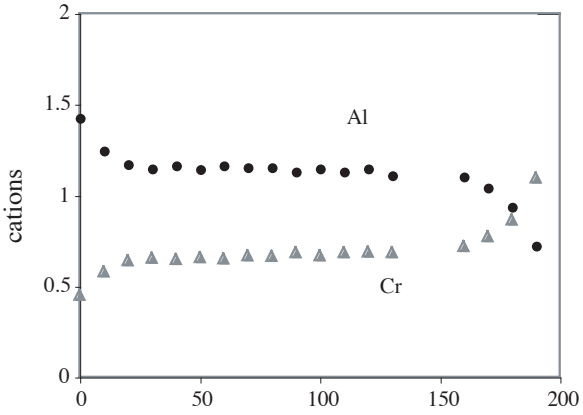

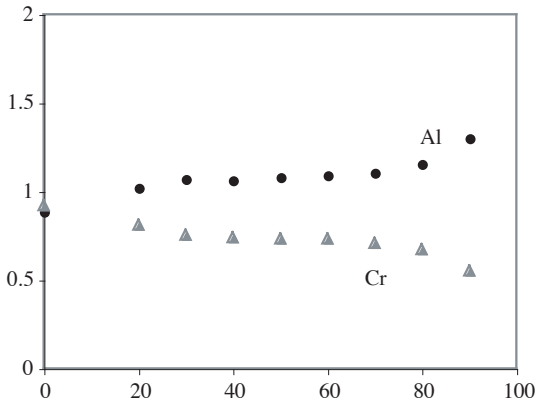

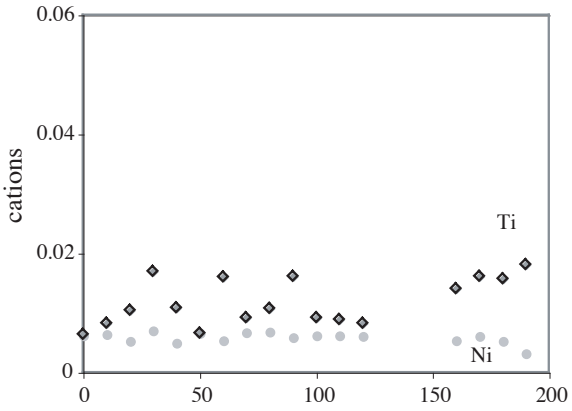

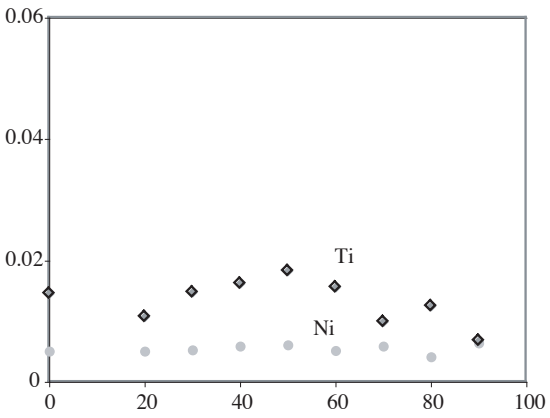

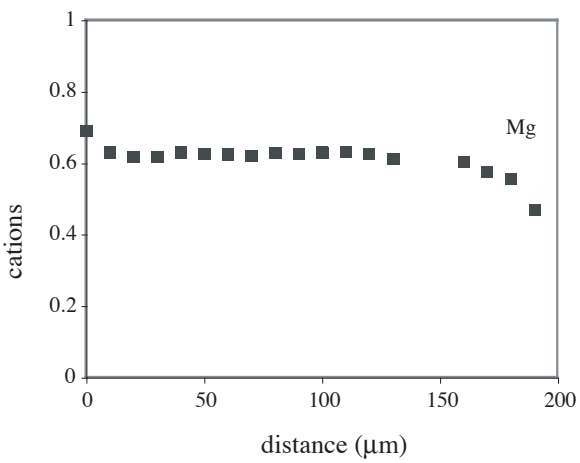

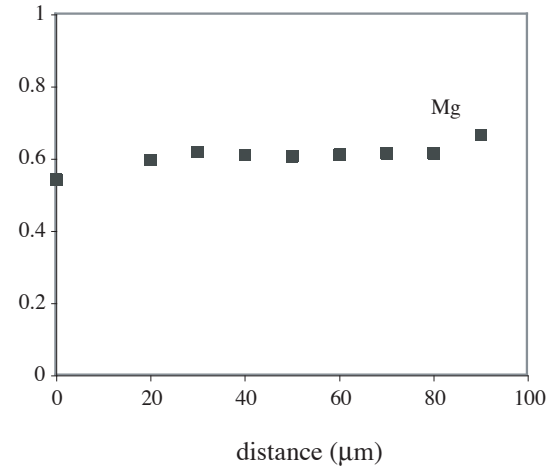

A2.6c: Spinel profils

Sample L04

distanc	0	10	20	30	40	50	60	80	90	100	110	120	140	150
SiO2	0.05	0.01	<0.01	<0.01	0.02	<0.01	<0.01	0.02	0.02	0.03	0.04	0.01	<0.01	0.01
TiO2	0.68	0.55	0.55	0.52	0.55	0.63	0.61	0.63	0.45	0.54	0.70	0.45	0.38	0.44
Al2O3	23.9	29.0	28.7	28.6	29.3	29.4	29.8	30.5	29.0	29.4	29.7	30.0	30.3	31.4
Cr2O3	35.0	31.0	31.4	31.8	29.8	30.7	29.8	29.2	28.8	29.0	28.9	28.3	28.2	27.3
Fe2O3	7.19	7.30	7.48	7.28	7.80	7.34	7.33	7.21	7.59	7.57	6.88	7.71	7.28	7.02
FeO	16.3	15.0	15.1	15.2	14.7	15.0	14.5	14.7	14.0	14.2	14.0	13.6	13.1	12.7
MnO	0.17	0.18	0.19	0.18	0.09	0.21	0.21	0.16	0.11	0.14	0.05	0.11	0.09	0.05
NiO	0.18	0.13	0.24	0.18	0.22	0.21	0.22	0.21	0.23	0.21	0.24	0.18	0.14	0.21
MgO	11.7	13.4	13.3	13.3	13.5	13.5	13.7	13.6	13.4	13.6	13.8	13.9	14.0	14.5
CaO	0.15	0.04	<0.01	0.02	<0.01	0.01	0.02	0.01	0.02	<0.01	<0.01	0.01	0.01	<0.01
Na2O	<0.01	<0.01	<0.01	0.01	<0.01	<0.01	<0.01	0.03	0.01	<0.01	<0.01	<0.01	0.02	0.02
ZnO	0.23	0.19	0.16	0.09	0.23	0.16	0.15	0.18	0.07	0.18	0.13	0.18	0.16	0.19
Total	95.6	96.8	97.2	97.2	96.1	97.2	96.4	96.4	93.7	94.8	94.6	94.5	93.8	93.8
Si	0.002	<0.001	<0.001	<0.001	0.001	<0.001	<0.001	0.001	0.001	0.001	0.001	<0.001	<0.001	<0.001
Ti	0.017	0.013	0.013	0.012	0.013	0.014	0.014	0.015	0.011	0.013	0.016	0.011	0.009	0.010
Al	0.902	1.051	1.039	1.036	1.065	1.061	1.079	1.099	1.079	1.081	1.091	1.101	1.116	1.146
Cr	0.889	0.754	0.763	0.772	0.728	0.742	0.723	0.706	0.718	0.714	0.713	0.697	0.697	0.670
Fe3	0.174	0.169	0.173	0.168	0.181	0.169	0.169	0.166	0.180	0.178	0.161	0.181	0.171	0.164
Fe2	0.438	0.385	0.388	0.390	0.379	0.384	0.372	0.377	0.368	0.369	0.366	0.355	0.342	0.329
Mn	0.005	0.005	0.005	0.005	0.003	0.006	0.006	0.004	0.003	0.004	0.001	0.003	0.002	0.001
Ni	0.005	0.003	0.006	0.005	0.006	0.005	0.005	0.005	0.006	0.005	0.006	0.005	0.004	0.005
Mg	0.560	0.615	0.611	0.608	0.621	0.616	0.627	0.621	0.631	0.632	0.642	0.644	0.654	0.668
Ca	0.005	0.001	<0.001	0.001	<0.001	<0.001	0.001	<0.001	0.001	<0.001	<0.001	<0.001	<0.001	<0.001
Na	<0.001	<0.001	<0.001	<0.001	<0.001	<0.001	<0.001	0.002	<0.001	<0.001	<0.001	<0.001	0.001	0.001
Zn	0.005	0.004	0.004	0.002	0.005	0.004	0.003	0.004	0.002	0.004	0.003	0.004	0.004	0.004

Sample L04

distanc	160	170	180	200	210	220	240	250	270	280	290	300	310
SiO2	0.01	<0.01	0.01	<0.01	0.02	<0.01	0.01	<0.01	0.01	<0.01	<0.01	0.01	<0.01
TiO2	0.43	0.53	0.62	0.66	0.59	0.53	0.64	0.58	0.59	0.51	0.58	0.57	0.63
Al2O3	30.7	30.7	30.6	32.0	31.8	32.2	31.8	31.8	31.5	31.1	30.4	29.8	28.4
Cr2O3	27.8	27.9	28.4	29.0	29.0	29.6	29.6	29.2	29.8	29.5	30.7	31.0	32.3
Fe2O3	7.31	7.88	7.16	6.56	7.20	7.00	6.88	6.98	7.03	7.53	7.28	7.20	7.30
FeO	12.7	13.3	13.7	14.6	14.6	14.6	14.9	14.6	14.7	14.5	15.3	15.2	16.0
MnO	0.14	0.20	0.08	0.11	0.09	0.13	0.15	0.14	0.16	0.21	0.03	0.04	0.13
NiO	0.25	0.23	0.20	0.18	0.19	0.24	0.24	0.22	0.24	0.24	0.21	0.20	0.17
MgO	14.2	14.1	14.1	14.2	14.3	14.4	14.0	14.2	14.2	14.0	13.7	13.6	13.0
CaO	0.01	0.04	<0.01	<0.01	<0.01	<0.01	<0.01	<0.01	<0.01	<0.01	<0.01	<0.01	0.01
Na2O	0.04	0.03	0.03	<0.01	<0.01	<0.01	0.04	<0.01	<0.01	0.02	<0.01	0.02	<0.01
ZnO	0.14	0.26	0.09	0.21	0.19	0.09	0.17	0.12	0.13	0.19	0.20	0.17	0.21
Total	93.8	95.2	95.0	97.5	97.9	98.9	98.49	97.94	98.3	97.9	98.4	97.9	98.1
Si	<0.001	<0.001	<0.001	<0.001	0.001	<0.001	<0.001	<0.001	<0.001	<0.001	<0.001	<0.001	<0.001
Ti	0.010	0.012	0.014	0.015	0.013	0.012	0.014	0.013	0.013	0.012	0.013	0.013	0.015
Al	1.128	1.114	1.112	1.133	1.122	1.126	1.120	1.124	1.111	1.105	1.080	1.067	1.023
Cr	0.684	0.680	0.694	0.690	0.688	0.694	0.698	0.693	0.704	0.703	0.730	0.744	0.781
Fe3	0.171	0.183	0.166	0.148	0.162	0.156	0.155	0.157	0.158	0.171	0.165	0.164	0.168
Fe2	0.332	0.342	0.353	0.367	0.365	0.363	0.373	0.366	0.369	0.366	0.386	0.386	0.409
Mn	0.004	0.005	0.002	0.003	0.002	0.003	0.004	0.004	0.004	0.006	0.001	0.001	0.003
Ni	0.006	0.006	0.005	0.004	0.005	0.006	0.006	0.005	0.006	0.006	0.005	0.005	0.004
Mg	0.659	0.649	0.648	0.636	0.638	0.637	0.623	0.635	0.631	0.626	0.615	0.615	0.592
Ca	<0.001	0.001	<0.001	<0.001	<0.001	<0.001	<0.001	<0.001	<0.001	<0.001	<0.001	<0.001	<0.001
Na	0.003	0.002	0.002	<0.001	<0.001	<0.001	0.003	<0.001	<0.001	0.001	<0.001	0.001	<0.001
Zn	0.003	0.006	0.002	0.005	0.004	0.002	0.004	0.003	0.003	0.004	0.004	0.004	0.005

A2.6c: Spinel profils

Sample L112, profil 1

distanc	10	30	40	50	70	80	90	100	110	120	130	150	160	170
SiO2	0.01	0.01	0.02	<0.01	0.01	0.01	0.01	0.02	0.01	0.02	<0.01	0.02	0.03	0.01
TiO2	2.54	0.94	0.74	0.79	0.56	0.77	0.52	0.70	0.54	0.61	0.56	1.10	0.69	0.80
Al2O3	23.0	27.6	28.5	29.5	30.0	30.7	30.9	30.9	30.8	31.0	31.2	31.2	31.4	31.4
Cr2O3	35.1	32.7	32.0	31.7	31.0	30.5	30.3	30.4	30.5	31.3	30.6	30.9	30.7	29.9
Fe2O3	5.65	7.43	8.82	7.04	7.91	7.08	7.36	7.75	7.87	6.77	7.26	6.19	7.24	7.25
FeO	22.2	18.1	15.8	16.8	16.1	15.8	15.5	15.2	15.7	15.3	15.4	15.6	15.2	15.2
MnO	0.18	0.05	0.18	0.17	0.09	0.09	0.14	0.13	0.11	0.10	0.06	0.06	0.13	0.16
NiO	0.20	0.22	0.19	0.26	0.27	0.23	0.27	0.31	0.28	0.27	0.22	0.25	0.27	0.30
MgO	9.6	12.1	13.7	12.8	13.3	13.6	13.7	14.0	13.7	14.0	13.9	14.1	14.1	14.1
CaO	0.11	0.02	0.02	<0.01	0.01	<0.01	<0.01	<0.01	<0.01	0.02	<0.01	<0.01	<0.01	<0.01
Na2O	<0.01	<0.01	<0.01	<0.01	<0.01	0.02	<0.01	0.04	0.01	<0.01	0.02	0.03	0.05	0.01
ZnO	0.15	0.12	0.10	0.14	0.15	0.12	0.17	0.15	0.21	0.12	0.16	0.25	0.18	0.16
Total	98.6	99.3	100.1	99.3	99.4	98.9	98.8	99.6	99.7	99.5	99.3	99.7	100.0	99.2
Si	<0.001	<0.001	0.001	<0.001	<0.001	<0.001	<0.001	0.001	<0.001	0.001	<0.001	0.001	0.001	<0.001
Ti	0.061	0.022	0.017	0.018	0.013	0.017	0.012	0.016	0.012	0.014	0.012	0.025	0.015	0.018
Al	0.860	0.994	1.007	1.049	1.060	1.084	1.092	1.083	1.082	1.087	1.093	1.089	1.092	1.099
Cr	0.883	0.791	0.759	0.756	0.736	0.723	0.718	0.714	0.718	0.734	0.720	0.725	0.718	0.703
Fe3	0.135	0.171	0.199	0.160	0.179	0.160	0.166	0.173	0.176	0.152	0.163	0.138	0.161	0.162
Fe2	0.590	0.463	0.395	0.425	0.403	0.396	0.388	0.378	0.390	0.381	0.384	0.387	0.376	0.379
Mn	0.005	0.001	0.005	0.005	0.002	0.002	0.004	0.003	0.003	0.003	0.002	0.001	0.003	0.004
Ni	0.005	0.005	0.005	0.006	0.007	0.006	0.007	0.008	0.007	0.007	0.005	0.006	0.006	0.007
Mg	0.453	0.549	0.611	0.578	0.595	0.608	0.610	0.620	0.607	0.620	0.616	0.622	0.622	0.623
Ca	0.004	0.001	0.001	<0.001	0.001	<0.001	<0.001	<0.001	<0.001	0.001	<0.001	<0.001	<0.001	<0.001
Na	<0.001	<0.001	<0.001	<0.001	<0.001	0.001	<0.001	0.002	0.001	<0.001	0.001	0.002	0.003	0.001
Zn	0.004	0.003	0.002	0.003	0.003	0.003	0.004	0.003	0.005	0.003	0.003	0.005	0.004	0.003

Sample L112, profil 1

distanc	180	190	200	210	220	230	240	270	280	290	300	310	330	340
SiO2	<0.01	<0.01	0.03	<0.01	<0.01	<0.01	0.03	0.02	<0.01	<0.01	0.03	0.01	<0.01	<0.01
TiO2	0.73	1.21	1.98	0.75	1.19	0.66	1.02	1.05	0.32	2.96	0.88	1.29	0.53	0.50
Al2O3	31.4	31.4	30.8	31.5	31.1	31.1	30.6	31.3	31.9	30.4	31.4	31.3	31.4	31.2
Cr2O3	30.7	30.5	30.3	30.5	30.8	30.8	30.4	30.5	30.3	29.9	31.4	30.8	31.5	31.2
Fe2O3	7.16	6.29	5.83	6.84	6.08	7.18	6.94	5.78	6.98	4.26	5.83	5.91	6.82	6.61
FeO	15.3	15.7	16.1	15.4	15.5	15.5	15.8	15.8	15.2	16.8	15.4	15.6	15.2	15.4
MnO	0.13	0.19	0.11	0.11	0.13	0.13	0.19	0.13	0.13	0.10	0.12	0.07	0.08	0.11
NiO	0.23	0.22	0.25	0.24	0.29	0.27	0.22	0.23	0.24	0.25	0.25	0.22	0.18	0.18
MgO	14.2	14.1	14.3	14.1	14.1	13.9	13.9	13.8	14.0	14.2	14.2	14.2	14.1	13.8
CaO	0.02	<0.01	0.01	0.01	0.01	0.03	<0.01	<0.01	<0.01	<0.01	<0.01	<0.01	<0.01	0.03
Na2O	0.04	0.01	0.01	0.01	0.02	<0.01	<0.01	<0.01	0.01	0.03	<0.01	0.01	0.05	0.03
ZnO	0.12	0.24	0.20	0.11	0.12	0.17	0.08	0.13	0.08	0.21	0.19	0.24	0.10	0.20
Total	100.1	99.9	99.9	99.5	99.3	99.7	99.1	98.8	99.2	99.1	99.6	99.6	99.9	99.13
Si	<0.001	<0.001	0.001	<0.001	<0.001	<0.001	0.001	0.001	<0.001	<0.001	0.001	<0.001	<0.001	<0.001
Ti	0.016	0.027	0.044	0.017	0.027	0.015	0.023	0.024	0.007	0.066	0.020	0.029	0.012	0.011
Al	1.093	1.093	1.072	1.100	1.088	1.088	1.078	1.102	1.118	1.068	1.095	1.091	1.092	1.095
Cr	0.717	0.713	0.708	0.714	0.724	0.722	0.718	0.720	0.713	0.705	0.734	0.721	0.735	0.736
Fe3	0.159	0.140	0.130	0.153	0.136	0.161	0.156	0.130	0.156	0.096	0.130	0.132	0.152	0.148
Fe2	0.378	0.388	0.398	0.382	0.386	0.384	0.395	0.396	0.377	0.419	0.382	0.385	0.376	0.383
Mn	0.003	0.005	0.003	0.003	0.003	0.003	0.005	0.003	0.003	0.003	0.003	0.002	0.002	0.003
Ni	0.006	0.005	0.006	0.006	0.007	0.006	0.005	0.006	0.006	0.006	0.006	0.005	0.004	0.004
Mg	0.622	0.623	0.632	0.623	0.625	0.616	0.617	0.616	0.618	0.632	0.625	0.628	0.622	0.612
Ca	0.001	<0.001	<0.001	<0.001	<0.001	0.001	<0.001	<0.001	<0.001	<0.001	<0.001	<0.001	<0.001	0.001
Na	0.002	<0.001	0.001	<0.001	0.001	<0.001	<0.001	<0.001	0.001	0.002	<0.001	0.001	0.003	0.002
Zn	0.003	0.005	0.004	0.002	0.003	0.004	0.002	0.003	0.002	0.005	0.004	0.005	0.002	0.004

A2.6c: Spinel profils

Sample L112, profil 1											**Sample L112, profil 2**			
distanc	**350**	**360**	**370**	**380**	**390**	**400**	**410**	**420**	**430**	**450**	**10**	**20**	**30**	**40**
SiO2	0.03	<0.01	<0.01	0.02	<0.01	0.02	<0.01	<0.01	0.03	0.30	0.13	<0.01	<0.01	<0.01
TiO2	1.39	0.58	0.79	0.70	0.80	0.71	0.93	0.64	1.02	0.63	0.86	0.73	0.55	0.47
Al2O3	30.6	30.9	30.5	30.6	30.6	30.5	31.0	31.4	33.1	36.6	29.2	29.6	30.4	31.3
Cr2O3	31.3	31.8	32.1	31.6	31.6	31.9	31.1	31.2	29.8	27.1	32.0	31.9	31.7	31.0
Fe2O3	6.20	6.48	6.48	6.79	6.78	6.39	6.00	6.60	4.94	4.47	5.95	6.70	6.77	6.62
FeO	16.1	15.7	15.6	15.2	15.7	15.5	15.5	15.2	16.6	14.8	18.5	16.7	15.9	15.3
MnO	0.14	0.07	0.00	0.07	0.11	0.13	0.08	0.09	0.17	0.15	0.08	0.10	0.18	0.07
NiO	0.25	0.19	0.25	0.25	0.27	0.22	0.18	0.22	0.21	0.17	0.25	0.17	0.24	0.22
MgO	14.1	13.9	14.0	14.0	13.8	13.9	14.0	14.2	13.8	15.2	11.9	12.9	13.4	13.9
CaO	0.03	0.02	0.01	0.01	0.01	<0.01	0.02	<0.01	<0.01	0.05	0.09	0.00	0.01	0.01
Na2O	<0.01	<0.01	0.02	0.04	<0.01	0.01	<0.01	0.02	<0.01	0.01	0.01	0.02	0.01	0.00
ZnO	0.12	0.11	0.10	0.17	0.20	0.18	0.20	0.18	0.07	0.20	0.17	0.16	0.16	0.12
Total	100.2	99.6	99.8	99.4	99.8	99.4	99.0	99.8	99.6	99.6	99.1	99.0	99.3	99.0
Si	0.001	<0.001	<0.001	0.001	<0.001	0.001	<0.001	<0.001	0.001	0.009	0.004	<0.001	<0.001	<0.001
Ti	0.031	0.013	0.018	0.016	0.018	0.016	0.021	0.014	0.023	0.014	0.020	0.017	0.012	0.011
Al	1.065	1.082	1.067	1.075	1.071	1.073	1.090	1.096	1.150	1.243	1.048	1.053	1.072	1.099
Cr	0.733	0.747	0.754	0.743	0.742	0.751	0.734	0.730	0.694	0.616	0.770	0.763	0.751	0.732
Fe3	0.138	0.145	0.145	0.152	0.152	0.143	0.135	0.147	0.110	0.097	0.136	0.152	0.153	0.149
Fe2	0.399	0.389	0.387	0.378	0.391	0.387	0.388	0.376	0.408	0.356	0.469	0.421	0.399	0.381
Mn	0.004	0.002	0.000	0.002	0.003	0.003	0.002	0.002	0.004	0.004	0.002	0.003	0.005	0.002
Ni	0.006	0.005	0.006	0.006	0.006	0.005	0.004	0.005	0.005	0.004	0.006	0.004	0.006	0.005
Mg	0.620	0.615	0.620	0.622	0.612	0.616	0.622	0.625	0.604	0.652	0.539	0.582	0.598	0.619
Ca	0.001	0.001	<0.001	<0.001	<0.001	<0.001	0.001	<0.001	<0.001	0.002	0.003	<0.001	<0.001	<0.001
Na	<0.001	<0.001	0.001	0.002	<0.001	0.001	<0.001	0.001	<0.001	0.001	<0.001	0.001	0.001	<0.001
Zn	0.003	0.002	0.002	0.004	0.004	0.004	0.004	0.004	0.002	0.004	0.004	0.004	0.004	0.003

Sample L112, profil 2														
distanc	**50**	**60**	**70**	**80**	**100**	**110**	**130**	**150**	**160**	**170**	**190**	**210**	**220**	**260**
SiO2	0.00	0.01	0.02	<0.01	0.02	0.07	0.01	0.04	<0.01	0.01	0.01	0.02	0.02	<0.01
TiO2	0.49	1.97	0.83	0.76	0.36	0.49	0.43	1.06	0.44	0.53	0.76	0.67	0.54	1.28
Al2O3	31.4	30.5	30.9	30.9	31.1	31.8	31.2	31.7	31.2	31.0	31.0	31.0	31.5	30.5
Cr2O3	31.2	30.6	31.1	30.9	32.0	31.8	30.6	30.9	30.6	30.2	30.7	31.0	31.0	30.7
Fe2O3	6.47	5.52	6.49	6.82	6.73	5.75	7.23	5.41	7.47	7.65	7.19	6.94	6.92	6.41
FeO	15.0	16.2	15.8	15.5	15.2	15.2	15.2	15.5	15.1	15.3	15.5	15.6	15.5	16.5
MnO	0.06	0.15	0.07	0.17	0.10	0.10	0.11	0.07	0.07	0.16	0.13	0.08	0.07	0.14
NiO	0.20	0.24	0.22	0.22	0.23	0.24	0.28	0.17	0.25	0.29	0.23	0.22	0.26	0.22
MgO	14.0	14.1	13.9	14.0	14.1	14.2	13.9	14.3	14.0	13.8	13.9	13.9	14.0	13.5
CaO	0.02	<0.01	<0.01	0.01	<0.01	0.02	0.01	0.02	<0.01	<0.01	<0.01	<0.01	<0.01	0.01
Na2O	0.04	0.01	<0.01	<0.01	<0.01	0.01	<0.01	0.01	0.01	<0.01	0.02	<0.01	0.01	<0.01
ZnO	0.19	0.14	0.17	0.08	0.18	0.11	0.12	0.10	0.17	0.22	0.16	0.14	0.13	0.17
Total	99.1	99.4	99.4	99.3	99.9	99.7	99.1	99.2	99.3	99.2	99.6	99.6	99.9	99.5
Si	<0.001	<0.001	0.001	<0.001	0.001	0.002	<0.001	0.001	<0.001	<0.001	0.000	0.001	0.001	<0.001
Ti	0.011	0.044	0.019	0.017	0.008	0.011	0.010	0.024	0.010	0.012	0.017	0.015	0.012	0.029
Al	1.101	1.068	1.084	1.085	1.084	1.105	1.096	1.107	1.095	1.091	1.086	1.085	1.098	1.073
Cr	0.734	0.720	0.732	0.728	0.749	0.742	0.722	0.723	0.719	0.713	0.721	0.729	0.724	0.726
Fe3	0.145	0.124	0.146	0.153	0.150	0.128	0.162	0.121	0.167	0.172	0.161	0.155	0.154	0.144
Fe2	0.374	0.403	0.393	0.386	0.375	0.375	0.379	0.384	0.374	0.382	0.386	0.388	0.383	0.413
Mn	0.001	0.004	0.002	0.004	0.003	0.003	0.003	0.002	0.002	0.004	0.003	0.002	0.002	0.004
Ni	0.005	0.006	0.005	0.005	0.006	0.006	0.007	0.004	0.006	0.007	0.006	0.005	0.006	0.005
Mg	0.622	0.627	0.616	0.620	0.621	0.626	0.619	0.632	0.622	0.615	0.616	0.616	0.617	0.602
Ca	0.001	<0.001	<0.001	<0.001	<0.001	0.001	<0.001	0.001	<0.001	<0.001	<0.001	<0.001	<0.001	<0.001
Na	0.002	0.001	<0.001	<0.001	<0.001	<0.001	<0.001	<0.001	<0.001	<0.001	0.001	<0.001	0.001	<0.001
Zn	0.004	0.003	0.004	0.002	0.004	0.003	0.003	0.002	0.004	0.005	0.003	0.003	0.003	0.004

A2.6c: Spinel profils

Sample L112, profil 2												**L112, profil 3**		
distanc	**270**	**280**	**290**	**300**	**310**	**320**	**330**	**340**	**350**	**360**	**370**	**10**	**20**	**30**
SiO2	0.01	0.02	<0.01	0.02	<0.01	<0.01	<0.01	0.01	<0.01	0.01	0.02	0.03	0.01	<0.01
TiO2	0.52	1.06	0.77	0.83	0.24	0.91	0.22	1.25	0.90	2.33	0.54	0.34	0.67	0.36
Al2O3	31.5	30.8	31.2	31.1	13.7	30.6	31.1	29.9	30.2	28.8	29.5	32.3	30.3	30.2
Cr2O3	30.9	30.5	30.2	31.1	24.3	30.6	30.8	31.0	30.7	31.1	31.6	27.7	30.7	31.6
Fe2O3	6.90	7.53	7.78	6.97	19.87	7.15	7.87	6.81	7.48	5.67	7.45	7.82	7.21	8.14
FeO	15.3	15.3	15.1	15.6	2.9	15.3	15.4	16.1	15.8	17.6	16.8	17.3	17.0	16.1
MnO	0.05	0.15	0.07	0.09	0.06	0.19	0.13	0.19	0.16	0.12	0.09	0.11	0.20	0.12
NiO	0.24	0.26	0.27	0.23	0.17	0.23	0.27	0.26	0.23	0.22	0.27	0.30	0.24	0.24
MgO	14.1	14.3	14.3	14.0	15.3	14.0	13.6	13.6	13.7	13.3	12.8	12.3	12.6	13.2
CaO	<0.01	<0.01	0.04	<0.01	<0.01	<0.01	0.02	0.02	0.02	0.01	<0.01	0.06	0.02	0.02
Na2O	<0.01	0.01	0.01	0.02	0.01	<0.01	0.01	0.03	0.02	<0.01	<0.01	0.01	0.03	0.04
ZnO	0.21	0.21	0.11	0.23	0.06	0.16	0.22	0.16	0.07	0.12	0.13	0.14	0.22	0.09
Total	99.7	100.1	99.9	100.3	76.5	99.2	99.6	99.3	99.2	99.3	99.2	98.4	99.2	100.2
Si	<0.001	0.001	<0.001	0.001	<0.001	<0.001	<0.001	<0.001	<0.001	<0.001	0.001	0.001	<0.001	<0.001
Ti	0.012	0.024	0.017	0.018	0.007	0.021	0.005	0.028	0.020	0.053	0.012	0.008	0.015	0.008
Al	1.100	1.074	1.088	1.082	0.637	1.078	1.090	1.057	1.067	1.025	1.050	1.148	1.076	1.060
Cr	0.723	0.712	0.705	0.726	0.758	0.721	0.725	0.734	0.726	0.741	0.755	0.660	0.731	0.745
Fe3	0.154	0.168	0.173	0.155	0.591	0.161	0.176	0.154	0.169	0.129	0.169	0.178	0.164	0.183
Fe2	0.379	0.379	0.374	0.386	0.097	0.383	0.384	0.403	0.395	0.445	0.423	0.438	0.429	0.402
Mn	0.001	0.004	0.002	0.002	0.002	0.005	0.003	0.005	0.004	0.003	0.002	0.003	0.005	0.003
Ni	0.006	0.006	0.007	0.006	0.005	0.006	0.006	0.006	0.006	0.005	0.007	0.007	0.006	0.006
Mg	0.621	0.628	0.630	0.618	0.900	0.624	0.605	0.606	0.610	0.596	0.578	0.552	0.566	0.587
Ca	<0.001	<0.001	0.001	<0.001	<0.001	<0.001	0.001	0.001	0.001	<0.001	<0.001	0.002	0.001	0.001
Na	<0.001	0.001	0.001	0.001	<0.001	<0.001	0.001	0.002	0.001	<0.001	<0.001	0.001	0.002	0.003
Zn	0.005	0.005	0.002	0.005	0.002	0.004	0.005	0.003	0.002	0.003	0.003	0.003	0.005	0.002

Sample L112, profil 3														
distanc	**40**	**50**	**60**	**70**	**90**	**100**	**110**	**120**	**130**	**140**	**150**	**160**	**170**	**190**
SiO2	0.03	0.01	0.01	<0.01	<0.01	<0.01	<0.01	<0.01	0.01	<0.01	<0.01	0.01	<0.01	0.04
TiO2	0.37	0.92	0.43	0.65	1.00	0.54	3.05	0.64	0.72	0.44	0.67	1.76	0.55	0.46
Al2O3	29.7	29.8	30.1	30.2	29.9	30.4	28.6	30.1	30.3	30.5	30.1	28.8	29.6	29.1
Cr2O3	32.2	32.1	32.1	31.8	31.2	32.1	30.6	31.7	32.1	32.5	32.3	32.2	33.3	32.6
Fe2O3	7.79	6.55	7.38	6.94	6.88	7.54	5.38	7.28	6.73	6.78	6.02	5.84	6.57	6.29
FeO	16.3	16.4	15.3	15.7	16.1	15.5	17.7	15.9	15.8	15.7	15.8	17.4	15.9	17.0
MnO	0.18	0.12	0.09	0.09	0.19	0.13	0.11	0.08	0.16	0.17	0.18	0.17	0.07	0.07
NiO	0.25	0.22	0.28	0.19	0.24	0.24	0.24	0.31	0.23	0.23	0.17	0.23	0.25	0.22
MgO	13.1	13.4	13.8	13.8	13.4	13.9	13.7	13.5	13.8	13.7	13.6	13.1	13.5	12.4
CaO	0.01	0.03	0.01	<0.01	<0.01	0.01	0.03	<0.01	<0.01	<0.01	0.02	<0.01	<0.01	0.03
Na2O	0.01	<0.01	0.01	<0.01	<0.01	0.04	<0.01	0.03	<0.01	0.01	<0.01	<0.01	0.02	0.01
ZnO	0.19	0.12	0.15	0.12	0.20	0.20	0.07	0.12	0.12	0.10	0.10	0.16	0.16	0.10
Total	100.1	99.6	99.7	99.5	99.0	100.5	99.4	99.6	99.9	100.1	98.9	99.7	99.9	98.3
Si	0.001	<0.001	<0.001	<0.001	<0.001	<0.001	<0.001	<0.001	<0.001	<0.001	<0.001	<0.001	<0.001	0.001
Ti	0.008	0.021	0.010	0.015	0.023	0.012	0.069	0.014	0.016	0.010	0.015	0.040	0.012	0.011
Al	1.046	1.050	1.058	1.063	1.059	1.060	1.013	1.060	1.061	1.066	1.065	1.020	1.043	1.046
Cr	0.761	0.760	0.757	0.752	0.741	0.750	0.727	0.750	0.756	0.763	0.768	0.767	0.786	0.787
Fe3	0.175	0.148	0.166	0.156	0.156	0.168	0.122	0.164	0.151	0.152	0.136	0.132	0.148	0.145
Fe2	0.407	0.411	0.383	0.392	0.404	0.383	0.446	0.398	0.392	0.389	0.397	0.437	0.397	0.434
Mn	0.005	0.003	0.002	0.002	0.005	0.003	0.003	0.002	0.004	0.004	0.005	0.004	0.002	0.002
Ni	0.006	0.005	0.007	0.005	0.006	0.006	0.006	0.008	0.006	0.006	0.004	0.006	0.006	0.006
Mg	0.585	0.598	0.613	0.613	0.602	0.611	0.612	0.601	0.611	0.607	0.607	0.590	0.601	0.565
Ca	<0.001	0.001	<0.001	<0.001	<0.001	<0.001	0.001	<0.001	<0.001	<0.001	0.001	<0.001	<0.001	0.001
Na	0.001	<0.001	0.001	<0.001	<0.001	0.002	<0.001	0.002	<0.001	0.001	<0.001	<0.001	0.001	<0.001
Zn	0.004	0.003	0.003	0.003	0.004	0.004	0.002	0.003	0.003	0.002	0.002	0.004	0.004	0.002

A2.6c: Spinel profils

Sample L112, profil 4

distanc	20	30	40	60	70	80	90	100	110	120	130	160	180	200
SiO2	<0.01	0.02	<0.01	0.02	<0.01	0.02	<0.01	0.02	0.02	<0.01	0.02	<0.01	0.01	0.01
TiO2	0.41	0.86	0.57	0.61	0.58	0.65	0.63	0.69	0.73	1.06	1.07	0.82	0.65	0.76
Al2O3	40.3	35.1	33.7	31.7	31.2	31.5	31.5	31.2	31.1	31.1	30.7	30.5	29.5	25.7
Cr2O3	22.8	26.6	28.7	30.3	30.8	31.0	31.1	30.9	31.9	31.4	31.8	32.0	32.3	35.6
Fe2O3	5.17	6.01	5.75	6.73	7.44	6.80	6.40	7.21	5.87	6.10	6.37	6.32	6.83	6.13
FeO	12.5	14.8	14.8	15.3	14.9	15.0	15.0	14.8	15.5	15.1	15.2	15.3	15.1	17.8
MnO	0.06	0.07	0.05	0.07	0.07	0.17	0.15	0.05	0.12	0.15	0.15	0.14	0.16	0.16
NiO	0.33	0.21	0.22	0.24	0.25	0.21	0.21	0.24	0.19	0.25	0.22	0.21	0.23	0.13
MgO	16.2	14.7	14.4	14.0	14.3	14.2	14.1	14.5	14.0	14.4	14.4	14.1	13.8	11.7
CaO	0.04	0.04	0.02	0.03	0.03	0.01	<0.01	<0.01	<0.01	<0.01	<0.01	<0.01	0.02	0.06
Na2O	0.04	0.02	<0.01	0.01	0.02	0.03	0.03	0.02	<0.01	<0.01	0.01	<0.01	0.01	<0.01
ZnO	0.28	0.19	0.11	0.22	0.18	0.16	0.19	0.20	0.19	0.20	0.23	0.21	0.13	0.09
Total	98.1	98.6	98.3	99.2	99.8	99.8	99.3	99.9	99.6	99.7	100.0	99.5	98.7	98.1
Si	<0.001	0.001	<0.001	0.001	<0.001	0.001	<0.001	0.001	0.001	<0.001	0.001	<0.001	<0.001	0.001
Ti	0.009	0.019	0.013	0.014	0.013	0.014	0.014	0.015	0.016	0.024	0.024	0.018	0.015	0.018
Al	1.357	1.212	1.176	1.111	1.088	1.097	1.101	1.087	1.087	1.084	1.068	1.069	1.047	0.942
Cr	0.516	0.617	0.671	0.711	0.721	0.724	0.730	0.722	0.749	0.734	0.742	0.752	0.769	0.878
Fe3	0.111	0.133	0.128	0.151	0.166	0.151	0.143	0.160	0.131	0.136	0.142	0.142	0.155	0.144
Fe2	0.298	0.362	0.367	0.381	0.369	0.370	0.372	0.366	0.386	0.373	0.376	0.381	0.380	0.464
Mn	0.002	0.002	0.001	0.002	0.002	0.004	0.004	0.001	0.003	0.004	0.004	0.004	0.004	0.004
Ni	0.008	0.005	0.005	0.006	0.006	0.005	0.005	0.006	0.005	0.006	0.005	0.005	0.006	0.003
Mg	0.690	0.643	0.636	0.618	0.630	0.627	0.626	0.637	0.618	0.636	0.634	0.624	0.621	0.543
Ca	0.001	0.001	0.001	0.001	0.001	<0.001	<0.001	<0.001	<0.001	<0.001	<0.001	<0.001	0.001	0.002
Na	0.002	0.001	<0.001	0.001	0.001	0.002	0.002	0.001	<0.001	<0.001	<0.001	<0.001	0.001	<0.001
Zn	0.006	0.004	0.002	0.005	0.004	0.004	0.004	0.004	0.004	0.004	0.005	0.005	0.003	0.002

Sample La2002-05, profil 3

distanc	10	20	30	40	60	70	80	90	100	110	120	130	140	150
SiO2	0.02	0.02	0.01	0.03	<0.01	0.01	<0.01	<0.01	0.02	0.01	0.03	0.01	<0.01	0.04
TiO2	0.16	0.16	0.17	0.33	0.68	0.57	0.65	0.70	0.58	0.73	0.79	0.67	1.18	0.70
Al2O3	50.5	46.7	44.9	40.6	31.6	29.8	29.0	29.2	28.3	27.9	27.3	27.0	26.8	31.0
Cr2O3	13.8	17.5	18.9	21.7	29.0	30.1	30.4	31.3	32.0	32.3	32.3	33.2	32.9	30.6
Fe2O3	4.11	4.73	5.14	5.25	7.27	7.80	8.18	7.55	7.84	7.30	8.02	7.50	7.29	6.80
FeO	10.1	11.0	11.4	12.8	15.8	16.5	16.6	16.6	16.4	16.8	16.8	17.1	17.1	15.4
MnO	0.05	0.10	0.11	0.11	0.15	0.19	0.20	0.20	0.21	0.15	0.22	0.11	0.20	0.17
NiO	0.35	0.28	0.28	0.20	0.21	0.21	0.22	0.26	0.24	0.23	0.21	0.17	0.14	0.18
MgO	18.9	18.0	17.6	16.1	13.5	12.8	12.7	12.8	12.8	12.5	12.5	12.2	12.4	13.9
CaO	0.02	<0.01	0.02	0.01	<0.01	<0.01	0.01	<0.01	<0.01	<0.01	0.01	0.01	0.04	0.07
Na2O														
ZnO	0.25	0.20	0.12	0.07	0.21	0.07	0.11	0.07	0.10	0.18	0.20	0.16	0.19	0.21
Total	98.3	98.7	98.6	97.2	98.5	98.2	98.0	98.6	98.5	98.1	98.2	98.1	98.2	99.0
Si	0.001	0.001	<0.001	0.001	<0.001	0.001	<0.001	<0.001	0.001	<0.001	0.001	<0.001	<0.001	0.001
Ti	0.003	0.003	0.004	0.007	0.015	0.013	0.015	0.016	0.013	0.017	0.018	0.016	0.027	0.016
Al	1.612	1.515	1.471	1.378	1.118	1.069	1.047	1.044	1.019	1.013	0.990	0.982	0.973	1.092
Cr	0.296	0.380	0.414	0.493	0.687	0.725	0.735	0.751	0.772	0.784	0.786	0.811	0.803	0.722
Fe3	0.084	0.098	0.107	0.114	0.164	0.179	0.188	0.173	0.180	0.169	0.186	0.175	0.169	0.153
Fe2	0.228	0.254	0.264	0.307	0.397	0.421	0.424	0.422	0.420	0.433	0.432	0.441	0.442	0.385
Mn	0.001	0.002	0.003	0.003	0.004	0.005	0.005	0.005	0.005	0.004	0.006	0.003	0.005	0.004
Ni	0.008	0.006	0.006	0.005	0.005	0.005	0.005	0.006	0.006	0.006	0.005	0.004	0.003	0.004
Mg	0.761	0.737	0.728	0.692	0.605	0.581	0.577	0.581	0.581	0.571	0.572	0.564	0.571	0.617
Ca	0.001	<0.001	0.001	<0.001	<0.001	<0.001	<0.001	<0.001	<0.001	<0.001	<0.001	<0.001	0.001	0.002
Na														
Zn	0.005	0.004	0.003	0.002	0.005	0.002	0.003	0.002	0.002	0.004	0.005	0.004	0.004	0.005

A2.6c: Spinel profils

Sample La2002-05, profil 4

distanc	10	20	30	50	60	70	80	90	100	130	140	150	160	170
SiO2	<0.01	0.02	0.01	<0.01	0.02	<0.01	<0.01	<0.01	0.01	<0.01	0.03	0.03	<0.01	<0.01
TiO2	0.10	0.21	0.22	0.27	0.49	0.53	0.50	0.55	0.69	0.58	0.59	0.49	0.52	0.57
Al2O3	56.43	48.51	42.44	36.05	33.66	32.41	31.55	31.23	31.29	31.07	30.93	31.15	31.44	31.1
Cr2O3	9.04	16.66	21.92	26.58	29.2	30.4	30.7	31.0	31.0	31.4	31.0	31.4	30.93	30.9
Fe2O3	3.43	3.46	4.45	5.52	5.29	5.45	5.70	6.26	5.69	4.27	5.96	6.00	6.14	6.19
FeO	7.7	9.8	11.8	13.6	14.5	15.1	14.9	14.8	15.1	16.2	15.0	15.1	14.8	14.9
MnO	0.05	0.09	0.09	0.15	0.15	0.17	0.09	0.25	0.21	0.12	0.16	0.14	0.17	0.14
NiO	0.45	0.34	0.27	0.18	0.24	0.17	0.27	0.21	0.20	0.15	0.23	0.20	0.26	0.21
MgO	21.0	18.8	17.1	15.1	14.5	14.1	14.0	14.1	14.0	12.9	13.9	14.0	14.0	14.1
CaO	0.01	0.03	0.03	0.01	0.02	<0.01	<0.01	<0.01	<0.01	0.01	0.01	0.02	<0.01	0.02
Na2O														
ZnO	0.17	0.28	0.15	0.16	0.10	0.13	<0.01	0.14	0.15	0.20	0.07	0.11	0.23	0.01
Total	98.4	98.2	98.4	97.6	98.2	98.4	97.7	98.5	98.2	96.9	97.9	98.7	98.6	98.0
Si	<0.001	0.001	<0.001	<0.001	0.001	<0.001	<0.001	<0.001	<0.001	<0.001	0.001	0.001	<0.001	<0.001
Ti	0.002	0.004	0.005	0.006	0.011	0.012	0.011	0.012	0.016	0.013	0.013	0.011	0.012	0.013
Al	1.741	1.560	1.408	1.249	1.175	1.139	1.119	1.102	1.106	1.118	1.098	1.098	1.107	1.100
Cr	0.187	0.359	0.488	0.617	0.684	0.715	0.730	0.733	0.734	0.758	0.738	0.744	0.731	0.734
Fe3	0.068	0.071	0.094	0.122	0.118	0.122	0.129	0.141	0.128	0.098	0.135	0.135	0.138	0.140
Fe2	0.169	0.224	0.277	0.333	0.360	0.376	0.374	0.371	0.378	0.413	0.378	0.379	0.371	0.374
Mn	0.001	0.002	0.002	0.004	0.004	0.004	0.002	0.006	0.005	0.003	0.004	0.003	0.004	0.004
Ni	0.010	0.008	0.006	0.004	0.006	0.004	0.007	0.005	0.005	0.004	0.006	0.005	0.006	0.005
Mg	0.819	0.765	0.716	0.661	0.639	0.625	0.629	0.627	0.625	0.589	0.625	0.622	0.625	0.629
Ca	<0.001	0.001	0.001	<0.001	0.001	<0.001	<0.001	<0.001	<0.001	<0.001	<0.001	0.001	<0.001	0.001
Na														
Zn	0.003	0.006	0.003	0.004	0.002	0.003	<0.001	0.003	0.003	0.005	0.002	0.003	0.005	<0.001

Sample La2002-05, profil 4

distanc	180	190	210	220	230	240	260	280	290	300	310	320	330	340
SiO2	<0.01	0.01	0.01	<0.01	0.01	0.01	<0.01	<0.01	<0.01	<0.01	0.01	0.02	<0.01	<0.01
TiO2	0.55	0.51	0.51	0.51	0.49	0.51	0.46	0.44	0.50	0.48	0.45	0.45	0.46	0.45
Al2O3	31.3	31.3	31.7	31.5	31.6	31.6	31.8	32.4	32.1	32.1	32.7	33.3	33.2	34.4
Cr2O3	31.1	31.2	30.7	30.9	31.2	30.9	30.8	30.5	30.1	30.7	30.3	30.2	29.7	28.8
Fe2O3	6.07	6.16	6.18	6.28	5.61	5.86	5.85	5.12	5.81	5.93	5.91	5.67	5.67	5.32
FeO	14.8	14.6	14.2	14.7	15.0	14.8	15.0	14.5	14.3	14.6	14.5	14.4	14.3	14.0
MnO	0.14	0.14	0.14	0.12	0.06	0.12	0.13	0.13	0.09	0.15	0.14	0.10	0.15	0.17
NiO	0.21	0.19	0.34	0.23	0.19	0.19	0.17	0.26	0.27	0.25	0.15	0.31	0.25	0.22
MgO	14.2	14.3	14.4	14.3	14.1	14.2	14.0	14.2	14.4	14.4	14.5	14.7	14.6	14.9
CaO	0.01	0.02	0.02	0.02	<0.01	0.01	0.03	0.02	<0.01	0.01	0.03	0.02	0.02	0.01
Na2O														
ZnO	0.09	0.19	0.09	0.10	0.08	0.08	0.16	0.18	0.18	0.08	0.14	0.13	0.14	0.11
Total	98.4	98.6	98.3	98.6	98.3	98.3	98.4	97.7	97.7	98.6	98.9	99.2	98.5	98.3
Si	<0.001	<0.001	<0.001	<0.001	<0.001	<0.001	<0.001	<0.001	<0.001	<0.001	<0.001	0.001	<0.001	<0.001
Ti	0.012	0.011	0.011	0.011	0.011	0.012	0.010	0.010	0.011	0.011	0.010	0.010	0.010	0.010
Al	1.103	1.102	1.115	1.108	1.114	1.114	1.119	1.143	1.133	1.124	1.140	1.153	1.158	1.193
Cr	0.735	0.736	0.723	0.728	0.737	0.730	0.728	0.721	0.714	0.722	0.708	0.701	0.695	0.669
Fe3	0.137	0.138	0.139	0.141	0.126	0.132	0.132	0.115	0.131	0.133	0.131	0.125	0.126	0.118
Fe2	0.369	0.364	0.356	0.366	0.374	0.369	0.374	0.362	0.358	0.362	0.359	0.353	0.354	0.345
Mn	0.004	0.004	0.004	0.003	0.002	0.003	0.003	0.003	0.002	0.004	0.003	0.002	0.004	0.004
Ni	0.005	0.005	0.008	0.005	0.005	0.005	0.004	0.006	0.007	0.006	0.003	0.007	0.006	0.005
Mg	0.632	0.635	0.642	0.634	0.629	0.633	0.625	0.633	0.641	0.637	0.641	0.644	0.643	0.653
Ca	<0.001	0.001	0.001	0.001	<0.001	<0.001	0.001	0.001	<0.001	<0.001	0.001	0.001	0.001	<0.001
Na														
Zn	0.002	0.004	0.002	0.002	0.002	0.002	0.004	0.004	0.004	0.002	0.003	0.003	0.003	0.002

A2.6c: Spinel profils

La2002-05, profil 4 L09, profil 1

distanc	350	360	10	20	30	40	50	60	70	80	90	100	110	120
SiO2	0.01	0.02	0.02	0.01	0.02	0.02	0.03	0.01	0.01	<0.01	0.04	0.01	0.03	<0.01
TiO2	0.41	0.25	0.39	0.45	0.49	0.42	0.37	0.38	0.32	0.34	0.35	0.32	0.30	0.39
Al2O3	36.5	38.8	35.1	35.7	35.4	35.7	35.7	36.0	36.1	36.1	35.8	36.1	36.1	36.2
Cr2O3	27.6	24.9	29.3	28.7	28.7	28.8	28.3	28.5	28.0	28.2	28.7	28.3	28.6	28.2
Fe2O3	4.47	4.71	5.10	4.60	4.95	4.71	4.82	5.05	4.67	4.71	4.90	4.99	4.80	4.81
FeO	13.4	12.8	14.9	14.9	15.1	14.7	14.5	14.8	14.4	14.9	14.8	14.5	14.8	14.7
MnO	0.10	0.09	0.21	0.15	0.20	0.13	0.21	0.17	0.17	0.18	0.18	0.24	0.22	0.19
NiO	0.23	0.19	0.26	0.23	0.21	0.22	0.20	0.27	0.21	0.21	0.28	0.22	0.24	0.22
MgO	15.5	16.0	14.7	14.7	14.6	14.8	14.8	14.8	14.9	14.6	14.8	14.9	14.7	14.9
CaO	0.03	0.04	0.01	<0.01	<0.01	0.02	<0.01	<0.01	0.01	<0.01	<0.01	0.01	<0.01	0.01
Na2O														
ZnO	0.10	0.17	0.11	0.14	0.15	0.26	0.12	0.18	0.08	0.18	0.25	0.21	0.24	0.15
Total	98.4	98.0	100.1	99.6	99.8	99.9	99.1	100.2	98.9	99.3	100.1	99.8	99.9	99.7
Si	<0.001	0.001	0.001	<0.001	0.001	0.001	0.001	<0.001	<0.001	<0.001	0.001	<0.001	0.001	<0.001
Ti	0.009	0.006	0.009	0.010	0.011	0.009	0.008	0.008	0.007	0.007	0.008	0.007	0.007	0.009
Al	1.250	1.318	1.199	1.220	1.211	1.218	1.226	1.224	1.239	1.235	1.220	1.230	1.228	1.234
Cr	0.634	0.568	0.672	0.659	0.658	0.660	0.651	0.650	0.644	0.647	0.656	0.647	0.653	0.645
Fe3	0.098	0.102	0.111	0.101	0.108	0.103	0.106	0.110	0.102	0.103	0.107	0.109	0.104	0.105
Fe2	0.326	0.307	0.361	0.363	0.367	0.357	0.354	0.356	0.351	0.361	0.358	0.352	0.357	0.355
Mn	0.002	0.002	0.005	0.004	0.005	0.003	0.005	0.004	0.004	0.005	0.005	0.006	0.005	0.005
Ni	0.005	0.004	0.006	0.005	0.005	0.005	0.005	0.006	0.005	0.005	0.006	0.005	0.006	0.005
Mg	0.673	0.687	0.634	0.635	0.631	0.639	0.643	0.638	0.645	0.633	0.635	0.640	0.635	0.641
Ca	0.001	0.001	<0.001	<0.001	<0.001	0.001	<0.001	<0.001	<0.001	<0.001	<0.001	<0.001	<0.001	<0.001
Na														
Zn	0.002	0.004	0.003	0.003	0.003	0.006	0.003	0.004	0.002	0.004	0.005	0.005	0.005	0.003

Sample L09, profil 1

distanc	130	140	160	170	190	200	210	220	230	240	250	270	280	290
SiO2	0.03	<0.01	<0.01	<0.01	0.04	0.01	0.01	0.01	0.01	0.01	0.03	0.04	0.01	0.06
TiO2	0.88	0.49	0.34	0.37	0.35	0.37	0.36	0.39	0.39	0.28	0.36	0.48	0.40	0.43
Al2O3	36.0	36.1	36.4	36.2	36.4	36.8	36.4	36.8	36.8	36.7	36.9	37.0	36.8	36.9
Cr2O3	28.1	28.2	27.8	27.8	27.6	27.8	28.1	27.5	27.8	27.9	27.9	27.6	27.3	28.0
Fe2O3	4.09	4.57	4.89	5.19	5.07	4.95	4.77	4.82	4.68	4.93	4.79	4.51	5.03	4.17
FeO	15.4	14.8	14.7	14.5	14.4	14.5	14.7	14.5	14.6	14.5	14.6	14.7	14.4	15.1
MnO	0.20	0.16	0.22	0.21	0.00	0.21	0.15	0.17	0.10	0.26	0.19	0.21	0.19	0.20
NiO	0.27	0.16	0.22	0.22	0.32	0.28	0.23	0.23	0.13	0.18	0.25	0.19	0.27	0.21
MgO	14.6	14.9	14.8	15.0	15.0	15.1	14.9	15.0	15.1	15.0	15.1	15.1	15.0	14.8
CaO	<0.01	<0.01	<0.01	<0.01	0.02	0.01	<0.01	<0.01	<0.01	<0.01	0.02	0.02	<0.01	0.01
Na2O														
ZnO	0.18	0.16	0.10	0.19	0.25	0.13	0.15	0.17	0.09	0.24	0.14	0.21	0.21	0.16
Total	99.8	99.6	99.4	99.7	99.5	100.2	99.8	99.5	99.7	99.9	100.2	100.0	99.6	100.0
Si	0.001	<0.001	<0.001	<0.001	0.001	<0.001	<0.001	<0.001	<0.001	<0.001	0.001	0.001	<0.001	0.002
Ti	0.019	0.011	0.008	0.008	0.008	0.008	0.008	0.008	0.008	0.006	0.008	0.010	0.009	0.009
Al	1.228	1.233	1.242	1.235	1.241	1.246	1.239	1.251	1.249	1.246	1.247	1.253	1.251	1.250
Cr	0.643	0.646	0.636	0.636	0.631	0.631	0.641	0.627	0.633	0.634	0.632	0.626	0.622	0.637
Fe3	0.089	0.100	0.107	0.113	0.110	0.107	0.104	0.105	0.101	0.107	0.103	0.097	0.109	0.090
Fe2	0.373	0.358	0.356	0.349	0.348	0.347	0.354	0.349	0.352	0.349	0.350	0.352	0.347	0.363
Mn	0.005	0.004	0.005	0.005	0.000	0.005	0.004	0.004	0.003	0.006	0.005	0.005	0.005	0.005
Ni	0.006	0.004	0.005	0.005	0.008	0.007	0.005	0.005	0.003	0.004	0.006	0.005	0.006	0.005
Mg	0.632	0.641	0.639	0.645	0.648	0.647	0.642	0.646	0.649	0.642	0.645	0.646	0.646	0.635
Ca	<0.001	<0.001	<0.001	<0.001	0.001	<0.001	<0.001	<0.001	<0.001	<0.001	0.001	0.001	<0.001	<0.001
Na														
Zn	0.004	0.003	0.002	0.004	0.005	0.003	0.003	0.004	0.002	0.005	0.003	0.004	0.004	0.003

A2.6c: Spinel profils

Sample L09, profil 1

distanc	300	310	320	330	340	350	360	370	380	390	400	410	420
SiO2	<0.01	<0.01	<0.01	<0.01	0.02	0.02	0.03	0.01	0.02	<0.01	<0.01	0.02	0.02
TiO2	0.34	0.35	0.35	0.36	0.34	0.67	0.31	0.36	1.27	0.36	0.45	0.37	0.38
Al2O3	37.2	37.0	37.5	37.2	37.3	36.9	37.0	37.2	36.5	37.0	36.5	35.8	35.0
Cr2O3	27.7	27.9	28.2	27.3	27.8	27.7	28.1	27.9	27.8	27.8	27.9	28.4	29.3
Fe2O3	4.78	4.43	4.63	5.07	4.46	3.70	4.87	4.52	3.64	4.86	4.76	4.66	4.99
FeO	14.8	14.7	15.0	14.3	14.7	15.3	14.4	14.6	15.6	14.7	15.2	15.5	16.3
MnO	0.17	0.21	0.17	0.17	0.13	0.10	0.17	0.18	0.16	0.21	0.19	0.15	0.18
NiO	0.26	0.21	0.22	0.24	0.23	0.25	0.28	0.23	0.26	0.22	0.23	0.29	0.20
MgO	15.0	14.9	15.1	15.2	15.1	14.7	15.2	15.1	14.9	15.0	14.6	14.3	13.8
CaO	<0.01	<0.01	<0.01	<0.01	<0.01	0.01	<0.01	<0.01	0.01	<0.01	<0.01	<0.01	<0.01
Na2O													
ZnO	0.22	0.19	0.20	0.22	0.19	0.16	0.21	0.19	0.20	0.20	0.24	0.04	0.15
Total	100.4	99.9	101.3	100.1	100.2	99.5	100.5	100.3	100.3	100.3	100.1	99.5	100.4
Si	<0.001	<0.001	<0.001	<0.001	0.001	0.001	0.001	<0.001	0.001	<0.001	<0.001	0.001	0.001
Ti	0.007	0.008	0.008	0.008	0.007	0.015	0.007	0.008	0.027	0.008	0.010	0.008	0.008
Al	1.256	1.254	1.253	1.256	1.259	1.257	1.246	1.254	1.234	1.249	1.240	1.228	1.200
Cr	0.627	0.635	0.632	0.619	0.629	0.632	0.634	0.633	0.631	0.630	0.637	0.653	0.673
Fe3	0.103	0.096	0.099	0.109	0.096	0.081	0.105	0.098	0.079	0.105	0.103	0.102	0.109
Fe2	0.353	0.354	0.356	0.343	0.353	0.371	0.344	0.350	0.375	0.353	0.367	0.377	0.397
Mn	0.004	0.005	0.004	0.004	0.003	0.003	0.004	0.004	0.004	0.005	0.005	0.004	0.005
Ni	0.006	0.005	0.005	0.006	0.005	0.006	0.007	0.005	0.006	0.005	0.005	0.007	0.005
Mg	0.639	0.639	0.638	0.650	0.643	0.632	0.649	0.645	0.639	0.640	0.627	0.620	0.600
Ca	<0.001	<0.001	<0.001	<0.001	<0.001	<0.001	<0.001	<0.001	<0.001	<0.001	<0.001	<0.001	<0.001
Na													
Zn	0.005	0.004	0.004	0.005	0.004	0.003	0.005	0.004	0.004	0.004	0.005	0.001	0.003

Sample L09, profil 2

distanc	10	20	30	40	50	60	70	80	90	100	110	120	130	140
SiO2	0.03	0.03	0.04	0.03	0.04	<0.01	<0.01	<0.01	0.02	0.01	0.02	<0.01	0.01	<0.01
TiO2	0.45	0.57	0.59	0.51	0.69	0.86	0.92	1.24	0.47	0.47	0.67	0.50	0.50	0.62
Al2O3	25.3	28.5	30.7	31.0	32.0	31.8	31.8	31.3	31.8	32.1	31.7	32.1	32.4	31.9
Cr2O3	38.8	35.9	33.8	33.4	32.9	32.5	32.6	32.8	32.8	32.5	32.6	32.7	32.4	32.4
Fe2O3	5.30	5.21	4.85	5.23	4.87	4.60	5.07	3.98	5.40	5.28	4.80	5.27	5.40	5.43
FeO	17.2	15.6	15.3	14.9	14.8	14.9	14.7	15.2	14.5	14.4	14.4	14.3	14.6	14.3
MnO	0.24	0.24	0.18	0.17	0.21	0.19	0.18	0.19	0.18	0.21	0.16	0.19	0.21	0.18
NiO	0.14	0.20	0.20	0.21	0.19	0.18	0.25	0.20	0.21	0.19	0.21	0.20	0.19	0.25
MgO	12.2	13.6	14.1	14.3	14.7	14.6	14.8	14.5	14.7	14.7	14.6	14.9	14.8	14.8
CaO	0.04	0.01	0.01	<0.01	0.01	<0.01	0.01	0.03	<0.01	<0.01	0.04	<0.01	<0.01	0.02
Na2O														
ZnO	0.12	0.29	0.14	0.21	0.17	0.14	0.30	0.24	0.10	0.31	0.25	0.20	0.15	0.28
Total	99.8	100.2	99.8	100.0	100.6	99.7	100.7	99.7	100.1	100.2	99.5	100.3	100.7	100.1
Si	0.001	0.001	0.001	0.001	0.001	<0.001	<0.001	<0.001	0.001	<0.001	0.001	<0.001	<0.001	<0.001
Ti	0.011	0.013	0.013	0.011	0.015	0.019	0.020	0.028	0.010	0.010	0.015	0.011	0.011	0.014
Al	0.915	1.006	1.071	1.079	1.100	1.103	1.095	1.091	1.098	1.108	1.102	1.106	1.112	1.102
Cr	0.940	0.849	0.792	0.780	0.761	0.757	0.753	0.766	0.761	0.754	0.761	0.756	0.747	0.751
Fe3	0.122	0.117	0.108	0.116	0.107	0.102	0.112	0.089	0.119	0.116	0.107	0.116	0.118	0.120
Fe2	0.442	0.391	0.379	0.368	0.362	0.367	0.360	0.375	0.355	0.354	0.356	0.350	0.357	0.351
Mn	0.006	0.006	0.004	0.004	0.005	0.005	0.004	0.005	0.005	0.005	0.004	0.005	0.005	0.005
Ni	0.004	0.005	0.005	0.005	0.004	0.004	0.006	0.005	0.005	0.005	0.005	0.005	0.004	0.006
Mg	0.555	0.605	0.623	0.631	0.640	0.641	0.643	0.637	0.644	0.641	0.644	0.648	0.642	0.646
Ca	0.001	<0.001	<0.001	<0.001	<0.001	<0.001	<0.001	0.001	<0.001	<0.001	0.001	<0.001	<0.001	0.001
Na														
Zn	0.003	0.006	0.003	0.005	0.004	0.003	0.007	0.005	0.002	0.007	0.006	0.004	0.003	0.006

A2.6c: Spinel profils

Sample L09, profil 2

distanc	160	170	190	200	210	220	230	240	250	260	270	280	290	300
SiO2	<0.01	0.01	0.03	0.03	<0.01	0.02	0.02	<0.01	0.71	0.01	0.07	0.01	0.02	0.03
TiO2	0.41	0.62	0.67	0.54	0.68	0.59	0.73	0.62	0.56	0.50	0.44	0.92	0.51	0.55
Al2O3	32.5	32.3	32.1	32.1	32.0	32.1	32.1	32.3	31.6	32.0	31.7	31.6	32.1	32.2
Cr2O3	32.1	32.3	32.5	32.2	32.4	31.7	32.8	32.0	31.2	32.0	31.9	32.5	32.4	31.9
Fe2O3	5.57	5.17	5.34	5.58	5.06	5.29	4.80	5.11	4.82	5.44	4.93	4.90	5.24	5.27
FeO	14.4	14.3	14.8	14.5	14.8	14.8	14.6	14.8	14.7	14.6	14.2	14.8	14.8	14.6
MnO	0.15	0.18	0.19	0.22	0.18	0.14	0.22	0.15	0.17	0.19	0.12	0.20	0.19	0.17
NiO	0.16	0.20	0.18	0.24	0.21	0.17	0.23	0.27	0.22	0.22	0.26	0.24	0.24	0.29
MgO	14.8	14.9	14.8	14.7	14.6	14.5	14.9	14.6	14.9	14.5	14.5	14.6	14.6	14.6
CaO	0.02	0.02	0.03	<0.01	0.01	0.01	0.01	0.01	0.05	<0.01	0.02	<0.01	<0.01	<0.01
Na2O														
ZnO	0.20	0.30	0.14	0.28	0.21	0.15	0.10	0.11	0.22	0.17	0.18	0.24	0.16	0.09
Total	100.2	100.3	100.8	100.4	100.1	99.4	100.5	99.9	99.1	99.6	98.4	100.0	100.3	99.8
Si	<0.001	<0.001	0.001	0.001	<0.001	0.001	0.001	<0.001	0.021	<0.001	0.002	<0.001	0.001	0.001
Ti	0.009	0.014	0.015	0.012	0.015	0.013	0.016	0.014	0.013	0.011	0.010	0.020	0.011	0.012
Al	1.119	1.111	1.103	1.107	1.107	1.116	1.105	1.117	1.100	1.110	1.113	1.094	1.109	1.116
Cr	0.741	0.747	0.750	0.744	0.752	0.739	0.757	0.742	0.727	0.746	0.752	0.756	0.751	0.741
Fe3	0.123	0.114	0.117	0.123	0.112	0.118	0.105	0.113	0.107	0.121	0.111	0.109	0.116	0.117
Fe2	0.351	0.350	0.361	0.355	0.364	0.364	0.356	0.364	0.364	0.359	0.354	0.364	0.363	0.359
Mn	0.004	0.004	0.005	0.006	0.005	0.004	0.005	0.004	0.004	0.005	0.003	0.005	0.005	0.004
Ni	0.004	0.005	0.004	0.006	0.005	0.004	0.005	0.006	0.005	0.005	0.006	0.006	0.006	0.007
Mg	0.646	0.648	0.641	0.641	0.637	0.638	0.647	0.637	0.654	0.638	0.645	0.641	0.635	0.641
Ca	0.001	0.001	0.001	<0.001	<0.001	<0.001	<0.001	<0.001	0.002	<0.001	0.001	<0.001	<0.001	<0.001
Na														
Zn	0.004	0.006	0.003	0.006	0.005	0.003	0.002	0.002	0.005	0.004	0.004	0.005	0.004	0.002

Sample L09, profil 2									Sample L09, profil 3					
distanc	310	330	350	360	370	380	390	400	10	20	30	40	50	70
SiO2	0.01	0.03	0.01	0.02	0.03	0.02	0.02	0.01	0.02	0.03	0.02	<0.01	0.03	0.00
TiO2	0.66	0.63	0.52	0.47	0.53	0.50	0.60	0.80	0.45	0.41	0.47	0.53	0.58	0.55
Al2O3	32.24	32.65	32.52	32.36	31.76	31.05	28.97	21.28	31.92	33.69	34.09	34.54	33.83	34.52
Cr2O3	31.99	31.96	32.23	32.64	32.68	33.59	35.37	41.77	30.80	29.23	28.98	29.40	29.25	28.85
Fe2O3	4.81	4.88	5.23	5.18	5.23	5.19	5.03	5.71	6.05	6.33	5.93	5.72	5.89	5.84
FeO	14.82	14.77	14.47	14.52	14.98	14.90	15.81	18.33	17.82	16.68	16.31	16.02	15.87	15.72
MnO	0.14	0.14	0.23	0.21	0.12	0.21	0.18	0.27	0.25	0.21	0.22	0.20	0.22	0.17
NiO	0.19	0.28	0.17	0.26	0.19	0.16	0.22	0.20	0.14	0.23	0.16	0.24	0.24	0.25
MgO	14.57	14.67	14.83	14.70	14.43	14.28	13.53	11.05	12.47	13.42	13.67	14.08	14.06	14.20
CaO	0.01	0.03	0.03	0.03	0.02	0.03	0.02	0.10	0.01	<0.01	<0.01	<0.01	<0.01	0.01
Na2O														
ZnO	0.11	0.17	0.13	0.26	0.20	0.32	0.23	0.16	0.21	0.20	0.25	0.25	0.05	0.13
Total	99.6	100.2	100.4	100.7	100.2	100.2	100.0	99.7	100.1	100.4	100.1	101.0	100.0	100.3
Si	<0.001	0.001	<0.001	0.001	0.001	0.001	0.001	<0.001	0.001	0.001	0.001	<0.001	0.001	<0.001
Ti	0.015	0.014	0.011	0.010	0.012	0.011	0.014	0.019	0.010	0.009	0.010	0.012	0.013	0.012
Al	1.119	1.125	1.118	1.112	1.100	1.079	1.022	0.789	1.119	1.164	1.177	1.179	1.167	1.184
Cr	0.745	0.739	0.744	0.753	0.759	0.783	0.837	1.038	0.724	0.677	0.671	0.673	0.677	0.664
Fe3	0.107	0.107	0.115	0.114	0.116	0.115	0.113	0.135	0.135	0.140	0.131	0.125	0.130	0.128
Fe2	0.365	0.361	0.353	0.354	0.368	0.367	0.396	0.482	0.443	0.409	0.400	0.388	0.388	0.383
Mn	0.003	0.004	0.006	0.005	0.003	0.005	0.005	0.007	0.006	0.005	0.006	0.005	0.005	0.004
Ni	0.005	0.007	0.004	0.006	0.005	0.004	0.005	0.005	0.003	0.005	0.004	0.006	0.006	0.006
Mg	0.639	0.639	0.645	0.639	0.632	0.628	0.603	0.518	0.553	0.586	0.597	0.608	0.613	0.616
Ca	<0.001	0.001	0.001	0.001	0.001	0.001	0.001	0.004	<0.001	<0.001	<0.001	<0.001	<0.001	<0.001
Na														
Zn	0.003	0.004	0.003	0.006	0.004	0.007	0.005	0.004	0.005	0.004	0.005	0.005	0.001	0.003

A2.6c: Spinel profils

Sample L09, profil 3

distanc	80	90	110	120	130	140	150	160	170	180	190	200	210	220
SiO2	<0.01	0.01	<0.01	0.03	0.03	0.01	0.02	<0.01	0.03	0.02	<0.01	<0.01	<0.01	0.02
TiO2	0.55	0.62	0.53	0.56	0.55	0.55	0.43	0.33	0.45	0.48	0.45	0.39	0.55	0.49
Al2O3	34.5	34.6	34.6	34.6	34.9	35.0	35.1	35.1	34.7	34.9	35.2	35.6	34.8	35.2
Cr2O3	28.7	28.5	28.6	29.1	28.5	28.4	28.6	28.5	28.6	28.4	28.4	28.5	28.6	28.2
Fe2O3	5.96	5.83	6.40	5.81	5.90	5.96	5.82	5.79	5.94	6.00	5.79	5.89	5.87	5.96
FeO	15.9	15.8	15.4	15.9	15.7	15.5	15.8	15.3	15.4	15.2	15.2	15.0	15.6	15.1
MnO	0.21	0.23	0.21	0.20	0.21	0.16	0.17	0.11	0.21	0.20	0.19	0.21	0.21	0.20
NiO	0.26	0.19	0.25	0.22	0.29	0.24	0.22	0.29	0.23	0.25	0.27	0.30	0.22	0.23
MgO	14.0	14.1	14.4	14.3	14.3	14.5	14.2	14.4	14.4	14.4	14.5	14.7	14.3	14.5
CaO	<0.01	0.02	0.02	<0.01	0.01	<0.01	0.01	<0.01	<0.01	<0.01	0.01	0.03	<0.01	0.01
Na2O														
ZnO	0.21	0.28	0.18	0.14	0.12	0.20	0.14	0.09	0.18	0.25	0.24	0.27	0.25	0.26
Total	100.2	100.2	100.6	100.8	100.5	100.5	100.6	99.8	100.1	100.2	100.3	100.8	100.3	100.2
Si	<0.001	<0.001	<0.001	0.001	0.001	<0.001	0.001	<0.001	0.001	0.001	<0.001	<0.001	<0.001	0.001
Ti	0.012	0.014	0.012	0.012	0.012	0.012	0.009	0.007	0.010	0.010	0.010	0.009	0.012	0.011
Al	1.184	1.188	1.181	1.182	1.192	1.194	1.198	1.204	1.190	1.194	1.203	1.207	1.190	1.201
Cr	0.661	0.656	0.656	0.665	0.654	0.651	0.656	0.655	0.659	0.653	0.651	0.649	0.657	0.647
Fe3	0.131	0.128	0.140	0.127	0.129	0.130	0.127	0.127	0.130	0.131	0.126	0.128	0.128	0.130
Fe2	0.387	0.385	0.374	0.384	0.381	0.375	0.383	0.372	0.374	0.370	0.369	0.361	0.378	0.367
Mn	0.005	0.006	0.005	0.005	0.005	0.004	0.004	0.003	0.005	0.005	0.005	0.005	0.005	0.005
Ni	0.006	0.004	0.006	0.005	0.007	0.006	0.005	0.007	0.005	0.006	0.006	0.007	0.005	0.006
Mg	0.609	0.612	0.622	0.616	0.617	0.624	0.614	0.624	0.623	0.625	0.624	0.629	0.618	0.628
Ca	<0.001	0.001	0.001	<0.001	<0.001	<0.001	<0.001	<0.001	<0.001	<0.001	<0.001	0.001	<0.001	<0.001
Na														
Zn	0.005	0.006	0.004	0.003	0.003	0.004	0.003	0.002	0.004	0.005	0.005	0.006	0.005	0.006

Sample L09, profil 3

distanc	230	240	250	260	270	280	290	300	310	320	330	340	350	360
SiO2	0.01	<0.01	0.03	0.01	0.02	0.01	0.06	0.01	0.02	<0.01	0.14	0.03	0.01	0.03
TiO2	0.48	0.42	0.44	0.46	0.47	0.38	0.43	0.51	0.56	0.47	0.40	0.47	0.42	0.47
Al2O3	35.1	35.3	35.8	36.0	36.6	36.8	36.1	35.7	35.6	35.4	35.4	35.2	35.5	35.1
Cr2O3	28.6	28.4	27.8	27.7	27.7	27.1	27.9	27.5	28.6	27.8	28.1	28.2	28.3	28.6
Fe2O3	5.79	5.70	5.67	5.75	5.16	5.26	5.72	5.39	5.24	5.47	5.72	5.99	5.61	5.82
FeO	15.0	15.2	15.3	15.0	15.1	14.9	15.1	15.0	15.3	15.1	15.3	15.1	15.2	15.4
MnO	0.20	0.19	0.21	0.22	0.11	0.23	0.11	0.19	0.17	0.20	0.18	0.20	0.20	0.19
NiO	0.18	0.21	0.18	0.25	0.25	0.21	0.25	0.25	0.29	0.20	0.15	0.31	0.20	0.25
MgO	14.7	14.5	14.6	14.7	14.8	14.8	14.9	14.6	14.7	14.5	14.6	14.5	14.5	14.5
CaO	<0.01	<0.01	0.01	0.02	<0.01	<0.01	<0.01	<0.01	0.01	0.03	<0.01	0.01	0.02	0.01
Na2O														
ZnO	0.21	0.20	0.14	0.16	0.23	0.26	0.19	0.12	0.14	0.05	0.20	0.20	0.18	0.14
Total	100.3	100.2	100.1	100.2	100.4	99.8	100.7	99.3	100.6	99.2	100.2	100.3	100.2	100.4
Si	<0.001	<0.001	0.001	<0.001	0.001	<0.001	0.002	<0.001	0.001	<0.001	0.004	0.001	<0.001	0.001
Ti	0.010	0.009	0.010	0.010	0.010	0.008	0.009	0.011	0.012	0.010	0.009	0.010	0.009	0.010
Al	1.198	1.207	1.219	1.223	1.239	1.251	1.221	1.225	1.210	1.217	1.208	1.201	1.213	1.196
Cr	0.654	0.651	0.636	0.632	0.628	0.617	0.633	0.634	0.651	0.642	0.642	0.646	0.647	0.655
Fe3	0.126	0.124	0.123	0.125	0.112	0.114	0.124	0.118	0.114	0.120	0.125	0.131	0.122	0.127
Fe2	0.364	0.369	0.370	0.362	0.363	0.358	0.363	0.366	0.368	0.368	0.371	0.366	0.368	0.372
Mn	0.005	0.005	0.005	0.006	0.003	0.006	0.003	0.005	0.004	0.005	0.004	0.005	0.005	0.005
Ni	0.004	0.005	0.004	0.006	0.006	0.005	0.006	0.006	0.007	0.005	0.004	0.007	0.005	0.006
Mg	0.633	0.626	0.628	0.634	0.635	0.634	0.636	0.632	0.631	0.631	0.630	0.628	0.627	0.625
Ca	<0.001	<0.001	<0.001	0.001	<0.001	<0.001	<0.001	<0.001	<0.001	0.001	<0.001	<0.001	0.001	<0.001
Na														
Zn	0.005	0.004	0.003	0.003	0.005	0.006	0.004	0.003	0.003	0.001	0.004	0.004	0.004	0.003

A2.6c: Spinel profils

Sample L09, profil 3														
distanc	**370**	**380**	**390**	**400**	**410**	**420**	**430**	**440**	**450**	**460**	**470**	**480**	**500**	**510**
SiO2	0.01	0.01	0.30	0.03	0.02	0.01	0.02	0.03	0.02	<0.01	<0.01	<0.01	0.01	<0.01
TiO2	0.43	0.58	0.42	0.47	0.37	0.37	0.40	1.84	0.35	0.40	0.36	0.40	0.44	0.49
Al2O3	35.3	35.2	35.3	35.2	35.2	34.9	35.1	34.1	35.3	35.0	35.0	35.1	35.1	35.2
Cr2O3	28.4	28.4	28.8	28.2	27.9	28.9	28.4	28.0	28.7	28.5	28.3	29.4	28.4	28.2
Fe2O3	5.91	5.97	5.09	5.98	6.31	5.78	5.73	4.43	5.82	5.86	5.90	5.68	5.67	5.95
FeO	15.1	15.3	15.7	15.5	15.2	15.2	15.3	16.4	15.3	15.3	15.0	15.6	15.3	15.1
MnO	0.18	0.17	0.13	0.21	0.17	0.21	0.21	0.21	0.19	0.22	0.22	0.23	0.26	0.26
NiO	0.25	0.23	0.19	0.25	0.25	0.22	0.21	0.21	0.26	0.30	0.18	0.27	0.24	0.20
MgO	14.6	14.6	14.6	14.3	14.5	14.4	14.4	14.4	14.5	14.3	14.4	14.3	14.4	14.5
CaO	<0.01	<0.01	0.06	0.01	<0.01	0.01	<0.01	<0.01	<0.01	0.02	<0.01	<0.01	<0.01	0.01
Na2O														
ZnO	0.17	0.32	0.21	0.23	0.16	0.24	0.18	0.31	0.19	0.19	0.22	0.30	0.15	0.28
Total	100.4	100.7	100.7	100.3	100.1	100.2	99.9	99.8	100.6	100.1	99.6	101.2	99.9	100.2
Si	<0.001	<0.001	0.009	0.001	0.001	<0.001	0.001	0.001	0.001	<0.001	<0.001	<0.001	<0.001	<0.001
Ti	0.009	0.013	0.009	0.010	0.008	0.008	0.009	0.040	0.008	0.009	0.008	0.009	0.010	0.011
Al	1.203	1.197	1.199	1.202	1.204	1.194	1.204	1.173	1.202	1.200	1.202	1.192	1.204	1.203
Cr	0.649	0.647	0.655	0.646	0.641	0.663	0.652	0.647	0.655	0.655	0.652	0.668	0.653	0.646
Fe3	0.129	0.130	0.110	0.130	0.138	0.126	0.126	0.097	0.127	0.128	0.130	0.123	0.124	0.130
Fe2	0.366	0.370	0.378	0.375	0.368	0.369	0.371	0.400	0.369	0.371	0.366	0.375	0.372	0.366
Mn	0.004	0.004	0.003	0.005	0.004	0.005	0.005	0.005	0.005	0.006	0.005	0.006	0.006	0.007
Ni	0.006	0.005	0.004	0.006	0.006	0.005	0.005	0.005	0.006	0.007	0.004	0.006	0.006	0.005
Mg	0.630	0.626	0.626	0.619	0.627	0.624	0.624	0.625	0.624	0.621	0.627	0.616	0.623	0.627
Ca	<0.001	<0.001	0.002	<0.001	<0.001	<0.001	<0.001	<0.001	<0.001	0.001	<0.001	<0.001	<0.001	<0.001
Na														
Zn	0.004	0.007	0.005	0.005	0.004	0.005	0.004	0.007	0.004	0.004	0.005	0.006	0.003	0.006

Sample L09, profil 3										**L110, profil 2**				
distanc	**520**	**530**	**540**	**550**	**560**	**570**	**580**	**600**	**610**	**20**	**30**	**50**	**60**	**70**
SiO2	0.01	0.02	<0.01	<0.01	0.01	<0.01	0.02	<0.01	0.05	0.03	0.01	0.02	0.08	0.01
TiO2	0.60	0.44	0.46	0.44	0.47	0.39	0.37	0.29	0.18	0.87	0.55	1.19	0.32	0.66
Al2O3	35.3	35.1	35.0	35.1	34.6	35.0	35.3	38.2	41.1	39.0	38.3	34.2	33.8	33.1
Cr2O3	28.4	28.8	28.4	28.7	29.3	29.0	28.4	25.9	23.5	25.5	25.8	28.0	27.9	29.0
Fe2O3	5.66	5.57	5.87	5.45	5.58	5.83	5.98	5.42	4.76	1.37	3.65	4.36	6.44	5.94
FeO	15.4	15.6	15.4	15.5	15.6	15.5	15.5	14.6	14.4	16.1	15.0	16.2	15.3	15.3
MnO	0.18	0.15	0.18	0.21	0.24	0.20	0.22	0.20	0.12	0.16	0.13	0.20	0.13	0.12
NiO	0.24	0.18	0.22	0.16	0.24	0.19	0.23	0.25	0.22	0.18	0.23	0.19	0.22	0.19
MgO	14.6	14.4	14.4	14.4	14.3	14.4	14.4	15.1	15.5	14.0	14.8	13.9	14.0	14.1
CaO	<0.01	<0.01	<0.01	0.01	<0.01	<0.01	0.01	<0.01	0.01	0.02	0.01	0.02	0.01	0.01
Na2O														
ZnO	0.22	0.21	0.22	0.11	0.12	0.27	0.15	0.18	0.23	0.28	0.15	0.11	0.06	0.14
Total	100.5	100.5	100.1	100.0	100.4	100.7	100.5	100.0	100.1	97.5	98.5	98.5	98.2	98.6
Si	<0.001	0.001	<0.001	<0.001	<0.001	<0.001	0.001	<0.001	0.001	0.001	<0.001	0.001	0.002	<0.001
Ti	0.013	0.010	0.010	0.010	0.010	0.008	0.008	0.006	0.004	0.019	0.012	0.026	0.007	0.015
Al	1.202	1.199	1.199	1.203	1.185	1.193	1.203	1.286	1.366	1.342	1.306	1.193	1.182	1.158
Cr	0.649	0.660	0.653	0.659	0.672	0.663	0.649	0.585	0.523	0.588	0.590	0.656	0.656	0.680
Fe3	0.123	0.121	0.128	0.119	0.122	0.127	0.130	0.117	0.101	0.030	0.080	0.097	0.144	0.133
Fe2	0.371	0.378	0.374	0.376	0.378	0.375	0.375	0.350	0.340	0.394	0.363	0.401	0.379	0.380
Mn	0.004	0.004	0.004	0.005	0.006	0.005	0.005	0.005	0.003	0.004	0.003	0.005	0.003	0.003
Ni	0.006	0.004	0.005	0.004	0.006	0.004	0.005	0.006	0.005	0.004	0.006	0.005	0.005	0.004
Mg	0.628	0.620	0.622	0.623	0.619	0.619	0.619	0.642	0.653	0.611	0.637	0.614	0.620	0.624
Ca	<0.001	<0.001	<0.001	<0.001	<0.001	<0.001	<0.001	<0.001	<0.001	0.001	<0.001	0.001	<0.001	<0.001
Na														
Zn	0.005	0.005	0.005	0.002	0.003	0.006	0.003	0.004	0.005	0.006	0.003	0.002	0.001	0.003

A2.6c: Spinel profils

L110, profil 2							**Sample L110, profil 2**				**L110, profil 3**			
distanc	**80**	**90**	**100**	**110**	**120**	**130**	**140**	**150**	**160**	**170**	**190**	**10**	**20**	**30**
SiO2	<0.01	0.03	<0.01	0.03	<0.01	<0.01	0.01	<0.01	0.01	0.20	0.05	0.02	0.02	<0.01
TiO2	0.83	0.32	0.61	2.64	0.63	0.87	1.42	0.87	0.51	0.44	0.88	0.31	0.21	0.19
Al2O3	32.4	32.5	31.7	29.9	31.3	31.1	30.6	30.8	30.2	30.3	27.8	40.7	40.0	38.3
Cr2O3	29.7	30.2	30.3	30.0	31.0	30.4	30.0	31.3	32.2	32.8	33.2	22.2	22.9	24.8
Fe2O3	5.71	5.85	6.65	4.87	6.19	6.30	6.00	5.87	6.02	4.66	6.20	3.17	4.21	4.04
FeO	15.6	15.1	15.5	17.3	15.5	15.8	16.2	15.9	16.2	16.5	17.4	17.7	17.3	17.3
MnO	0.14	0.22	0.16	0.16	0.00	0.13	0.19	0.19	0.17	0.10	0.15	0.09	0.18	0.12
NiO	0.23	0.18	0.22	0.20	0.22	0.16	0.30	0.27	0.15	0.20	0.23	0.28	0.28	0.29
MgO	14.0	13.9	13.8	13.7	13.9	13.7	13.5	13.6	13.2	13.0	12.3	12.9	13.1	12.9
CaO	0.02	0.02	<0.01	<0.01	<0.01	0.01	<0.01	0.01	<0.01	<0.01	<0.01	0.05	0.05	0.03
Na2O														
ZnO	0.09	0.10	0.23	0.20	0.21	0.16	0.24	0.20	0.12	0.23	0.15	0.13	0.20	0.20
Total	98.6	98.5	99.2	99.1	98.9	98.5	98.5	98.8	98.7	98.4	98.4	97.6	98.4	98.2
Si	<0.001	0.001	<0.001	0.001	<0.001	<0.001	<0.001	<0.001	<0.001	0.006	0.002	0.001	0.001	<0.001
Ti	0.019	0.007	0.014	0.060	0.014	0.020	0.032	0.020	0.012	0.010	0.020	0.007	0.005	0.004
Al	1.136	1.141	1.112	1.058	1.103	1.098	1.086	1.087	1.072	1.078	1.007	1.402	1.372	1.326
Cr	0.700	0.712	0.712	0.711	0.730	0.720	0.713	0.741	0.768	0.784	0.806	0.514	0.526	0.576
Fe3	0.128	0.131	0.149	0.110	0.139	0.142	0.136	0.132	0.137	0.106	0.143	0.070	0.092	0.089
Fe2	0.388	0.377	0.386	0.434	0.387	0.397	0.409	0.398	0.408	0.418	0.447	0.434	0.422	0.425
Mn	0.004	0.005	0.004	0.004	0.000	0.003	0.005	0.005	0.004	0.003	0.004	0.002	0.004	0.003
Ni	0.006	0.004	0.005	0.005	0.005	0.004	0.007	0.007	0.004	0.005	0.006	0.007	0.007	0.007
Mg	0.619	0.618	0.614	0.613	0.617	0.612	0.606	0.606	0.593	0.586	0.562	0.561	0.567	0.564
Ca	0.001	0.001	<0.001	<0.001	<0.001	<0.001	<0.001	<0.001	<0.001	<0.001	<0.001	0.002	0.002	0.001
Na														
Zn	0.002	0.002	0.005	0.004	0.005	0.004	0.005	0.004	0.003	0.005	0.003	0.003	0.004	0.004

Sample L110, profil 3										**Sample L147, profil 4**				
distanc	**40**	**80**	**90**	**100**	**110**	**120**	**130**	**140**	**150**	**0**	**10**	**20**	**30**	**40**
SiO2	0.02	<0.01	0.02	0.02	<0.01	<0.01	<0.01	0.01	0.04	0.03	0.04	0.03	0.02	0.00
TiO2	0.16	0.41	0.37	0.41	1.52	0.53	0.68	0.57	0.70	0.77	0.82	0.92	2.25	1.05
Al2O3	36.8	29.0	28.2	29.3	28.3	28.9	28.64	26.8	24.4	30.4	31.0	30.2	29.6	30.8
Cr2O3	26.5	32.4	32.9	32.5	32.2	32.4	33.2	34.4	36.3	33.3	32.5	32.9	31.7	30.5
Fe2O3	3.89	5.97	6.51	6.10	5.64	6.91	5.96	6.94	6.56	4.30	4.24	3.99	4.11	4.84
FeO	18.7	19.0	18.8	17.7	18.0	16.9	17.0	17.0	17.7	18.9	19.4	18.6	20.0	18.6
MnO	0.18	0.20	0.16	0.15	0.19	0.16	0.16	0.10	0.18	0.17	0.18	0.15	0.23	0.09
NiO	0.18	0.20	0.22	0.16	0.25	0.12	0.14	0.20	0.18	0.20	0.22	0.19	0.23	0.15
MgO	11.9	11.0	11.1	12.0	12.3	12.5	12.58	12.2	11.4	11.7	11.6	11.9	11.9	11.9
CaO	0.01	0.03	0.01	0.02	<0.01	0.03	0.05	0.03	0.14	0.03	0.01	0.01	0.01	<0.01
Na2O										0.02	<0.01	0.01	0.01	<0.01
ZnO	0.33	0.21	0.11	0.14	0.16	0.18	0.06	0.25	0.22	0.20	0.22	0.17	0.16	0.19
Total	98.7	98.4	98.4	98.5	98.6	98.7	98.4	98.49	97.77	100.0	100.3	99.0	100.1	98.1
Si	0.001	<0.001	0.001	0.001	<0.001	<0.001	<0.001	<0.001	0.001	0.001	0.001	0.001	0.001	<0.001
Ti	0.004	0.010	0.009	0.009	0.035	0.012	0.016	0.013	0.017	0.017	0.019	0.021	0.051	0.024
Al	1.284	1.054	1.027	1.055	1.022	1.037	1.031	0.974	0.905	1.077	1.096	1.079	1.050	1.107
Cr	0.621	0.789	0.804	0.785	0.779	0.781	0.801	0.838	0.904	0.791	0.770	0.787	0.754	0.734
Fe3	0.087	0.139	0.151	0.140	0.130	0.158	0.137	0.161	0.156	0.097	0.096	0.091	0.093	0.111
Fe2	0.462	0.489	0.487	0.453	0.461	0.431	0.433	0.438	0.466	0.475	0.486	0.470	0.503	0.473
Mn	0.004	0.005	0.004	0.004	0.005	0.004	0.004	0.003	0.005	0.004	0.005	0.004	0.006	0.002
Ni	0.004	0.005	0.006	0.004	0.006	0.003	0.003	0.005	0.005	0.005	0.005	0.005	0.006	0.004
Mg	0.525	0.504	0.510	0.545	0.559	0.569	0.572	0.561	0.533	0.526	0.518	0.538	0.533	0.541
Ca	<0.001	0.001	<0.001	0.001	<0.001	0.001	0.002	0.001	0.005	0.001	<0.001	<0.001	<0.001	<0.001
Na										0.001	<0.001	0.001	<0.001	<0.001
Zn	0.007	0.005	0.002	0.003	0.004	0.004	0.001	0.006	0.005	0.004	0.005	0.004	0.004	0.004

A2.6c: Spinel profils

Sample L147, profil 4

distance	**0**	**10**	**20**	**30**	**40**	**50**	**60**	**70**	**80**	**90**	**100**	**110**	**120**	**130**
SiO2	0.03	0.04	0.03	0.02	<0.01	0.56	0.10	0.01	0.03	<0.01	0.03	0.02	0.02	0.01
TiO2	0.77	0.82	0.92	2.25	1.05	0.44	0.37	0.60	1.12	0.61	0.83	0.68	0.74	0.78
Al2O3	30.4	31.0	30.2	29.6	30.8	32.9	32.5	31.6	31.1	31.2	30.8	30.5	30.3	30.1
Cr2O3	33.3	32.5	32.9	31.7	30.5	33.3	32.5	30.7	31.4	30.6	31.2	32.1	32.4	33.6
Fe2O3	4.30	4.24	3.99	4.11	4.84	0.00	3.13	5.67	5.06	6.22	6.24	6.12	5.92	5.51
FeO	18.9	19.4	18.6	20.0	18.6	20.2	19.4	17.3	18.3	17.5	16.7	16.2	16.5	17.4
MnO	0.17	0.18	0.15	0.23	0.09	0.13	0.24	0.18	0.15	0.15	0.14	0.11	0.09	0.15
NiO	0.20	0.22	0.19	0.23	0.15	0.12	0.16	0.23	0.22	0.17	0.31	0.18	0.23	0.18
MgO	11.7	11.6	11.9	11.9	11.9	11.3	11.0	12.6	12.4	12.5	13.1	13.4	13.3	12.8
CaO	0.03	0.01	0.01	0.01	<0.01	0.04	0.01	<0.01	0.04	0.04	0.01	0.01	0.01	0.01
Na2O	0.02	<0.01	0.01	0.01	<0.01	0.02	0.16	<0.01	0.01	<0.01	0.01	0.01	0.01	0.03
ZnO	0.20	0.22	0.17	0.16	0.19	0.22	0.23	0.23	0.23	0.21	0.16	0.23	0.14	0.23
Total	100.0	100.3	99.0	100.1	98.1	99.2	99.8	99.1	100.2	99.1	99.5	99.5	99.6	100.8
Si	0.001	0.001	0.001	0.001	0.000	0.017	0.003	0.000	0.001	0.000	0.001	0.001	0.001	0.000
Ti	0.017	0.019	0.021	0.051	0.024	0.010	0.008	0.013	0.025	0.014	0.019	0.015	0.017	0.018
Al	1.077	1.096	1.079	1.050	1.107	1.162	1.147	1.117	1.094	1.105	1.085	1.074	1.067	1.053
Cr	0.791	0.770	0.787	0.754	0.734	0.788	0.770	0.728	0.741	0.727	0.736	0.758	0.766	0.790
Fe3	0.097	0.096	0.091	0.093	0.111	0.000	0.071	0.128	0.114	0.141	0.141	0.138	0.133	0.123
Fe2	0.475	0.486	0.470	0.503	0.473	0.506	0.486	0.433	0.457	0.441	0.418	0.405	0.413	0.431
Mn	0.004	0.005	0.004	0.006	0.002	0.003	0.006	0.005	0.004	0.004	0.004	0.003	0.002	0.004
Ni	0.005	0.005	0.005	0.006	0.004	0.003	0.004	0.006	0.005	0.004	0.007	0.004	0.005	0.004
Mg	0.526	0.518	0.538	0.533	0.541	0.504	0.490	0.565	0.552	0.559	0.585	0.597	0.592	0.569
Ca	0.001	<0.001	<0.001	<0.001	<0.001	0.001	<0.001	<0.001	0.001	0.001	<0.001	<0.001	<0.001	<0.001
Na	0.001	<0.001	0.001	<0.001	<0.001	0.001	0.009	<0.001	0.001	<0.001	0.001	0.001	<0.001	0.002
Zn	0.004	0.005	0.004	0.004	0.004	0.005	0.005	0.005	0.005	0.005	0.004	0.005	0.003	0.005

Sample L147, profil 4				**Sample L241, profil 1**										
distance	**140**	**150**	**160**	**0**	**10**	**20**	**30**	**40**	**60**	**70**	**80**	**90**	**100**	**110**
SiO2	0.03	0.02	0.07	0.04	<0.01	<0.01	0.03	<0.01	0.02	0.05	0.02	0.02	0.02	0.01
TiO2	0.69	1.02	0.31	0.31	0.39	0.48	0.78	0.49	0.73	0.42	0.50	0.74	0.42	0.41
Al2O3	30.2	29.6	30.4	43.4	36.9	34.1	33.6	33.8	33.9	33.6	33.8	33.0	33.4	32.9
Cr2O3	32.6	32.2	32.1	20.4	25.6	27.9	28.5	28.1	28.3	29.0	29.1	29.8	29.0	29.8
Fe2O3	5.53	4.69	2.63	5.14	7.33	7.49	7.33	7.57	6.72	7.22	7.19	6.95	7.45	7.61
FeO	18.2	18.8	26.4	12.8	15.1	15.4	15.7	15.0	15.4	15.3	15.2	15.4	15.0	14.9
MnO	0.09	0.06	0.31	0.16	0.17	0.15	0.16	0.07	0.18	0.17	0.05	0.10	0.10	0.16
NiO	0.16	0.19	0.09	0.28	0.28	0.23	0.30	0.21	0.23	0.29	0.29	0.25	0.26	0.26
MgO	12.1	11.7	6.2	16.6	14.7	14.2	14.3	14.5	14.4	14.3	14.6	14.5	14.5	14.6
CaO	<0.01	0.01	0.01	0.11	0.04	0.02	0.03	0.03	0.02	<0.01	0.01	<0.01	0.01	<0.01
Na2O	0.04	0.01	0.01	0.02	0.03	0.01	0.01	0.02	0.01	0.02	<0.01	0.02	<0.01	0.01
ZnO	0.19	0.11	0.60	0.15	0.11	0.19	0.21	0.16	0.18	0.17	0.19	0.24	0.19	0.17
Total	99.8	98.4	99.1	99.5	100.6	100.1	101.0	100.0	99.9	100.6	100.9	101.0	100.4	100.8
Si	0.001	0.001	0.002	0.001	<0.001	<0.001	0.001	<0.001	0.001	0.001	0.001	0.001	0.001	<0.001
Ti	0.016	0.024	0.007	0.007	0.008	0.011	0.017	0.011	0.016	0.009	0.011	0.016	0.009	0.009
Al	1.069	1.068	1.123	1.427	1.248	1.172	1.149	1.164	1.166	1.154	1.155	1.131	1.148	1.130
Cr	0.775	0.777	0.797	0.450	0.579	0.643	0.655	0.650	0.653	0.668	0.666	0.685	0.670	0.686
Fe3	0.125	0.108	0.062	0.108	0.158	0.165	0.160	0.166	0.148	0.158	0.157	0.152	0.164	0.167
Fe2	0.459	0.481	0.692	0.299	0.361	0.377	0.382	0.367	0.375	0.372	0.369	0.373	0.365	0.362
Mn	0.002	0.002	0.008	0.004	0.004	0.004	0.004	0.002	0.004	0.004	0.001	0.002	0.003	0.004
Ni	0.004	0.005	0.002	0.006	0.007	0.005	0.007	0.005	0.005	0.007	0.007	0.006	0.006	0.006
Mg	0.543	0.532	0.291	0.690	0.630	0.618	0.619	0.631	0.626	0.622	0.630	0.626	0.630	0.632
Ca	<0.001	<0.001	<0.001	0.003	0.001	0.001	0.001	0.001	0.001	<0.001	<0.001	<0.001	<0.001	<0.001
Na	0.002	0.001	0.001	0.001	0.002	0.001	<0.001	0.001	0.001	0.001	<0.001	0.001	<0.001	0.001
Zn	0.004	0.003	0.014	0.003	0.002	0.004	0.005	0.003	0.004	0.004	0.004	0.005	0.004	0.004

A2.6c: Spinel profils

Sample L241, profil 1						**Sample L241, profil 2**							
distance	**120**	**130**	**160**	**180**	**190**	**0**	**20**	**30**	**40**	**50**	**60**	**70**	**80**	**90**
SiO2	0.01	0.03	0.03	0.04	0.03	0.03	0.05	<0.01	0.04	0.02	0.01	0.01	<0.01	0.01
TiO2	0.38	2.32	0.64	0.69	0.76	0.62	0.48	0.67	0.73	0.83	0.70	0.45	0.57	0.32
Al2O3	33.3	32.4	31.8	26.0	19.2	24.0	28.9	30.7	30.4	31.2	31.4	31.8	33.6	38.9
Cr2O3	29.8	29.8	30.9	35.9	43.5	37.4	34.2	32.3	31.6	31.6	31.5	30.4	29.1	24.7
Fe2O3	6.76	4.70	6.63	7.08	6.01	6.88	6.42	6.61	7.21	6.63	6.36	7.46	6.72	6.04
FeO	15.0	17.2	16.0	17.1	19.8	17.2	16.1	15.4	15.6	16.1	15.8	15.4	15.7	13.9
MnO	0.14	0.18	0.13	0.13	0.26	0.25	0.15	0.18	0.25	0.17	0.12	0.10	0.17	0.02
NiO	0.26	0.29	0.23	0.22	0.12	0.20	0.21	0.22	0.25	0.26	0.22	0.25	0.18	0.28
MgO	14.4	14.1	13.7	12.2	9.9	11.7	13.4	14.0	13.8	13.9	13.9	14.0	14.2	15.7
CaO	<0.01	<0.01	0.03	0.12	0.14	0.05	0.03	<0.01	0.01	<0.01	<0.01	<0.01	0.01	0.04
Na2O	0.03	0.04	0.01	0.04	0.02	0.03	0.01	<0.01	0.02	0.01	0.01	0.01	0.01	<0.01
ZnO	0.20	0.20	0.23	0.25	0.15	0.16	0.14	0.23	0.14	0.16	0.18	0.23	0.20	0.16
Total	100.2	101.3	100.3	99.8	99.9	98.5	100.1	100.4	100.1	100.7	100.3	100.1	100.5	100.1
Si	<0.001	0.001	0.001	0.001	0.001	0.001	0.002	<0.001	0.001	0.001	<0.001	<0.001	<0.001	<0.001
Ti	0.008	0.051	0.014	0.016	0.018	0.015	0.011	0.015	0.016	0.018	0.016	0.010	0.013	0.007
Al	1.147	1.110	1.103	0.938	0.722	0.886	1.021	1.070	1.065	1.082	1.093	1.105	1.155	1.302
Cr	0.688	0.687	0.721	0.867	1.097	0.924	0.810	0.754	0.742	0.734	0.734	0.710	0.672	0.555
Fe3	0.149	0.103	0.147	0.163	0.144	0.162	0.145	0.147	0.161	0.147	0.141	0.166	0.148	0.129
Fe2	0.366	0.419	0.395	0.437	0.528	0.451	0.402	0.380	0.386	0.395	0.390	0.379	0.383	0.329
Mn	0.003	0.005	0.003	0.003	0.007	0.007	0.004	0.005	0.006	0.004	0.003	0.003	0.004	<0.001
Ni	0.006	0.007	0.005	0.005	0.003	0.005	0.005	0.005	0.006	0.006	0.005	0.006	0.004	0.006
Mg	0.626	0.612	0.604	0.557	0.470	0.543	0.596	0.619	0.610	0.608	0.612	0.616	0.616	0.665
Ca	<0.001	<0.001	0.001	0.004	0.005	0.002	0.001	<0.001	<0.001	<0.001	<0.001	<0.001	<0.001	0.001
Na	0.002	0.002	0.001	0.002	0.001	0.002	0.001	<0.001	0.001	0.001	<0.001	0.001	<0.001	<0.001
Zn	0.004	0.004	0.005	0.006	0.003	0.004	0.003	0.005	0.003	0.003	0.004	0.005	0.004	0.003

Annexe A2.5: profiles of minerals and data set associated

A2.5d: plagioclase profiles

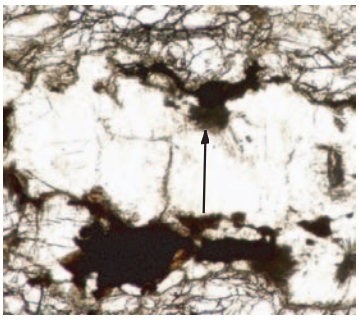

Sample L112, profil 1, proto-mylonite
distance: 310 µm

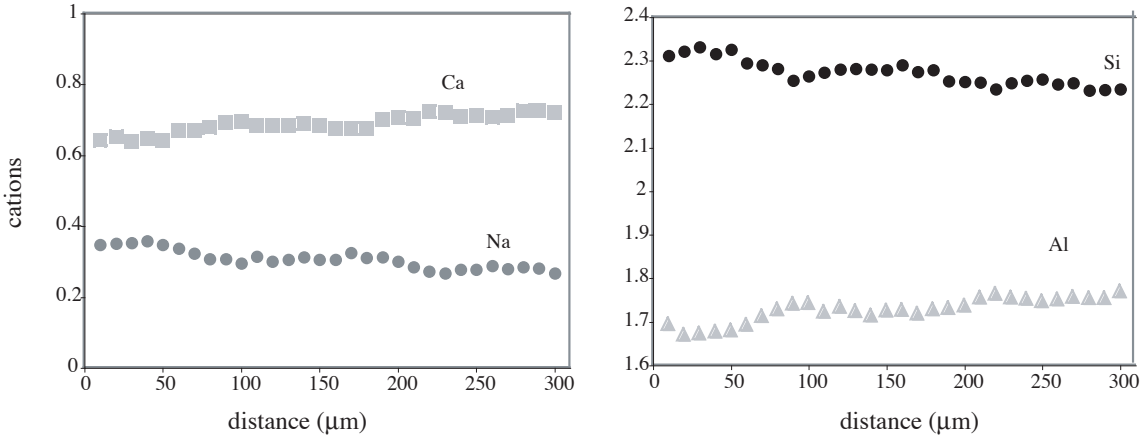

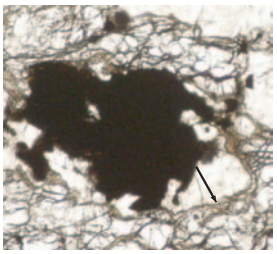

Sample L112, profil 2, proto-mylonite
distance: 190 µm

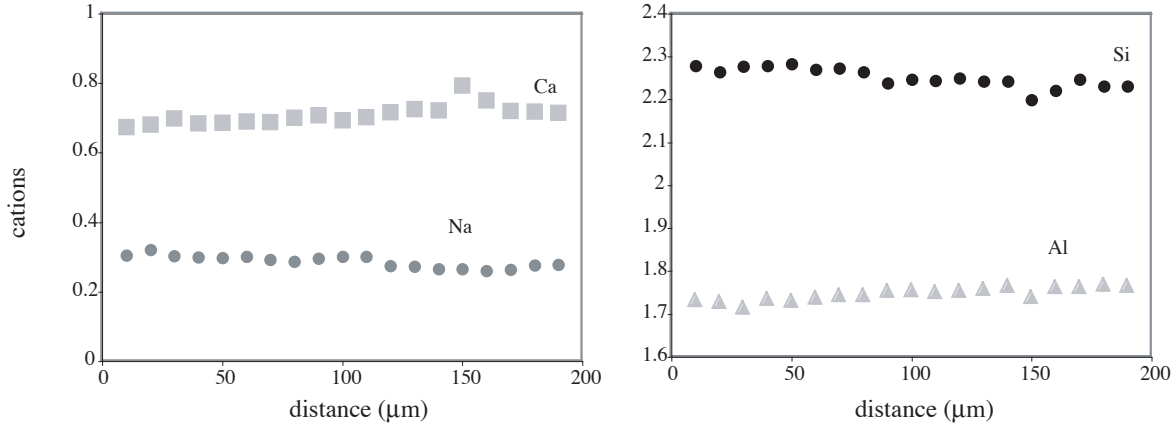

Annexe A2.5: profiles of minerals and data set associated

A2.5d: plagioclase profiles

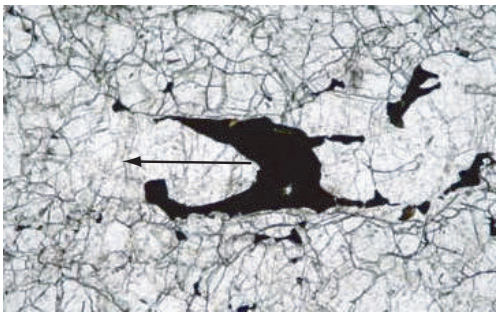

Sample La2002-05, section 1, proto-mylonite
distance: 611 µm

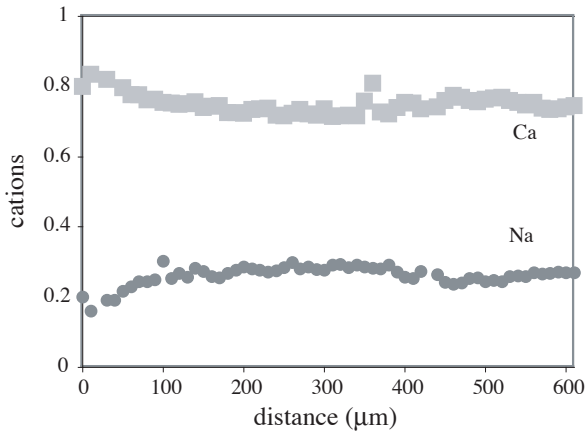

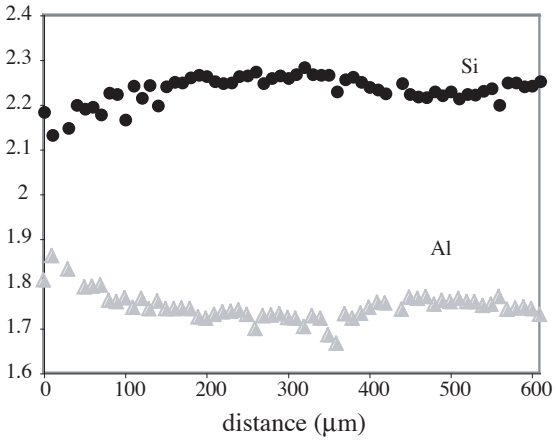

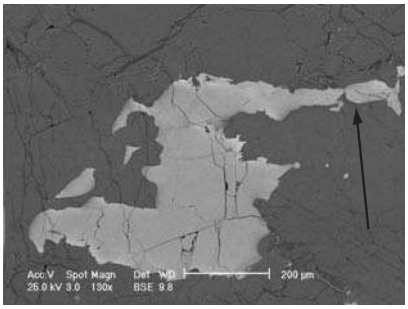

Sample L241, section 1, CGSGc
distance: 300 µm

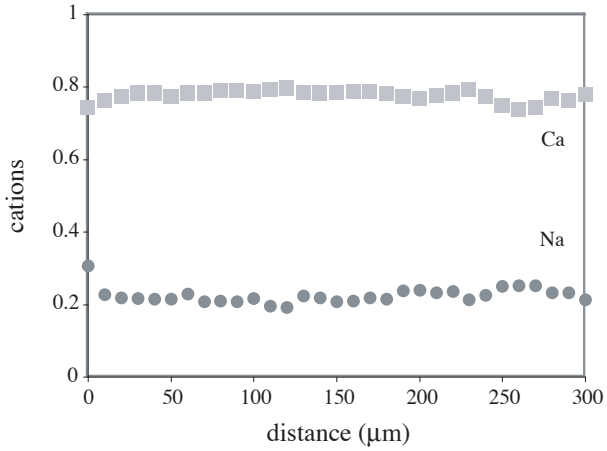

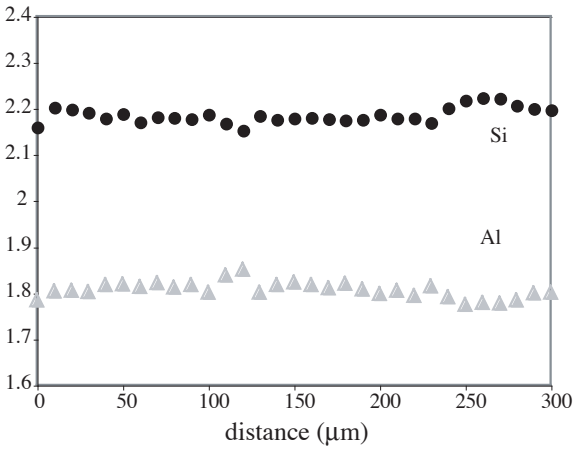

A2.6d: Plagioclase profils

Sample L112, profil 1

distanc	10	20	30	40	50	60	70	80	90	100	110	120	130	140
SiO2	51.3	51.3	51.8	51.5	51.6	51.0	50.8	50.4	50.1	50.0	49.7	50.7	50.8	50.6
Al2O3	31.9	31.3	31.5	31.7	31.6	31.9	32.2	32.4	32.8	32.7	32.0	32.7	32.5	32.2
Fe2O3	0.10	0.10	0.08	0.03	0.12	0.08	0.09	0.06	0.06	0.07	0.14	0.05	0.08	0.06
FeO	<0.01	<0.01	<0.01	<0.01	<0.01	<0.01	<0.01	<0.01	<0.01	<0.01	<0.01	<0.01	<0.01	<0.01
CaO	13.3	13.5	13.3	13.5	13.3	13.9	13.9	14.0	14.4	14.3	14.0	14.2	14.2	14.3
Na2O	3.98	4.01	4.05	4.11	3.99	3.87	3.69	3.50	3.53	3.36	3.54	3.45	3.50	3.58
K2O	<0.01	<0.01	<0.01	<0.01	<0.01	<0.01	0.01	0.01	0.01	<0.01	0.01	<0.01	<0.01	<0.01
Total	100.5	100.1	100.7	100.8	100.5	100.8	100.6	100.4	100.8	100.4	99.3	101.0	101.1	100.7
Si	2.31	2.32	2.33	2.32	2.33	2.29	2.29	2.28	2.25	2.26	2.27	2.28	2.28	2.28
Al	1.69	1.67	1.67	1.68	1.68	1.69	1.71	1.73	1.74	1.74	1.72	1.73	1.72	1.71
Fe3	0.004	0.003	0.003	0.001	0.004	0.003	0.003	0.002	0.002	0.003	0.005	0.002	0.003	0.002
Fe2	<0.001	<0.001	<0.001	<0.001	<0.001	<0.001	<0.001	<0.001	<0.001	<0.001	<0.001	<0.001	<0.001	<0.001
Ca	0.643	0.653	0.640	0.649	0.642	0.672	0.671	0.680	0.693	0.695	0.685	0.683	0.685	0.691
Na	0.348	0.352	0.354	0.358	0.349	0.338	0.323	0.307	0.309	0.295	0.314	0.301	0.305	0.313
K	<0.001	<0.001	<0.001	<0.001	<0.001	<0.001	0.001	0.001	0.001	<0.001	<0.001	<0.001	<0.001	<0.001
Anorthit	0.65	0.65	0.64	0.65	0.65	0.67	0.68	0.69	0.69	0.70	0.69	0.69	0.69	0.69
Albite	0.35	0.35	0.36	0.36	0.35	0.33	0.33	0.31	0.31	0.30	0.31	0.31	0.31	0.31

Sample L112, profil 1

distanc	150	160	170	180	190	200	210	220	230	240	250	260	270	280
SiO2	50.5	50.6	49.7	49.5	49.1	49.6	50.0	49.2	49.9	49.9	50.0	49.6	49.8	49.3
Al2O3	32.4	32.4	31.8	31.8	32.0	32.5	33.1	32.9	33.1	32.9	32.8	32.8	33.0	32.9
Fe2O3	0.12	0.00	0.13	0.11	0.06	0.14	0.11	0.20	0.19	0.13	0.12	0.15	0.11	0.11
FeO	<0.01	0.06	<0.01	<0.01	<0.01	<0.01	<0.01	<0.01	<0.01	<0.01	<0.01	<0.01	<0.01	<0.01
CaO	14.2	13.9	13.8	13.7	14.2	14.5	14.6	14.9	14.9	14.7	14.7	14.6	14.7	15.0
Na2O	3.50	3.49	3.67	3.49	3.52	3.41	3.26	3.10	3.06	3.18	3.17	3.29	3.18	3.24
K2O	<0.01	<0.01	0.01	<0.01	<0.01	<0.01	<0.01	<0.01	<0.01	0.01	<0.01	0.01	<0.01	<0.01
Total	100.6	100.5	99.1	98.6	98.8	100.1	101.0	100.3	101.2	100.8	100.9	100.5	100.7	100.5
Si	2.28	2.29	2.27	2.28	2.25	2.25	2.25	2.23	2.25	2.26	2.26	2.25	2.25	2.23
Al	1.72	1.73	1.72	1.73	1.73	1.74	1.76	1.76	1.76	1.75	1.75	1.75	1.76	1.75
Fe3	0.004	0.000	0.005	0.004	0.002	0.005	0.004	0.007	0.007	0.004	0.004	0.005	0.004	0.004
Fe2	<0.001	0.002	<0.001	<0.001	<0.001	<0.001	<0.001	<0.001	<0.001	<0.001	<0.001	<0.001	<0.001	<0.001
Ca	0.686	0.675	0.677	0.677	0.701	0.706	0.705	0.723	0.721	0.709	0.713	0.708	0.712	0.726
Na	0.306	0.306	0.326	0.312	0.314	0.300	0.284	0.273	0.268	0.278	0.278	0.288	0.279	0.285
K	<0.001	<0.001	0.001	<0.001	<0.001	<0.001	<0.001	<0.001	<0.001	0.001	<0.001	0.001	<0.001	<0.001
Anorthit	0.69	0.69	0.68	0.69	0.69	0.70	0.71	0.73	0.73	0.72	0.72	0.71	0.72	0.72
Albite	0.31	0.31	0.33	0.32	0.31	0.30	0.29	0.27	0.27	0.28	0.28	0.29	0.28	0.28

A2.6d: Plagioclase profils

Sample L112, profil 1			**Sample L112, profil 2**											
distanc	**290**	**300**	**10**	**20**	**30**	**40**	**50**	**60**	**70**	**80**	**90**	**100**	**110**	**120**
SiO2	49.1	49.2	49.1	48.6	50.5	50.4	50.6	50.0	50.2	50.3	48.7	48.2	48.3	49.8
Al2O3	32.7	33.0	31.6	31.4	32.3	32.5	32.5	32.5	32.7	32.8	32.4	32.0	32.0	32.9
Fe2O3	0.10	0.14	0.24	0.19	0.14	0.11	0.09	0.05	0.07	0.15	0.13	0.10	0.08	0.13
FeO	<0.01	<0.01	<0.01	<0.01	<0.01	<0.01	0.01	<0.01	0.02	<0.01	<0.01	<0.01	<0.01	<0.01
CaO	14.9	14.8	13.6	13.6	14.5	14.1	14.2	14.2	14.2	14.5	14.4	13.9	14.1	14.8
Na2O	3.19	3.04	3.39	3.56	3.48	3.40	3.41	3.43	3.33	3.29	3.31	3.34	3.34	3.14
K2O	0.01	<0.01	0.02	0.01	<0.01	0.01	0.01	0.01	<0.01	<0.01	<0.01	0.01	<0.01	<0.01
Total	100.1	100.2	97.9	97.4	100.9	100.5	100.8	100.2	100.5	101.0	98.9	97.6	97.8	100.7
Si	2.234	2.236	2.279	2.264	2.278	2.279	2.283	2.269	2.273	2.265	2.239	2.246	2.244	2.250
Al	1.754	1.770	1.732	1.727	1.714	1.734	1.730	1.737	1.743	1.743	1.753	1.754	1.750	1.753
Fe3	0.003	0.005	0.008	0.007	0.005	0.004	0.003	0.002	0.002	0.005	0.004	0.003	0.003	0.004
Fe2	<0.001	<0.001	<0.001	<0.001	<0.001	<0.001	<0.001	<0.001	0.001	<0.001	<0.001	<0.001	<0.001	<0.001
Ca	0.727	0.721	0.674	0.680	0.699	0.684	0.686	0.690	0.688	0.700	0.708	0.694	0.703	0.717
Na	0.282	0.268	0.306	0.322	0.304	0.299	0.298	0.302	0.292	0.287	0.295	0.302	0.301	0.275
K	0.001	<0.001	0.001	0.001	<0.001	0.001	<0.001	<0.001	<0.001	<0.001	<0.001	<0.001	<0.001	<0.001
Anorthit	0.72	0.73	0.69	0.68	0.70	0.70	0.70	0.70	0.70	0.71	0.71	0.70	0.70	0.72
Albite	0.28	0.27	0.31	0.32	0.30	0.30	0.30	0.30	0.30	0.29	0.29	0.30	0.30	0.28

Sample L112, profil 2								**Sample La2002-05, profil 1**						
distanc	**130**	**140**	**150**	**160**	**170**	**180**	**190**	**0**	**10**	**30**	**40**	**50**	**60**	**70**
SiO2	49.6	49.7	47.6	48.7	49.7	48.9	48.2	47.8	46.8	46.4	47.5	48.1	48.3	46.3
Al2O3	33.0	33.2	31.9	32.8	33.1	32.9	32.4	33.6	34.6	33.57	31.61	33.37	33.48	32.37
Fe2O3	0.07	0.10	0.10	0.18	0.18	0.14	0.31	0.22	0.30	0.26	0.19	0.16	0.13	0.14
FeO	<0.01	<0.01	<0.01	<0.01	<0.01	<0.01	<0.01	<0.02	<0.03	<0.04	<0.05	<0.06	<0.07	<0.08
CaO	15.0	14.9	16.0	15.4	14.9	14.7	14.4	16.35	17.09	16.53	17.57	16.32	15.93	15.39
Na2O	3.11	3.04	2.96	2.95	3.01	3.13	3.10	2.26	1.82	2.14	2.13	2.45	2.61	2.67
K2O	<0.01	0.01	0.02	0.01	<0.01	0.01	0.01	<0.01	<0.01	<0.01	0.01	<0.01	0.02	0.04
Total	100.7	100.9	98.7	100.1	100.8	99.7	98.4	100.2	100.6	99.0	99.0	100.4	100.5	96.9
Si	2.24	2.24	2.20	2.22	2.25	2.23	2.23	2.19	2.13	2.15	2.20	2.19	2.20	2.18
Al	1.76	1.77	1.74	1.76	1.76	1.77	1.77	1.81	1.86	1.83	1.73	1.79	1.79	1.80
Fe3	0.002	0.004	0.004	0.006	0.006	0.005	0.011	0.008	0.010	0.009	0.007	0.006	0.004	0.005
Fe2	<0.001	<0.001	<0.001	<0.001	<0.001	<0.001	<0.001	<0.001	<0.001	<0.001	<0.001	<0.001	<0.001	<0.001
Ca	0.725	0.722	0.794	0.750	0.721	0.719	0.714	0.800	0.835	0.820	0.873	0.796	0.776	0.776
Na	0.273	0.266	0.265	0.261	0.264	0.277	0.278	0.201	0.161	0.192	0.192	0.216	0.230	0.243
K	<0.001	<0.001	0.001	0.001	<0.001	<0.001	0.001	<0.001	<0.001	<0.001	0.001	<0.001	0.001	0.002
Anorthit	0.73	0.73	0.75	0.74	0.73	0.72	0.72	0.80	0.84	0.81	0.82	0.79	0.77	0.76
Albite	0.27	0.27	0.25	0.26	0.27	0.28	0.28	0.20	0.16	0.19	0.18	0.21	0.23	0.24

A2.6d: Plagioclase profils

Sample La2002-05, profil 1

distanc	80	90	110	120	130	140	150	160	170	180	190	200	210	220
SiO2	49.1	49.0	49.4	48.0	49.3	47.6	49.5	49.5	49.7	49.7	49.9	49.9	49.6	49.2
Al2O3	32.9	32.9	32.6	32.4	32.5	32.3	32.6	32.5	32.7	32.5	32.2	32.2	32.4	32.2
Fe2O3	0.19	0.16	0.13	0.07	0.12	0.04	0.08	0.07	0.12	0.10	0.14	0.11	0.05	0.10
FeO	<0.01	<0.01	<0.01	<0.01	<0.01	<0.01	<0.01	<0.01	<0.01	0.02	<0.01	<0.01	<0.01	0.00
CaO	15.6	15.7	15.5	15.1	15.4	15.3	15.2	15.3	15.4	14.9	14.9	14.9	15.1	15.0
Na2O	2.8	2.8	2.9	3.0	2.9	3.1	3.1	2.9	2.9	3.0	3.2	3.3	3.2	3.1
K2O	0.01	<0.01	0.01	0.01	<0.01	0.02	0.01	0.01	0.01	<0.01	0.01	<0.01	<0.01	0.01
Total	100.6	100.5	100.6	98.6	100.2	98.3	100.5	100.3	100.9	100.2	100.3	100.3	100.4	99.6
Si	2.23	2.22	2.24	2.22	2.24	2.20	2.24	2.25	2.25	2.26	2.27	2.26	2.25	2.25
Al	1.76	1.76	1.75	1.77	1.74	1.76	1.74	1.74	1.74	1.74	1.72	1.72	1.73	1.74
Fe3	0.007	0.005	0.004	0.003	0.004	0.002	0.003	0.003	0.004	0.003	0.005	0.004	0.002	0.003
Fe2	<0.001	<0.001	<0.001	<0.001	<0.001	<0.001	<0.001	<0.001	<0.001	0.001	<0.001	<0.001	<0.001	<0.001
Ca	0.761	0.762	0.753	0.749	0.751	0.756	0.740	0.744	0.745	0.724	0.726	0.723	0.735	0.735
Na	0.243	0.249	0.253	0.267	0.257	0.282	0.273	0.259	0.256	0.268	0.278	0.287	0.280	0.277
K	<0.001	<0.001	0.001	0.001	<0.001	0.001	0.001	0.001	<0.001	<0.001	0.001	<0.001	<0.001	<0.001
Anorthit	0.76	0.75	0.75	0.74	0.75	0.73	0.73	0.74	0.74	0.73	0.72	0.72	0.72	0.73
Albite	0.24	0.25	0.25	0.26	0.26	0.27	0.27	0.26	0.26	0.27	0.28	0.28	0.28	0.27

Sample La2002-05, profil 1

distanc	230	240	250	260	270	280	290	300	310	320	330	340	370	380
SiO2	49.6	49.9	50.1	50.0	47.7	49.9	50.0	49.9	50.3	50.4	50.1	50.1	49.8	50.2
Al2O3	32.5	32.5	32.5	31.7	31.1	32.4	32.4	32.3	32.4	31.9	32.3	32.2	32.4	32.4
Fe2O3	0.11	0.10	0.11	0.14	0.14	0.12	0.16	0.12	0.13	0.11	0.07	0.10	0.12	0.06
FeO	0.00	0.00	0.00	0.00	0.00	0.00	0.00	0.00	0.00	0.00	0.00	0.00	<0.01	<0.01
CaO	15.2	14.8	14.8	14.8	14.5	14.9	14.8	15.2	14.8	14.7	14.8	14.8	15.0	15.0
Na2O	3.1	3.1	3.3	3.4	3.1	3.3	3.2	3.2	3.3	3.3	3.2	3.3	3.2	3.3
K2O	0.01	0.00	0.00	0.02	0.07	0.00	0.01	0.00	0.01	0.03	0.00	0.00	<0.01	<0.01
Total	100.5	100.4	100.7	100.1	96.7	100.5	100.6	100.6	100.9	100.5	100.5	100.5	100.4	101.0
Si	2.25	2.26	2.27	2.27	2.25	2.26	2.27	2.26	2.27	2.28	2.27	2.27	2.257	2.263
Al	1.74	1.74	1.73	1.70	1.73	1.73	1.73	1.72	1.72	1.70	1.73	1.72	1.732	1.721
Fe3	0.004	0.004	0.004	0.005	0.005	0.004	0.006	0.004	0.005	0.004	0.003	0.004	0.004	0.002
Fe2	<0.001	<0.001	<0.001	<0.001	<0.001	<0.001	<0.001	<0.001	<0.001	<0.001	<0.001	<0.001	<0.001	<0.001
Ca	0.737	0.718	0.716	0.723	0.734	0.722	0.717	0.736	0.714	0.715	0.717	0.716	0.727	0.722
Na	0.271	0.275	0.285	0.299	0.281	0.286	0.280	0.277	0.291	0.293	0.284	0.292	0.280	0.292
K	0.001	<0.001	<0.001	0.001	0.004	<0.001	0.001	<0.001	0.001	0.002	<0.001	<0.001	<0.001	<0.001
Anorthit	0.73	0.72	0.72	0.71	0.72	0.72	0.72	0.73	0.71	0.71	0.72	0.71	0.72	0.71
Albite	0.27	0.28	0.29	0.29	0.28	0.28	0.28	0.27	0.29	0.29	0.28	0.29	0.28	0.29

A2.6d: Plagioclase profils

Sample La2002-05, profil 1

distanc	390	400	410	440	450	460	470	480	490	500	510	520	530	540
SiO2	49.6	49.4	49.4	49.6	48.8	48.7	48.8	49.2	48.9	49.1	48.9	48.8	49.0	49.1
Al2O3	32.4	32.7	32.9	32.6	32.9	32.9	33.1	32.8	32.9	32.9	33.1	32.7	32.9	32.7
Fe2O3	0.15	0.10	0.10	0.10	0.10	0.09	0.13	0.08	0.17	0.11	0.13	0.14	0.07	0.14
FeO	<0.01	<0.01	<0.01	<0.01	<0.01	<0.01	<0.01	<0.01	<0.01	<0.01	<0.01	<0.01	<0.01	<0.01
CaO	15.2	15.5	15.5	15.3	15.6	15.9	15.8	15.7	15.5	15.7	15.8	15.8	15.6	15.5
Na2O	3.1	2.9	2.9	3.0	2.8	2.7	2.7	2.9	2.9	2.8	2.8	2.8	2.9	3.0
K2O	<0.01	<0.01	<0.01	<0.01	0.03	0.01	0.01	0.01	<0.01	<0.01	<0.01	0.01	<0.01	<0.01
Total	100.5	100.6	100.8	100.5	100.2	100.3	100.5	100.7	100.4	100.5	100.8	100.1	100.6	100.4
Si	2.252	2.240	2.235	2.248	2.225	2.218	2.218	2.230	2.221	2.23	2.2	2.2	2.2	2.2
Al	1.732	1.746	1.757	1.742	1.769	1.766	1.770	1.753	1.762	1.7592	1.7661	1.7579	1.7581	1.7495
Fe3	0.005	0.004	0.004	0.003	0.003	0.003	0.005	0.003	0.006	0.004	0.00	0.00	0.00	0.00
Fe2	<0.001	<0.001	<0.001	<0.001	<0.001	<0.001	<0.001	<0.001	<0.001	<0.001	<0.001	<0.001	<0.001	<0.001
Ca	0.739	0.754	0.752	0.742	0.759	0.775	0.768	0.760	0.757	0.763	0.768	0.769	0.759	0.754
Na	0.272	0.258	0.253	0.264	0.243	0.237	0.240	0.254	0.255	0.244	0.248	0.244	0.258	0.261
K	<0.001	<0.001	<0.001	<0.001	0.002	0.001	<0.001	0.001	<0.001	<0.001	<0.001	<0.001	<0.001	<0.001
Anorthit	0.73	0.75	0.75	0.74	0.76	0.77	0.76	0.75	0.75	0.76	0.76	0.76	0.75	0.74
Albite	0.27	0.26	0.25	0.26	0.24	0.23	0.24	0.25	0.25	0.24	0.24	0.24	0.25	0.26

Sample La2002-05, profil 1								L241, profil 1						
distanc	550	560	570	580	590	600	610	10	20	30	40	50	60	70
SiO2	49.4	46.1	49.6	49.6	49.6	49.5	49.8	48.5	48.5	48.1	48.1	48.1	47.3	48.0
Al2O3	32.8	31.5	32.5	32.6	32.8	32.6	32.4	33.7	33.8	33.5	34.1	33.9	33.5	34.0
Fe2O3	0.07	0.12	0.14	0.12	0.09	0.09	0.08	0.08	0.07	0.11	0.07	0.08	0.09	0.14
FeO	<0.01	<0.01	<0.01	<0.01	<0.01	<0.01	<0.01	<0.01	<0.01	<0.01	<0.01	<0.01	<0.01	<0.01
CaO	15.4	14.8	15.2	15.1	15.2	15.2	15.4	15.7	15.9	16.0	16.1	15.9	15.9	16.07
Na2O	3.0	2.9	3.0	3.0	3.1	3.1	3.1	2.6	2.5	2.46	2.46	2.44	2.57	2.36
K2O	0.01	0.03	0.01	<0.01	0.01	0.03	0.01	0.01	0.03	<0.01	<0.01	<0.01	0.01	0.02
Total	100.7	95.4	100.4	100.4	100.8	100.5	100.7	100.5	100.8	100.2	100.8	100.3	99.4	100.6
Si	2.2	2.2	2.2	2.2	2.2	2.24	2.25	2.203	2.199	2.193	2.180	2.190	2.172	2.182
Al	1.7528	1.7704	1.7411	1.7443	1.7469	1.74	1.73	1.804	1.806	1.803	1.818	1.819	1.814	1.822
Fe3	0.002	0.004	0.005	0.00	0.003	0.003	0.003	0.003	0.002	0.004	0.003	0.003	0.003	0.005
Fe2	<0.001	<0.001	<0.001	<0.001	<0.001	<0.001	<0.001	<0.001	<0.001	<0.001	<0.001	<0.001	<0.001	<0.001
Ca	0.748	0.754	0.738	0.735	0.736	0.741	0.745	0.762	0.773	0.783	0.783	0.774	0.782	0.783
Na	0.259	0.269	0.266	0.268	0.272	0.269	0.269	0.228	0.218	0.218	0.216	0.215	0.229	0.208
K	0.001	0.002	<0.001	<0.001	0.001	0.002	0.001	0.001	0.002	<0.001	<0.001	<0.001	0.001	0.001
Anorthit	0.74	0.74	0.74	0.73	0.73	0.73	0.73	0.77	0.78	0.78	0.78	0.78	0.77	0.79
Albite	0.26	0.26	0.27	0.27	0.27	0.27	0.27	0.23	0.22	0.22	0.22	0.22	0.23	0.21

A2.6d: Plagioclase profils

Sample L241, profil 1

distanc	**80**	**90**	**100**	**110**	**120**	**130**	**140**	**150**	**160**	**170**	**180**	**190**	**200**	**210**
SiO2	47.6	47.8	48.4	47.1	48.1	48.0	48.0	47.9	48.0	48.0	46.6	48.0	47.2	46.7
Al2O3	33.6	33.9	33.8	34.3	33.7	34.1	34.1	33.9	33.9	34.1	32.8	33.5	33.1	32.6
Fe2O3	0.17	0.17	0.15	0.15	0.07	0.14	0.08	0.11	0.14	0.21	0.15	0.17	0.16	0.12
FeO	<0.01	<0.01	<0.01	<0.01	<0.01	<0.01	<0.01	<0.01	<0.01	<0.01	<0.01	<0.01	<0.01	<0.01
CaO	16.1	16.2	16.3	16.3	16.1	16.1	16.1	16.2	16.2	16.1	15.4	15.7	15.7	15.6
Na2O	2.37	2.35	2.47	2.18	2.54	2.49	2.37	2.38	2.49	2.45	2.63	2.71	2.59	2.62
K2O	0.01	0.03	0.02	0.02	0.04	<0.01	<0.01	<0.01	<0.01	<0.01	<0.01	0.02	0.02	0.04
Total	99.9	100.5	101.0	100.1	100.6	100.8	100.6	100.5	100.8	100.9	97.6	100.1	98.7	97.7
Si	2.18	2.18	2.19	2.15	2.18	2.18	2.18	2.18	2.18	2.18	2.18	2.19	2.18	2.18
Al	1.81	1.82	1.80	1.85	1.80	1.82	1.82	1.82	1.81	1.82	1.81	1.80	1.81	1.79
Fe3	0.006	0.006	0.005	0.005	0.003	0.005	0.003	0.004	0.005	0.007	0.005	0.006	0.005	0.004
Fe2	<0.001	<0.001	<0.001	<0.001	<0.001	<0.001	<0.001	<0.001	<0.001	<0.001	<0.001	<0.001	<0.001	<0.001
Ca	0.791	0.790	0.788	0.797	0.785	0.783	0.785	0.788	0.787	0.782	0.773	0.768	0.776	0.783
Na	0.210	0.208	0.216	0.193	0.223	0.218	0.209	0.210	0.219	0.215	0.238	0.239	0.233	0.237
K	0.001	0.002	0.001	0.001	0.003	<0.001	<0.001	<0.001	<0.001	<0.001	<0.001	0.001	0.001	0.002
Anorthit	0.79	0.79	0.78	0.80	0.78	0.78	0.79	0.79	0.78	0.78	0.76	0.76	0.77	0.766
Albite	0.21	0.21	0.22	0.20	0.22	0.22	0.21	0.21	0.22	0.22	0.24	0.24	0.23	0.232

Sample L241, profil 1

distanc	**220**	**230**	**240**	**250**	**260**	**270**	**280**	**290**
SiO2	47.2	48.1	48.6	49.1	49.1	48.5	48.4	48.4
Al2O3	33.5	33.2	33.0	33.4	33.4	33.3	33.6	33.6
Fe2O3	0.12	0.14	0.16	0.18	0.18	0.14	0.14	0.24
FeO	<0.01	<0.01	<0.01	<0.01	<0.01	<0.01	<0.01	<0.01
CaO	16.1	15.8	15.3	15.2	15.3	15.8	15.7	16.0
Na2O	2.40	2.54	2.84	2.87	2.87	2.65	2.64	2.42
K2O	0.04	<0.01	0.01	0.03	<0.01	0.02	0.02	<0.01
Total	99.3	99.8	100.0	100.8	100.9	100.4	100.4	100.6
Si	2.17	2.20	2.22	2.22	2.22	2.21	2.20	2.20
Al	1.82	1.79	1.77	1.78	1.78	1.78	1.80	1.80
Fe3	0.004	0.005	0.006	0.006	0.006	0.005	0.005	0.008
Fe2	<0.001	<0.001	<0.001	<0.001	<0.001	<0.001	<0.001	<0.001
Ca	0.794	0.775	0.750	0.738	0.743	0.769	0.762	0.780
Na	0.214	0.226	0.251	0.252	0.251	0.234	0.233	0.214
K	0.003	<0.001	0.001	0.002	<0.001	0.001	0.001	<0.001
Anorthit	0.79	0.77	0.75	0.75	0.75	0.77	0.77	0.79
Albite	0.21	0.23	0.25	0.25	0.25	0.23	0.23	0.22

A2.7: Thermometry

		Brey and Kholer (2 prx)	Brey and Kholer	witt & eickschen Seck 91		Ballhaus
	n=				n=	
Porphyroclasts core (P=10Kbar)						
hydrous mylonite						
L187d	4		902 ± 7	1032 ± 7	3	944 ± 35
mylonite						
L04	3		956 ± 10	1106 ± 25	3	1136 ± 65
L104	3		951 ± 29	1096 ± 27		
average			*954 ± 4*	*1101 ±7*		
proto-mylonite						
L112	3		1022 ± 18	1080 ± 26	2	992 ± 49
La2002-05	4		1012 ± 4	1045 ± 8	3	1109 ± 4
average			*1017 ± 7*	*1063 ± 25*		*1051 ± 83*
FGSG						
L09	5		944 ± 56	1085 ± 27		
L110	4		995 ± 28	1053 ± 10	4	972 ± 20
average			*970 ± 36*	*1069 ± 23*		
CGSG						
L13	4		969 ± 16	1014 ± 14	2	759 ± 31
L147	4		977 ± 38	1028 ± 39	3	885 ± 21
L241	4		934 ± 13	1049 ± 18	3	1128 ± 5
average			*960 ± 23*	*1030 ± 18*		*924 ± 188*
CGSG north						
W2	3		1010 ± 38	1086 ± 38		
L195	3		996 ± 35	1054 ± 46		
average			*1003 ± 10*	*1070 ± 23*		
Intermediate plateau in porhyroclasts (P=10Kbar)						
proto-mylonite						
La2002-05	3		972 ± 16	967 ± 27		
CGSG central						
L147	4		1005 ± 34	968 ± 11		
L241	4		929 ± 20	992 ± 7		
average			*967 ± 54*	*980 ± 17*		
Porphyroclasts rims (P=5Kbar)						
hydrous mylonite						
L187d	4	770 ± 5	798 ± 6	826 ± 24		
mylonite						
L04	2	918 ± 9	840 ± 36	734 ± 7		
L104	3	805 ± 27	841 ± 35	825 ± 52		
average		*862 ± 80*	*841 ± 1*	*779 ± 65*		
proto-mylonite						
L112	2	841 ± 35	916 ± 33	817 ± 82		
La2002-05	1	868	889	765		
average		*855 ± 19*	*903 ± 19*	*791 ± 37*		

A2.7: Thermometry

		n=	Brey and Kholer (2 prx)	Brey and Kholer	witt & eickschen Seck 91	n=	Ballhaus
Porphyroclasts rims (P=5Kbar)							
FGSG							
	L09	2	843 ± 6	859 ± 42	855 ± 69		
	L110	2	816 ± 54	958 ± 49	919 ± 20		
	average		*830 ± 19*	*909 ± 70*	*887 ± 46*		
CGSG central							
	L13	2	888 ± 76	933 ± 55	895 ± 5		
	L147	4	728 ± 22	956 ± 17	907 ± 11		
	L241	2	810 ± 56	872 ± 18	903 ± 6		
	average		*809 ± 80*	*920 ± 43*	*901 ± 6*		
CGSG north							
	W2	5	805 ± 99	919 ± 49	904 ± 22		
	L195	2	622 ± 1	609 ± 31	632 ± 12		
	average		*714 ± 130*	*764 ± 219*	*768 ± 192*		
Neoblasts (P=5 Kbar)							
hydrous mylonite							
	L187	3	800 ± 25	825 ± 11	693 ± 9	2	631 ± 30
mylonite							
	L04	6	859 ± 16	870 ± 49	737 ± 25	4	774 ± 53
	L104	4	921 ± 18	887 ± 14	798 ± 48		
	average		*890 ± 44*	*879 ± 12*	*768 ± 43*		
proto-mylonite							
	L112	2	776 ± 65	889 ± 12	776 ± 16	4	707 ± 78
	La2002-05	4	836 ± 49	892 ± 37	771 ± 61	3	812 ± 20
	average		*806 ± 42*	*891 ± 2*	*773 ± 3*		*760 ± 74*
FGSG							
	L09	3	947 ± 42	960 ± 17	883 ± 31	4	806 ± 55
	L110	3	828 ± 42	863 ± 34	807 ± 65	4	781 ± 32
	average		*888 ± 84*	*912 ± 69*	*845 ± 54*		*794 ± 18*
opx imp core(ol + liq -> opx + liq) (P=10Kbar)							
mylonite							
	L04	6		851 ± 17	771 ± 21		
	L104	3		913 ± 10	863 ± 2		
	average			*882 ± 44*	*817 ± 65*		
proto-mylonite							
	L112	3		895 ± 14	943 ± 59		
	La2002-05	3		980 ± 18	877 ± 25		
	average			*938 ± 60*	*910 ± 47*		
FGSG							
	L110	5		1071 ± 140	929 ± 17		

A2.7: Thermometry

		n=	Brey and Kholer (2 prx)	Brey and Kholer	witt & eickschen Seck 91
opx imp core(ol + liq -> opx + liq) (P=10Kbar)					
CGSG c					
	L13	5		1009 ± 31	923 ± 15
	L147	4		970 ± 23	964 ± 28
	L241	5		927 ± 58	822 ± 64
	average			*969 ± 41*	*903 ± 73*
CGSGn					
	W2	4		937 ± 70	865 ± 23
	L195	5		957 ± 39	936 ± 61
	average			*947 ± 14*	*900 ± 50*
opx imp rim (ol + liq -> opx + liq) (P= 10 kbar)					
mylonite					
	L104	2		885 ± 8	776 ± 28
proto-mylonite					
	La2002-05	2		896 ± 5	791 ± 10
FGSG					
	L110	5		883 ± 19	813 ± 23
CGSGc					
	L147	4		929 ± 41	826 ± 89
CGSGn					
	L195	5		945 ± 31	901 ± 103
opx imp (cpx + liq -> opx + plg) (P=10Kbar)					
hydrous-mylonite					
	L187	3		977 ± 216	1066 ± 25
FGSG					
	L09	5		946 ± 33	1019 ± 94
CGSGc					
	L13	5		977 ± 29	1073 ± 70
CGSGn					
	L195	5		900 ± 33	1223 ± 28

A2.8a: structural data set from northern and central part

stop	foliation		layering		lineatio	mafic dikes		stop	foliation		layering		lineatio	mafic dikes	
	strike	*dip*	*strike*	*dip*	*strike*	*strike*	*dip*		*strike*	*dip*	*strike*	*dip*	*strike*	*strike*	*dip*
L1	20	90			110			**L61**					20		
L2	15	68	15	68				**L63**			165	30			
L3	35	90				145	90	**L69**			200	17			
L4	10	85	10	85		20	84	**L70**			180	15			
L5	25	90	200	60	110			**L72**			110	38			
L6	25	90	30	80		25	90	**L74**	75	85	75	85			
L7	35	73	35	73				**L75**	70	80				165	90
L8	45	78	45	78				**L78**	40	82	55	82			
L9	45	74						**L79**	20	71	20	71			
L10	43	61	43	60	135			**L80**	40	75	40	75			
L11					100			**L81**	25	62	25	62			
L12					115			**L82**	10	60	10	60			
L13			110	38	120	300	52	**L83**	30	60					
L14			110	38				**L84**	5	65	5	65			
L15	65	90	105	52				**L85**	35	82	40	56			
L17			20	85				**L86**	25	65					
L18			45	90				**L87**	200	76	10	95			
L19	60	90	60	90				**L88**	190	82	10	85			
L20	30	80						**L89**	10	85					
L21	50	90						**L90**	20	90					
L22	333	28						**L91**	15	70					
L23	160	90						**L92**	35	60	35	60			
L24			115	22					30	80	30	70			
L27			35	24				**L93**	10	86					
L28			255	15				**L95**	220	50					
L30	80	75	80	75		328	80	**L96**	220	65	220	77			
						135	90	**L97**	35	85	35	85			
L31						328	82	**L98**			45	80			
L32	45	80	45	80				**L99**	45	77	45	77			
L33	65	90	65	90	155			**L102**	80	90					
L34	65	90			155			**L103**	20	90					
L35	90	90	90	90				**L104**	200	80					
L36	15	60	15	60				**L105**	15	80					
L37			235	81				**L106**	35	75	35	60			
L38			25	65				**L107**	195	85					
L39			105	60		25	44	**L108**	215	50					
L40			95	66				**L109**	235	65					
L41	80	55	80	55				**L110**			60	90			
L42	80	65	80	65		80	65	**L111**			25	75			
L43			80	66		350	90	**L112**	40	85					
L44			80	60		355	58	**L113**	70	90	70	90			
L45	65	70	65	70				**L115**	70	85					
L46						344	74	**L117**	70	90					
L48	100	45	100	45	10			**L118**	45	85	60	50			
L49	25	65						**L119**	20	90					
L50	125	90			35	35	65	**L120**	15	90					
L51						355	60	**L121**	45	85					
L53	75	90						**L122**	45	90					
L54					40			**L123**	40	90					
L55	130	70						**L124**	30	90				130	90
L56	170	90	80	39	80			**L125**	215	85				270	60
L57	70	90						**L126**	65	90	65	90			
L58	70	90						**L127**	65	90	65	90			
L59	50	80						**L128**	60	70	60	70			
L60	45	60	45	60	135			**L130**	50	90					

stop	strike foliation	dip	strike layering	dip	line	strike dikes	dip
L131	25	90					
L132	150	85				305	90
L133	130	85	130	85			
L134	305	90					
L135	155	46					
L136	250	56	250	56			
L137			10	85		140	90
L138	70	90	70	90		90	90
L139	295	70	295	70			
L140						325	40
L141	35	75					
L142	60	75					
L143	55	90	55	90		60	90
L144	65	85	65	85			
L145	35	65					
L146	55	90					
L147	60	70					
L148	75	80					
L149	75	70					
L150	50	65					
L151	70	90					
L152	55	85	55	85			
L154	70	90					
L155	80	90	80	90		70	72
						170	85
L156	25	90					
L157	35	90					
L158	60	90				145	90
L159	60	75					
L160	40	75	40	75		55	90
L161	80	90				130	90
						60	65
L162							
L163	65	65	65	65			
L164	60	50	60	50			
L165	80	85	80	85		20	65
						20	90
L166			255	70			
L167	80	90					
L168	260	75					
L169	215	40					
L170	65	65					
L171	45	80					
L172	245	85					
L173	40	70				340	85
L174	45	75	45	75			
L175	70	50	70	50			
L176							
L177			105	80			
L178							
L179	100	68				345	45
L180							
L181	70	60					
L182							
L183	90	80					
L184	5	75			95		
L185	80	60	80	60			

stop	strike foliation	dip	strike layering	dip	line	strike dikes	dip
L186	225	75					
	205	75					
L187	90	90					
	130	85	120	90			
	140	90					
L188			60	10	35		
L189					115		
L191			195	45			
L192					90		
L193	90	90			30		
L194			45	20			
L195	330	20	330	20	65		
L197	160	70					
L198	160	90					
L203					5		
L205	75	55					
L206	310	70					
L207	35	35					
L208	35	75					
L210	0	80					
L211	40	60					
L212	225	50					
L213	30	80			120		
L215	5	40					
L217	58	85					
L218	15	89	45	50			
L219	27	86	51	57	115		
L220	205	71	46	65			
L221	24	80					
L222	37	80	64	56	155		
L223	27	74					
L224	33	85	62	53			
L225	36	89					
L227	45	85	67	59	125		
L228	75	65	75	65			
L229	74	50					
L230	45	75	78	45		305	73
			100	50	230		
L233	215	75					
L234	195	64					
L235	20	89					
L238	285	89					
L240	172	61					
L241	63	69	64	58			
L242	45	80	74	54			
L243	61	70	75	59			
L244			71	71			
L245	250	69					
L246	55	85	75	69			

A2.8b: structural data set from southern part

Stop	foliation		layering		lineatic	mafic dikes		Stop	foliation		layering		lineatic	mafic dikes	
	direction	*dip*	*direction*	*dip*		*direction*	*dip*		*direction*	*dip*	*direction*			*direction*	*dip*
A1	120	60			10			**A56**	135	30				350	80
A2								**A57**	190	55			80	185	40
A3	140	80	140	80		25	80	**A58**	70	25				215	45
A4	355	25				15	70	**A59**	180	20				255	75
	110	50						**A60**	205	40			115	215	85
A5	145	85				15	70							20	85
						15	78	**A61**						215	70
						185	78	**A62**	10	80				65	60
A6	145	55						**A63**	175	40					
A7	115	45						**A64**	65	60				210	60
A8								**A65**	130	75				220	80
A9	35	55				35	40	**A66**						210	90
A10	135	65						**A67**	115	75				265	20
A11	210	80				205	80							240	55
A12	125	75						**A68**	120	65					
A13	145	48						**A69**						25	85
A14	150	75						**A70**	75	30				300	65
A15	160	77						**A71**						330	75
	135	45						**A72**						290	80
A16								**A73**	345	70					
A17								**A74**							
A18	130	50				35	55	**A75**	15	90					
A19	50	45				225	30	**A76**	185	85					
A20								**A77**						165	40
A21	290	80						**A78**	175	50					
A22	150	55			100			**A79**	215	45			90		
A23									165	35					
A24								**A80**	215	60					
A25						210	75	**A81**							
A26					20			**A82**	190	85					
A27	195	70						**A83**	200	85					
A28								**A84**	85	45					
A29								**A85**	145	75					
A30			330	80	60			**A86**	215	35					
A31	55	90				60	90	**A87**	20	90					
A32	70	90				220	40	**A88**	215	85					
A33								**A89**	115	35				15	75
A34								**A90**	145	0				115	90
A35	235	45						**A91**	155	70					
A36															
A37								**A92**			105	45		65	75
A38								**A93**	135	40					
A39								**A94**					20	120	90
A40			155	80				**A95**	120	45				170	90
A41			150	70		130	90	**A96**							
A42			265	70		185	95	**A97**	145	75					
						270	20	**A98**							
A43					90			**A99**							
A44	165	90						**A100**							
A45	170	70						**A101**	170	15				210	90
A46	330	75	305	60		245	65	**A102**							
A47								**A103**							
A48	350	30													
A49	315	90													
A50	180	25													
A51	20	80			165										
A52															
A53	175	65													
A54	265	65													
A55	240	90			80										

APPENDIX 3

DIKES AND ZIRCON

Annexe A3.1: Layering outcrops

A3.2b: from the central part of the massif

Outcrop L05, Gran Costa

L88, Pian della Copa

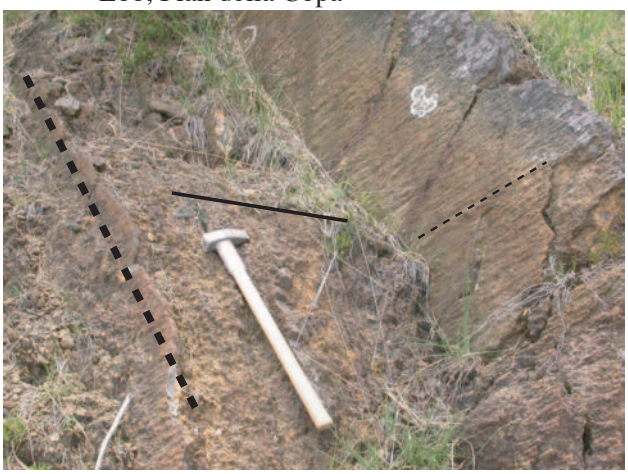

L220, Grange di Germagnano

L165, north of Maddalene

layering
foliation
lineation

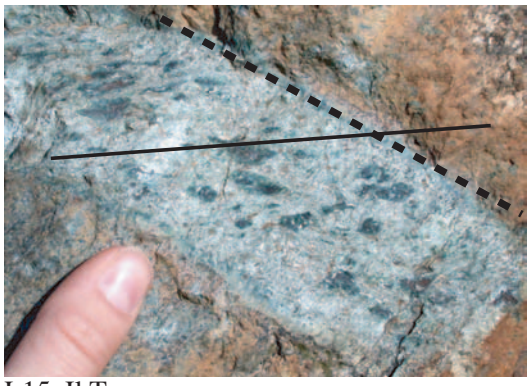

L15, Il Turu

L187, Fasa bela

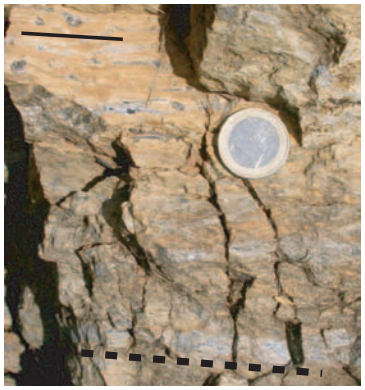

L04, Gran Costa

L08, Gran Costa

Annexe A3.2: dikes outcrops

A3.2a: dikelets from the central part of the massif

L31, Pte Barolo

L31, Pte Barolo

L161, Mionda

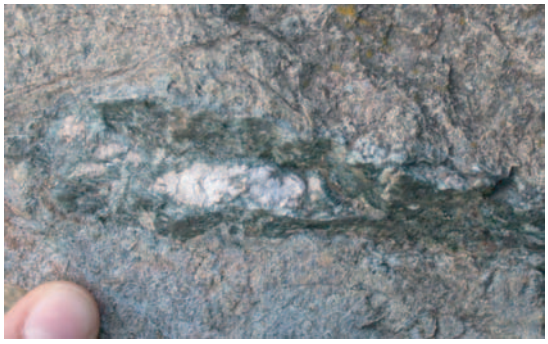

L51, Il Diazo

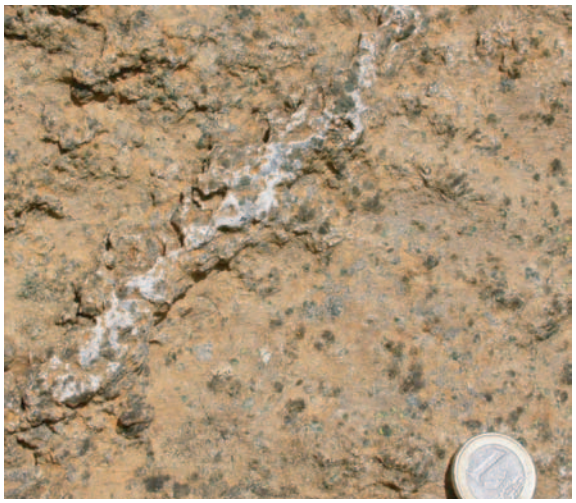

Monte Colombano

L165, north Maddalene

Annexe A3.2: dikes outcrops

A3.2b: gabbros from the southern part of the massif

A19, East of Alpi prato Pare

A64, south of Mte Cuo

dunite dunite lherzolite

A42, Alpi prato Pare

▬ ▬ ▬ layering

A79, North of Montecopretto

A91, NW Monte Musine

A91

A91

Annexe A3.2: dikes outcrops

A3.2c: basaltic dikes

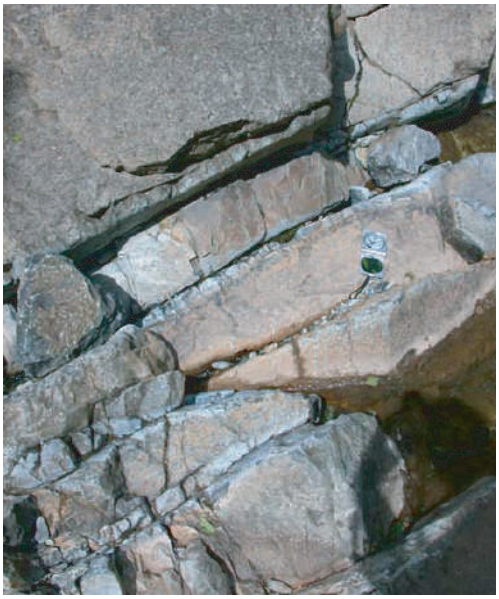

L59, south of Tese village

L153, Traves

L91, Gran Costa

L165, north Maddalene

V14, Muanda piantegrandi

V14, Muanda piantegrandi

Annexe A3.3: SEM picture of zircon

A165

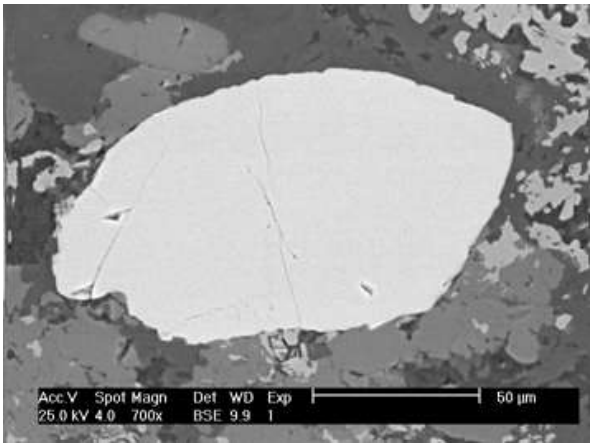

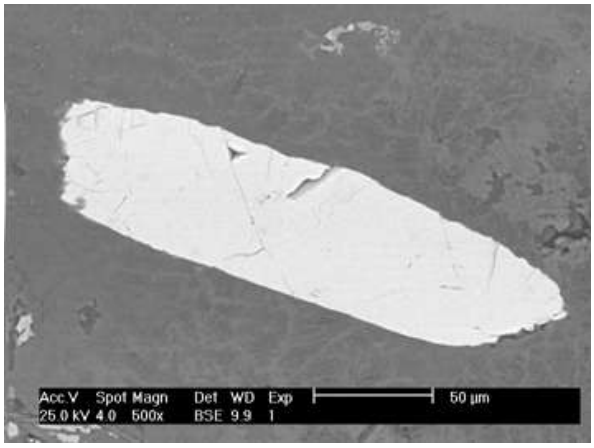

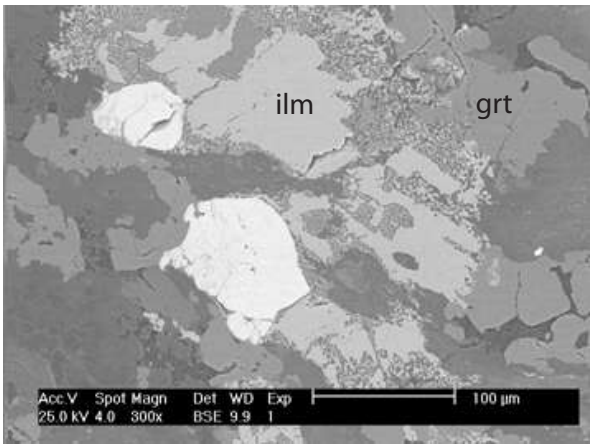

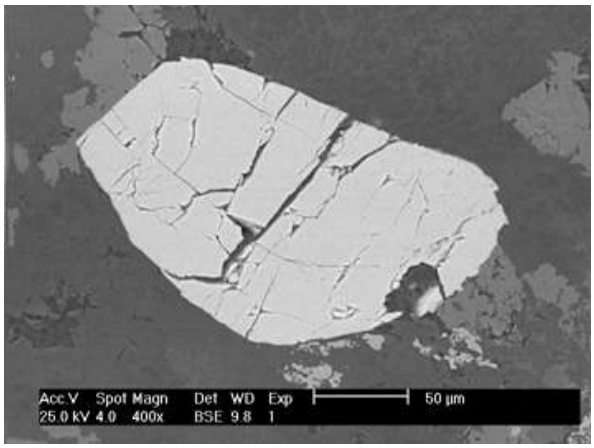

A71

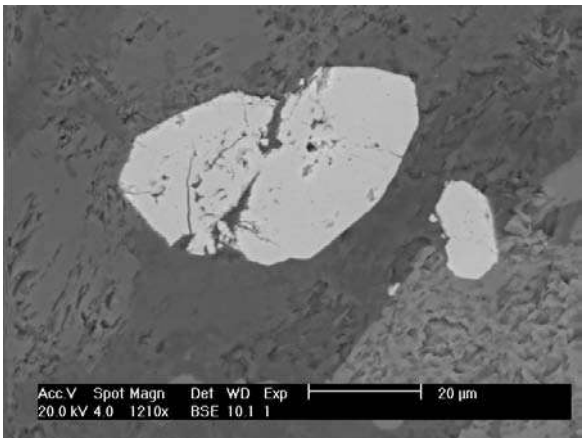

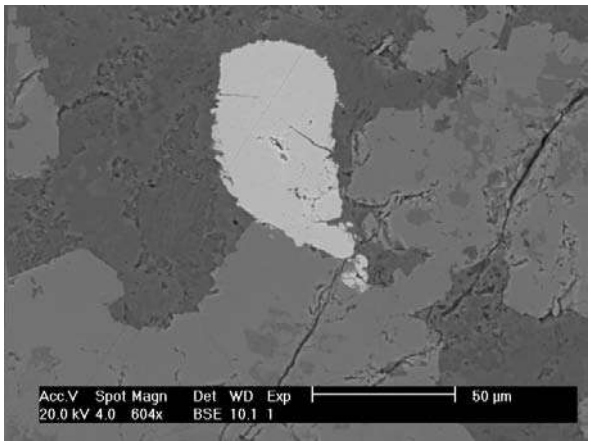

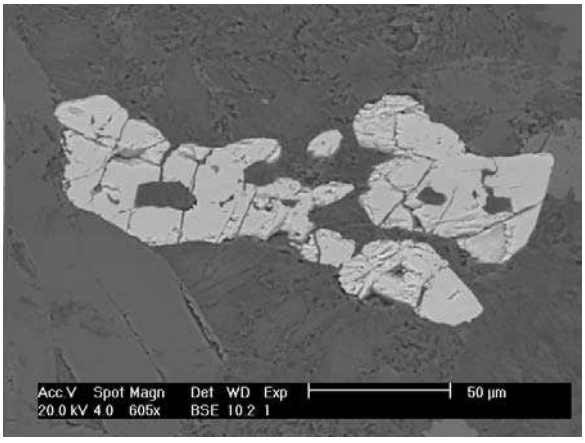

Annexe A3.3: SEM picture of zircon

A91

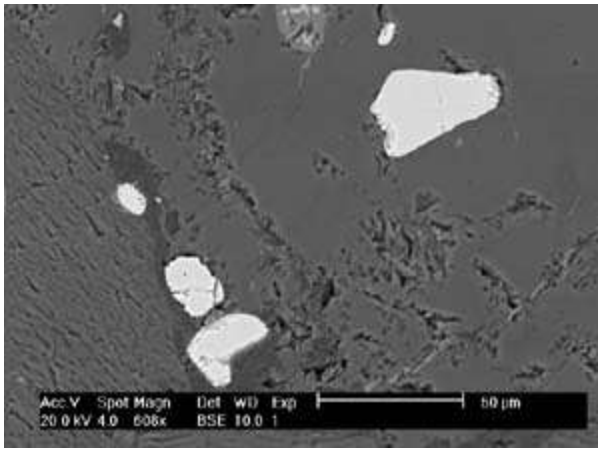

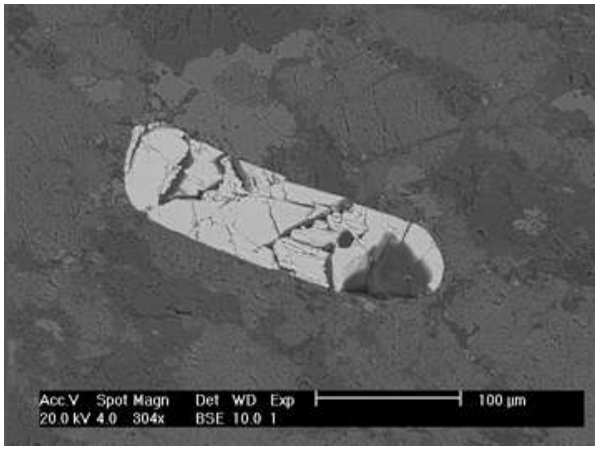

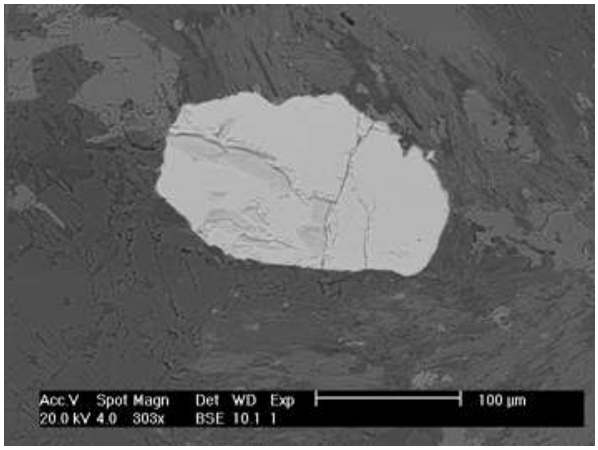

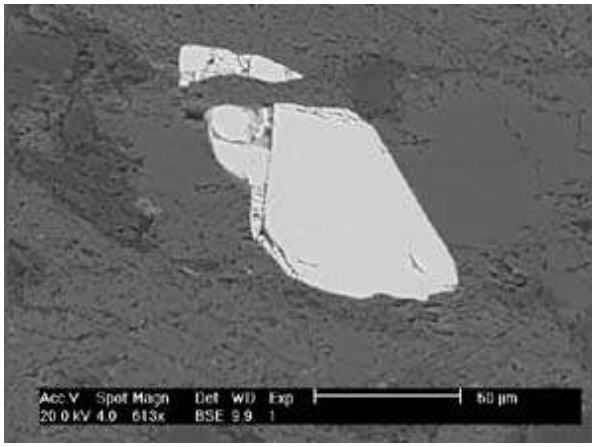

Annexe A3.4: Cathodo-luminscence zircon picture

A3.4a: L165

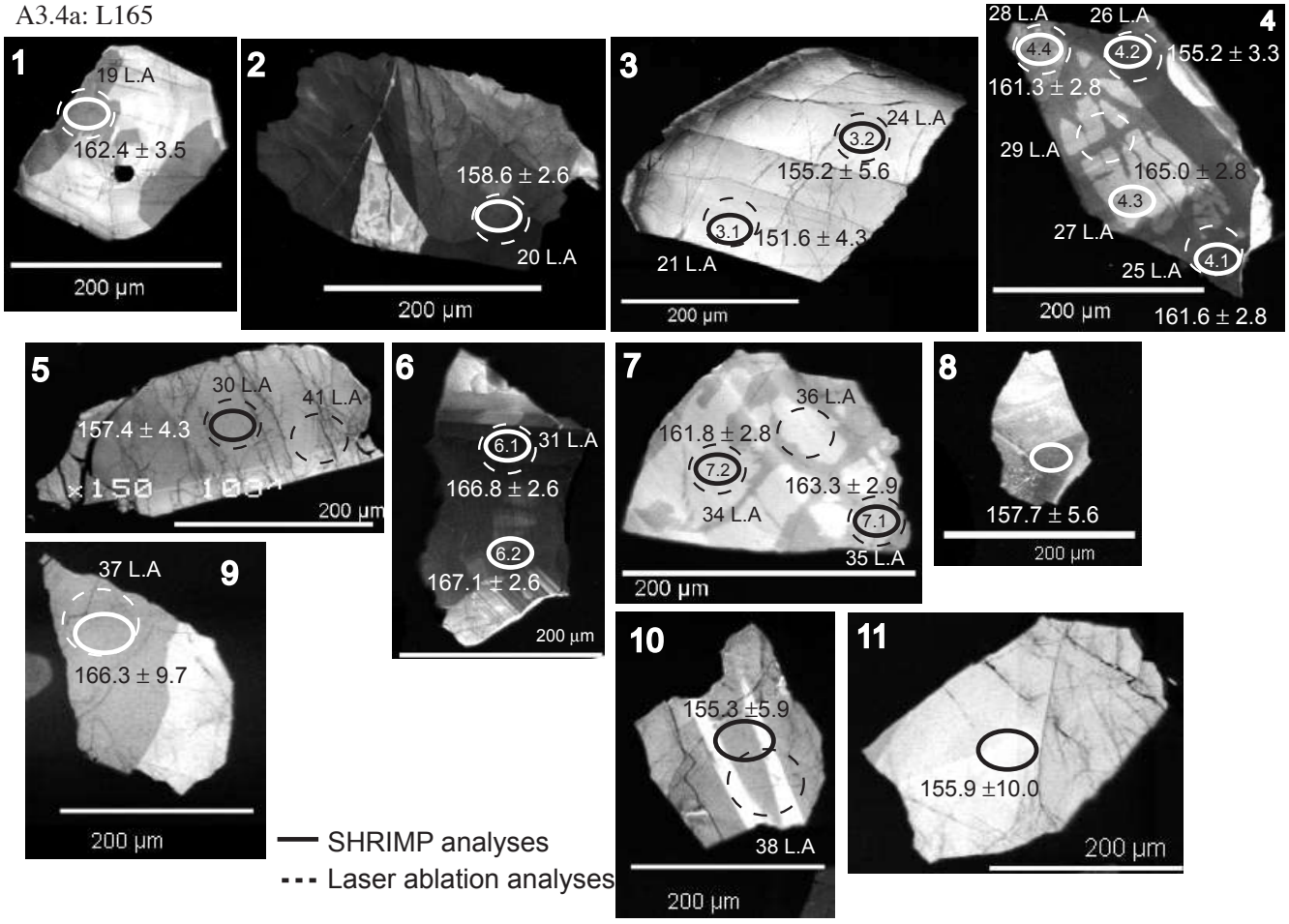

A3.4b: A71

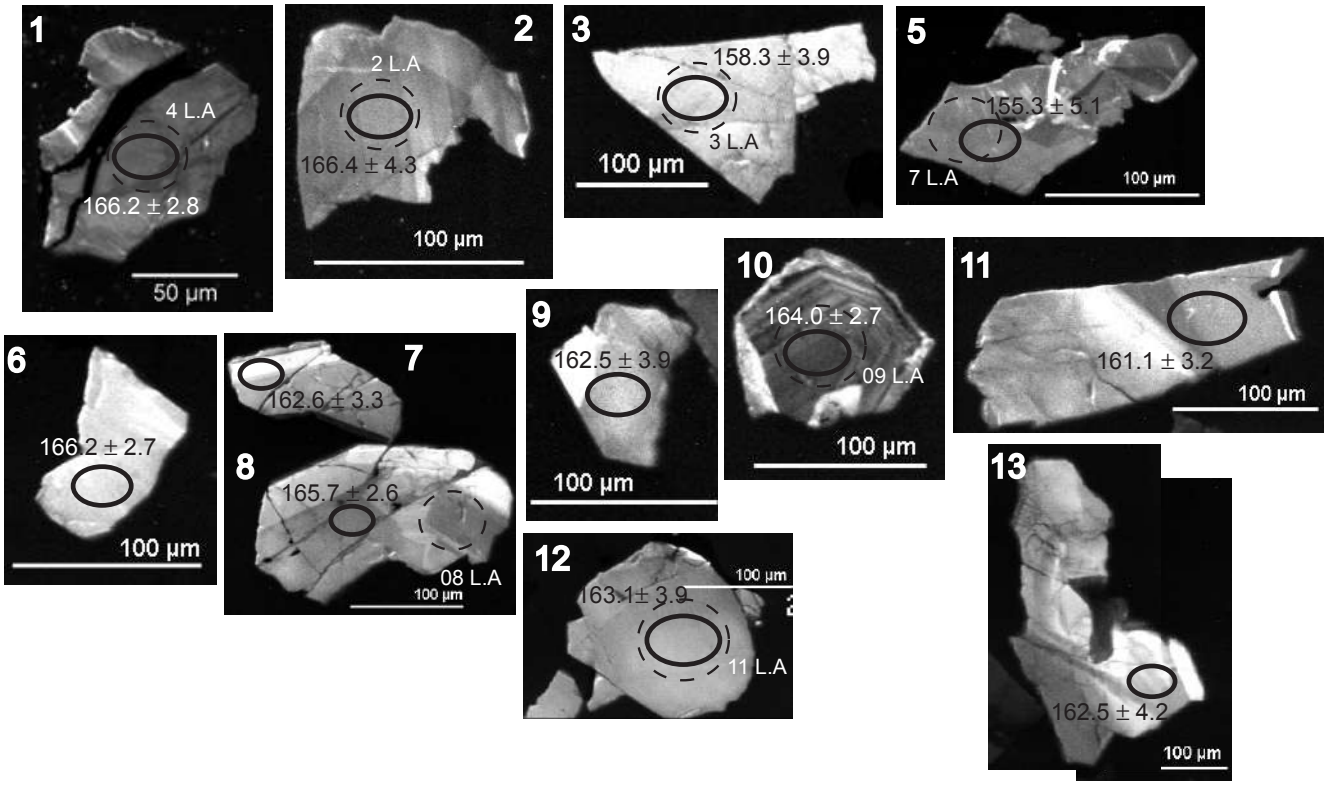

Annexe A3.4: Cathodo-luminscence zircon picture

A3.4c: A91

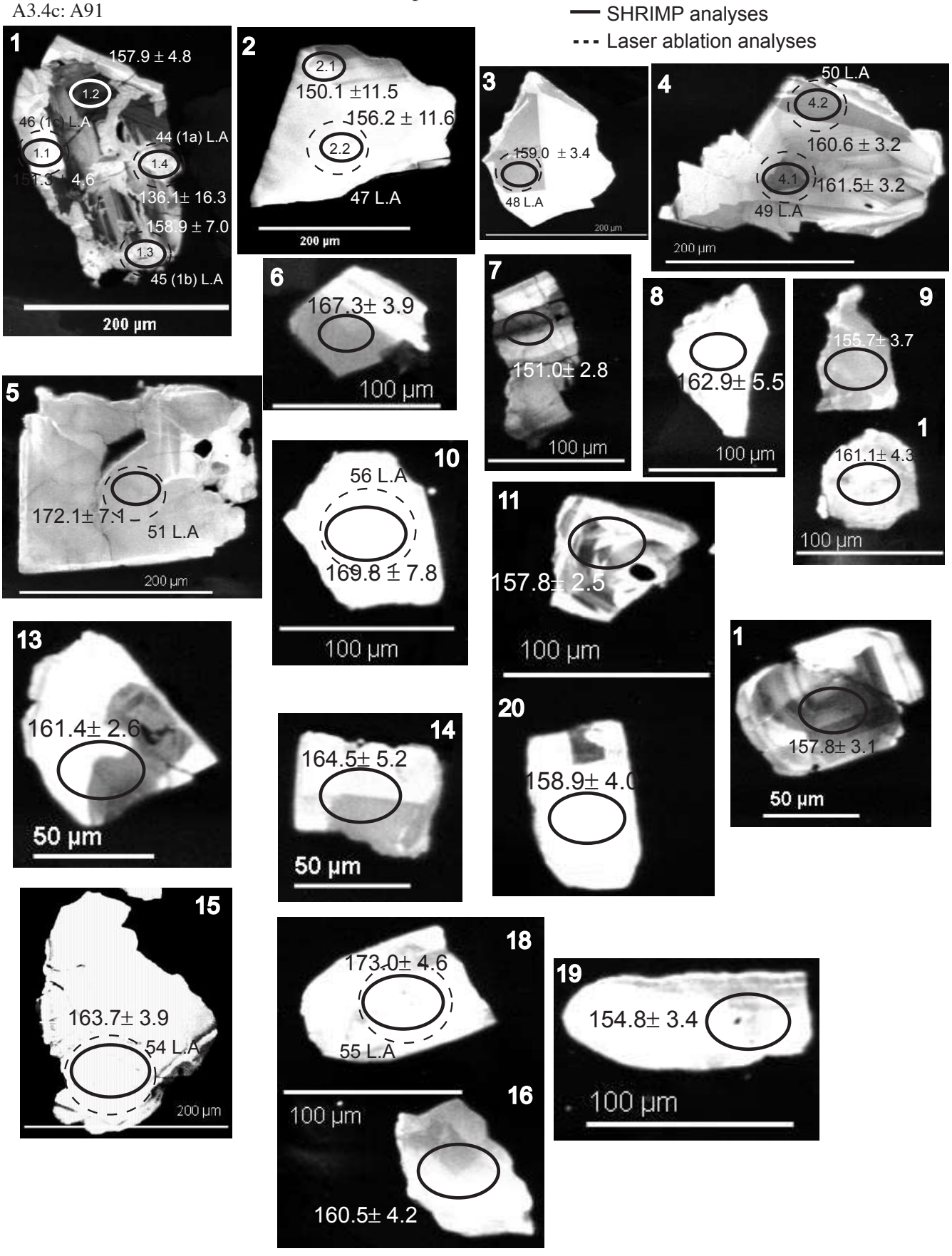

APPENDIX 4

ZIRCON OF GRANULITE (B11) (CD)

APPENDIX 5

PUBLICATION AND SELECTED COMMUNICATION (CD)

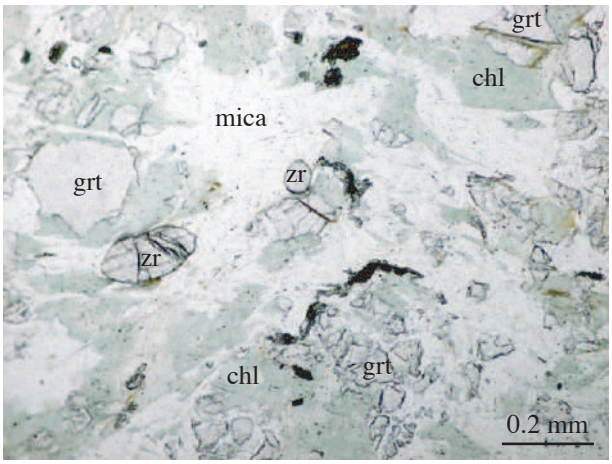
grt
chl
mica
grt
zr
zr
chl
grt
0.2 mm

Annexe A4.2: Cathodo-luminscence zircon picture, sample B11

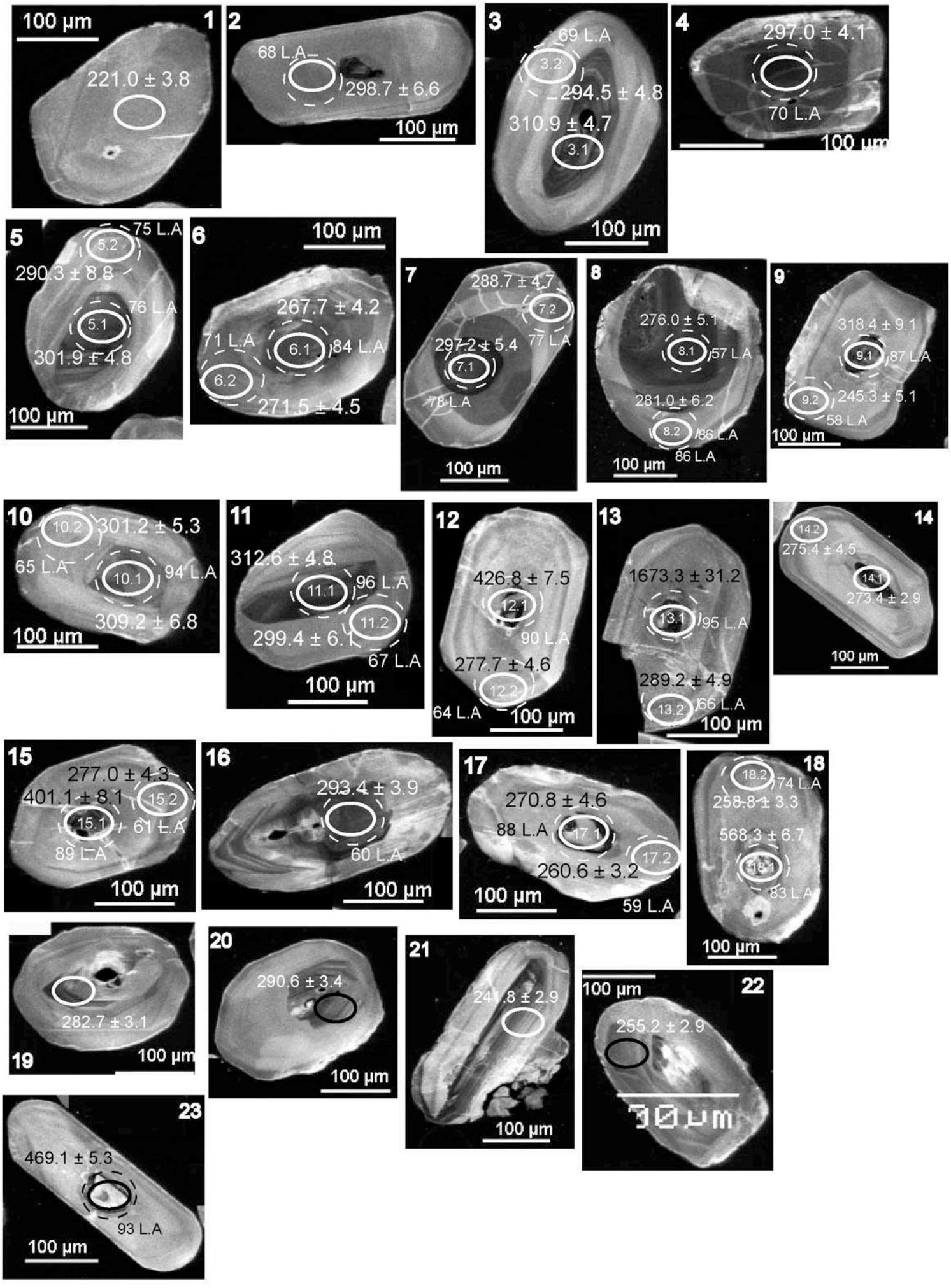

B11	**P**	**Ti**	**Sr**	**Y**	**Nb**	**La**	**Ce**	**Pr**	**Nd**	**Sm**	**Eu**	**Gd**	**Tb**	**Dy**
B118	2905	61	0.9	3245	13	bdl	6	0.31	10.4	48.6	3.3	338	104	693
B119	1904	103	0.9	3657	8	bdl	13	0.31	7.9	24.6	1.1	128	42	432
B119	1886	103	0.9	3650	8	bdl	13	0.31	7.9	24.6	1.1	128	42	431
B1115	247	13	0.1	194	1	0.01	1	0.02	0.5	1.3	0.1	8	3	26
B1112	1810	109	1.0	2901	10	bdl	15	0.36	8.5	21.8	1.0	116	36	365
B116	2010	127	1.1	4028	14	bdl	18	0.38	9.5	23.7	1.7	132	45	475
B1118	225	15	0.1	280	1	bdl	1	0.04	0.8	2.0	0.1	13	4	39
B116	579	12	0.2	650	2	bdl	2	0.12	2.4	5.8	0.2	25	7	75
B118	296	14	0.1	220	1	0.02	1	0.03	0.7	2.0	0.2	11	3	31
B1113	1841	96	0.9	2992	8	bdl	13	0.42	8.0	21.3	1.0	106	36	366
B1111	1327	123	0.9	3836	10	bdl	15	0.41	8.6	25.5	1.7	149	52	512
B112	1914	106	0.8	3076	11	bdl	17	0.43	10.2	32.9	1.9	155	48	432
B113	1873	112	0.9	4471	8	bdl	14	0.50	9.9	31.6	1.7	164	53	553
B115	345	12	0.2	405	1	0.01	1	0.04	1.0	3.1	0.1	16	5	48
B117	1279	116	0.7	3166	10	bdl	12	0.40	7.4	21.8	1.5	134	45	441
B1110	1354	116	0.8	3086	11	bdl	13	0.35	7.9	22.7	1.6	135	46	435
B1116	3824	128	17.8	8055	14	0.16	19	0.95	16.9	44.0	2.4	239	80	869
B113	1074	14	0.3	1391	3	0.02	3	0.21	3.9	8.6	0.5	47	14	159
B1110	470	16	0.1	412	2	bdl	2	0.066	1.301	3.4	0.1	16	5	49
B1111	1050	17.33	0.3	1326.3	2	bdl	3	0.216	4.1	8.9	0.5	43	13.05	142.8
B115	6212	143	2.0	14984	22	0.24	31	1.77	38.2	89.2	4.7	458	150	1623
B117	3221	103	1.1	3335	13	bdl	11	1.13	28.9	128.3	4.8	624	149	803
B114	19653	66	4.0	46079	14	bdl	2	0.27	9.1	44	11.3	522	363	5557
B1118	919	13	0.9	1697	7	bdl	55	0.10	1.7	4.8	1.0	27	10	141
B1113	521	31	0.7	1389	8	0.20	29	0.10	1.5	4.5	0.9	32	11	133
B119	388	11	0.2	269	1	0.05	0.3	0.03	0.5	1.2	0.1	7	3	34
B1117	689	11	0.6	459	2	0.05	1	0.03	0.6	1.3	0.2	8	3	44
B11_15	239	12	0.7	435	2	0.04	10	0.02	0.4	0.7	0.2	5	2	31
B11_12	281	10	0.3	516	4	0.02	59	0.06	1.1	2.3	0.8	10	3	41
B11_23	264	10	0.2	328	1	bdl	10	0.09	1.4	2.3	1.1	9	3	32

Grain spot	U (ppm)	Th (ppm)	Th/U	Pb* (ppm)	Pb comm 206 %	uncorrected 207Pb/206Pb	uncorrected 238U/206Pb	206Pb/238U ± (1)	**ages (Ma) 206Pb/238U 208 cor**	CL structure
B11.1.1	153	48	0.32	4.6	0.14	0.056 ±2	28.6 ±0.5	0.0349 ±6	**221 ± 4**	external rim
B11-21.1	430	165	0.38	14.1	0.12	0.052 ±1	26.1 ±0.3	0.0383 ±4	**242 ± 3**	external rim
B11.9.2	190	52	0.27	6.4	0.24	0.053 ±1	25.7 ±0.5	0.0389 ±8	**245 ± 5**	external rim
B11-22.1	463	208	0.45	16.1	0.01	0.053 ±1	24.8 ±0.3	0.0404 ±4	**255 ± 3**	external rim
B11-18.2	165	50	0.30	5.8	0.21	0.053 ±1	24.4 ±0.3	0.041 ±5	**259 ± 3**	external rim
B11-17.2	170	45	0.26	6.0	0.03	0.053 ±1	24.2 ±0.3	0.0413 ±5	**261 ± 3**	external rim
B11.6.1	371	144	0.39	13.5	-0.18	0.052 ±1	23.6 ±0.4	0.0423 ±6	**268 ± 4**	external rim
B11.6.2	165	47	0.29	6.1	0.02	0.056 ±1	23.2 ±0.4	0.040o ±7	**272 ± 5**	external rim
B11-14.2	209	56	0.27	7.8	0.08	0.053 ±2	22.9 ±0.4	0.0437 ±7	**275 ± 4**	external rim
B11.8.1	619	13	0.02	23.3	0.07	0.052 ±1	22.8 ±0.4	0.0438 ±8	**276 ± 5**	external rim
B11-15.2	223	56	0.25	8.4	0.16	0.053 ±1	22.7 ±0.3	0.0440 ±7	**277 ± 4**	external rim
B11.12.2	174	52	0.30	6.6	0.03	0.056 ±1	22.7 ±0.4	0.0440 ±8	**278 ± 5**	external rim
B11.8.2	190	56	0.29	7.3	0.10	0.052 ±2	22.4 ±0.5	0.0446 ±10	**281 ± 6**	external rim
B11.7.2	182	52	0.29	7.2	0.08	0.055 ±1	21.8 ±0.3	0.0458 ±7	**289 ± 5**	internal rim
B11.13.2	137	44	0.32	5.4	0.10	0.053 ±1	21.8 ±0.4	0.0459 ±8	**289 ± 5**	internal rim
B11.5.2	177	54	0.31	7.0	-0.17	0.052 ±1	21.7 ±0.6	0.0460 ±14	**290 ± 9**	internal rim
B11.3.2	185	51	0.28	7.4	0.37	0.051 ±1	21.3 ±0.3	0.0469 ±7	**295 ± 5**	internal rim
B11.2.1	225	72	0.32	9.2	0.08	0.052 ±1	21.1 ±0.5	0.0475 ±10	**299 ± 7**	internal rim
B11.11.2	183	52	0.28	7.5	-0.01	0.054 ±1	21.0 ±0.4	0.0475 ±9	**299 ± 6**	internal rim
B11.10.2	158	52	0.33	6.7	0.26	0.054 ±2	20.3 ±0.4	0.0493 ±10	**309 ± 7**	internal rim
B11-16.1	542	233	0.43	21.7	0.30	0.055 ±1	21.4 ±0.3	0.0467 ±6	**293 ± 4**	external core
B11-19.1	549	216	0.39	21.2	0.23	0.053 ±1	22.3 ±0.2	0.0449 ±5	**283 ± 3**	external core
B11-20.1	422	157	0.37	16.8	0.20	0.053 ±2	21.6 ±0.2	0.0462 ±5	**291 ± 3**	external core
B11.4.1	920	6	0.01	37.3	0.00	0.053 ±3	21.2 ±0.3	0.0471 ±7	**297 ± 4**	external core
B11.7.1	964	41	0.04	39.1	-0.01	0.054 ±1	21.2 ±0.4	0.0472 ±9	**297 ± 5**	external core
B11.10.1	332	160	0.48	13.7	0.48	0.056 ±1	20.8 ±0.3	0.0481 ±8	**301 ± 5**	external core
B11.5.1	441	179	0.41	18.1	-0.16	0.052 ±1	20.9 ±0.3	0.0479 ±7	**302 ± 5**	external core
B11.3.1	629	305	0.48	26.7	0.01	0.052 ±1	20.2 ±0.3	0.0494 ±7	**311 ± 5**	external core
B11.11.1	660	327	0.50	28.2	0.09	0.053 ±1	20.1 ±0.3	0.0497 ±7	**313 ± 5**	external core
B11.9.1	819	17	0.02	35.6	-0.04	0.079 ±8	19.8 ±0.6	0.0506 ±15	**318 ± 9**	inherited core
B11-17.1	801	58	0.07	40.8	0.12	0.057 ±1	16.9 ±0.2	0.0593 ±8	**371 ± 5**	inherited core
B11-15.1	894	138	0.15	49.4	0.09	0.059 ±1	15.6 ±0.3	0.0643 ±13	**401 ± 8**	inherited core
B11.12.1	1249	774	0.62	75.2	2.30	0.058 ±1	14.3 ±0.2	0.0701 ±11	**427 ± 8**	inherited core
B11-23.1	350	108	0.31	22.7	0.20	0.056 ±2	13.2 ±0.1	0.0756 ±8	**469 ± 5**	inherited core
B11-18.1	394	201	0.51	31.8	1.79	0.062 ±1	10.7 ±0.1	0.0938 ±10	**568 ± 7**	inherited core
B11.13.1	689	252	0.37	176.0	0.40	0.170 ±2	3.4 ±0.1	0.2976 ±60	**1673 ± 31**	inherited core

B11

Ho	Er	Tm	Yb	Lu	Hf	Ta	Th	U	Th\U	Eu/Eu*
106	221	26	170	21	148823	17.79	144	6986	0.02	0.017
122	378	58	397	46	127925	3.91	531	1982	0.27	0.015
121	377	58	396	46	127481	3.91	529	1979	0.27	0.015
6	17	2	15	2	10793	0.54	39	151	0.26	0.017
95	294	45	311	38	126930	4.67	558	1755	0.32	0.014
131	453	82	684	102	129684	6.12	760	2263	0.34	0.021
9	23	3	16	2	10857	0.57	44	141	0.31	0.016
21	76	13	101	15	9884	0.75	127	324	0.39	0.015
7	22	3	21	3	10461	0.50	49	163	0.30	0.024
96	300	44	297	35	128530	4.21	482	1891	0.26	0.015
122	319	41	254	28	128065	5.26	499	1635	0.31	0.020
98	280	41	289	36	125459	5.40	775	2388	0.32	0.020
145	457	69	455	54	131138	3.67	533	1910	0.28	0.017
14	49	8	58	8	11222	0.38	49	155	0.32	0.011
99	252	32	188	21	131078	4.54	469	1639	0.29	0.019
99	245	29	178	20	128412	5.28	517	1708	0.30	0.021
260	958	180	1584	237	120370	5.76	1092	3016	0.36	0.017
47	185	35	279	45	9366	1.02	286	553	0.52	0.017
13	46	8	66	10	9850	0.77	115	246	0.47	0.013
43	166	31	260	40	9117	0.9298	202	449	0.45	0.018
486	1814	337	2910	434	113837	8.30	2484	5663	0.44	0.017
113	216	26	160	20	144819	8.03	770	8042	0.10	0.013
1567	5200	864	6458	860	144385	19.07	51	10448	0.00	0.040
55	285	68	680	121	10541	2.57	249	392	0.64	0.063
46	209	46	428	74	9212	2.31	655	1267	0.52	0.049
9	34	7	56	9	11777	0.44	18	700	0.03	0.032
15	74	19	203	38	10295	1.90	32	593	0.05	0.038
13	76	21	245	52	10266	0.91	118	713	0.17	0.067
15	78	20	214	42	9415	1.45	729	693	1.05	0.122
11	52	12	122	23	9890	0.51	70	132	0.53	0.187

EXHUMATION OF MANTLE LITHOSPHERE: FIELD RELATIONS, AND INTERACTION PROCESSES BETWEEN MAGMATISM AND DEFORMATION (FIELD TRIP TO THE NORTHERN LANZO PERIDOTITE)

Mary-Alix Kaczmarek*,**,✉** and **Othmar Müntener******

** Institute de Géologie, Université de Neuchâtel, Rue Emile Argand 11, CH-2007 Neuchâtel, Switzerland.*
*** Institute of Geological Sciences, University of Bern, Baltzerstr. 1-3, CH-3012 Bern, Switzerland*
✉ *Corresponding author, email: othmar.muntener@geo.unibe.ch.*

Keywords: *Lanzo peridotite, melt migration, deformation, ophiolites, granulites. Western Alps.*

ABSTRACT

The Lanzo peridotite plays a key role in exploring the effects of deformation and magmatism in a system evolving from rifting to sea floor spreading. In this field guide we present new field observations, structural and petrological data that constrain the exhumation evolution of the northern Lanzo peridotites during the opening of the Piemonte Ligurian ocean. Gabbroic dikes ranging from troctolite to gabbronorite to oxide gabbros and plagiogranites indicate fractionation of mafic magmas in a relatively thick thermal lithosphere. This lithosphere was thinned by a large shear zone separating different mantle domains. The thermal evolution of the shear zone is recorded by porphyroclastic to mylonitic plagioclase peridotites. Later, at least parts of the mantle rocks were exhumed to the ocean floor, as indicated by widespread serpentinization, rodingitization of mafic dikes, local occurrences of ophicarbonates and metabasalts. Possible origins of crustal remnants (pre-alpine granulite) within the serpentinites are discussed.

GEOLOGICAL OVERVIEW

The Lanzo peridotites are part of the high-pressure belt of the Western Alps (Fig. 1), which was formed during Upper Cretaceous - Early Tertiary subduction along the Eastern border of the Liguria-Piemonte Ocean and which includes other eclogite facies ophiolites such as Saas Zermatt and Mt. Viso (e.g. Lombardo and Pognante, 1982). To the northwest the peridotites are bounded by serpentinites and their oceanic cover (Fig. 2). To the north, the thinned continental crust of the Sesia zone is exposed, which consists of 3 units (Dal Piaz, 1999): the eclogitic micaschists, gneiss minuti and a monometamorphic sedimentary sequence, and the diorite-kinzigite units (lower crust). The paleogeographic position of the Sesia zone is subject of some debate. It either formed the most distal part of the Adriatic continental margin (Dal Piaz, 1999), or an extensional allochthon separated from the Adriatic margin by a window of exhumed continental man-

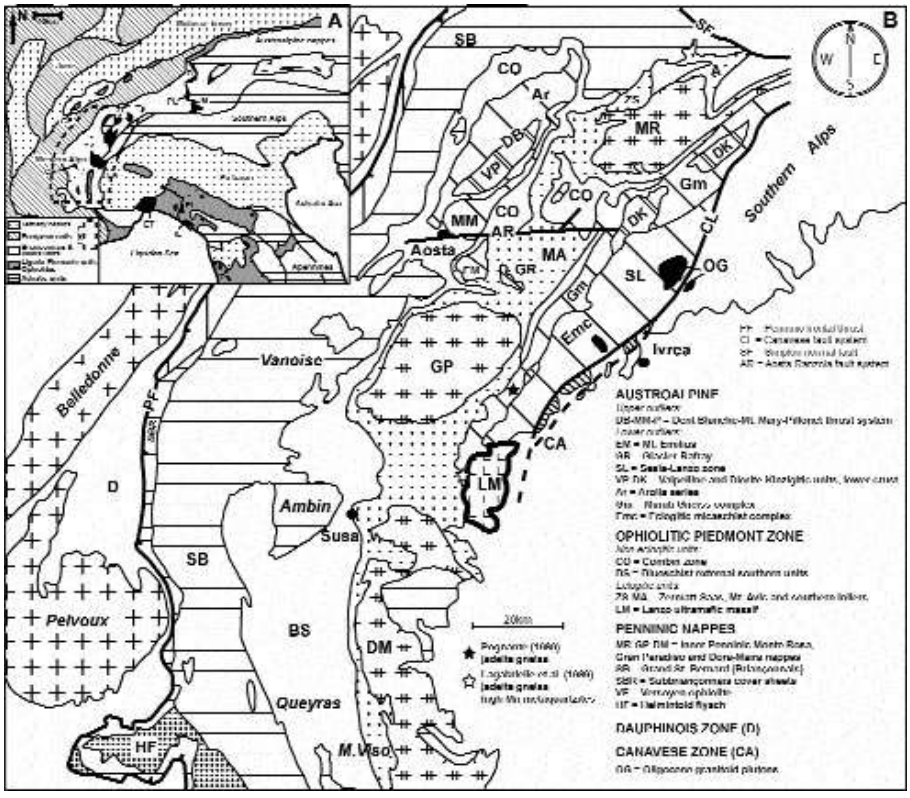

Fig. 1 - General tectonic-geologic overview of the Western Alps (modified after Dal Piaz, 1999) and the location of the Lanzo massif.

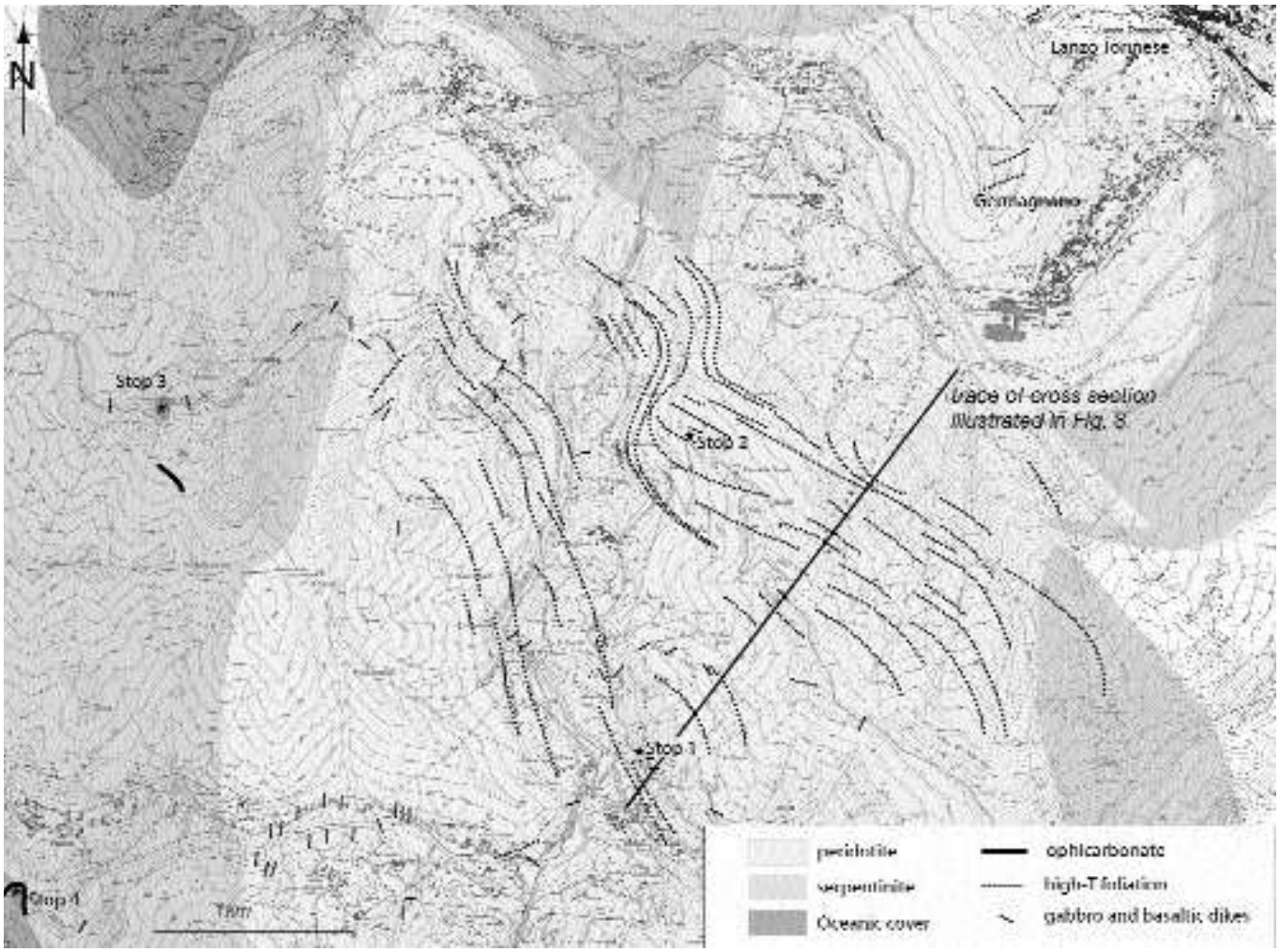

Fig. 2 - Topographic map of the Lanzo Nord area visited during the fieldtrip. The major foliation of the peridotite rocks and gabbroic dikes are indicated.

tle (Froitzheim and Manatschal, 1996), or is part of Europe (Fudral and Deville, 1986).

Peridotites and gabbroic dikes are partially transformed into eclogite facies rocks during Alpine metamorphism. The peridotite core is surrounded by serpentinized peridotites and strongly foliated serpentinites, mainly composed of antigorite and diopside, and minor olivine, chlorite, magnetite and titanian-clinohumite. In places the top of the mantle rocks is covered by ophicarbonate breccias (Fig. 3). Depending on whole rock composition, gabbroic dikes developed different high-pressure mineral parageneses (chloritoid, talc, garnet, ± kyanite (Kienast and Pognante, 1988; Pelletier and Müntener, 2005), indicating peak metamorphic conditions of ~550-620°C and pressures in excess of 2.0 GPa (Pelletier and Müntener, 2005). Within the serpentinites, gabbro and basaltic dikes are partially transformed into metarodingites (Figs. 2, 3), consisting of Ca-rich garnet, diopside, chlorite, epidote, titanite, vesuvianite and Ca-amphibole. Rodingitization most probably occurred during exposure of the ultramafic rocks on the ocean floor by circulation of fluids associated with serpentinization of mantle rocks, increasing Ca and decreasing Na of the bulk rock (Evans et al., 1979; Pognante et al., 1985).

There are large areas with little high-pressure overprint, where mantle processes are well preserved. In the northern part of the Lanzo massif, the remnants of a high-temperature mantle shear zone are exposed, separating a fragment of a former subcontinental mantle lithosphere (spinel to plagioclase peridotites with abundant pyroxenites) from a mantle hybrid (mainly plagioclase peridotites, dunites in the western part, pyroxenites, abundant gabbroic dikes and a few basalts; e.g., Bodinier et al., 1991). The outcrop of the shear zone extends over an area of ~2 km long and several hundreds of meters large (Fig. 2).

EXCURSION ROUTE

The aim of the excursion to the Lanzo north peridotite is to visit structures and rock types that are related to the spatial and temporal evolution of deformation and magmatism in a system undergoing exhumation to the seafloor, during the incipient opening of the Liguria-Piemonte Ocean. We start with a group of small outcrops near Maddelene (Fig. 2) where the field relations between pyroxenite layering, peridotite foliation and intrusion of gabbroic dikes can be studied (Stop 2) before inspecting a traverse of a high-temperature mantle shear zone (Gran Costa, Stop 1), visiting mainly the footwall and its increasing deformation gradient towards the mylonite zone. We will continue with a cross section from peridotites to serpentinized peridotites and shall discuss the importance of granulites enclosed within the Lanzo peridotites (Combasistel, Stop 3). Finally, time permitting, we will visit some rocks of the oceanic cover of

the Lanzo peridotites (ophicarbonates, mafic rocks, Lassieri, Stop 4), or gneiss and calcschists in the area of Richiaglio (see Fig. 17).

Gabbroic rocks in the Lanzo peridotite: fractional crystallization in a thick thermal lithosphere (Stop 1)

Within the unmetamorphosed parts of the Lanzo peridotite, mafic rocks can be separated into 3 groups (Boudier, 1978; Boudier and Nicolas, 1972):

(1) an oldest 'indigenous' group of troctolites to olivine gabbronorites and olivine gabbros, a few centimeters to several decameters long and frequently occurring 'en echelon' with diffuse contacts to the surrounding lherzolites. This type is frequently found in the southwestern part of the Lanzo massif (see Field Trip part I), but can also be recognized in the lower parts of Rio Ordagna (Fig. 2).

(2) An intrusive group of troctolites, olivine gabbros, gabbronorites to oxide gabbros and rare plagiogranites, with sharp contacts and chilled margins towards the peridotite. These gabbroic dikes can be followed over tens of meters in the field and may be found all over the Lanzo peridotite. Locally, the gabbros are cut by or grade into high temperature shear zones (Fig. 4a). Within these shear zones cm-sized amphibole phenocrysts are common and are associated with ilmenite, apatite and rare zircon. Ilmenite is often xenomorphic between plagioclase, pyroxenes and amphibole, indicating late stage magmatic crystallization (Desmurs et al., 2001; Tribuzio et al., 2000). Previously, the hornblende-bearing gabbros were interpreted to be of metamorphic origin (Compagnoni et al., 1984; Pognante et al., 1985). Rarely, zircon-rich plagiogranites cut deformed peridotites. They either represent late stage differentiates from the main gabbros (Desmurs et al., 2002,; Tribuzio et al., 2000), or, alternatively, they represent the products of hydrous partial melting of gabbro cumulates (Koepke et al., 2005).

(3) Porphyritic basaltic dikes of MORB affinity crosscutting peridotites, gabbros and shear zones (Pognante et al., 1985).

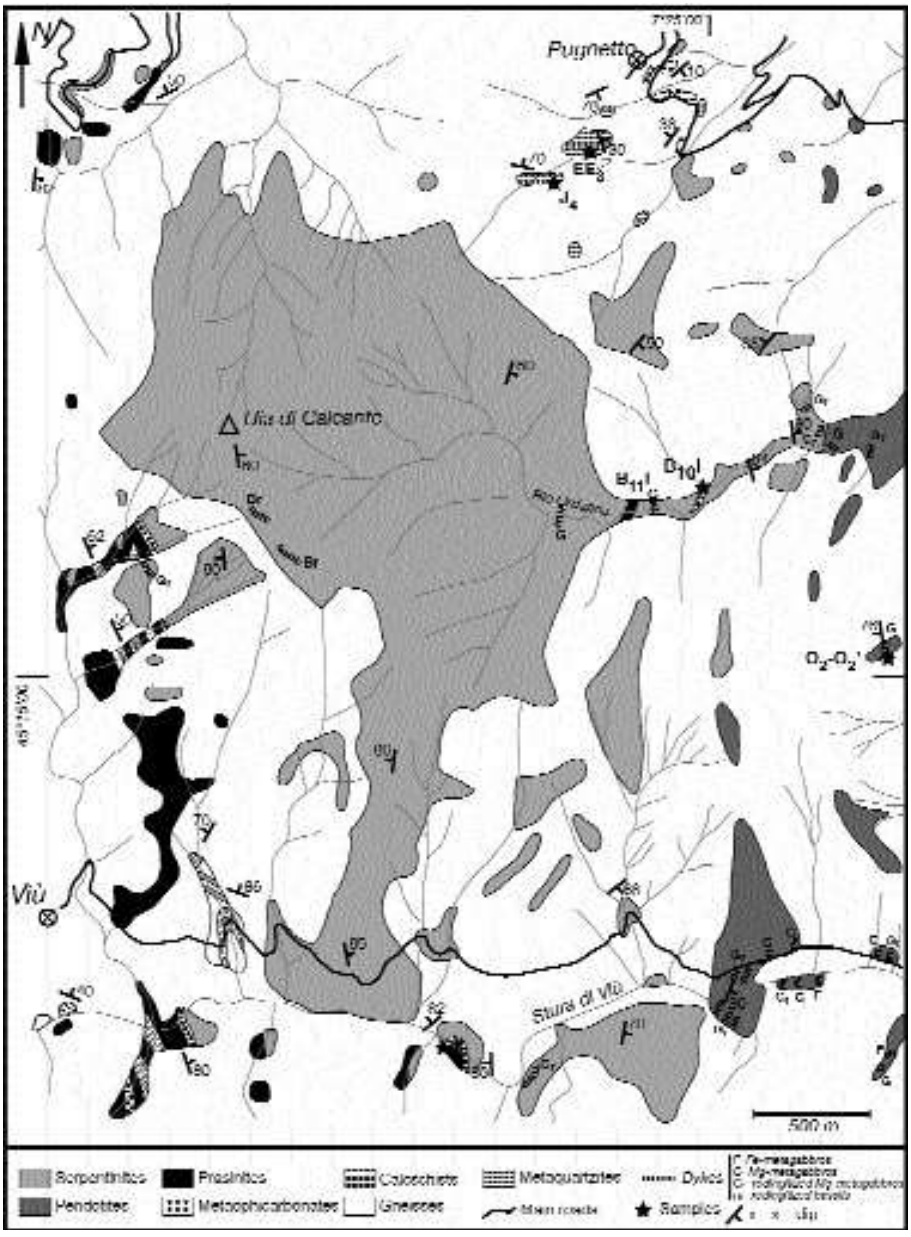

Fig. 3 - Simplified geological map of the northwestern part of the Lanzo massif, illustrating serpentinite-sedimentary cover contacts and the occurrence of a metaophicarbonates, prasinites, chlorite-phengite gneisses, phengite-quartz calcschists successions along the contact (Pelletier and Müntener, 2005).

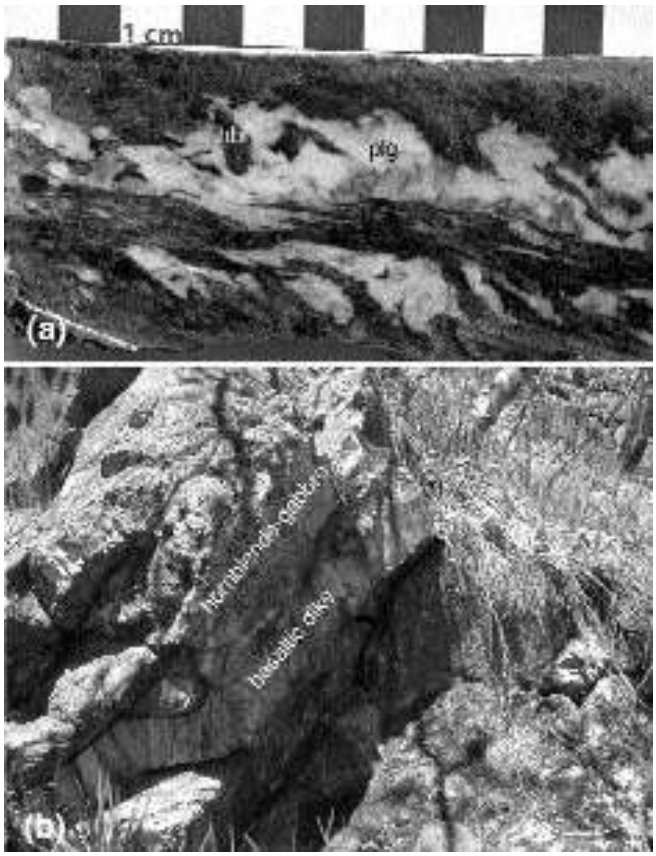

Fig. 4 - (a) Handspecimen of mylonitic oxide gabbro L165b. Note that mafic phases (hornblende, zircon, apatite and ilmenite) are concentrated in the centre of the shear zone, indicating late stage mylonitisation and migration of highly differentiated liquid. (b) Basaltic dike crosscutting differentiated apatite-amphibole-gabbros, Val della Torre.

Age determinations of gabbroic rocks

Zircons were studied by cathodoluminescence (CL) and analysed with SHRIMP II for U-Pb dating and LA-ICP-MS for trace element determination. CL imaging of zircon reveals magmatic zoning cut by an unzoned recrystallized domains (Fig. 5). U-Pb dating of 3 samples indicates an age of magmatism of about 160 Ma (Kaczmarek et al., 2005), similar to other Western Alps ophiolitic gabbros. Trace element chemistry of zircon by LA-ICP-MS indicates a positive Ce anomaly and a variable Eu negative anomaly (Fig. 6). The Eu anomaly suggests plagioclase fractionation in the magma and is consistent with the magmatic origin of the zircon.

Geochemistry

The Lanzo gabbros show highly variable bulk rock compositions (Pognante et al., 1985; Bodinier et al., 1986). In terms of mineralogy and major elements, the gabbros from the northeastern part of Lanzo are generally more evolved than those from the southwestern part. Chondrite normalized REE data, compiled in Fig. 7, illustrate that most of the gabbroic dikes represent cumulates with little or no trapped liquid indicating efficient extraction of interstitial liquids (Bodinier et al., 1986). Fig. 7 also illustrates calculated liquid compositions derived from cpx from dunites, harzburgites and primitive troctolite to olivine gabbros (Piccardo et al., 2005). These data are similar to basaltic dikes (Pognante et al., 1985) supporting the idea that 'indigenous' group 1 gabbros are cumulates that formed in equilibrium with liquids, that were extracted to form basalts.

High-temperature shear zones in the mantle (Stop 2)

One of the major discoveries along mid-ocean ridges and along ocean-continent transitions in the past decades was the observation that mantle rocks can be exposed over several kilometers. There is a general consensus that the final deformation occurred along low-temperature detachment faults, but there is little observational data about the deep, high-temperature deformation that presumably preceded detachment faulting, or alternatively, represents the deep roots of detachment faults.

The shear zone in the northern Lanzo peridotite is ~2 km wide, and oriented NW-SE with a sub-vertical foliation (Fig. 2). Pyroxenitic layering and high temperature foliations are parallel in the ultra-mylonite zone (Fig. 2). In contrast, they are discordant in less deformed rocks, with re-orientation of the pyroxene in the pyroxenitic layering parallel to the high-temperature foliation. Several cross sections indicate that the deformation is not symmetrically distributed along the shear zone. There is a relatively sharp transition (about 400 to 500 m) from weakly deformed porphyroclastic peridotites (grain size up to 1.5 cm) to ultramylonites (grain size ~50 µm or less) on the northern side of the mylonite. The southern part of the shear zone, however, shows a much smoother transition. Reconstructing the main deformational features in 3D indicates that this shear zone is

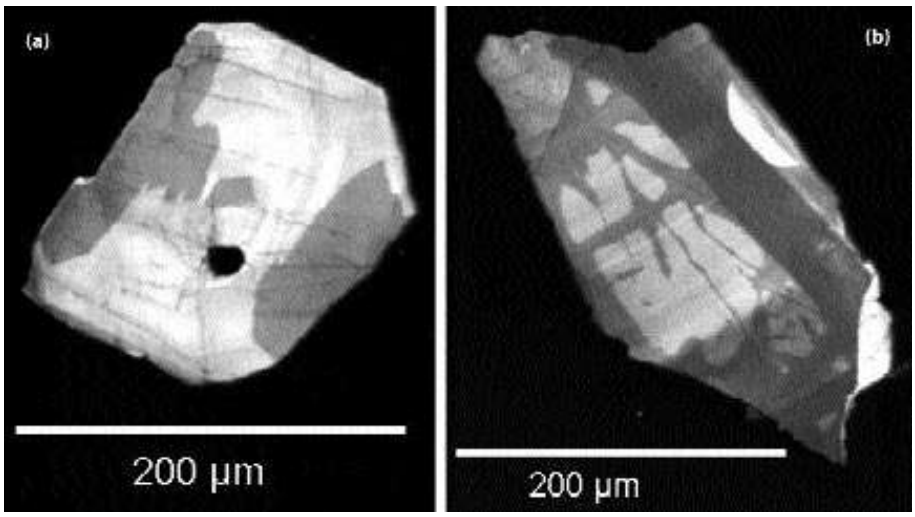

Fig. 5 - Cathodo-luminescence (CL) images of zircons from oxide gabbro 165b. Note the internal structure of the zircon, indicating several stages of zircon crystallization and corrosion. U-Pb ages of the different zones, however, are the same within error and indicate a middle Jurassic age of crystallization (Kaczmarek et al., in preparation).

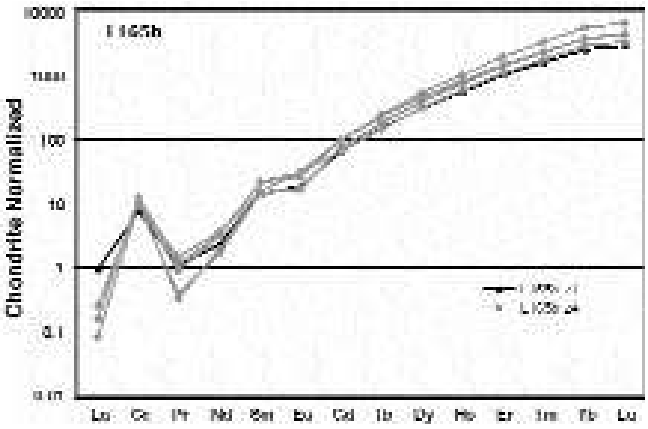

Fig. 6 - REE spectra of zircons from hbl-oxide gabbro 165b. The chondrite normalized REE spectra are smooth with a regular increase in HREE. Note the weak negative Eu anomaly, indicating that zircons crystallized from differentiated liquids (Kaczmarek et al., in preparation).

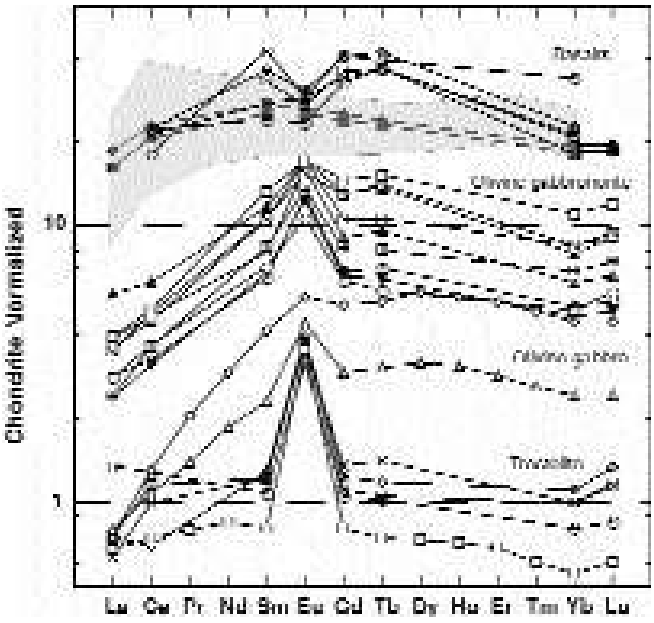

Fig. 7 - Geochemical variation of gabbroic rocks from the Lanzo peridotite. (a) Chondrite normalized REE spectra of different gabbroic dikes ranging from troctolite, olivine gabbro, and gabbronorite. Positive Eu anomalies in troctolite and olivine gabbronorite are indicative of a cumulate origin. (gabbro data from Bodinier et al., 1986; Piccardo et al., 2005; basalt data from Pognante et al., 1985). Gray shaded area is the range of calculated liquids from cpx in dunite, harzburgite and olivine gabbros (Piccardo et al., 2005), which is similar to the measured basalt data from Pognante et al. (1985). Note that Gd values for the data of Bodinier et al. (1986) are interpolated between Tb and Sm.

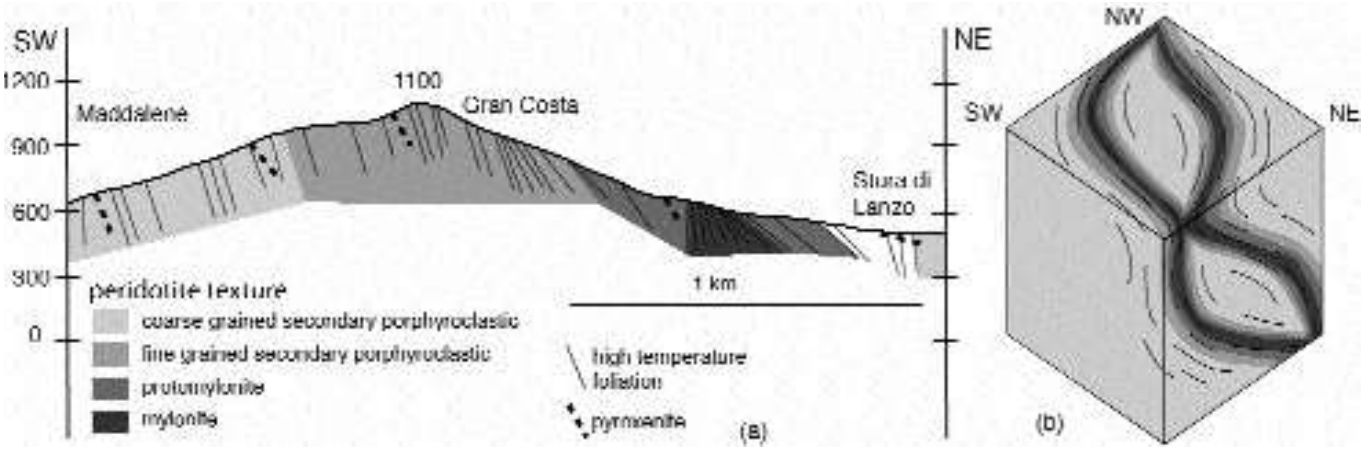

Fig. 8 - (a) Schematic cross section of the peridotite mylonite zone, illustrating the relationships between high temperature foliations and pyroxenite layers. For profile location, see Fig. 2. (b) Schematic model of an anastomozing shear zone, which could explain the irregular distibution of peridotite mylonites in the field.

anastomozing (Fig. 8), with progressive localization of deformation with increasing strain. Mylonites thus include areas of less deformed regions (Fig. 8).

Preliminary grain size analyses indicate 4 types of microstructures from “porphyroclastic” with magmatic and impregnation textures (olivine grain size: 0.2 to 1.05 mm, aspect ratios: 1.6 to 2) to ultra-mylonitic (grain size: < 0.05 to 0.15 mm, aspect ratios ~ 1.6) with extremely stretched (aspect ratio up to 10:1) porphyroclastic opx (Fig. 9). There is a clear difference in the recrystallized grain size between ‘monomineralic’ bands of olivine and ‘polycrystalline bands’ (Fig. 9). Typical peridotite mylonite bands consist of olivine (ol) + clinopyroxene (cpx) + opx + plagioclase (plg) + Cr-Al spinel ± Ti hornblende and enclose coarse porphyroclasts of pyroxene or polycrystalline bands of olivine. Some cpx porphyroclasts show signs of previous reaction textures with a melt (cpx_1 + liq _ opx + plg ± ol; Fig. 10). This indicates that the mylonite formation postdates cpx-corroding melt/rock reactions.

Detailed mineral chemical investigations by SEM and by electron microprobe (EMS) revealed that porphyroclastic pyroxenes and spinel are strongly zoned in some elements, suggesting disequilibrium mineral compositions. Cores of pyroxenes are rich in Al and poor in Ti and probably indicate equilibration in the spinel peridotite facies (Fig. 10). Large pyroxene porphyroclasts record processes of melt infiltration and melt/rock reaction, which is reflected by complex zonation patterns of Ti. Rim compositions of pyroxenes

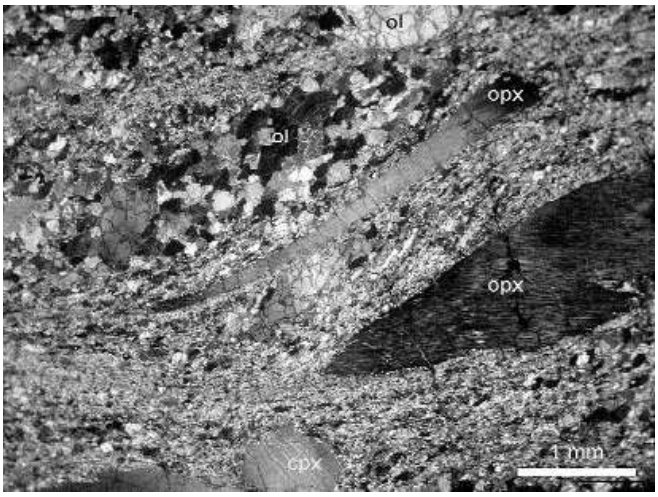

Fig. 9 - Microphotograph of a peridotite mylonite illustrating the localization of deformation and the very fine grained recrystallization products. Orthopyroxene might be extremely stretched with aspect ratios up to 10:1. The mylonitic matrix consists of olivine, cpx, opx, spinel, plagioclase and rarely Ti-hornblende testifying high temperature dynamic recrystallization. With of micrograph is 0.7 cm (Sample L04).

as well as small, recrystallized grains within the mylonite indicate equilibration under plagioclase facies conditions (Fig. 11) and relatively low temperatures (800 to 900°C, based on single opx and two pyroxene thermometry, e.g., Brey and Köhler, 1990). Spinel porphyroclasts show strongly variable Mg# and Cr#. Zoning of spinel seems to be unrelated to its microstructural setting and indicates disequilibrium conditions (Fig. 12), probably related to rapid cooling and incomplete re-equilibration during fast exhumation.

Our results indicate that melt migration and high-temperature deformation are juxtaposed both in time and space. Melt-rock reaction may cause grain size reduction, which in turn led to localization of deformation. Observations indicate that actively deforming peridotite mylonite might suppress brittle failure and that ascending gabbros might terminate and partially crystallize along actively deforming shear zones. Field observations also indicate that gabbros are asymmetrically distributed with respect to the shear zone. A schematic model to illustrate these speculations is shown in Fig. 13, where melt-assisted extension in the deep parts of the lithosphere might be important. Similar models are currently debated for the origin of oceanic core complexes (e.g., Escartin et al., 2003; Tucholke et al., 2001; Tucholke et al., 1998).

Granulite facies remnants in the Lanzo mantle (Stop 3)

Phengite-bearing mafic gneisses with intercalated quartz-feldspar-rich bands interpreted as leucosomes were found within the serpentinites along the Ordagna river (B_{11}, for location see Figs. 2, 3) and are separated from the serpentinites by an intensely foliated metaophicarbonate zone about 10 m wide. The leucosomes form a discontinuous and thin network between more mafic parts. Locally, a faint banding between mafic layers and quartz-feldspar-rich leucosomes are reminiscent of migmatites. The mafic gneiss is dominated by greenschist facies assemblages, consisting of chlorite, actinolite, epidote, titanite, and albite porphyrob-

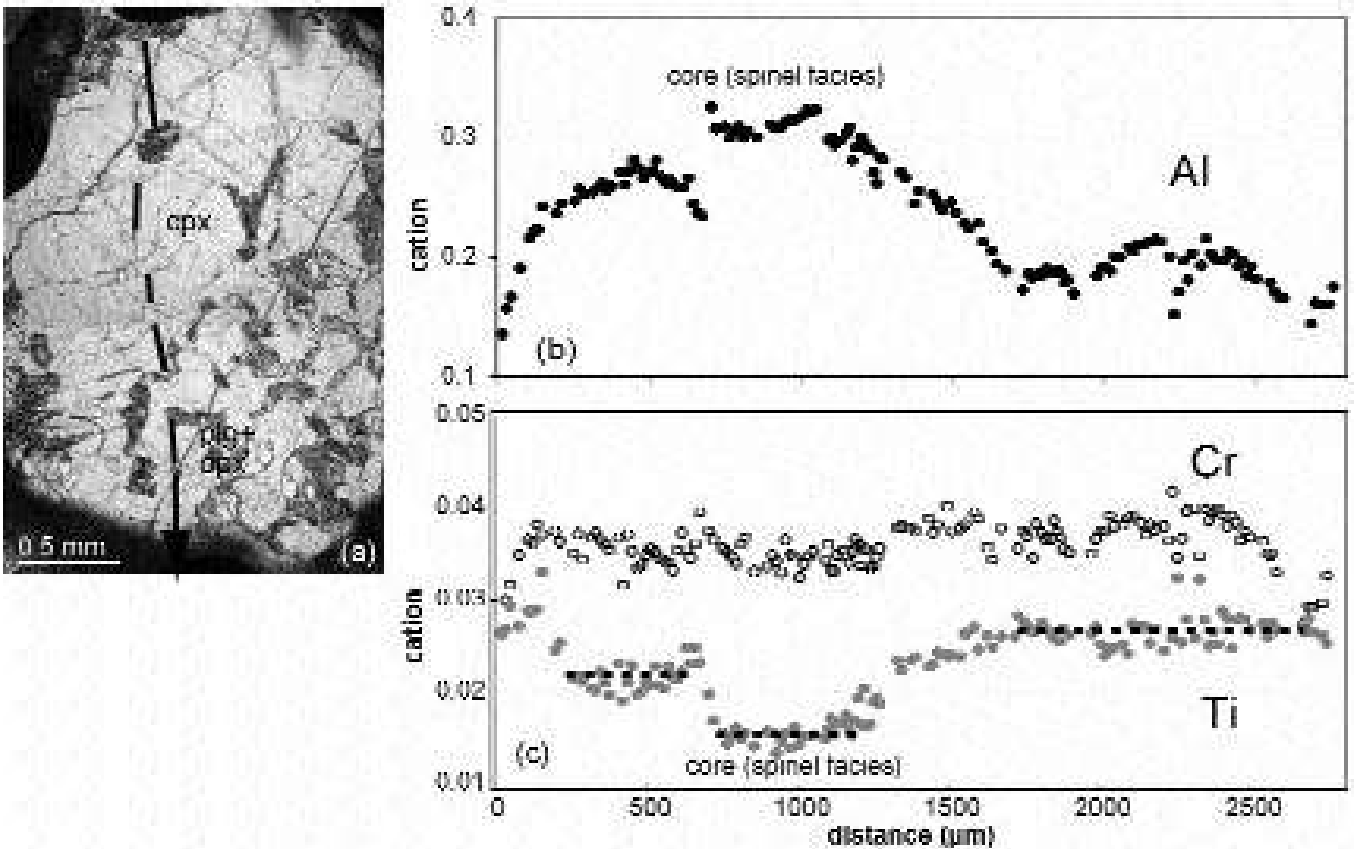

Fig. 10 - Textural and compositional variation of clinopyroxene porphyroclasts in a plagioclase peridotite. (a) Microphotograph showing a cpx crystal that has partially been replaced by intergrown orthopyroxene + plagioclase, similar to the textures found in Lanzo south (Müntener and Piccardo, 2003; Piccardo et al., 2004). Variation of Al (panel b), Cr and Ti (panel c) suggests equlibration of the core in the spinel peridotite facies. Decreasing Al, increasing Ti and the microtextures indicate that the transition from spinel to plagioclase facies is accompanied by melt/rock reaction with a cpx-undersaturated liquid.

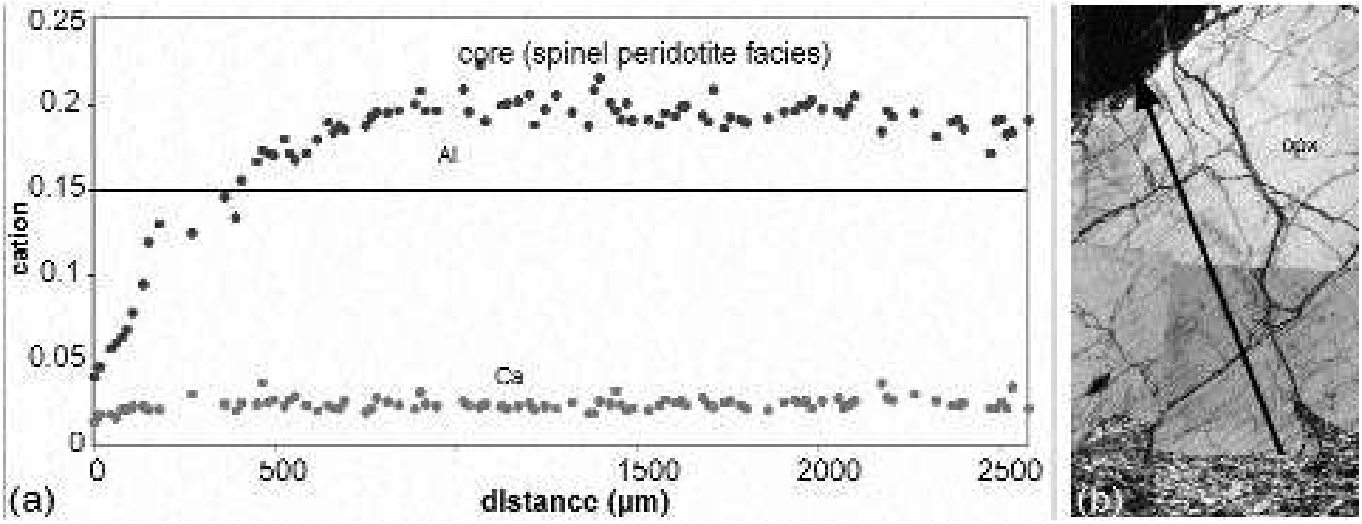

Fig. 11 - Compositional variation of large orthopyroxene porphyroclast, which is embedded in a peridotite mylonite. Note the complete equilibration of Ca, while Al shows a plateau in the core, which is diffusively requilibrated towards the rim. Rim compositions correspond to small opx granoblasts in the matrix. Ca-in opx thermometry indicates temperatures of ~ 850°C (Kaczmarek and Müntener, unpublished).

lasts. High-pressure relics are phengite (Si ~3.6), glaucophane (only present in actinolite core), garnet rims around pre-Alpine garnet-porphyroclasts, quartz, rutile and zoisite. Accessory zircon crystals are abundant in this rock. The intercalation of mafic gneisses and quartz-rich leucosomes is similar to 'polymetamorphic paraschists' of Pognante (1989). Fe-Mg thermometry applied to phengite-garnet rim pairs indicates peak metamorphic conditions of ~ 500°C, at pressures exceeding 1 GPa (Pelletier and Müntener, 2005). The only relics documenting a pre-Alpine history are zoned garnets (Fig. 14d) and zircon crystals. Garnets show little zoning and have small rims with decreasing Mg# and increasing grossular and spessartine contents. The cores show a large plateau of nearly constant composition (Fig. 14b), high pyrope and low grossular contents, similar to some garnets from the high-temperature granulite-facies basement rocks in the Sesia zone (II DK or polymetamorphic paraschists: Pognante, 1989). The association is equivalent to rocks known in the II DK in the Sesia Zone, interpreted as pre-Alpine lower continental crust.

CL images of the numerous zircon crystals reveal metamorphic rims surrounding detrital cores (Fig. 15). The cores yield ages from Devonian to Proterozoic, as expected for a detrital population. CL imaging indicates two different domains in the metamorphic rims. A dark inner rim surrounding the detrital core, which was dated at ~ 304 Ma, and an outer rim dated at ~ 293 Ma (Kaczmarek et al., 2005, and in preparation). Zircon REE patterns from the granulitic sample show a positive slope from Gd to Lu for the core and a near flat pattern for the external rim, suggesting equilibration with garnet (Fig. 16). Composition of garnets, trace element equilibrium between garnet and zircon (Rubatto, 2002), and the U-Pb ages strongly suggest that the protolith of the phengite gneisses were equilibrated under granulite facies conditions in post-Variscan pre-Alpine times (Kaczmarek et al., 2005).

The oceanic cover of the Lanzo peridotite (Stop 4)

Detailed mapping along the Western border of the Lanzo massif revealed a series of metamorphosed oceanic rocks covering the serpentinized peridotites between Pugnetto and Richiaglio (Figs. 1, 3, 17). This succession includes from bottom to top (Lagabrielle et al., 1989; Pelletier and Müntener, 2005): serpentinized peridotites, local ophicarbonates, metabasites, metaquartzites, phengite-quartz-calcschists and marbles, locally containing eclogite facies basaltic pebbles,

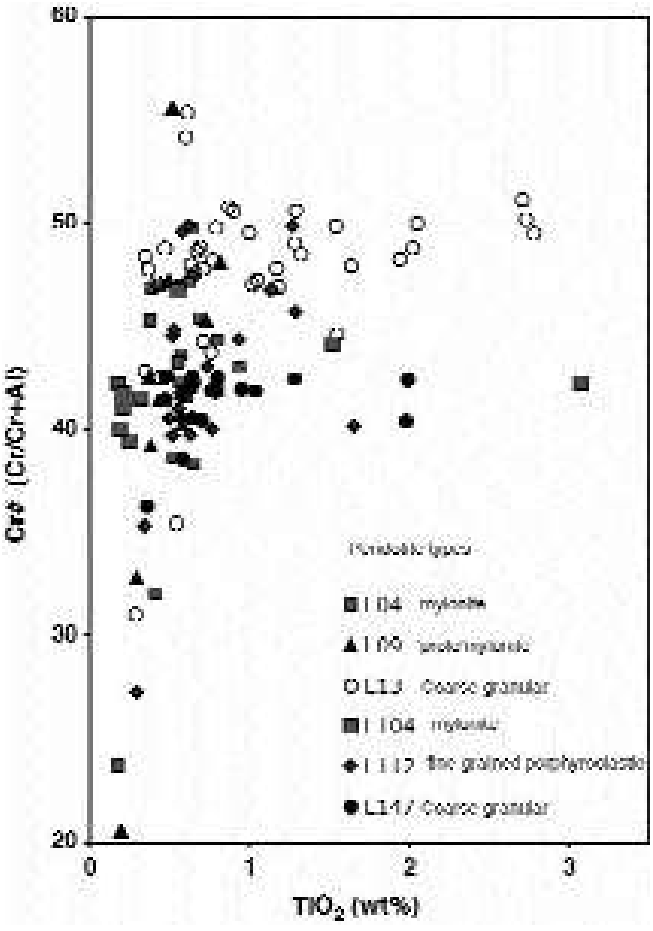

Fig. 12 - Spinel Cr# (molar Cr/Cr+Al) vs TiO_2 from variably deformed plagioclase peridotites from Lanzo Nord, indicating an extreme chemical variability within single samples. Note that the chemical disequilibrium of spinel is independent on the microstructure, and suggest rapid cooling rates (Kaczmarek and Müntener, unpublished).

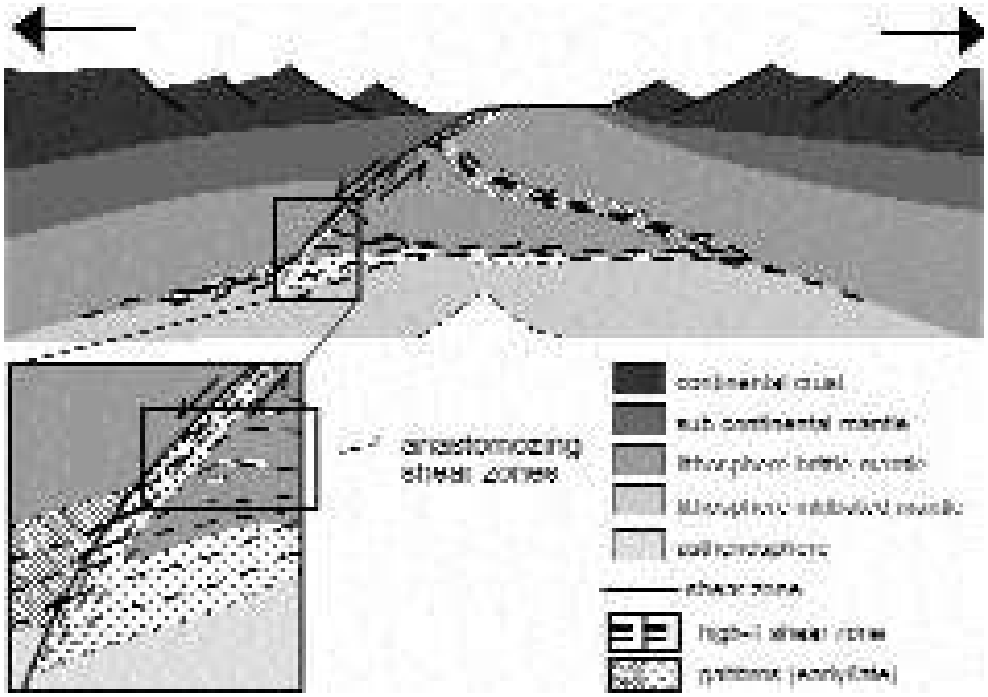

Fig. 13 - A simplified model illustrating the potential tectonic significance of the Lanzo shear zone in the framework of the formation of ocean-continent transition zones and mantle exhumation. Migrating mafic melts might terminate along large shear zones, crystallize and get exhumed to shallower crustal levels. This could explain the observation of abundant gabbroic dikes in the 'footwall' of the shear zone.

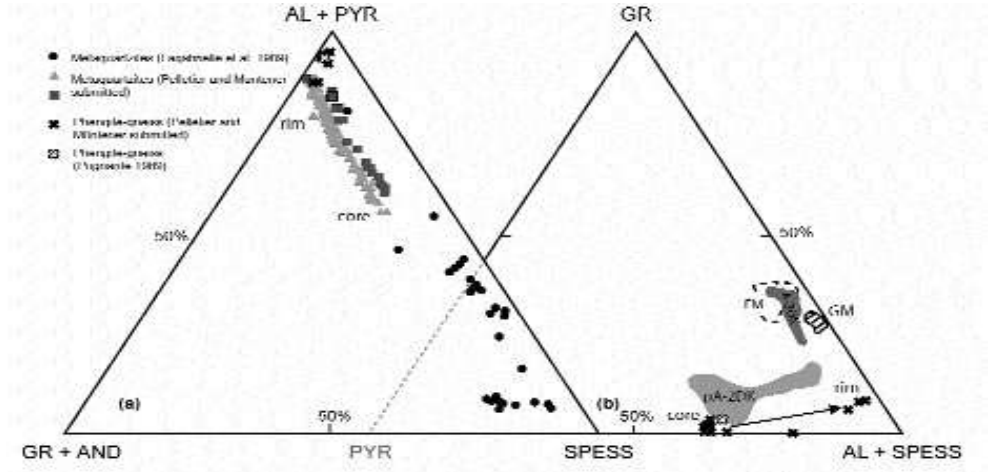

Fig. 14 - (a) compositional variation of garnet from granulites and from Mesozoic metasediments from the cover of the Lanzo peridotite. Mn-rich garnets show a prograde metamorphic evolution with Mn-rich cores and progressive decrease towards the rim (Lagabrielle et al., 1989; Pelletier and Müntener, 2005). (b) Granulite garnet cores are almandine-pyrope solid solutions, with very low Mn and Ca content. The garnets from the Lanzo granulite are similar to garnet from lower crustal rocks from the Sesia zone (Pognante, 1989). (c) compositional profile of garnet from the granulites show high Mg# in the core and low Ca and Mn contents, suggesting previous high temperature equilibration. (d) BSE image showing the incomplete reequilibration of garnet during Alpine metamorphism. GM- gneiss minuti; EM- eclogitic micaschists; pA-2DK- pre-Alpine garnets from the "seconda zona dioritica-kinzigitica"; A-2DK- Alpine garnets from the "seconda zona dioritica-kinzigitica". Modified from Pelletier and Müntener (2005).

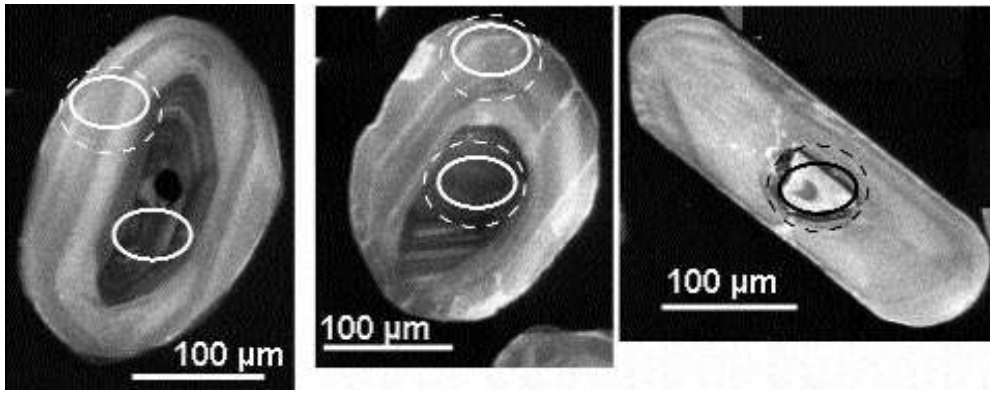

Fig. 15 - Cathodo-luminescence (CL) images of zircons from granulite B11. Circles represent approximate diameter of SHRIMP spot analyses, stippled lines is the approximate diameter of Laser Ablation ICP-MS analysis of zircons. Most analyses provide an age between 300 and 290 Ma. Note the inherited cores in some zircons, indicating a sedimentary protolith of the granulites.

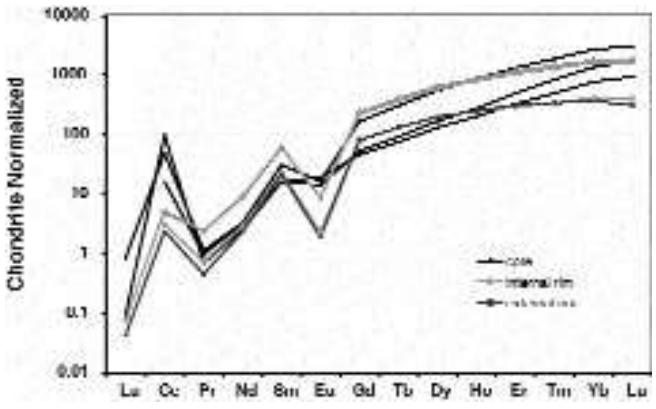

Fig. 16 - REE spectra of zircons from granulites. Note that the cores show typical igneous pattern, with large positive Ce and negative Eu anomalies, and smooth increase in HREE. In contrast the inner and outer rim both show reduced or absent Eu anomalies and a less fractionated HREE pattern, indicating equilibration with garnet (e.g., Rubatto, 2002).

and fine-grained leucocratic-gneisses. Metaquarzites were also found in the northern area near Pugnetto and are associated with calcschists (Fig. 3). Although most of the lithological contacts are strongly overprinted by Alpine deformation and metamorphism, two important field observations strongly suggest that at least parts of the Lanzo peridotites once formed the ocean-floor of the Jurassic Liguria Piemonte Ocean: (1) Serpentinite schists (detritus?) and blocs of eclogitized mafic rocks within marbles (Fig. 17) indicate that erosion of ultramafic and mafic rocks occurred contemporaneously with pelagic sedimentation of carbonate rocks (Lagabrielle et al., 1989). (2) The local occurrence of ophicarbonate rocks, covered by metabasites, suggests that the serpentinized peridotites were (at least partially) exposed on the ocean floor.

The occurrence of gneisses and lower crust rocks within the oceanic cover of the Lanzo peridotite is more difficult to explain. Either (1) they represent stratigraphic or tectonic intercalations of acidic material within the oceanic sediments, similar to occurrences in the Western Alps (Lago Nero unit, Chenaillet ophiolite: Polino and Lemoine, 1984) the eastern Central Alps (Err-Platta nappe: Manatschal and Nievergelt, 1997), the northern Apennine (Marroni et al., 1998) and the Iberia ocean-continent transition (Manatschal et al., 2001), or (2) alternatively, these rocks are tectonically imbricated during (early) collision between the Lanzo peridotites and the Sesia zone, a contact that shows a polyphase deformation history (Spalla et al., 1983). The former hypothesis suggests a close paleogeographic connection between the continental crust and the Lanzo peridotites in the Late Jurassic, where continental sources are not too far away from the oceanic crust. This would imply that lower crustal continental and oceanic units were already juxtaposed in Mesozoic times, a typical feature of ocean-continent transition zones (Manatschal et al., 2001; Müntener and Hermann, 2001). Associations of oceanic sediments with exhumed lower crustal and mantle rocks have been described in the eastern Central Alps (Müntener et al., 2000) and the present-day Iberia margin (Manatschal et al., 2001). If this interpretation holds for the Sesia-Lanzo connection, it would have several important consequences for the origin and paleogeographic setting of the Lanzo peridotites, fostering the model of a continental to oceanic mantle transition in the Lanzo peridotite (Bodinier et al., 1991).

Acknowledgments

Our work is supported by the Swiss National Science foundation (Grants Nr. 200020-103646/2 and 21-66923.01), which is gratefully acknowledged. We thank the participants of the Peridotite Workshop 2005 for lively and inspiring discussions during the fieldtrip. Comments from R. Tribuzio and Y. Lagabrielle improved the final version of the manuscript.

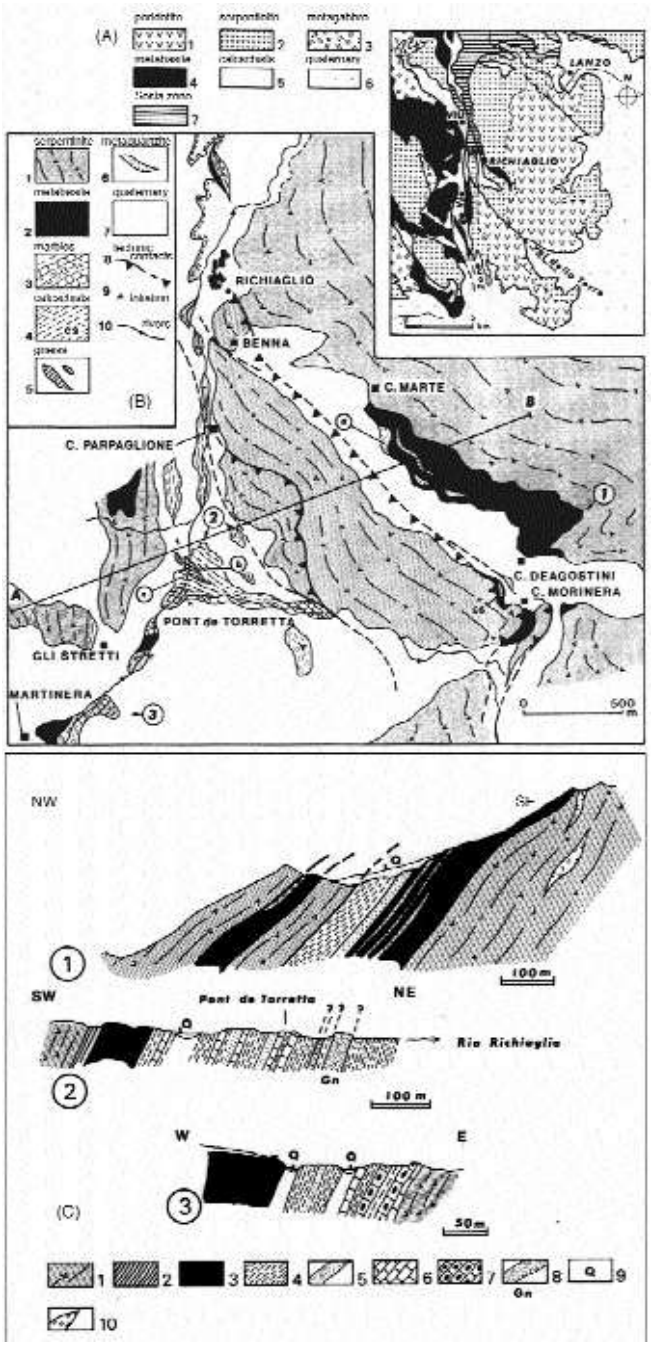

Fig. 17 - The Lanzo massif and its sedimentary cover along the western contact near Richiaglio, taken from Lagabrielle et al. (1989). (a) Overview map, (b) Simplified geological map of the Lanzo peridodite body, surrounding rocks and location of cross section. (c) Detailed cross sections showing the relationships between the serpentinite basement and associated metasediments and metavolcanics. (1) serpentinized peridotites, (2) foliated serpentinites, (3) metabasites, (4) calcschists, (5) Mn-rich garnet metaquartzites, (6) phyllitic marbles, (7) marbles with blocs of eclogites, (8) finegrained leucogneiss, (9) quaternary, (10) pegmatitic gabbro dikes with the serpentinites.

REFERENCES

Bodinier J.L., Guiraud M., Dupuy C. and Dostal J., 1986. Geochemistry of basic dikes in the Lanzo massif (Western Alps): petrogenetic and geodynamic implications. Tectonophysics, 128: 75-95.

Bodinier J.L., Menzies M.A. and Thirlwall M.F., 1991. Continental to oceanic mantle transition: REE and Sr-Nd isotopic geochemistry of the Lanzo lherzolite massif. J. Petrol., Special Lherzolite Issue, p. 191-210.

Boudier F., 1978. Structure and petrology of the Lanzo peridotite massif (Piedmont Alps). Geol. Soc. Am. Bull., 89: 1574-1591.

Boudier F. and Nicolas A., 1972. Fusion partielle gabbroïque dans la lherzolite de Lanzo (Alpes piémontaises). Schweiz. Mineral. Petrogr. Mitt., 52: 39-56.

Brey G.P. and Köhler T., 1990. Geothermobarometry in four-phase lherzolites II. New thermobarometers, and practical assesment of existing thermobarometers. J. Petrol. 31: 1353-1378.

Compagnoni R., Radicati di Bronzolo F. and Sandrone R., 1984. Kaersutite-bearing mylonitic gabbro from the Lanzo peridotite (Western Italian Alps). Geol. Mijn., 63: 189-196.

Dal Piaz G.V., 1999. The Austroalpine-Piedmont nappe stack and the puzzle of western Alpine Tethys. In: G. Gosso (Ed.), Third workshop on Alpine geological studies. Mem. Soc. Geol. It., 53: 155-176.

Desmurs L., Manatschal G. and Bernoulli D., 2001. The Steinmann trinity revisited: exhumation and magmatism along an ocean-continent transition: the Platta nappe, eastern Switzerland. In: R.C.L. Wilson, R.B. Withmarsh, B. Taylor and N. Froitzheim (Eds.), Non-volcanic rifting of continental margins: A comparison of evidence from land and sea 187. Geol. Soc. London Spec. Publ., p. 235-266.

Desmurs L., Müntener O. and Manatschal G., 2002. Onset of magmatic accretion within magma-poor passive margins: A case study from the Err-Platta ocean-continent transition, Eastern Switzerland. Contrib. Mineral. Petrol., 144: 365-382.

Escartin J., Mevel C., MacLeod C.J. and McCaig A.M., 2003. Constraints on deformation conditions and the origin of oceanic detachments: The Mid-Atlantic ridge core complex at 15°45'N. Geochem. Geophys. Geosyst. 4, doi: 10.1029/2002GC000472.

Evans B.W., Trommsdorff V. and Richter W., 1979. Petrology of an eclogite-metarodingite suite at Cima di Gagnone, Ticino, Switzerland. Am. Miner., 64: 15-31.

Froitzheim N. and Manatschal G., 1996. Kinematics of Jurassic rifting, mantle exhumation, and passive-margin formation in the Austroalpine and Penninic nappes (eastern Switzerland). Geol. Soc. Am. Bull., 108: 1120-1133.

Fudral S. and Deville E., 1986. La zone Sesia existe-t-elle? Nouvelles observations sur les enveloppes métasédimentaires du massif cristallin pré-triasique de Sesia au Nord du Mont Ciucrin (Alpes occidentales-région de Lanzo-Italie). C.R. Acad. Sci. Paris, 302: 1021-1026.

Kaczmarek M.-A., Rubatto D. and Müntener O., 2005. SHRIMP U-Pb zircon dating of gabbro and granulite from the peridotite massif of Lanzo (Italy). Geophys. Res. Abs., 7: 03098.

Kienast J.R. and Pognante U., 1988. Chloritoid-bearing assemblages in eclogitized metagabbros of the Lanzo peridotite body (Western Italian Alps). Lithos 21 (1): 1-11.

Koepke J., Feig S.T. and Snow J., 2005. Hydrous partial melting within the lower oceanic crust. Terra Nova, 17: 286-291.

Lagabrielle Y., Fudral S. and Kienast J.-R., 1989. La couverture océanique des ultrabasites de Lanzo (Alpes occidentales): arguments lithostratigraphiques et pétrologiques, or [The oceanic cover of the Lanzo peridotite body (Western Italian Alps): lithostratigraphic and petrological evidences]. Geodin. Acta (Paris), 3: 43-55.

Lombardo B. and Pognante U., 1982. Tectonic implications in the evolution of the Western Alps ophiolite metagabbros. Ofioliti, 7: 371-394.

Manatschal G., Froitzheim N., Turrin B. and Rubenach M., 2001. The role of detachment faulting in the formation of an ocean-continent transition: insights from the Iberia abyssal plain. In: R.C.L. Wilson, R.B. Withmarsh, B. Taylor and N. Froitzheim (Eds.), Non-volcanic rifting of continental margins: A comparison of evidence from land and sea. Geol. Soc. London Spec. Publ., 187: 405-428.

Manatschal G. and Nievergelt P., 1997. A continent ocean transition recorded in the Err and Platta nappes (eastern Switzerland). Ecl. Geol. Helv., 90: 3-27.

Marroni M., Molli G., Montanini A. and Tribuzio R., 1998. The association of continental crust rocks with ophiolites in the Northern Apennines (Italy): implications for the continent-ocean transition in the Western Tethys. Tectonophysics, 292: 43-66.

Müntener O. and Hermann J., 2001. The role of lower crust and continental upper mantle during formation of non-volcanic passive margins: Evidence from the Alps. In: R.C.L. Wilson, R.B. Withmarsh, B. Taylor and N. Froitzheim (Eds.), Non-volcanic rifting of continental margins: A comparison of evidence from land and sea. Geol. Soc. London Spec. Publ., 187: 267-288.

Müntener O., Hermann J. and Trommsdorff V., 2000. Cooling history and exhumation of lower crustal granulites and upper mantle (Malenco, Eastern Central Alps). J. Petrol., 41: 175-200.

Müntener O. and Piccardo G.B., 2003. Melt migration in ophiolitic peridotites: the message from Alpine-Apennine peridotites and implications for embryonic ocean basins. In: Y. Dilek and P.T. Robinson (Eds.), Ophiolites in Earth history. Geol. Soc. London Spec. Publ., 218: 69-89.

Pelletier L. and Müntener O., 2005. High pressure metamorphism of the Lanzo peridotite and its oceanic cover, and some consequences for the Sesia-Lanzo zone (northwestern Italian Alps). Lithos, submitted.

Piccardo G.B., Müntener O., Zanetti A., Romairone A., Bruzzone S., Poggi E. and Spagnolo G., 2004. The Lanzo South peridotite: Melt/peridotite interaction in the mantle lithosphere of the Jurassic Ligurian Tethys. Ofioliti 29 (1): 37-62.

Piccardo G.B., Zanetti A., Müntener O., Poggi E. and Spagnolo G., 2005. Melt/peridotite interaction in the Lanzo South peridotite: field, textural and geochemical evidence. Lithos, submitted.

Pognante U., 1989. Lawsonite, blueschist and eclogite formation in the southern Sesia zone (western Alps, Italy). Eur. J. Mineral., 1: 89-104.

Pognante U., Rösli U. and Toscani L., 1985. Petrology of ultramafic and mafic rocks from the Lanzo peridotite body (Western Alps). Lithos, 18: 201-214.

Polino R. and Lemoine M., 1984. Détritisme mixte d'origine continentale et océanique dans les sédiments jurassico-crétacés supra-ophiolitiques de la Téthys ligure: la série du Lago Nero (Alpes occidentales franco-italiennes). C.R. Acad. Sci. Paris, 298: 359-364.

Rubatto D., 2002. Zircon trace element geochemistry: partitioning with garnet and the link between U-Pb ages and metamorphism. Chem. Geol., 184 (1-2): 123-138.

Spalla M.I., De Maria L., Gosso G., Miletto M. and Pognante U., 1983. Deformazione e metamorfismo della zona Sesia-Lanzo meridionale al contatto con la falda piemontese e con il massiccio di Lanzo, Alpi occidentali. Mem. Soc. Geol. It., 26: 499-514.

Tribuzio R., Tiepolo M. and Vannucci R., 2000. Evolution of gabbroic rocks from the Northern Apennine ophiolites (Italy): Comparison with the lower oceanic cust from modern slow spreading ridges. In: Y. Dilek, E.M. Moores, D. Elthon and A. Nicolas (Eds.), Ophiolites and oceanic crust: new insights from field studies and Ocean Drilling Program. Geol. Soc. Am. Spec. Paper, 349: 129-138.

Tucholke B.E., Fujioka K., Ishihara T., Hirth G. and Kinoshita M., 2001. Submersible study of an oceanic megamullion in the central North Atlantic. J. Geophys. Res. 106 (B8): 16145-16161.

Tucholke B.E., Lin J. and Kleinrock M.C., 1998. Megamullions and mullion structure defining oceanic metamorphic core complexes on the Mid-Atlantic ridge. J. Geophys. Res., 103 (B5): 9857-9866.

Received, October 2, 2005
Accepted, November 28, 2005

Juxtaposition of melt migration and high-temperature shear zones in the Lanzo peridotite (Italy).

Kaczmarek M-A.[1] and Müntener O.[1]
[1]*Institut de Géologie de Neuchâtel, rue Emile Argand 11, 2007 Neuchâtel- Suisse, email: mary-alix.kaczmarek@unine.ch*

The plagioclase peridotite massif of Lanzo is composed of 3 zones (north, central and south) which are separated by shear zones. In all 3 units numerous intrusive rocks can be observed. In order to determine the relationships between high temperature deformation and emplacement of igneous rocks, we investigate in detail the shear zone between the northern and the central part of the Lanzo peridotite. Field and petrological work allowed a broad study on the spatial distribution of peridotite deformation and relation with intrusive gabbros.

The shear zone including peridotite mylonite which separates the northern from the central body has a dimension of > 1500 meters length to at least 250 meters wide. The foliation is sub-vertical and dips to the NE. Progressive deformation towards the mylonite is reflected by the parallelization of pyroxenite bands. A series of gabbroic dikes ranging from olivine gabbro to kaersutite-bearing diorites is observed south of the mylonite zone, dipping steeply to the NW to N. The gabbroic dikes are discordant to the mylonitic foliation and are generally weakly deformed. Few gabbros have been found in the mylonite zone, they are partially discordant to the foliation but others are parallel to the mylonite. The spatial distribution of gabbro dikes relative to the peridotite mylonite varies from north to the south. They are much more abundant in the south. Thin section observations and SEM analysis of the peridotite mylonite reveal two parageneses: Porphyroclasts of olivine (ol), clinopyroxene (cpx), orthopyroxene (opx) and spinel (spl) are embedded in an extremely finegrained matrix of ol, cpx, opx, spl, and plagioclase (plg). Many opx porphyroclasts have aspect ratios up to 20:1. Thermobarometry of porphyroclastic mineral assemblages in the peridotite indicate very high temperatures (>1100°C-1250°C [Pognante et al., 1985]). In the mylonites, ol-rich zones are separated from opx-cpx-spl-plg rich zones. The grain size between the two bands is remarkably different with recrystallized olivines being much larger than recrystallized pyroxenes and spinel. In addition, olivine shows a strong lattice preferred orientation [Boudier, 1978].

Our preliminary observations indicate that actively deforming peridotite mylonite might suppress brittle failure and that ascending gabbros might terminate and crystallize along actively deforming shear zone. This is supported by the observation that gabbros are asymmetrically distributed with respect to the shear zone. If true, 'gabbro-rich zone' might be the footwall of high-temperature mylonitic shear zone. Such shear zones are a prerequisite for concave-downward detachment models where deeper and hotter mantle rocks are exhumed towards mid ocean ridges.

Boudier, F. [1978]; Geol Soc. Am Bull 89,1574-1591
Pognante, U., Rösli, U. and Toscani, L. [1985], Lithos 18, 201-214

Juxtaposition of melt migration and high-temperature shear zones (Lanzo, Italy).

M-A. KACZMAREK AND O. MÜNTENER

Institut de Géologie de Neuchâtel, rue Emile Argand 11, 2007 Neuchâtel, Switzerland.

Peridotite mylonite shear zones are commonly found in peridotite massifs [e.g. 1] and in peridotites dredged and drilled from the ocean floor [2-3] and may accommodate much of the deformation during magma-starved periods of (ultra-)slow spreading. Solid state reaction-induced grain size reduction is often assumed as an important process, but the potential role of melt-enhanced reactions is less well known. To provide constraints on the rheological weakening of mantle lithosphere, we investigate the mutual relationships between high-temperature deformation, melt-rock reaction and emplacement of plutonic rocks.

Results of a field study in the north of the Lanzo massif (N-Italy) reveals that a shear zone including peridotite mylonite has a dimension of > 1500 meters length to at least 250 meters wide. Petrological data and preliminary grain size analyses indicate 4 types of microstructures from porphyroclastic (grain size: 0.2 to 1.05 mm, aspect ratios between 1.6 and 2) to ultra-mylonitic (grain size: <0.05 to 0.15 mm, aspect ratios below 1.6). Typical peridotite mylonite bands consist of olivine (ol) + clinopyroxene (cpx) + orthopyroxene (opx) + plagioclase (plg) + Cr-Al spinel +/- Ti hornblende and enclose coarse porphyroclasts of pyroxene or polycrystalline bands of olivine. Some cpx porphyroclasts show signs of previous reaction textures with a melt (cpx_1 +liq -> opx + plg ± ol), a texture which is common in the southern Lanzo massif [4]. This indicates that the mylonite formation postdates cpx-corroding melt/rock reaction. On the other hand, a series of discordant gabbroic dikes ranging from ol-gabbro to kaersutite-bearing diorites are abundant on one side of the mylonite zone only and are generally weakly deformed.

Our preliminary results indicate that melt migration and high temperature deformation are juxtaposed both in time and space. Melt-rock reaction may caused grain size reduction which in turn led to localisation of deformation. Melt-enhanced shearing might be a prerequisite for the formation of large-scale detachment faults and oceanic core complexes at mid-ocean ridges.

References

[1] Vissers R.L.M., Drury M.R., Hoogerduijn-Strating E.H. and Van Der Wal D. (1991) *Geology* **19**, 990-993.

[2] Jaroslow G.E., Hirth G. and Dick H.J.B. (1996) *Tectonophysics* **256**, 17-37.

[3] ODP leg 209, preliminary reports.

[4] Müntener O. Piccardo G.B. (2003), *Geol Soc London Spec Publ*, **218,** in press.

SHRIMP U-Pb zircon dating of gabbro and granulite from the peridotite massif of Lanzo (Italy).

Kaczmarek, M.-A.[1,2], Rubatto, D.[3] and Müntener, O.[2]

(1) Institute of Geology, University of Neuchâtel, rue Emile Argand, 2007 Neuchâtel, Switzerland
(2) Institute of Geological Sciences, University of Bern, Baltzerst. 1, 3012 Bern, Switzerland
(3) Department of Earth and Marine Sciences The Australian National University, Canberra ACT 0200, Australia.

The Lanzo peridotite in the Western Alps is one of the largest plagioclase peridotite massifs. Its oceanic and Alpine metamorphic evolution have been matter of debate. The massif is subdivided into 3 parts, the southern, central and northern body, which are separated by shear zones. The numerous gabbroic dikes in the Lanzo massif can be separated into 2 groups (Boudier and Nicolas 1972; Boudier 1978)): (I) an oldest 'indigenous' group of troctolite to olivine gabbro, frequently occurring 'en echelon' with fuzzy contacts to the surrounding lherzolites and interpreted as genetically related to the plagioclase lherzolites. (II) An intrusive group of troctolite, olivine gabbros, gabbronorites to Fe-Ti gabbros, with usually sharp contacts towards the peridotite. We sampled zircon-bearing Fe-Ti gabbros from the second group in the central and southern part of the massif. In addition, one granulite sample situated in the serpentinized NW part of the massif was studied.

Fe-Ti gabbros contain a magmatic paragenesis composed of brown amphibole, ilmenite, pyroxene, apatite and zircon and a metamorphic paragenesis with garnet, chlorite, chloritoid, talk, and retrograde green amphibole. Zircons were studied by cathodoluminescence (CL) and analysed with SHRIMP II for U-Pb dating and LA-ICP-MS for trace element determination. CL imaging of zircon reveals magmatic zoning cross cut by a unzoned recrystallized domains. U-Pb dating of three samples indicates an age of magmatism of 160 to 163 Ma, similar to other Western Alps ophiolitic gabbros. In one sample, some zircon domains are as young as (150-151 Ma). Trace element chemistry of zircon by LA-ICP_MS indicates a positive Ce anomaly and a variable Eu negative anomaly. The Eu anomaly suggest plagioclase fractionation in the magma and is in line with the magmatic origin of the zircon. The recrystallized domains show some degree of trace element perturbation.

The granulitic sample is mainly composed of quartz, garnet, albite, white mica, rutile, titanite, ilmenite and chlorite. CL images of the numerous zircon crystals reveal metamorphic rims surrounding detrital cores. The cores yield ages from ~ 400 to ~ 1670 Ma as expected for a detrital population. CL imaging indicates two different domains in the metamorphic rims. A dark inner rim surrounding the detrital core, which was dated at ~ 304 Ma, and an outer rim dated at around 293 Ma. Such metamorphic ages are well known in the Austroalpine basement such as Ivrea or Sesia Zones. Zircon REE patterns from the granulitic sample show a positive slope from Gd to Lu for the core and a near flat pattern for the external rim. Analyses also indicate lower content of U for the core (132 to 1267ppm) than the rim (most around 2000 ppm). The internal and external rims can be distinguished on the basis of different U contents and trace element composition

Shear zone and melt impregnation in the peridotitic massif of Lanzo (Italy).

Kaczmarek M-A.(1,2*) and Müntener O.(2)
(1) Institute of Geology, University of Neuchâtel, rue Emile Argand, 2007 Neuchâtel, Switzerland
(2) Institute of Geological Sciences, University of Bern, Baltzerst. 1, 3012 Bern, Switzerland
mary-alix.kaczmarek@unine.ch; Othmar.Muntener@geo.unibe.ch

Mylonitic mantle shear zone are commonly found in peridotite massifs (e.g. Vissers et al., 1991) and in the oceanic lithosphere (Jaroslow et al. 1996, preliminary report ODP leg 209), may control the strength of the mantle lithosphere (Vissers et al., 1995) during magma-starved periods of (ultra-)slow spreading. Previous works in the Lanzo massif indicate the presence of shear zone (Boudier, 1978) and pervasive magma flow (Bodinier et al., 1986). Solid-state reaction-induced grain size reduction is often assumed as an important process, but the role of melt-enhanced reactions is less well known. To provide constraints on the rheological weakening of mantle lithosphere, we investigate the mutual relationships between high-temperature deformation, melt-rock reaction and emplacement of plutonic rocks in the plagioclase peridotite massif of Lanzo.
Fieldwork in the north of the Lanzo massif (N-Italy) reveals that a peridotite mantle shear zone has a dimension of > 1500 meters length to at least 250 meters wide with a sub-vertical foliation and dips to the NE. A series of discordant gabbroic dikes ranging from ol-gabbro to kaersutite-bearing diorites are abundant on the south of the mylonite and are generally weakly deformed. Petrological data and preliminary grain size analyses indicate 4 types of microstructures from “proto-granular” with magmatic and impregnate texture (grain size: 0.2 to 1.05 mm, aspect ratios: 1.6 to 2) to ultra-mylonitic (grain size: <0.05 to 0.15 mm, aspect ratios ~ 1.6) with porphyroclastic orthopyroxene (opx) extremely stretch (aspect ration up to 10:1). This classification reveals a dissymmetric deformation repartition: the interval from ultra-mylonitic rock to proto-granular rocks is smaller in the north (close to 1 km) than in the south (> to 2 km). close to the foliation for area with smalls grains (< 50 μm) and discordant orientation in rich olivine area with grain size around 100μm or more. Typical peridotite mylonite bands consist of olivine (ol) + clinopyroxene (cpx) + opx + plagioclase (plg) + Cr-Al spinel +/- Ti hornblende and enclose coarse porphyroclasts of pyroxene or polycrystalline bands of olivine. Some cpx porphyroclasts show signs of previous re-action textures with a melt (cpx_1 +liq -> opx + plg ± ol), a texture which is common in the southern Lanzo massif (Müntener and Piccardo, 2003). This indicates that the mylonite formation postdates cpx-corroding melt/rock reaction. Thermobarometry of porphyroclastic mineral assemblages in the peridotite indicate very high temperatures (>1100°C-1250°C [Pognante et al., 1985]), and preliminary results of blasts crystallization condition indicate temperature close to 850°C.
Our preliminary results indicate that melt migration and high temperature deformation are juxtaposed both in time and space. Melt-rock reaction may caused grain size reduction which in turn led to localisation of deformation. Observations indicate that actively deforming peridotite mylonite might suppress brittle failure and that ascending gabbros might terminate and crystallize along actively deforming shear zone. This is supported by the observation that gabbros are asymmetrically distributed with respect to

the shear zone. If true, 'gabbro-rich zone' might be the footwall of high-temperature mylonitic shear zone.

Boudier, F., 1978. Structure and petrology of the Lanzo peridotite massif (Piedmont Alps). Geologicclas Society of America Bulletin, 89: 1574-1591.
Bodinier, J.L., Giraud M., Dupuy C. and Dostal J.,1986. Geochemistry of basic dykes in the Lanzo massif (w.A.) Tectonophysics, 128: 77-95
Jaroslow et al. 1996.
Müntener, O., and Piccardo, G., 2003.
Pognante 1985.
Preliminary report ODP leg 209.
Vissers et al., 1991.
Vissers et al., 1995.

High temperature shear zones and melt impregnation in the upper mantle (Lanzo massif, Italy). Implications for continental breakup.

Kaczmarek, M.-A.[1,2], Müntener O.[2]

(1) Institute of Geology, University of Neuchâtel, rue E. Argand 11, 2009 Neuchâtel, Suisse

(2) Institute of Geological Sciences, University of Bern, Baltzerstr. 1, 3012 Bern, Suisse

Different mantle domains characterize present-day and ancient ocean-continent transition zones and many of them show signs of melt/rock reaction, but their relationships to deformation processes in the thermal boundary layer are poorly understood. The transition from melt-poor to -rich regions is likely to be an important rheological boundary. To constrain the rheological weakening of mantle lithosphere, we investigate the relationships between deformation, melt-rock reaction and mafic dike emplacement in the Lanzo peridotite massif (NW-Italy).

Between the northern and central parts of the massif, deformation textures are coarse-grained secondary granular (CGSG) to mylonite and hydrous-mylonite (HM). CGSG shows weakly deformed, porphyroclastic zones and domains of igneous recrystallization. Mylonite and HM show a fine-grained, polycrystalline matrix (ol, pl, cpx, opx, sp, Ti-hbl), enclosing porphyroclasts. HM contains hydrated fine-grained areas composed of chlorite and hbl. The spatial distribution of deformation is asymmetric with respect to the mylonite and increase from S to N. Discordant gabbroic dikes are asymmetrically distributed and concentrated in the southern part of the shear zone.

The pyroxene chemistry is correlated with grain size: porphyroclastic, high Al, low Ti cpx cores are irregularly replaced by lower Al, high Ti cpx. Thermometry indicates 1100-1030°C (cores) and lower equilibration temperatures for neoblasts (850-855°C). Corroded cpx porphyroclasts and interstitial opx surrounding ol demonstrate that (sp) peridotites reacted with melts during deformation. Spinel compositions cover the entire range from spinel to plagioclase peridotites, indicating disequilibrium.

The preservation of chemical disequilibrium of spinel and pyroxenes in the footwall of the shear zone suggests rapid temperature decrease from near-solidus conditions to the conditions of chlorite and hbl stability. Steep thermal gradients between infiltrated and lithospheric peridotites are compatible with numerical models that predict the exhumation of hot mantle material beneath thinned continental crust prior to the exposure on the seafloor. Melt migration in the footwall suggests that the shear zone acted as a permeability barrier.

(higher U and lower HREE in the internal rim). This indicated that the two rims formed in different conditions, and thus their age reflects different metamorphic stages. The presence of a granulite body zone within the Lanzo serpentinite, testify for a complicated history of the Lanzo massif. This body is probably derived from the nearby Sesia Zone and was incorporated in the serpentinite during Jurassic tectonics or, more likely, in Alpine times.

Boudier, F. (1978). "Structure and petrology of the Lanzo peridotite massif (Piedmont Alps)." Geological Society of America Bulletin **89**: 1574-1591.
Boudier, F. and A. Nicolas (1972). "Fusion partielle gabbroïque dans la lherzolite de Lanzo (Alpes piémontaises)." Schweizerische Mineralogische und Petrographische Mitteilungen **52**: 39-56.

REFERENCES

Aldiss, D.T., 1981. Plagiogranites from the ocean crust and ophiolites. Nature, 289: 577-578.
Allan, J.F. and Dick, H.J.B., 1996. Cr-rich spinel as a tracer for melt migration and melt-wall rock interaction in the mantle: Hess Deep, Leg 147. Proceedings of the Ocean Drilling Program, Scientific results, 147: 157-172.
Allegre, C.J. and Turcotte, D.L., 1986. Implications of a two-component marble-cake mantle. Nature, 323(6084): 123-127.
Ballhaus, C., Berry, R.F. and Green, D.H., 1991. High pressure experimental calibration of the olivine-orthopyroxene-spinel oxygen geobarometer; implications for the oxidation state of the upper mantle. Contributions to Mineralogy and Petrology, 107(1): 27-40.
Beccaluva, L., Macciotta, G., Piccardo, G.B. and Zeda, O., 1984. Petrology of lherzolitic rocks from the Northern Apennine ophiolites. Lithos, 17: 299-316.
Bedini, R.M., Bodinier, J.L., Dautria, J.M. and Morten, L., 1997. Evolution of LILE-enriched small melt fractions in the lithospheric mantle; a case study from the East African Rift. Earth and Planetary Sciences Letters, 153(1-2): 67-83.
Bente, K. and Lensch, G., 1981. Studies of retromorphosed dikes of southern Lanzo peridotite massif, Italian Western Alps. Schweizerische Mineralogische und Petrographische Mitteilungen, 61(2-3): 297-303.
Berthé, D., Choukroune, P. and Gapais, D., 1979. Orientation preferentielle du quartz et orthogneissification progressive en regime cisaillant: l'exemple du cisaillement sud-armoricain. Bulletin de Minéralogie, 102: 265-272.
Beslier, M.O., Cornen, G. and Girardeau, J., 1996. Tectono-metamorphic evolution of peridotites from the ocean/continent tansition of the Iberai abyssal plain margin. Proceedings of the Ocean Drilling Program, Scientific Results, 149: 397-412.
Bill, M., Bussy, F., Cosca, M., Masson, H. and Hunziker, J.C., 1997. High-precision U-Pb and 40Ar/39Ar dating of an Alpine ophiolite (Gets nappe, French Alps). Eclogae Geologicae Helvetiae, 90: 43-54.
Bill, M., Nagler, T.F. and Masson, H., 2000. Major, minor, trace element, Sm-Nd and Sr isotope compositions of mafic rocks from the earliest oceanic crust of the Alpine Tethys. Schweizerische Mineralogische und Petrographische Mitteilungen, 80: 131-145.
Black, L.P. Kamo, S. L., Williams, I., Mundil, R., Davis, D. W., Korsch, R. J. and Foudoulis, C., 2003. The application of SHRIMP to Phanerozoic geochronology; a critical appraisal of four zircon standards. Chemical Geology, 200: 171-188.
Blackman, D.K., Cann, J.R., Janssen, B. and Smith, D.K., 1998. Origin of extensional core complexes: evidence from the Mid-Atlantic at Atlantis Fracture Zone. Journal of Geophysical Research, 103(B9): 21,315-21,333.
Bodinier, J.L., 1988a. Geochemistry and petrogenesis of the Lanzo peridotite body, Western Alps. Tectonophysics, 149: 67-88.
Bodinier, J.L. and Godard, M., 2003. Orogenic, ophiolitic and abyssal peridotites. Treatise on Geochemistry, 2: 103-170.
Bodinier, J.L., Guirard, M., Dupuy, C. and Dostal, J., 1986. Geochemistry of basic dikes in the Lanzo massif (Western Alps): petrogenetic and geodynamic implications. Tectonophysics, 128: 77-95.
Bodinier, J.L., Menzies, M.A. and Thirlwall, M.F., 1991. continental to oceanic mantle transition -REE and Sr-Nd isotopic geochemistry of the Lanzo lherzolite massif. Journal of Petrology, Special Lherzolite Issue: 191-210.
Bonatti, E., Brunelli, D., Fabretti, P., Ligi, M., Portaro, R. A. and Seyler, M., 2001. Steady-state creation of crust-free lithopshere at colds spots in mid-ocean ridges. Geology, 29(11): 979-982.
Borghini, G., Rampone, E., Crispini, L., De Ferrari, R. and Godard, M., 2007. Origin and emplacement of ultramafic-mafic intrusions in the Erro-Tobbio mantle peridotite (Ligurian Alps, Italy). Lithos, 94(1-4): 210-229.
Borsi, L., Schärer, U., Gaggero, L. and Crispini, L., 1996. Age, origin and geodynamic significance of plagiogranites in lherzolites and gabbros of the Piedmont-Liguria ocean basin. Earth and Planetary Science Letters, 140: 227-241.
Boudier, F., 1972. Relations lherzolites-gabbro-dunite dans le massif de Lanzo (Alpes Piémontaises): exemple de fusion partielle, Université de Nantes, Nantes, 106 pp.
Boudier, F., 1978. Structure and petrology of the Lanzo peridotite massif (Piedmont Alps). Geological Society of America Bulletin, 89(10): 1574-1591.
Boudier, F., Ceuleneer, G. and Nicolas, A., 1988. Shear zones, thrusts and related magmatism in the Oman ophiolite; initiation of thrusting on an oceanic ridge. Tectonophysics, 151(1-4): 275-296.
Boudier, F. and Nicolas, A., 1972. Fusion partielle gabbroique dans la lherzolite de Lanzo (Alpes Piémontaises). Bulletin Suisse de Minéralogie et de Pétrographie, 52(1): 39-56.
Boudier, F. and Nicolas, A., 1977. Structural controls on partial melting in the Lanzo peridotites. Bulletin - Oregon, Department of Geology and Mineral Industries, 96: 63-78.
Boudier, F. and Nicolas, A., 1982. Stress and strain estimates in the Lanzo peridotite massif (western Alps). Collection internationales, CNRS Paris, 272: 221-228.
Bown, J. and White, R.S., 1994. Variation with spreading rate of oceanic crustal thickness and geochemistry. Earth and Planetary Science Letters, 121: 435-439.
Brey, G.P. and Köhler, T., 1990. Geothermobarometry in four-phase lherzolites II. New thermobarometers, and practical assessment of existing thermobarometers. Journal of Petrology, 31(6): 1353-1378.
Cannat, M., 1993. Emplacement of mantle rocks in the seafloor at mid-ocean ridges. Journal of Geophysical Research, 98(B3): 4163-4172.
Cannat, M., 1996. How thick is the magmatic crust at slow spreading oceanic ridges? Journal of Geophysical Research, 101(B2): 2847-2857.

Cannat, M., Bideau, D. and Bougault, H., 1992. Serpentinized peridotites and gabbros in the Mid-Atlantic Ridge axial valley at 15 degrees 37'N and 16 degrees 52'N. Earth and Planetary Sciences Letters, 109(1-2): 87-106.

Cannat, M., Chatin, F., Whitechurch, H. and Ceuleneer, G., 1997a. II. Gabbroic rocks trapped in the upper mantle at the mid-atlantic ridge. Proceedings of the Ocean Drilling Program, Scientific results, 153: 243-264.

Cannat, M. Lagabrielle, Y., Bougault, H., Casey, J., de Coutures, N., Dmitriev, L., Fouquet, Y., 1997b. Ultramafic and gabbroic exposures at the Mid-Atlantic ridge: geological mapping in the 15°N region. Tectonophysics, 279: 193-213.

Cannat, M., Mével, C. and Stakes, D., 1991. Normal ductile shear zones at an oceanic spreading ridge: tectonic evolution of site 735 gabbros (Southwest Indian Ridge). Proceedings of the Ocean Drilling Program, Scientific Results, 118: 415-429.

Ceuleneer, G., Nicolas, A. and Boudier, F., 1988. Mantle flow patterns at an oceanic spreading centre; the Oman peridotites record. Tectonophysics, 151(1-4): 1-26.

Compagnoni, R., 1977. The Sesio-Lanzo Zone; high pressure-low temperature metamorphism in the austroalpine continental margin. Rendiconti della Società Italiana di Mineralogia e Petrologia, 33(2): 335-374.

Compagnoni, R. and Sandrone, R., 1979. Il massicio di Lanzo nel quadro del metamorphismo alpino. S. I. M. P, 35(2): 842.

Compston, W., Williams, I., Kirschvink, J.L., Zhang, Z. and Ma, G., 1992. Zircon U-Pb ages for the Early Cambrian time-scale. Journal of the Geological Society of London, 149(2): 171-184.

Compston, W., Williams, I. and Meyer-Charles, E., 1984. U-Pb geochronology of zircons from lunar breccia 73217 using a sensitive high mass resolution ion microprobe. Journal of Geophysical Research, 89: 525-534.

Coogan, L.A. and Hinton, R.W., 2006. Do the trace element compositions of detrital zircons require Hadean continental crust? Geology, 34(8): 633-636.

Corfu, F., Hanchar, J.M., Hoskin, P.W.O. and Kinny, P., 2003. Atlas of Zircon Textures. In: J.M. Hanchar and P.W.O. Hoskin (Editors), Zircon. Reviews in Mineralogy and Geochemistry. Mineralogical Society of America and Geochemical Society, Washington, DC, pp. 469-500.

Costa, S. and Caby, R., 2001. Evolution of the Ligurian Tethys in the Western Alps: Sm/Nd and U/Pb geochronology and rare-earth element geochemistry of the Montgenevre ophiolite, France. Chemical Geology, 175: 449-466.

Dal Piaz, G.V., 1974. High-pressure and low-temperature metamorphism within the structural evolution of the Alpine-Apennine ophiolitic basin; Part I, Paleogeographic considerations. Bollettino della Societa Geologica Italiana, 93(2): 437-467.

Dal Piaz, G.V., 1988. Revised setting of the Piedmont zone in the northern Aosta valley, western Alps. Ofioliti, 13(2-3): 157-162.

Decandia, F.A. and Elter, P., 1972. La "zona" ofiolitifera del Bracco nel settore compreso fra Levanto e la Val Graveglia (Appennino ligure), Memorie della Società Geologica Italiana, pp. 503-530.

Dennis, A.J. and Secor, D.T., 1987. A model for the development of crenulations in shear zones with applications from the Southern Appalachian Piedmont. Journal of Structural Geology, 9: 809-817.

Desmurs, L., 2001. Mantle evolution and magmatism in an evolving ocean-continent transition: The Platta nappe, eastern Switzerland, Swiss Federal Institute of Technology Zurich, 159 pp.

Desmurs, L., Müntener, O. and Manatschal, G., 2002. Onset of magmatic accretion within a magma-poor rifted margin: a case study from the Platta ocean-continent transition, eastern Switzerland. Contrib Mineral Petrol, 144: 365-382.

Dick, H.J.B., 1989. Abyssal peridotites, very slow spreading ridges and ocean ridge magmatism. Geological Society Special Publication of London, 42: 71-105.

Dick, H.J.B., 1994. ODP looks through tectonic windows. JOI/USSAC newsletter, 7(2): 1-3.

Dick, H.J.B. and Bullen, T., 1984. Chromian spinel as a petrogenetic indicator in abyssal and alpine-type peridotites and spatially associated lavas. Contributions to Mineralogy and Petrology, 86(1): 54-64.

Dick, H.J.B., Fisher, R.L. and Bryan, W.B., 1984. Mineralogic variability of the uppermost mantle along mid-ocean ridges. Earth and Planetary Science Letters, 69: 88-106.

Dick, H.J.B., Lin, J. and Schouten, H., 2003. An ultraslow-spreading class of ocean ridge. Nature, 426(6965): 405-412.

Dick, H.J.B. and Natland, J.H., 1996. Late-stage melt evolution and transport in the shallow mantle beneath the East Pacific Rise. Proceedings of the Ocean Drilling Program, Scientific results, 147: 103-134.

Dick, H.J.B., Natland, J. H., Alt, J. C., Bach, W., Bideau, D., Gee, J. S., Haggas, S., Hertogen, J. G. H., Hirth, G., Holm, P. M., Ildefonse, B., Iturrino, G. J., John, B. E., Kelley, D. S., Kikawa, E., Kingdon, A., LeRoux, P. J., Maeda, J., Meyer, P. S., Miller, D. J., Naslund, H. R., Niu, Y. L., Robinson, P. T., Snow, J., Stephen, R. A., Trimby, P. W., Worm, H. U. and Yoshinobu, A., 2000. A long in situ section of the lower ocean crust: results of ODP Leg 176 drilling at the Southwest Indian ridge, Earth and Planetary Science Letters, pp. 31-51.

Dick, H.J.B., Schouten, H., Meyer, P. S., Gallo, D. G., Bergh, H., Tyce, R., Patriat, P., Johnson, K. T. M., Snow, J. and Fisher, A., 1991. Tectonic evolution of the Atlantis II fracture zone. Proceedings of the Ocean Drilling Program, Scientific Results, 118: 359-398.

Dietrich, V.J., 1969. Die ophiolite des Oberhalbsteins (Graubünden) und das Ophiolithmaterial des ostschweizerischen Molasseablagerungen, ein petrographischer Vergleich, Bern, 179 pp.

Dijkstra, H.A., Drury, M.R. and Vissers, R.L.M., 2001. Structural petrology of plagioclase peridotites in the west Othris Mountains (Greece): melt impregnation in the mantle lithosphere. Journal of Petrology, 42(1): 5-24.

Dijkstra, H.A., Drury, M.R., Vissers, R.L.M. and Newman, J., 2002. On the role of melt-rock reaction in mantle shear zone

formation in the Othris peridotite massif (Greece). Journal of Structural Geology, 24: 1431-1450.
Droop, G.T.R., Lombardo, B. and Pognante, U., 1990. Formation and distribution of eclogite facies rocks in the Alps. In: D.A. Carswell (Editor), Eclogite facies rocks. Blackie, Glasgow and London, pp. 225-259.
Drury, M.R. and Fitz Gerald, J.D., 1998. Mantle rheology: insights from laboratory studies of deformation and phases transition. In: I. Jackson (Editor), The earth's mantle: composition, structure, and evolution. Cambridge University Press, Cambridge, pp. 503-559.
Drury, M.R., Hoogerduijn Strating, E.H. and Vissers, R.L.M., 1990. Shear zone structures and microstructures in mantle peridotites from the Voltri Massif, Ligurian Alps, N.W. Italy. Geologie en Mijnbouw, 69(1): 3-17.
Eggins, S.M., Rudnick, R.L. and McDonough, W.F., 1998. The composition of peridotites and their minerals; a laser-ablation ICP-MS study. Earth and Planetary Science Letters, 154(1-4): 53-71.
Elthon, D., 1992. Chemical trends in abyssal peridotites; refertilization of depleted suboceanic mantle. Journal of Geophysical Research, 97(6).
Ernst, W.G. and Piccardo, G.B., 1979. Petrogenesis of some Ligurian Peridotites; I Mineral and bulk-rock chemistry. Geochimica and Cosmochimica Acta, 43(2): 219-238.
Florineth, D. and Froitzheim, N., 1994. Transition from continental to oceanic basement in the Tasna nappe (Engadine window, Graubünden, Switzerland): evidence for Ealy Cretaceous opening of the Valais ocean. Schweizerisches Mineralogische und Petrographische Mitteilungen, 74: 437-448.
Frey, F.A., Suen, C.J. and Stockman, H.W., 1985. The Ronda high temperature peridotite: geochemistry and petrogenesis. Geochimica et Cosmochimica Acta, 49: 2469-2491.
Froitzheim, N. and Eberli, G.P., 1990. Extensional detachment faulting in the evolution of a Tethys passive continental margin, Eastern Alps, Switzerland. Geological Society of America Bulletin, 102: 1297-1308.
Froitzheim, N. and Manatschal, G., 1996. Kinematics of Jurassic rifting, mantle exhumation, and passive margin formation in the Austroalpine and Penninic nappes (Eastern Switzerland). Geological Society of America Bulletin, 108(9): 1120-1133.
Froitzheim, N., Schmid, S.M. and Frey, M., 1996. Mesozoic paleogeography and timing of eclogite-facies metamorphism in the Alps: A working hypothesis. Eclogae Geologicae Helvetiae, 89(1): 81-110.
Furusho, M. and Kanagawa, K., 1999. Transformation-induced strain localization in a lherzolite mylonite from the Hidaka metamorphic belt of the central Hokkaido, Japan. Tectonophysics, 313: 411-432.
Garrido, C. J. and Bodinier, J.L., 1999. Diversity of mafic rocks in the Ronda peridotite: evidence for pervasive melt-rock reaction during heating of subcontinental lithosphere by upwelling asthenosphere. Journal of Petrology, 40(5): 729-754.
Gasparik, T., 1987. Orthopyroxene thermometry in simple and complex systems. Contributions to Mineralogy and Petrology, 96: 357-370.
Gebauer, D., Tilton, G.R., Schertl, H.-P. and Schreyer, W., 1993. Eocene/Oligocene ultrahigh-pressure metamorphism in the Dora Maira Massif (Western Alps) and it s geodynamic implications. Terra Nova, 5(Terra abstract): 10.
Girardeau, J. and Mercier, J.-C.C., 1992. Evidence for plagioclase-lherzolite intrusion in the Mid-Atlantic Ridge, DSDP Leg 37. In: L.M. Parsons , B.J. Murton and P. Browning (Editors), Ophiolite and their modern oceanic analogues. Geological Society Special Publications. Geological Society of London, London, pp. 241-250.
Godard, M., Jousselin, D. and Bodinier, J.L., 2000. Relationships between geochemistry and structure beneath a paleo-spreading centre: a study of the mantle section in the Oman ophiolite. Earts and Planetary Science Letters, 180: 133-148.
Handy, M.R., 1989. Deformation regimes and the rheological evolution of fault zones in the lithosphere: the effects of pressure, temperature, grainsize and time. Tectonophysics, 163: 119-152.
Hart, S.R. and Dunn, T., 1993. Experimental cpx/melt partitioning of 24 trace elements. Contributions to Mineralogy and Petrology, 113(1): 1-8.
Hellebrand, E., Snow, J., Dick, H.J.B. and Hofmann, A.W., 2001. Coupled major and trace elements as indicators of the extent of melting in mid-ocean-ridge peridotites. Nature, 410: 677-681.
Hellebrand, E., Snow, J., Mostefaoui, S. and Hoppe, P., 2005. Trace element distribution between orthopyroxene and clinopyroxene in periodotites from the Gakkel Ridge; a SIMS and NanoSIMS study. Contributions to Mineralogy and Petrology, 150(5): 486-504.
Hellebrand, E., Snow, J.E., Dick, H.J.B., Devey, C.W. and Hofmann, A.W., 1999. Reactive crack flow in the oceanic mantle: an ion probe study on cpx from vein-bearing abyssal peridotites. Ofioliti, 24: 106-107.
Hellebrand, E., Snow, J.E. and Mühe, R., 2002. Mantle melting beneath Gakkel Ridge (Artic Ocean): abyssal peridotite spinel compositions. Chemical Geology, 182: 227-235.
Herwegh, M., Berger, A. and Ebert, A., 2005. Grain coarsening maps: a new tool to predict microfabric evolution of polymineralic rocks. Geological Society of America, 33(10): 801-804.
Hiess, J., Nutman, A., Bennett, V. and Holden, P., 2006. Ti zircon thermometry applied to metamorphic and igneous systems. Geochimica et Cosmochimica Acta, 70(18): A250.
Hinton, R.W. and Upton, B.G.J., 1991. The chemistry of zircon: variations within and between large crystals from syenite and alkali basalts xenoliths. Geochimica et Cosmochimica Acta, 55: 3287-3302.
Hirth, G. and Kohlstedt, D.L., 1995a. Experimental constraints on the dynamics of the partially molten upper mantle; 2,

Deformation in the dislocation creep regime. Journal of Geophysical Research, 100(8): 15441-15449.
Hirth, G. and Kohlstedt, D.L., 1995b. Experimental constraints on the dynamics of the partially molten upper mantle; Deformation in the diffusion creep regime. Journal of Geophysical Research, 100(2): 1981-2001.
Hofmann, A.W., 1988. Chemical differentiation of the Earth; the relationship between mantle, continental crust, and oceanic crust. Earth and Planetary Sciences Letters, 90(3): 297-314.
Hoogerduijn Strating, E.H., Rampone, E., Piccardo, G.B., Drury, M.R. and Vissers, R.L.M., 1993. Subsolidus emplacement of mantle peridotite during incipient oceanic rifting and opening of the Mesozoic Tethys (Voltri massif, NW Italy). Journal of Petrology, 34(5): 901-927.
Ionov, D.A., Savoyant, L. and dupuy, C., 1992. Application of the ICP-MS technique to trace element analysis of peridotites and their minerals. Geostandards Newsletter, 16: 311-315.
Jagoutz, E., Palme, H., Baddenhausen, H., Blum, K., Cendales, G., Dreibus, G., spettel, B., Lorenz, V. and Vanke, H., 1979. The abundance of major, minor and trace elements in the earth's mantle as derived from primitive ultramafic nodules. Geochimica and Cosmochimica Acta, 11(2031-2050).
Jaroslow, G.E., Hirth, G. and Dick, H.J.B., 1996. Abyssal peridotite mylonites: implications for grain-size sensitive flow and strain localization in the oceanic lithopshere. Tectonophysics, 256: 17-37.
Jochum, K.P., Seufert, H.M. and Thirlwall, M.F., 1990. Multi-element analysis of 15 international standard rocks by isotope-disolution spark source mass spectrometry. Geostandards Newsletter, 14: 469-473.
Johnson, K.T.M. and Dick, H.J.B., 1992. Open system melting and temporal and spatial variation of peridotite and basalt at the Atlantis II fracture zone. Journal of Geophysical Research, 97(6): 9219-9241.
Johnson, K.T.M., Dick, H.J.B. and Shimizu, N., 1990. Melting in the oceanic upper mantle: an ion microprobe study of diopsides in abyssal peridotites. Journal of Geophysical Research, 95(B3): 2661-2678.
Kaczmarek, M.-A. and Müntener, O., 2005. Exhumation of mantle lithosphere: field relations, and interaction processes between magmatism and deformation (Field trip to the northern Lanzo peridotite). Ofioliti, 30(2): 125-134.
Kelemen, P.B., Dick, H.J.B. and Quick, J.E., 1992. Formation of harzburgite by pervasive melt/rock reaction in the upper mantle. Nature, 358: 635-641.
Kelemen, P.B. et al., 2004. ODP Leg 209 drills into mantle peridotite along the Mid-Atlantic Ridge from 14 degrees N to 16 degrees N. Joint Oceanographic Institutions for Deep Earth Sampling Journal, 30(1): 14-19.
Kelemen, P.B., Koga, K. and Shimizu, N., 1997. Geochemistry of gabbro sills in the crust-mantle transition zone of the Oman ophiolite: implications for the origin of the oceanic lower crust. Earth and Planetary Science, 146: 475-488.
Kelemen, P.B., Shimizu, N. and Salters, V.J.M., 1995. Extraction of mid-ocean-ridge basalt from the upwelling mantle by focused flow of melt in dunite channels. Nature, 375: 747-753.
Kienast, J.R. and Pognante, U., 1988. Chloritoid-bearing assemblages in eclogitized metagabbros of the Lanzo peridotite body (western Italian Alps). Lithos, 21(1): 1-11.
Kinzler, R.J., 1997. Melting of mantle peridotite at pressures approaching the spinel to garnet transition; application to mid-ocean ridge basalt petrogenesis. Journal of Geophysical Research, 102(1): 853-874.
Klemme, S. and O'Neill, H.S.C., 2000. The near-solidus transition from garnet lherzolite to spinel lherzolite. Contributions to Mineralogy and Petrology, 138: 237-248.
Koepke, J., Feig, S.T. and Snow, J., 2005. Hydrous partial melting within the lower oceanic crust, Terra Nova, pp. 286-291.
Lagabrielle, Y. and Cannat, M., 1990. Alpine Jurassic ophiolites resemble the modern central Atlantic basement. Geology, 18(4): 319-322.
Lagabrielle, Y., Fudral, S. and Kienast, J.-R., 1989. La couverture océanique des ultrabasites de Lanzo (Alpes Occidentales): arguments lithostratigraphiques et pétrologiques. Geodinamica Acta, 4(1): 43-55.
Lagabrielle, Y. and Lemoine, M., 1997. Alpine, Corsican and Apennine ophiolites: the slow-spreading ridge model. C. R. Acad. Sci. Paris, 325: 909-920.
Langmuir, C., Fornari, D., Colodner, D., Charlou, J. L., Costa, I., Desbruyeres, D., Desonie, D., Emerson, T., Fiala-Medioni, A., Fouquet, Y., Humphris, S., Saldanha, L., Sours-Page, R., Thatcher, M., Tivey, M., van Dover, C., von Damm, K., Wiese, K and Wilson, C. J. N., 1993. Geological setting and characteristics of the Lucky strike vent field at 37 degrees 17'N on the Mid-Atlantic Ridge, AGU 1993 fall meeting. American Geophysical Union, Washington, DC, United States, San Francisco, pp. 99.
Lardeaux, J.M. and Spalla, M.I., 1991. From granulites to eclogites in the Sesia zone (Italian Western Alps): a record of the opening and closure of the Piemont ocean. Journal of Metamorphic Geology, 9: 35-59.
Lavier, L.L. and Manatschal, G., 2006. A mechanism to thin the continental lithosphere at magma-poor margins, Nature, pp. 324-328.
Lemoine, M. Arnaud-Vanneau, A., Arnaud, H., Bas, T., Bourbon, M., Dumont, T., Gidon, M., de Graciansky, P.-C., Megard-Galli, J., Rudkiewicz, J.-L. and Tricart, P., 1986. Etapes et modalités de la subsidence d'une paléo-marge passive : les Alpes occidentales au mésozoique. Bulletin des Centres de Recherche et d'Exploration-Production d'Elf-Aquitaine, 10(1): 143-149.
Lemoine, M., Tricart, P. and Boillot, G., 1987. Ultramafic and gabbroic ocean floor of the Ligurian Tethys (Alps, Corsica, Apennines): In search of a genetic model. Geology, 15: 622-625.
Lemoine, M. Tricart, P., Caby, R., Carpena, J., Lagabrielle, Y., Polino, R. and De Wever, P., 1985. Radiometric versus stratigraphic dating of the Western Alps ophiolites; contradictions, problems, geodynamic implications. Ofioliti,

10(2-3): 525.
Lenoir, X., Garrido, C.J., Bodinier, J.L. and Dautria, J.M., 2000. Contrasting lithospheric mantle domains beneath the Massif Central (France) revealed by geochemistry of peridotite xenoliths. Earth and Planetary Sciences Letters, 181: 359-375.
Lenoir, X., Garrido, C.J., Bodinier, J.L., Dautria, J.M. and Gervilla, F., 2001. The recrystallization front of the Ronda peridotite: Evidence for melting and thermal erosion of subcontinental lithospheric mantle beneath the Alboran basin. Journal of Petrology, 42: 141-158.
Lombardo, B. and Pognante, U., 1982. Tectonic implications in the evolution of the Western Alps ophiolite metagabbros. Ofioliti, 2/3: 371-394.
Lombardo, B., Rubatto, D. and Castelli, D., 2002. Ion microprobe U-Pb dating of zircon from a Monviso metaplagiogranite: implications for the evolution of the Piedmont-Liguria Tethys in the western Alps. Ofioliti, 27(2): 109-117.
Ludwig, K.R., 2003. Isoplot/Ex version 3.0. A geochronological toolkit for Microsoft Excel. Berkeley Geochronological Centre Spec. Publication.
Mainprice, D., 1997. Modelling the anisotropic seismic properties of partially molten rocks found at mid-ocean ridges. Tectonophysics, 279: 161-179.
Manatschal, G., 2004. New models for evolution of magma-poor rifted margins based on a review of data and concepts from West Iberai and the Alps. International Journal of Earth Sciences, 93: 432-466.
Manatschal, G. and Bernoulli, D., 1999. Architecture and tectonic evolution of nonvolcanic margins; present-day Galicia and ancient Adria. Tectonics, 18(6): 1099-1119.
Manatschal, G. and Nievergelt, P., 1997. A continent-ocean transition recorded in the Err and Plata nappes (Eastern Switzerland). Eclogae Geologicae Helvetiae, 90(1): 3-27.
Marroni, M., Molli, G., Montanini, A. and Tribuzio, R., 1998. The association of continental crust rocks with ophiolites in the Northern Apennines (Italy); implications for the continent-ocean transition in the western Tethys. Tectonophysics, 292(1-2): 43-66.
McDonough, W.F. and Sun, S.S., 1995. The composition of the Earth. Chemical Geology, 120: 223-253.
Menzies, M.A., 1973. Mineralogy and partial melt textures within an ultramafic-mafic body, Greece. Contributions to Mineralogy and Petrology, 42(4): 273-285.
Mercier, J.-C.C. and Nicolas, A., 1975. Textures and fabrics of upper-mantle peridotites as illustrated by xenoliths from basalts. Journal of Petrology, 16(2): 454-487.
Michael, P.J. and Bonatti, E., 1985. Peridotite composition from th eNorth Atlantic; regional and tectonic variations and implications for partial melting. Earth and Planetary Science Letters, 73: 91-104.
Michael, P.J., Langmuir, C., Dick, H. J. B., Snow, J. E., Goldstein, S. L., Graham, D. W., Lehnert, K., Kurras, G., Jokat, W., Mühe, R and Edmonds, H. N., 2003. magmatic and amagmatic seafloor generation at the ultra-slow-spreading Gakkel ridge, Artic Ocean. Nature, 423: 956-961.
Müntener, O. and Hermann, J., 1996. The Val Malenco lower crust-upper crust mantle complex and its field relations (Italian Alps). Schweizerisches Mineralogische und Petrographische Mitteilungen, 76: 475-500.
Müntener, O., Hermann, J. and Trommsdorff, V., 2000. Cooling History and Exhumation of Lower-Crustal Granulite and Upper Mantle (Malenco, Eastern Central Alps). Journal of Petrology, 41(2): 175-200.
Müntener, O. and Manatschal, G., 2006. High degrees of melting recorded by spinel harzburgites of the Newfoundland margin: The role of inheritance and consequences for the evolution of the southern North Atlantic. Earth and Planetary Science Letters, 252: 437-452.
Müntener, O., Pettke, T., Desmurs, L., Meier, M. and Schaltegger, U., 2004. Refertilization of mantle peridotite in embryonic ocean basins: trace element and Nd isotopic evidence and implications for crust-mantle relationships. Earth and Planetary Sciences Letters, 221: 293-308.
Müntener, O. and Piccardo, G.B., 2003. Melt migration in ophiolitic peridotites: the message from Alpine-Apennine peridotites and implications for embryonic ocean basins. The Geological Society of London, Special publications, 218, 69-89pp.
Müntener, O., Piccardo, G.B., Polino, R. and Zanetti, A., 2005. Revisiting the Lanzo peridotite (NW-Italy): “asthenospherization” of ancient mantle lithosphere. Ofioliti, 30(2): 111-124.
Newman, J., Lamb, W.M., Drury, M.R. and Vissers, R.L.M., 1999. Deformation processes in a peridotite shear zone: reaction-softening by an H2O-deficient, continuous net transfert reaction. Tectonopysics, 303: 193-222.
Nicolas, A., 1986. A melt extraction model based on structural studies in mantle peridotites. Journal of petrology, 27(4): 999-1022.
Nicolas, A., 1989. Structures of ophiolites and dynamics of oceanic lithosphere. Petrology and Structural Geology Series, 4. Kluwer Academic Publishers, Dordrecht / Boston / London, 367 pp.
Nicolas, A., Bouchez, J.-L. and Boudier, F., 1972. Kinematic interpretation of plastic deformations in the lherzolite Massif of Lanzo (Piedmont Alps); comparison with other massifs. Tectonophysics, 14(2): 143-171.
Nicolas, A., Bouchez, J.-L., Boudier, F. and Mercier, J.-C.C., 1971. Textures, structures and fabrics due to solid state flow in some european lherzolites. Tectonophysics, 12(1): 55-86.
Nicolas, A., Boudier, F. and Ceuleneer, G., 1988. Mantle flow patterns and magma chambers at ocean ridges; evidence from the Oman Ophiolite. Marine Geophysical Researchers, 9(4): 293-310.

Nicolas, A. and Dupuy, C., 1984. Origin of ophiolitic and oceanic ophiolites. Tectonopysics, 110(3-4): 177-187.
Niida, K. and Green, D.H., 1999. Stability and chemical composition of pargasitic amphibole in MORB pyrolite under upper mantle conditions. Contributions to Mineralogy and Petrology, 135: 18-40.
Ohnenstetter, M., Ohnenstetter, D., Vidal, Ph., Cornichet, J., Hermitte, D. and Mace, J., 1981. Crystallization and age of zircon from Corsican ophiolitic albitites: consequences for oceanic expansion in the Jurassic times. Earth and Planetary Science Letters, 54: 397-408.
Olgaard, D.L. and Evans, B., 1988. Grain growth in synthetic marbles with added mica and water. Contrib Mineral Petrol, 100(2): 246-260.
Ozawa, K. and Takahashi, N., 1995. P-T history of mantle diapir: the Horoman peridotite complex, Hokkaido, northern Japan. Contribution to Mineral Petrology, 120: 223-248.
Passchier, C.W., 1991. Geometric constraints on the development of shear bands in rocks. Geologie en Mijnbouw, 70: 203-211.
Pearce, N. J. G., Perkins, W. T., Westgate, J. A., Gorton, M. P., Jackson, S. E., Neal, C. R. and Chenery, S. P., 1996. A compilation of new and published major and trace element data for NIST SRM 610 and NIST SRM 612 glass reference materials. Geostandards Newsletter, 21(1): 115-144.
Pelletier, L., 2003. Relation entre une croûte océanique et sa couverture sédimentaire. L'exemple du massif de Lanzo (Alpes piémontaises, Italie), Diplôme de Géologie BENEFRI, Neuchâtel.
Pelletier, L. and Müntener, O., 2006. High pressure metamorphism of the Lanzo peridotite and its oceanic cover, and some consequences for the Sesia-Lanzo zone (northwestern Italian Alps). Lithos, 90: 111-130.
Péron-Pinvidic, G., Manatschal, G., Minshull, T.A. and Sawyer, D.S., 2007. The tectono-sedimentary evolution of the deep iberia-newfoundland margins: evidence for a complex break-up history. Tectonics, in press.
Peters, T. and Stettler, A., 1987. Radiometric age, thermobarometry, and mode of emplacement of the Totalp peridotite in the Eastern Swiss Alps. Schweizerische Mineralogische und Petrographische Mitteilungen, 67(3): 285-294.
Piccardo, G.B., 1976. Petrology of the lherzolite massif of Suvero, La Spezia. Ofioliti, 1(2): 279-317.
Piccardo, G.B., 2003. Mantle processes during ocean formation; petrologic records in peridotites from the Alpine-Apennine ophiolites. Episodes, 26(3): 193-199.
Piccardo, G.B., Müntener, O. and Zanetti, A., 2004a. Alpine-Apennine ophiolitic peridotites: new concepts on their composition and evolution. Ofioliti, 29(1): 63-74.
Piccardo, G.B., Müntener, O., Zanetti, A., Romairone, A., Bruzzone, S., Poggi, E. and Spagnolo, G., 2004b. The Lanzo south peridotite: melt/peridotite interaction in the mantle lithosphere of the Jurassic Ligurian Tethys. Ofioliti, 29(1): 37-62.
Piccardo, G.B., Rampone, E. and Vannucci, R., 1990. Upper mantle evolution during continental rifting and ocean formation; evidences from peridotite bodies of the Western Alpine-Northern Apennine system. Mémoires de la Société Géologique de France, Nouvelle Serie, 156: 323-333.
Piccardo, G.B., Zanetti, A. and Müntener, O., 2007. Melt/peridotite interaction in the Lanzo South peridotite: field, textural and geochemical evidence. Lithos, 94(1-4): 181-209.
Piccardo, G.B., Zanetti, A., Poggi, E., Spagnolo, G. and Müntener, O., 2006. Melt/peridotite interaction in the Lanzo South peridotite: field, textural and geochemical evidence. Lithos, in press.
Platt, J.P., 1984. Secondary cleavage in ductile shear zones. Journal of Structural Geology, 6: 439-442.
Platt, J.P. and Vissers, R.L.M., 1980. Extensional structures in anisotropic rocks. Journal of Structural Geology, 2: 397-410.
Pognante, U., 1989a. Lawsonite, blueschiste and eclogite formation in the southern Sesia zone (western Alps, Italy). European Journal of Mineralogy, 1: 89-104.
Pognante, U., 1989b. Tectonic implications of lawsonite formation in the Sesia zone (Western Alps). tectonophysics, 162: 219-227.
Pognante, U., Rösli, U. and Toscani, L., 1985. Petrology of ultramafic and mafic rocks from the Lanzo peridotite body (western Alps). Lithos, 18: 201-214.
Protocoll, P.c., 1972. Penrose field conference on ophiolites. Geotimes, 17(24-25).
Puschnig, A.R., 1998. The Forno unit (Rhetic Alps): Evolution of an ocean floor sequence from rifting to Alpine orogeny, Swiss Federal Institute of Technology, Zurich.
Quick, J.E., 1981. Petrology and petrogenesis of the Trinity Peridotite, an upper mantle diapir in the eastern Klamath Mountains, northern California. Journal of Geophysical Research, 86(12): 11837-11863.
Rampone, E., Hofmann, A. W., Piccardo, G. B., Vannucci, R., Bottazzi, P. and Ottolini, L., 1995. Petrology, mineral and isotope geochemistry of the external Liguride peridotites (Northern Apennines, Italy). Journal of Petrology, 36(1): 81-105.
Rampone, E., Hofmann, A. W., Piccardo, G. B., Vannucci, R., Bottazzi, P. and Ottolini, L., 1996. Trace element and isotope geochemistry of depleted peridotites from an N-MORB type ophiolite (Internal Liguride, N. Italy). Contributions to Mineralogy and Petrology, 123(1): 61-76.
Rampone, E., Hofmann, A.W. and Raczek, I., 1998. Isotopic contrast within the Internal Liguride ophiolite (N.Italy): the lack of a genetic mantle-crust link. Earth and Planetary Science Letters, 163: 175-189.
Rampone, E., Romairone, A., Abouchami, W., Piccardo, G.B. and Hofmann, A.W., 2005. Chronology, petrology and isotope geochemistry of the Erro-Tobbio peridotites (Ligurian Alps, Italy): records of late Paleozoic lithospheric extension.

Journal of Petrology, 46(4): 799-827.
Reddy, S.M., Timms, N. E., Trimby, P. W., Kinny, P. D., Buchan, C. and Blake, K., 2006. Crystal-plastic deformation of zircon: A defect in the assumption of chemical robustness. Geological Society of America, 34(4): 257-260.
Roeder, P.L. and Emslie, R.F., 1970. Olivine-liquid equilibrium. Contributions to Mineralogy and Petrology, 29: 275-289.
Rubatto, D. and Gebauer, D., 2000. Use of cathodoluminescence for U-Pb zircon dating by ion microprobe; some examples from the Western Alps. In: M. Pagel, V. Barbin, P. Blanc and D. Ohnenstetter (Editors), Cathodoluminescence in Geosciences. Springer, Berlin, pp. 373-400.
Rubatto, D., Gebauer, D. and Fanning, M., 1998. Jurassic formation and Eocene subduction of the Zermatt_Saas-Fee ophiolites: implications for the geodynamic evolution of the Central and western Alps. Contributions to Mineralogy and Petrology, 132: 269-287.
Rubatto, D. and Hermann, J., 2003. Zircon formation during fluid circulation in eclogites (Monviso, Western Alps): Implications for Zr and Hf budget in subduction zones. Geochimica et Cosmochimica Acta, 67(12): 2173-2187.
Rutter, E.H. and Brodie, K.H., 1988. Rheological behaviour of the lower crust. Ricerca Scientifica ed Educazione Permanente, 65A(58-59).
Sandrone, R., Leardi, L., Rossetti, P. and Compagnoni, R., 1986. P-T conditions for the eclogitic re-equilibration of the metaophiolotes from Val d'Ala di Lanzo (internal Piemontese zone, Western Alps). Journal of metamorphic Geology, 4: 161-178.
Sautter, V., Jaoul, O. and Abel, F., 1988. Aluminium diffusion in diposide using the 27Al(p, g)28Si nuclear reaction: Preliminary results. Earth and Planetary Science Letters, 89: 109-114.
Schaltegger, U., Desmurs, L., Manatschal, G., Müntener, O., Meier, M., Frank, M. and Bernoulli, D., 2002. The transition from rifting to sea-floor spreading within a magma-poor rifted margin: field and isotopic constraints. Terra Nova, 14: 156-162.
Schärer, U., Girardeau, J., Cornen, G. and Boillot, G., 2000. 138-121 Ma asthenospheric magmatism prior to continental break-up in the North Atlantic and geodynamic implications. Earth and Planetary Science Letters, 181(4): 555-572.
Schmid, S.M., Fügenschuh, B., Kissling, E. and Schuster, R., 2004. Tectonic map and overtall architecture of the Alpine orogen. Eclogae Geologicae Helvetiae, 97: 93-117.
Schwartz, J.J., John, B. E., Cheadle, M. J., Miranda, E. A., Grimes, C. B., Wooden, J. L. and Dick, H. J. B., 2005. Dating the growth of oceanic crust at a slow spreading ridge. Science, 310: 654-657.
Serri, G., 1980. Chemistry and petrology of gabbroic complexes from the northern Apennine ophiolites. In: A. Panayiotou (Editor), Ophiolites; Proceedings, International ophiolite symposium, pp. 296-313.
Sibson, R.H., 1977. Kinetic shear resistance, fluid pressures and radiation efficiency during seismic faulting. Pure and Applied Geophysics, 115(1-2): 387-400.
Smith, C.A., Sisson, V.B., Avé Lallemant, H.G. and Copeland, P., 1999. Two contrasting pressure-temperature-time paths in the Villa de Cura blueschist belt, Venezuela: Possible evidence for Late Cretaceous initiation of subduction in the Caribbean. Geological Society of America Bulletin, 111(6): 831-848.
Spalla, M.I., De Maria, L., Gosso, G., Miletto, M. and Pognante, U., 1983. deformazione e metamorfismo della zona Sesia-Lanzo meridionale al contatto con la falda piemontese e con il massiccio de Lanzo, Alpi Occidentali. Memoria della Societa Geologica Italiana, 26: 499-514.
Spry, A.H., 1969. The interpretation of the textures of peridotites, eclogites and granulites. Special Publication - Geological Society of Australia, 2: 307-321.
Stacey, J.S. and Kramers, J.D., 1975. Approximation of terrestrial lead isotope evolution by a two-stage model. Earth and Planetary Science Letters, 26(2): 207-221.
Suhr, G., Seck, H.A., Shimizu, N., Guenther, D. and Jenner, G., 1998. Infiltration of refractory melts into the lowermost oceanic crust; evidence from dunite- and gabbro-hosted clinopyroxenes in the Bay of Islands Ophiolite. Contributions to Mineralogy and Petrology, 131(2-3): 136-154.
Sun, S.S. and McDonough, W.F., 1989. Chemical and isotopic systemaics of oceanic basalts: Implications for mantle composition and processes. In: A.D. Sanders and M.J. Norry (Editors), Magmatism in the ocean basins. Special Publication Geological Society of London, London, pp. 313-345.
Timms, N.E., Kinny, P.D. and Reddy, S.M., 2006. Enhanced diffusion of Uranium and Thorium linked to crystal plasticity in zircon. Geochemical Transactions, 7(10).
Tribuzio, R., Thirlwall, M.F. and Vannucci, R., 2004. Origin of the gabbro-peridotite association from the northern apennine ophiolites (Italy). Journal of Petrology, 45(6): 1109-1124.
Trommsdorff, V., Piccardo, G.B. and Montrasio, A., 1993. From magmatism through metamorphism to sea floor emplacement of subcontinental Adria lithosphere during pre-Alpine rifting (Malenco, Italy). Schweizerische Mineralogische und Petrographische Mitteilungen, 73(2): 191-203.
Tucholke, B.E., Lin, J. and Kleinrock, M.C., 1998. Megamullions and mullion structure defining oceanic metamorphic core complexes on the Mid-Atlantic Ridge. Journal of Geophysical Research, 103(B5): 9857-9866.
Tucholke, B.E., Sawyer, D.S. and Sibuet, J.C., 2006. Breakup of the Newfoundland-Iberia rift. In: G. Karner, G. Manatschal and L. Pinheiro (Editors), MARGINS Theoretical and experimental.
Van der Pluijm, B.A. and Marshak, S., 2004. Earth structure, and introduction to structural and geology tectonics.
Van der Wal, D. and Bodinier, J.L., 1996. Origin of the recrystallization front in the Ronda peridotite by km-scale pervasive

porous melt flow. Contributions to Mineralogy and Petrology, 122: 387-405.
Vannucci, R., Piccardo, G. B., Rivalenti, G., Zanetti, A., Rampone, E., Ottilini, L., Oberti, R., Mazzucchelli, M. and Bottazzi, P ., 1995. Origin of LREE-depleted amphiboles in the subcontinental mantle. Geochimica and Cosmochimica Acta, 59(9): 1763-1771.
Villiger, S., Ulmer, P., Müntener, O. and Thompson, A.B., 2004. The liquid line of descent of anhydrous, mantle-derived, tholeiitic liquids by fractional and equilibrium crystallization; an experimental study at 1.0 GPa. Journal of Petrology, 45(12): 2369-2388.
Vissers, R.L.M., Drury, M.R., Hoogerduijn Strating, E.H., Spiers, C.J. and Van der Wal, D., 1995. Mantle shear zone and their effect on lithosphere strength during continental break-up. Tectonopysics, 249: 155-171.
Vissers, R.L.M., Drury, M.R., Hoogerduijn Strating, E.H. and Van der Wal, D., 1991. Shear zones in the upper mantle; a case study in an Alpine lherzolite massif. Geology, 19(10): 990-993.
Vissers, R.L.M., Drury, M.R., Newman, J. and Fliervoet, T.F., 1997. Mylonitic deformation in upper mantle peridotites of the North Pyrenean Zone (France): implications for strength and strain localization in the lithospere. Tectonopysics, 279: 303-325.
Von der Handt, A., Seyler, M., Snow, J.E. and Hellebrand, E., 2002. Geochemistry of plagioclase peridotites from the southwest Indian Ridge (63° to 65°E). Geochimica and Cosmochimica Acta, 68(11S): 706.
Warren, J.M. and Hirth, G., 2006. Grain size sensitive deformation mechanisms in naturally deformed peridotites. Earth and Planetary Science Letters, 248: 438-450.
Watson, E.B. and Harrison, T.M., 2005. Zircon thermometer reveals minimum melting conditions on earliest earth. Science, 308: 841-844.
Watson, E.B., Hayden, L. A., Wark, D. A., Cherniak, D. J., Thomas, J. B. and Manchester, J. E., 2006. New crystallization thermometers for zircon, rutile and sphene; calibrations, diffusion considerations, and applications. Geological Society of America, 38(2): 5.
Weissert, H.J. and Bernoulli, D., 1985. A transform margin in the Mesozoic Thetys: evidence from the Swiss Alps. Geologische Rundschau, 74: 731-745.
White, S.H. and Knipe, R.J., 1978. Transformation- and reaction-enhanced ductility in rocks. Journal of the Geological Society of London, 135(5): 513-516.
Whitmarsh, R.B., Manatschal, G. and Minshull, T.A., 2001. Evolution of magma-poor continental margins from rifting to seafloor spreading, Nature, pp. 150-154.
Witt-Eickschen, G. and Seck, H.A., 1991. Solubility of Ca and Al in orthopyroxene from spinel peridotite; an improved version of an empirical geothermometer. Contributions to Mineralogy and Petrology, 106(4): 431-439.
Workman, R.K. and Hart, S.R., 2005. Major and trace element composition of the depleted MORB mantle (DMM). Earth and Planetary Science Letters, 231: 53-72.